

UNIVERZITA PALACKÉHO V OLOMOUCI

Přírodovědecká fakulta
Laboratoř růstových regulátorů



Molekulární mechanismus působení vybraných inhibitorů proteinkinas

DISERTAČNÍ PRÁCE

Autor:	Mgr. Markéta Kovalová
Studijní obor:	P1527 Biologie
Studijní program:	1501V019 Experimentální biologie
Forma studia:	Prezenční
Vedoucí práce:	prof. RNDr. Vladimír Kryštof, Ph.D.
Rok:	2024

„Prohlašuji, že jsem předloženou disertační práci vypracovala samostatně za použití citované literatury.“

V Olomouci dne.....

.....

„Ráda bych poděkovala svému školiteli prof. RNDr. Vladimíru Kryštofovi, Ph.D. za odborné vedení, jeho cenné rady, věcné připomínky a podporu po celou dobu mého doktorského studia. Dále také Mgr. Haně Dostálové, Mgr. Miroslavu Peřinovi, Mgr. Jakobovi Bělíčkoví a Mgr. Marii Fedrové za jejich pomoc a neutuchající optimismus. Taktéž bych chtěla poděkovat Mgr. Evě Řezníčkové, Ph.D., Mgr. Radku Jordovi, Ph.D. a všem ostatním spoluautorům za spolupráci na společných publikacích. V neposlední řadě bych chtěla poděkovat celému týmu Katedry experimentální biologie a zejména pak Janě Hudcové a Mgr. Veronice Vojáčkové.“

Projekty v této práci byly podpořeny Univerzitou Palackého v Olomouci (IGA_PrF_2023_012), Evropskou Unií – Next Generation EU (Národní ústav pro výzkum rakoviny, program EXCELES, LX22NPO5102) a Grantovou agenturou ČR (21-06553S, 23-05462S).

Bibliografická identifikace

Jméno a příjmení autora	Markéta Kovalová
Název práce	Molekulární mechanismus působení vybraných inhibitorů proteinkinas
Typ práce	Disertační
Pracoviště	Laboratoř růstových regulátorů, Přírodovědecká fakulta, Univerzita Palackého v Olomouci
Vedoucí práce	Prof. RNDr. Vladimír Kryštof, Ph.D.
Rok obhajoby práce	2024

Abstrakt

Cyklin dependentní kinasy (CDK) představují klíčové regulátory nejen transkripčního cyklu a jejich funkce je v nádorových buňkách často narušena. To, společně s transkripční závislostí nádorů, představuje slibné důvody pro využití inhibice transkripčních CDK v nádorové terapii a v posledních letech byla představena řada slibných tCDK inhibitorů. První část této disertační práce je zaměřena na využití již známých inhibitorů tCDK v léčbě leukemií s KMT2A translokací, jejichž aplikace by mohla být přínosem ve srovnání se standardizovanou léčbou. V druhé části práce je představen nový trisubstituovaný pyrazolo[4,3-*d*]pyrimidinový derivát, LGR6768, který inhiboval CDK7 v nanomolárních koncentracích. Tento inhibitor vykazoval slibné antileukemické účinky a jeho aplikace ovlivnila buněčný cyklus i transkripci a vedla k apoptose nádorových buněk. Poslední část této práce vychází z optimalizace duálního FLT3/CDK9 inhibitoru. Ta vedla k vývoji nového ATP-kompetitivního FLT3 inhibitoru a také duálního degradéru FLT3/CDK9, jejichž testování a charakterizace byla zaměřena na leukemie s FLT3-ITD mutací.

Klíčová slova	cyklin-dependentní kinasa, transkripce, inhibitor, leukemie
Počet stran	92
Počet příloh	4
Jazyk	Český

Bibliographical identification

Autor's first name and surname	Markéta Kovalová
Title	Molecular mechanism of action of selected protein kinase inhibitors
Type of thesis	Ph.D. thesis
Department	Laboratory of Growth Regulators, Faculty of Science, Palacký University
Supervisor	Prof. RNDr. Vladimír Kryštof, Ph.D.
The year of presentation	2024

Abstract

Cyclin-dependent kinases (CDK) are key regulators of the transcriptional cycle, and they are often deregulated in cancer cells. Together with the transcriptional addiction of tumours, this provides a promising rationale for the use of transcriptional CDK inhibitors in cancer therapy, and several promising tCDK inhibitors have been introduced in recent years. The first part of this thesis focuses on known inhibitors of tCDK in the treatment of leukaemia with KMT2A translocation, whose application could be beneficial compared to standard therapy. The second part presents a novel pyrazolo[4,3-*d*]pyrimidine derivative, LGR6768, which inhibited CDK7 in the nanomolar range. This inhibitor showed promising anti-leukaemic potential and its application affected cell cycle, transcription, and induced apoptosis of cancer cells. The last part of the thesis is based on the optimisation of dual FLT3/CDK9 inhibitor, which led to the development of new ATP-competitive FLT3 inhibitor and also dual FLT3/CDK9 degrader. The characterisation and testing of these compounds was focused on leukaemia with FLT3-IDT mutation.

Keywords	Cyclin-dependent kinase, transcription, inhibitor, leukaemia
Number of pages	92
Number of appendices	4
Language	Czech

OBSAH

SEZNAM POUŽITÝCH ZKRATEK	8
1 ÚVOD A CÍLE PRÁCE	11
2 TRANSKRIPČNÍ CYKLUS A JEHO REGULACE	13
2.1 CDK v regulaci transkripčního cyklu	14
2.1.1 Cyklin dependentní kinasa 7	15
2.1.2 Cyklin dependentní kinasy 8 a 19	18
2.1.3 Cyklin dependentní kinasa 9	19
2.1.4 Cyklin dependentní kinasa 10	21
2.1.5 Cyklin dependentní kinasa 11	22
2.1.6 Cyklin dependentní kinasy 12 a 13	23
2.1.7 Cyklin dependentní kinasa 20	25
3 PATOLOGICKÁ DEREGULACE TRANSKRIPČNÍHO CYKLU	27
3.1 Změny v transkripčních CDK	28
3.2 Transkripční faktor Myc	30
3.3 Translokace lysinmethyltransferasy <i>KMT2A</i>	31
3.3.1 <i>KMT2A</i> -r leukemie	33
4 INHIBITORY TRANSKRIPČNÍCH CYKLIN DEPENDENTNÍCH KINAS	35
4.1 Inhibitory CDK7	37
4.2 Inhibitory CKD8/19	41
4.3 Inhibitory CDK9	42
5 METODIKA	46
5.1 Buněčné kultury	46
5.2 Analýza cytotoxicity	47
5.3 Analýza exprese genů	47
5.4 Analýza buněčného cyklu	48
5.5 SDS PAGE a imunodetekce	48
5.6 Detekce aktivity kaspas 3/7	49
6 KOMENTOVANÉ VÝSLEDKY A DISKUZE	50
6.1 Inhibitory CDK v léčbě leukemií s <i>KMT2A</i> translokací	50
6.2 CDK7 jako potenciální terapeutický cíl	55
6.3 Od CDK inhibice k inhibici FLT3	61

7	ZÁVĚR.....	67
8	SEZNAM POUŽITÉ LITERATURY.....	70
9	CURRICULUM VITAE.....	89
10	SEZNAM PŘÍLOH	91

SEZNAM POUŽITÝCH ZKRATEK

9G8 – Serine/arginine-rich splicing factor 7
ACTB – Actin beta
AFF1 – AF4/FMR2 family member 1
AFF4 – ALF transcription elongation factor 4
ALL – Acute lymphoblastic leukaemia
AML – Acute myeloid leukaemia
ATM – ATM Serine/Threonine Kinase
B2M – Beta-2-microglobulin
BARD1 – BRCA1-associated RING domain protein 1
Bcl-2 – Apoptosis regulator Bcl-2
BCR – Breakpoint cluster region
BRCA1 – Breast cancer type 1 susceptibility protein
CAK – CDK-activating kinase
CDK – Cyclin-dependent kinase
CDKi – CDK inhibitor
CK1 δ – Casein kinase 1 δ
CKM – CDK8 kinase module
CML – chronic myeloid leukaemia
CNG – Copy-number gain
CNL – Copy-number loss
CNV – Copy-number variations
CTD – C-terminal domain
DDR – DNA damage response
DOT1L – Histone-lysine N-methyltransferase, H3 lysine-79 specific
DSIF – DRB sensitivity-inducing factor
DLT – Dose limiting toxicity
E2F1 – Transcription factor E2F1
ELL2 – RNA polymerase II elongation factor ELL2
EFS – Event free survival
ER – Estrogen receptor
ETS2 – Protein C-ets-2
FLT3 – FMS-like tyrosine kinase 3
FP – Fusion partner
GAPDH – Glyceraldehyde-3-phosphate dehydrogenase
GI₅₀ – Half maximal growth concentration
GSK3 α – Glycogen synthase kinase-3 alpha
HR+ – hormone-receptor positive
HER2 – Human epidermal growth factor receptor 2
HGSOC – High-grade serous ovarian cancer
Hox – Homeobox protein
IC₅₀ – Half maximal inhibitory concentration
IMDM - Iscove's Modified Dulbecco's Medium

ITD – Internal tandem duplication
JAK – Janus kinase
Kin28 – Serine/threonine-protein kinase KIN28
KMT – Histone-lysine N-methyltransferase
LEDGF – Lens epithelium-derived growth factor
Mcl-1 – Induced myeloid leukemia cell differentiation protein Mcl-1
Med – Mediator of RNA polymerase II transcription subunit
MEIS-1 – Meis homeobox 1
MePCE – 7SK snRNA methylphosphate capping enzyme
miRNA – MicroRNA
MLL1 – Mixed-lineage leukemia 1
MLLT – MLLT super elongation complex subunit
MM – Multiple myeloma
MYB – MYB proto-oncogene,
MYC – Myc proto-oncogene
NELF – Negative elongation factor
NHL – Non-Hodgkin's lymphoma
OS – Overall survival
p53 – Cellular tumor antigen p53
PAGE - Polyacrylamide gel electrophoresis
PDX – Patient derived xenograft
PIC – Preinitiation complex
PR – Partial response
PRC1 – Polycomb Repressive Complex 1
PROTAC – Proteolysis targeting chimera
PTD – Partial tandem duplication
P-TEFb – Positive transcription elongation factor
RFS – Recurrent-free survival
RHD – Replication-dependent histone
RNAPII – RNA polymerase II
RNPS1 – RNA-binding protein with serine-rich domain 1
Rpb1 – DNA-directed RNA polymerase II subunit RPB1
RPL13A – Ribosomal protein L13a
RPMI - Roswell Park Memorial Institute Medium
RSR – Replication stress response
RTS – Receptor tyrosine kinase
RUNX – RUNX family transcription factor
SD – Stable disease
SDS - Sodium dodecyl sulfate
SEC – Super-elongation factor
siRNA – Small interfering RNA
snoRNA – Small nucleolar RNA
snRNA – Small nuclear RNA
Srb10 – Meiotic mRNA stability protein kinase SSN3

STAT – Signal transducer and activator of transcription
tCDK – Transcriptional cyclin-dependent kinase
TCF – T cell factor
TD – Tandem duplication
TES – Transcription end site
TF – Transcription factor
TGI – Tumor growth inhibition
TNBC – Triple-negative breast cancer
TP53 – Tumor Protein P53
TRIM28 – Tripartite motif containing 28
WT – Wild type
 α -MEM - Minimum Essential Medium α

1 ÚVOD A CÍLE PRÁCE

Proteinkinasy představují klíčové regulátory široké škály buněčných procesů včetně regulace proliferace a diferenciaci buněk, transkripce, apoptosy či buněčného metabolismu. Zprostředkovávají přenos γ -fosfátové skupiny z ATP na cílový substrát vedoucí ke konformační změně substrátu a ovlivnění jeho aktivity. Deregulace proteinkinas, způsobená změnami v expresi či mutacemi, je pozorována u řady onemocnění včetně nádorových, neurodegenerativních či zánětlivých (Manning *et al.*, 2002; Rask-Andersen *et al.*, 2014)

Mezi proteinkinasy patří i rodina cyklin-dependentních kinas (CDK). Jedná se o skupinu serin/threonin kinas, jejichž katalytická aktivita je závislá na regulační podjednotce, kterým je obvykle protein cyklin. V genomu člověka bylo popsáno 21 genů kódujících CDK a většina z nich specificky váže pouze jeden nebo několik málo z 30 známých cyklinů. Na základě strukturních a funkčních studií byly CDK rozděleny do dvou podrodin – CDK regulující buněčný cyklus (CDK1-6 a CDK14-18) a CDK regulující transkripci (CDK7-13, CDK19 a CDK20) (Malumbres *et al.*, 2009; Malumbres, 2014; Wood *et al.*, 2018). Mimo tyto hlavní dva procesy jsou však zapojeny do regulace široké plejády dalších buněčných procesů, jako jsou například opravy DNA (Blazek *et al.*, 2011; Nepomuceno *et al.*, 2017), sestřih RNA (Hu *et al.*, 2003), epigenetické modifikace (Ebmeier *et al.*, 2017) či neurogeneze (Jessberger *et al.*, 2009) a spermatogeneze (Mikolcevic *et al.*, 2012). Struktura CDK je dvoualočná, obdobně jako struktura většiny kinas. Menší aminoterminální lalok je tvořený primárně β -skládanými listy. Ty jsou spojené flexibilní pantovou oblastí s α -helixy tvořící větší karboxy-terminální lalok. Mezi tyto oblasti je vmezeřeno konzervativní aktivní místo složené z ATP-vazebné domény, cyklin-vazebné domény a T-aktivační smyčky (Whittaker *et al.*, 2017; Wood *et al.*, 2018).

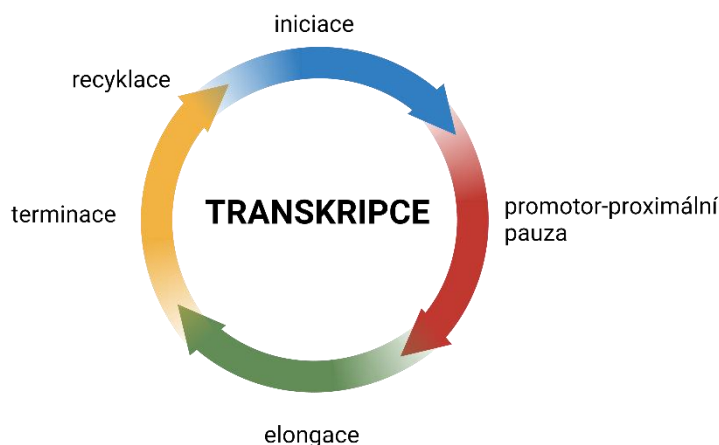
Pro svoji esenciální roli a častou deregulaci v rámci nádorových onemocnění představují CDK slibné terapeutické cíle již několik dekad. Vývoj selektivních inhibitorů však komplikuje vysoká strukturní similarita a konzervativnost ATP-vazebné domény. Prvotní ATP-kompetitivní inhibitory vykazovaly velmi omezenou selektivitu, což společně s nedostatečným pochopením mechanismu účinku vedlo k jejich toxicitě a u většiny z nich také k selhání v klinických testováních. Nicméně v průběhu let byla objevena řada strukturních odlišností mezi jednotlivými CDK, které umožnily vývoj nových selektivních, nejen ATP-kompetitivních, inhibitorů. Některé již byly schváleny pro léčbu (např. CDK4/6

specifické inhibitory palbociclib, abemaciclib, ribociclib a trilaciclib) a velká řada z nich je testována v klinických studiích (Whittaker *et al.*, 2017; Zhang *et al.*, 2021a).

Tato disertační práce je zaměřena na charakterizaci nových nízkomolekulárních inhibitorů transkripčních cyklin-dependentních kinas, které byly navrženy a připraveny na pracovišti školitele, s cílem pochopit jejich mechanismu účinku a ověřit možnosti jejich využití jako protinádorová léčiva se zaměřením na leukemická onemocnění.

2 TRANSKRIPČNÍ CYKLUS A JEHO REGULACE

Transkripci protein-kódujících genů lze považovat za několika krokový regulovaný cyklický proces, vykazující řadu paralel s buněčným cyklem, a lze tedy hovořit o transkripčním cyklu (Obr. 1). Transkripce protein-kódujících genů je řízená RNA polymerasou II (RNAPII) a v rámci jedné buňky se zároveň odehrávají tisíce transkripčních cyklů. Každý tento cyklus je složen z několika kroků, a to z tvorby preiniciačního komplexu (PIC) a jeho interakce s oblastí promotoru, iniciace transkripce, promotor-proximální pauzy, elongace, terminace a fáze recyklace komponent transkripčního cyklu (Galbraith *et al.*, 2019; Parua *et al.*, 2020; Vervoort *et al.*, 2022).



Obr. 1: Schematické znázornění transkripčního cyklu (upraveno dle Vervoort *et al.*, 2022; vytvořeno pomocí BioRender.com).

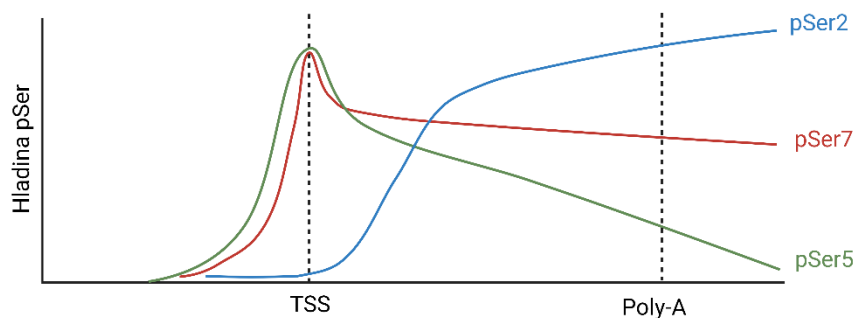
Prvním krokem transkripčního cyklu je sestavení PIC, obsahující RNAPII a řadu transkripčních faktorů (TFIIA, TFIIB, TFIID, THIIIE, TFIIF a THIIH). Před jeho sestavením dochází k zapojení mediátorového komplexu, který vytváří most mezi oblastí promotoru a enhanceru. Po sestavení PIC dochází k iniciaci transkripce za zapojení kinasové domény TFIIH. Krátce po proběhnutí transkripce, zhruba 30-60 nukleotidů, následuje tzv. promotor-proximální pauza indukovaná faktory DSIF (*DRB sensitivity-inducing factor*) a NELF (*negative elongation factor*). Za uvolnění transkripčního aparátu z pauzy je zodpovědný super-elongační komplex (SEC) obsahující pozitivní transkripční elongační faktor b (P-TEFb) a následně dochází k produktivní elongaci transkriptu. Po opuštění promotor-proximální pauzy může dojít k re-inicaci transkripce. Transkripční faktory

a mediátor setrvávají v oblasti promotoru po iniciaci a re-iniciaci nového cyklu je tak časově méně náročná než prvotní iniciace (Wu *et al.*, 2021; Vervoort *et al.*, 2022).

Proces transkripce je přísně regulován na dvou vzájemně propojených úrovních. První regulace se odehrává na úrovni 3D organizace chromatinu a jeho modulátorů. Druhá úroveň zahrnuje transkripční faktory (TF), transkripční fosfatasy a transkripční cyklin dependentní kinasy (tCDK) s jejich vazebnými cykliny (Lee *et Young*, 2013; Vervoort *et al.*, 2022). Bezchybná regulace transkripce je nezbytná pro správné ustanovení buněčné identity a funkci buněk. Její narušení pak vede k řadě nejen nádorových onemocnění. Následující text bude zaměřen na regulaci transkripce na úrovni jednotlivých transkripčních cyklů se zaměřením na transkripční CDK.

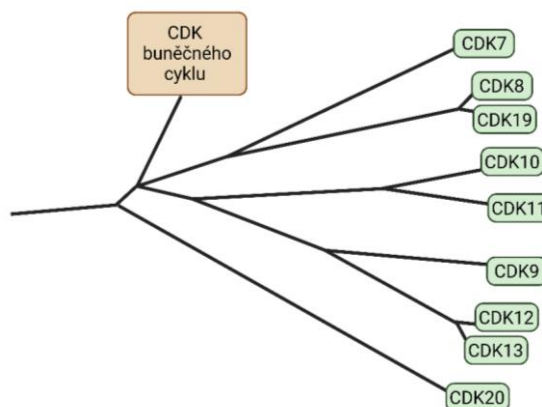
2.1 CDK v regulaci transkripčního cyklu

Transkripční CDK hrají významnou regulační roli v průběhu celého procesu transkripce, jelikož přímo ovlivňují aktivitu RNAPII. RNAPII je klíčovým enzymem v celém procesu transkripce a její regulace je založena na reverzibilní fosforylaci C-terminální domény (CTD). CTD je doménou velké podjednotky (Rpb1) RNAPII a je složena z několika opakování konzervativní heptaptidové sekvence – Tyr₁-Ser₂-Pro₃-Thr₄-Ser₅-Pro₆-Ser₇ (YSPTSPS). Každý Ser, Thr a Tyr může být fosforylován a to například právě komplexem CDK/cyklin, které fosforylují serinová residua (pSer_{2/5/7}). V průběhu transkripce se hladiny fosforylací jednotlivých serinových residuí mění (Obr. 2) a tyto změny hrají klíčovou roli. Ovlivňují nejen aktivitu polymerasy, ale také regulují postupnou rekrutaci dalších regulátorů transkripce (Corden, 1990; Galbraith *et al.*, 2019; Parua *et Fisher*, 2020). Esenciální roli tCDK podporuje také skutečnost, že jejich deficiencie je embryonálně letální (Li *et al.*, 2004; Westerling *et al.*, 2007; Ganuza *et al.*, 2012; Dickinson *et al.*, 2016; Juan *et al.*, 2016; Snouffer *et al.*, 2017; Nováková *et al.*, 2019). Výjimkou je CDK19, jejíž ztráta embryonálně letální není a neovlivňuje ani délku života (Mogila *et al.*, 2022).



Obr. 2: Změny v hladinách pSer modifikací RNAPII CTD v průběhu transkripce protein kódujících genů (upraveno dle (Constantin *et al.*, 2022); vytvořeno pomocí BioRender.com).

Na základě evoluční příbuznosti bylo do skupiny tCDK zařazeno devět kinas (Obr. 3), přičemž zapojení do regulace transkripce je nejlépe pochopeno u CDK7, CDK8/19 a CDK9. Mimo tyto tři kinasy patří mezi tCDK také CDK10, CDK11-13 a CDK20. O těchto kinasach máme zatím velmi málo informací, avšak v posledních letech se taktéž stávají předmětem výzkumu.

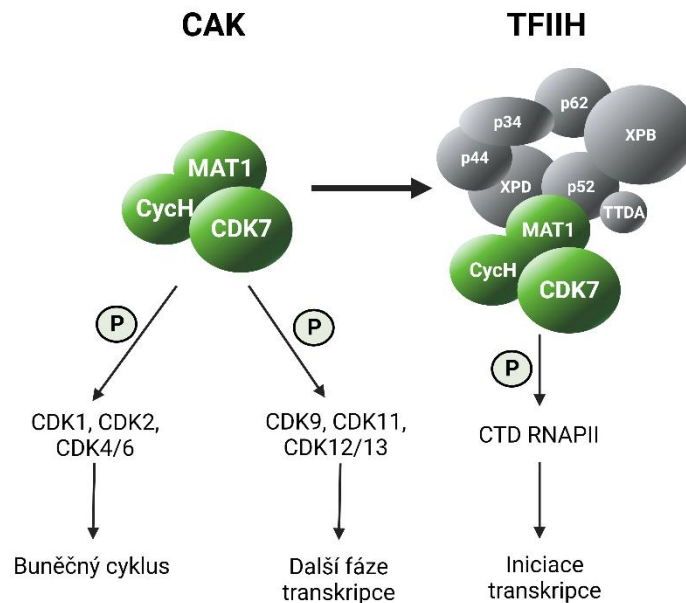


Obr. 3: Schematické znázornění evolučních vztahů mezi cyklin-dependentními kinasami se zaměřením na transkripční CDK (upraveno dle Malumbres, 2014; vytvořeno pomocí BioRender.com).

2.1.1 Cyklin dependentní kinasa 7

CDK7 je evolučně řazena do skupiny transkripčních CDK, svou činností však ovlivňuje nejen transkripci, ale přes aktivaci dalších CDK také buněčný cyklus (Obr. 4). CDK7 je také někdy označována jako CDK-aktivační kinasa (CAK) a tvoří, společně s cyklinem H a proteinem MAT1, trimerní komplex. Tento komplex může fungovat samostatně nebo

jako součást desetipodjednotkového transkripčního faktoru TFIIF (Malumbres, 2014; Li *et al.*, 2022).



Obr. 4: Role CDK7 v regulaci transkripce a buněčného cyklu (vytvořeno pomocí BioRender.com).

TFIIF je obecný transkripční faktor, který hraje roli při iniciaci transkripce. Jeho podjednotky disponují helikasovou, ATP-asovou a také kinasovou aktivitou, kterou zprostředkovává právě CDK7. CDK7 je zodpovědná za fosforylaci CTD RNAPII predominantně v pozici Ser5 (Roy *et al.*, 1994; Li *et al.*, 2022). Tato fosforylace umožní uvolnění RNAPII z oblasti promotoru a zahájí tak transkripci (Wong *et al.*, 2014). CDK7 prostřednictvím pSer5 CTD může regulovat také ko-transkripční vazbu 5' methylguanositinové čepičky (Ebmeier *et al.*, 2017; Noe Gonzalez *et al.*, 2018).

In vitro experimenty s CDK7 i jejím kvasinkovým orthologem Kin28 ukázaly roli také při fosforylaci Ser7. Tato fosforylace je pravděpodobně závislá na předchozí fosforylaci Ser5. Substituce residuí Ser5 za alanin vedla k poklesu hladin pSer7. Naopak stejná substituce residuí Ser2 či Ser7 neměla na fosforylaci Ser5 vliv (Akhtar *et al.*, 2009).

Fosforylaci CTD však role CDK7 při regulaci transkripce nekončí. Svou aktivitou ovlivňuje také promotor-proximální pauzu. Její inhibice vede k narušení výměny TFIIF za DSIF, rekrutace NELF a následného ustanovení promotor-proximální pauzy. Tento efekt byl pozorován u genů *GAPDH*, *p21* či *c-Myc* (Glover-Cutter *et al.*, 2009; Larochelle *et al.*, 2012) a může být pouze genově specifický. Studie (Ebmeier *et al.*, 2017), která zahrnovala

celogenomovou Chip-seq analýzu ukázala, že inhibice CDK7 buněk vedla ke zvýšení tzv. RNAPII pausing indexu (poměr mezi množstvím RNAPII v oblasti -30 až +300 bází vzhledem k místu zahájení transkripce a množstvím RNAPII v oblasti od +301 bází). Tento nárůst byl v souladu s pozorovaným zahájením produktivní elongace indukovaným CDK7. V tomto případě CDK7 fosforylovala Thr168 v aktivační T-smyčce CDK9 čímž zapříčinila její aktivaci. Aktivní CDK9 následně fosforylovala CTD RNAPII a další TF, což vedlo k uvolnění transkripčního aparátu z promotor-proximální pauzy (Larochelle *et al.*, 2012). Inhibice CDK7 také vedla k celkové redukci pSer2 směrem ke 3' konci genů. Zároveň však byl signál pSer2 posunut až do oblasti hraničící s 3' koncem transkripční oblasti, s čímž korelovalo pozorované oddálení terminace transkripce (Ebmeier *et al.*, 2017).

Jak již vyplývá z názvu CAK, tento trimerní komplex slouží k aktivaci dalších CDK přes fosforylaci threoninů v aktivační T-smyčce (Whittaker *et al.*, 2017; Li *et al.*, 2022). V předchozím odstavci byla zmíněna aktivace CDK9 (Larochelle *et al.*, 2012). Z dalších transkripčních kinas CDK7 aktivuje také CDK11 (Thr219), CDK12 (Thr893) a CDK13 (Thr871) (Larochelle *et al.*, 2006; Rimel *et al.*, 2020). Jejich aktivací CDK7 dále nepřímo reguluje transkripci. Podobně je také schopna nepřímo regulovat buněčný cyklus skrze aktivaci CDK1 (Thr161), CDK2 (Thr160) a také CDK4/6 (Thr172/Thr177) (Fesquet *et al.*, 1993; Russo *et al.*, 1996; Ganuza *et al.*, 2012; Bisteau *et al.*, 2013). V případě buněčného cyklu je následkem inaktivace/inhibice CDK7 mimo jiné pokles ve fosforylaci podřízených CDK a také zastavení v G1 či G2/M fázích (Ganuza *et al.*, 2012; Patel *et al.*, 2018; Olson *et al.*, 2019; Marineau *et al.*, 2022).

Mezi další role CDK7 patří také regulace transkripčních faktorů jako například p53 či E2F1 (Ko *et al.*, 1997; Lu *et al.*, 1997; Vandel *et al.*, 1999), estrogenového a androgenového receptoru či alfa receptoru kyseliny retinové (Rochette-Egly *et al.*, 1997; Chen *et al.*, 2000; Lee *et al.*, 2000) a regulace epigenetických modifikací (Glover-Cutter *et al.*, 2009; Ebmeier *et al.*, 2017).

CDK7 ovlivňuje velkou řadu procesů, nicméně její role v řízení globální transkripce je sporná. Výsledky některých studií naznačují, že aktivita CDK7 není nezbytně nutná pro fosforylaci Ser5 nebo globální transkripci. Esenciální role CDK7 tedy možná nespočívá v přímém regulaci RNAPII, ale spíše v regulaci dalších CDK a TF (Ganuza *et al.*, 2012; Donovan *et al.*, 2022). To také podporuje pozorovaný efekt CDK7 selektivního inhibitoru

YKL-5-124. Jeho aplikace vedla k ovlivnění buněčného cyklu, avšak neovlivnila globální transkripci a fosforylaci CTD RNAPII (Olson *et al.*, 2019).

2.1.2 Cyklin dependentní kinasy 8 a 19

CDK8 a její paralog CDK19 vytvářejí společně s cyklinem C (cycC) a proteiny Med12 a Med13 CDK8-kinasový modul (CKM). Prvotní testy na kvasinkách popsaly represivní funkci Srb10 (ortholog CDK8) prostřednictvím fosforylace CTD a zabránění sestavení funkčního PIC (Hengartner *et al.*, 1998). Dlouhou dobu tak byla CDK8 považována pouze za negativní regulátor transkripce. V rámci regulace transkripce však CDK8 zastává několik funkcí od regulace globální transkripce, kdy inhibuje re-iniciaci transkripce, až po regulaci konkrétních signálních drah pomocí fosforylace specifických transkripčních faktorů (Wu *et al.*, 2021).

Primární role CDK8 je spojována s mediátorovým komplexem regulujícím sestavení pre-iniciačního komplexu na počátku transkripce. Jedná se o velký multiproteinový komplex složený z 30 proteinů a lze jej rozdělit na 2 části – jádro mediátorového komplexu a CKM. Tyto 2 podjednotky spolu mohou buď interagovat (CDK8-mediátorový komplex), nebo fungovat odděleně (Wu *et al.*, 2021). Represivní funkce CKM je založena na kompetici s RNAPII o vazbu do jádra mediátorového komplexu. Interakce CKM s jádrem mediátorového komplexu znemožní vazbu RNAPII, a tedy iniciaci transkripce (Knuesel *et al.*, 2009; Tsai *et al.*, 2013). Tato represivní funkce CKM je však nezávislá na fosforylační aktivitě CDK8 (Elmlund *et al.*, 2006; Knuesel *et al.*, 2009). Inhibice pomocí CKM není omezená pouze na inhibici při prvotním sestavení PIC, ale je schopna interagovat s PIC po jeho sestavení a inhibovat tak re-iniciaci transkripce (Knuesel *et al.*, 2009).

Další represivní role CDK8 spočívá v regulaci aktivity komplexu CDK7/cycH. CDK8 katalyzuje fosforylaci cycH v místě Ser5/304, což negativně ovlivňuje aktivitu CDK7/cycH a následně celého transkripčního faktoru TFIIH nezbytného v raných fázích transkripce (Akoulitchev *et al.*, 2000).

I přes zmíněné negativní regulace transkripce, CDK8 může fungovat také jako pozitivní regulátor transkripce, avšak pravděpodobně pouze v případě specifických genů. Deplece CDK8 vede k narušení rekrutace CDK7 a CDK9, ovlivnění podřízených fosforylací CTD a také rychlosti elongace. Zmíněný efekt byl pozorován například u genů zapojených

do odpovědi na sérové růstové faktory (*serum response network*) nebo genů exprimovaných při reakci na hypoxii (Donner *et al.*, 2010; Galbraith *et al.*, 2013).

Mezi další substráty CDK8 patří několik transkripčních faktorů. Pomocí jejich fosforylace CDK8 řídí nejen jejich aktivitu a expresi podřízených genů, ale také například jejich degradaci. Příkladem mohou být transkripční faktory STAT1, STAT3 a STAT5 (Bancerek *et al.*, 2013), E2F1 (Morris *et al.*, 2008; Zhao *et al.*, 2013) nebo Smad (Alarcón *et al.*, 2009). Svou aktivitou ovlivňuje i signální dráhu Notch (Fryer *et al.*, 2004).

V průběhu lidské evoluce došlo k replikací genů *CDK8*, *Med12* a *Med13* za vzniku jejich paralogů *CDK19*, *Med12L* a *Med13*. CDK8 a CDK19 vykazují vysokou sekvenční shodu v doméně vázající cyklin C, a podobně jako CDK8 vytváří CDK19 kinasový komplex CDK19/cycC/Med12/Med13 (Bourbon, 2008; Daniels *et al.*, 2013; Wu *et al.*, 2021). Ve většině tkání jsou tyto kinasy ko-exprimovány až na pár výjimek, které vykazující vyšší expresi CDK8 či naopak CDK19. Podobně se funkce těchto dvou paralogů z velké části překrývá, nicméně například u nádorových buněk karcinomu kolorekta byly objeveny odlišné soubory genů ovlivněné CDK8 nebo CDK19, což naznačuje specializaci jednotlivých kinas (Galbraith *et al.*, 2013).

2.1.3 Cyklin dependentní kinasa 9

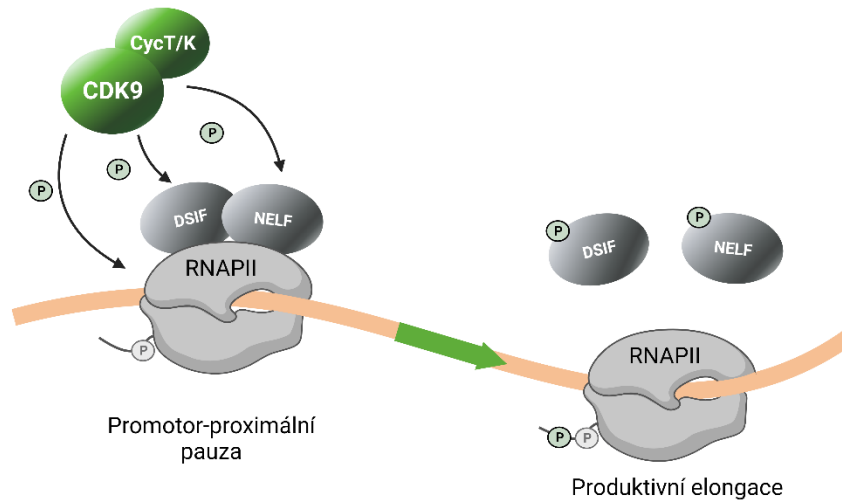
CDK9 je známá zejména pro svou nezbytnou roli v procesu elongace transkripce. Společně s cykliny skupiny T (cycT1, cycT2a a cycT2b) nebo cyklinem K vytváří P-TEFb komplex, který tuto fázi transkripce reguluje (Peng *et al.*, 1998; Fu *et al.*, 1999). V lidských buňkách je CDK9 exprimována ve 2 isoformách – CDK9₅₅ a CDK9₄₂, které se liší svojí molekulovou hmotností a lokalizací (Morales *et* Giordano, 2016; Egloff, 2021). Navíc obě isoformy odlišně interagují s proteinem Ku70, který je zapojen do oprav DNA, což naznačuje jejich další možné rozdílné funkce (Liu *et al.*, 2010). Nicméně v publikovaných experimentech není vždy detekovaná isoforma definována, avšak prvotní objev CDK9 se vztahuje k isoformě CDK9₄₂, a ta je také obecně více exprimovaná (Graña *et al.*, 1994; Egloff, 2021).

Primární role CDK9 je spojována s uvolněním RNAPII z promotor-proximální pauzy, což vede k zahájení produktivní elongace (Obr. 5). Pro efektivní narušení této pauzy je nezbytná fosforylace tří substrátů CDK9 (Cheng *et* Price, 2007). Prvním z nich jsou serinová residua CTD RNAPII. V případě CDK9 je fosforylační aktivita obecně

spojována se Ser2, nicméně některé studie ukázaly také její schopnost fosforylovat i Ser5 (Ramanathan *et al.*, 2001; Shim *et al.*, 2002; Glover-Cutter *et al.*, 2009; Ebmeier *et al.*, 2017). Navíc CDK9 pravděpodobně preferenčně fosforyluje již dříve fosforylované CTD, např. ty obsahující pSer7 (Marshall *et al.*, 1996; Czudnochowski *et al.*, 2012). Naopak předchozí fosforylace Ser2 a Ser5 zabraňovaly fosforylační aktivitě CDK9. Tato studie však také popsala CDK9 jako primárně Ser5 kinasu. Role P-TEFb, a tedy CDK9, byla rovněž významně popsána v souvislosti s transkripcí viru HIV (Zhu *et al.*, 1997; Garber *et al.*, 1998); v tomto modelu byla také pozorována schopnost CDK9 měnit substrátovou specifitu v závislosti na přítomnosti/nepřítomnosti specifického proteinu Tat. V nepřítomnosti Tat CDK9 fosforylovala Ser2 a za fosforylaci Ser5 byla zodpovědná CDK7. Přítomnost Tat proteinu však umožnila CDK9 fosforylovat Ser2 i Ser5 (Zhou *et al.*, 2000). Podobně i u lidských buněk byly pozorovány změny v substrátové specifitě P-TEFb. Konkrétně fosforylace Tyr1 CTD vedla k nárůstu hladiny pSer2, přičemž změny v hladinách pSer5 nebyly detekovány. Nicméně v případě nefosforylované CTD P-TEFb preferenčně fosforylovala Ser5. Inhibice pTyr1 také vedla k akumulaci RNAPII v oblasti promotoru a došlo tedy k narušení uvolnění RNAPII z promotor-proximální pauzy (Mayfield *et al.*, 2019). Zmíněná fosforylace CTD navíc také ovlivňuje interakce mezi RNAPII a DSIF, dalším substrátem CDK9 zapojeným do promotor-proximální pauzy, přičemž DSIF interaguje s nefosforovanou formou RNAPII (Wada *et al.*, 1998).

DSIF je schopen fungovat jako negativní i pozitivní regulátor transkripce, a to na základě jeho fosforylačního stavu. Je složen ze dvou podjednotek – hSpt5 a hSpt4. CDK9, jakožto součást P-TEFb, je zodpovědná za fosforylaci podjednotky hSpt5, a to konkrétně Thr4 v C-terminálního regionu. Tato fosforylace je nezbytná pro aktivační funkci DSIF a blokuje jeho represivní aktivitu (Ivanov *et al.*, 2000; Yamada *et al.*, 2006).

Posledním substrátem v regulaci promotor-proximální pauzy je NELF. Jedná se o multiproteinový komplex složený ze čtyř podjednotek, který interaguje s DSIF. Fosforylace podjednotky NELF-E vede k disociaci NELF z elongačního komplexu (Yamaguchi *et al.*, 1999; Fujinaga *et al.*, 2004). P-TEFb je schopný fosforylovat také podjednotku NELF-A (Lu *et al.*, 2016). Substrátová specifita byla v tomto případě pravděpodobně ovlivněna dalšími transkripčními faktory, které rekrutují P-TEFb.



Obr. 5: Zapojení CDK9 v při uvolnění promotor-proximální pauzy (upraveno dle Vervoot, 2020; vytvořeno pomocí BioRender.com)

CDK9 je také zapojena v pozdějších fázích transkripce, kde ovlivňuje sestřih a úpravy 3' konce vznikající RNA (Pirngruber *et al.*, 2009; Lenasi *et Barboric*, 2010; Laitem *et al.*, 2015; Parua *et al.*, 2018). Při zajištění produktivní elongace a úprav vznikající RNA CDK9 pravděpodobně spolupracuje s CDK12 a CDK13 (Egloff, 2021).

Mimo transkripci hraje CDK9 významnou roli i při kontrole stability genomu. Například v komplexu s cycK, ne však cycT1 či cycT2, je zapojená do odpovědi na replikační stres (RSR, *replication stress response*) (Yu *et al.*, 2010). Také hraje roli v odpovědi na poškození DNA (DDR, *DNA damage response*), kdy interaguje s BRCA1 a BARD1, jakožto důležitými proteiny při DDR, a pravděpodobně reguluje opravy DNA homologní rekombinací (Nepomuceno *et al.*, 2017). Navíc její deplece zvýšila citlivost buněk k radiační terapii (Storch *et Cordes*, 2016; Nepomuceno *et al.*, 2017).

2.1.4 Cyklin dependentní kinasa 10

I přesto, že byla CDK10 popsána již téměř před 30 lety (Graña *et al.*, 1994; Guen *et al.*, 2017), její funkce začíná být více pochopena až v posledních letech. Po dlouhou dobu byla totiž považována za sirotčí CDK bez známého cyklinu. CDK10 vytváří komplex s cyklinem Q (dříve cyklin M) (Guen *et al.*, 2013), avšak studie (Zimmermann *et al.*, 2016) popsala také interakci s cyklinem G2. V lidských buňkách je CDK10 exprimována v několika isoformách

(Crawford *et al.*, 1999; Sergère *et al.*, 2000), přičemž kratší isoformy pravděpodobně nevytváří komplex s cycQ (Guen *et al.*, 2013).

Rozsáhlejší studie zabývající se zejména substráty CDK10 byla zveřejněna teprve v roce 2022 (Düster *et al.*, 2022). Tato studie poprvé popsala CDK10 jako CTD kinasu, přičemž CDK10 je schopna fosforylovat Ser2, Ser5 a v menší míře i Ser7. Pro svou kinasovou aktivitu nepotřebovala předchozí fosforylace CTD a ve srovnání s CDK7 a CDK9 byla její kinasová aktivita nižší.

Mezi substráty CDK10 patří i další proteiny zapojené do regulace transkripce. Jedním z nich je protein MePCE (Düster *et al.*, 2022), což je RNA metyltransferasa zodpovědná za tvorbu 5' methylguanosinové čepičky u 7SK malé jaderné RNA (snRNA). Navíc MePCE, společně s 7SK snRNA a několika dalšími proteiny, vytváří komplex zodpovědný za inaktivaci P-TEFb (Egloff *et al.*, 2018; Yang *et al.*, 2019). Dalším substrátem je protein TRIM28 (Düster *et al.*, 2022), který je zapojený do regulace celé řady procesů, například DDR dráhy, regulace proteinu p53 či epiteliálně-mesenchymální transice, a jeho zvýšená exprese je asociována s horší prognózou některých nádorových onemocnění (Czerwińska *et al.*, 2017; Yang *et al.*, 2023). CDK10 interaguje také s transkripčním faktorem ETS2 (Kasten *et al.*, 2001).

Další pravděpodobné substráty CDK10 jsou zapojené do regulace široké plejády buněčných procesů, například úprav miRNA, regulace translace, či signálních drah růstových faktorů a řady dalších (Düster *et al.*, 2022). Nicméně role CDK10 a přesný mechanismus jejího zapojení do těchto procesů ještě zbývá objasnit.

2.1.5 Cyklin dependentní kinasa 11

V lidském genomu jsou dva vysoce podobné geny (*CDK11A* a *CDK11B*) (Gururajan *et al.*, 1998) kódující několik variant CDK11 a pomocí alternativního sestřihu vzniká četné množství isoform. Primárně jsou exprimovány isoformy CDK11^{p110} a CDK11^{p58} (Trembley *et al.*, 2004). Třetí častá isoforma CDK11^{p46} vzniká proteolytickým štěpením kaspasami z delších isoform v průběhu apoptosy (Beyaert *et al.*, 1997). Isoformy CDK11 tvoří komplexy s několika isoformami cyklinů L1 a L2 (Loyer *et al.*, 2008). Primárně je CDK11 spojována s regulací sestřihu pre-mRNA. CDK11^{p110} je schopna interagovat se sestřihovými faktory RNPS1 a 9G8. Navíc protein 9G8 je fosforylačním substrátem CDK11^{p110}

a imunodeplece CDK11^{p110} v sestřihovém testu vedla k poklesu sestřihu testovaného β -globinu (Loyer *et al.*, 1998; Hu *et al.*, 2003). Isoforma p110 je schopna interakce také s několika elongačními faktory. Imunoprecipitační analýza prokázala interakci CDK11^{p110} s elongačními faktory TFIIS, ELL2 a TFIIF a také RNAPII. Nicméně žádný z těchto proteinů nebyl přímým substrátem CDK11 (Trembley *et al.*, 2002).

Mimo zmíněné obecné regulace bylo popsáno zapojení CDK11 do regulace transkripce specifické skupiny genů – replikačně dependentních histonů (RHD) nezbytných pro sbalení nově nasyntetizované DNA. V tomto případě byla pozorována rekrutace CDK11 specifickými TF do oblasti RHD genů, kde byla zodpovědná primárně za fosforylaci Ser2 CTD směrem ke 3' konci transkriptů. Tato fosforylace je spojována jak s elongační fází, tak slouží i jako platforma pro vazbu faktorů zapojených do úprav 3' konce. Ve srovnání s CDK9, jakožto primární kinasou fosforylující CTD v místě Ser2, byla však tato fosforylace méně efektivní (Gajdušková *et al.*, 2020).

Dále bylo popsáno zapojení CDK11 mimo regulaci transkripce, a to konkrétně v regulaci G2/M fáze buněčného cyklu (isoforma p58) (Petretti *et al.*, 2006) a v apoptose (isoforma p46) (Lahti *et al.*, 1995).

2.1.6 Cyklin dependentní kinasy 12 a 13

CDK12 vytváří komplex s cyklinem K. Je jednou z dalších kinas, které fosforylují CTD doménu RNAPII, a je pravděpodobně primárně zapojena v pozdějších fázích transkripce (Lukasik *et al.*, 2021; Vervoort *et al.*, 2022). *In vitro* testy ukázaly schopnost CDK12 fosforylovat CTD primárně v místě Ser2, ale i Ser5 (Bartkowiak *et al.*, 2010; Blazek *et al.*, 2011; Böskén *et al.*, 2014; Bartkowiak *et al.*, 2015; Tellier *et al.*, 2020). Studie (Zhang *et al.*, 2016) popsala lokalizaci CDK12 v rámci genomu pomocí celogenomové CHIP-seq analýzy. CDK12 byla detekována v oblasti enhancerů, kde se shodovala s RNAPII a také s acetylační značkou H3K27_{Ac}, která je spojována s aktivními enhancery. Dále byla také lokalizována v oblasti protein-kódujících genů, kde se opět překrývala se signálem RNAPII, což naznačuje, že může postupovat s RNAPII v procesu elongace. Nicméně v této studii vedla aplikace CDK12/13 selektivního inhibitoru THZ531 k redukci pouze pSer2 směrem ke 3' konci genů a úroveň pSer5 nebyla ovlivněna (Zhang *et al.*, 2016). Nezbytnost CDK12 v elongační fázi transkripce podporuje také pozorované snížení rychlosti elongace, slabší vazba elongačních faktorů na chromatin a celková represe globální transkripce při její

inhibici. Taktéž byl pozorován pokles v hladinách pSer2 i pSer5 (Tellier *et al.*, 2020). Na druhou stranu knock-out CDK12 neovlivnil globální úroveň transkripce a snížil expresi pouze malého množství genů. Významnou část však tvořily geny s dlouhými transkripty, a to zejména geny zapojené DDR. To potvrdily i testy se selektivním inhibítorem CDK12/13 THZ531. CDK12/cycK tedy hraje důležitou roli při odpovědi buňky na poškození DNA. CDK12 taktéž ovlivňuje stabilitu genomu, jelikož deplece CDK12/cycK indukuje signalizaci DDR i bez vnějšího poškození DNA. Navíc vede k akumulaci buněk v G2/M fázi, což naznačuje možnou aktivaci kontrolního bodu pro poškození DNA (Blazek *et al.*, 2011; Liang *et al.*, 2015; Zhang *et al.*, 2016).

Mezi další možné role CDK12 patří zapojení do úprav pre-mRNA a tvorby 3'konce. CDK12 interaguje se sestřihovým aparátem a její deplece v buňkách rakoviny prsu vedla k alternativnímu sestřihu genů s dlouhými transkripty. Aplikace CDK12/13 inhibítora THZ531 vedla k redukci ko-transkripčního sestřihu v buňkách Non-Hodgkinova lymfomu (NHL), rakoviny děložního čípku a chronické myeloidní leukemie (CML). Navíc knock-down CDK12 ovlivnil, mimo jiné, expresi genů zapojených do úprav RNA (Bartkowiak *et al.*, 2015; Liang *et al.*, 2015; Tien *et al.*, 2017; Magnuson *et al.*, 2022). Prostřednictvím pSer2 tak CDK12 také pravděpodobně ovlivňuje formování 3'konce mRNA (Davidson *et al.*, 2014)

CDK13 sdílí vysokou sekvenční homologii s CDK12 a podobně jako CDK12 vytváří komplex s cyklinem K. Je tedy možné, že tyto kinasy mají podobnou funkci vzhledem ke strukturální podobnosti a stejnému vazebnému cyklinu (Choi *et al.*, 2020; Vervoort *et al.*, 2022). Podobně jako CDK12, i CDK13 je schopna fosforylovat CTD (Bartkowiak *et al.*, 2010). Nicméně studie zaměřující se na změny v expresi genů vlivem ztráty CDK12 a CDK13 pozorovaly rozdíly mezi cílovými geny ovlivněnými CDK12 a CDK13. I přes velký překryv v ovlivněných genech (například geny zapojené do úprav RNA), knock-down CDK13 neovlivnil DDR geny, a naopak byla ukázána regulace genů zapojených do translace či energetického metabolismu. Na rozdíl od CDK12, CDK13 také významně ovlivnila expresi snRNA a malých jadérekových RNA (snoRNA) (Blazek *et al.*, 2011; Liang *et al.*, 2015).

I přes částečně odlišné funkce CDK12 a CDK13 některé studie naznačují jejich vzájemnou kooperaci. Duální inhibice CDK12 a CDK13 vedla k indukci buněčné smrti v sub-mikromolárních koncentracích, což odpovídalo efektu CDK12/13 duálního inhibítora

THZ531 (Zhang *et al.*, 2016; Fan *et al.*, 2020). Oproti tomu inhibice pouze CDK12 nebo CDK13 měla sice vliv na buněčný cyklus, nicméně aplikace relativně vysokých dávek nevedla k indukci buněčné smrti ($IC_{50} > 10 \mu M$). Podobně inhibice obou kinas ovlivnila expresi více genů než inaktivace každé zvlášť. Duální inhibice vedla také k redukci fosforylace CTD, zejména Ser2, a redukci obsazenosti RNAPII směrem ke 3'konci genů a u místa konce transkripce (TES, *transkription end site*). Na rozdíl od předchozích studií zde nebyl rozlišen vliv inhibice CDK12 a CDK13 na hladiny pSer (zejména pak u CDK12), což naznačuje vzájemnou kooperaci. Pozorován byl také efekt na rychlost elongace a procesivitu RNAPII, který byl u duální inhibice větší ve srovnání se selektivní inhibicí CDK12 nebo CDK13 (Fan *et al.*, 2020).

2.1.7 Cyklin dependentní kinasa 20

Jednou z nejméně prozkoumaných tCDK je CDK20 (Malumbres, 2014). Podobně jako CDK7, CDK20 interaguje s cycH a také kasein kinasou 2 (Qiu *et al.*, 2008). Prvotní studie identifikovaly CDK20 jako další kinasu s CAK aktivitou (Kaldis *et al.*, 2000) zodpovědnou za aktivaci CDK2. Inhibice CDK20 vedla k poklesu fosforylace CDK2 v místě Thr160 doprovázeného akumulací buněk v G1 fázi buněčného cyklu. Dlouho trvající knock-down pomocí siRNA narušil aktivitu CDK2 a také buněčnou proliferaci. CAK aktivita CDK20 byla ve srovnání s CDK7 slabší (Liu *et al.*, 2004). Podobné výsledky ukázala také studie na nádorových buňkách gliomu (Ng *et al.*, 2007). Nicméně funkce CDK20 jako další CAK je značně kontroverzní. Studie (Wohlbold *et al.*, 2006) sice pozorovala vliv CDK20 na proliferaci buněk, nicméně již nepozorovala vliv na aktivaci CDK2. Dle této studie CAK aktivita CDK20 pravděpodobně vyplývá z její interakce s CDK7. Podobně ani studie na vzorcích rakoviny ovarií nepozorovala vliv CDK20 na pCDK2. Knock-down CDK20 však vedl ke snížení exprese cyklinu D1, který je regulátorem buněčného cyklu. Zvýšená exprese CDK20 také ovlivnila proliferaci nádorových buněk *in vitro* a růst nádoru *in vivo* (Wu *et al.*, 2009). Zdali tedy CDK20 má CAK aktivitu, případně za jakých podmínek, není zcela jisté, nicméně prokazatelně ovlivňuje proliferaci buněk a růst nádorů.

Mezi další role CDK20 patří například podpora ciliogeneze, procesu nezbytného v savčí embryogenezi, skrz zapojení do Hedgehog signální dráhy (Snouffer *et al.*, 2017), a je také zapojena do aktivace β -katenin/TCF signální dráhy (Feng *et al.*, 2011).

Mimo tzv. obecnou CDK20 (dále jen CDK20) zmíněnou výše, byla popsána druhá varianta tzv. srdeční CDK20. Tato isoforma je menší a její exprese je tkáňově specifická, a to konkrétně v srdci, játrech a ledvinách. Od CDK20 se srdeční isoforma také liší vazebnými partnery. Nicméně obě tyto isoformy podporují růst a přežití srdečních buněk (Qiu *et al.*, 2008).

3 PATOLOGICKÁ DEREGULACE TRANSKRIPČNÍHO CYKLU

Deregulace transkripce byla popsána u řady onemocnění včetně neurodegenerativních, autoimunitních, zánětlivých, kardiovaskulárních či diabetu. Významně také přispívá k rozvoji nádorových onemocnění (Lee *et Young*, 2013; Parnell *et al.*, 2014; Jin *et al.*, 2019). Onkogenní deregulace se může odehrávat jak na úrovni jednotlivých lokusů, ale taktéž na úrovni globální transkripce a tím ovlivnit velkou část genomu (Lee *et Young*, 2013; Vervoort *et al.*, 2022). V této kapitole budou dále popsány změny, které přímo souvisí s tCDK, ať už jejich mutace, zvýšená exprese nebo změny jejich modulátorů, jako je například KMT2A a Myc.

Nádorové buňky často vykazují „transkripční závislost“ (*transcriptional addiction*). Tento jev vychází z onkogenní závislosti, kdy nádorové buňky jsou pro udržení svého maligního fenotypu absolutně závislé na jednom či více onkogenech, které byly zapojené již při tumorogenezi (Weinstein *et Joe*, 2008). Transkripční závislost rozšiřuje koncept onkogenní závislosti o další genetické a epigenetické změny vedoucí právě k deregulaci transkripce. Závislost nádorů na kontinuální aktivitě komponent transkripčního aparátu vede k jejich citlivosti k jakémukoli narušení transkripce (Bradner *et al.*, 2017). Řada klíčových onkogenů má krátký poločas rozpadu, a to jak na úrovni mRNA, tak na úrovni proteinů. V případě některých nádorových onemocnění je pozorována závislost na kontinuální transkripci těchto onkogenů. Příkladem může být závislost na anti-apoptickém proteinu Mcl-1, kterou vykazují zejména hematologické malignity (Bolomsky *et al.*, 2020). Typickým příkladem nádoru závislého na Mcl-1 je mnohočetný myelom (MM; Derenne *et al.*, 2002; Zhang *et al.*, 2002). Exprese Mcl-1 je u pacientů s MM často zvýšena, a to jak v době diagnózy, tak zejména při relapsu. (Wuillème-Toumi *et al.*, 2005) zkoumali expresi proteinu Mcl-1 u 51 pacientů, z toho 26 v relapsu, a porovnávali je s expresí Mcl-1 u 7 zdravých dárců. Zvýšená exprese Mcl-1 korelovala nejen s progresí onemocnění (abnormální exprese u 81 % v relapsu oproti 52 % při diagnóze), ale také s horší prognózou onemocnění, kdy pacienti s abnormální expresí vykazovali kratší čas přežití bez známek choroby (EFS, *event free survival*). Z hematologických malignit byla závislost na Mcl-1 prokázána také u akutní myeloidní leukemie (AML; (Glaser *et al.*, 2012) i u NHL (Kuramoto *et al.*, 2002) a podobně jako u pacientů s MM zvýšená exprese souvisela s nepříznivou prognózou a taktéž s progresí onemocnění. Závislost na Mcl-1 byla také prokázána u některých solidních tumorů, kde opět často souvisí s horší prognózou a může být i zodpovědná za rezistenci nádorových buněk (Zhang *et al.*, 2011; Goodwin *et al.*, 2015;

Campbell *et al.*, 2018; Campbell *et al.*, 2021; Wang *et al.*, 2021b; Fu *et al.*, 2022). Inhibice transkripce pomocí inhibitorů některých tCDK může vést k narušení exprese *MCL-1*, případně dalších anti-apoptických genů, a tedy k indukci apoptosy nádorových buněk (Kwiatkowski *et al.*, 2014; Hu *et al.*, 2019; Borowczak *et al.*, 2022b; Li *et al.*, 2022; Kovalová *et al.*, 2023b; Sher *et al.*, 2023).

K deregulaci transkripce může vést řada procesů. Níže v textu jsou zmíněné události tzv. přímé deregulace transkripce (Vervoort *et al.*, 2022). Konkrétně změny, které ovlivňují tCDK, ať už to jsou přímo jejich mutace či aberantní exprese, anebo změny v proteinech, které s nimi interagují, jako je například transkripční faktor Myc nebo methyltransferasa KMT2A.

3.1 Změny v transkripčních CDK

K narušení transkripce může docházet např. v důsledku mutací, změn v počtu kopií či změn v expresi tCDK. V některých případech tyto změny vedou k horší prognóze. Z velké části však důsledek těchto změn nebyl doposud pochopen.

Rozsáhlou studií genomických změn v buňkách s abnormální expresí tCDK a jejich vazebných cyklinů provedli Shan *et al.* (2020). Ve své studii analyzovali data z více než 10 000 tumorů se zaměřením na změny v počtu kopií (CMV, *copy-number variations*), a to jak ztráty v počtu kopií (CNL, *copy-number loss*), tak nárůst v počtu kopií (CNG, *copy-number gain*). Dále byl analyzován výskyt mutací či fúzí. V případě tCDK byly detekovány primárně CNL a u téměř všech tCDK se vyskytovaly CNL alespoň u jednoho nádorového typu. Výjimku tvořily pouze *CDK9*, *CDK12* a *CDK13*. Nejčastěji byly tyto změny detekovány v *CDK7*, a to ve 27 % testovaných tumorů. Většinou šlo o heterozygotní ztráty a homozygotní delece byly detekovány výjimečně. Nicméně důsledky těchto změn nebyly studovány. V případě tCDK byly detekovány i CNG. Například v *CDK8*, a to u pacientů s karcinomem kolorekta. U těchto pacientů má *CDK8* onkogenní potenciál (Firestein *et al.*, 2008).

Výskyt mutací je u tCDK relativně výjimečný, zejména u *CDK7*, *CDK9*, *CDK10* nebo *CDK20*. Nejčastější dochází k mutacím v genu *CDK12* (Shan *et al.*, 2020; COSMIC, 2023). Ve studii Shan *et al.* (2020) se jednalo o jedinou tCDK, u níž byly nalezeny mutace

ve více nádorových typech. Tyto mutace byly rozprostřené napříč celým genem *CDK12* a většinou byly heterozygotní. Mutace *CDK12* byly pozorovány například u pacientek se serózním karcinomem ovarií vysokého stupně (HGSOC, *high-grade serous ovarian cancer*) a zahrnovaly nesmyslné mutace, indely či mutace měnící smysl kodonu (Bell *et al.*, 2011; Popova *et al.*, 2016). Inaktivace genu *CDK12* způsobila genomickou nestabilitu a vedla k rozvoji tzv. CDK12 TD-plus fenotypu. Ten je charakterizován vysokým počtem (stovkami) tandemových duplikací (TD) s velikostí do 10 Mb, a nachází se zhruba u 4 % HGSOC (Popova *et al.*, 2016). Zvýšený výskyt TD při detekované mutaci genu *CDK12* byl pozorován i u některých pacientů s metastazující kastročně-rezistentní rakovinou prostaty (Quigley *et al.*, 2018; Wu *et al.*, 2018b; Reimers *et al.*, 2020). Obecně je u rakoviny prostaty mutace *CDK12* asociována s rychlejším rozvojem metastáz a kastroční rezistence ve srovnání s kohortami pacientů nesoucí mutaci v genu *TP53* či genech zapojených do homologní rekombinace jako je *BRCA1*, *BRCA2* a *ATM* (Reimers *et al.*, 2020). Mutace v genu *CDK12* byly detekovány také v mnoha dalších nádorech, a to například u cholangiokarcinomu, karcinomu žaludku a kolorekta, difúzního velkobuněčného B-lymfomu, karcinomu endometria a řady dalších (Lui *et al.*, 2018). Vzácné jsou taktéž fúze genů kódujících tCDK, nicméně několik jich bylo detekováno, a to zejména opět u *CDK12*, následně i *CDK13*, *CDK8* a *CDK19* (Shan *et al.*, 2020).

Poslední možností narušení transkripce skrz tCDK je změna v jejich expresi. Jedná se také o nejčastější změny, přičemž může docházet jak k aberantnímu snížení, tak i zvýšení exprese. Tyto změny bývají v některých případech asociovány s horším průběhem nemoci, a to například s rozvojem metastáz, relapsem či nižší mírou přežití a v některých případech souvisejí i s horší odpovědí na chemoterapeutickou léčbu. Důsledky změn expresí jednotlivých tCDK se zabývala již celá řada studií. Problémem některých z nich je však velmi nízký počet zahrnutých pacientů (Feng *et al.*, 2011; Zhou *et al.*, 2015; Zhao *et al.*, 2017; Ma *et al.*, 2019; Kim *et al.*, 2020; Ma *et al.*, 2021). V případě CDK7 byl popsán negativní vliv vyšší exprese mRNA i proteinu CDK7 na klinické výsledky například u pacientů s triple-negativním karcinomem prsu (TNBC, *triple-negative breast cancer*), a to zejména na dobu přežití specifickou pro karcinom prsu a přežití bez návratu nemoci (RFS, *recurrent-free survival*) (Li *et al.*, 2017). Podobně vyšší exprese *CDK7* byla detekována u osteosarkomu ve srovnání se vzorky normální kostní dřeně či svalové tkáně, a i zde měla negativní vliv na RFS. Testování zahrnovalo také vzorky 91 pacientů, které byly rozděleny na základě intenzity imunohistochemického barvení na vzorky s nízkou nebo

vysokou expresí CDK7. V tomto případě vyšší exprese korelovala s rozvojem metastáz, návratem nemoci a nižším celkovým přežitím (OS, *overall survival*) pacientů (Ma *et al.*, 2021). Podobná korelace mezi vysokou expresí proteinu, rozvojem metastáz a nižším OS u pacientů s osteosarkomem byla pozorována také u CDK9 (Ma *et al.*, 2019).

V některých případech může mít také negativní dopad ztráta exprese. Jedním z příkladů je CDK10, u níž byla pozorována snížená exprese ve srovnání s nenádorovou tkání například u rakoviny prsu. Exprese CDK10 byla asociována s nižšími stádii nemoci a nepřítomností metastáz v lymfatických uzlinách. OS pacientů pozitivních na CDK10 bylo také signifikantně vyšší (You *et al.*, 2015). Při zaměření na ER+ rakoviny prsu u pacientů léčených tamoxifenem nízká exprese *CDK10* opět výrazně korelovala s nižším přežitím pacientů. Navíc byla spojena s rezistencí k tamoxifenu (Iorns *et al.*, 2008).

3.2 Transkripční faktor Myc

Další možný mechanismus deregulace transkripce je založený na aberantní rekrutaci P-TEFb do promotor-proximální pauzy, za kterou je zodpovědný TF Myc. Myc rodina obsahuje tři proto-onkogeny – *C-MYC* (dále pouze *MYC*), *MYCN* a *MYCL*. Tyto tři geny kódují transkripční faktory, které jsou zapojené do řady fyziologických procesů. TF Myc je zapojen do regulace proliferace, diferenciaci či apoptosy. Myc je globální regulátor transkripce který potencionálně ovlivňuje zhruba 15 % genomu (Chen *et al.*, 2018; Wang *et al.*, 2021a).

V rámci tumorogeneze hraje Myc významnou roli. Jedná se o jeden z nejčastěji deregulovaných genů v rámci lidských tumorů. Často dochází ke zvýšení jeho exprese například jako následek chromosomálních translokací či CMV nebo také deregulací nadřizovaných signálních drah či aktivací super-enhancerů u *MYC* genu (Kalkat *et al.*, 2017; Chen *et al.*, 2018; Baluapuri *et al.*, 2020; Vervoort *et al.*, 2022). Při iniciaci tumorogeneze však většinou *MYC* nepracuje samostatně, ale synergisticky s dalšími událostmi jako je například ztráta p53 či aktivace anti-apoptického proteinu Bcl-2. Řada nádorů pak vykazuje onkogenní závislost na *MYC* podobně jako tomu je u *MCL-1* a suprese *MYC* vede k jejich regresi (Gabay *et al.*, 2014; Dhanasekaran *et al.*, 2022).

Myc interaguje s řadou transkripčních faktorů a ovlivňuje tak proces transkripce. Mezi nimi i P-TEFb (Lourenco *et al.*, 2021). Jejich interakce vede k rekrutaci P-TEFb

do oblasti promotor-proximální pauzy, čímž podporuje produktivní elongaci genů (Kanazawa *et al.*, 2003; Gargano *et al.*, 2007; Rahl *et al.*, 2010). Aberantní aktivace Myc tedy vede ke zvýšení transkripce, a to nejen Myc-cílových genů (Wang *et al.*, 2021a).

3.3 Translokace lysinmethyltransferasy *KMT2A*

MLL1/KMT2A translokace představují genetické aberace, které souvisí s rozvojem leukemických onemocnění. Původní označení *MLL1* (*mixed-lineage leukemia 1*) souvisí se změnou buněčné linie (lymfoblastické za myeloidní a naopak), ke které dochází v průběhu nemoci, a to zejména při relapsu. Tato záměna je vzácná, nicméně často je asociována právě s *MLL1* translokací (Dorantes-Acosta *et Pelayo*, 2012; Rossi *et al.*, 2012; Rayes *et al.*, 2016). Nedávno byl gen *MLL1* na základě své biologické funkce přejmenován na *KMT2A* (lysinmethyltransferasa 2A). V současnosti se však v literatuře setkáme s obojím označením tohoto genu a s ním asociovanými leukemií. V tomto textu bude dále používán nový název *KMT2A*.

Leukemie s translokací genu *KMT2A* jsou časté zejména v pediatrické onkologii a označují se jak *KMT2A*-r leukemie. Tato translokace se vyskytuje zhruba v 75-80 % leukemií u kojenců do 1 roku a 5-10 % leukemií u dětí a dospělých, a to jak u myeloidních (AML), tak i lymfoblastických (ALL) leukemií s převažujícím výskytem u ALL. Obecně mají tyto leukemie špatnou prognózu a nízkou míru přežití (Marschalek, 2017; Chan *et Chen*, 2019; Li *et Song*, 2021; Meyer *et al.*, 2023). Výskyt *KMT2A* translokací byl také pozorován u AML souvisejících s léčbou, a to jako následek léčby primárních nádorů pomocí inhibitorů topoisomerasy II (Super *et al.*, 1993; Sandler *et al.*, 1997; Felix, 2001).

Gen *KMT2A* se nachází na chromosomu 11 v oblasti 11q23 (Ziemin-van der Poel *et al.*, 1991) a kóduje zhruba 500 kDa velký, několikadoménový jaderný protein spadající do rodiny histon-lysinmethyltransferas (KMT), katalyzujících transfer jedné až tří methylových skupin z S-adenosinmethylthioninu na lysinová residua histonů, zejména pak histonu H3. U lidí bylo doposud popsáno 24 KMT, které jsou zapojené do methylace histonů. V případě *KMT2A* se jedná zejména o trimethylaci H3K4 (H3K4_{met3}) v oblasti promotorů (Guenther *et al.*, 2005). Tato značka je obecně asociována právě s oblastí promotorů transkripčně aktivních genů (Santos-Rosa *et al.*, 2002; Kimura, 2013). Závislost

na této methylační značce byla pozorována například u některých *Hox* genů (Wang *et al.*, 2009).

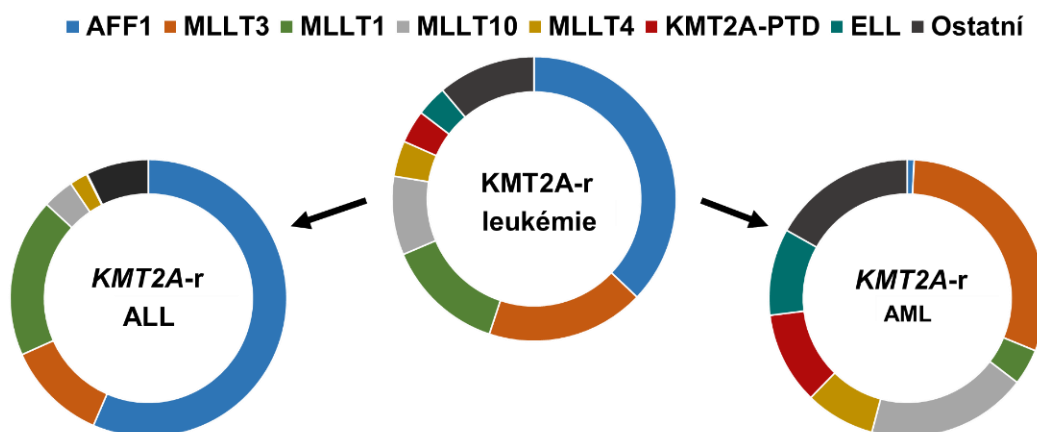
V rámci post-translačních modifikací dochází ke štěpení KMT2A proteinu taspasou 1 za vzniku 2 fragmentů – 320kDa velký KMT2A-N fragment a 180 kDa velký KMT2A-C fragment. Tyto fragmenty dimerizují za vzniku výsledného funkčního KMT2A proteinu (Hsieh *et al.*, 2003a; Hsieh *et al.*, 2003b; Yokoyama et Cleary, 2008). N-koncová část (KMT2A-N) je primárně zodpovědná za rozpoznání a vazbu KMT2A proteinu do cílového genu, kdežto C-koncová část (KMT2A-C) zprostředkovává katalytickou aktivitu proteinu. Výsledný heterodimer interaguje s řadou proteinů za vzniku velkého KMT2A komplexu. Mezi interagujícími proteiny jsou například menin, LEDGF, WRAD komplex, histonacetyltransferasy a řada dalších. Ty jsou zapojené například do vazby komplexu do oblasti cílových genů nebo zvyšují jeho methylační aktivitu (Yokoyama et Cleary, 2008; Patel *et al.*, 2009; Huang *et al.*, 2012; Winters et Bernt, 2017; Li et Song, 2021). Díky kooperaci s acetyltransferásami, KMT2A způsobuje i acylaci histonů. Methylační a acetylační aktivita tohoto multiproteinového komplexu je úzce provázána a experimentální důkazy naznačují, že acetylace zprostředkovaná KMT2A je při hematopoéze pravděpodobně významnější než její methylační aktivita (Mishra *et al.*, 2014).

I přesto, že ještě zbývá objasnit přesný mechanismus vlivu KMT2A na cílové geny, je jasné, že se chová jako pozitivní regulátor transkripce a ovlivňuje iniciaci transkripce RNAPII genů (Guenther *et al.*, 2005). Jeho vliv byl popsán zejména při embryonálním vývoji a hematopoese. Homozygotní delece genu *KMT2A* byla letální v embryonálním stádiu, heterozygotní myši vykazovaly retardaci růstu a narušení segmentační identity. Pozorováno bylo také narušení hematopoese, a to zejména anémie a snížené množství krevních destiček (Yu *et al.*, 1995; Yagi *et al.*, 1998). Vliv KMT2A na regulaci exprese byl pozorován zejména u genů skupiny *Hox*, včetně genu *Hoxa9* (Yu *et al.*, 1995; Milne *et al.*, 2002; Wang *et al.*, 2009). *Hox* geny patří do skupiny homeobox genů, které kódují transkripční faktory regulující embryonální vývoj. V dospělosti jsou zapojeny zejména do regulace normální, ale i maligní hematopoese. S KMT2A leukemiemi souvisí zejména gen *Hoxa9*, který je exprimován, společně se svými kofaktory *Meis1* a *Pbx1*, v kmenových buňkách a raných progenitorech. S diferenciací krevních buněk exprese *Hoxa9* klesá (Pineault *et al.*, 2002; Argiropoulos et Humphries, 2007; Alharbi *et al.*, 2013; Collins et Hess, 2016). Deficience *Hoxa9* vedla ke sníženému množství lymfocytů, granulocytů a myeloidních a erytroidních progenitorů. Dále byl pozorováno zmenšení sleziny

doprovázené poklesem v množství B-lymfocytů a zmenšení brzlíku (Lawrence *et al.*, 1997). Jeho zvýšená exprese naopak vede k expansi hematopoetických kmenových buněk a proliferaci myeloidních progenitorů. Po delší době přispívá zvýšená exprese *Hoxa9* k rozvoji AML (Kroon *et al.*, 1998; Thorsteinsdottir *et al.*, 2002).

3.3.1 *KMT2A*-r leukemie

Jak již bylo zmíněno, gen *KMT2A* často podléhá mutacím, přičemž nejfrekventovanější je translokace genu za vzniku fúzních proteinů. Nejčastěji vznikají fúzní proteiny *KMT2A*-r, nicméně byly popsány i případy reciprokých fúzí r-*KMT2A*. Také byl popsán výskyt delecí, parciálních tandemových duplikací (PTD) či inzercí genu *KMT2A* (Meyer *et al.*, 2019; Meyer *et al.*, 2023). Nejnovější studie Meyer *et. al* (2023) zahrnující 3401 pacientů popsala přes 130 možných přestaveb genu *KMT2A*, přičemž tyto přestavby zahrnují více než 100 různých fúzních partnerů (FP). Většina přestaveb (n = 2895) však zahrnovala pouze 6 FP – *AFF1*, *MLLT3*, *MLLT1*, *MLLT10*, *AFDN/MLLT4* a *ELL*. Významně byly také zastoupeny *KMT2A*-PTD. Zastoupení jednotlivých FP se lišilo dle věku a typu leukemie. Mezi pacienty byl častější výskyt ALL (n = 2182) než AML (n = 1116). Zastoupení FP je znázorněno na Obr. 6.



Obr. 6: Schematické znázornění zastoupení fúzních partnerů u *KMT2A*-r leukemií (upraveno podle Meyer *et. al.*, 2023).

Na genu *KMT2A* se nacházejí 2 oblasti, ve kterých dochází ke zlomu a následné fúzi s FP. Jedná se o tzv. *breakpoint cluster region* – BCR1 a BCR2. Majoritní část zlomů se odehrává v oblasti BCR1, která se nachází zhruba mezi exony 7 a 13. Minoritně také

dochází ke zlomům v oblasti BCR2, která se nachází mezi intronem 19 a exonem 24. Mimo tyto oblasti byly popsány případy zlomu v 2. intronu, které nevedly k sestavení funkčního proteinu. Další zlom byl nalezen v oblasti mezi introny 35 a 36, který vedl ke vzniku fúzního proteinu obsahujícího téměř celý protein KMT2A. Mohlo by se jednat o třetí a velmi vzácný bod zlomu (BCR3). Nicméně tento zlom byl popsán v roce 2021 a byl pozorován doposud pouze u 2 pacientů. Pro jeho potvrzení je třeba více případů (Meyer *et al.*, 2019; Meyer *et al.*, 2021; Meyer *et al.*, 2023).

KMT2A část vzniklých fúzních proteinů si zachovává svoji původní funkci, a to vazbu do promotorů cílových genů a ovlivnění jejich transkripce. Nicméně předešlé studie ukázaly, že cílové geny KMT2A-wt a KMT2A-r se ne vždy shodují. Shodné cílové geny reguluje například KMT2A-MLLT1, naopak KMT2A-MLLT3 reguluje odlišný soubor genů. V obou případech ale KMT2A-r proteiny regulují pouze malé množství genů, mezi nimiž však stále figuruje *Hoxa9* (Wang *et al.*, 2011; Xu *et al.*, 2016).

Vniklé fúzní proteiny narušují transkripci cílových genů a v závislosti na fúzním partnerovi se mechanismus deregulace transkripce liší. Jednou z možností je interakce s elongačním komplexem SEC. Například protein ELL je přímo součástí SEC (Shilatifard *et al.*, 1996). Další KMT2A fúzní partner AFF1 interaguje s P-TEFb jakožto součástí SEC. Svou vazbou do SEC a interakcí s P-TEFb stimuluje jeho kinasovou aktivitu. Přímou či nepřímou přes AFF1 interagují se SEC také další FP, konkrétně MLLT1, MLLT3 (Erfurth *et al.*, 2004; Monroe *et al.*, 2011). Druhou možností je vazba na histon methyltransferasu DOT1L, která je zodpovědná za metylaci H3K79_{me2/3}. Ta je spojována s aktivně transkribovanými geny (Slany, 2016). Vazba s DOT1L byla popsána u proteinů MLLT1, MLLT3, a MLLT10 (Okada *et al.*, 2005; Mueller *et al.*, 2009; Monroe *et al.*, 2011). Další popsaná varianta deregulace cílových genů je inhibice polycomb represivního komplexu (PRC1), který je zapojený do regulace například *Hox* genů. Inhibice PRC1 byla popsána v případě fúzního proteinu KMT2A-MLLT1 (Maethner *et al.*, 2011). Výše zmíněné interakce vedou k narušení transkripce a leukemogenesi.

Jak již bylo zmíněno, *Hox* geny hrají významnou roli v KMT2A leukemiích a jejich exprese je v těchto leukemiích zvýšena. Zajímavostí však je, že KMT2A translokace ve skutečnosti nevedla u AML pacientů přímo ke zvýšené expresi *Hox* genů, úroveň jejich exprese je totiž shodná s expresí v normálních hematopoetických kmenových buňkách (Spencer *et al.*, 2015).

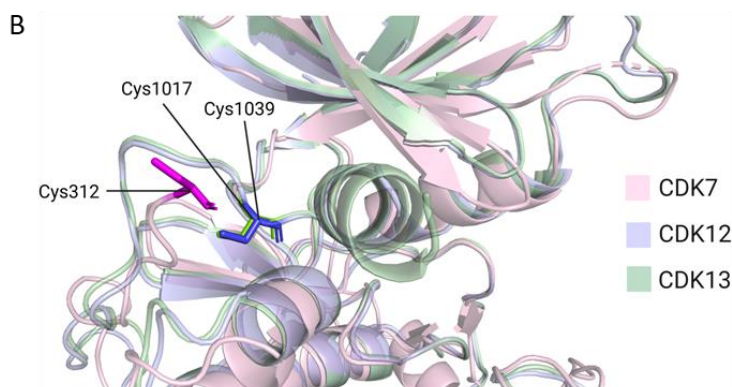
4 INHIBITORY TRANSKRIPČNÍCH CYKLIN DEPENDENTNÍCH KINAS

Již několik dekád jsou CDK cílem při vývoji protinádorových léčiv. První CDK inhibitory však vykazovaly velmi nízkou selektivitu a inhibovaly několik CDK zároveň. Mezi ně patří CDK inhibitory první (flavopiridol/alvociclib, roscovitine/seliciclib) i druhé (dinaciclib, CYC065, SNS-032, AT7519) generace. I přes velké množství klinických testů jejich zavedení do praxe bylo zatím neúspěšné (Whittaker *et al.*, 2017; Heptinstall *et al.*, 2018; Ettl *et al.*, 2022). Nicméně v současnosti je v klinickém testování (NCT03604783) látka TP-1287, což je pro-léčivo zmíněného flavopiridolu (Kim *et al.*, 2017). Problém prvotních inhibitorů spočíval zejména v nízké selektivitě a s tím související toxicitou, ale taktéž nepochopením přesného mechanismu účinku. Tento nedostatek také bránil vhodné selekci pacientů (Asghar *et al.*, 2015; Ettl *et al.*, 2022). Neúspěch první a druhé generace vedl ke snaze o vývoj selektivních CDK inhibitorů a k lepšímu pochopení jejich mechanismu účinku. Průlom způsobil vývoj selektivních CDK4/6 inhibitorů (palbociclib, abemaciclib, ribociclib a trilaciclib), které jsou doposud zatím jako jediné schválené pro léčebné použití (Fry *et al.*, 2004; Bisi *et al.*, 2016; Kim, 2017; Syed, 2017).

Většina CDK inhibitorů funguje jako reversibilní ATP-kompetitivní látky. Konzervativnost aktivního místa však omezuje jejich selektivitu. To vedlo k rozvoji dalších přístupů inhibice CDK. Jednou z dalších zkoumaných cest je interakce s méně konzervativními částmi kinasy, což se uplatňuje zejména u alosterických či kovalentních inhibitorů. Kovalentní inhibitory CDK většinou interagují s cysteinovými residui v blízkosti ATP-vazebné kapsy (Sánchez-Martínez *et al.*, 2015; Chaikuad *et al.*, 2018; Sánchez-Martínez *et al.*, 2019; Lukasik *et al.*, 2021). Jejich vývoj byl z počátku brzděn obavami z jejich reaktivity a s tím související neselektivity. I přesto však kovalentní inhibitory přináší řadu výhod jako například delší účinek a možnost aplikace nižších dávek (Sutanto *et al.*, 2020; Boike *et al.*, 2022). V průběhu let bylo pro léčbu nádorových onemocnění schváleno již několik kovalentních inhibitorů, mimo jiné i například BTK inhibitory ibrutinib, acalabrutinib a zanubrutinib či EGFR inhibitor osimertinib (Honigberg *et al.*, 2010; Cross *et al.*, 2014; Wu *et al.*, 2016; Guo *et al.*, 2019). První kovalentní inhibitor cílicí na tCDK byl inhibitor THZ1, který kovalentně interaguje s cysteinovým residuem 312 (Cys312) mimo ATP-vazebnou kapsu. Podobně byly cysteinová residua v blízkosti aktivního místa nalezena taktéž u CDK12 (Cys1039) i CDK13 (Cys1017) (Obr. 7) a i s těmito residui je THZ1 schopen interagovat (Kwiatkowski *et al.*, 2014). Struktura THZ1 inspirovala vývoj velké

řady dalších, nejen kovalentních, CDK inhibitorů (Kovalová *et al.*, 2023a; Příloha I) a některé z nich již vstoupily do klinického testování.

A	CDK7_HUMAN	MKYFSNRPGP-TP---GCQLPRPNC CPV -----E-----TL	317
	CDK8_HUMAN	DPYFLEDPLPTSDVFAGCQIPYPKREFLTEEEPDDKGDKNQOQQGNNH-----	381
	CDK9_HUMAN	HDFFWSDPM-----PSDLKGLSTHLSMFEY-LAPPRRKG----SQITQQSTNQSRN	359
	CDK10_HUMAN	SSYFKEKPLP-CE---PELMPTFPHHR-----NKRAAPA-----TSEGQS	355
	CD11A_HUMAN	HEYFRETPLP-ID---PSMFPTWPAKS-----EQQRVKRG--TSRPPEGGL	748
	CD11B_HUMAN	HEYFRETPLP-ID---PSMFPTWPAKS-----EQQRVKRG--TSRPPEGGL	760
	CDK12_HUMAN	SDFLKDVVELSKMA---PPDLPHW----QD CHEL -WSKRRRQRQSGVVVEEPPPSKTSR	1067
	CDK13_HUMAN	CEFLRDVEPSKMP---PPDLPLW----QD CHEL -WSKRRRQKQMGMTDDVSTI-KAPR	1044
	CDK19_HUMAN	DPYFQEDPLPTLDVFAGCQIPYPKREFLNEDDPEEKGDKNQOQQNQHQOQPTAPPQAAA	391
	CDK20_HUMAN	HQYFFTAPLP-AH---PSELPIPQRLG-----G-----PA	310



Obř. 7: Srovnání podobnosti transkripčních CDK. (A) Sekvenční alignment části transkripčních CDK v oblasti aktivního místa. Cystein v blízkosti aktivního místa u jednotlivých kinas je zvýrazněn červeně. (B) Struktura aktivního místa vybraných CDK se zvýrazněným cysteinem.

Dalším možným přístupem je cílená degradace CDK s využitím chimérických konjugátů indukujících proteolýzu (PROTAC, *proteolysis targeting chimera*). Jedná se o heterobifunkční molekuly složené z inhibitoru CDK propojeného linkerem k ligandu schopnému vázat E3 ubiquitin ligasu. S těmito proteiny tvoří PROTAC ternární komplex, jehož výsledkem je polyubiquitinace a proteasomální degradace cílové CDK (Békés *et al.*, 2022; Ettl *et al.*, 2022). Aplikace PROTAC konjugátů skrývá také několik výhod ve srovnání s konvenčními kinasovými inhibitory. Příkladem může být schopnost překonání rezistence vzniklé například zvýšenou expresí cílových proteinů nebo některými mutacemi. Zároveň byla pozorována vyšší selektivita ve srovnání s klasickými inhibitory. V neposlední řadě PROTAC funguje jako katalyzátor interakce mezi cílovým proteinem a E3 ubiquitin ligasou. Pro kompletní degradaci cílového proteinu tak není vyžadováno velké množství konjugátu, a to zejména u proteinů s pomalým obratem (Sánchez-Martínez *et al.*, 2019; Hughes *et al.*, 2021; Békés *et al.*, 2022). Do klinického testování vstoupily PROTAC konjugáty poprvé v roce 2019, konkrétně konjugáty cílicí na androgenový či estrogenový receptor

(NCT03888612, NCT04072952). V případě tCDK je vývoj PROTAC konjugátů zaměřený zejména na CDK9, kde bylo představeno již několik degradérů (Robb *et al.*, 2017; Bian *et al.*, 2018; Olson *et al.*, 2018; King *et al.*, 2021; Qiu *et al.*, 2021). Dále byly popsány i degradéry zaměřené na CDK7 (Du *et al.*, 2021; Nam *et al.*, 2022), CDK8 (Hatcher *et al.*, 2018) či CDK12 (Niu *et al.*, 2022).

Za poslední roky bylo popsáno velké množství tCKD inhibitorů s větší či menší selektivitou (Huang *et al.*, 2022; Li *et al.*, 2022; Vervoort *et al.*, 2022). Z toho důvodu se následující text zaměřuje pouze na inhibitory, které jsou prezentovány jako selektivní tCDK inhibitory a byly nebo aktuálně stále jsou v klinickém testování. Jejich struktury jsou znázorněny na Obr. 8-10. Do klinického testování se doposud dostaly pouze inhibitory CDK7, CDK8/19 a CDK9.

4.1 Inhibitory CDK7

Díky svojí duální roli jak v regulaci buněčného cyklu, tak v regulaci transkripce, představuje CDK7 velmi slibný cíl při nádorové terapii. V poslední dekádě bylo vyvinuto již několik selektivních CKD7 inhibitorů (CDK7i). V preklinických testech většina CDK7i způsobuje pokles fosforylace jednoho či více serinů CTD RNAPII – konkrétně Ser5, Ser7 a taktéž Ser2, jehož fosforylace je asociována s CDK9. Dále je také pozorován vliv na buněčný cyklus, a to zejména na fosforylaci cílových kinas CAK – CDK1 a CDK2 a s tím související zastavení buněčného cyklu v G1 či G2/M fázi (Ali *et al.*, 2009; Kwiatkowski *et al.*, 2014; Patel *et al.*, 2018; Choi *et al.*, 2019; Olson *et al.*, 2019; Gaur *et al.*, 2023). Nicméně nový, velmi selektivní CDK7 inhibitor YKL-5-124 způsoboval pouze zmíněný efekt na buněčný cyklus bez vlivu na fosforylaci CTD RNAPII a globální transkripci (Olson *et al.*, 2019). Není tedy zcela jasné, jestli pozorovaný vliv na transkripci působením některých CDK7 inhibitorů je přímým důsledkem inhibice CDK7 nebo jiných CDK. Je tedy nezbytné lépe porozumět důsledkům selektivní inhibice CDK7, případně její degradace či deplece.

Prvním selektivním inhibitorem CDK7, který vstoupil do klinického testování, byl samuraciclub (CT7001/ICEC0942). Vznikl strukturální optimalizací prvního selektivního CDK7 inhibitoru BS-181 (Ali *et al.*, 2009). Samuraciclub byl testován na 117 kinasach, kde prokázal selektivitu vůči CDK7. Antiproliferační aktivita byla testována na panelu 60 nádorových linií, přičemž mediánová GI₅₀ byla 0,25 μM. Při srovnání cytotoxického

účinku na nádorové a nenádorové prsní buňky byly nádorové buněčné linie 2-3x citlivější než linie nenádorové. Aplikace vedla k typickému CDK7i fenotypu, s poklesem pSer2/5/7, G2/M bloku a indukci apoptosy (Patel *et al.*, 2018). V roce 2017 vstoupil do klinického testování (NCT03363893) jako monoterapie na solidní tumory s následným zaměřením jako monoterapie na TNBC, případně v kombinaci s fulvestrantem (ER antagonist) u HR+/HER2- rakovinu prsu u pacientů s předešlou léčbou pomocí CDK4/6i. V první fázi studie byla stanovena maximální tolerovaná dávka na 360 mg/denně, aplikace vyšších dávek vedla k toxicitě limitující dávku (DLT, *dose limiting toxicity*). Většina vedlejších účinků byla gastrointestinální, nízkého stupně a snadno zvládnutelná pomocí standardní terapie. Pouze v 6 případech se vyskytly vážné vedlejší účinky, které souvisely s aplikací samuraciclibu. V rámci hematologického profilu byl často zaznamenán mírný pokles v počtu krevních destiček a pouze ve 3 případech byla detekována trombocytopenie stupně 3 (G3) a vyšší, nicméně po vysazení samuraciclibu došlo k rychlému srovnání stavu. V rámci první testované skupiny (monoterapie na solidní tumory) byla u 52,8 % zaznamenána stabilizace nemoci (SD) s viditelným benefitem u kastročně-rezistentní rakoviny prostaty. V případě monoterapie u TNBC byla zaznamenána částečná odpověď na léčbu (PR; *partial response*) u jednoho pacienta (5 %) a u 11 došlo k SD (55 %). Kombinovaná terapie samuraciclibu a fulvestrantu byla dobře tolerována, u 13 pacientů (52 %) došlo k SD a u tří pacientů (12 %) došlo PR. V žádné testované skupině nedošlo k celkové odpovědi na léčbu (Coombes *et al.*, 2023). Příznivé výsledky vedly k rozšíření klinických studií na samuraciclib. V současné době je testován v několika kombinacích na lokálně pokročilých nebo metastatických ER+/HER2- rakovinách prsu, a to konkrétně v kombinaci se selektivními degradéry estrogenového receptoru giredestrantem (NCT04802759) nebo elacestrantem (NCT05963997) a v kombinaci s fulvestrantem, kde je porovnávána účinnost s monoterapií fulvestrantu (NCT05963984).

THZ1 byl jedním z prvních kovalentních inhibitorů zacilujících na tCDK (Kwiatkowski *et al.*, 2014). Vzhledem ke své špatné metabolické stabilitě nevstoupil do klinického testování, nicméně byl inspirací pro vývoj řady nových inhibitorů, a to včetně SY-1365 (mevocielib) od firmy Syros Pharmaceuticals. SY-1365 vznikl optimalizací struktury THZ1 a inhiboval CDK7 v řádu stovek nM. Antiproliferativní účinky SY-1365 byly prokázány na panelu 386 buněčných linií obsahujících 26 nádorových typů. Největší citlivost vykazovaly leukemické linie, přičemž hodnoty IC₅₀ se pohybovaly v nanomolárních koncentracích u většiny testovaných nádorových typů. Aplikace SY-1365 vedla k typickým

projevům CDK7i a účinky byly pozorovány taktéž na myších modelech *in vivo* leukemií, karcinomu vaječníků a TNBC. SY-1365 prokázal synergistický efekt s BH3 mimetikem venetoclaxem (Hu *et al.*, 2017; Konstantinopoulos *et al.*, 2018; Hu *et al.*, 2019). Všechna tato zjištění podpořila zahájení klinického testování v roce 2017 (NCT03134638) na pokročilé solidní tumory, rakovinu vaječníků a prsu, a to jako monoterapie nebo v kombinaci s karboplatinou (inhibitor DNA syntézy) nebo fulvestrantem. Prvotní data ze studie ukázala, že pro dosažení klinické aktivity látky by bylo nezbytné navýšit dávku či zvýšit frekvenci dávkování, což by však vytvořilo dávkovací plán, který by příliš zatěžoval pacienty. Z toho důvodu se společnost Syros rozhodla ukončit testování intravenózního SY-1365 a upřednostnit orálně podávaný novější CDK7 inhibitor SY-5609 (Syros Pharmaceuticals, 2019).

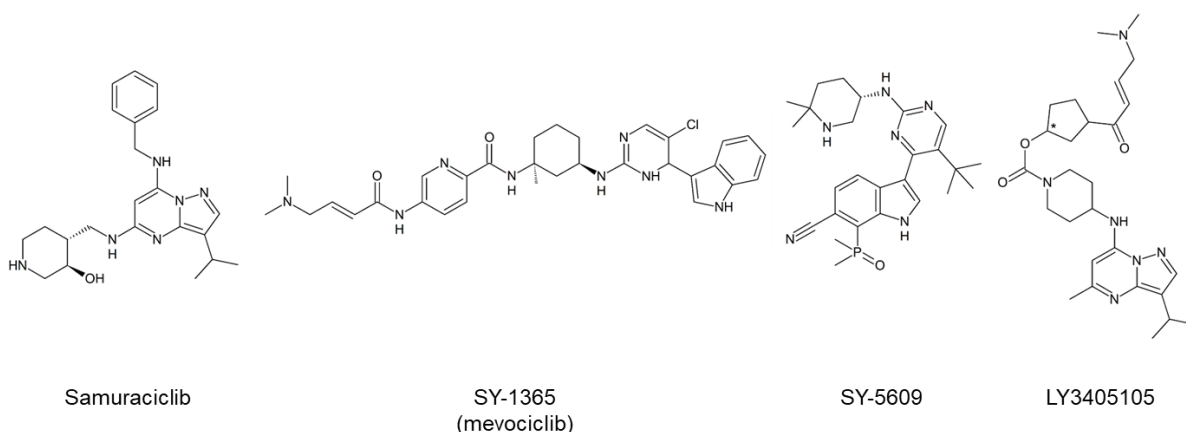
SY-5609 je nekovalentním nástupcem SY-1365, jedná se o vysoce selektivní inhibitor CDK7 v porovnání s CDK2/9/12. Nicméně při kinasovém testování na 485 kinasách bylo 9 dalších kinas inhibováno $\geq 70\%$, a to včetně CDK13,16,17 a 18 (Marineau *et al.*, 2022). V rámci *in vivo* testování SY-5609 prokázal účinek na několika myších modelech, a to včetně malobuněčného karcinomu plic, HGSOc a TNBC. U všech modelů byla pozorována minimálně 50% inhibice růstu tumoru (TGI; *tumor growth inhibition*) a u více než poloviny modelů aplikace látky vedla k 95 % TGI bez náznaku opětovného růstu po 21 dnech. Všechny tyto pozitivní výsledky vedly ke spuštění klinického testování na solidní tumory jako monoterapie případně v kombinaci s dalšími léčivy (NCT04247126, NCT04929223). Prvotní výsledky z fáze I pro pokročilé solidní tumory (monoterapie) a HR+ rakovinu prsu (kombinace s fulvestrantem) vedly ke stanovení tolerované dávky na 3 mg/denně. Většina pozorovaných vedlejších účinků byla úrovně G1-2. Odpověď na SY-5609 vykazovala mezi pacienty vysokou variabilitu. Došlo tedy k navýšení kohort pacientů s rakovinou prsu a plic pro studium efektu SY-5609 na homogennější populaci pacientů (Sharma *et al.*, 2021; Roth, 2022).

LY3405105 je dalším kovalentním inhibitorem CDK7, který byl v klinickém testování. Tato látka inhibovala CDK7 s $IC_{50} = 93$ nM, přičemž zbylé testované kiny z rodiny CDK byly inhibovány v mikromolárních koncentracích. Selektivita byla celkově testována na 320 kinasách, data však byla publikována pouze pro rodinu CDK. Aplikace vedla k poklesu fosforylace RNAPII na Ser5 a v sub-mikromolárních koncentracích inhibovala proliferaci buněčných linií karcinomu prsu, plic, ovarií, žaludku a kolorekta a prokázala účinky i na několika PDX (*patient derived xenograft*) (Coates *et al.*, 2019).

V roce 2018 vstoupil inhibitor LY3405105 do fáze I klinického testování (NCT03770494), nicméně ta byla ukončena kvůli nedostatečné účinnosti.

V klinickém testování jsou také další dva CDK7 inhibitory, u nichž doposud nebyla publikována struktura. Prvním z nich je Q901, který vykazoval skvělou selektivitu vůči CDK7 v rámci CDK rodiny. V preklinických testech vykazoval účinky *in vivo* u řady xenograftů (HGSOC, CRPR, karcinom pankreatu, kolorekta, ER+ prsu) (Yu *et al.*, 2020; Yu *et al.*, 2022). V roce 2022 vstoupil do fáze I/II klinického testování (NCT05394103) pro pokročilé/metastatické rakoviny jako monotepapie nebo v kombinaci s pembrolizumabem (anti-PD-1).

Druhým CDK7i (bez zveřejněné struktury) v klinickém testování je XL102 (AUR102). Jedná se o velmi selektivní CDK7i, který prokázal anti-proliferační aktivitu na širokém panelu buněčných linií, přičemž u většiny testovaných linií se hodnoty IC_{50} pohybovaly v rozmezí 100 – 200 nM. *In vivo* aktivita byla prokázána na xenograftech difúzního velkobuněčného B-lymfomu, AML a TNBC, kdy v dávce 30 mg/kg a vyšší byla zaznamenána regrese tumoru (Satyam *et al.*, 2020; Gaur *et al.*, 2023). Do fáze I klinického testování vstoupil XL102 v roce 2021 (NCT04726332) a je testován na pokročilých solidních tumorech jako monoterapie či v kombinaci s fulvestrantem, prednisonem (kortikosteroid) či abirateronem (CYP17A1 inhibitor). Prvotní data z fáze z klinického testování, které zahrnuje testování dávky, ukazují dobrou tolerabilitu a nebyla pozorována DLT. Studie stále pokračuje a bude následovat rozšíření kohort pacientů (Patnaik *et al.*, 2023).



Obr. 8: Struktury CDK7i v klinickém testování.

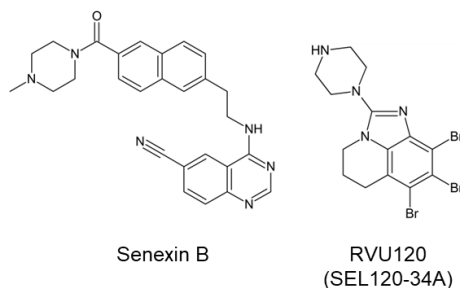
4.2 Inhibitory CKD8/19

CDK8 a její paralog CDK19 jsou součástí mediátorového komplexu regulující transkripci a představují tedy taktéž potencionální terapeutický cíl v léčbě rakoviny. Nicméně za určitých podmínek může mít CDK8 i tumor-supresorovou funkci a v tento moment je její inhibice nežádoucí. Její proto-onkogenní funkce souvisí zejména s její upregulací či mutací. Navíc byla také pozorována spojitost mezi CDK8-mediátor zprostředkovanou transkripci a rozvojem metastáz či rezistence k léčivům (Wu *et al.*, 2021). Pozitivní efekt aplikace inhibitorů CDK8/19 byl pozorován u rakoviny prostaty (Offermann *et al.*, 2022), AML (Rzymiski *et al.*, 2017) či ER+ rakoviny prsu (McDermott *et al.*, 2017).

Prvním CDK8/19 inhibitorem, který vstoupil do klinického testování, byl senexin B (BCD-115, SNX2-1-165). Tento inhibitor vykazoval vysokou selektivitu vůči CDK8/19 při kinasovém testování na více než 450 kinasách. V preklinickém testování účinně inhiboval proliferaci u TNBC buněčných linií a prokázal synergistické účinky s dalšími léčivy několika subtypů rakoviny prsu. Aplikace senexinu B *in vivo* vedla k TGI u TNBC xenograftů (Robinson *et al.*, 2013; McDermott *et al.*, 2017; Ding *et al.*, 2022). Senexin B byl testován v kombinaci s endokrinní terapií ve fázi I klinického testování na ER+/HER2-rakovinu prsu (NCT03065010). Studie byla dokončena, nicméně výsledná data nebyla doposud publikována.

Druhým CDK8/19 inhibitorem, který vstoupil do klinického testování, je RVU120 (dříve SEL120-34A). V kinasových testech účinně inhiboval CDK8 a CDK19. Preklinické testy prokázaly jeho antileukemickou aktivitu *in vitro* i *in vivo* u CDX (*cell line-derived xenograft*) myších modelů. Citlivost buněčných linií korelovala s hladinami pSTAT5 a pSTAT1 (Rzymiski *et al.*, 2017). Citlivost k RVU120 byla pozorována také u TNBC buněčných linií a xenograftů, přičemž i zde citlivost korelovala s pSTAT, tentokrát pSTAT3 (Rzymiski *et al.*, 2022). Aktuálně je RVU120 testován ve dvou klinických studiích. První studie (NCT04021368) je fáze I u pacientů s relabující/refrakterní AML a myelodysplastickým syndromem s vysokým rizikem (HR-MDS). Druhá studie (NCT0505225) zahrnuje fázi I a II u pacientů s relabujícím/refrakterním metastazujícím či pokročilým solidním tumorem. V případě studie na hematologických malignitách jsou doposud zveřejněny výsledky 19 pacientů (16 AML, 3 HR-MDS), podávání inhibitoru bylo dobře tolerováno a nebyla pozorována DLS. Z vedlejších účinků byla nejčastější febrilní neutropenie a trombocytopenie, přičemž většina (84 %) vedlejších účinků byla G3-G4.

V průběhu studie bylo zaznamenáno několik SD a 1 kompletní remise (Abboud *et al.*, 2022). Podobné výsledky byly zjištěny i ve studii na solidních tumorech (Dziadziunsko *et al.*, 2022). Obě studie nadále pokračují a došlo k navýšení aplikované dávky.



Obr. 9: Struktury CDK8/19i v klinickém testování.

4.3 Inhibitory CDK9

Vzhledem k esenciální roli CDK9 v elongační fázi transkripce má význam použití inhibitorů v nádorech s narušenou transkripcí, jako je popsáno například u nádorů s *MYC* amplifikací (Blake *et al.*, 2019; Hashiguchi *et al.*, 2019). Nicméně význam CDK9 inhibice byl popsán i u dalších typů nádorů, například u karcinomu prostaty (Richters *et al.*, 2021), osteosarkomu (Ma *et al.*, 2019), mnohočetného myelomu (Lim *et al.*, 2020; Borowczak *et al.*, 2022a) nebo karcinomu prsu (Wei *et al.*, 2021; Noblejas-López *et al.*, 2022). V preklinických testech vedlo použití CDK9 inhibitorů k poklesu fosforylace Ser2 CTD RNAPII, exprese proteinů Myc a Mcl-1 a indukci apoptosy (Lim *et al.*, 2020; Alsfouk, 2021; Huang *et al.*, 2022).

První selektivní CDK9 inhibitor, který vstoupil do klinického testování, byl atuveciclib (BAY-1143572). Atuveciclib vykazoval slibnou selektivitu v rámci CDK rodiny a v preklinických testech také *in vivo* antileukemické účinky u AML xenograftů (Lücking *et al.*, 2017). Díky slibným preklinickým výsledkům vstoupil atuveciclib do fáze I klinického testování na pokročilé malignity (NCT01938638) a leukemie (NCT02345382). V průběhu prvotní studie však maximální tolerované dávky vedly k neutropenii a nižší dávky byly naopak bez efektu (Bayer, 2017). Z toho důvody společnost Bayer zrušila veškeré další testování atuveciclibu a zaměřila se na vývoj dalších sloučenin.

Optimalizace atuveciclibu vedla k identifikaci enitociclibu (VIP152/BAY-1251152), který vykazoval lepší biochemickou (IC_{50} CDK9 = 3 nM) i buněčnou účinnost (IC_{50} MOLM-13 = 29 nM) ve srovnání s atuveciclibem (IC_{50} CDK9 = 13 nM; IC_{50} MOLM-13 = 310 nM). Při rozsáhlém kinomovém testování zahrnující mimo jiné celou CDK

rodinu vykazoval enitociclib selektivitu vůči CDK9 při aplikaci 100 nM, kdy residuální aktivitu nižší než 25 % vykazovala již jen kinasa GSK3 α . Nicméně při navýšení koncentrace na 1 μ M enitociclib inhiboval řadu dalších kinas včetně CDK4 (residuální aktivita CDK4/D1 = 21 % a CDK4/D3 = 25 %) a CDK7 (residuální aktivita 5%). Nicméně v případě CDK7 další testy její inhibici nepotvrdily (Lücking *et al.*, 2021). K podobným výsledkům dospěli i Wells *et al.* (2020), kteří měřili procentuální inhibici CDK v živých buňkách. Zde byla detekována procentuální inhibice >75 % mimo CDK9 také u CDK3, CDK4 a CDK6 (Wells *et al.*, 2020). Nicméně enitociclib vykazoval antileukemické účinky *in vivo* v případě AML a CLL xenograftů a také dobrou tolerabilitu (Lücking *et al.*, 2021; Sher *et al.*, 2023). Vstoupil tedy do klinického testování jako monoterapie nebo v kombinaci s dalšími léčivy (NCT02745743, NCT02635672, NCT04978779, NCT05371054) se zaměřením zejména na hematologické malignity, solidní tumory, ale i Richterův syndrom. Prvotní testy u pacientů s AML neprokázaly žádný efekt, avšak enitociclib vykazoval dobrou tolerabilitu (Byrne *et al.*, 2018). Výsledky ze studie NCT04978779 ukazují opět příznivou farmakokinetiku, tolerabilitu a monoterapie byla vyhodnocena jako bezpečná. Navíc u části pacientů byla pozorována pozitivní reakce na léčbu. U 7 pacientů se solidními tumory došlo k zastavení progresu nemoci a u dvou pacientů s vysoce maligním (*high-grade*) B-buněčným lymfomem došlo k remisi (Diamond *et al.*, 2022). Tato studie společně s dalšími stále probíhá.

V roce 2020 byl představen inhibitor AZD4573, který je uváděn jako selektivní inhibitor CDK9, nicméně v nanomolárních koncentracích inhibuje taktéž CDK1/2/3/4/6, GSK3 α a GSK3 β . AZD4573 vykazoval antileukemické účinky v MV4-11 xenograftech (Barlaam *et al.*, 2020; Cidado *et al.*, 2020) a vstoupil do fáze I a II klinického testování jako monoterapie (NCT03263637, NCT05140382) nebo v kombinaci s acalabrutinibem (NCT04630756). Všechny testy jsou zaměřeny na hematologické malignity. Prvotní výsledky studie NCT03263637 naznačují bezpečnost AZD4573, nicméně 69,2 % pacientů ve studii NCT04630756 vykazovalo nežádoucí účinky stupně 3 a vyšší, zejména neutropenii a trombocytopenii. I přesto však 63,6 % pacientů na léčbu zareagovalo, přičemž 36,4 % s kompletní remisí (Brummendorf *et al.*, 2022; Strati *et al.*, 2022). Studie tedy i nadále probíhá.

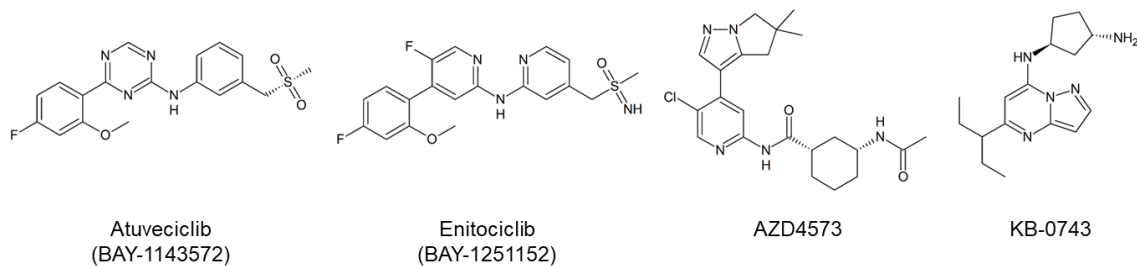
Dalším CDK9 inhibitorem v klinickém testování je inhibitor KB-0742 firmy Kronos-Bio, který inhibuje CDK9 při 6 nM a při kinasovém testu vykazoval 50x vyšší selektivitu vůči CDK9 v porovnání s ostatními CDK. KB-0742 prokázal protinádorový

účinek *in vitro* i *in vivo* u xenograftů AML, neuroblastomu s *MYCN* amplifikací, malobuněčného karcinomu plic, osteosarkomu a karcinomu prostaty. Jeho aplikace vedla taktéž k narušení exprese genů souvisejících s rakovinou prostaty (Richters *et al.*, 2021; Day *et al.*, 2022; Saffran *et al.*, 2022). V roce 2021 tento inhibitor vstoupil do fáze I/II klinického testování pro relabující a refrakterní solidní nádory a NHL (NCT04718675). Tato studie v první fázi testuje farmakokinetické a farmakodynamické vlastnosti látky v rozdílných dávkách. V druhé fázi pak dojde k navýšení kohort pacientů a testování bezpečnosti a farmakodynamických vlastností látky v nádoru. Studie aktuálně stále nabírá pacienty a doposud nebyly zveřejněny žádné oficiální výsledky.

V klinickém testování jsou další 2 CDK9i, u nichž nebyly publikovány struktury. Prvním z nich je inhibitor PRT2527, který vstoupil v roce 2021 do klinického testování na solidní tumory (NCT05159518) a v roce 2022 taktéž na hematologické malignity (NCT05665530). CDK9 inhibuje již v koncentraci 0,98 nM a byl testován na panelu se 117 kinasami, včetně rodiny CDK. Nicméně data jsou zveřejněna pouze pro CDK1-7, přičemž inhibitor vykazuje 35x-1000x vyšší selektivitu k CDK9 ve srovnání s CDK1-7. *In vitro* inhiboval PRT2527 proliferaci řady buněčných linií zahrnující AML, ALL, CLL i linie rakoviny prsu, kastročně-rezistentní rakoviny prostaty, sarkomu, melanomu či primárních buněk adenoidního cystického karcinomu. Citlivé byly zejména linie solidních tumorů s *MYC* amplifikací. *In vivo* vedla aplikace PRT2527 k redukci růstu nádorů u PDX pankreatického duktálního adenokarcinomu a rakoviny prsu, obojí s *MYC* amplifikací a taktéž u PDX rakoviny prostaty. Efekt byl pozorován také u CDX AML (Zhang *et al.*, 2021b; Federici *et al.*, 2022). Prvotní výsledky ze studie NCT05159518 na solidních tumorech s 18 pacienty ukázaly několik vedlejších účinků většinou stupně 1-2 (G1-2), případně 3-4 (G3-4) bez závislosti na podávané dávce. Výjimku tvořila neutropenie. U 5 pacientů vedla aplikace k SD, u žádného nedošlo ke zlepšení nemoci (PR/CR) (Henry *et al.*, 2023). Obě studie probíhají a stále nabírají pacienty.

Posledním selektivním CDK9 inhibitorem v klinickém testování je GFH009. U tohoto inhibitoru taktéž není známá struktura a doposud bylo publikováno velmi omezené množství preklinických dat. Látka vykazovala antiproliferanční aktivitu u linie MV4-11 a její aplikace vedla k inhibici pSer2 RNAPII, exprese Mcl-1 a vedla k indukci štěpení kaspasy-3. Aplikace GFH009 *in vivo* vedla k inhibici růstu tumoru u MV4-11 myšího xenograftu (Zhou *et al.*, 2022). V letech 2020 a 2023 vstoupil do 2 klinických studií zaměřených na hematologické malignity (NCT04588922, NCT05934513). Prvotní data ze studie

NCT04588922 od 14 AML pacientů a 16 pacientů s lymfomem ukazují na tolerovatelnost látky. Mezi nejčastější vedlejší účinky patřila anemie a pokles v počtu bílých krvinek a neutrofilů, většinou s vážností G1-G2. U tří pacientů byla zaznamenána G3 pneumonie související s léčbou. U čtyřech pacientů s lymfomem došlo ke stabilizaci nemoci, u pacientů s AML nebyla zaznamenána reakce na léčbu (Qi *et al.*, 2022).



Obr. 10: Struktury CDK9i v klinickém testování.

5 METODIKA

5.1 Buněčné kultury

Lidské nádorové linie byly získány z European Collection of Authenticated Cell Culture, German Collection of Microorganisms and Cell Cultures, Cell Line Service, American Tissue Culture Collection nebo byly darovány doc. Janem Bouchalem z Univerzity Palackého v Olomouci. Všechny buněčné linie byly kultivovány ve vhodném médiu doplněné o 10% fetální bovinní sérum, streptomycin (100 µg/ml), penicilin (100 IU/ml) a glutamin (4 mM) a kultivovány v 37°C a 5% CO₂. Seznam použitých buněčných linií s kulturačním médiem a zdrojem je shrnut v Tab. 1.

Tab. 1: Seznam použitých lidských nádorových linií

Buněčná linie	Nádorový typ	Zdroj	Kultivační médium
22Rv1	karcinom prostaty	LF UP*	RPMI
BT474	karcinom prsu	LF UP*	DMEM
CCFR-CEM	ALL	ECACC	RPMI
DU145	karcinom prostaty	LF UP*	RPMI
G361	Melanom	ECACC	DMEM
HL-60	AML	ECACC	IMDM
K562	CML	ECACC	DMEM
LAPC4	karcinom prostaty	LF UP*	DMEM
MCF7	karcinom prsu	ECACC	DMEM
MINO	Lymfom	ATCC	RPMI
ML-2	AML	DMSZ	RPMI
MOLM-13	AML	DSMZ	RPMI
MV4-11	AML	Cell line service	RPMI
RS4-11	ALL	DSMZ	α-MEM
SEM	ALL	DSMZ	IMDM
SKBR3	karcinom prsu	ATCC	DMEM
THP-1	AML	DSMZ	RPMI
U937	AML	DSMZ	RPMI

AML – akutní myeloidní leukemie; ALL – akutní lymfoblastická leukemie; CML – chronická myeloidní leukemie; ATCC - American Tissue Culture Collection; DSMZ - German Collection of Microorganisms and Cell Cultures; ECACC - European Collection of Authenticated Cell Culture

* Buňky byly získány z Ústavu patologie Lékařské fakulty Univerzity Palackého Olomouc.

5.2 Analýza cytotoxicity

Pro analýzu cytotoxických účinků studovaných látek byla použita metoda Calcein AM, která je založena na hydrolýze calceinu AM intracelulárními esterasami živých buněk na silně fluorescenční calcein.

Buněčné linie byly vysazeny do 96-jamkové mikrotitrační desky a následující den byly ovlivněny požadovanými koncentracemi testovaných látek. Po 72hodinové inkubaci byl ke vzorkům přidán roztok Calceinu AM a po další 4hodinové inkubaci byla změřena fluorescence při 485/538 nm (excitace/emise) na fluorimetru Fluoreskan Ascent (Labsystem).

5.3 Analýza exprese genů

Buněčné linie určené pro analýzu exprese genů byly vysazeny na Petriho kultivační misky, ovlivněny testovanými látkami o příslušné koncentraci, sklizeny do lyzačního pufru a zamrazeny v -80 °C. Následovala izolace RNA pomocí RNeasy plus mini kitu (QIAGEN). V rámci izolace byla ze vzorků odstraněna gDNA. Koncentrace RNA byla stanovena pomocí spektrofotometru DeNovix. Stabilita RNA byla ověřena pomocí agarózové elektroforézy. Vzorky s intaktní RNA obsahovaly 2 jasné bandy odpovídající 28S a 18S RNA. Vyzolovaná RNA byla přepsána do cDNA pomocí SensiFAST cDNA Synthesis Kit (Bioline). Pro ověření efektivity transkripce byl do vzorku přidán RNA spike I (TATAA). Vlastní analýza genové exprese byla provedena pomocí qPCR za využití SensiFAST SYBR No-ROX kitu (Bioline) na přístroji CFX96 Real-time PCR Detection System (Biorad). Používané primery (Tab. 2) byly navrženy pomocí programu Primer Blast (Ye *et al.*, 2012) a nasyntetizovány firmou Generi biotech. Raw data byla vyhodnocena v programu CFX Maestro Software (Biorad Laboratories, ver 2.2) a relativní normalizovaná exprese byla stanovena pomocí metody delta delta Ct (Livak *et Schmittgen*, 2001). Exprese studovaných genů byla vztažena vždy k minimálně 2 referenčním genům, jejichž exprese byla v rámci daných experimentálních podmínek vyhodnocena jako nejstabilnější pomocí programů CFX Maestro Software (Biorad Laboratories, ver 2.2) nebo RefFinder (Xie *et al.*, 2012; Xie *et al.*, 2023).

Tab. 2: Sekvence použitých primerů

Gen	Forward primer	Reverse primer
<i>ACTB</i>	GCACCACACCTTCTACAAT	GTCTCAAACATGATCTGGGT
<i>B2M</i>	CACCCCCACTGAAAAAGATG	AGCAAGCAAGCAGAATTTGG
<i>BCL-2</i>	ATGTGTGTGGAGAGCGTCA	ACAGCCAGGAGAAATCAAACAG
<i>FLT3</i>	GGAATGGGTGCTTTGCGATT	CAGCACCTTATGTCCGTCCC
<i>GAPDH</i>	TCCAAAATCAAGTGGGGCGA	TGGTTCACACCCATGACGAA
<i>HOXA9</i>	CCTGACTGACTATGCTTGTGGT	ACTCTTTCTCCAGTTCCAGGG
<i>MCL-1</i>	AGTTGTACCGGCAGTCG	TTTGATGTCCAGTTTCCGAAG
<i>MEIS1</i>	CGTCACAAAAAGCGTGGCAT	ATGGTGAGTCCCGTGTCTTG
<i>MYB</i>	TCTCCAGTCATGTTCCATACCC	TGTGTGGTTCTGTGTTGGTAGC
<i>MYC</i>	TACAACACCCGAGCAAGGAC	AGCTAACGTTGAGGGGCATC
<i>RPL13A</i>	CGACAAGAAAAAGCGGATGG	TTCTCTTCTCTTCTCTCTCC
<i>RUNX1</i>	CACTGTGATGGCTGGCAATG	CTTGCGGTGGGTTTGTGAAG
<i>RUNX2</i>	TCTGGCCTTCCACTCTCAGT	TGCAGGTAGGTGTGGTAGT

5.4 Analýza buněčného cyklu

Testované buněčné linie byly vysazeny na Petriho kultivační misky a následující den byly ovlivněny testovanými látkami. Po 24/48/72hodinové inkubaci byly buňky sklizeny a fixovány ve vychlazeném 70% ethanolu přes noc. Následující den proběhla rehydratace vzorků v PBS, denaturace pomocí 2M HCl s 0,5% Tritonem X-100 a neutralizace pomocí 0,1M Na₂B₄O₇ (pH = 8,5). Vzorky byly poté značeny propidium jodidem (výsledná koncentrace 100 µg/ml) po dobu půl hodiny s následným měřením relativního obsah jaderné DNA pomocí průtokové cytometrie s využitím přístroje BD FACS Verse (FACSuite software, verze 1.0.6.) a 488 nm excitačního laseru. Pro analýzu buněčného cyklu byl použit software ModFit LT (Verity Software House, verze 4.1.7).

5.5 SDS PAGE a imunodetekce

Vzorky určené pro imunodetekci proteinů byly ovlivněny testovanými látkami, sklizeny a poté 20 minut lyzovány v extrakčním RIPA pufru (20 mM TRIS pH = 7,4; 100 mM NaCl; 2 mM EGTA; 5 mM EDTA; 0,2% Nonidet P-40 pH = 7,4; před použitím přidáno: 1 mM DTT; 1 mM PMSF; 1 mM Na₂VO₃; 2 mM NaF; 0,5 µg/ml leupeptin a 2 µg/ml aprotinin). Následně byly vzorky sonikovány pomocí ultrazvukového homogenizátoru

a zcentrifugovány. Koncentrace proteinů v lyzátu byla stanovena spektrofotometrickou Bradfordovou metodou (Bradford, 1976). Pro vyrovnání koncentrace byly vzorky doplněny o vzorkovací pufr (0,3 M TRIS pH = 6,8; 10% SDS; 50% glycerol; 0,05% bromfenolová modř; 5% 2-merkaptoethanol) a poté byly denaturovány při 95 °C po dobu 3 minut.

Proteiny byly separovány s využitím polyakrylamidové elektroforézy za denaturujících podmínek a poté byly přeneseny na nitroceluloseovou membránu pomocí metody western blotting. Membrány byly blokovány v 3% BSA, inkubovány s primárními protilátkami přes noc, promyty a nakonec inkubovány se sekundárními protilátkami konjugovanými s křenuvou peroxidasou. Aktivita peroxidasy byla detekována s využitím Super-Signal West Pico reagents (Merck) a CCD kamery LAS-4000 (FujiFilm). Použité protilátky jsou vždy specifikovány v příslušné publikaci.

5.6 Detekce aktivity kaspas 3/7

Buněčné lyzáty určené pro detekci aktivity kaspas 3/7 byly napipetovány do 96-jamkové mikrotitrační destičky s výslednou koncentrací proteinů 15 µg. Ke vzorkům byl přidán fluorescenčně značený substrát Ac-DEVD-AMC (Enzo Life Sciences) a reakční pufr (25 nM PIPES, 2 mM MgCl₂, 2 mM EGTA, 5 mM DTT, pH 7.3). Po inkubaci při laboratorní teplotě ve tmě následovala detekce fluorescenčního signálu při 355/460 nm (excitace/emise) s využitím fluorimetru Fluoreskan Ascent (Labsystem).

6 KOMENTOVANÉ VÝSLEDKY A DISKUZE

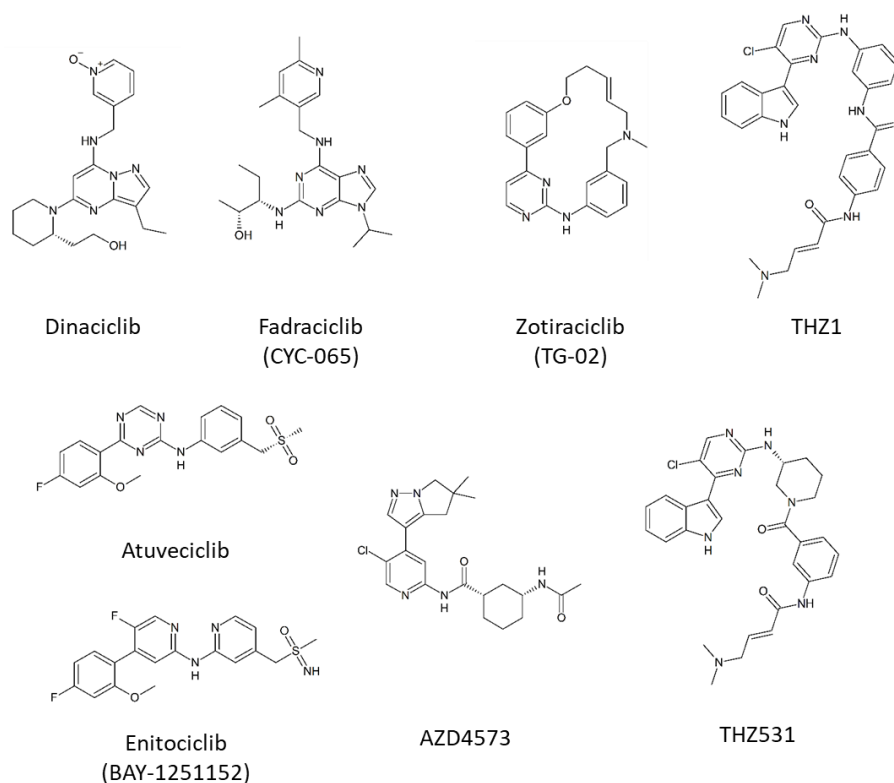
6.1 Inhibitory CDK v léčbě leukemií s *KMT2A* translokací

Inhibitory tCDK skrývají velký potenciál v protinádorové léčbě (Huang *et al.*, 2022; Li *et al.*, 2022; Vervoort *et al.*, 2022). Vzhledem k tomu, že CDK9 je v některých případech zapojena do *KMT2A*-r patogeneze, mohla by její selektivní inhibice představovat další terapeutický přístup v léčbě leukemií s *KMT2A* translokací. Tento typ leukemií je charakteristický špatnou odpovědí na standardizovaný léčebný protokol zejména u pacientů s ALL. Vývoj nových cílených léčiv, případně znovu-využití již schválených, by mohlo vést k zefektivnění léčby těchto leukemií (Tsakaneli *et Williams*, 2021; Górecki *et al.*, 2023; Kamens *et al.*, 2023).

Dílčím cílem práce bylo prověřit možnost využití inhibitorů tCDK pro léčbu leukemií s *KMT2A* translokacemi. Pro tuto část práce bylo zvoleno 8 různých CDK inhibitorů zahrnující pan-selektivní inhibitory, ale i selektivní inhibitory CDK7, CDK9 nebo CDK12/13. Selektivita jednotlivých inhibitorů popsána v původních publikacích je shrnuta v Tab. 3, jejich struktury jsou znázorněny na Obr. 11.

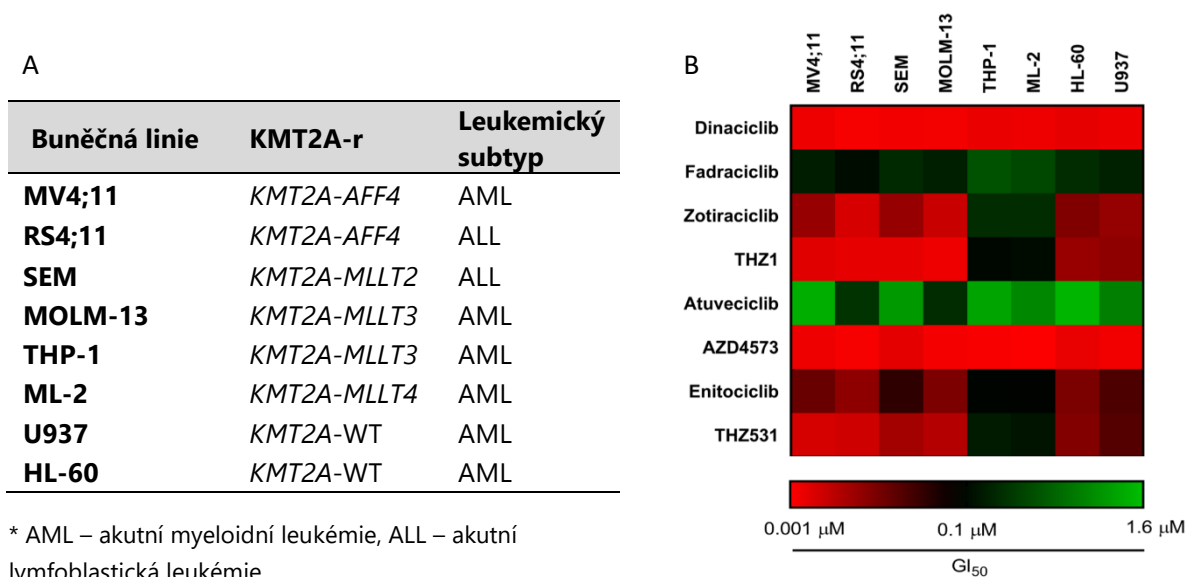
Tab. 3: Testované inhibitory CDK a jejich primárně uváděné kinasové cíle

Inhibitor	Publikované cíle	Primární publikace
Dinaciclib	CDK1, CDK2, CDK5, CDK9	Parry <i>et al.</i> (2010)
Fadraciclib	CDK2, CDK5, CDK9	Frame <i>et al.</i> (2020)
Zotiraciclib	CDK2, JAK, FLT3	William <i>et al.</i> (2012)
THZ1	CDK7	Kwiatkowski <i>et al.</i> (2014)
Atuveciclib	CDK9	Lücking <i>et al.</i> (2017)
AZD4573	CDK9	Barlaam <i>et al.</i> (2018)
Enitociclib	CDK9	Luecking <i>et al.</i> (2017)
THZ531	CDK12, CDK13	Zhang <i>et al.</i> (2016)



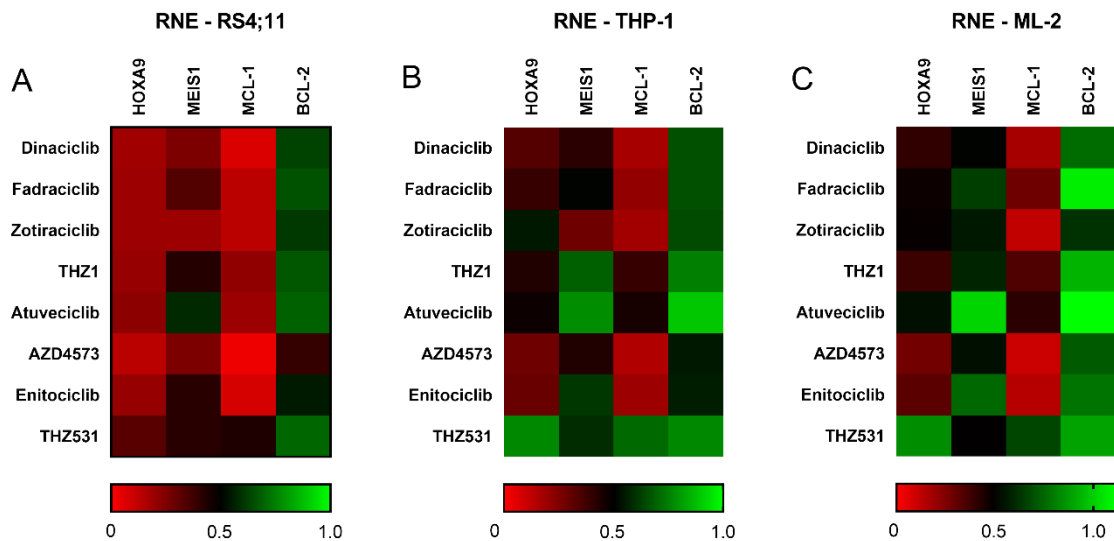
Obr. 11: Struktury použitých inhibitorů

Tyto látky byly nejprve testovány pro svou antiproliferační aktivitu na panelu leukemických linií zahrnující linie s translokací genu *KMT2A* (*KMT2A-r*) a i s původní nemutovanou variantou (*KMT2A-WT*) (Obr. 12A). Většina inhibitorů vykazovala na všech použitých leukemických liniích antiproliferační aktivitu s hodnotami GI_{50} v nanomolárních až submikromolárních koncentracích (Obr. 12B). V rámci *KMT2A-r* linií nebyl pozorován vliv fúzního partnera na citlivost vůči studovaným inhibitorům. Navíc tyto linie vykazovaly obdobnou citlivost jako linie *KMT2A-WT*, a to i v případě CDK9 selektivních inhibitorů. Přičemž u těchto inhibitorů byla očekávána vyšší citlivost vzhledem k patogenezi *KMT2A-r* leukemií.



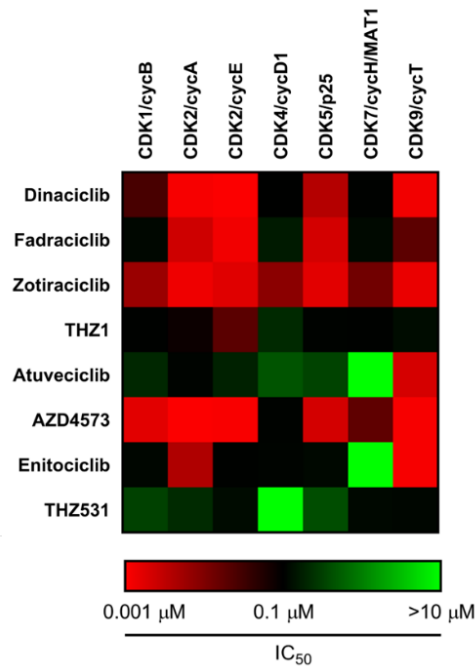
Obr. 12: (A) Seznam použitých buněčných linií. (B) Grafické znázornění antiproliferační aktivity testovaných inhibitorů na buněčných liniích *KMT2A-r* nebo *KMT2A-WT*.

Dále byl studován vliv testovaných látek na expresi genů zapojených do patogeneze *KMT2A-r* leukemií (*HOXA9*, *MEIS-1*) a apoptosy (*MCL-1*, *BCL-2*) (Armstrong *et al.*, 2002; Wong *et al.*, 2007; Faber *et al.*, 2009). Látky byly testovány na třech buněčných liniích s rozdílnou translokací genu *KMT2A*, konkrétně RS4;11, THP-1 a ML-2. V případě buněčné linie RS4;11 je přítomný fúzní partner (*AFF4*) součástí SEC, podobně jako P-TEFb (Lin *et al.*, 2010). Taktéž byly popsány interakce mezi *MLLT3*, nacházející se u linie THP-1, a komponentami transkripčního aparátu (Erfurth *et al.*, 2004; Monroe *et al.*, 2011). Navíc *MLLT3* patří mezi nejčastější fúzní partnery genu *KMT2A* (Meyer *et al.*, 2023). Testované látky byly aplikovány na buněčné linie v koncentraci 1 μM po dobu 2 hodin. Většina aplikovaných látek vedla k poklesu exprese genů *HOXA9* a *MCL-1* (Obr. 13). Oproti tomu například exprese genu *BCL-2* zůstala ve většině případů stabilní, což pravděpodobně souvisí s jeho vyšší stabilitou. Nicméně při porovnání efektu jednotlivých inhibitorů na studované geny nebyl ani zde pozorován výrazně odlišný efekt selektivních CDK9 inhibitorů ve srovnání s ostatními CDK inhibitory. Pozorovaný efekt spíše koreloval s cytotoxickými účinky použitých inhibitorů. Podobně byl studován vliv inhibitorů na hladiny fosorylace RNAPII a hladiny proteinů Mcl-1 a MEIS-1 u linií s *KMT2A* translokací. Předběžné výsledky imunoanalýzy také neodhalily specifický efekt CDK9 inhibitorů u *KMT2A-r* leukemických linií.



Obr. 13: Grafické znázornění relativní normalizované exprese studovaných genů po aplikaci vybraných inhibitorů u linií (A) RS4;11, (B) THP-1 a (C) ML-2. Látky byly aplikovány po dobu 2 hodin v koncentraci 1 μ M. Exprese genů byla normalizovaná ke genům *RPL13A* a *ACTB* v případě linie RS4;11, genům *RPL13A* a *GAPDH* v případě linie THP-1 a genům *RPL13A* a *B2M* v případě linie ML-2.

Získané výsledky nenaznačily žádný specifický efekt inhibice CDK9 u buněčných linií nesoucí translokaci v genu *KMT2A*. Nicméně v průběhu prováděných experimentů byla publikována studie Wells *et al.* (2020), zaměřující se na selektivitu známých CDK inhibitorů. V této studii bylo poukázáno na problematiku neselektivity inhibitorů, které jsou často popisovány jako selektivní, a to včetně některých inhibitorů zahrnutých v této práci. Podobné zjištění o nesprávně popisované selektivitě inhibitorů byla taktéž publikována kolektivem z pracoviště školitele (Jorda *et al.*, 2018; Hendrychová *et al.*, 2021). Z tohoto důvodu jsme se rozhodli otestovat selektivitu vybraných inhibitorů interním standardizovaným kinetickým testem. Naše výsledky korelují s výsledky Wells *et al.* (2020) a zejména u inhibitoru AZD4573 byla zjištěna jeho omezená selektivita (Obr. 14).



Obr. 14: Grafické znázornění inhibičních aktivit vybraných inhibitorů na panelu CDK.

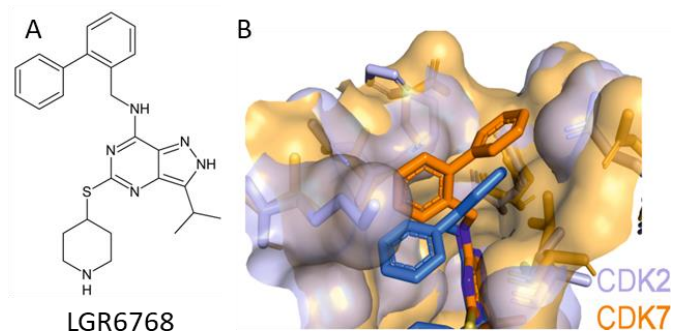
Z důvodu nedostatečné selektivity většiny použitých inhibitorů a také neprůkaznosti prozatímních výsledků jsme se rozhodli v této práci nepokračovat. Z testovaných látek vykazovaly inhibitory atuveciclib a enitociclib vyšší míru selektivity vůči CDK9. CDK9 inhibovaly v nanomolárních koncentracích a hodnoty IC₅₀ pro další CDK byly alespoň 10x vyšší. Lze tedy předpokládat, že pokud by selektivní inhibice CDK9 vedla ke specifickému účinku u *KMT2A*-r leukemií, byl by tento efekt pozorován alespoň u těchto inhibitorů. Podobnou studii se zaměřením na CDK9 inhibitory u *KMT2A*-r leukemií provedli (Garcia-Cuellar *et al.*, 2014). Tato studie je zaměřena zejména na účinky flavopiridolu a inhibitoru PC585, kdy popisuje benefiční inhibici CDK9 u *KMT2A*-r leukemií. Flavopiridol je však pan-selektivní inhibitor CDK a i přesto, že PC585 je popisován jako vysoce selektivní CDK9 inhibitor, data potvrzující takovéto tvrzení nebyla publikována. Pozorované výsledky nelze tedy s jistotou přisuzovat inhibici CDK9. Nicméně jak naše, tak data publikovaná ve studii Garcia-Cuellar *et al.* (2014) mohou naznačovat, že selektivní i neselektivní inhibice CDK9 by mohla být u leukemií s *KMT2A*-r translokací benefiční, a to zejména ve srovnání se standardizovanou léčbou, která má velmi často pouze malou účinnost. Pro přesné pochopení mechanismu účinku CDK případně CDK9 inhibitorů u *KMT2A*-r leukemií je však potřeba provést další testování.

6.2 CDK7 jako potenciální terapeutický cíl

Cyklin-dependentní kinasa 7, jakožto duální regulátor transkripce i buněčného cyklu, představuje slibný terapeutický cíl v protinádorové léčbě. Zvýšená exprese CDK7 byla popsána v řadě nádorů, jako je například triple-negativní karcinom prsu, karcinom ovarií či hepatocelulární karcinom. Často také koreluje s agresivitou tumoru a horší prognózou pacientů. V posledním desetiletí byla představena celá řada selektivních CDK7 inhibitorů a šest z nich je aktuálně v klinickém testování (shrnutí v **(Kovalová *et al.*, 2023a; Příloha I)**).

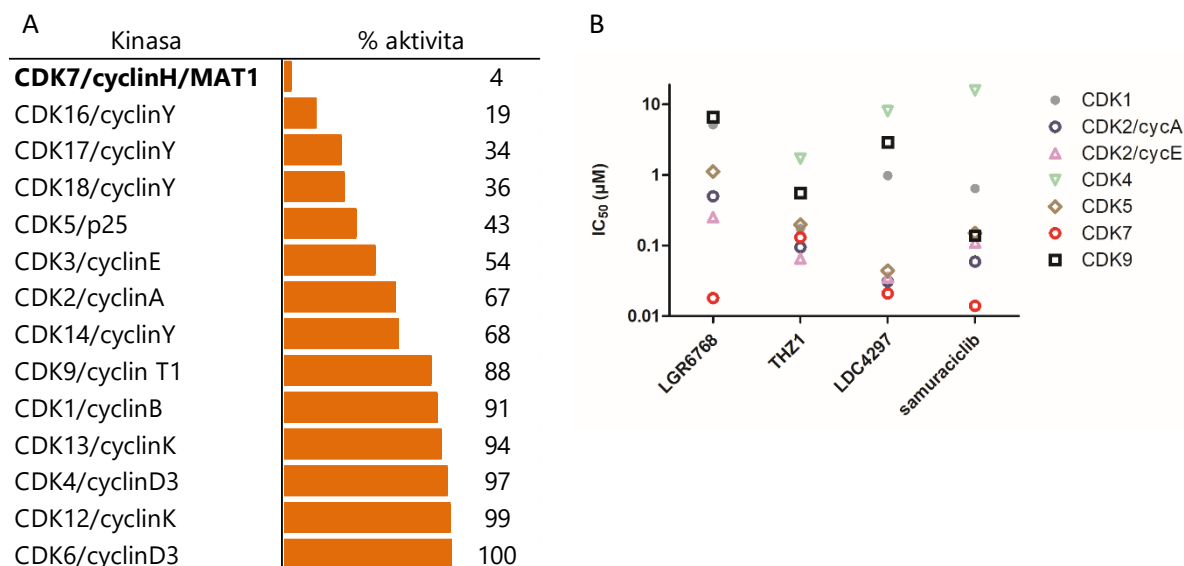
V dřívějších pracích publikovaných autory z pracoviště školitele bylo popsáno několik sérií velmi účinných 3,5,7-trisubstituovaných pyrazolo[4,3-*d*]pyrimidinů, které jakožto panselektivní CDK inhibitory vykazovaly silné protinádorové účinky *in vitro* a *in vivo* (Jorda *et al.*, 2011; Řezníčková *et al.*, 2015; Vymětalová *et al.*, 2016; Jorda *et al.*, 2019). Optimalizací těchto látek vznikl nový trisubstituovaný derivát pyrazolo[4,3-*d*]pyrimidinu, LGR6768 (Obr. 15A.), který selektivně inhibuje CDK7 **(Kovalová *et al.*, 2023b; Příloha II)**.

Pro pochopení selektivity byla nejprve porovnána jeho orientace v aktivním místě CDK2 a CDK7 na základě nově určené struktury kokryystalu (PDB ID 8B54), resp. modelu. I přes strukturní podobnost CDK2 a CDK7 byly pozorovány změny ve vazebné pozici LGR6768 v aktivních místech. Aktivní místo CDK7 je mnohem širší a otevřenější možným vazbám. LGR6768 je tedy v mnohem relaxovanější pozici a piperidinová část zasahuje hlouběji do aktivního místa. Hlavní rozdíl je v orientaci bifenyly. V případě CDK2 bifenyl směřuje do aktivního místa, kdežto u CDK7 se nachází na jeho okraji a směřuje ven. Tyto změny v orientaci by mohly být způsobeny rozdíly ve struktuře okraje aktivního místa mezi CDK2 a CDK7. Odlišná orientace bifenyly koresponduje s rozdílnými orientacemi benzylaminového substituentu u samuracilibu, pozorovanými taktéž mezi CDK2 a CDK7 (Greber *et al.*, 2021). Důležitá je také mimo jiné substituce Ile10 (CDK2) za Leu18 (CDK7), s nímž bifenylový substituent vytváří hydrofobní interakce. Získané výsledky (Obr. 15B) naznačují, že pro selektivitu LGR6768 vůči CDK7 je klíčová orientace a interakce bifenylového substituentu.



Obr. 15: (A) Struktura látky LGR6768. (B) Srovnání vazebné pozice LGR6768 v CDK7 (oranžová) a CDK2 (modrá).

Pro stanovení selektivity bylo provedeno komerční kinomové testování na panelu 50 kinas, které zahrnovaly známé vedlejší cíle příbuzných pyrazolo[4,3-*d*]pyrimidinů (Jorda *et al.*, 2019) a purinových isosterů, jako jsou roscovitin a CR8 (Bettayeb *et al.*, 2008). Kinomové testování potvrdilo selektivní redukci aktivity CDK7 na 4 % a to při aplikování 1 μ M koncentrace látky. Pouze dvě další kinasy byly signifikantně inhibovány – CDK16 (Obr. 16A) a CK1 δ (**Příloha II, Fig. S4**), obě s residuální aktivitou 19 %. Vzhledem k vysoké strukturní podobnosti v rámci rodiny CDK byla látka LGR6768 také testována interním standardizovaným kinetickým testem pro určení selektivity vůči některým CDK. Koncentračně závislé měření prokázalo potentní inhibici CDK7 v nízkých nanomolárních hodnotách s $IC_{50} = 20$ nM, přičemž hodnota byla nejméně 12x nižší než hodnoty IC_{50} pro zbylé testované CDK (**Příloha II, Tab. S2**). Nakonec byla selektivita LGR6768 porovnána s dalšími CDK7 inhibitory, konkrétně THZ1, LDC4297 a samuracilibem (Obr. 16B). Látka LGR6768 vykazovala vyšší míru selektivity v porovnání s inhibitory LDC4297 a samuracilibem.



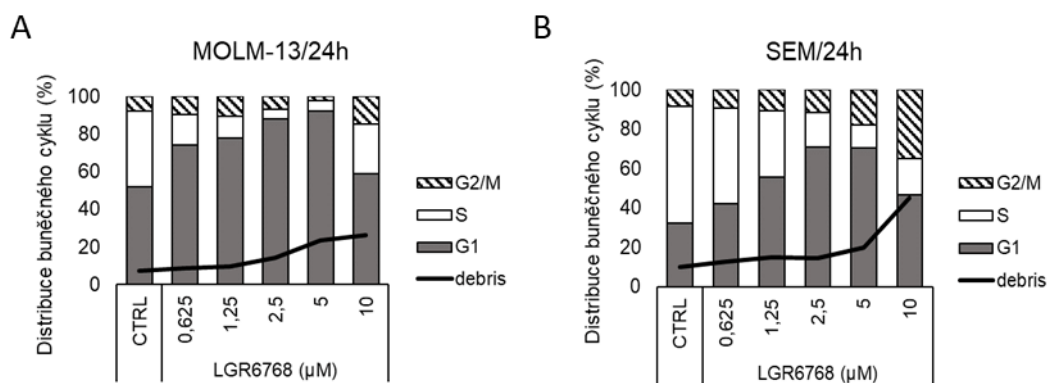
Obr. 16: (A) Selektivita LGR6768 vůči CDK při aplikaci látky v koncentraci 1 μM . (B) Srovnání inhibice vybraných CDK látkou LGR6768 a vybranými známými CDK7 inhibitory.

CDK7, jakožto součást CAK, je zapojena do regulace buněčného cyklu skrz fosforylaci T-smyčky CDK1 a CDK2 v místech Thr161, respektive Thr162. Imunoanalýza na buněčné nádorové linii SEM ukázala pokles ve fosforylaci obou kinas v závislosti na koncentraci (**Příloha II, Fig. 3C**) a době působení (**Příloha II, Fig. 3D**) aplikované látky LGR6768. Byla taktéž pozorována očekávaná defosforylace CTD RNAPII (**Příloha II, Fig. 3C, D**). Detekovaný pokles nebyl tak dramatický jako u méně selektivního CDK7 inhibitoru THZ1 (Kwiatkowski *et al.*, 2014) a naše výsledky více odpovídají novému selektivnímu inhibitoru YKL-5-124, který vykazoval pouze minimální efekt na fosforylaci CTD RNAPII (Olson *et al.*, 2019).

V předchozích studiích vykazovaly některé CDK7 inhibitory antileukemické účinky na AML i ALL liniích a taktéž AML xenograftech (Kwiatkowski *et al.*, 2014; Hu *et al.*, 2019; Park *et al.*, 2020; Abudureheman *et al.*, 2021). Z tohoto důvodu byla látka LGR6768 testována na panelu buněčných linií 10 hematologických malignit (5 AML, 3 ALL, 1 lymfom, 1 CML). Pozorovaná antiproliferační aktivita látky u leukemických buněčných linií dosahovala hodnot GI_{50} v rozmezí od 0,44 μM po 4,4 μM . Výjimku tvořily méně citlivé linie K562 a CCRF-CEM ($GI_{50} > 5 \mu\text{M}$). Látka byla testována také na buněčných liniích odvozených od jiných nádorových typů (karcinom prsu, prostaty, melanom). Tyto buněčné linie vykazovaly nižší citlivost vůči LGR6768 ve srovnání s AML a ALL liniemi, což naznačuje antileukemický potenciál látky (**Příloha II, Fig. 4A**). Ve srovnání se známými

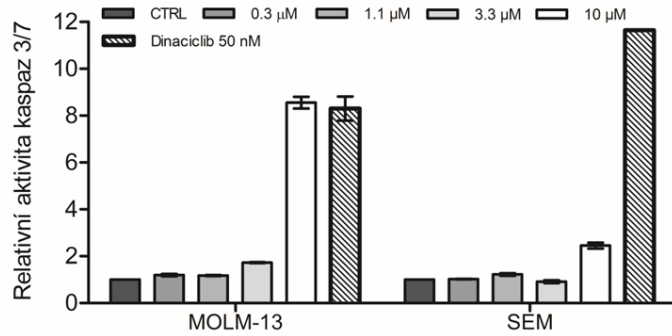
CDK7 inhibitory THZ1 (Kwiatkowski *et al.*, 2014) a SY-1365 (Hu *et al.*, 2019) vykazuje látka LGR6768 slabší antiproliferační aktivitu. Nicméně obě tyto látky jsou kovalentními inhibitory, na rozdíl od LGR6768. To by mohlo vysvětlovat vyšší potenci látek vůči nádorovým buněčným liniím.

Inhibice CDK7 často vede k narušení buněčného cyklu, což je doprovázeno poklesem počtu buněk v S-fázi, a naopak nárůstem počtu buněk v G1 či G2/M fázi v závislosti na buněčné linii a koncentraci inhibitoru (Ali *et al.*, 2009; Kelso *et al.*, 2014; Choi *et al.*, 2019; Olson *et al.*, 2019; Marineau *et al.*, 2022; Gaur *et al.*, 2023). Aplikace látky po dobu jednoho dne vedla ke koncentračně závislému G1 bloku u linie SEM i MOLM-13 již v nejnižších koncentracích (Obr. 17). Nejvyšší aplikovaná koncentrace (10 μM) pak vedla k signifikantní apoptose doprovázené G2/M blokem.



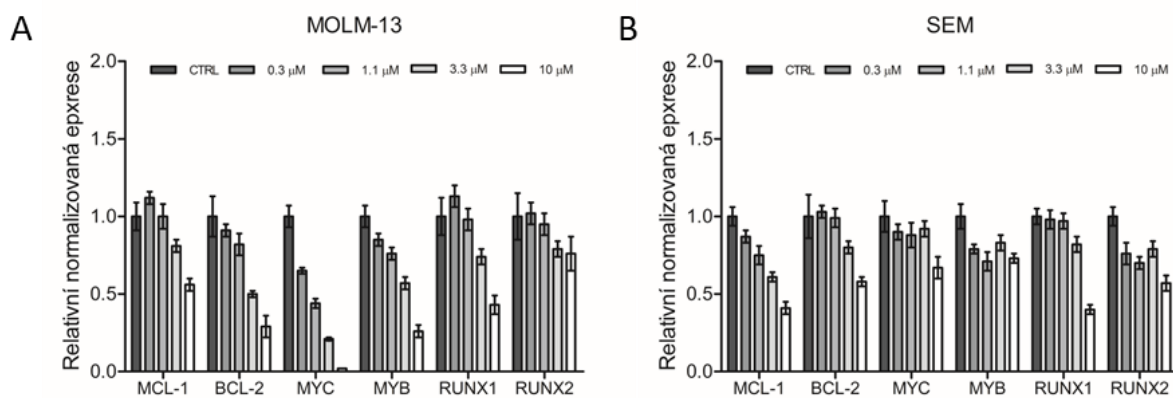
Obr. 17: Vliv LGR6768 na buněčný cyklus linií (A) MOLM-13 a (B) SEM po 24 hodinách.

Pro-apoptický efekt látky byl dále studován pomocí imunoanalýzy na buněčných liniích MV4-11, MOLM-13 a SEM (**Příloha II, Fig. 5A**). Látka byla aplikována po dobu 24 hodin ve vzrůstající koncentraci. Efekt látky byl pozorován pouze v nejvyšší aplikované koncentraci (10 μM), kdy bylo detekováno štěpení apoptického markeru PARP-1 a také fragmenty caspasy-7 a caspasy-9. Aplikace látky vedla také k mírnému snížení hladiny anti-apoptického proteinu Mcl-1, avšak hladiny anti-apoptického proteinu Bcl-2 zůstaly stabilní. To je pravděpodobně způsobeno jeho vyšší stabilitou. Podobné výsledky již byly popsány u jiných CDK7 inhibitorů (Kwiatkowski *et al.*, 2014; Patel *et al.*, 2018; Hu *et al.*, 2019; Gaur *et al.*, 2023). Pro-apoptický účinek látky byl v souladu s imunoanalýzou potvrzen i fluorimetrickým kaspasovým testem, a to na buněčných liniích MOLM-13 i SEM po 24hodinovém ovlivnění látkou LGR6768 (Obr. 18).



Obr. 18: Relativní aktivita kaspas 3/7 v buněčných liniích MOLM-13 a SEM po ovlivnění látkou LGR6768 nebo dinacilíbem po dobu 24 hodin.

Vzhledem ke změnám na proteinové úrovni byl studován vliv látky LGR6768 na expresi genů hrající významnou roli při apoptose, hematopoese nebo v AML patogenezi (*BCL-2*, *MCL-1*, *RUNX*, *MYC*, *MYB*) (Obr. 19). U většiny těchto genů byly již dříve popsány změny v transkripci vlivem působení některých inhibitorů tCDK (Kwiatkowski *et al.*, 2014; Zeng *et al.*, 2018; Hu *et al.*, 2019; Cidado *et al.*, 2020; Abudureheman *et al.*, 2021). Vzrůstající dávky LGR6768 vedly k poklesu exprese anti-apoptických genů *MCL-1* a *BCL-2*. Změny byly detekovány již po 4 hodinách, což naznačuje rychlou inhibici a schopnost indukovat apoptosu. U většiny genů došlo alespoň k dvojnásobnému poklesu exprese, který byl koncentračně závislý. V případě genu *MYC* u linie MOLM-13 došlo k rapidnímu poklesu exprese na < 1 % hladiny exprese kontrol. To by mohlo být vysvětleno vysokou sensitivitou linie MOLM-13 k látce LGR6768.



Obr. 19: Relativní normalizovaná exprese genů souvisejících s apoptosou a kódující transkripční faktory souvisejících s patogenezí hematologických malignit u buněčných linií (A) MOLM-13 a (B) SEM. Buňky byly ovlivněny vzrůstající koncentrací látky LGR6768 po dobu 4 hodin. Exprese genů byla normalizovaná k referenčním genům *GAPDH* a *RPL13A* (MOLM-13) nebo *GAPDH* a *B2M* (SEM).

Vzhledem k duální roli při regulaci buněčného cyklu i transkripce představuje cílení na CDK7 zajímavou terapeutickou možností v léčbě nádorových onemocnění (Diab *et al.*, 2020; Li *et al.*, 2022; Kovalová *et al.*, 2023a; Příloha I). V této části byla popsána látka LGR67468, nový pyrazolo[4,3-*d*]pyrimidinový derivát, který účinně a selektivně inhibuje CDK7. Účinky této látky odpovídají dalším popsaným CDK7 inhibitorům (Hu *et al.*, 2019; Olson *et al.*, 2019; Gaur *et al.*, 2023).

6.3 Od CDK inhibice k inhibici FLT3

Poslední část této práce je věnována studiu mechanismu působení duálních inhibitorů kinas s antileukemickými účinky, ať již na bázi konvenčních ATP kompetitivních inhibitorů, nebo na bázi proteolýzu indukujícího chimérického konjugátu (PROTAC), který indukuje specifickou degradaci cílových kinas, konkrétně CDK9 a onkogenní kinasy FLT3.

FMS-like tyrosin kinasa (FLT3) je jednou z 56 receptorových tyrosin kinas (RTS). Její exprese je asociována primárně s ranými hematopoetickými buňkami a je nezbytná pro proliferaci a diferenciaci hematopoetických progenitorů (Kazi *et Rönstrand*, 2019). Zhruba u 30 % pacientů s AML je detekována aktivační mutace ve *FLT3*. Nejčastěji se jedná o interní tandemovou duplikaci (ITD) v juxtamembránové doméně, která vede k dimerizaci FLT3 bez přítomnosti ligandu. Méně časté jsou bodové mutace v kinasové doméně, které způsobují konstitutivní aktivaci FLT3 (Meshinchi *et Appelbaum*, 2009; Daver *et al.*, 2021). Vzhledem k významu FLT3 v patologii AML došlo v posledních letech k vývoji několika FLT3 inhibitorů. Přičemž midostaurin (Levis, 2017), gilteretinib (Dhillon, 2019) a quizartinib (Zarrinkar *et al.*, 2009) byly již schváleny FDA pro léčbu AML pacienty s FLT3 mutací. Nicméně odpověď na FLT3 inhibitory je často limitována rozvojem rezistence.

Výchozím bodem pro tuto část práce byla série 2,6,9-trisubstituovaných purinů, které silně inhibovaly CDK a některé z nich také FLT3 (Gucký *et al.*, 2018). Jedna z neúčinnějších modelových látek této série (BPA311) inhibovala cílové kinasy v nanomolárních koncentracích a podobně vysoká účinnost byla pozorována také v leukemických buňkách exprimujících onkogenní variantu *FLT3*-ITD. Modifikací struktury BPA311 byly získány další nové látky s odlišným mechanismem účinku – kompetitivní inhibitor **34f** (Břehová *et al.*, 2023; Příloha III) a proteolýzu indukující chimérický konjugát PROTAC 13 (Řezníčková *et al.*, 2022; Příloha IV).

Nové kompetitivní inhibitory byly získány racionální modifikací již výše zmíněných trisubstituovaných purinů (Gucký *et al.*, 2018); konkrétně byly navrženy, připraveny a studovány isosterní trisubstituované deriváty s rozdílnými heterocyklickými jádry místo purinu jako jsou thieno[3,2-*d*]pyrimidiny, pyrazolo[1,5-*a*]pyrimidiny, imidazo[4,5-*b*]pyridiny, pyrido[4,3-*d*]pyrimidiny a imidazo[1,2-*b*]pyridaziny (Břehová *et al.*, 2023; Příloha III). Všechny látky byly testovány pro svou inhibiční aktivitu vůči rekombinantní *FLT3*-ITD, CDK2 a některé i CDK9. Cílem bylo potlačení CDK inhibiční aktivity a zvýšení aktivity vůči FLT3.

Z připravených látek vykazovaly nejzajímavější aktivity deriváty imidazo[1,2-*b*]pyridazinů a pro detailnější charakterizaci účinků byla z této skupiny vybrána látka **34f**. Interní standardizované kinetické testování odhalilo účinnou inhibici rekombinantní *FLT3*-ITD již v nanomolárních koncentracích. Oproti látce BPA311 z předchozí série došlo rovněž k vylepšení selektivity. Kinasy CDK2 a CDK9 byly inhibovány sub-mikromolárními koncentracemi (Tab. 4), o řád vyššími než látkou BPA311. Inhibiční aktivita **34f** vůči *FLT3*-ITD byla také srovnatelná se známými inhibitory, jako jsou quizartinib (0,010 μ M) a gilteritinib (0,012 μ M).

Tab. 4: Inhibiční aktivita látky **34f** a inhibitoru BPA 311

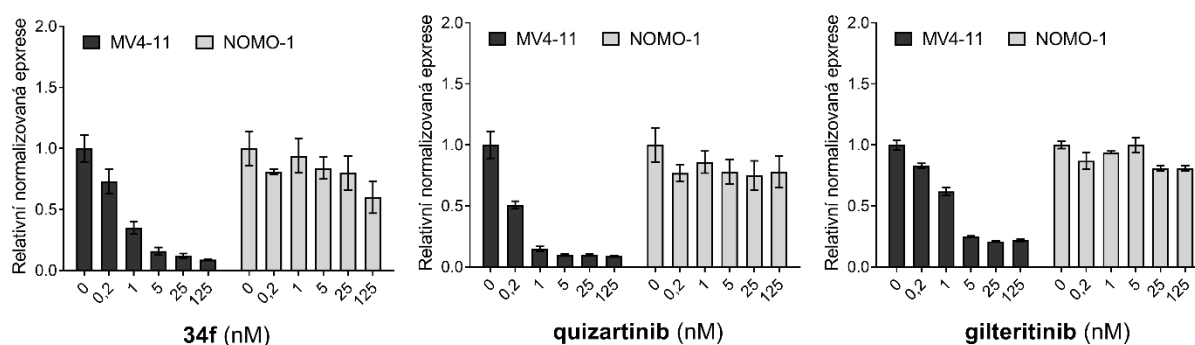
Inhibitor	IC ₅₀ ± SD (μ M)		
	FLT3-IDT	CDK2	CDK9
34f	0,004 ± 0,002	0,493 ± 0,091	0,146 ± 0,054
BPA 311	0,002 ± 0,001	0,028 ± 0,009	0,037 ± 0,009

Antiproliferační aktivita látek byla testována na souboru 7 hematologických malignit. Soubor zahrnoval linie nesoucí *FLT3*-ITD, které jsou plně závislé na *FLT3* signalizaci (MV4-11, MOLM-13) a také několik *FLT3* independentních linií (Tab. 5; **Příloha III., Tab. 7**). Látka **34f** vykazovala silnou antiproliferační aktivitu na *FLT3*-ITD buněčných liniích MV4-11 a MOLM-13 s hodnotami GI₅₀ v jednotkách nanomolů, oproti tomu linie nezávislé na *FLT3* signalizaci byly inhibovány s hodnotami GI₅₀ v jednotkách mikromolů. Získané výsledky antiproliferační aktivity byly srovnatelné se standardními *FLT3* inhibitory (quizartinib a gilteretinib).

Tab. 5: Antiproliferační aktivita látky **34f** a standardních *FLT3* inhibitorů

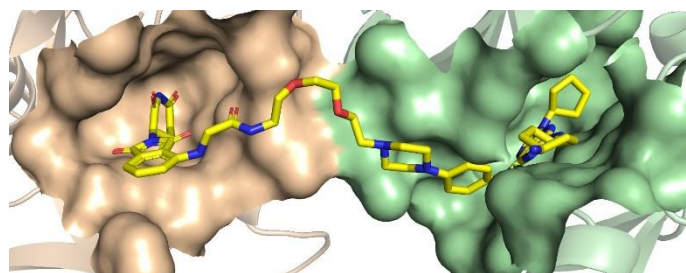
Buněčná linie	GI ₅₀ ± SD (μ M)		
	34f	quizartinib	gilteritinib
MV4-11	0,007 ± 0,004	0,003 ± 0,001	0,026 ± 0,009
MOLM-13	0,009 ± 0,006	0,004 ± 0,004	0,034 ± 0,013
CCRF-CEM	1,768 ± 0,261	> 10	2,771 ± 0,229
NOMO-1	4,275 ± 0,818	> 10	1,601 ± 0,226

Další analýza potvrdila FLT3-dependenční mechanismus účinku látky **34f**. Aplikace látky ve vzrůstajících koncentracích po dobu 1 hodiny vedla ke koncentračně závislému poklesu fosforylace FLT3 a také podřízených proteinů u buněčné linie MV4-11 (**Příloha III, Fig. 4A**). Aktivační mutace *FLT3-ITD* vede k narušení exprese specifického setu genů včetně například zvýšení exprese genu *MYC* (Kim *et al.*, 2007; Ohanian *et al.*, 2014; Basit *et al.*, 2018; Bogdanov *et al.*, 2023). Taktéž se jedná o klíčový onkogen, jehož deregulace často přispívá k rozvoji hematologických malignit. Aplikace látky **34f** po dobu 4 hodin vedla k signifikantnímu poklesu exprese genu *MYC* u FLT3-dependenční linie MV4-11, oproti tomu exprese tohoto genu nebyla výrazně ovlivněna u FLT3-independentní linie NOMO-1. Podobný efekt byl pozorován také po aplikaci inhibitorů quizaritnibu a gilteritinibu (Obr. 20).



Obr. 20: Relativní normalizovaná exprese genu *MYC* u buněčných linií MV4-11 a NOMO-1. Buňky byly ovlivněny látkou **34f** či komerčním inhibitorem quizartinibem nebo gilteritinibem po dobu 4 hodin. Exprese genů byla normalizovaná ke genům *GAPDH* a *RPL13A*.

Druhá část práce, věnovaná charakterizaci účinku PROTAC, taktéž vychází z duálních kompetitivních inhibitorů CDK a FLT3 (Gucký *et al.*, 2018). Jejich konverze na PROTAC vycházela z molekulárního modelování, jímž byla určena orientace látky BPA311 v aktivních místech kinas CDK9 a FLT3. Ethylový zbytek mířící ven z aktivního místa byl zvolen vhodným místem pro prodloužení linkerem propojující BPA311 a pomalidomid, který byl vybrán jakožto známý a používaný ligand ubiquitinligasy CRBN (**Řezníčková *et al.*, 2022; Příloha IV**). Délka a chemická struktura linkeru byla navržena opět pomocí molekulárního modelování a částečně byla inspirována předešlými publikacemi (Burslem *et al.*, 2018; Huang *et al.*, 2018; Olson *et al.*, 2018).



Obr. 21: Predikovaná vazba látky PROTAC 13 (žlutá) do FLT3 (zelená) a CRBN (oranžová).

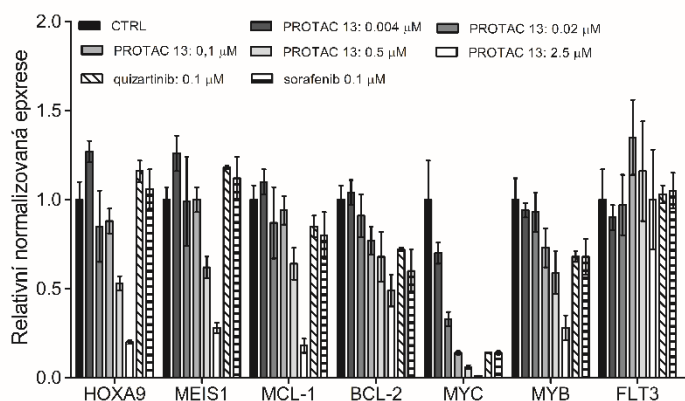
Získaný PROTAC 13 (Obr. 21) vykazoval slibnou antiproliferační aktivitu na buněčných liniích AML nesoucích *FLT3*-ITD (MV4-11, MOLM-13) s hodnotami GI_{50} v nanomolárních koncentracích. Naopak hodnoty GI_{50} u leukemických liniích bez *FLT3*-ITD byly alespoň 20x vyšší (Tab. 6; **Příloha IV, Tab. 1**). Ve srovnání s parentální látkou BPA311 nedošlo ke zlepšení antiproliferační aktivity, nicméně byla zachována citlivost a selektivita buněčných linií s *FLT3*-ITD (**Příloha IV, Tab. 1**). Podobně byla také zachována aktivita parentální látky vůči FLT3 (2% residuální aktivita) a CDK9 (3% a 8% residuální aktivita) (**Příloha IV, Fig. S2**).

Tab. 6: Antiproliferační aktivita látky PROTAC 13 na panelu leukemických linií

Buněčná linie	$IC_{50} \pm SD$ (μM)
	PROTAC 13
MV4-11	0,047 \pm 0,029
MOLM-13	0,119 \pm 0,031
RS4;11	1,014 \pm 0,208
HL60	6,122 \pm 2,383
THP-1	9,993 \pm 0,012

Vliv PROTAC 13 na hladiny proteinů FLT3 a CDK9 byl následně ověřován pomocí imunanalýzy. Látka byla testována na buněčné linii MV4-11 a její aplikace přes noc vedla ke koncentračně závislé degradaci proteinů FLT3 a CDK9, a to již od 100 nM (**Příloha IV, Fig. 2A**). Oproti tomu aplikace standardních FLT3 inhibitorů quizartinibu a sorafenibu neovlivnila CDK9, a naopak vedla k nárůstu hladiny FLT3 proteinu. Tento efekt je pozorován při dlouhodobém ovlivnění FLT3 inhibitory (Reiter *et al.*, 2018) a potenciálně může mít vliv na rozvoj rezistence (Weisberg *et al.*, 2011).

Efekt PROTAC 13 na CDK9, jakožto klíčového regulátoru transkripce, lze pozorovat na poklesu exprese genů zapojených do patogeneze AML. Pro potvrzení mechanismu účinku byly vybrány geny hrající roli při hematopoese, apoptose a iniciaci AML jako jsou *HOXA9*, *MEIS-1*, *MCL-1*, *BCL-2*, *MYC* a *MYB*. Aplikace látky PROTAC 13 na buněčnou linii MV4-11 po dobu 4 hodin vedla ke koncentračně závislému poklesu exprese studovaných genů (Obr. 22). Zároveň však aplikace látky neovlivnila expresi genu *FLT3*, což potvrzuje její mechanismus účinku. Pro srovnání efektu látky s komerčními FLT3 inhibitory byla linie MV4-11 ovlivněna také sorafenibem a quizartinibem. Nicméně v jejich případě nebyl pozorován tak silný efekt inhibice na expresi vybraných genů, což naznačuje potenciální terapeutický benefit inhibice CDK9 u AML.



Obr. 22: Relativní normalizovaná exprese genů zapojených do AML patogeneze u buněčné linie MV4-11. Buňky byly ovlivněny látkou PROTAC 13 či komerčními inhibitory quizartinibem nebo sorafenibem po dobu 4 hodin. Exprese genů byla normalizovaná ke genům *GAPDH* a *RPL13A*.

Akutní myeloidní leukemie je agresivním typem leukemií a zhruba u třetiny pacientů se nachází onkogenní mutace v genu *FLT3*. Pro tyto typy leukemie již bylo schváleno použití některých FLT3 inhibitorů (Zarrinkar *et al.*, 2009; Levis, 2017; Dhillon, 2019) a další jsou v klinickém testování. Dlouhodobá aplikace těchto inhibitorů je však doprovázena rozvojem rezistence (Wu *et al.*, 2018a). V rámci této disertační práce byl popsán nový imidazo[1,2-*b*]pyridazinový inhibitor FLT3 (látka **34f**) a taktéž proteolýzu indukující chimérický konjugát, PROTAC 13, který selektivně degraduje FLT3 a CDK9. Strukturní optimalizací došlo u řady látek k omezení inhibice CDK, což naznačuje, že CDK9 inhibiční aktivita nemusí být klíčová pro aktivitu látek. Naopak primární roli zde pravděpodobně hraje

inhibice FLT3. I přesto však experimenty s PROTAC 13 naznačují, že selektivní degradace CDK9 může být významným příspěvkem k účinnosti.

7 ZÁVĚR

Nádorové buňky často vykazují transkripční závislost a jsou tedy kriticky dependentní na kontinuální expresi transkriptů s krátkým poločasem rozpadu. Příkladem mohou být transkripty antiapoptických genů nebo klíčových onkogenních transkripčních faktorů. Společně s častou deregulací exprese transkripčních CDK to představuje pádné důvody pro zkoumání tCDK jako možných terapeutických cílů v onkologii. Takle možnost je studována již řadu let od vývoje první generace pan-selektivních CDK inhibitorů, které blokovaly nejen buněčný cyklus, ale také inhibovaly tCDK. Tyto první inhibitory často pozbývaly biochemickou selektivitu. Jejich toxicita byla způsobena ovlivněním většího množství cílů a taktéž jejich aplikace komplikovala pochopení důležitosti tCDK v protinádorové odpovědi. I přesto významně přispěly k vnímání tCDK jako slibných terapeutických cílů. Intenzivní výzkum částečně vyřešil problematiku selektivity, alespoň vůči některým CDK. Příkladem mohou být palbociclib nebo ribociclib selektivně cílicí na CDK4/6, a které byly eventuálně schválené jako protinádorová léčiva. Tato skutečnost potvrdila, že dostatečné selektivity lze dosáhnout i u velmi příbuzných enzymů, jako jsou CDK. Také to podnítilo vývoj řady nových selektivnějších inhibitorů zaměřujících se nejen na tCDK.

První část této práce byla zaměřena na využití inhibitorů transkripčních CDK v léčbě leukemií s *KMT2A* translokací. Tyto translokace jsou časté zejména u kojenců do 1 roku a jejich následkem je deregulace transkripce řady klíčových onkogenů. Jedním z mechanismů deregulace je interakce fúzních partnerů se super-elongačním komplexem, který je složený z velké řady proteinů včetně CDK9 (Li *et al.*, 2021; Meyer *et al.*, 2023). Inhibice CDK9 by mohla být možným terapeutickým řešením. Část této práce se zaměřila na testování více či méně selektivních inhibitorů CDK zahrnujících i tři inhibitory, které byly popsány jako CDK9 selektivní. Ověřena byla jejich antiproliferační aktivita na panelu leukemických linií obsahujících jak linie s translokací genu *KMT2A* (*KMT2A-r*), tak linie obsahující nemutovanou variantu (*KMT2A-wt*). Dále byl studován vliv těchto inhibitorů na expresi genů a proteinů zapojených do patogeneze *KMT2A-r* leukemií. Předběžné výsledky žádného z těchto testů neodhalily specifický efekt CDK9 inhibitorů u *KMT2A-r* linií. Navíc u některých studovaných inhibitorů byla odhalena jejich nízká selektivita, což byl paralelně potvrzeno i nezávisle (Wells *et al.*, 2020). Ze získaných dat nelze jednoznačně určit, zdali cílená inhibice CDK9 byla významně efektivní u *KMT2A-r* leukemií. Nicméně

i přesto byly testované buněčné linie citlivé k některým tCDKi a jejich obecná inhibice by mohla být přínosem.

Druhá a hlavní část této práce byla zaměřena na inhibici CDK7. Vzhledem k duální roli při regulaci buněčného cyklu i transkripce, představuje cílení na CDK7 zajímavou terapeutickou možností v léčbě nádorových onemocnění a již bylo popsáno několik kovalentních i kompetitivních inhibitorů, které selektivně inhibují CDK7. Několik z nich je aktuálně v klinickém testování (Patel *et al.*, 2018; Satyam *et al.*, 2020; Yu *et al.*, 2020; Marineau *et al.*, 2022). V této části byl popsán nový trisubstituovaný derivát pyrazolo[4,3-*d*]pyrimidinu, látka LGR6768, která účinně a selektivně inhibuje CDK7. Selektivita inhibice byla potvrzena kinetickými experimenty s rekombinantními enzymy a podpořena strukturní analýzou. LGR6768 ukázala antileukemický potenciál a její aplikace vedla ke snížení fosforylace substrátů CDK7, včetně CDK1, CDK2 a mírně i CTD RNAPII. Analýza buněčného cyklu ukázala blokaci v G1 fázi po aplikaci látky. Ve vyšších koncentracích došlo k indukci apoptosy doprovázené G2/M blokem, aktivací kaspas a štěpení proteinu PARP-1. Navíc, aplikace látky LGR6768 vedla ke snížení exprese hematologických onkogenů. Naše i další publikované výsledky naznačují, že inhibice CDK7 jako terapeutická možnost v léčbě nádorových onemocnění stojí za další zkoumání.

Poslední část byla zaměřena na akutní myeloidní leukemie s mutací *FLT3-ITD*, která souvisí s vyšší mírou relapsu a horší prognózou. Tato část práce vycházela z optimalizace dříve publikované látky BPA311 (Gucký *et al.*, 2018), která potently inhibovala CDK a FLT3. První optimalizací došlo k vývoji imidazo[1,2-*b*]pyridazinu, látky **34f**, u níž došlo k vylepšení selektivity vůči *FLT3-ITD* a potlačení její CDK inhibiční aktivity. Látka prokázala slibné antiproliferační účinky u buněčných liniích nesoucí *FLT3-ITD* srovnatelné se standardními inhibitory. Oproti tomu buněčné linie s nemutovanou formou FLT3 vykazovaly několikanásobně nižší citlivost, což dokazuje FLT3-dependentní mechanismus účinku látky. Aplikace látky vedla také k narušení fosforylace FLT3 a podřízené signalizace a také snížení exprese genu *MYC*. Druhou optimalizací vznikl proteolýzu indukující chimérický konjugát PROTAC 13, jakožto duální degradér CDK9 a FLT3. Tato látka taktéž vykazovala slibné antiproliferační účinky u buněčných liniích s *FLT3-ITD* a mechanismus účinku byl potvrzen pomocí imunoanalýzy, kde byla pozorována koncentračně závislá degradace cílových proteinů. Efekt látky, v souvislosti s cílovou degradací CDK9, byl prokázán pomocí analýzy exprese genů, kde byl pozorován pokles v expresi onkogenů zapojených do patogeneze AML.

Získaná data této dizertační práce přispívají k pochopení role inhibice tCDK v léčbě nádorových onemocnění a jsou v souladu s již dříve publikovanými daty. Přestože se transkripční inhibitory zaměřují na globální transkripci, jsou relativně selektivní vůči maligním buňkám. To je pravděpodobně způsobeno již zmíněnou citlivostí nádorových buněk na kontinuální expresi specifických onkogenů. Stále je však třeba lépe porozumět molekulárním mechanismům, které řídí transkripční cyklus, a důsledkům jeho inhibice. Moderní techniky, jako je CRISPR/Cas9, mohou hrát důležitou roli v tomto poznání a také v racionálním designu nových terapeutických strategií pro léčbu nádorových onemocnění.

8 SEZNAM POUŽITÉ LITERATURY

- Abboud, C., Sr., Zaucha, J. M., Solomon, S. R., Bradley, T., Mouhayar, E., Angelosanto, N., ... Lech Marañda, E. (2022). CDK 8/19 Kinase Inhibitor RVU120 in Patients with AML or Higher-Risk MDS: Safety and Efficacy Results from New Dose Escalation Cohorts. *Blood*, *140*, 6228-6229.
- Abudurehman, T., Xia, J., Li, M.-H., Zhou, H., Zheng, W.-W., Zhou, N., ... Duan, C.-W. (2021). CDK7 Inhibitor THZ1 Induces the Cell Apoptosis of B-Cell Acute Lymphocytic Leukemia by Perturbing Cellular Metabolism. *Frontiers in Oncology*, *11*.
- Akhtar, M. S., Heidemann, M., Tietjen, J. R., Zhang, D. W., Chapman, R. D., Eick, D., & Ansari, A. Z. (2009). TFIID Kinase Places Bivalent Marks on the Carboxy-Terminal Domain of RNA Polymerase II. *Molecular Cell*, *34*(3), 387-393.
- Akoulitchev, S., Chuikov, S., & Reinberg, D. (2000). TFIID is negatively regulated by cdk8-containing mediator complexes. *Nature*, *407*(6800), 102-106.
- Alarcón, C., Zaromytidou, A.-I., Xi, Q., Gao, S., Yu, J., Fujisawa, S., ... Massagué, J. (2009). Nuclear CDKs Drive Smad Transcriptional Activation and Turnover in BMP and TGF-beta Pathways. *Cell*, *139*(4), 757-769.
- Alharbi, R. A., Pettengell, R., Pandha, H. S., & Morgan, R. (2013). The role of HOX genes in normal hematopoiesis and acute leukemia. *Leukemia*, *27*(5), 1000-1008.
- Ali, S., Heathcote, D. A., Kroll, S. H. B., Jogalekar, A. S., Scheiper, B., Patel, H., ... Coombes, R. C. (2009). The Development of a Selective Cyclin-Dependent Kinase Inhibitor That Shows Antitumor Activity. *CANCER RESEARCH*, *69*(15), 6208-6215.
- Alsouk, A. (2021). Small molecule inhibitors of cyclin-dependent kinase 9 for cancer therapy. *Journal of Enzyme Inhibition and Medicinal Chemistry*, *36*(1), 693-706.
- Argiropoulos, B., & Humphries, R. K. (2007). Hox genes in hematopoiesis and leukemogenesis. *Oncogene*, *26*(47), 6766-6776.
- Armstrong, S. A., Staunton, J. E., Silverman, L. B., Pieters, R., den Boer, M. L., Minden, M. D., ... Korsmeyer, S. J. (2002). MLL translocations specify a distinct gene expression profile that distinguishes a unique leukemia. *Nature Genetics*, *30*(1), 41-47.
- Asghar, U., Witkiewicz, A. K., Turner, N. C., & Knudsen, E. S. (2015). The history and future of targeting cyclin-dependent kinases in cancer therapy. *Nature Reviews Drug Discovery*, *14*(2), 130-146.
- Baluapuri, A., Wolf, E., & Eilers, M. (2020). Target gene-independent functions of MYC oncoproteins. *Nature Reviews Molecular Cell Biology*, *21*(5), 255-267.
- Bancerek, J., Poss, Zachary C., Steinparzer, I., Sedlyarov, V., Pfaffenwimmer, T., Mikulic, I., ... Kovarik, P. (2013). CDK8 Kinase Phosphorylates Transcription Factor STAT1 to Selectively Regulate the Interferon Response. *Immunity*, *38*(2), 250-262.
- Barlaam, B., Casella, R., Cidado, J., Cook, C., De Savi, C., Dishington, A., ... Yao, T. (2020). Discovery of AZD4573, a Potent and Selective Inhibitor of CDK9 That Enables Short Duration of Target Engagement for the Treatment of Hematological Malignancies. *Journal of Medicinal Chemistry*, *63*(24), 15564-15590.
- Barlaam, B., Savi, C. D., Drew, L., Ferguson, A. D., Ferguson, D., Gu, C., ... Shao, W. (2018). Abstract 1650: Discovery of AZD4573, a potent and selective inhibitor of CDK9 that enables transient target engagement for the treatment of hematologic malignancies. *CANCER RESEARCH*, *78*(13_Supplement), 1650-1650.
- Bartkowiak, B., & Greenleaf, A. L. (2015). Expression, Purification, and Identification of Associated Proteins of the Full-length hCDK12/CyclinK Complex*. *Journal of Biological Chemistry*, *290*(3), 1786-1795.
- Bartkowiak, B., Liu, P., Phatnani, H. P., Fuda, N. J., Cooper, J. J., Price, D. H., ... Greenleaf, A. L. (2010). CDK12 is a transcription elongation-associated CTD kinase, the metazoan ortholog of yeast Ctk1. *Genes & Development*, *24*(20), 2303-2316.
- Bartkowiak, B., Yan, C., & Greenleaf, A. L. (2015). Engineering an analog-sensitive CDK12 cell line using CRISPR/Cas. *Biochimica et Biophysica Acta (BBA) - Gene Regulatory Mechanisms*, *1849*(9), 1179-1187.

- Basit, F., Andersson, M., & Hultquist, A. (2018). The Myc/Max/Mxd Network Is a Target of Mutated Flt3 Signaling in Hematopoietic Stem Cells in Flt3-ITD-Induced Myeloproliferative Disease. *Stem Cells International*, 2018, 3286949.
- Bayer. (2017). An open-label Phase I dose-escalation study to characterize the safety, tolerability, pharmacokinetics, and maximum tolerated dose of BAY1143572 given in a once-daily or an intermittent dosing schedule in subjects with advanced malignancies. <https://clinicaltrials.bayer.com/study/16519/>
- Békés, M., Langley, D. R., & Crews, C. M. (2022). PROTAC targeted protein degraders: the past is prologue. *Nature Reviews Drug Discovery*, 21(3), 181-200.
- Bell, D., Berchuck, A., Birrer, M., Chien, J., Cramer, D. W., Dao, F., ... Data coordination, c. (2011). Integrated genomic analyses of ovarian carcinoma. *Nature*, 474(7353), 609-615.
- Bettayeb, K., Oumata, N., Echalié, A., Ferandin, Y., Endicott, J. A., Galons, H., & Meijer, L. (2008). CR8, a potent and selective, roscovitine-derived inhibitor of cyclin-dependent kinases. *Oncogene*, 27(44), 5797-5807.
- Beyaert, R., Kidd, V. J., Cornelis, S., Van de Craen, M., Denecker, G., Lahti, J. M., ... Fiers, W. (1997). Cleavage of PITSLRE Kinases by ICE/CASP-1 and CPP32/CASP-3 during Apoptosis Induced by Tumor Necrosis Factor *. *Journal of Biological Chemistry*, 272(18), 11694-11697.
- Bian, J., Ren, J., Li, Y., Wang, J., Xu, X., Feng, Y., ... Li, Z. (2018). Discovery of Wogonin-based PROTACs against CDK9 and capable of achieving antitumor activity. *Bioorganic Chemistry*, 81, 373-381.
- Bisi, J. E., Sorrentino, J. A., Roberts, P. J., Tavares, F. X., & Strum, J. C. (2016). Preclinical Characterization of G1T28: A Novel CDK4/6 Inhibitor for Reduction of Chemotherapy-Induced Myelosuppression. *Molecular Cancer Therapeutics*, 15(5), 783-793.
- Bisteau, X., Paternot, S., Colleoni, B., Ecker, K., Coulonval, K., De Groote, P., ... Roger, P. P. (2013). CDK4 T172 Phosphorylation Is Central in a CDK7-Dependent Bidirectional CDK4/CDK2 Interplay Mediated by p21 Phosphorylation at the Restriction Point. *PLOS Genetics*, 9(5), e1003546.
- Blake, D. R., Vaseva, A. V., Hodge, R. G., Kline, M. P., Gilbert, T. S. K., Tyagi, V., ... Der, C. J. (2019). Application of a MYC degradation screen identifies sensitivity to CDK9 inhibitors in KRAS-mutant pancreatic cancer. *Science Signaling*, 12(590), 1-15.
- Blazek, D., Kohoutek, J., Bartholomeeusen, K., Johansen, E., Hulinkova, P., Luo, Z., ... Peterlin, B. M. (2011). The Cyclin K/Cdk12 complex maintains genomic stability via regulation of expression of DNA damage response genes. *Genes & Development*, 25(20), 2158-2172.
- Bogdanov, K., Kudryavtseva, E., Fomicheva, Y., Churkina, I., Lomaia, E., Girshova, L., ... Zaritsky, A. (2023). Shift of N-MYC Oncogene Expression in AML Patients Carrying the FLT3-ITD Mutation. *Pathophysiology*, 30(3), 296-313.
- Boike, L., Henning, N. J., & Nomura, D. K. (2022). Advances in covalent drug discovery. *Nature Reviews Drug Discovery*, 21(12), 881-898.
- Bolomsky, A., Vogler, M., Köse, M. C., Heckman, C. A., Ehx, G., Ludwig, H., & Caers, J. (2020). MCL-1 inhibitors, fast-lane development of a new class of anti-cancer agents. *Journal of Hematology & Oncology*, 13(1), 173.
- Borowczak, J., Szczerbowski, K., Ahmadi, N., & Szyllberg, Ł. (2022a). CDK9 inhibitors in multiple myeloma: a review of progress and perspectives. *Medical Oncology*, 39(4), 39.
- Borowczak, J., Szczerbowski, K., Maniewski, M., Zdrenka, M., Słupski, P., Antosik, P., ... Szyllberg, Ł. (2022b). The Prognostic Role of CDK9 in Bladder Cancer. *Cancers*, 14(6), 1492.
- Bösken, C. A., Farnung, L., Hintermair, C., Merzel Schachter, M., Vogel-Bachmayr, K., Blazek, D., ... Geyer, M. (2014). The structure and substrate specificity of human Cdk12/Cyclin K. *Nature Communications*, 5(1), 3505.
- Bourbon, H.-M. (2008). Comparative genomics supports a deep evolutionary origin for the large, four-module transcriptional mediator complex. *Nucleic Acids Research*, 36(12), 3993-4008.
- Bradford, M. M. (1976). A rapid and sensitive method for the quantitation of microgram quantities of protein utilizing the principle of protein-dye binding. *Analytical Biochemistry*, 72(1), 248-254.

- Bradner, J. E., Hnisz, D., & Young, R. A. (2017). Transcriptional Addiction in Cancer. *Cell*, *168*(4), 629-643.
- Brummendorf, T. H., Medd, P., Koch, R., Stilgenbauer, S., Sharma, S., He, Y., ... Kater, A. P. (2022). Safety, Tolerability, Pharmacokinetics (PK) and Preliminary Antitumor Activity of the Cyclin-Dependent Kinase-9 (CDK9) Inhibitor AZD4573 in Relapsed/Refractory Hematological Malignancies: A Phase 1 First-in-Human Study. *Blood*, *140*(Supplement 1), 3126-3127.
- Břehová, P., Řezníčková, E., Škach, K., Jorda, R., Dejmek, M., Vojáčková, V., ... Kryštof, V. (2023). Inhibition of FLT3-ITD Kinase in Acute Myeloid Leukemia by New Imidazo[1,2-b]pyridazine Derivatives Identified by Scaffold Hopping. *Journal of Medicinal Chemistry*, *66*(16), 11133-11157.
- Burslem, G. M., Song, J., Chen, X., Hines, J., & Crews, C. M. (2018). Enhancing Antiproliferative Activity and Selectivity of a FLT-3 Inhibitor by Proteolysis Targeting Chimera Conversion. *Journal of the American Chemical Society*, *140*(48), 16428-16432.
- Byrne, M., Frattini, M. G., Ottmann, O. G., Mantzaris, I., Wermke, M., Lee, D. J., ... Cordoba, R. (2018). Phase I Study of the PTEFb Inhibitor BAY 1251152 in Patients with Acute Myelogenous Leukemia. *Blood*, *132*, 4055-4055.
- Campbell, K. J., Dhayade, S., Ferrari, N., Sims, A. H., Johnson, E., Mason, S. M., ... Blyth, K. (2018). MCL-1 is a prognostic indicator and drug target in breast cancer. *Cell Death & Disease*, *9*(2), 19.
- Campbell, K. J., Mason, S. M., Winder, M. L., Willemsen, R. B. E., Cloix, C., Lawson, H., ... Tait, S. W. G. (2021). Breast cancer dependence on MCL-1 is due to its canonical anti-apoptotic function. *Cell Death & Differentiation*, *28*(9), 2589-2600.
- Cidado, J., Boiko, S., Proia, T., Ferguson, D., Criscione, S. W., San Martin, M., ... Drew, L. (2020). AZD4573 Is a Highly Selective CDK9 Inhibitor That Suppresses MCL-1 and Induces Apoptosis in Hematologic Cancer Cells. *Clinical Cancer Research*, *26*(4), 922-934.
- Eli Lilly and Company. (2019). Preparation of pyrazolopyrimidinyl aminopyridines as CDK7 inhibitors for the treatment of cancer. US20190144456.
- Collins, C. T., & Hess, J. L. (2016). Deregulation of the HOXA9/MEIS1 axis in acute leukemia. *Current Opinion in Hematology*, *23*(4).
- Constantin, T. A., Greenland, K. K., Varela-Carver, A., & Bevan, C. L. (2022). Transcription associated cyclin-dependent kinases as therapeutic targets for prostate cancer. *Oncogene*, *41*(24), 3303-3315.
- Coombes, R. C., Howell, S., Lord, S. R., Kenny, L., Mansi, J., Mitri, Z., ... Krebs, M. G. (2023). Dose escalation and expansion cohorts in patients with advanced breast cancer in a Phase I study of the CDK7-inhibitor samuraciclib. *Nature Communications*, *14*(1), 4444.
- Corden, J. L. (1990). Tails of RNA polymerase II. *Trends in Biochemical Sciences*, *15*(10), 383-387.
- COSMIC Catalogue of Somatic Mutations in Cancer (září 2023): <https://cancer.sanger.ac.uk/cosmic>
- Crawford, J., Ianzano, L., Savino, M., Whitmore, S., Cleton-Jansen, A.-M., Settasatian, C., ... Savoia, A. (1999). The PISSLRE Gene: Structure, Exon Skipping, and Exclusion as Tumor Suppressor in Breast Cancer. *Genomics*, *56*(1), 90-97.
- Cross, D. A. E., Ashton, S. E., Ghyorghi, S., Eberlein, C., Nebhan, C. A., Spitzler, P. J., ... Pao, W. (2014). AZD9291, an Irreversible EGFR TKI, Overcomes T790M-Mediated Resistance to EGFR Inhibitors in Lung Cancer. *Cancer Discovery*, *4*(9), 1046-1061.
- Czerwińska, P., Mazurek, S., & Wiznerowicz, M. (2017). The complexity of TRIM28 contribution to cancer. *Journal of Biomedical Science*, *24*(1), 63.
- Czudnochowski, N., Böskén, C. A., & Geyer, M. (2012). Serine-7 but not serine-5 phosphorylation primes RNA polymerase II CTD for P-TEFb recognition. *Nature Communications*, *3*(1), 842.
- Daniels, D. L., Ford, M., Schwinn, M. K., Benink, H., Galbraith, M. D., Amunugama, R., ... Urh, M. (2013). Mutual Exclusivity of MED12/MED12L, MED13/13L, and CDK8/19 Paralogs Revealed within the CDK-Mediator Kinase Module. (S2), 004.
- Daver, N., Venugopal, S., & Ravandi, F. (2021). FLT3 mutated acute myeloid leukemia: 2021 treatment algorithm. *Blood Cancer Journal*, *11*(5), 104.

- Davidson, L., Muniz, L., & West, S. (2014). 3' end formation of pre-mRNA and phosphorylation of Ser2 on the RNA polymerase II CTD are reciprocally coupled in human cells. *Genes & Development*, 28(4), 342-356.
- Day, M. A., Saffran, D. C., Hood, T., Obholzer, N., Pandey, A., Lin, C. Y., ... DiMartino, J. (2022). Abstract 2565: CDK9 inhibitor KB-0742 is active in preclinical models of small-cell lung cancer. *CANCER RESEARCH*, 82(12_Supplement), 2565-2565.
- Derenne, S., Monia, B., Dean, N. M., Taylor, J. K., Rapp, M.-J. e., Harousseau, J.-L., ... Amiot, M. (2002). Antisense strategy shows that Mcl-1 rather than Bcl-2 or Bcl-xL is an essential survival protein of human myeloma cells. *Blood*, 100(1), 194-199.
- Dhanasekaran, R., Deutzmann, A., Mahauad-Fernandez, W. D., Hansen, A. S., Gouw, A. M., & Felsher, D. W. (2022). The MYC oncogene — the grand orchestrator of cancer growth and immune evasion. *Nature Reviews Clinical Oncology*, 19(1), 23-36.
- Dhillon, S. (2019). Gilteritinib: First Global Approval. *Drugs*, 79(3), 331-339.
- Diab, S., Yu, M., & Wang, S. (2020). CDK7 Inhibitors in Cancer Therapy: The Sweet Smell of Success? *Journal of Medicinal Chemistry*, 63(14), 7458-7474.
- Diamond, J. R., Boni, V., Lim, E., Nowakowski, G., Cordoba, R., Morillo, D., ... Moreno, V. (2022). First-in-Human Dose-Escalation Study of Cyclin-Dependent Kinase 9 Inhibitor VIP152 in Patients with Advanced Malignancies Shows Early Signs of Clinical Efficacy. *Clinical Cancer Research*, 28(7), 1285-1293.
- Dickinson, M. E., Flenniken, A. M., Ji, X., Teboul, L., Wong, M. D., White, J. K., ... Center, R. B. (2016). High-throughput discovery of novel developmental phenotypes. *Nature*, 537(7621), 508-514.
- Ding, X., Sharko, A. C., McDermott, M. S. J., Schools, G. P., Chumanevich, A., Ji, H., ... Broude, E. V. (2022). Inhibition of CDK8/19 Mediator kinase potentiates HER2-targeting drugs and bypasses resistance to these agents in vitro and in vivo. *Proceedings of the National Academy of Sciences*, 119(32), e2201073119.
- Donner, A. J., Ebmeier, C. C., Taatjes, D. J., & Espinosa, J. M. (2010). CDK8 is a positive regulator of transcriptional elongation within the serum response network. *Nature Structural & Molecular Biology*, 17(2), 194-199.
- Donovan, M. G., Galbraith, M. D., & Espinosa, J. M. (2022). Multi-omics investigation reveals functional specialization of transcriptional cyclin dependent kinases in cancer biology. *Scientific Reports*, 12(1), 22505.
- Dorantes-Acosta, E., & Pelayo, R. (2012). Lineage Switching in Acute Leukemias: A Consequence of Stem Cell Plasticity? *Bone Marrow Research*, 2012, 406796.
- Dana-Farber Cancer Institute, Inc. (2021). Pyrrolopyrazole derivatives as degraders of cyclin-dependent kinase 7 (CDK7) and preparation and uses thereof. WO2021026109.
- Düster, R., Ji, Y., Pan, K.-T., Urlaub, H., & Geyer, M. (2022). Functional characterization of the human Cdk10/Cyclin Q complex. *Open Biology*, 12(3), 210381.
- Dziadziunszko, R., Garralda, E., Angelosanto, N., Rzymyski, T., Dudziak, R., Brzózka, K., ... Lugowska, I. (2022). Phase I/II trial of RVU120 (SEL120), a CDK8/CDK19 inhibitor in patients with relapsed/refractory metastatic or advanced solid tumors. *Journal of Clinical Oncology*, 40(16_suppl), e15091.
- Ebmeier, C. C., Erickson, B., Allen, B. L., Allen, M. A., Kim, H., Fong, N., ... Taatjes, D. J. (2017). Human TFIIH Kinase CDK7 Regulates Transcription-Associated Chromatin Modifications. *Cell Reports*, 20(5), 1173-1186.
- Egloff, S. (2021). CDK9 keeps RNA polymerase II on track. *Cellular and Molecular Life Sciences*, 78(14), 5543-5567.
- Egloff, S., Studniarek, C., & Kiss, T. (2018). 7SK small nuclear RNA, a multifunctional transcriptional regulatory RNA with gene-specific features. *Transcription*, 9(2), 95-101.
- Elmlund, H., Baraznenok, V., Lindahl, M., Samuelsen, C. O., Koeck, P. J. B., Holmberg, S., ... Gustafsson, C. M. (2006). The cyclin-dependent kinase 8 module sterically blocks Mediator interactions with RNA polymerase II. *Proceedings of the National Academy of Sciences*, 103(43), 15788-15793.
- Erfurth, F., Hemenway, C. S., de Erkenez, A. C., & Domer, P. H. (2004). MLL fusion partners AF4 and AF9 interact at subnuclear foci. *Leukemia*, 18(1), 92-102.

- Ettl, T., Schulz, D., & Bauer, R. J. (2022). The Renaissance of Cyclin Dependent Kinase Inhibitors. *Cancers*, *14*(2), 293.
- Faber, J., Krivtsov, A. V., Stubbs, M. C., Wright, R., Davis, T. N., van den Heuvel-Eibrink, M., ... Armstrong, S. A. (2009). HOXA9 is required for survival in human MLL-rearranged acute leukemias. *Blood*, *113*(11), 2375-2385.
- Fan, Z., Devlin, J. R., Hogg, S. J., Doyle, M. A., Harrison, P. F., Todorovski, I., ... Johnstone, R. W. (2020). CDK13 cooperates with CDK12 to control global RNA polymerase II processivity. *Science Advances*, *6*(18), 1-18.
- Federici, E., Civenni, G., Kokanovic, A., Sandrini, G., Guarrera, L., Mosole, S., ... Catapano, C. V. (2022). Abstract 5471: PRT2527, a novel highly selective cyclin-dependent kinase 9 (CDK9) inhibitor, is active in preclinical models of prostate cancer. *CANCER RESEARCH*, *82*(12_Supplement), 5471-5471.
- Felix, C. A. (2001). Leukemias related to treatment with DNA topoisomerase II inhibitors*. *Medical and Pediatric Oncology*, *36*(5), 525-535.
- Feng, H., Cheng, A. S. L., Tsang, D. P., Li, M. S., Go, M. Y., Cheung, Y. S., ... Sung, J. J. Y. (2011). Cell cycle-related kinase is a direct androgen receptor-regulated gene that drives β -catenin/T cell factor-dependent hepatocarcinogenesis. *The Journal of Clinical Investigation*, *121*(8), 3159-3175.
- Fesquet, D., Labbé, J. C., Derancourt, J., Capony, J. P., Galas, S., Girard, F., ... Cavadore, J. C. (1993). The MO15 gene encodes the catalytic subunit of a protein kinase that activates cdc2 and other cyclin-dependent kinases (CDKs) through phosphorylation of Thr161 and its homologues. *The EMBO Journal*, *12*(8), 3111-3121.
- Firestein, R., Bass, A. J., Kim, S. Y., Dunn, I. F., Silver, S. J., Guney, I., ... Hahn, W. C. (2008). CDK8 is a colorectal cancer oncogene that regulates β -catenin activity. *Nature*, *455*(7212), 547-551.
- Frame, S., Saladino, C., MacKay, C., Atrash, B., Sheldrake, P., McDonald, E., ... Zheleva, D. (2020). Fadraciliclib (CYC065), a novel CDK inhibitor, targets key pro-survival and oncogenic pathways in cancer. *PLOS ONE*, *15*(7), e0234103.
- Fry, D. W., Harvey, P. J., Keller, P. R., Elliott, W. L., Meade, M., Trachet, E., ... Toogood, P. L. (2004). Specific inhibition of cyclin-dependent kinase 4/6 by PD 0332991 and associated antitumor activity in human tumor xenografts. *Molecular Cancer Therapeutics*, *3*(11), 1427-1438.
- Fryer, C. J., White, J. B., & Jones, K. A. (2004). Mastermind Recruits CycC:CDK8 to Phosphorylate the Notch ICD and Coordinate Activation with Turnover. *Molecular Cell*, *16*(4), 509-520.
- Fu, D., Pfannenstiel, L., Demelash, A., Phoon, Y. P., Mayell, C., Cabrera, C., ... Gastman, B. (2022). MCL1 nuclear translocation induces chemoresistance in colorectal carcinoma. *Cell Death & Disease*, *13*(1), 63.
- Fu, T.-J., Peng, J., Lee, G., Price, D. H., & Flores, O. (1999). Cyclin K Functions as a CDK9 Regulatory Subunit and Participates in RNA Polymerase II Transcription*. *Journal of Biological Chemistry*, *274*(49), 34527-34530.
- Fujinaga, K., Irwin, D., Huang, Y., Taube, R., Kurosu, T., & Peterlin, B. M. (2004). Dynamics of Human Immunodeficiency Virus Transcription: P-TEFb Phosphorylates RD and Dissociates Negative Effectors from the Transactivation Response Element. *Molecular and Cellular Biology*, *24*(2), 787-795.
- Gabay, M., Li, Y., & Felsher, D. W. (2014). MYC Activation Is a Hallmark of Cancer Initiation and Maintenance. *Cold Spring Harbor Perspectives in Medicine*, *4*(6), 1-13.
- Gajdušková, P., Ruiz de los Mozos, I., Rájecký, M., Hluchý, M., Ule, J., & Blazek, D. (2020). CDK11 is required for transcription of replication-dependent histone genes. *Nature Structural & Molecular Biology*, *27*(5), 500-510.
- Galbraith, Matthew D., Allen, Mary A., Bensard, Claire L., Wang, X., Schwinn, Marie K., Qin, B., ... Espinosa, Joaquín M. (2013). HIF1A Employs CDK8-Mediator to Stimulate RNAPII Elongation in Response to Hypoxia. *Cell*, *153*(6), 1327-1339.
- Galbraith, M. D., Bender, H., & Espinosa, J. M. (2019). Therapeutic targeting of transcriptional cyclin-dependent kinases. *Transcription*, *10*(2), 118-136.

- Ganuza, M., Sáiz-Ladera, C., Cañamero, M., Gómez, G., Schneider, R., Blasco, M. A., ... Barbacid, M. (2012). Genetic inactivation of Cdk7 leads to cell cycle arrest and induces premature aging due to adult stem cell exhaustion. *The EMBO Journal*, *31*(11), 2498-2510.
- Garber, M. E., Wei, P., & Jones, K. A. (1998). HIV-1 Tat interacts with cyclin T1 to direct the P-TEFb CTD kinase complex to TAR RNA. *Cold Spring Harb Symp Quant Biol*, *63*, 371-380.
- Garcia-Cuellar, M. P., Füller, E., Mäthner, E., Breitingner, C., Hetzner, K., Zeitlmann, L., ... Slany, R. K. (2014). Efficacy of cyclin-dependent-kinase 9 inhibitors in a murine model of mixed-lineage leukemia. *Leukemia*, *28*(7), 1427-1435.
- Gargano, B., Amente, S., Majello, B., & Lania, L. (2007). P-TEFb is a Crucial Co-Factor for Myc Transactivation. *Cell Cycle*, *6*(16), 2031-2037.
- Gaur, T., Poddutoori, R., Khare, L., Bagal, B., Rashmi, S., Patkar, N., ... Hasan, S. K. (2023). Novel covalent CDK7 inhibitor potently induces apoptosis in acute myeloid leukemia and synergizes with Venetoclax. *Journal of Experimental & Clinical Cancer Research*, *42*(1), 186.
- Glaser, S. P., Lee, E. F., Trounson, E., Bouillet, P., Wei, A., Fairlie, W. D., ... Strasser, A. (2012). Anti-apoptotic Mcl-1 is essential for the development and sustained growth of acute myeloid leukemia. *Genes & Development*, *26*(2), 120-125.
- Glover-Cutter, K., Larochelle, S., Erickson, B., Zhang, C., Shokat, K., Fisher, R. P., & Bentley, D. L. (2009). TFIIH-Associated Cdk7 Kinase Functions in Phosphorylation of C-Terminal Domain Ser7 Residues, Promoter-Proximal Pausing, and Termination by RNA Polymerase II. *Molecular and Cellular Biology*, *29*(20), 5455-5464.
- Goodwin, C. M., Rossanese, O. W., Olejniczak, E. T., & Fesik, S. W. (2015). Myeloid cell leukemia-1 is an important apoptotic survival factor in triple-negative breast cancer. *Cell Death & Differentiation*, *22*(12), 2098-2106.
- Górecki, M., Kozioł, I., Kopystecka, A., Budzyńska, J., Zawitkowska, J., & Lejman, M. (2023). Updates in KMT2A Gene Rearrangement in Pediatric Acute Lymphoblastic Leukemia. *Biomedicines*, *11*(3), 821.
- Graña, X., De Luca, A., Sang, N., Fu, Y., Claudio, P. P., Rosenblatt, J., ... Giordano, A. (1994). PITALRE, a nuclear CDC2-related protein kinase that phosphorylates the retinoblastoma protein in vitro. *Proceedings of the National Academy of Sciences*, *91*(9), 3834-3838.
- Greber, B. J., Remis, J., Ali, S., & Nogales, E. (2021). 2.5-Å-resolution structure of human CDK-activating kinase bound to the clinical inhibitor ICEC0942. *Biophysical Journal*, *120*(4), 677-686.
- Gucký, T., Řezníčková, E., Radošová Muchová, T., Jorda, R., Klejová, Z., Malínková, V., ... Kryštof, V. (2018). Discovery of N2-(4-Amino-cyclohexyl)-9-cyclopentyl-N6-(4-morpholin-4-ylmethyl-phenyl)-9H-purine-2,6-diamine as a Potent FLT3 Kinase Inhibitor for Acute Myeloid Leukemia with FLT3 Mutations. *Journal of Medicinal Chemistry*, *61*(9), 3855-3869.
- Guen, V. J., Gamble, C., Flajolet, M., Unger, S., Thollet, A., Ferandin, Y., ... Colas, P. (2013). CDK10/cyclin M is a protein kinase that controls ETS2 degradation and is deficient in STAR syndrome. *Proceedings of the National Academy of Sciences*, *110*(48), 19525-19530.
- Guen, V. J., Gamble, C., Lees, J. A., & Colas, P. (2017). The awakening of the CDK10/Cyclin M protein kinase. *Oncotarget*, *8*(30), 50174-50186.
- Guenther, M. G., Jenner, R. G., Chevalier, B., Nakamura, T., Croce, C. M., Canaani, E., & Young, R. A. (2005). Global and Hox-specific roles for the MLL1 methyltransferase. *Proceedings of the National Academy of Sciences*, *102*(24), 8603-8608.
- Guo, Y., Liu, Y., Hu, N., Yu, D., Zhou, C., Shi, G., ... Wang, Z. (2019). Discovery of Zanubrutinib (BGB-3111), a Novel, Potent, and Selective Covalent Inhibitor of Bruton's Tyrosine Kinase. *Journal of Medicinal Chemistry*, *62*(17), 7923-7940.
- Gururajan, R., Lahti, J. M., Grenet, J., Easton, J., Gruber, I., Ambros, P. F., & Kidd, V. J. (1998). Duplication of a Genomic Region Containing the Cdc2L1-2 and MMP21-22 Genes on Human Chromosome 1p36.3 and their Linkage to D1Z2. *Genome Research*, *8*(9), 929-939.
- Hashiguchi, T., Bruss, N., Best, S., Lam, V., Danilova, O., Paiva, C. J., ... Danilov, A. V. (2019). Cyclin-Dependent Kinase-9 Is a Therapeutic Target in MYC-Expressing Diffuse Large B-Cell Lymphoma. *Molecular Cancer Therapeutics*, *18*(9), 1520-1532.

- Hatcher, J. M., Wang, E. S., Johannessen, L., Kwiatkowski, N., Sim, T., & Gray, N. S. (2018). Development of Highly Potent and Selective Steroidal Inhibitors and Degraders of CDK8. *ACS Medicinal Chemistry Letters*, 9(6), 540-545.
- Hendrychová, D., Jorda, R., & Kryštof, V. (2021). How selective are clinical CDK4/6 inhibitors? *Medicinal Research Reviews*, 41(3), 1578-1598.
- Hengartner, C. J., Myer, V. E., Liao, S.-M., Wilson, C. J., Koh, S. S., & Young, R. A. (1998). Temporal Regulation of RNA Polymerase II by Srb10 and Kin28 Cyclin-Dependent Kinases. *Molecular Cell*, 2(1), 43-53.
- Henry, J. T., Orr, D., Basu-Mallick, A., Spira, A., Lihou, C., Sharma, N., ... Patel, M. R. (2023). Abstract CT173: A phase 1, open-label, multicenter, dose-escalation study of PRT2527, a cyclin-dependent kinase 9 (CDK9) inhibitor, in adult patients (pts) with advanced solid tumors. *CANCER RESEARCH*, 83, CT173.
- Heptinstall, A. B., Adiyasa, I., Cano, C., & Hardcastle, I. R. (2018). Recent advances in CDK inhibitors for cancer therapy. *Future Medicinal Chemistry*, 10(11), 1369-1388.
- Honigberg, L. A., Smith, A. M., Sirisawad, M., Verner, E., Loury, D., Chang, B., ... Buggy, J. J. (2010). The Bruton tyrosine kinase inhibitor PCI-32765 blocks B-cell activation and is efficacious in models of autoimmune disease and B-cell malignancy. *Proceedings of the National Academy of Sciences*, 107(29), 13075-13080.
- Hsieh, J. J. D., Ernst, P., Erdjument-Bromage, H., Tempst, P., & Korsmeyer, S. J. (2003a). Proteolytic Cleavage of MLL Generates a Complex of N- and C-Terminal Fragments That Confers Protein Stability and Subnuclear Localization. *Molecular and Cellular Biology*, 23(1), 186-194.
- Hsieh, J. J. D., Cheng, E. H. Y., & Korsmeyer, S. J. (2003b). Taspase1: A Threonine Aspartase Required for Cleavage of MLL and Proper HOX Gene Expression. *Cell*, 115(3), 293-303.
- Hu, D., Mayeda, A., Trembley, J. H., Lahti, J. M., & Kidd, V. J. (2003). CDK11 Complexes Promote Pre-mRNA Splicing *. *Journal of Biological Chemistry*, 278(10), 8623-8629.
- Hu, S., Ke, N., Ren, Y., Miljovska, S., Rajagopal, N., McKeown, M., ... Fritz, C. C. (2017). Abstract 1151: SY-1365, a potent and selective CDK7 inhibitor, exhibits promising anti-tumor activity in multiple preclinical models of aggressive solid tumors. *CANCER RESEARCH*, 77, 1151-1151.
- Hu, S., Marineau, J. J., Rajagopal, N., Hamman, K. B., Choi, Y. J., Schmidt, D. R., ... Olson, E. R. (2019). Discovery and Characterization of SY-1365, a Selective, Covalent Inhibitor of CDK7. *CANCER RESEARCH*, 79(13), 3479-3491.
- Huang, H.-T., Dobrovolsky, D., Paulk, J., Yang, G., Weisberg, E. L., Doctor, Z. M., ... Gray, N. S. (2018). A Chemoproteomic Approach to Query the Degradable Kinome Using a Multi-kinase Degradator. *Cell Chemical Biology*, 25(1), 88-99.
- Huang, J., Gurung, B., Wan, B., Matkar, S., Veniaminova, N. A., Wan, K., ... Lei, M. (2012). The same pocket in menin binds both MLL and JUND but has opposite effects on transcription. *Nature*, 482(7386), 542-546.
- Huang, Z., Wang, T., Wang, C., & Fan, Y. (2022). CDK9 inhibitors in cancer research. *RSC Medicinal Chemistry*, 13(6), 688-710.
- Hughes, S. J., Testa, A., Thompson, N., & Churcher, I. (2021). The rise and rise of protein degradation: Opportunities and challenges ahead. *Drug Discovery Today*, 26(12), 2889-2897.
- Chaikuad, A., Koch, P., Laufer, S. A., & Knapp, S. (2018). The Cysteinome of Protein Kinases as a Target in Drug Development. *Angewandte Chemie International Edition*, 57(16), 4372-4385.
- Chan, A. K. N., & Chen, C.-W. (2019). Rewiring the Epigenetic Networks in MLL-Rearranged Leukemias: Epigenetic Dysregulation and Pharmacological Interventions. *Frontiers in Cell and Developmental Biology*, 7, 1-15.
- Chen, D., Riedl, T., Washbrook, E., Pace, P. E., Coombes, R. C., Egly, J.-M., & Ali, S. (2000). Activation of Estrogen Receptor β by S118 Phosphorylation Involves a Ligand-Dependent Interaction with TFIID and Participation of CDK7. *Molecular Cell*, 6(1), 127-137.
- Chen, H., Liu, H., & Qing, G. (2018). Targeting oncogenic Myc as a strategy for cancer treatment. *Signal Transduction and Targeted Therapy*, 3(1), 5.

- Cheng, B., & Price, D. H. (2007). Properties of RNA Polymerase II Elongation Complexes Before and After the P-TEFb-mediated Transition into Productive Elongation*. *Journal of Biological Chemistry*, 282(30), 21901-21912.
- Choi, S. H., Kim, S., & Jones, K. A. (2020). Gene expression regulation by CDK12: a versatile kinase in cancer with functions beyond CTD phosphorylation. *Experimental & Molecular Medicine*, 52(5), 762-771.
- Choi, Y. J., Kim, D. H., Yoon, D. H., Suh, C., Choi, C.-M., Lee, J. C., ... Rho, J. K. (2019). Efficacy of the novel CDK7 inhibitor QS1189 in mantle cell lymphoma. *Scientific Reports*, 9(1), 7193.
- Iorns, E., Turner, N. C., Elliott, R., Syed, N., Garrone, O., Gasco, M., ... Ashworth, A. (2008). Identification of CDK10 as an Important Determinant of Resistance to Endocrine Therapy for Breast Cancer. *Cancer Cell*, 13(2), 91-104.
- Ivanov, D., Kwak, Y. T., Guo, J., & Gaynor, R. B. (2000). Domains in the SPT5 Protein That Modulate Its Transcriptional Regulatory Properties. *Molecular and Cellular Biology*, 20(9), 2970-2983.
- Jessberger, S., Gage, F. H., Eisch, A. J., & Lagace, D. C. (2009). Making a neuron: Cdk5 in embryonic and adult neurogenesis. *Trends in Neurosciences*, 32(11), 575-582.
- Jin, W., Qazi, T. J., Quan, Z., Li, N., & Qing, H. (2019). Dysregulation of Transcription Factors: A Key Culprit Behind Neurodegenerative Disorders. *The Neuroscientist*, 25(6), 548-565.
- Jorda, R., Havlíček, L., McNae, I. W., Walkinshaw, M. D., Voller, J., Štunc, A., ... Kryštof, V. (2011). Pyrazolo[4,3-d]pyrimidine Bioisostere of Roscovitine: Evaluation of a Novel Selective Inhibitor of Cyclin-Dependent Kinases with Antiproliferative Activity. *Journal of Medicinal Chemistry*, 54(8), 2980-2993.
- Jorda, R., Havlíček, L., Štunc, A., Tušková, D., Daumová, L., Alam, M., ... Kryštof, V. (2019). 3,5,7-Substituted Pyrazolo[4,3-d]pyrimidine Inhibitors of Cyclin-Dependent Kinases and Their Evaluation in Lymphoma Models. *Journal of Medicinal Chemistry*, 62(9), 4606-4623.
- Jorda, R., Hendrychová, D., Voller, J., Řezníčková, E., Gucký, T., & Kryštof, V. (2018). How Selective Are Pharmacological Inhibitors of Cell-Cycle-Regulating Cyclin-Dependent Kinases? *Journal of Medicinal Chemistry*, 61(20), 9105-9120.
- Juan, H. C., Lin, Y., Chen, H. R., & Fann, M. J. (2016). Cdk12 is essential for embryonic development and the maintenance of genomic stability. *Cell Death & Differentiation*, 23(6), 1038-1048.
- Kaldis, P., & Solomon, M. J. (2000). Analysis of CAK activities from human cells. *European Journal of Biochemistry*, 267(13), 4213-4221.
- Kalkat, M., De Melo, J., Hickman, K. A., Lourenco, C., Redel, C., Resetca, D., ... Penn, L. Z. (2017). MYC Deregulation in Primary Human Cancers. *Genes*, 8(6), 151.
- Kamens, J. L., Nance, S., Koss, C., Xu, B., Cotton, A., Lam, J. W., ... Gruber, T. A. (2023). Proteasome inhibition targets the KMT2A transcriptional complex in acute lymphoblastic leukemia. *Nature Communications*, 14(1), 809.
- Kanazawa, S., Soucek, L., Evan, G., Okamoto, T., & Peterlin, B. M. (2003). c-Myc recruits P-TEFb for transcription, cellular proliferation and apoptosis. *Oncogene*, 22(36), 5707-5711.
- Kasten, M., & Giordano, A. (2001). Cdk10, a Cdc2-related kinase, associates with the Ets2 transcription factor and modulates its transactivation activity. *Oncogene*, 20(15), 1832-1838.
- Kazi, J. U., & Rönstrand, L. (2019). FMS-like Tyrosine Kinase 3/FLT3: From Basic Science to Clinical Implications. *Physiological Reviews*, 99(3), 1433-1466.
- Kelso, T. W. R., Baumgart, K., Eickhoff, J., Albert, T., Antrecht, C., Lemcke, S., ... Meisterernst, M. (2014). Cyclin-Dependent Kinase 7 Controls mRNA Synthesis by Affecting Stability of Preinitiation Complexes, Leading to Altered Gene Expression, Cell Cycle Progression, and Survival of Tumor Cells. *Molecular and Cellular Biology*, 34(19), 3675-3688.
- Kim, E. S. (2017). Abemaciclib: First Global Approval. *Drugs*, 77(18), 2063-2070.
- Kim, J., Cho, Y.-J., Ryu, J.-Y., Hwang, I., Han, H. D., Ahn, H. J., ... Lee, J.-W. (2020). CDK7 is a reliable prognostic factor and novel therapeutic target in epithelial ovarian cancer. *Gynecologic Oncology*, 156(1), 211-221.
- Kim, K.-T., Baird, K., Davis, S., Piloto, O., Levis, M., Li, L., ... Small, D. (2007). Constitutive Fms-like tyrosine kinase 3 activation results in specific changes in gene expression in myeloid leukaemic cells. *British Journal of Haematology*, 138(5), 603-615.

- Kim, W., Haws, H., Peterson, P., Whatcott, C. J., Weitman, S., Warner, S. L., ... Siddiqui-Jain, A. (2017). Abstract 5133: TP-1287, an oral prodrug of the cyclin-dependent kinase-9 inhibitor alvocidib. *CANCER RESEARCH*, 77, 5133-5133.
- Kimura, H. (2013). Histone modifications for human epigenome analysis. *Journal of Human Genetics*, 58(7), 439-445.
- King, H. M., Rana, S., Kubica, S. P., Mallareddy, J. R., Kizhake, S., Ezell, E. L., ... Natarajan, A. (2021). Aminopyrazole based CDK9 PROTAC sensitizes pancreatic cancer cells to venetoclax. *Bioorganic & Medicinal Chemistry Letters*, 43, 128061.
- Knuesel, M. T., Meyer, K. D., Bernecky, C., & Taatjes, D. J. (2009). The human CDK8 subcomplex is a molecular switch that controls Mediator coactivator function. *Genes & Development*, 23(4), 439-451.
- Ko, L. J., Shieh, S.-Y., Chen, X., Jayaraman, L., Tamai, K., Taya, Y., ... Pan, Z.-Q. (1997). p53 Is Phosphorylated by CDK7-Cyclin H in a p36MAT1-Dependent Manner. *Molecular and Cellular Biology*, 17(12), 7220-7229.
- Konstantinopoulos, P. A., Hodgson, G., Rajagopal, N., Johannessen, L., Liu, J. F., Kirschmeier, P. T., ... Matulonis, U. A. (2018). Abstract 1525: SY-1365, a selective CDK7 inhibitor, exhibits potent antitumor activity against ovarian cancer models in vitro and in vivo. *CANCER RESEARCH*, 78, 1525-1525.
- Kovalová, M., Baraka, J. P., Mik, V., Jorda, R., Luo, L., Shao, H., & Kryštof, V. (2023a). A patent review of cyclin-dependent kinase 7 (CDK7) inhibitors (2018-2022). *Expert Opinion on Therapeutic Patents*, 33(2), 67-87.
- Kovalová, M., Havlíček, L., Djukic, S., Škerlová, J., Peřina, M., Pospíšil, T., ... Kryštof, V. (2023b). Characterization of new highly selective pyrazolo[4,3-d]pyrimidine inhibitor of CDK7. *Biomedicine & Pharmacotherapy*, 161, 114492.
- Kroon, E., Kros, J., Thorsteinsdottir, U., Baban, S., Buchberg, A. M., & Sauvageau, G. (1998). Hoxa9 transforms primary bone marrow cells through specific collaboration with Meis1a but not Pbx1b. *The EMBO Journal*, 17(13), 3714-3725.
- Kuramoto, K., Sakai, A., Shigemasa, K., Takimoto, Y., Asaoku, H., Tsujimoto, T., ... Katoh, O. (2002). High expression of MCL1 gene related to vascular endothelial growth factor is associated with poor outcome in non-Hodgkin's lymphoma. *British Journal of Haematology*, 116(1), 158-161.
- Kwiatkowski, N., Zhang, T., Rahl, P. B., Abraham, B. J., Reddy, J., Ficarro, S. B., ... Gray, N. S. (2014). Targeting transcription regulation in cancer with a covalent CDK7 inhibitor. *Nature*, 511(7511), 616-620.
- Lahti, J. M., Xiang, J., Heath, L. S., Campana, D., & Kidd, V. J. (1995). PITSLRE protein kinase activity is associated with apoptosis. *Molecular and Cellular Biology*, 15(1), 1-11.
- Laitem, C., Zaborowska, J., Isa, N. F., Kufs, J., Dienstbier, M., & Murphy, S. (2015). CDK9 inhibitors define elongation checkpoints at both ends of RNA polymerase II-transcribed genes. *Nature Structural & Molecular Biology*, 22(5), 396-403.
- Larochelle, S., Amat, R., Glover-Cutter, K., Sansó, M., Zhang, C., Allen, J. J., ... Fisher, R. P. (2012). Cyclin-dependent kinase control of the initiation-to-elongation switch of RNA polymerase II. *Nature Structural & Molecular Biology*, 19(11), 1108-1115.
- Larochelle, S., Batliner, J., Gamble, M. J., Barboza, N. M., Kraybill, B. C., Blethrow, J. D., ... Fisher, R. P. (2006). Dichotomous but stringent substrate selection by the dual-function Cdk7 complex revealed by chemical genetics. *Nature Structural & Molecular Biology*, 13(1), 55-62.
- Lawrence, H. J., Helgason, C. D., Sauvageau, G., Fong, S., Izon, D. J., Humphries, R. K., & Largman, C. (1997). Mice Bearing a Targeted Interruption of the Homeobox Gene HOXA9 Have Defects in Myeloid, Erythroid, and Lymphoid Hematopoiesis. *Blood*, 89(6), 1922-1930.
- Lee, D. K., Duan, H. O., & Chang, C. (2000). From Androgen Receptor to the General Transcription Factor TFIIH: Identification of CDK Activating kinase (CAK) as an Androgen Receptor N-terminal Associated Coactivator *. *Journal of Biological Chemistry*, 275(13), 9308-9313.
- Lee, Tong I., & Young, Richard A. (2013). Transcriptional Regulation and Its Misregulation in Disease. *Cell*, 152(6), 1237-1251.

- Lenasi, T., & Barboric, M. (2010). P-TEFb stimulates transcription elongation and pre-mRNA splicing through multilateral mechanisms. *RNA Biology*, 7(2), 145-150.
- Levis, M. (2017). Midostaurin approved for FLT3-mutated AML. *Blood*, 129(26), 3403-3406.
- Li, B., Ni Chonghaile, T., Fan, Y., Madden, S. F., Klinger, R., O'Connor, A. E., ... Gallagher, W. M. (2017). Therapeutic Rationale to Target Highly Expressed CDK7 Conferring Poor Outcomes in Triple-Negative Breast Cancer. *CANCER RESEARCH*, 77(14), 3834-3845.
- Li, T., Inoue, A., Lahti, J. M., & Kidd, V. J. (2004). Failure To Proliferate and Mitotic Arrest of CDK11p110/p58-Null Mutant Mice at the Blastocyst Stage of Embryonic Cell Development. *Molecular and Cellular Biology*, 24(8), 3188-3197.
- Li, X., & Song, Y. (2021). Structure, function and inhibition of critical protein–protein interactions involving mixed lineage leukemia 1 and its fusion oncoproteins. *Journal of Hematology & Oncology*, 14(1), 56.
- Li, Z.-M., Liu, G., Gao, Y., & Zhao, M.-G. (2022). Targeting CDK7 in oncology: The avenue forward. *Pharmacology & Therapeutics*, 240, 108229.
- Liang, K., Gao, X., Gilmore, J. M., Florens, L., Washburn, M. P., Smith, E., & Shilatifard, A. (2015). Characterization of Human Cyclin-Dependent Kinase 12 (CDK12) and CDK13 Complexes in C-Terminal Domain Phosphorylation, Gene Transcription, and RNA Processing. *Molecular and Cellular Biology*, 35(6), 928-938.
- Lim, S.-L., Xu, L., Han, B.-C., Shyamsunder, P., Chng, W.-J., & Koeffler, H. P. (2020). Multiple myeloma: Combination therapy of BET proteolysis targeting chimeric molecule with CDK9 inhibitor. *PLOS ONE*, 15(6), e0232068.
- Lin, C., Smith, E. R., Takahashi, H., Lai, K. C., Martin-Brown, S., Florens, L., ... Shilatifard, A. (2010). AFF4, a Component of the ELL/P-TEFb Elongation Complex and a Shared Subunit of MLL Chimeras, Can Link Transcription Elongation to Leukemia. *Molecular Cell*, 37(3), 429-437.
- Liu, H., Herrmann, C. H., Chiang, K., Sung, T.-L., Moon, S.-H., Donehower, L. A., & Rice, A. P. (2010). 55K isoform of CDK9 associates with Ku70 and is involved in DNA repair. *Biochemical and Biophysical Research Communications*, 397(2), 245-250.
- Liu, Y., Wu, C., & Galaktionov, K. (2004). p42, a Novel Cyclin-dependent Kinase-activating Kinase in Mammalian Cells*. *Journal of Biological Chemistry*, 279(6), 4507-4514.
- Livak, K. J., & Schmittgen, T. D. (2001). Analysis of Relative Gene Expression Data Using Real-Time Quantitative PCR and the 2- $\Delta\Delta$ CT Method. *Methods*, 25(4), 402-408.
- Lourenco, C., Resetca, D., Redel, C., Lin, P., MacDonald, A. S., Ciaccio, R., ... Penn, L. Z. (2021). MYC protein interactors in gene transcription and cancer. *Nature Reviews Cancer*, 21(9), 579-591.
- Loyer, P., Trembley, J. H., Grenet, J. A., Busson, A., Corlu, A., Zhao, W., ... Lahti, J. M. (2008). Characterization of Cyclin L1 and L2 Interactions with CDK11 and Splicing Factors: Influence Of Cyclin L Isoforms On Splice Site Selection*. *Journal of Biological Chemistry*, 283(12), 7721-7732.
- Loyer, P., Trembley, J. H., Lahti, J. M., & Kidd, V. J. (1998). The RNP protein, RNPS1, associates with specific isoforms of the P34CDC2 related PITSLRE protein kinase in vivo. *Journal of Cell Science*, 111(11), 1495-1506.
- Lu, H., Fisher, R. P., Bailey, P., & Levine, A. J. (1997). The CDK7-cycH-p36 Complex of Transcription Factor IIIH Phosphorylates p53, Enhancing Its Sequence-Specific DNA Binding Activity In Vitro. *Molecular and Cellular Biology*, 17(10), 5923-5934.
- Lu, X., Zhu, X., Li, Y., Liu, M., Yu, B., Wang, Y., ... Chen, R. (2016). Multiple P-TEFbs cooperatively regulate the release of promoter-proximally paused RNA polymerase II. *Nucleic Acids Research*, 44(14), 6853-6867.
- Lücking, U., Kosemund, D., Böhnke, N., Lienau, P., Siemeister, G., Denner, K., ... von Nussbaum, F. (2021). Changing for the Better: Discovery of the Highly Potent and Selective CDK9 Inhibitor VIP152 Suitable for Once Weekly Intravenous Dosing for the Treatment of Cancer. *Journal of Medicinal Chemistry*, 64(15), 11651-11674.
- Lücking, U., Scholz, A., Lienau, P., Siemeister, G., Kosemund, D., Bohlmann, R., ... Brands, M. (2017). Identification of Atuveciclib (BAY 1143572), the First Highly Selective, Clinical PTEFb/CDK9 Inhibitor for the Treatment of Cancer. *ChemMedChem*, 12(21), 1776-1793.

- Luecking, U. T., Scholz, A., Kosemund, D., Bohlmann, R., Briem, H., Lienau, P., ... Brands, M. (2017). Abstract 984: Identification of potent and highly selective PTEFb inhibitor BAY 1251152 for the treatment of cancer: from p.o. to i.v. application via scaffold hops. *CANCER RESEARCH*, 77(13_Supplement), 984-984.
- Lui, G. Y. L., Grandori, C., & Kemp, C. J. (2018). CDK12: an emerging therapeutic target for cancer. *Journal of Clinical Pathology*, 71(11), 957-962.
- Lukasik, P., Zaluski, M., & Gutowska, I. (2021). Cyclin-Dependent Kinases (CDK) and Their Role in Diseases Development-Review. *International Journal of Molecular Sciences*, 22(6).
- Ma, H., Dean, D. C., Wei, R., Hornicek, F. J., & Duan, Z. (2021). Cyclin-dependent kinase 7 (CDK7) is an emerging prognostic biomarker and therapeutic target in osteosarcoma. *Therapeutic Advances in Musculoskeletal Disease*, 13, 1-15.
- Ma, H., Seebacher, N. A., Hornicek, F. J., & Duan, Z. (2019). Cyclin-dependent kinase 9 (CDK9) is a novel prognostic marker and therapeutic target in osteosarcoma. *EBioMedicine*, 39, 182-193.
- Maethner, E., Breiting, C., Garcia-Cuellar, M.-P., Hess, J. L., & Slany, R. K. (2011). MLL-ENL Inhibits Polycomb Repressive Complex 1 to Achieve Efficient Transformation of Hematopoietic Cells. *Blood*, 118(21), 2443-2443.
- Magnuson, B., Bedi, K., Narayanan, I. V., Bartkowiak, B., Blinkiewicz, H., Paulsen, M. T., ... Ljungman, M. (2022). CDK12 regulates co-transcriptional splicing and RNA turnover in human cells. *iScience*, 25(9).
- Malumbres, M. (2014). Cyclin-dependent kinases. *Genome Biology*, 15(6), 122.
- Malumbres, M., Harlow, E., Hunt, T., Hunter, T., Lahti, J. M., Manning, G., ... Wolgemuth, D. J. (2009). Cyclin-dependent kinases: a family portrait. *Nature Cell Biology*, 11(11), 1275-1276.
- Manning, G., Whyte, D. B., Martinez, R., Hunter, T., & Sudarsanam, S. (2002). The Protein Kinase Complement of the Human Genome. *Science*, 298(5600), 1912-1934.
- Marineau, J. J., Hamman, K. B., Hu, S., Alnemy, S., Mihalich, J., Kabro, A., ... Chuaqui, C. (2022). Discovery of SY-5609: A Selective, Noncovalent Inhibitor of CDK7. *Journal of Medicinal Chemistry*, 65(2), 1458-1480.
- Marshall, N. F., Peng, J., Xie, Z., & Price, D. H. (1996). Control of RNA Polymerase II Elongation Potential by a Novel Carboxyl-terminal Domain Kinase*. *Journal of Biological Chemistry*, 271(43), 27176-27183.
- Marschalek, R. (2017). MLL☆ *Reference Module in Life Sciences*: Elsevier.
- Mayfield, J. E., Irani, S., Escobar, E. E., Zhang, Z., Burkholder, N. T., Robinson, M. R., ... Zhang, Y. (2019). Tyr1 phosphorylation promotes phosphorylation of Ser2 on the C-terminal domain of eukaryotic RNA polymerase II by P-TEFb. *eLife*, 8, e48725.
- McDermott, M. S. J., Chumanovich, A. A., Lim, C.-u., Liang, J., Chen, M., Altilla, S., ... Broude, E. V. (2017). Inhibition of CDK8 mediator kinase suppresses estrogen dependent transcription and the growth of estrogen receptor positive breast cancer. *Oncotarget*, 8(8), 12558-12575.
- Meshinchi, S., & Appelbaum, F. R. (2009). Structural and Functional Alterations of FLT3 in Acute Myeloid Leukemia. *Clinical Cancer Research*, 15(13), 4263-4269.
- Meyer, C., Larghero, P., Almeida Lopes, B., Burmeister, T., Gröger, D., Sutton, R., ... Marschalek, R. (2023). The KMT2A recombinome of acute leukemias in 2023. *Leukemia*, 37(5), 988-1005.
- Meyer, C., Larghero, P., Lopes, B., Caye-Eude, A., Cavé, H., Külp, M., ... Marschalek, R. (2021). Targeted Next Generation Sequencing Reveals a Third Breakpoint Cluster Region and New Partner Genes in the KMT2A Recombinome. *Blood*, 138(Supplement 1), 3327-3327.
- Meyer, C., Lopes, B. A., Caye-Eude, A., Cavé, H., Arfeuille, C., Cucchini, W., ... Marschalek, R. (2019). Human MLL/KMT2A gene exhibits a second breakpoint cluster region for recurrent MLL-*USP2* fusions. *Leukemia*, 33(9), 2306-2340.
- Mikolcevic, P., Sigl, R., Rauch, V., Hess, M. W., Pfaller, K., Barisic, M., ... Geley, S. (2012). Cyclin-Dependent Kinase 16/PCTAIRE Kinase 1 Is Activated by Cyclin Y and Is Essential for Spermatogenesis. *Molecular and Cellular Biology*, 32(4), 868-879.
- Milne, T. A., Briggs, S. D., Brock, H. W., Martin, M. E., Gibbs, D., Allis, C. D., & Hess, J. L. (2002). MLL Targets SET Domain Methyltransferase Activity to Hox Gene Promoters. *Molecular Cell*, 10(5), 1107-1117.

- Mishra, B. P., Yang, W., Zaffuto, K. M., Artinger, E. L., Li, B. E., Cheng, C., ... Ernst, P. (2014). The histone methyltransferase activity of mll1 is dispensable for hematopoiesis and leukemogenesis. *Experimental Hematology*, 42(8), S18.
- Mogila, V., Bruter, A. A., Varlamova, E. A., Korshunova, D. S., Tatarskiy, V. V., Shtil, A. A., & Roninson, I. B. (2022). Abstract 6003: Developing Mediator kinase deficient mouse models of CDK8/19 inhibitor therapy. *CANCER RESEARCH*, 82, 6003-6003.
- Monroe, S. C., Jo, S. Y., Sanders, D. S., Basrur, V., Elenitoba-Johnson, K. S., Slany, R. K., & Hess, J. L. (2011). MLL-AF9 and MLL-ENL alter the dynamic association of transcriptional regulators with genes critical for leukemia. *Experimental Hematology*, 39(1), 77-86.
- Morales, F., & Giordano, A. (2016). Overview of CDK9 as a target in cancer research. *Cell Cycle*, 15(4), 519-527.
- Morris, E. J., Ji, J.-Y., Yang, F., Di Stefano, L., Herr, A., Moon, N.-S., ... Dyson, N. J. (2008). E2F1 represses β -catenin transcription and is antagonized by both pRB and CDK8. *Nature*, 455(7212), 552-556.
- Mueller, D., García-Cuellar, M.-P., Bach, C., Buhl, S., Maethner, E., & Slany, R. K. (2009). Misguided Transcriptional Elongation Causes Mixed Lineage Leukemia. *PLOS Biology*, 7(11), e1000249.
- Nam, K., Kim, J., Park, D., Seo, M., Jeon, Y., & Yu, D. Qurient Co., Ltd. (2022) Compounds for degradation of cyclin-dependent kinase 7 (CDK7). WO2022248682.
- Nepomuceno, T. C., Fernandes, V. C., Gomes, T. T., Carvalho, R. S., Suarez-Kurtz, G., Monteiro, A. N., & Carvalho, M. A. (2017). BRCA1 recruitment to damaged DNA sites is dependent on CDK9. *Cell Cycle*, 16(7), 665-672.
- Ng, S. S. M., Cheung, Y.-T., An, X.-M., Chen, Y. C., Li, M., Hoi-Yee Li, G., ... Lin, M. C. (2007). Cell Cycle-Related Kinase: A Novel Candidate Oncogene in Human Glioblastoma. *JNCI: Journal of the National Cancer Institute*, 99(12), 936-948.
- Niu, T., Li, K., Jiang, L., Zhou, Z., Hong, J., Chen, X., ... Zhu, C.-L. (2022). Noncovalent CDK12/13 dual inhibitors-based PROTACs degrade CDK12-Cyclin K complex and induce synthetic lethality with PARP inhibitor. *European Journal of Medicinal Chemistry*, 228, 114012.
- Noblejas-López, M. d. M., Gandullo-Sánchez, L., Galán-Moya, E. M., López-Rosa, R., Tébar-García, D., Nieto-Jiménez, C., ... Ocaña, A. (2022). Antitumoral Activity of a CDK9 PROTAC Compound in HER2-Positive Breast Cancer. *International Journal of Molecular Sciences*, 23(10), 5476.
- Noe Gonzalez, M., Sato, S., Tomomori-Sato, C., Conaway, J. W., & Conaway, R. C. (2018). CTD-dependent and -independent mechanisms govern co-transcriptional capping of Pol II transcripts. *Nature Communications*, 9(1), 3392.
- Nováková, M., Hampl, M., Vrábek, D., Procházková, J., Petrežselyová, S., Procházková, M., ... Kohoutek, J. (2019). Mouse Model of Congenital Heart Defects, Dysmorphic Facial Features and Intellectual Developmental Disorders as a Result of Non-functional CDK13. *Frontiers in Cell and Developmental Biology*, 7, 1-19.
- Offermann, A., Joerg, V., Becker, F., Roesch, M. C., Kang, D., Lemster, A.-L., ... Perner, S. (2022). Inhibition of Cyclin-Dependent Kinase 8/Cyclin-Dependent Kinase 19 Suppresses Its Pro-Oncogenic Effects in Prostate Cancer. *The American Journal of Pathology*, 192(5), 813-823.
- Ohanian, M., Kantarjian, H. M., Rozovski, U., Loghavi, S., Huh, Y., Abruzzo, L., ... Cortes, J. E. (2014). Clinical significance of MYC expression in acute myeloid leukemia. *Journal of Clinical Oncology*, 32(15_suppl), 7094-7094.
- Okada, Y., Feng, Q., Lin, Y., Jiang, Q., Li, Y., Coffield, V. M., ... Zhang, Y. (2005). hDOT1L Links Histone Methylation to Leukemogenesis. *Cell*, 121(2), 167-178.
- Olson, C. M., Jiang, B., Erb, M. A., Liang, Y., Doctor, Z. M., Zhang, Z., ... Gray, N. S. (2018). Pharmacological perturbation of CDK9 using selective CDK9 inhibition or degradation. *Nature Chemical Biology*, 14(2), 163-170.
- Olson, C. M., Liang, Y., Leggett, A., Park, W. D., Li, L., Mills, C. E., ... Gray, N. S. (2019). Development of a Selective CDK7 Covalent Inhibitor Reveals Predominant Cell-Cycle Phenotype. *Cell Chemical Biology*, 26(6), 792-803.

- Park, S. Y., Kim, K. Y., Jun, D. Y., Hwang, S.-K., & Kim, Y. H. (2020). G1 Cell Cycle Arrest and Extrinsic Apoptotic Mechanisms Underlying the Anti-Leukemic Activity of CDK7 Inhibitor BS-181. *Cancers*, *12*(12), 3845.
- Parnell, G. P., Gatt, P. N., Krupa, M., Nickles, D., McKay, F. C., Schibeci, S. D., ... Booth, D. R. (2014). The autoimmune disease-associated transcription factors EOMES and TBX21 are dysregulated in multiple sclerosis and define a molecular subtype of disease. *Clinical Immunology*, *151*(1), 16-24.
- Parry, D., Guzi, T., Shanahan, F., Davis, N., Prabhavalkar, D., Wiswell, D., ... Lees, E. M. (2010). Dinaciclib (SCH 727965), a Novel and Potent Cyclin-Dependent Kinase Inhibitor. *Molecular Cancer Therapeutics*, *9*(8), 2344-2353.
- Parua, P. K., Booth, G. T., Sansó, M., Benjamin, B., Tanny, J. C., Lis, J. T., & Fisher, R. P. (2018). A Cdk9-PP1 switch regulates the elongation-termination transition of RNA polymerase II. *Nature*, *558*(7710), 460-464.
- Parua, P. K., & Fisher, R. P. (2020). Dissecting the Pol II transcription cycle and derailing cancer with CDK inhibitors. *Nature Chemical Biology*, *16*(7), 716-724.
- Patel, A., Dharmarajan, V., Vought, V. E., & Cosgrove, M. S. (2009). On the Mechanism of Multiple Lysine Methylation by the Human Mixed Lineage Leukemia Protein-1 (MLL1) Core Complex. *Journal of Biological Chemistry*, *284*(36), 24242-24256.
- Patel, H., Periyasamy, M., Sava, G. P., Bondke, A., Slafer, B. W., Kroll, S. H. B., ... Ali, S. (2018). ICEC0942, an Orally Bioavailable Selective Inhibitor of CDK7 for Cancer Treatment. *Molecular Cancer Therapeutics*, *17*(6), 1156-1166.
- Patnaik, A., Barve, M., Bhave, M., Subbiah, V., Rasco, D., Bhatt, A., ... Shapiro, G. (2023). Abstract P4-01-35: A Phase 1 Study of the Oral CDK7 Inhibitor XL102 as a Single Agent and in Combination Therapy in Patients With Advanced Solid Tumors (QUARTZ-101): Initial Results From the Dose-Escalation Stage. *CANCER RESEARCH*, *83*, P4-01-35.
- Peng, J., Zhu, Y., Milton, J. T., & Price, D. H. (1998). Identification of multiple cyclin subunits of human P-TEFb. *Genes & Development*, *12*(5), 755-762.
- Petretti, C., Savoian, M., Montembault, E., Glover, D. M., Prigent, C., & Giet, R. (2006). The PITSLRE/CDK11p58 protein kinase promotes centrosome maturation and bipolar spindle formation. *EMBO reports*, *7*(4), 418-424.
- Pineault, N., Helgason, C. D., Lawrence, H. J., & Humphries, R. K. (2002). Differential expression of Hox, Meis1, and Pbx1 genes in primitive cells throughout murine hematopoietic ontogeny. *Experimental Hematology*, *30*(1), 49-57.
- Pirngruber, J., Shchebet, A., & Johnsen, S. A. (2009). Insights into the function of the human P-TEFb component CDK9 in the regulation of chromatin modifications and co-transcriptional mRNA processing. *Cell Cycle*, *8*(22), 3636-3642.
- Popova, T., Manié, E., Boeva, V., Battistella, A., Goundiam, O., Smith, N. K., ... Stern, M.-H. (2016). Ovarian Cancers Harboring Inactivating Mutations in CDK12 Display a Distinct Genomic Instability Pattern Characterized by Large Tandem Duplications. *CANCER RESEARCH*, *76*(7), 1882-1891.
- Qi, J., Zhou, K., Qian, W., Zang, A., Kadia, T. M., Lipsky, A. H., ... Wang, J. (2022). First in Human (FIH) Study of GFH009, a Highly Selective Cyclin-Dependent Kinase 9 (CDK9) Inhibitor, in Patients with Relapsed/Refractory (r/r) Hematologic Malignancies. *Blood*, *140*(Supplement 1), 9473-9474.
- Qiu, H., Dai, H., Jain, K., Shah, R., Hong, C., Pain, J., ... Depre, C. (2008). Characterization of a Novel Cardiac Isoform of the Cell Cycle-related Kinase That Is Regulated during Heart Failure*. *Journal of Biological Chemistry*, *283*(32), 22157-22165.
- Qiu, X., Li, Y., Yu, B., Ren, J., Huang, H., Wang, M., ... Bian, J. (2021). Discovery of selective CDK9 degraders with enhancing antiproliferative activity through PROTAC conversion. *European Journal of Medicinal Chemistry*, *211*, 113091.
- Quigley, D. A., Dang, H. X., Zhao, S. G., Lloyd, P., Aggarwal, R., Alumkal, J. J., ... Feng, F. Y. (2018). Genomic Hallmarks and Structural Variation in Metastatic Prostate Cancer. *Cell*, *174*(3), 758-769.
- Rahl, P. B., Lin, C. Y., Seila, A. C., Flynn, R. A., McCuine, S., Burge, C. B., ... Young, R. A. (2010). c-Myc Regulates Transcriptional Pause Release. *Cell*, *141*(3), 432-445.

- Ramanathan, Y., Rajpara, S. M., Reza, S. M., Lees, E., Shuman, S., Mathews, M. B., & Pe'ery, T. (2001). Three RNA Polymerase II Carboxyl-terminal Domain Kinases Display Distinct Substrate Preferences. *Journal of Biological Chemistry*, 276(14), 10913-10920.
- Rask-Andersen, M., Zhang, J., Fabbro, D., & Schiöth, H. B. (2014). Advances in kinase targeting: current clinical use and clinical trials. *Trends in Pharmacological Sciences*, 35(11), 604-620.
- Rayes, A., McMasters, R. L., & O'Brien, M. M. (2016). Lineage Switch in MLL-Rearranged Infant Leukemia Following CD19-Directed Therapy. *Pediatric Blood & Cancer*, 63(6), 1113-1115.
- Reimers, M. A., Yip, S. M., Zhang, L., Cieslik, M., Dhawan, M., Montgomery, B., ... Chou, J. (2020). Clinical Outcomes in Cyclin-dependent Kinase 12 Mutant Advanced Prostate Cancer. *European Urology*, 77(3), 333-341.
- Reiter, K., Polzer, H., Krupka, C., Maiser, A., Vick, B., Rothenberg-Thurley, M., ... Greif, P. A. (2018). Tyrosine kinase inhibition increases the cell surface localization of FLT3-ITD and enhances FLT3-directed immunotherapy of acute myeloid leukemia. *Leukemia*, 32(2), 313-322.
- Richters, A., Doyle, S. K., Freeman, D. B., Lee, C., Leifer, B. S., Jagannathan, S., ... Koehler, A. N. (2021). Modulating Androgen Receptor-Driven Transcription in Prostate Cancer with Selective CDK9 Inhibitors. *Cell Chemical Biology*, 28(2), 134-147.
- Rimel, J. K., Poss, Z. C., Erickson, B., Maas, Z. L., Ebmeier, C. C., Johnson, J. L., ... Taatjes, D. J. (2020). Selective inhibition of CDK7 reveals high-confidence targets and new models for TFIIF function in transcription. *Genes & Development*, 34(21-22), 1452-1473.
- Robb, C. M., Contreras, J. I., Kour, S., Taylor, M. A., Abid, M., Sonawane, Y. A., ... Rana, S. (2017). Chemically induced degradation of CDK9 by a proteolysis targeting chimera (PROTAC). *Chemical Communications*, 53(54), 7577-7580.
- Robinson, I. B., Porter, D. C., & Wentland, M. P. Senex Biotechnology Inc. (2013) CDK8/CDK19 selective inhibitors and preparation and use thereof in anti-metastatic and chemopreventative methods for cancer. WO2013116786.
- Rochette-Egly, C., Adam, S., Rossignol, M., Egly, J.-M., & Chambon, P. (1997). Stimulation of RAR β ; Activation Function AF-1 through Binding to the General Transcription Factor TFIIF and Phosphorylation by CDK7. *Cell*, 90(1), 97-107.
- Rossi, J. G., Bernasconi, A. R., Alonso, C. N., Rubio, P. L., Gallego, M. S., Carrara, C. A., ... Felice, M. S. (2012). Lineage switch in childhood acute leukemia: An unusual event with poor outcome. *American Journal of Hematology*, 87(9), 890-897.
- Roth, D. A. Syros Pharmaceuticals, Inc. (2022) Synthesis and dosing regimens for indole based cyclin-dependent kinase 7 inhibitors treating cancers. WO2022082056.
- Roy, R., Adamczewski, J. P., Seroz, T., Vermeulen, W., Tassan, J.-P., Schaeffer, L., ... Egly, J.-M. (1994). The MO15 cell cycle kinase is associated with the TFIIF transcription-DNA repair factor. *Cell*, 79(6), 1093-1101.
- Russo, A. A., Jeffrey, P. D., & Pavletich, N. P. (1996). Structural basis of cyclin-dependent kinase activation by phosphorylation. *Nature Structural Biology*, 3(8), 696-700.
- Rzymiski, T., Mikula, M., Żyłkiewicz, E., Dreas, A., Wiklik, K., Gołas, A., ... Brzózka, K. (2017). SEL120-34A is a novel CDK8 inhibitor active in AML cells with high levels of serine phosphorylation of STAT1 and STAT5 transactivation domains. *Oncotarget*, 8(20), 33779-33795.
- Rzymiski, T., Sroka-Porada, A., Kozakowska, M., Głowniak-Kwitek, U., Bukowska-Strakova, K., Obacz, M., ... Brzózka, K. (2022). Multiomics Analysis Confirms Effective Target Engagement for RVU120 - a First-in-Class CDK8/19 Kinase Inhibitor in AML and MR-MDS Patients and Reveals the Mechanism of Action. *Blood*, 140(Supplement 1), 5939-5940.
- Řezníčková, E., Krajčovičová, S., Peřina, M., Kovalová, M., Soral, M., & Kryštof, V. (2022). Modulation of FLT3-ITD and CDK9 in acute myeloid leukaemia cells by novel proteolysis targeting chimera (PROTAC). *European Journal of Medicinal Chemistry*, 243, 114792.
- Řezníčková, E., Weitensteiner, S., Havlíček, L., Jorda, R., Gucký, T., Berka, K., ... Strnad, M. (2015). Characterization of a Pyrazolo[4,3-d]pyrimidine Inhibitor of Cyclin-Dependent Kinases 2 and 5 and Aurora A With Pro-Apoptotic and Anti-Angiogenic Activity In Vitro. *Chemical Biology & Drug Design*, 86(6), 1528-1540.

- Saffran, D., Poon, E., Ibanez, G., Nakashima, J., Naffar-Abu Amara, S., Noe, C., ... Lin, C. Y. Abstract 208: Regulation of oncogenic transcription and tumor growth in pediatric cancers by the CDK9 inhibitor KB-0742 (2022) EORTC NCI AACR
- Sandler, E. S., Friedman, D. J., Mustafa, M. M., Winick, N. J., Bowman, W. P., & Buchanan, G. R. (1997). Treatment of children with epipodophyllotoxin-induced secondary acute myeloid leukemia. *Cancer*, 79(5), 1049-1054.
- Sánchez-Martínez, C., Gelbert, L. M., Lallena, M. J., & de Dios, A. (2015). Cyclin dependent kinase (CDK) inhibitors as anticancer drugs. *Bioorganic & Medicinal Chemistry Letters*, 25(17), 3420-3435.
- Sánchez-Martínez, C., Lallena, M. J., Sanfeliciano, S. G., & de Dios, A. (2019). Cyclin dependent kinase (CDK) inhibitors as anticancer drugs: Recent advances (2015–2019). *Bioorganic & Medicinal Chemistry Letters*, 29(20), 126637.
- Santos-Rosa, H., Schneider, R., Bannister, A. J., Sherriff, J., Bernstein, B. E., Emre, N. C. T., ... Kouzarides, T. (2002). Active genes are tri-methylated at K4 of histone H3. *Nature*, 419(6905), 407-411.
- Satyam, L. K., Poddutoori, R., Thiyagarajan, S., Mukherjee, S., Kaza, L. N., Charamanna, K., ... Samajdar, S. (2020). 170 Poster - Potent anti-tumor activity of AUR102, a selective covalent inhibitor of CDK7. *European Journal of Cancer*, 138, S47.
- Sergère, J.-C., Thuret, J.-Y., Le, G., Edgardo, R., Carosella, D., & Leteurtre, F. (2000). Human CDK10 Gene Isoforms. *Biochemical and Biophysical Research Communications*, 276(1), 271-277.
- Shan, W., Yuan, J., Hu, Z., Jiang, J., Wang, Y., Loo, N., ... Zhang, L. (2020). Systematic Characterization of Recurrent Genomic Alterations in Cyclin-Dependent Kinases Reveals Potential Therapeutic Strategies for Cancer Treatment. *Cell Reports*, 32(2), 107884.
- Sharma, M., Bashir, B., Hamilton, E., Juric, D., Papadopoulos, K., Richardson, D., ... Kelly, M. (2021). Tolerability and preliminary clinical activity of SY-5609, a highly potent and selective oral CDK7 inhibitor, in patients with advanced solid tumors. *Annals of Oncology*, 32, S587-S588.
- Sher, S., Whipp, E., Walker, J., Zhang, P., Beaver, L., Williams, K., ... Lapalombella, R. (2023). VIP152 is a selective CDK9 inhibitor with pre-clinical in vitro and in vivo efficacy in chronic lymphocytic leukemia. *Leukemia*, 37(2), 326-338.
- Shilatifard, A., Lane, W. S., Jackson, K. W., Conaway, R. C., & Conaway, J. W. (1996). An RNA Polymerase II Elongation Factor Encoded by the Human ELL Gene. *Science*, 271(5257), 1873-1876.
- Shim, E. Y., Walker, A. K., Shi, Y., & Blackwell, T. K. (2002). CDK-9/cyclin T (P-TEFb) is required in two postinitiation pathways for transcription in the *C. elegans* embryo. *Genes & Development*, 16(16), 2135-2146.
- Slany, R. K. (2016). The molecular mechanics of mixed lineage leukemia. *Oncogene*, 35(40), 5215-5223.
- Snouffer, A., Brown, D., Lee, H., Walsh, J., Lupu, F., Norman, R., ... Eggenschwiler, J. (2017). Cell Cycle-Related Kinase (CCRK) regulates ciliogenesis and Hedgehog signaling in mice. *PLOS Genetics*, 13(8), e1006912.
- Spencer, D. H., Young, M. A., Lamprecht, T. L., Helton, N. M., Fulton, R., O'Laughlin, M., ... Ley, T. J. (2015). Epigenomic analysis of the HOX gene loci reveals mechanisms that may control canonical expression patterns in AML and normal hematopoietic cells. *Leukemia*, 29(6), 1279-1289.
- Storch, K., & Cordes, N. (2016). The impact of CDK9 on radiosensitivity, DNA damage repair and cell cycling of HNSCC cancer cells. *Int J Oncol*, 48(1), 191-198.
- Strati, P., Kim, T. M., Danilov, A. V., Cheah, C. Y., Yoon, D. H., Jurczak, W., ... Gregory, G. (2022). Phase 1b/2a Study of AZD4573 (CDK9i) and Acalabrutinib in Patients with Relapsed/Refractory Diffuse Large B-Cell Lymphoma (r/r DLBCL): Results from Dose-Escalation. *Blood*, 140(Supplement 1), 6656-6658.
- Super, H. J., McCabe, N. R., Thirman, M. J., Larson, R. A., Le Beau, M. M., Pedersen-Bjergaard, J., ... Rowley, J. D. (1993). Rearrangements of the MLL gene in therapy-related acute myeloid

- leukemia in patients previously treated with agents targeting DNA-topoisomerase II. *Blood*, 82(12), 3705-3711.
- Sutanto, F., Konstantinidou, M., & Dömling, A. (2020). Covalent inhibitors: a rational approach to drug discovery. *RSC Medicinal Chemistry*, 11(8), 876-884.
- Syed, Y. Y. (2017). Ribociclib: First Global Approval. *Drugs*, 77(7), 799-807.
- Syros Pharmaceuticals, I. Prioritizing development of SY-5609, its oral CDK7 inhibitor, and discontinuing further development of SY-1365, its intravenous CDK7 inhibitor (2019) <https://ir.syros.com/press-releases/detail/170/syros-announces-update-on-selective-cdk7-inhibitor-portfolio>
- Tellier, M., Zaborowska, J., Caizzi, L., Mohammad, E., Velychko, T., Schwalb, B., ... Murphy, S. (2020). CDK12 globally stimulates RNA polymerase II transcription elongation and carboxyl-terminal domain phosphorylation. *Nucleic Acids Research*, 48(14), 7712-7727.
- Thorsteinsdottir, U., Mamo, A., Kroon, E., Jerome, L., Bijl, J., Lawrence, H. J., ... Sauvageau, G. (2002). Overexpression of the myeloid leukemia-associated Hoxa9 gene in bone marrow cells induces stem cell expansion. *Blood*, 99(1), 121-129.
- Tien, J. F., Mazloomian, A., Cheng, S.-W. G., Hughes, C. S., Chow, C. C. T., Canapi, L. T., ... Morin, G. B. (2017). CDK12 regulates alternative last exon mRNA splicing and promotes breast cancer cell invasion. *Nucleic Acids Research*, 45(11), 6698-6716.
- Trembley, J. H., Hu, D., Hsu, L.-C., Yeung, C.-Y., Slaughter, C., Lahti, J. M., & Kidd, V. J. (2002). PITSLRE p110 Protein Kinases Associate with Transcription Complexes and Affect Their Activity *. *Journal of Biological Chemistry*, 277(4), 2589-2596.
- Trembley, J. H., Loyer, P., Hu, D., Li, T., Grenet, J., Lahti, J. M., & Kidd, V. J. (2004). Cyclin Dependent Kinase 11 in RNA Transcription and Splicing *Progress in Nucleic Acid Research and Molecular Biology*, 77, 263-288.
- Tsai, K.-L., Sato, S., Tomomori-Sato, C., Conaway, R. C., Conaway, J. W., & Asturias, F. J. (2013). A conserved Mediator-CDK8 kinase module association regulates Mediator-RNA polymerase II interaction. *Nature Structural & Molecular Biology*, 20(5), 611-619.
- Tsakaneli, A., & Williams, O. (2021). Drug Repurposing for Targeting Acute Leukemia With KMT2A (MLL)-Gene Rearrangements. *Frontiers in Pharmacology*, 12, 1-12.
- Vandel, L., & Kouzarides, T. (1999). Residues phosphorylated by TFIIF are required for E2F-1 degradation during S-phase. *The EMBO Journal*, 18(15), 4280-4291.
- Vervoort, S. J., Devlin, J. R., Kwiatkowski, N., Teng, M., Gray, N. S., & Johnstone, R. W. (2022). Targeting transcription cycles in cancer. *Nature Reviews Cancer*, 22(1), 5-24.
- Vymětalová, L., Havlíček, L., Šturc, A., Skrášková, Z., Jorda, R., Pospíšil, T., ... Kryštof, V. (2016). 5-Substituted 3-isopropyl-7-[4-(2-pyridyl)benzyl]amino-1(2)H-pyrazolo[4,3-d]pyrimidines with anti-proliferative activity as potent and selective inhibitors of cyclin-dependent kinases. *European Journal of Medicinal Chemistry*, 110, 291-301.
- Wada, T., Takagi, T., Yamaguchi, Y., Watanabe, D., & Handa, H. (1998). Evidence that P-TEFb alleviates the negative effect of DSIF on RNA polymerase II-dependent transcription in vitro. *The EMBO Journal*, 17(24), 7395-7403.
- Wang, C., Zhang, J., Yin, J., Gan, Y., Xu, S., Gu, Y., & Huang, W. (2021a). Alternative approaches to target Myc for cancer treatment. *Signal Transduction and Targeted Therapy*, 6(1), 117.
- Wang, H., Guo, M., Wei, H., & Chen, Y. (2021b). Targeting MCL-1 in cancer: current status and perspectives. *Journal of Hematology & Oncology*, 14(1), 67.
- Wang, P., Lin, C., Smith, E. R., Guo, H., Sanderson, B. W., Wu, M., ... Shilatifard, A. (2009). Global Analysis of H3K4 Methylation Defines MLL Family Member Targets and Points to a Role for MLL1-Mediated H3K4 Methylation in the Regulation of Transcriptional Initiation by RNA Polymerase II. *Molecular and Cellular Biology*, 29(22), 6074-6085.
- Wang, Q.-f., Wu, G., Mi, S., He, F., Wu, J., Dong, J., ... Thirman, M. J. (2011). MLL fusion proteins preferentially regulate a subset of wild-type MLL target genes in the leukemic genome. *Blood*, 117(25), 6895-6905.
- Wei, D., Wang, H., Zeng, Q., Wang, W., Hao, B., Feng, X., ... Chen, X.-H. (2021). Discovery of Potent and Selective CDK9 Degradators for Targeting Transcription Regulation in Triple-Negative Breast Cancer. *Journal of Medicinal Chemistry*, 64(19), 14822-14847.
- Weinstein, I. B., & Joe, A. (2008). Oncogene addiction. *CANCER RESEARCH*, 68(9), 3077-3080.

- Weisberg, E., Ray, A., Nelson, E., Adamia, S., Barrett, R., Sattler, M., ... Griffin, J. D. (2011). Reversible Resistance Induced by FLT3 Inhibition: A Novel Resistance Mechanism in Mutant FLT3-Expressing Cells. *PLOS ONE*, 6(9), e25351.
- Wells, C. I., Vasta, J. D., Corona, C. R., Wilkinson, J., Zimprich, C. A., Ingold, M. R., ... Robers, M. B. (2020). Quantifying CDK inhibitor selectivity in live cells. *Nature Communications*, 11(1), 2743.
- Westerling, T., Kuuluvainen, E., & Maäkelaä, T. P. (2007). Cdk8 Is Essential for Preimplantation Mouse Development. *Molecular and Cellular Biology*, 27(17), 6177-6182.
- Whittaker, S. R., Mallinger, A., Workman, P., & Clarke, P. A. (2017). Inhibitors of cyclin-dependent kinases as cancer therapeutics. *Pharmacology & Therapeutics*, 173, 83-105.
- William, A. D., Lee, A. C. H., Goh, K. C., Blanchard, S., Poulsen, A., Teo, E. L., ... Dymock, B. W. (2012). Discovery of Kinase Spectrum Selective Macrocycle (16E)-14-Methyl-20-oxa-5,7,14,26-tetraazatetracyclo[19.3.1.1(2,6).1(8,12)]heptacosal(25),2(26),3,5,8(27),9,11,16,21,23-decaene (SB1317/TG02), a Potent Inhibitor of Cyclin Dependent Kinases (CDKs), Janus Kinase 2 (JAK2), and Fms-like Tyrosine Kinase-3 (FLT3) for the Treatment of Cancer. *Journal of Medicinal Chemistry*, 55(1), 169-196.
- Winters, A. C., & Bernt, K. M. (2017). MLL-Rearranged Leukemias—An Update on Science and Clinical Approaches. *Frontiers in Pediatrics*, 5, 1-21
- Wohlbold, L., Larochelle, S., Liao, J. C. F., Livshits, G., Singer, J., Shokat, K. M., & Fisher, R. P. (2006). The Cyclin-Dependent Kinase (CDK) Family Member PNQALRE/CCRK Supports Cell Proliferation but has no Intrinsic CDK-Activating Kinase (CAK) Activity. *Cell Cycle*, 5(5), 546-554.
- Wong, Koon H., Jin, Y., & Struhl, K. (2014). TFIIH Phosphorylation of the Pol II CTD Stimulates Mediator Dissociation from the Preinitiation Complex and Promoter Escape. *Molecular Cell*, 54(4), 601-612.
- Wong, P., Iwasaki, M., Somervaille, T. C. P., So, C. W. E., & Cleary, M. L. (2007). Meis1 is an essential and rate-limiting regulator of MLL leukemia stem cell potential. *Genes & Development*, 21(21), 2762-2774.
- Wood, D. J., & Endicott, J. A. (2018). Structural insights into the functional diversity of the CDK–cyclin family. *Open Biology*, 8(9), 180112.
- Wu, D., Zhang, Z., Chen, X., Yan, Y., & Liu, X. (2021). Angel or Devil ? - CDK8 as the new drug target. *European Journal of Medicinal Chemistry*, 213, 113043.
- Wu, G.-Q., Xie, D., Yang, G.-F., Liao, Y.-J., Mai, S.-J., Deng, H.-X., ... Kung, H.-F. (2009). Cell cycle-related kinase supports ovarian carcinoma cell proliferation via regulation of cyclin D1 and is a predictor of outcome in patients with ovarian carcinoma. *International Journal of Cancer*, 125(11), 2631-2642.
- Wu, J., Zhang, M., & Liu, D. (2016). Acalabrutinib (ACP-196): a selective second-generation BTK inhibitor. *Journal of Hematology & Oncology*, 9(1), 21.
- Wu, M., Li, C., & Zhu, X. (2018a). FLT3 inhibitors in acute myeloid leukemia. *Journal of Hematology & Oncology*, 11(1), 133.
- Wu, Y.-M., Cieřlik, M., Lonigro, R. J., Vats, P., Reimers, M. A., Cao, X., ... Chinnaiyan, A. M. (2018b). Inactivation of CDK12 Delineates a Distinct Immunogenic Class of Advanced Prostate Cancer. *Cell*, 173(7), 1770-1782
- Wuillème-Toumi, S., Robillard, N., Gomez, P., Moreau, P., Le Gouill, S., Avet-Loiseau, H., ... Bataille, R. (2005). Mcl-1 is overexpressed in multiple myeloma and associated with relapse and shorter survival. *Leukemia*, 19(7), 1248-1252.
- Xie, F., Wang, J., & Zhang, B. (2023). RefFinder: a web-based tool for comprehensively analyzing and identifying reference genes. *Functional & Integrative Genomics*, 23(2), 125.
- Xie, F., Xiao, P., Chen, D., Xu, L., & Zhang, B. (2012). miRDeepFinder: a miRNA analysis tool for deep sequencing of plant small RNAs. *Plant Molecular Biology*, 80(1), 75-84.
- Xu, J., Li, L., Xiong, J., denDekker, A., Ye, A., Karatas, H., ... Dou, Y. (2016). MLL1 and MLL1 fusion proteins have distinct functions in regulating leukemic transcription program. *Cell Discovery*, 2(1), 16008.
- Yagi, H., Deguchi, K., Aono, A., Tani, Y., Kishimoto, T., & Komori, T. (1998). Growth Disturbance in Fetal Liver Hematopoiesis of Mll-Mutant Mice. *Blood*, 92(1), 108-117.

- Yamada, T., Yamaguchi, Y., Inukai, N., Okamoto, S., Mura, T., & Handa, H. (2006). P-TEFb-Mediated Phosphorylation of hSpt5 C-Terminal Repeats Is Critical for Processive Transcription Elongation. *Molecular Cell*, *21*(2), 227-237.
- Yamaguchi, Y., Takagi, T., Wada, T., Yano, K., Furuya, A., Sugimoto, S., ... Handa, H. (1999). NELF, a Multisubunit Complex Containing RD, Cooperates with DSIF to Repress RNA Polymerase II Elongation. *Cell*, *97*(1), 41-51.
- Yang, Y., Eichhorn, C. D., Wang, Y., Cascio, D., & Feigon, J. (2019). Structural basis of 7SK RNA 5'- γ -phosphate methylation and retention by MePCE. *Nature Chemical Biology*, *15*(2), 132-140.
- Yang, Y. Q., Tan, S. M., Han, Y. Q., Huang, L. S., Yang, R. Q., Hu, Z. F., ... Zhou, Y. J. (2023). The role of tripartite motif-containing 28 in cancer progression and its therapeutic potentials. *Frontiers in Oncology*, *13*. 1-19
- Ye, J., Coulouris, G., Zaretskaya, I., Cutcutache, I., Rozen, S., & Madden, T. L. (2012). Primer-BLAST: A tool to design target-specific primers for polymerase chain reaction. *BMC Bioinformatics*, *13*(1), 134.
- Yokoyama, A., & Cleary, M. L. (2008). Menin Critically Links MLL Proteins with LEDGF on Cancer-Associated Target Genes. *Cancer Cell*, *14*(1), 36-46.
- You, Y., Li, H., Qin, X., Zhang, Y., Song, W., Ran, Y., & Gao, F. (2015). Decreased CDK10 expression correlates with lymph node metastasis and predicts poor outcome in breast cancer patients - a short report. *Cellular Oncology*, *38*(6), 485-491.
- Yu, B. D., Hess, J. L., Horning, S. E., Brown, G. A. J., & Korsmeyer, S. J. (1995). Altered Hox expression and segmental identity in Mll-mutant mice. *Nature*, *378*(6556), 505-508.
- Yu, D., Jeon, Y., Lee, S.-J., Kim, J., & Nam, K. (2022). Abstract 2574: Q901; a highly selective covalent cdk7 inhibitor inducing substantial anti-tumor effect in a broad spectrum of solid tumor lineages. *CANCER RESEARCH*, *82*, 2574-2574.
- Yu, D., Jeon, Y., Park, D., Seo, M., Ahn, W., Kim, J., ... Nam, K. (2020). Abstract 4855: Development of highly selective CDK7 inhibitor Q901 for solid tumors. *CANCER RESEARCH*, *80*, 4855-4855.
- Yu, D. S., Zhao, R., Hsu, E. L., Cayer, J., Ye, F., Guo, Y., ... Cortez, D. (2010). Cyclin-dependent kinase 9–cyclin K functions in the replication stress response. *EMBO reports*, *11*(11), 876-882.
- Zarrinkar, P. P., Gunawardane, R. N., Cramer, M. D., Gardner, M. F., Brigham, D., Belli, B., ... Bhagwat, S. S. (2009). AC220 is a uniquely potent and selective inhibitor of FLT3 for the treatment of acute myeloid leukemia (AML). *Blood*, *114*(14), 2984-2992.
- Zeng, M., Kwiatkowski, N. P., Zhang, T., Nabet, B., Xu, M., Liang, Y., ... Gray, N. S. (2018). Targeting MYC dependency in ovarian cancer through inhibition of CDK7 and CDK12/13. *eLife*, *7*, e39030.
- Zhang, B., Gojo, I., & Fenton, R. G. (2002). Myeloid cell factor-1 is a critical survival factor for multiple myeloma. *Blood*, *99*(6), 1885-1893.
- Zhang, H., Guttikonda, S., Roberts, L., Uziel, T., Semizarov, D., Elmore, S. W., ... Lam, L. T. (2011). Mcl-1 is critical for survival in a subgroup of non-small-cell lung cancer cell lines. *Oncogene*, *30*(16), 1963-1968.
- Zhang, M., Zhang, L., Hei, R., Li, X., Cai, H., Wu, X., ... Cai, C. (2021a). CDK inhibitors in cancer therapy, an overview of recent development. *American journal of cancer research*, *11* 5, 1913-1935.
- Zhang, T., Kwiatkowski, N., Olson, C. M., Dixon-Clarke, S. E., Abraham, B. J., Greifenberg, A. K., ... Gray, N. S. (2016). Covalent targeting of remote cysteine residues to develop CDK12 and CDK13 inhibitors. *Nature Chemical Biology*, *12*(10), 876-884.
- Zhang, Y. W., Lu, L., Wang, M., Rominger, D., Ruepp, S., Gallagher, K., ... Vaddi, K. (2021b). Abstract P237: PRT2527 is a potent and selective CDK9 inhibitor that demonstrates anti-cancer activity in preclinical models of hematological malignancies and solid tumors with MYC amplification. *Molecular Cancer Therapeutics*, *20*, P237-P237.
- Zhao, B.-w., Chen, S., Li, Y.-F., Xiang, J., Zhou, Z.-W., Peng, J.-S., & Chen, Y.-b. (2017). Low Expression of CDK10 Correlates with Adverse Prognosis in Gastric Carcinoma. [Research Paper]. *Journal of Cancer*, *8*(15), 2907-2914.

- Zhao, J., Ramos, R., & Demma, M. (2013). CDK8 regulates E2F1 transcriptional activity through S375 phosphorylation. *Oncogene*, *32*(30), 3520-3530.
- Zhou, F., Tang, L., Le, S., Ge, M., Cicic, D., Xie, F., ... Lu, Q. (2022). In Vitro and In Vivo Studies Support GFH009, a Selective CDK9 Inhibitor, As a Potential Treatment for Hematologic Cancers. *Blood*, *140*(Supplement 1), 7808-7809.
- Zhou, M., Halanski, M. A., Radonovich, M. F., Kashanchi, F., Peng, J., Price, D. H., & Brady, J. N. (2000). Tat Modifies the Activity of CDK9 To Phosphorylate Serine 5 of the RNA Polymerase II Carboxyl-Terminal Domain during Human Immunodeficiency Virus Type 1 Transcription. *Molecular and Cellular Biology*, *20*(14), 5077-5086.
- Zhou, Y., Han, C., Li, D., Yu, Z., Li, F., Li, F., ... Kan, Q. (2015). Cyclin-dependent kinase 11p110 (CDK11p110) is crucial for human breast cancer cell proliferation and growth. *Scientific Reports*, *5*(1), 10433.
- Zhu, Y., Pe'ery, T., Peng, J., Ramanathan, Y., Marshall, N., Marshall, T., ... Price, D. H. (1997). Transcription elongation factor P-TEFb is required for HIV-1 Tat transactivation in vitro. *Genes & Development*, *11*(20), 2622-2632.
- Ziemin-van der Poel, S., McCabe, N. R., Gill, H. J., Espinosa, R., Patel, Y., Harden, A., ... Rowley, J. D. (1991). Identification of a gene, MLL, that spans the breakpoint in 11q23 translocations associated with human leukemias. *Proceedings of the National Academy of Sciences*, *88*(23), 10735-10739.
- Zimmermann, M., Arachchige-Don, A. P. S., Donaldson, M. S., Patriarchi, T., & Horne, M. C. (2016). Cyclin G2 promotes cell cycle arrest in breast cancer cells responding to fulvestrant and metformin and correlates with patient survival. *Cell Cycle*, *15*(23), 3278-3295.

9 CURRICULUM VITAE

Jméno: Markéta Kovalová
Narozena: 30.10.1993 v Hranicích
Bydliště: M. J. Husa 1390, 751 31 Lipník nad Bečvou

Vzdělání:

2018 – nyní Experimentální biologie – doktorské studium
Univerzita Palackého v Olomouci, Přírodovědecká fakulta

2016 – 2018 Molekulární a buněčná biologie – navazující magisterské studium
Univerzita Palackého v Olomouci, Přírodovědecká fakulta

2013 – 2016 Molekulární a buněčná biologie – bakalářské studium
Univerzita Palackého v Olomouci, Přírodovědecká fakulta

Pedagogická činnost:

2019 LRR/BUBCV – Cvičení z buněčné biologie

2019 – 2022 LRR/IZVB – Informační zdroje v biologii a medicíně (podíl na výuce)

Zahraniční stáž:

2020 – 3 měsíce Institute for Medical Biochemistry, University of Veterinary Medicine, Vienna (prof. Florian Grebien)

Publikační činnost:

1. Břehová, P., Řezníčková, E., Škach, K., Jorda, R., Dejmek, M., Vojáčková, V., Šála, M., **Kovalová, M.**, Dračínský, M., Dolníková, A., Strmeň, T., Kinnertová, M., Chalupský, K., Dvořáková, A., Gucký, T., Mertlíková Kaiserová, H, Klener, P., Nencka, R., Kryštof, V. (2023). Inhibition of FLT3-ITD Kinase in Acute Myeloid Leukemia by New Imidazo[1,2-*b*]pyridazine Derivatives Identified by Scaffold Hopping. *J Med Chem*, 66(16), 11133-11157.
2. **Kovalová, M.***, Baraka, J. P.*, Mik, V., Jorda, R., Luo, L., Shao, H., Kryštof, V. (2023) A patent review of cyclin-dependent kinase 7 (CDK7) inhibitors (2018-2022). *Expert Opin Ther Patents* 33 (2), 67-87 *Sdílené prouautorství
3. **Kovalová, M.**, Havlíček, L., Djukic, S., Škerlová, J., Peřina, M., Pospíšil, T., Řezníčková, E., Řezáčová, P., Jorda, R., Kryštof, V. (2023) Characterization of new highly selective pyrazolo 4,3-*d* pyrimidine inhibitor of CDK7. *Biomed Pharmacother* 161, 114492

4. Peřina, M., Kiss, M. A., M3ty3n, G., Szczyrb3v3, E., Eli33, M., Œtudent, V., Kurf3rstov3, D., **Kovalov3, M.**, Mada, L., Bouchal, J., Frank, 3., Jorda, R. (2023) A-ring-fused pyrazoles of dihydrotestosterone targeting prostate cancer cells via the downregulation of the androgen receptor. *Eur J Med Chem* 249, 115086
5. 3ezn33kov3, E., Kraj3ovi3ov3, S., Peřina, M., **Kovalov3, M.**, Soral, M., KryŒtof, V. (2022) Modulation of FLT3-ITD and CDK9 in acute myeloid leukaemia cells by novel proteolysis targeting chimera (PROTAC). *Eur J Med Chem* 243, 114792
6. Barghash, R. F., Eldehna, W. M., **Kovalov3, M.**, Voj33kov3, V., KryŒtof, V., Abdel-Aziz, H. A. (2022) One-pot three-component synthesis of novel pyrazolo 3,4-b pyridines as potent antileukemic agents. *Eur J Med Chem* 227, 113952

Konfere3n3 pŕ3sp3vky:

- **Kovalov3 M.**, Jorda R, Havl33ek L, 3ezn33kov3, E., KryŒtof, V.: Transcriptional kinase CDK7 as a drug target. Chemistry and biology of phytohormones and related substances, 2023, kv3ten 21-23, Velk3 Losiny, 3R. 3stn3 prezentace.
- **Kovalov3, M.**, Grebien, F., KryŒtof, V.: Establishment of novel AML cellular models using CRISPR/Cas9 technologies. Chemistry and biology of phytohormones and related substances, 2022, kv3ten 15.-17., Bystŕice nad PernŒtejnem, 3R. 3stn3 prezentace.
- **Kovalov3, M.**, Jorda, R., Havl33ek, L., 3ezn33kov3, E., KryŒtof, V.: Transcriptional CDKs: potential targets in the treatment of leukemia. Chemistry and biology of phytohormones and related substances, 2021, z3ř3 12.-14., Malenovice, 3R. 3stn3 prezentace.
- **Kovalov3, M.**, Jorda, R., KryŒtof V: TRANSCRIPTIONAL CDKs: The way to go? Chemistry and biology of phytohormones and related substances, 2019, kv3ten 19.-21., Luha3ovice, 3R. 3stn3 prezentace.

10 SEZNAM PŘÍLOH

Tato disertační práce shrnuje a odkazuje na následující seznam publikací, které jsou přiloženy a v textu označovány jako příloha I-IV.

Příloha I:

Kovalová, M.*, Baraka, J. P.*, Mik, V., Jorda, R., Luo, L., Shao, H., Kryštof, V. (2023) A patent review of cyclin-dependent kinase 7 (CDK7) inhibitors (2018-2022). *Expert Opin Ther Patents* 33 (2), 67-87 *Sdílené prvouautorství

MK se jako sdílená první autorka podílela na sepsání patentové rešerše shrnující patentové přihlášky podané v letech 2018-2022, které se zabývaly vývojem inhibitorů a degradérů CDK7. Podílela se na revizi manuskriptu.

Příloha II:

Kovalová, M., Havlíček, L., Djukic, S., Škerlová, J., Peřina, M., Pospíšil, T., Řezníčková, E., Řezáčová, P., Jorda, R., Kryštof, V. (2023) Characterization of new highly selective pyrazolo 4,3-d pyrimidine inhibitor of CDK7. *Biomed Pharmacother* 161, 114492

MK jako první autorka optimalizovala a provedla buněčné experimenty analyzující expresi studovaných genů a proteinů, buněčný cyklus a aktivitu kaspáz. Interpretovala získaná data. Podílela se na sepsání manuskriptu a jeho revizi.

Příloha III:

Břehová, P., Řezníčková, E., Škach, K., Jorda, R., Dejmek, M., Vojáčková, V., Šála, M., **Kovalová, M.**, Dračínský, M., Dolníková, A., Strmeň, T., Kinnertová, M., Chalupský, K., Dvořáková, A., Gucký, T., Mertlíková Kaiserová, H., Klener, P., Nencka, R., Kryštof, V. (2023). Inhibition of FLT3-ITD Kinase in Acute Myeloid Leukemia by New Imidazo[1,2-*b*]pyridazine Derivatives Identified by Scaffold Hopping. *J Med Chem*, 66(16), 11133-11157.

MK jako spoluautorka zoptimalizovala a provedla buněčné experimenty analýzy exprese genů a interpretovala získaná data.

Příloha IV:

Řezníčková, E., Krajčovičová, S., Peřina, M., **Kovalová, M.**, Sural, M., Kryštof, V. (2022) Modulation of FLT3-ITD and CDK9 in acute myeloid leukaemia cells by novel proteolysis targeting chimera (PROTAC). *Eur J Med Chem* 243, 114792

MK jako spoluautorka zoptimalizovala a provedla buněčné experimenty analýzy exprese genů a interpretovala získaná data.

PŘÍLOHA I

Kovalová M*, Baraka JP*, Mik V, Jorda R, Luo L, Shao H, Kryštof V. (2023)
A patent review of cyclin-dependent kinase 7 (CDK7) inhibitors (2018-2022).
Expert Opin Ther Patents 33 (2), 67-87 *Sdílené prvoautorství

<https://doi.org/10.1080/13543776.2023.2195547>

A patent review of cyclin-dependent kinase 7 (CDK7) inhibitors (2018-2022)

Markéta Kovalová, Joseph Peter Baraka, Václav Mik, Radek Jorda, Lei Luo, Hao Shao & Vladimír Kryštof

To cite this article: Markéta Kovalová, Joseph Peter Baraka, Václav Mik, Radek Jorda, Lei Luo, Hao Shao & Vladimír Kryštof (2023) A patent review of cyclin-dependent kinase 7 (CDK7) inhibitors (2018-2022), Expert Opinion on Therapeutic Patents, 33:2, 67-87, DOI: [10.1080/13543776.2023.2195547](https://doi.org/10.1080/13543776.2023.2195547)

To link to this article: <https://doi.org/10.1080/13543776.2023.2195547>



© 2023 The Author(s). Published by Informa UK Limited, trading as Taylor & Francis Group.



Published online: 10 Apr 2023.



Submit your article to this journal [↗](#)



Article views: 223







View related articles [↗](#)



View Crossmark data [↗](#)

A patent review of cyclin-dependent kinase 7 (CDK7) inhibitors (2018–2022)

Markéta Kovalová ^{a*}, Joseph Peter Baraka^{b*}, Václav Mik ^a, Radek Jorda ^a, Lei Luo^b, Hao Shao^b
and Vladimír Kryštof ^{a,c}

^aDepartment of Experimental Biology, Faculty of Science, Palacký University Olomouc, Olomouc, Czech Republic; ^bCollege of Pharmaceutical Sciences, Southwest University, Chongqing, China; ^cInstitute of Molecular and Translational Medicine, Faculty of Medicine and Dentistry, Palacký University Olomouc, Olomouc, Czech Republic

ABSTRACT

Introduction: Cyclin-dependent kinase 7 (CDK7) is a member of the CDK family of serine/threonine protein kinases and participates in the regulation of the cell cycle and mRNA transcription. CDK7 is emerging as a possible drug target in oncology and six exciting drug candidates have already undergone early evaluation in clinical trials.

Areas covered: This review examines CDK7 inhibitors as anticancer drugs reported in patents published in the online databases of the World Intellectual Property Organization and European Patent Office in the 2018–2022 period. This review provides an overview of available inhibitors, including their chemical structures, biochemical profile and stage of development.

Expert opinion: Small-molecule CDK7 inhibitors represent attractive pharmacological modalities for the treatment of various cancer types. Highly potent and selective inhibitors have been discovered and many of them show promising results in several preclinical cancer models. Developed compounds act on the kinase by various mechanisms, including traditional ATP competition, irreversible binding to tractable cysteine 312 outside the active site of CDK7, and induced protein degradation by proteolysis targeting chimeras. Ongoing preclinical research and clinical trials should reveal which strategy will provide the highest benefits.

ARTICLE HISTORY

Received 18 January 2023
Accepted 22 March 2023

KEYWORDS

CAK; cancer; cyclin-dependent kinase 7; kinase inhibitor; PROTAC

1. Introduction



Cyclin dependent kinases (CDKs) constitute a family of serine/threonine protein kinases that form active complexes with corresponding cyclins to regulate cell cycle transitions and transcription [1]. CDK7 associates with cyclin H and MAT1 to form the CDK-activating kinase (CAK) complex, directing cell cycle transitions by phosphorylating the T-loop of cell cycle CDKs, such as CDK1, 2, 4 and 6 [2,3]. CDK7 is also a component of the general transcription factor IIH (TFIIH), facilitating transcription initiation by phosphorylating the C-terminal domain (CTD) heptapeptide repeats of RNA polymerase II (RNAP II) at Ser5 and Ser7 residues [4,5]. In addition, CDK7 phosphorylates CDK9, a component of positive transcription elongation factor b (P-TEFb), which in turn, phosphorylates the Ser2 residue of the RNAP II CTD to allow productive transcription elongation [6].

CDK7 has been intensively pursued as anticancer drug target due to its dysregulated cell cycle control and transcription in cancer cells [2]. The overexpression of CDK7 has been observed in different cancer types, such as mantle cell lymphoma [7], breast cancer [8], multiple myeloma [9], colorectal cancer [10], gastric cancer [11], ovarian cancer [12], oral squamous cell carcinoma [13], glioblastoma [14], and hepatocellular carcinoma [15], and is correlated with tumor

aggressiveness and a poor prognosis. CDK7 has also been found to directly phosphorylate or regulate the expression of oncogenic transcription factors, such as c-Myc [16], androgen receptor [17] and estrogen receptor [18]. CDK7 inhibitors have shown efficacy in animal models of most of the abovementioned cancers. In addition, CDK7 inhibition could trigger immune-response signaling [19] by inducing DNA replication stress and genome instability and synergize with anti-PD-1 therapy by inhibiting c-Myc activity to suppress PD-L1 expression [20]. These findings suggest that CDK7 inhibitors, as single agents or combined with other anticancer agents, have the potential to be translated into novel therapeutics.

In addition to cancer, CDK7 is involved in the pathogenesis of autosomal dominant polycystic kidney disease (ADPKD) [21]. Cellular metabolism is altered in ADPKD patients and is driven by super-enhancers (SE)-associated genes. CDK7 is required for the assembly and maintenance of SEs, rendering it a potential target for the treatment of ADPKD. CDK7 is upregulated in ADPKD patients, and its expression is correlated with the disease severity. The inhibition of CDK7 delayed abnormal cyst growth and slowed disease progression in ADPKD mouse models [22]. These results suggest that CDK7 is a promising therapeutic target for ADPKD treatment.

The discovery of highly selective CDK7 inhibitors has been challenging considering that there are 20 members in the CDK

CONTACT Vladimír Kryštof  vladimir.krystof@upol.cz  Department of Experimental Biology, Faculty of Science, Palacký University Olomouc, Šlechtitelů 27, Olomouc 78371, Czech Republic
^{*}Both authors contributed equally.

Article highlights

- CDK7 is a promising therapeutic target for the treatment of cancer.
- Small molecule inhibitors with various mechanisms of action are exploited, including ATP competitors, covalent binders and PROTACs
- Selective CDK7 inhibitors have shown encouraging results in preclinical cancer models.
- Six CDK7 inhibitors have entered phase I/II clinical trials and four of them are still active.
- This review covers CDK7 modulators published in the peer-reviewed literature and patents over the past 5 years

family and that the ATP binding site is highly conserved. Highly selective CDK7 inhibitors have been identified over the past few years, and six of them have entered clinical trials. In this review, we summarize all the efforts in the field, including CDK7 inhibitors reported both in the peer-reviewed literature and patent applications. In addition, we briefly discuss the rationale for and future challenges in developing CDK7 inhibitors as therapeutic agents.

2. Overview of CDK7 inhibitors

There has been a long-lasting interest in pursuing CDK7 as a therapeutic target, and the selective CDK7 inhibitors reported in the peer-reviewed literature have inspired the discovery of many of these reported in recent patents applications, especially the BS-181 and the THZ1 series. Over the last few years, several reviews covering inhibitors of CDK7 and other transcriptional CDKs have been published [23–25]. In this section, we summarize the CDK7 inhibitors reported in the peer-reviewed literature and provide updates regarding their clinical development (Table 1).

The first identified CDK inhibitors possess relatively low selectivity and interact equipotently with more CDKs, including cell cycle regulating CDK1 and CDK2 and transcriptional CDK7 and

CDK9. Suffering from polypharmacology, the anticancer activity of these compounds could not be clearly linked to a single kinase. To identify a potent and selective CDK7 inhibitor, Ali et al. started with roscovitine (**1**), a first-generation pan-CDK inhibitor, using a computational approach [26]. Purine was replaced by pyrazolo[1,5-*a*]pyrimidine based on computational calculations of the free solvation energies of several heterocyclic rings. Molecular docking suggested that there was extra space next to the ethyl substituent, which could be used to improve CDK7 specificity. Removing the hydroxyethyl moiety and replacing the remaining propyl side chain with a 1,6-diaminohexyl substituent resulted in the selective CDK7 inhibitor BS-181 (**2**) with an IC_{50} of 21 nM. BS-181 only inhibited CDK2 with an IC_{50} less than 1 μ M when tested against other CDKs and 69 additional kinases, with a 35-fold higher selectivity for CDK7 over CDK2. BS-181 inhibited the growth of different types of cancer cells with IC_{50} values ranging from 11.7 to 37 μ M. In MCF-7 cells, BS-181 inhibited RNAP II CTD Ser2/5 phosphorylation, induced cell apoptosis and arrested the cell cycle at the G1 phase [26]. BS-181 inhibited the growth of breast cancer MCF-7 and gastric cancer BGC823 xenografts in mice via intraperitoneal injection [27].

Further optimization of this scaffold led to the orally bioavailable CDK7 inhibitor samuraciliclib (**3**, CT7001, ICEC0942) [10]. Samuraciliclib inhibited CDK7 with an IC_{50} of 40 nM and was 45-, 15-, 230-, and 30-fold more selective for CDK7 over CDK1, CDK2, CDK5, and CDK9, respectively. When screened against a panel of 117 diverse kinases at 10 μ M, an additional five kinases, ERK8, STK33, CHK2, CLK2, and PHK, were inhibited to a similar extent as CDK2. Samuraciliclib inhibited the growth of 60 cell lines with a median GI_{50} of 0.25 μ M. It also decreased RNAP II CTD Ser2/5/7, CDK1 Thr161 and CDK2 Thr160 phosphorylation in a dose- and time-dependent manner in HCT116 colon cancer cells, resulting in an enrichment of cells in the G2/M phase. Treatment with samuraciliclib for 24 hours induced caspase 3/7 and PARP cleavage,

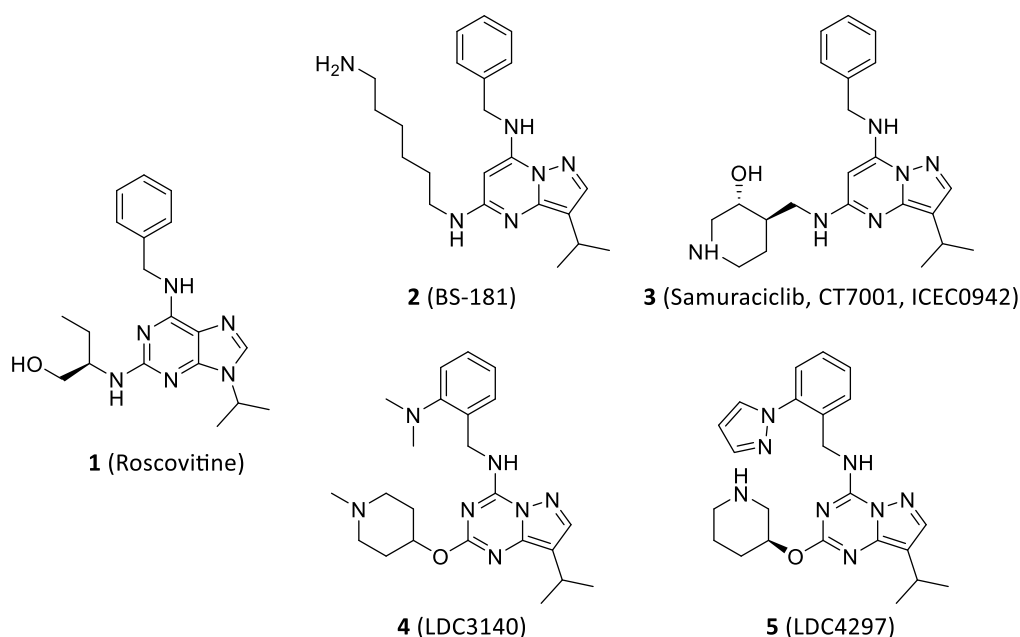


Table 1. CDK7 inhibitors in clinical trials.

Compound	Company	Trial Number	Condition/disease	Clinical Phase Status
SY-1365 (Mevociclib)	Syros Pharmaceuticals	NCT03134638	Advanced solid tumor, ovarian and breast cancer.	I; terminated (2021; business reasons)
Samuraciclib (CT7001, ICEC0942) LY3405105	Carrick Therapeutics Eli Lilly and Company	NCT03363893 NCT03770494	Advanced solid malignancies, TNBC, CRPC, HR ⁺ /HER2 ⁻ BC Solid tumor, TNBC, ovarian cancer, soft tissue sarcoma, epithelioid sarcoma, bladder cancer	I/II; active, not recruiting I; terminated (2021; lack of efficacy)
SY-5609	Syros Pharmaceuticals	NCT04247126	Advanced solid tumors, breast cancer, SCLC, pancreatic cancer	I; active not recruiting
Q901	Qurient Company	NCT04929223 NCT05394103	Metastatic colorectal cancer Advanced solid tumors, Advanced or metastatic ovarian cancer, CRPC, endometrial cancer, HR ⁺ /HER2 ⁻ BC, colorectal cancer, SCLC, pancreatic cancer	I; recruiting I/II; recruiting
XL102 (AUR102)	Exelixis	NCT04726332	Solid tumors, ovarian cancer, TNBC, HR ⁺ BC, mCRPC	I; recruiting

Notes: TNBC – triple-negative breast cancer; HR⁺/HER2⁻ BC - hormone receptor positive/HER2 negative breast cancer; CRPC – castration-resistant prostate cancer; SCLC – small cell lung cancer; mCRPC – metastatic castration-resistant prostate cancer.

indicating programmed cell death. In addition, such treatment showed antitumor effects either as a single agent in xenografts of both breast and colorectal cancers or combined with tamoxifen in ER⁺ breast cancer xenografts [10].

Recently, a high-resolution cryo-EM structure of human CAK complexed with samuraciclib (PDB ID: 7B5O and 7B5Q) was resolved [28], which explained its selectivity for CDK7 over CDK2 along with the CDK2-samuraciclib crystal structure previously reported (PDB ID: 5JQ5) [29]. The pyrazolopyrimidine core of samuraciclib formed hydrogen bonds with the hinge residue in a similar fashion, Met94 in CDK7 and Leu83 in CDK2 (Figure 1). However, the conformations of both six-ring-bearing substituents of samuraciclib were vastly different. The benzylamine moiety adopted a “ring-up” conformation when bound to CDK7 and a “ring-down” conformation when bound to CDK2. The difference in one residue (Ile10 in CDK2/Leu18 in CDK7) and a slight shift of the protein backbone near the C-terminus of the interdomain linker (around CDK2 Leu83/CDK7 Met94) might account for the distinct benzylamine orientation. The hydroxy group of the 3-hydroxypiperidine ring pointed toward the active site in CDK7 and adopted an OH-in conformation, whereas it pointed toward

the solvent and a neighboring β -strand in CDK2 with an OH-out conformation [28].

The phase 1 clinical trial results of samuraciclib in patients with advanced solid tumors were disclosed at the ESMO Congress 2021 [30]. Neutropenia and significant myelosuppression associated with other CDK inhibitors were not observed. Once daily, 240 mg and 360 mg were determined as clinically relevant doses, with 360 mg once per day as the recommended phase II dose. Fifty-seven percent (25/44) of RECIST-evaluable patients exhibited evidence of disease control. In the expansion cohort, 12 of 20 patients with TNBC had stable disease. In another single-arm cohort, 31 patients with advanced HR⁺/HER2⁻ BC who progressed on their prior CDK4/6 received both samuraciclib and fulvestrant, and the RECIST evaluation showed evidence of a reduction in the tumor burden [31]. The treatment was generally well tolerated with mild adverse drug effects. Samuraciclib showed an acceptable pharmacokinetic and safety profile with evidence of antitumor activity [30]. Based on the promising preclinical and clinical results, a phase 2 clinical trial will be jointly sponsored by Carrick and Menarini to evaluate the combination of samuraciclib and Menarini’s oral estrogen receptor degrader elacestrant in patients with CDK4/6i-resistant HR⁺ BC in 2023.

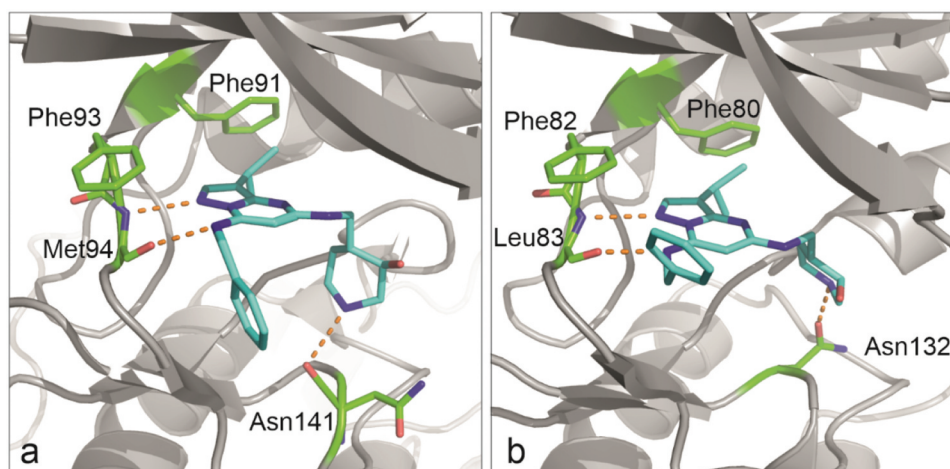


Figure 1. (a) Cryo-EM structure of the CAK-samuraciclib complex (PDB ID: 7B5Q); (b) crystal structure of CDK2-samuraciclib (PDB ID: 5JQ5). The kinases are shown as gray cartoon, the inhibitors are cyan. Nitrogen and oxygen atoms are shown in blue and red, respectively. Hydrogen bonds are denoted by orange dashed lines. Key residues are presented in the stick representation. The images were generated by PyMOL.

LDC3140 (**4**) and LDC4297 (**5**) were identified from a medicinal chemistry campaign by screening a kinase-biased library centered on BS-181 and other known ATP-competitive kinase inhibitors against CDK7 and a subsequent synthesis of 600 analogs [32]. Both compounds inhibited CDK7 with an IC_{50} less than 5 nM. LDC3140 was over 770-fold selective for CDK7 over the other CDKs tested, including CDK1/2/4/6/9. LDC4297 exhibited a much lower specificity for CDK7 than for the other CDKs, particularly CDK2 (IC_{50} = 6 nM) and CDK1 (IC_{50} = 54 nM). Both compounds decreased RNAP II phosphorylation at Ser5/7 and showed distinct physiological responses at relatively low and high concentrations [32].

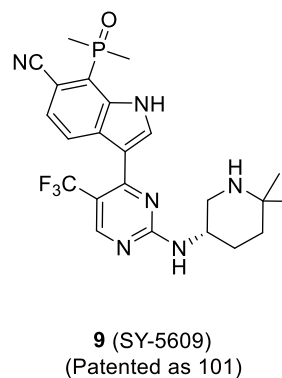
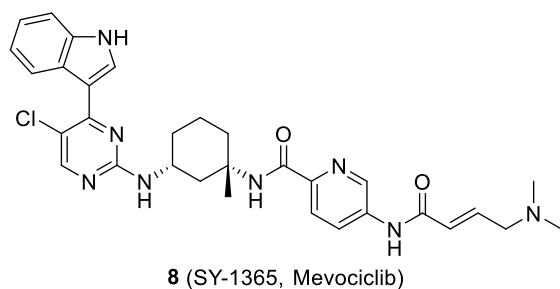
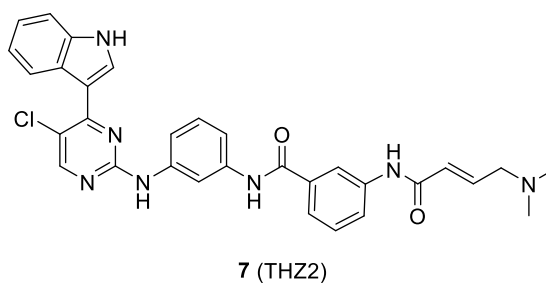
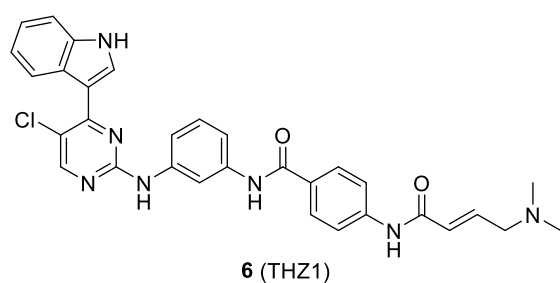
THZ1 (**6**) was the first covalent CDK7 inhibitor identified from a cell-based screening and kinase selectivity profiling of an in-house ATP-site-directed kinase inhibitor library by the Gray group [33]. THZ1 inhibited CDK7 by forming a covalent bond with Cys312 located outside the ATP binding site using its acrylamide moiety, which contributed to its activity to a large extent. THZ1 inhibited CDK7 in a time-dependent manner with an IC_{50} of 238 nM at 1 mM ATP and inhibited CDK12/13 (IC_{50} = 893 and 628 nM, respectively) covalently due to a conserved cysteine at a similar position [34]. Molecular docking showed that the aminopyrimidine of THZ1 formed hydrogen bonds with the hinge region residue Met94, and the chlorine atom interacted with the phenylalanine gatekeeper residue (Phe91) [33]. The acrylamide moiety was located in close proximity to Cys312 to form a covalent bond. This model was confirmed by the recently solved cryo-EM structure of the CAK-THZ1 complex (PDB ID: 6XD3, Figure 2a) [35].

THZ1 was screened against a diverse panel of over 1,000 cancer cell lines and had an IC_{50} less than 200 nM among 53% of these tested. A bioinformatic analysis showed that these

sensitive cell lines were characterized by the overexpression of (proto-) oncogenic transcription factors and factors involved in RNAP II-driven transcriptional regulation. THZ1 efficiently killed T-cell acute lymphoblastic leukemia (T-ALL) cell lines with misregulation of T-cell lineage-specific transcription factors at low nM and induced cell apoptosis via the downregulation of the antiapoptotic proteins MCL1 and XIAP. THZ1 also reduced RNAP II Ser2/5/7 phosphorylation and CDK1/2 T-loop phosphorylation and arrested the cell cycle at the G2 phase. THZ1 reduced the global mRNA levels at a high dose, whereas it preferentially decreased only a subset of genes at a low dose, especially *RUNX1*, which contains a large SE domain [33]. THZ1 showed efficacy in cancers addicted to oncogenic transcription factors and SE-associated genes, including T-ALL [33], SCLC [36], melanoma [37], T-cell lymphomas and multiple myeloma xenografted models [38]. However, THZ1 suffered from being a substrate of ABC drug transporters and poor metabolic stability ($T_{1/2}$ of 45 min in mouse plasma, CL = 129 mL/min/kg), limiting its *in vivo* investigations.

Moving the acrylamide of THZ1 from the *para*- to *meta*-position on the benzamide resulted in THZ2 (**7**), which retained selective CDK7 inhibition and improved the half-life 5-fold *in vivo*. In addition, THZ2 blocked tumor growth in a TNBC cell line and patient-derived xenograft (PDX) models [39].

The iterative optimization of the linker between the pyrimidine ring and covalent warhead in THZ1 led to a more metabolically stable analog, SY-1365 (**8**, mevociclib), which had the lowest plasma clearance of 5.6 mL/min/kg and highest k_{inac}/K_i of $0.131 \mu M^{-1} s^{-1}$ in this series [40]. The docking of SY-1365 to CDK7 demonstrated improved shape complementarity and possible stronger hydrophobic interactions between



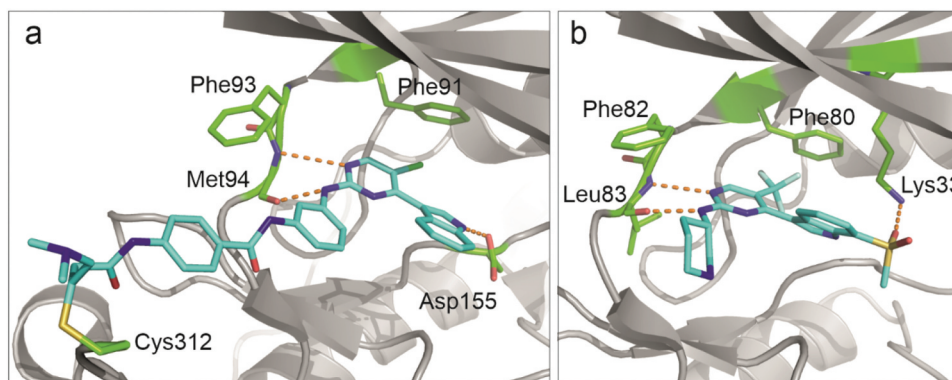


Figure 2. (a) Cryo-EM structure of the CAK-THZ1 complex (PDB ID: 6XD3); (b) crystal structure of SY-5609 analog in CDK2 (PDB ID: 7RA5). The kinases are presented as gray cartoon, the inhibitors are cyan. Nitrogen, oxygen and sulfur atoms are shown in blue, red and yellow, respectively. Hydrogen bonds are denoted by orange dashed lines. Key residues are presented in the stick representation. The images were generated by PyMOL.

the chiral cyclohexane-1,3-diamine ring and the solvent accessible surface of CDK7, which likely contributed to the increased potency compared with that of THZ1. SY-1365 inhibited CDK7 with an IC_{50} of 369 nM at 2 mM ATP without compound preincubation, whereas the IC_{50} of the other CDKs was 2 mM or greater, including CDK2, CDK9 and CDK12. Seven other kinases (out of 468) were inhibited greater than 90% by SY-1365 at 1 μ M in a kinome screen.

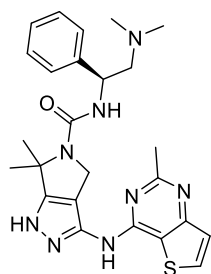
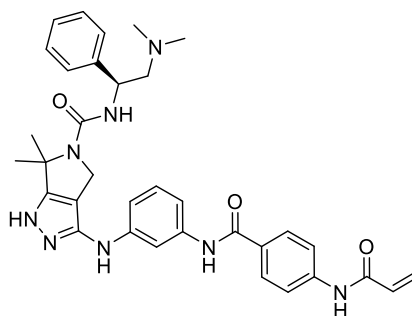
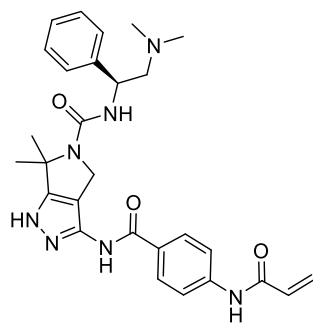
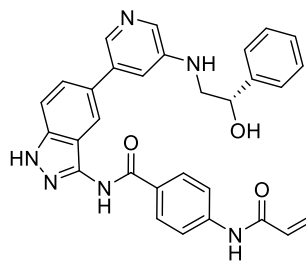
The antiproliferative activity of SY-1365 was evaluated in 386 human cell lines representing 26 cancer types. Most of them showed significant growth inhibition and cell killing in the nanomolar range. SY-1365 inhibited RNAP II CTD phosphorylation at Ser2/5/7 and CDK2 Thr160 phosphorylation in a dose- and time-dependent manner in several cell lines. SY-1365 preferentially downregulated SE-related oncogenic transcription factor genes, such as *MYC*, and the most significantly enriched pathways affected by SY-1365 were cell cycle-related and DNA damage repair-related, especially those related to homologous recombination repair and mismatch repair. SY-1365 showed antitumor activities in multiple xenograft models at a dose of 30 or 40 mg/kg once or twice per week, including acute myeloid leukemia (AML; Kasumi-1 and ML-2), ovarian (OVCAR3 and a patient-derived model OV15398), and TNBC PDX models [41–44].

In May 2017, a phase I clinical trial of SY-1365 was initiated with expansions in ovarian and breast cancer [45]. SY-1365 showed linear pharmacokinetics and manageable adverse events in a dose regime ranging from 2–64 mg/m², and target engagement was proven by the dose-dependent regulation of gene expression in PBMCs [46]. In the expansion portion, SY-1365 was evaluated as a single agent in patients with high-grade serous ovarian cancer (HGSOC) and relapsed clear cell ovarian cancer and in combination with other anticancer agents in patients with HGSOC and metastatic CDK4/6 inhibitor-resistant HR⁺ BC. Peri-infusional adverse events were observed due to the IV administration routine, which could be reduced by lowering the doses and extending the infusion times. The best response observed across the expansion cohorts was stable disease in 42% and 64% in the single-agent and combination cohorts, respectively [47]. Based on preclinical and clinical data, Syros believes that higher doses or more frequent dosing will be needed for clinical activity,

which could create an overly burdensome dosing schedule for patients. Syros decided to discontinue the clinical development of SY-1365 and prioritize its oral non-covalent CDK7 inhibitor SY-5609 (**9**) [48] patented in 2020 [49]. SY-5609 showed excellent selectivity toward CDK7 (binding of its analog to CDK7 is shown in Figure 2b) and *in vitro* and *in vivo* potency [48]. Based on these promising data, SY-5609 entered a phase I clinical trial (NCT04247126). Since it was patented during the period covered by this paper, SY-5609 is described in detail in the patent section below (chapter 3.2.).

The covalent warhead of THZ1 (**6**) was used in the further development of other CDK7 inhibitors. It was hybridized with a pyrrolidinopyrazole core from the known PAK4 inhibitor PF-3758309 (**10**), which impacts CDK7 as an off-target [50,51]. The hybridization led to YKL-1-116 (**11**) [52], which retained the potent inhibition of CDK7 (IC_{50} = 7.6 nM) but suboptimal antiproliferative activity in cells. Further optimization of the linker length between the aminopyrazole core and covalent warhead resulted in YKL-5-124 (**12**), with similar potency against CDK7 (IC_{50} = 9.7 nM), but higher potency against cancer cells [34]. YKL-5-124 is inactive against CDK12/13 up to 100 μ M and more than 130-fold selective for CDK7 over CDK2/9 (IC_{50} of 1.3 and 3.02 μ M, respectively). Its high selectivity was proven by KiNativ profiling, and CDK7 was the only target bound by 1 μ M YKL-5-124 in Jurkat extracts. Molecular docking studies showed that the 3-aminopyrazolopyrrolidine core formed hydrogen bonds with the hinge region residues Asp92 and Met94, and two additional hydrogen bonds with Lys41 and Asn141 were observed. The acrylamide moiety of YKL-5-124 was positioned in proximity to residue Cys312 to form a covalent bond. The treatment of HAP1 cells with YKL-5-124 inhibited the phosphorylation of CDK1 Thr161 and CDK2 Thr160, caused cell arrest at the G1/S transition, and downregulated the expression of E2F-driven genes. In contrast to THZ1, treatment with YKL-5-124 did not induce cell apoptosis or affect RNAP II CTD phosphorylation [34].

Compound B2 (**13**) was a potent CDK7 inhibitor scaffold-hopped from YKL-5-124 [22]. The aminopyrazole moiety of YKL-5-124 was retained to maintain the hydrogen bonds with the hinge region and the benzoyl motif as the linker to attach the covalent warhead. A pyridine ring was introduced to form a hydrogen bond with Asn142. Molecular docking

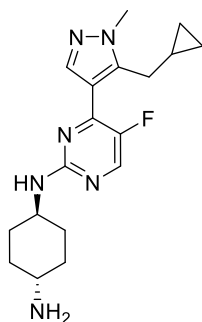
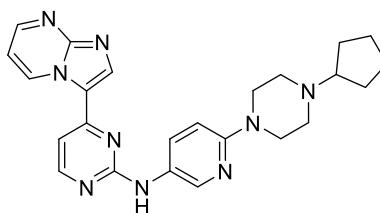
**10** (PF-3758309)**11** (YKL-1-116)**12** (YKL-5-124)**13** (B2)

suggested that the modification of pyridine at C5 should be tolerated since there was enough space around this region. The iterative optimization of the substituents at the pyridine C5 position and the addition of the Michael acceptor moiety resulted in the most potent compound B2. It inhibited CDK7 with an IC_{50} value of 4 nM and showed over 100-fold selectivity over the CDKs tested. Compound B2 was further assessed for selectivity using a 51 kinase diversity panel, and nine of them were inhibited by more than 50% at 1 μ M, especially GSK3 β with 99% inhibition. B2 inhibited GSK3 β with an IC_{50} of 148 nM and was 37-fold selective for CDK7 over GSK3 β . Compound B2 had acceptable pharmacokinetic properties with a $T_{1/2}$ of 3.44 h and good exposure after subcutaneous administration. B2 showed efficacy in an *in vitro* MDCK cyst

model, an *ex vivo* embryonic kidney cyst model and an ADPKD mouse model with minimal toxicity.

Compound A86 (**14**) was discovered in a cell-based screen as a potent CKI α inhibitor, but it also binds to CDK7 and CDK9 with K_D values of 0.34 nM and 5.4 nM, respectively [53]. A86 effectively killed AML cells by stabilizing of p53 and suppressing the transcription of SE-driven oncogenes. A86 showed efficacy in MLL-AF9 and several patient-derived AML xenograft models.

Compound 9q (**15**) is a dual CDK7/9 inhibitor optimized from a pan-selective CDK inhibitor. Compound 9q inhibited CDK7 and CDK9 with IC_{50} values of 55 nM and 38 nM, respectively. However, it also weakly inhibited CDKs 1–6 to a lesser extent [54]. Compound 9q inhibited the growth of a panel of

**14** (A86)**15** (9q)

cells with a low micromolar IC_{50} . This compound reduced the phosphorylation of RNAP II Ser2/5 and induced cell apoptosis in MV4–11 cells, arresting the cell cycle at the sub-G1 phase.

Recently, the preclinical data of several other promising CDK7 inhibitors were presented, but their structures have not yet been disclosed. One of them is Q901, a highly selective CDK7 inhibitor developed by the Korean company Qurient. Q901 triggered G1 cell cycle arrest in cells and inhibited tumor growth in an ER⁺ BC xenograft model, CDK4/6 inhibitor-resistant PDX model, and many other solid tumors [55,56]. Q901 was evaluated in a broad spectrum of solid tumor cell lines and was found to be more potent in TP53 wild-type cancer cells than in TP53 mutant cells. POLR2A was identified as a potential pharmacodynamic marker due to a dose-response increase in POLR2A expression upon Q901 treatment and a correlation with the tumor growth inhibition rate [57]. Q901 is currently undergoing a phase 1 clinical trial in adult patients with advanced solid tumors via intravenous infusion and selected advanced solid tumors with a cohort expansion at the recommended phase 2 dose (NCT05394103).

XL102, formerly known as AUR102, is a potent, orally bioavailable and highly selective covalent CDK7 inhibitor [58] that was discovered by Aurigene and is currently developed by joint efforts with Exelixis. XL102 induced cell death in various cancer cell lines and caused tumor regression in multiple xenograft models. XL102 under investigation in a phase 1 clinical trial as a single agent and in combination in patients with advanced solid tumors (QUARTZ-10, NCT047263321), including HR⁺ BC, TNBC, epithelial ovarian cancer, and mCRPC. The preliminary data from the dose-escalation stage of the trial showed that XL102 reached its T_{max} within 1–3 hours and had a half-life of 5–9 hours. XL102 was well tolerated at the doses evaluated, and treatment-emergent adverse events were observed at high doses but were low grade and reversible. No objective responses were observed at the data cutoff, and patients with stable disease remained in the study. XL102 will be further evaluated in patients in a single-agent dose-escalation cohort, a tumor-specific cohort and a combination cohort [59].

QS1189 is a pyrazolo-triazine-based inhibitor discovered by Qurient, the originator of clinical candidate Q901. QS1189 inhibits CDK7 with an IC_{50} of 15 nM, but it also shows similar inhibition of other CDKs, including CDK16, CDK2 and CDK5 [7]. QS1189 inhibited the growth of mantle cell lymphoma (MCL) cells with IC_{50} values between 50 and 250 nM. Similar to other CDK7 inhibitors, QS1189 decreased RNAP II CTD Ser2/5/7 phosphorylation and downregulated genes involved in transcriptional regulation and the cell cycle in MCL cells. QS1189 induced G2/M cell cycle arrest and cell apoptosis as evidenced by cleaved PARP and Caspase 3.

YPN-005 is highly selective for CDK7 from Yungjin Pharmaceutical with an IC_{50} of 31 nM and inhibited 7 other kinases over 90% at 1 μ M in a 468 kinase panel screen, including CDK13, CDK19, CSNK1A1, CSNK1D, CSNK1E, MAPK15, and MAPK10 [60]. YPN-005 showed potent antiproliferative effects in SCLC cells, cisplatin- or etoposide-resistant cells, and organoids derived from SCLC patients. Similar to other CDK7 inhibitors, YPN-005 treatment significantly decreased the phosphorylation of the RNAP II CTD and significantly inhibited tumor growth in xenograft models established from the SCLC cell line H209 and cisplatin- or etoposide-resistant H209 cells. Another study [61] showed its antileukemic potential both *in*

vitro and *in vivo*. YPN-005 induced apoptosis and suppressed the expression of c-MYC, FLT3 and STAT5. An *ex vivo* proliferation inhibition assay in primary leukemic cells also showed higher sensitivity in AML cells with FLT3-ITD mutation.

Finally, UD-017 is a potent CDK7 inhibitor with an IC_{50} of 16 nM from Ube Industries that is at least 300-fold more selective for CDK7 over other CDKs [62]. The compound was tested in a panel of 313 kinases, and only 4 other kinases (AMPK α 2/ β 1/ γ 1, AMPK α 1/ β 1/ γ 1, haspin, and GSK3 β) were inhibited over 90% at 1 μ M, but the IC_{50} values were hundreds of nM. UD-017 potently inhibited the growth of a wide range of cancer cells, and c-Myc expression correlated well with its antiproliferative activities [63]. Specifically, UD-017 inhibited the proliferation of the HCT-116 cell line (GI_{50} = 19 nM), and its *in vitro* application led to a decrease in RNAP II CTD, CDK1 and CDK2 phosphorylation, and the induction of apoptosis. It showed *in vivo* efficacy in HCT-116 xenografts alone and in combination with 5-FU [64,65]. UD-017 also strongly inhibited tumor growth in multiple PDX models, including non-small cell lung cancer (LXFL1121), pleura mesothelioma (PXF541), gastric cancer (GXA3067) and sarcoma (SXF5117) [66].

Combinations of several drugs are often used and have been shown to be beneficial in cancer treatment. To date, CDK7 inhibitors have shown *in vitro* and *in vivo* synergistic effect in combination with BH3 mimetics [9,40], BET inhibitors [67], antiestrogens [10,58], p53-activating agents [52] and immunotherapy [19,20]. This strategy has also been tested in the clinical trials particularly for samuraciclib, SY-1365 and SY-5609. Abovementioned treatment strategies have already been reviewed in detail in several papers [5,23,24].

3. New patent literature concerning CDK7 inhibitors

The documents were retrieved from the online databases of the World Intellectual Property Organization (www.wipo.int) and European Patent Office (espacenet.com) and cross-checked in the databases of the American Chemical Society (scifinder.cas.org) and Elsevier (reaxys.com). Duplicate and irrelevant documents not covering small-molecule inhibitors were removed manually, and the remaining patents were sorted according to the chemical similarity of the described compounds. In some cases, the subject compounds have clear similarities to existing agents, and the patents cover only slightly modified analogs that bind CDKs in the same manner. More often, the similarity is less obvious, but at least some structural motifs are conserved.

3.1. THZ1 and THZ2 analogs

The discovery of THZ1 (**6**), the first covalent CDK7 inhibitor, has inspired many researchers, including the team at Chongqing Medical University, who disclosed a series of eight analogs (e.g. example **16**) in which the indole moiety of THZ1 was replaced with various anilines [68]. Further modifications (e.g. addition of the methoxy or methyl group) were introduced on the distal phenyl ring bearing a warhead for covalent attachment to the target protein [68]. All compounds showed similar inhibitory activities on CDK7 at a 200 nM

concentration, reaching more than 97%, comparable to THZ1 used as a positive control. The compounds also inhibited the proliferation of the human cancer cell lines MDA-MB-231 and A549 with calculated IC_{50} values below 25 nM.

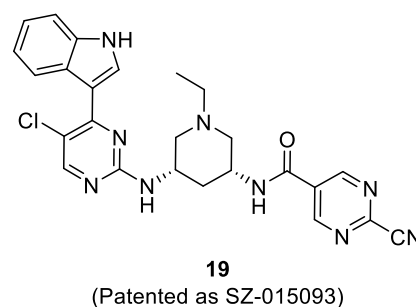
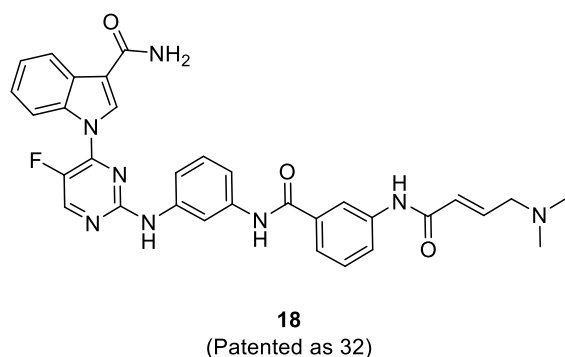
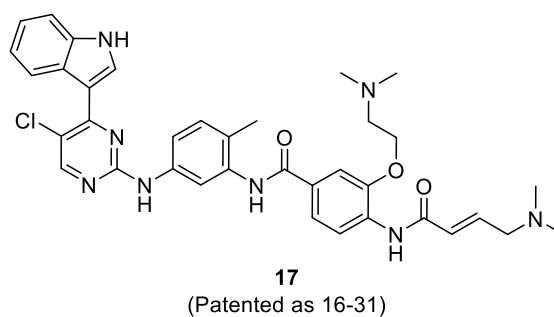
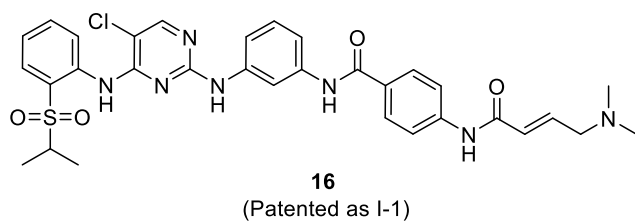
Encouraged by the striking selectivity of THZ1 and especially THZ2 (**7**), in recent years, several companies have focused on 3-pyrimidin-4-yl-indoles and isosteric 3-pyrimidin-4-yl-pyrrolo[2,3-*b*]pyridines. In this respect, Longtaishen Pharmaceutical Technology Company published a document protecting THZ2 derivatives bearing an additional chain at the benzene ring distal to indole [69]. Compound **17** exhibited interesting inhibitory activity against CDK7 (IC_{50} = 6 nM). In addition, Ancureall Pharmaceuticals Company disclosed THZ2 analogs, in which indole is attached reversely and further modified by carboxamide function [70]. Their set of compounds was tested only to determine the antiproliferative potential in the MOLM-13 cell line. Compound **18** exhibited improved antiproliferative activity (IC_{50} < 1 nM) compared to THZ1 (IC_{50} = 1–10 nM). Information regarding potency or selectivity toward CDK7 was not presented, but the structural similarity to the parental inspiration is obvious.

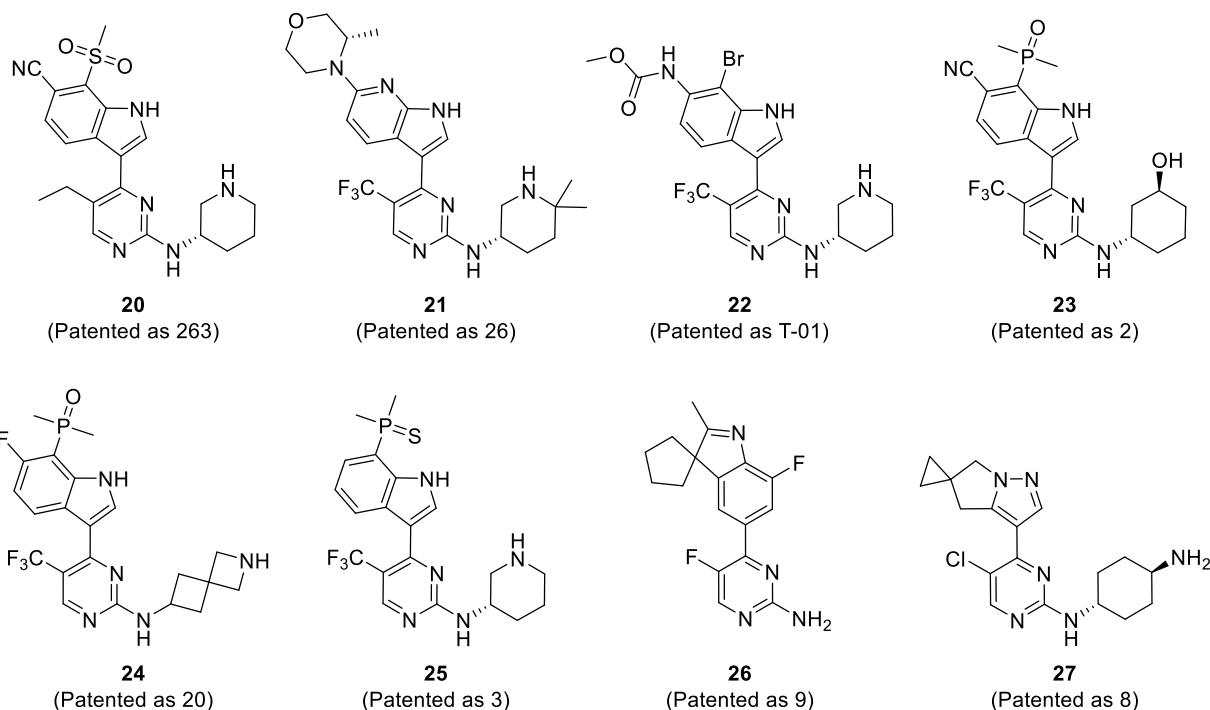
Suzhou Sinovent Pharmaceutical Technology presented set of SY-1365 (**8**) analogs that lacked typical methylsulfonyl or dimethylfosforyl functions [71–73]. Compound **19** displayed CDK7 IC_{50} of 1.06 nM without preincubation, and the IC_{50} decreased below 0.5 nM after 60 minutes. No additional data regarding its selectivity or *in vitro* and *in vivo* potency were shown [73].

One of the most active and successful companies focusing on research investigating pyrimidinylindole derivatives is Syros Pharmaceuticals, the originator of the clinical candidate SY-1365 (**8**) (see Table 1). They published two patents in 2019

describing compounds related to THZ1 and SY-1365, both significantly simplified [74,75]. Most of the presented compounds exhibited great selectivity toward CDK7 with IC_{50} values below 30 nM and IC_{50} values \geq 500 nM for the other tested kinases, including CDK2, CDK9, and CDK12. All compounds were tested *in vitro* on ovarian and TNBC cell lines; the most potent compounds blocked their proliferation at < 100 nM concentrations. Another large set consisting of 268 compounds was disclosed in 2021 [76]. The compounds showed a wide range of selectivity and potency. For example, **20** effectively inhibited CDK7 (IC_{50} < 20 nM), displayed strong selectivity against CDK2/9/12 (IC_{50} > 5 μ M) and exhibited nanomolar inhibition of proliferation of HCC70 and A673 cell lines.

Importantly, Syros Pharmaceuticals presented another clinical candidate, SY-5609 (**9**). The synthesis, preclinical and first clinical data are covered in several patents [49,77–79]. SY-5609 showed excellent selectivity toward CDK7 among the tested kinases. The K_D of SY-5609 was 0.065 nM, and the selectivity was determined as a ratio of K_i/K_D (CDK7) with values of 40,000, 13,000, and 15,000 for kinases CDK2, CDK9, and CDK12, respectively. SY-5609 was screened against 485 kinases at a 1 μ M concentration; the compound inhibited only 9 kinases \geq 70% (including CDK13, CDK16, CDK17, and CDK18) [48]. The compound was shown to be effective *in vivo* in several PDX, including TNBC, SCLC, and HGSOc. The compound induced at least 50% tumor growth inhibition (TGI) in all models, and in more than half of the models, it led to more than 95% TGI without any evidence of regrowth for 21 days after the last dose. Due to positive outcomes in preclinical *in vivo* studies and its great tolerability, SY-5609 entered phase I clinical trials for advanced solid tumors as a single agent and HR⁺ breast





cancer in combination with fulvestrant (NCT04247126). The first results [79] led to the establishment of the maximum tolerated dose as 3 mg/daily. SY-5609 showed approximately dose-proportional pharmacokinetics and moderate to high interpatient variability. This clinical trial is still ongoing with expansions to several cancer types to study the effect in more homogenous patient populations.

GT Apeiron Therapeutics presented another large group of closely related compounds with a 3-pyrimidin-4-yl-pyrrolo[2,3-*b*]pyridine core with a wide range of selectivity and potency [80–82]. Selectivity was profiled within the group of CDK7, CDK2, CDK9, and CDK12. Compounds potently and selectively inhibited CDK7 with $IC_{50} < 20$ nM, and the proliferation of the cancer cell lines HCC70 and A2780 was inhibited in the nanomolar range. The compounds also showed enhanced membrane permeability and reflux rate compared to the comparative compound with a similar structure [83]. Compound **21** exhibited great selectivity toward CDK7 ($IC_{50} = 9.5$ nM) over CDK2/9/12 ($IC_{50} > 10$ μ M) and effectively inhibited the tested cell lines in tens of nM.

Additional compounds inspired by SY-5609 were disclosed by TYC Medicines, who presented compounds based on the pyrimidinylindole core [84]. Similar to previous companies, they tested their first set of compounds in term of kinase selectivity using CDK7, CDK2, CDK9, and CDK12. Example **22** inhibited CDK7 at less than 50 nM, whereas the other kinases were more than 10-fold less sensitive. *In vitro* proliferation assays showed that this compound effectively inhibited the proliferation of breast, ovarian, colorectal, and lung cancer cells. All tested cell lines were inhibited in the nanomolar range, and **22** inhibited proliferation more effectively than SY-5609 in most tested cell lines. The studies also showed that **22** has improved pharmacokinetic parameters compared with SY-5609.

A gap in the chemical space was further filled by Jiangsu Simcere Pharmaceutical Company, who presented a small group of similar pyrimidinylindole derivatives related to SY-5609 [85,86]. Compound **23**, which has a cyclohexyl ring instead of piperidine, presented great selectivity toward CDK7 with an IC_{50} of 2.3 nM. The other tested CDKs (i.e. CDK1, CDK2, CDK4, CDK6, CDK9, and CDK12) were inhibited in the micromolar range. Closely related compounds based again on the 3-[(4-trifluoromethyl)pyrimidin-3-yl]indole core with similar potency and selectivity were disclosed by Guangzhou Fermion Technology [87]. The pyrimidine ring was substituted at the C2 position either by an aminocyclohexylamino or piperidin-3-ylamino group or by bicyclic or nitrogen-containing spirocyclic moieties linked to the pyrimidine via an amino or methylamino group (e.g. **24**). In some cases, the hydrogen atom at the C7 position on the indole ring was substituted by a fluorine or cyano group, whereas the C8 position was occupied mostly by dimethylphosphoryl or sulfur-containing functional groups. The most selective compounds inhibited CDK7 at less than 10 nM and additionally tested kinases (CDK2, CDK9, and CDK12) at over 1000 nM. Few related indole derivatives bearing dimethylthiophosphoryl functionality were published in a patent by Newsoara Biopharma [88]. Compound **25** was the most potent, with an IC_{50} of 3.6 nM, but again, no details concerning its selectivity or *in vitro* and *in vivo* activity were provided.

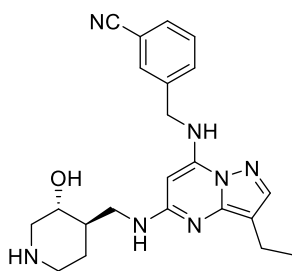
Two additional patents protect compounds resembling THZ1/THZ2 only partly. A group of 38 aminopyrimidines (prepared by Shanghai Lingda Biomedical) are linked to indole or various other fused six- and five-membered nitrogen-containing heterocycles (e.g. indazole, benzo[*d*]imidazole, imidazo[1,2-*a*]pyridine, or tetrahydropyrazolo[4,3-*c*]

pyrimidine) and these are CDK7 inhibitors capable of strongly targeting CDK9 [89]. The first set of inhibitors is represented by 2,4,5-trisubstituted pyrimidines with conserved fluorine atom at the C5 position. The C2 position of pyrimidine was substituted by an amino, aminocyclohexylamino or aminocyclohexanecarboxamido group. The other set of inhibitors consisted of 4,6-disubstituted pyrimidines with the same substituents described above. The CDK7 IC_{50} values of the most active compounds ranged from 20–100 nM; **26** caused a > 80% decrease in CDK7/9 activity tested at 1 and 0.1 μ M concentrations.

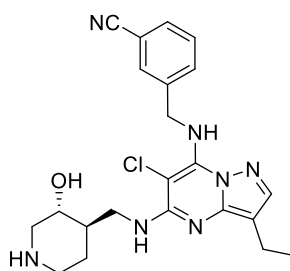
A series of 2-aminopyrimidines substituted with pyrazoles or pyrrolo[1,2-*b*]pyrazoles were disclosed by Beijing Guohong Biomedical Technology [90]. Most compounds showed nanomolar inhibitory activity on both CDK7 and CDK9 and reasonable selectivity over CK1 α [90]. The proliferation of the AML cell lines MV-4-11 and MOLM-13 was inhibited by **27** with IC_{50} values of 94 and 32 nM, respectively. Moreover, the synergistic effect of **27** and the p53 activator eprenetapopt in various tumor cell lines and its pharmacokinetic data have been described.

3.2. Pyrazolopyrimidines

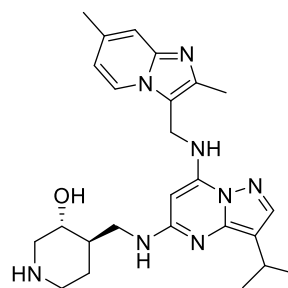
Pyrazolo[1,5-*a*]pyrimidine is a core structure of samuraciclib (CT7001/ICEC0942, **3**), an ATP-competitive, selective inhibitor of CDK7, first-in-class used in clinical trials for the treatment of patients with advanced TNBC, developed by Carrick Therapeutics. In the patent disclosed by the same company, more potent samuraciclib analogs were published [91]. The substitution of ethyl instead of isopropyl at position 3 of the pyrazolo[1,5-*a*]pyrimidine core and introduction of a cyano group to the *meta* position of the benzyl ring in the case of **28** resulted in a 4-fold improvement in CDK7 inhibition in comparison to that of samuraciclib. Furthermore, the presence of a chlorine atom at the pyrazolo[1,5-*a*]pyrimidine C6 position further increased the potency of **29** with a CDK7 IC_{50} value of 4.2 nM and even higher selectivity (CDK2/CDK7 ratio = 571, CDK9/CDK7 ratio = 40). Some derivatives also showed better pharmacokinetic properties in comparison to samuraciclib, such as a lower affinity to human plasma protein and lower efflux ratio, both in two models of multidrug resistant cell lines MDCK-MDR1 and MDCK-BCRP.



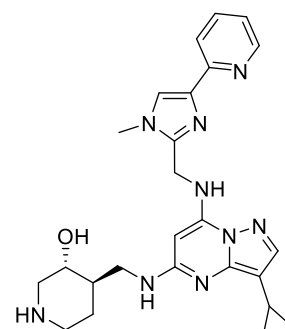
28
(Patented as APPAMP-003)



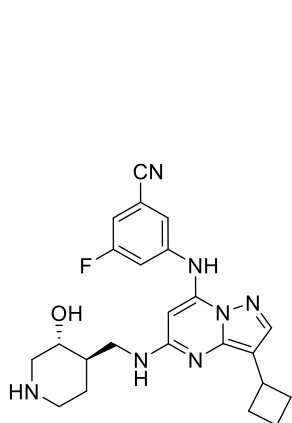
29
(Patented as APPAMP-004)



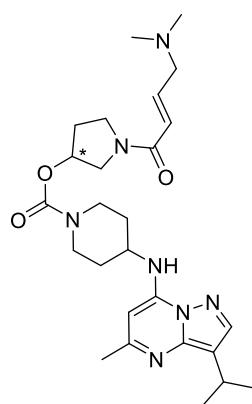
30
(Patented as H-APPAMP-015)



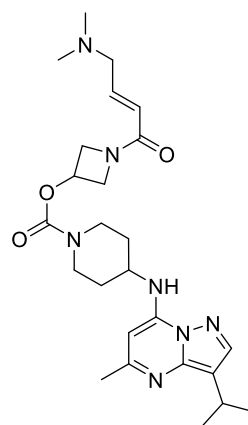
31
(Patented as PPA-024)



32
(Patented as I-55)

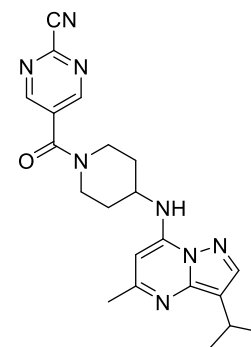


33 (LY3405105)
(Patented as I - mixture of enantiomers)



34
(Patented as II, (*S*)-isomer)

36
(Patented as F10)



35
(Patented as III, (*R*)-isomer)

37
(Patented as SZ-015249)

The same company subsequently presented a series of 45 analogs of samuraciclib, with a benzylamino group at the C7 position substituted with various heterocyclic methylamines [92]. Their inhibitory activity was tested on CDK7 and CDK12, and most compounds showed higher preferences for CDK12. However, compound **30** with a 2,7-dimethylimidazo[1,2-*a*]pyridine-3-methylamino substituent effectively and selectively inhibited CDK7 with an IC_{50} value of 3 nM and a CDK7/CDK12 ratio of 0.01.

Another group of structurally related inhibitors invented by Carrick Therapeutics showed similar activity and selectivity toward CDK7 and CDK12 [93]. The C3 and C5 positions of the pyrazolo[1,5-*a*]pyrimidine core were occupied by substituents similar to those in the previous group, whereas the C7 position was substituted by various heterobiaryl methylamino functionalities. Five compounds showed CDK7 IC_{50} values < 100 nM and CDK7/CDK12 ratios from 1 to 4. The highest CDK7 inhibitory activity was observed in **31** with an IC_{50} value = 17 nM (CDK7/12 = 2.8). Moreover, compound **31** inhibited the viability of A673 cells with IC_{50} = 96.4 nM.

The Translational Genomics Research Institute disclosed another series of potent CDK7 inhibitors structurally related to samuraciclib [94]. The differences from samuraciclib include modifications of all three substituted positions. The hydroxypiperidin-4-ylmethylamine moiety at the C5 position was replaced by piperidin-3-ylamino or piperidin-3-yloxy groups in some compounds, and isopropyl at the C3 position was changed to cyclopropyl or cyclobutyl. Finally, C7 benzylamine was shortened to substituted aniline (e.g. **32**). Several compounds exhibited CDK7 IC_{50} values up to 100 nM. Unfortunately, no information regarding the compound selectivity or activity on cancer cell lines was provided. Much more distinct compounds built on pyrazolo[1,5-*a*]pyrimidine were described in the patent application prepared by Eli Lilly and Company [95]. This document describes the clinical candidate LY3405105 (**33**) and its *S* (**34**) and *R* (**35**) enantiomers. The substitution at the C5 position on the pyrazolo[1,5-*a*]pyrimidine ring was limited to a methyl group, and benzylamine at the C7 position was replaced by a 4-aminopiperidine moiety. This substituent was further equipped with an α,β -unsaturated carbonyl head (intended for covalent attachment to a cysteine residue on CDK7), which was attached via a pyrrolidin-3-yloxy carbonyl bridge. LY3405105 and **35** displayed IC_{50} values of 17.3 nM and 48.7 nM without preincubation with CDK7 and 2.37 nM and 5.06 nM after 3 h preincubation, respectively. The compounds reduced the phosphorylation of Ser5 in the RNAP II CTD and transcription of *c-Myc*. The selectivity of LY3405105 was tested in a panel of 320 kinases; however, the results were shown only for a set of 11 CDKs. LY3405105 was interestingly selective for CDK7 (IC_{50} = 93 nM), with IC_{50} values equal to 2.83 μ M (CDK4), 6.32 μ M (CDK9), 7.41 μ M (CDK19), 8.08 μ M (CDK6), and > 9 μ M for the other CDKs. The proliferation inhibition of various cancer cell lines was dose dependent, with IC_{50} values ranging from 14–48 nM. In addition, LY3405105 demonstrated significant activity in several human cancer xenograft models.

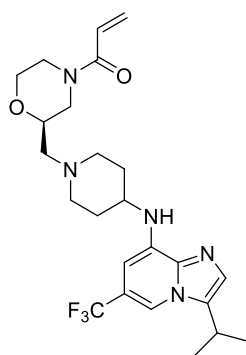
The results of antiproliferative and growth inhibition studies of more than 150 cancer cell lines indicated that loss-of-function mutations in the *ARID1A*, *KMT2C* or *RB1* genes represent potential biomarkers for possible patient selection strategies. In 2018, LY3405105 entered a phase I clinical trial for solid tumors (NCT03770494), but the trial was terminated due to a lack of sufficient efficacy.

One highly potent and selective CDK7 inhibitor, **36**, that is structurally closely related to LY3405105 was presented by Longtaishen Medical Technology [96]. The substitution of the pyrrolidine ring by azetidine slightly increased the CDK7 potency compared to both parent molecule enantiomers. The application of compound **36** at 10 and 200 nM concentrations resulted in 41% and 93% decreases in CDK7 activity, respectively. No such strong inhibitory effect was observed in the other CDKs (CDK1/2/4/6/9) even at a 1 μ M concentration. In comparison to the *S*-enantiomer of homologous LY3405105 (**34**), compound **36** displayed a higher antiproliferative effect both *in vitro* in MDA-MB-231, MDA-MB-468, A549, and NCI-H1299 cancer cell lines and *in vivo* in nude mouse xenografts.

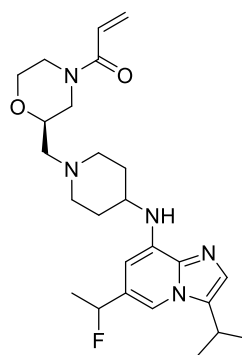
The last group of CDK7 inhibitors with this core was revealed by Suzhou Sinovent Pharmaceutical Technology [97]. These compounds are structurally related to compounds **33** and **36** from the previous patents with isopropyl, methyl and piperidine-4-ylamino groups at the C3, C5 and C7 positions of the pyrazolo[1,5-*a*]pyrimidine core, respectively. However, different aromatic heterocycles bearing cyano group were attached to the nitrogen atom of the piperidine or aminocyclohexyl moiety via amide bond. The IC_{50} values of CDK7 inhibition were determined after 60 min of incubation of the inhibitor with the enzyme, and the most potent compounds reached single-digit nanomolar activity (e.g. **37**).

3.3. Imidazopyridines

A small group of imidazopyridine derivatives, developed as analogs of the mentioned pyrazolo[1,5-*a*]pyrimidine LY3405105 (**33**) [95], were described by Eli Lilly and Company [98]. The compounds effectively inhibited CDK7 in the nanomolar range, whereas CDK9 was inhibited in the micromolar range. Moreover, the IC_{50} values of CDK7 decreased approximately 10 times when the enzyme was preincubated with the compounds for 3 hours (66 nM and 6 nM, respectively), indicating the expected irreversible mechanism of inhibition. The selectivity toward CDK7 over CDK9 was also confirmed by a mechanistic analysis of the inhibition of RNAP II CTD phosphorylation at Ser5 over Ser2 as target sites for CDK7 and CDK9, respectively; the data correlated with the biochemical assays. Compound **38** was chosen for screening in a panel of 468 human kinases, revealing great selectivity for CDK7; the only kinase with a residual activity less than 35% was CDK7 (residual activity of 4% at 0.2 μ M). The *in vitro* and *in vivo* effect were analyzed with compound **39**. This compound potently inhibited cell proliferation in the low nanomolar range and showed efficacy in breast xenografts.



38
(Patented as 8)

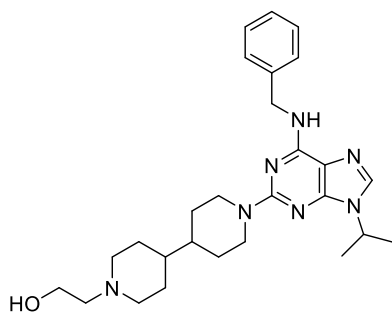


39
(Patented as 1)

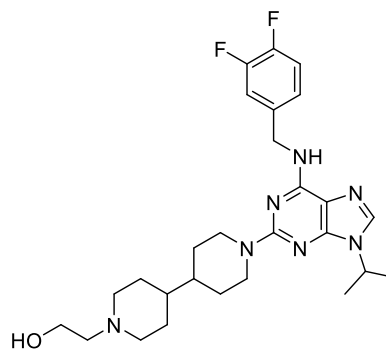
3.4. Purines

Some of the first CDK inhibitors, such as roscovitine (**1**), were identified among trisubstituted purines. Although these compounds had relatively low selectivity across CDKs, Tianjin University of Science and Technology developed isoform-specific purine derivatives as CDK7 inhibitors [99]. Trisubstituted derivative **40** was assayed against a broad spectrum of kinases and inhibited CDK7 activity by 88%. The other tested kinases were inhibited by less than 50%, with the exception of CLK2

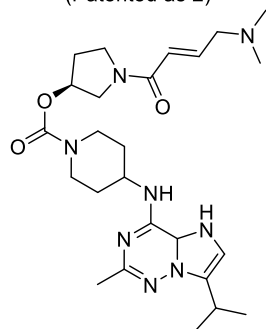
and CLK4 kinases, which were inhibited by 90 and 92%, respectively. In proliferation assays, this compound was shown to be less effective with IC_{50} values in the micromolar range. Another compound, **41**, was the most effective in *in vitro* tests, with IC_{50} values in the nanomolar range in most tested cell lines. The application of **41** also effectively inhibited angiogenesis (HUVECs, chicken embryo chorioallantoic membrane vascular experiment). However, no information regarding the selectivity of this compound was presented.



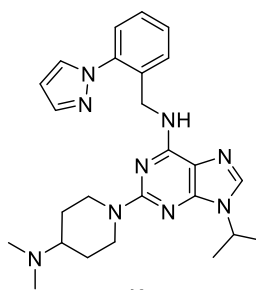
40
(Patented as 2)



41
(Patented as 9)



42
(Patented as SZ-015268)



43
(Patented as VII-3)

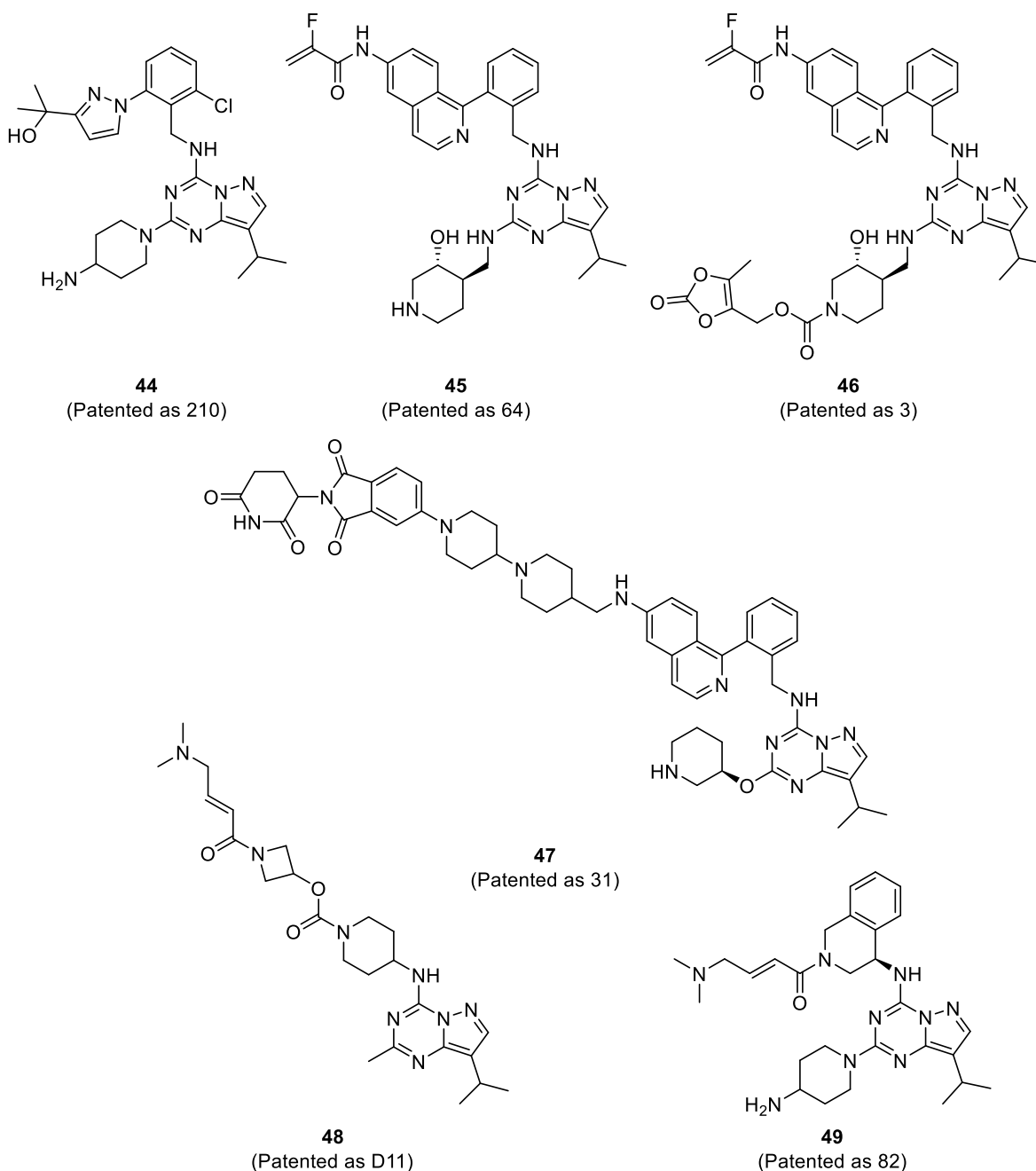
Suzhou Sinovent Pharmaceuticals presented a group of compounds with purine and various isosteric heterocyclic cores [100]. The tested compounds inhibited CDK7 activity and the proliferation of HCC70 and OVCAR-3 cells in the nanomolar range, but no additional data regarding selectivity were presented. Compound **42** belongs to the purine-isosteric imidazo[2,1-*f*][1,2,4]triazines and was the most potent compound with an IC_{50} = 23.6 nM for the inhibition of CDK7. It also inhibited cell proliferation at similar concentrations and was shown to be effective in HCT-116 colon xenograft models.

Additionally, Taizhou EOC Pharma claimed over one hundred potential CDK7 inhibitors based on several heterocyclic

motifs, including purines and isosteric heterocycles [101]. The pattern of substitutions clearly corresponds to LDC4297 (**5**). Approximately twenty tested compounds were potent toward CDK7 with IC_{50} values below 100 nM, but the selectivity is unknown. The example purine derivative **43** showed efficacy in breast (MCF7, T47D, and HCC70) and ovarian (OVCAR-3) cancer cell lines with IC_{50} values below 200 nM.

3.5. Pyrazolotriazines

Large and attractive series of pyrazolo[1,5-*a*] [1,3,5] triazine and pyrazolo[1,5-*a*]pyrimidine derivatives related to roscovitine



(1), samuraciclib (**3**) and especially LDC4297 (**5**) were disclosed by Qurient along with the Lead Discovery Center [102,103]. The most interesting reversible compounds inhibit CDK7 with IC_{50} values below 100 nM and simultaneously show at least 200-fold selectivity over CDK1, CDK2, and CDK5 [102]. Compound **44** was further profiled in a panel of 28 different CDK/cyclin complexes, revealing that the IC_{50} of CDK7 was 15 nM, whereas the other CDKs were much less sensitive ($IC_{50} > 3 \mu M$). Compound **44** also showed efficacy in several cancer cell lines and an OVCAR-3 xenograft model. Covalent compounds, from the second patent [103], are structurally similar to the above mentioned library but all possess the usual Michael acceptor within the side chain pointing outward the active site of CDK7 supposed to attack its Cys312 (example **45**). It is claimed that these compounds display more than 500-fold selectivity for CDK7 over CDK1/2/5. Their proliferation potency was demonstrated in H460, MV4-11, and A2780 cell lines, which were blocked by sub/micromolar concentrations.

Compound **45** was further optimized by Qurient, who prepared twenty prodrugs of **45** with improved ADME parameters [104]. The described prodrugs of **45** bear various groups modifying the hydroxyl or cyclic amine of the piperidine, such as acyls, carboxylates, valine, etc. The pharmacokinetic parameters after oral administration were substantially improved, and the application of **46** (40 mg/kg qd) displayed the strongest antitumor effect in A2780 xenografts in mice among the five tested prodrugs.

Qurient remained focused on pyrazolotriazine derivatives and recently presented a set of CDK7 degraders [105]. The compounds contain either VHL or CRBN ligands attached at various positions to the CDK7 inhibitor via linkers of different lengths and structures. Most presented compounds potently ($IC_{50} < 100$ nM) and selectively inhibited CDK7 (more than 500-fold selectivity over CDK1, CDK2 and CDK5). The authors claim that the compounds also exhibit high affinity to E3 ubiquitin ligase (K_D typically ≤ 100 nM), although the data were not shown. The application of the compounds to the A2780 cell line resulted in a dose-dependent degradation of CDK, and the most potent compounds exhibited a half-maximal degradation concentration (DC_{50}) < 100 nM. The

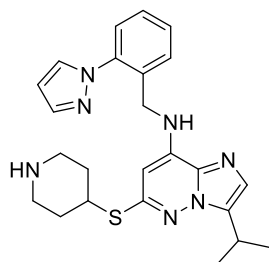
strongest effect was observed with **47**, which caused a large decrease in the CDK7 levels at 12 nM.

Another set of pyrazolo[1,5-*a*][1,3,5]triazine derivatives was developed by Longtaishen Medical Technology [96,106]. The example compounds bear isopropyl or methyl moieties at the 2 and 8 positions, respectively, and a long chain at the 4-position containing an unsaturated carbonyl moiety, supposedly positioned to bind Cys312 of CDK7. The authors several potent CDK7 inhibitors with selectivity over CDK1, CDK2, CDK4, CDK6, and CDK9. Compound **48** [96] inhibited CDK7 by 95% at 200 nM. The other tested kinases were inhibited by less than 34% when applied at 1000 nM. In addition, **48** showed *in vitro* and *in vivo* anticancer activity. Compounds substituted similarly are claimed by Shanghai Lingda Biomedical, who presented a hundred pyrazolo[1,5-*a*][1,3,5]triazines with low nanomolar potency against CDK7 and some selectivity over CDK9 [107]. Compound **49** belongs to the most potent derivatives with $IC_{50} = 2.4$ nM, but additional selectivity profiling and *in vitro* or *in vivo* data were not shown.

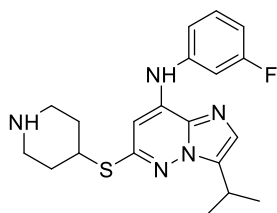
3.6. Imidazopyrazines and imidazopyridazines

Additional isosteres of LDC4297 (**5**) with imidazo[1,2-*a*]pyrazines and imidazo[1,2-*b*]pyridazine skeletons were prepared by the Translation Genomics Research Institute [108]. These compounds share structural similarity to LDC4297, with correspondingly positioned isopropyl and piperidine and pyrazolylphenyl moiety (e.g. **50**), which was even reduced to small function on the phenyl (e.g. **51**). Most compounds are characterized by potency against CDK7 ($IC_{50} < 100$ nM), but information regarding selectivity was not provided. The antiproliferative activity of selected compounds was determined in a panel of six cell lines with different origins (MiaPaCa2, HPAC, Kasumi1, MDA-MB-231, A2780, and A673); $GI_{50} < 1 \mu M$ illustrates the effect of the most potent compound **51**.

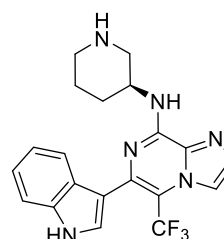
Completely differently substituted imidazo[1,2-*a*]pyrazines were claimed by Scinnohub Pharmaceutical [109]. Only information regarding the potency to CDK7 is mentioned, and 27 compounds display IC_{50} values below 10 nM. The nanomolar inhibition value ($GI_{50} = 10$ nM) in the antiproliferative assay of A2780 cells is also presented for the most potent derivative **52**.



50
(Patented as 62)



51
(Patented as 44)



52
(Patented as 43)

3.7. Dihydropyrrolopyrazoles

The Dana Faber Cancer Institute introduced a library of YKL-5-124 (**12**) derivatives containing 33 compounds with covalent binding moiety [110]. Most compounds bear methyl on the pyrazole ring and the phenyl ring, bearing the reactive allyl group is replaced by various other cycles, such as in **53**. The potency of CDK7 is characterized by an IC_{50} value < 100 nM. Another patent [111] showed both covalent and reversible inhibitors, with **54** as the most potent example with $IC_{50} = 10.8$ nM for CDK7 and > 4.5 μ M for both CDK2 and CDK9.

YKL-5-124 also served as a basis for development of several proteolysis targeting chimeras (PROTACs) [112]. These conjugates should represent a set of new chemical tools for CDK7 knockdown and may provide a potential treatment modality for CDK7-associated cancers and autoimmune disorders. In total, 34 pyrrolo[3,4-*c*]pyrazole derivatives were claimed, and their potency at 1 μ M in Jurkat cells was screened by a western blot analysis, leading to the identification of lead **55**. Proteasome-dependent CDK7 degradation as an expected mechanism of action was confirmed by additional experiments.

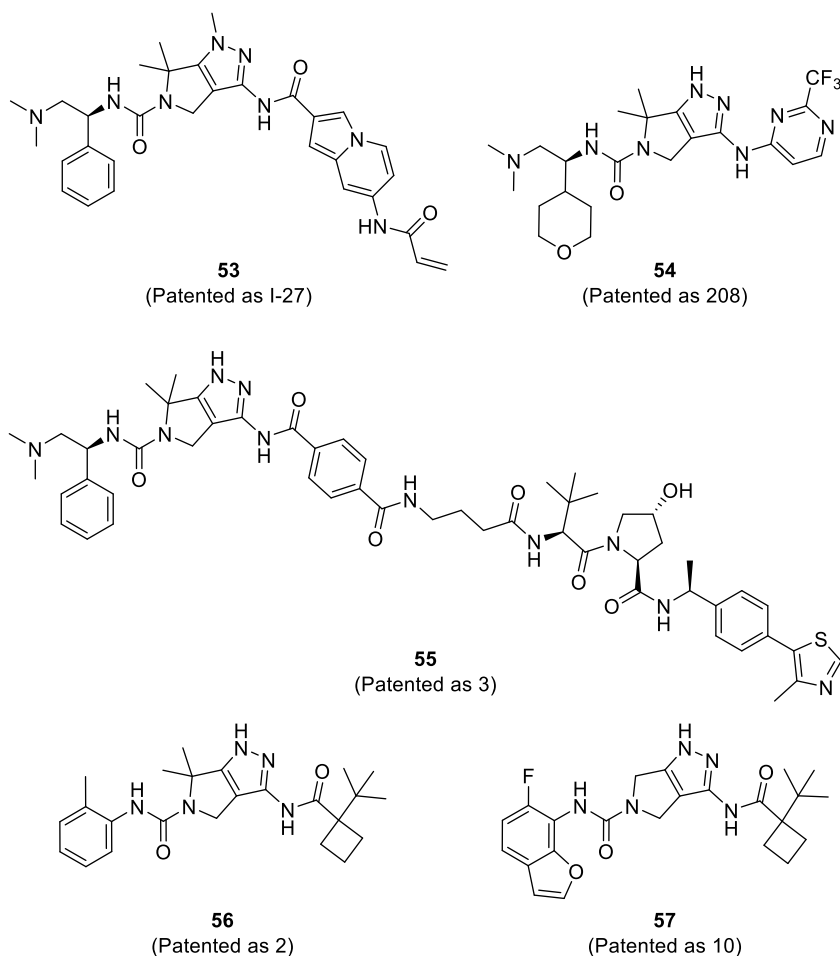
Also Ube Industries reported a series of 11 inhibitors built on the dihydropyrrolopyrazole core that are also structurally related to YKL-5-124 (**56** and **57**) [113]. The authors described not only

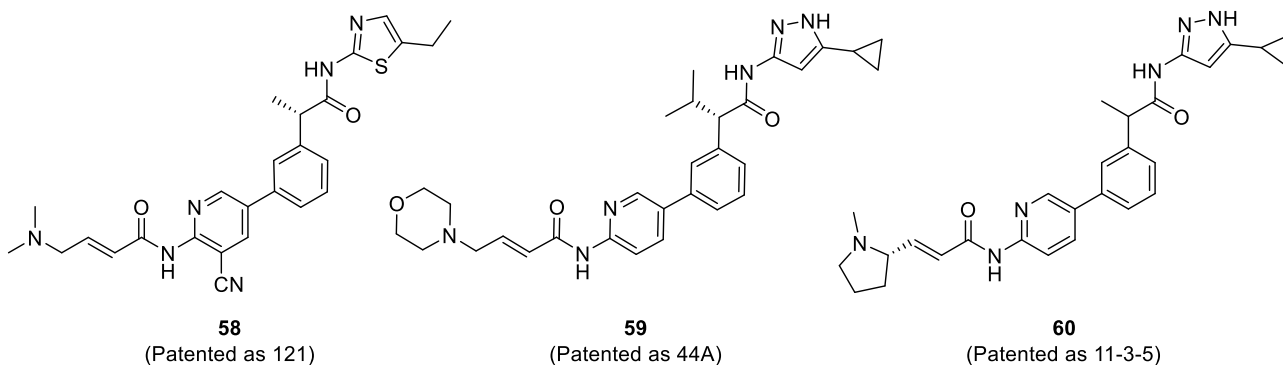
promising CDK7 inhibitory activities with K_i values ≤ 50 nM and selectivity over PLK1 and CDK2 ($K_i \geq 5$ μ M or $K_i \geq 300$ nM, respectively) but also preliminary *in vivo* data.

3.8. Phenylpyridines

Phenylpyridine derivatives with a typical reactive enone moiety in the side chain disclosed by the Korean company Yungjin Pharmaceutical (who developed clinical candidate YPN-005) display high CDK7 inhibitory activity with IC_{50} values in the single digit nanomolar range [114–116]. The compounds have low inhibitory activity against CDK2 and CDK5 with supposedly high selectivity based on an assay of a set of 468 kinases. The proliferation of all cancer cell lines is blocked by nanomolar doses; compound **58** exhibited an increased effect on cancer cell lines derived from AML with $GI_{50} < 1$ nM. These compounds also reduced the phosphorylation level of RNAP II CTD and the expression of c-Myc and Mcl-1 in cancer cells [114].

Similar derivatives, but with limited information regarding their potency and selectivity against CDK7 [117,118], were reported by Aurigene Discovery Technologies, who developed one of the clinically tested CDK7 inhibitors XL102 (mentioned in chapter 2). Example inhibitor **59** [118] inhibited the proliferation





of DU-145 cells and showed a synergistic effect with docetaxel. Finally, Longtaishen Pharmaceutical Technology presented phenylpyridine derivatives, and some of them potently inhibited CDK7; for example, the application of 0.2 μM compound **60** resulted in a 99% decrease in CDK7 activity [119].

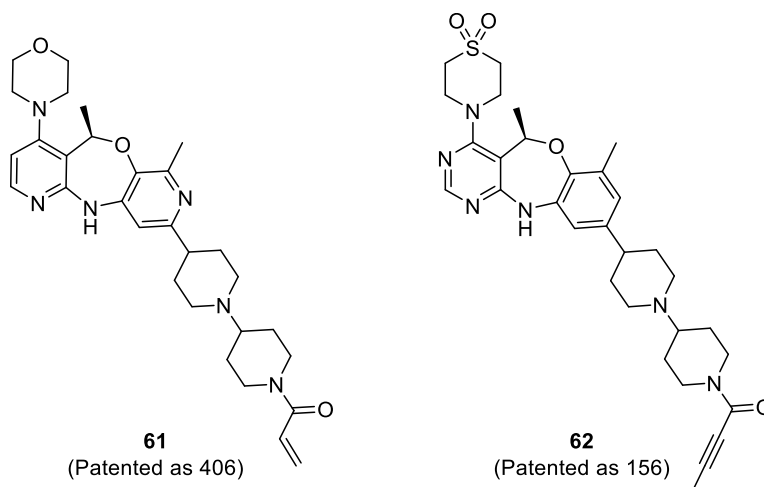
3.9. Tricyclic 1,4-oxazepines

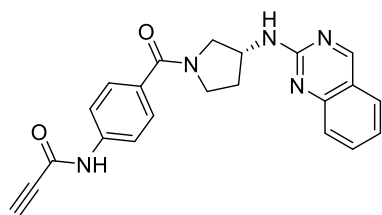
Highly original compounds that are structurally distinct from most other CDK inhibitors have been developed by Janssen Pharmaceutica; these compounds were constructed on a tricyclic core containing 1,4-oxazepine [120,121]. The first group of inhibitors contains mostly 4-morpholinylpyridine fused by 7-methyl-1,4-oxazepine to a phenyl or pyridyl ring, which is further substituted by two linked nonaromatic heterocycles terminated with an α,β -unsaturated carbonyl warhead as in compound **61** [120]. In the other group of Janssen inhibitors [121], 4-morpholinylpyridine was replaced by 4-thiomorpholinylpyrimidine as in compound **62**. Both compound series were tested to detect their antiproliferative activity using an isogenic cell line pair expressing wild-

type CDK7 or its C312S mutant designed to be insensitive to covalent binders. Whereas the IC_{50} values of the inhibition of wild-type CDK7 were in the single-digit nanomolar range, the mutant was dramatically less sensitive ($> 10 \mu\text{M}$), confirming the mode of action of the inhibitors.

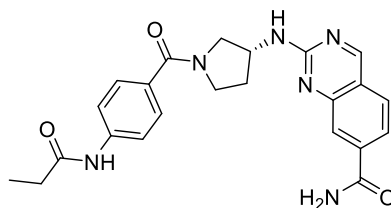
3.10. Quinazolines and pyridopyrimidines

This chapter summarizes two groups of structurally distinct compounds consisting of two fused six-membered rings. The inhibitors from the first group, disclosed by Kinnate Biopharm, were based on quinazoline, isoquinoline or dihydropyrido[2,3-*d*]pyrimidine scaffolds [122]. The side chains attached to the heterocyclic core and terminated with propionic acid residues or different warheads for covalent modifications (acrylamide, 4-dimethylaminobut-2-enamide, propiolamide or vinylsulfonamide) were formed primarily by 4-aminobenzoylpyrrolidin-3-ylamino or 4-aminobenzoylpiperidin-3-ylamino groups (e.g. **63**). The CDK inhibitory activity was tested in recombinant CDK2, CDK7 and CDK12. The compounds were able to inhibit all these CDK isoforms but with preferences for CDK12. The highest activity was observed in **64**, which had the IC_{50} values below 100 nM

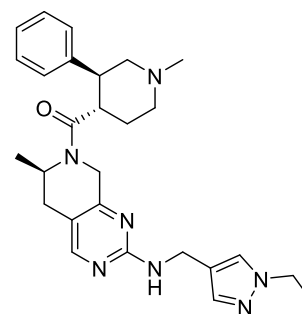




63
(Patented as 70)



64
(Patented as 57)



65
(Patented as 58)

for all tested CDKs. Interestingly, in the case of compound **64**, the 4-aminobenzoylpyrrolidine-3-ylamino was modified by a propionic acid residue instead of an α,β -unsaturated carbonyl or vinyl-sulfonamide reactive group.

The other group of more than 200 potent CDK7 inhibitors structurally based on 1,2,3,4-tetrahydro-2,6-naphthyridine or 5,6,7,8-tetrahydropyrido[3,4-*d*]pyrimidine, including for example **65**, was disclosed by Janssen Pharmaceutica [123]. Various *N*-alkyl-3-phenylpiperidin-4-carbonyl functionalities were attached to the nitrogen atom on the saturated ring of the core heterocycle, whereas the pyrimidine ring was substituted by diverse cyclic/heterocyclic amines or heterocyclic methylamines. The compounds displayed high CDK7 inhibitory activity with IC_{50} values in the single-digit nanomolar range. Moreover, the prepared compounds effectively inhibited the phosphorylation of Ser5 in the RNAP II CTD in A549 cells. Nevertheless, no information regarding the compounds' selectivity or anti-proliferative activity was provided.

4. Conclusion

The interest in pursuing CDK7 as a therapeutic target has been ongoing for at least one decade, and significant progress has been achieved in the past few years. The field of CDK7 inhibitors is continuously growing, spanning diverse chemical classes and promising kinase selectivity. In addition, the available compounds possess different mechanisms of inhibition, including conventional competition, irreversible binding and specific induction of CDK7 degradation by heterobifunctional compounds. The new compounds disclosed in 58 patent applications published during the reviewed period, i.e. from 2018 to 2022, span over 15 chemotypes. We classified and summarized the chemical structures and their biochemical and biological properties, providing researchers with a comprehensive update of the field, including exciting clinical candidates.

5. Expert opinion

Cancer cells often display transcriptional addiction, i.e. a state in which they are critically dependent on the continuous production of short life time transcripts, their processing and stability,

including those encoding antiapoptotic proteins and oncogenic transcription factors. This, together with the high expression of CDK7 in many cancer types, provides a strong rationale for examining this kinase as a possible target and in parallel stimulates the development of its modulators as drugs for oncology.

In fact, this possibility has been investigated since the discovery that the early generation of pan-selective CDK inhibitors not only block the cell cycle but also potently inhibit transcriptional CDKs (tCDKs). Although early inhibitors usually lacked biochemical selectivity, showed connected toxicities and complicated the understanding of the importance of tCDKs in the antitumor response, they significantly contributed to gaining knowledge regarding the involvement of tCDKs in cancer biology. Intense research has partly solved problems related to potency and selectivity, at least toward some CDKs, such as CDK4-targeting palbociclib or ribociclib, which have been eventually approved as drugs. These stories clearly confirm that selectivity can be obtained even within closely related enzymes of the CDK family.

Luckily, CDK7 also belongs to kinases for which promising inhibitors were developed. At least partly, this has been possible due to the presence of a unique cysteine residue located at the entry to the active site of CDK7, which is tractable by irreversible binders. Although covalent drugs often display significant off-target toxicities related to the presence of reactive function, the first CDK7 irreversible inhibitor, SY-1365 (**8**), has already reached clinical trials, followed by other candidates, such as Q901 and XL102. The high number of patents for irreversible binders published during the reviewed period indicates an unflagging interest in this field.

Selectivity over other CDKs (and other more distinct kinases) could also be obtained with reversible compounds as in the case of samuraciclib (**3**), SY-5609 (**9**), and other clinical candidates. A wealth of patent applications describing similar inhibitors without a reactive group and acting as ATP competitors were also published during the reviewed period. The results of clinical research will hopefully answer the question of whether the toxicity of covalent compounds is manageable and whether reversible drugs provide higher safety. However, a clear answer could be masked by other pharmacological parameters, including selectivity, which usually contributes to target and off-target activity and toxicity.

Nevertheless, the genetic inactivation of CDK7 shows that it is dispensable for global transcription and does not lead to any negative consequences in adult tissues [124]. This finding can have two interesting and partly contradictory implications, indicating that (i) the toxicity of selective CDK7 inhibitors could be low but also that (ii) selective CDK7 inhibition could be compensated by other kinases, and highly selective compounds could not have a sufficient effect. In particular, the second option raises further questions because not all tCDKs, which could have compensatory roles, are tumor-promoting; under some contexts, they could even have opposite functions (for example, CDK8 also has a tumor suppressive role [125]), and their inactivation thus can be counterproductive.

However, another fascinating concept of CDK7 modulation employs induced protein degradation. Developed PROTACs can shed light on possible compensations. In addition, it could help explore other possible functions of CDK7. Some kinases, including partly related CDK6 and CDK9, also play noncatalytic roles and regulate transcription by providing a protein scaffold for interaction with other transcription regulators [126]. It is tempting to speculate that if CDK7 also belongs to this group of multimodal regulators, not only its degradation but also the inactivation of its enzymatic role could eliminate all possible functions, leading to a more pronounced effect.

A deeper understanding of CDK7 biology, eventually allowing the identification of specific genes selectively dependent on CDK7, could translate into better selection of specific cancer types and improvement of such personalized therapeutic strategies. Interest in potent CDK7 inhibitors is continuing, and we expect that further development will reveal the true value of this therapeutic strategy.

Funding

This paper was funded by the European Union - Next Generation EU (National Institute for Cancer Research, programme EXCELES, Project No. LX22NPO5102), Czech Science Foundation (21-06553S) and Palacký University Olomouc (IGA_2022_007).

Declaration of interest

H Shao was supported by the grant from Department of Science & Technology of Hunan Province (2021JJ41015). The authors have no other relevant affiliations or financial involvement with any organization or entity with a financial interest in or financial conflict with the subject matter or materials discussed in the manuscript apart from those disclosed.

Reviewer disclosures

Peer reviewers on this manuscript have no relevant financial or other relationships to disclose.

ORCID

Markéta Kovalová  <http://orcid.org/0000-0001-8394-1700>

Václav Mik  <http://orcid.org/0000-0002-8515-3035>

Radek Jorda  <http://orcid.org/0000-0002-4905-7126>

Vladimír Kryštof  <http://orcid.org/0000-0001-5838-2118>

References

Papers of special note have been highlighted as either of interest (*) or of considerable interest () to readers.**

- Satyanarayana A, Kaldis P. Mammalian cell-cycle regulation: several Cdks, numerous cyclins and diverse compensatory mechanisms. *Oncogene*. 2009;28 :2925–2939.
- Fisher RP. Cdk7: a kinase at the core of transcription and in the crosshairs of cancer drug discovery. *Transcription*. 2019;10:47–56.
- Asghar U, Witkiewicz AK, Turner NC, et al. The history and future of targeting cyclin-dependent kinases in cancer therapy. *Nat Rev Drug Discov*. 2015;14:130–146.
- Akhtar MS, Heidemann M, Tietjen JR, et al. TFIIH kinase places bivalent marks on the carboxy-terminal domain of RNA polymerase II. *Mol Cell*. 2009;34:387–393.
- Vervoort SJ, Devlin JR, Kwiatkowski N, et al. Targeting transcription cycles in cancer. *Nat Rev Cancer*. 2022;22:5–24. .
- Comprehensive review about transcriptional CDKs and their inhibition**
- Larochelle S, Amat R, Glover-Cutter K, et al. Cyclin-dependent kinase control of the initiation-to-elongation switch of RNA polymerase II. *Nat Struct Mol Biol*. 2012;19:1108–1115.
- Choi YJ, Kim DH, Yoon DH, et al. Efficacy of the novel CDK7 inhibitor QS1189 in mantle cell lymphoma. *Sci Rep*. 2019;9:7193.
- Li B, Ni Chonghaile T, Fan Y, et al. Therapeutic rationale to target highly expressed CDK7 conferring poor outcomes in triple-negative breast cancer. *Cancer Res*. 2017;77:3834–3845.
- Zhang Y, Zhou L, Bandyopadhyay D, et al. The covalent CDK7 inhibitor THZ1 potently induces apoptosis in multiple myeloma cells in vitro and in vivo. *Clin Cancer Res*. 2019;25:6195–6205.
- Patel H, Periyasamy M, Sava GP, et al. ICEC0942, an orally bioavailable selective inhibitor of CDK7 for cancer treatment. *Mol Cancer Ther*. 2018;17:1156–1166.
- Naseh G, Mohammadifard M, Mohammadifard M. Upregulation of cyclin-dependent kinase 7 and matrix metalloproteinase-14 expression contribute to metastatic properties of gastric cancer. *IUBMB Life*. 2016;68:799–805.
- Zhang Z, Peng H, Wang X, et al. Preclinical efficacy and molecular mechanism of targeting CDK7-dependent transcriptional addiction in ovarian cancer. *Mol Cancer Ther*. 2017;16:1739–1750.
- Jiang L, Huang R, Wu YP, et al. Overexpression of CDK7 is associated with unfavourable prognosis in oral squamous cell carcinoma. *Pathology*. 2019;51:74–80.
- Meng W, Wang JJ, Wang BC, et al. CDK7 inhibition is a novel therapeutic strategy against GBM both in vitro and in vivo. *Cancer Manag Res*. 2018;10:5747–5758.
- Tsang FH, Law CT, Tang TC, et al. Aberrant super-enhancer landscape in human hepatocellular carcinoma. *Hepatology*. 2019;69:2502–2517.
- Chipumuro E, Marco E, Christensen CL, et al. CDK7 inhibition suppresses super-enhancer-linked oncogenic transcription in MYCN-driven cancer. *Cell*. 2014;159:1126–1139.
- Lee DK, Duan HO, Chang C. From androgen receptor to the general transcription factor TFIIH. Identification of cdk activating kinase (CAK) as an androgen receptor NH(2)-terminal associated coactivator. *J Biol Chem*. 2000;275:9308–9313.
- Chen D, Riedl T, Washbrook E, et al. Activation of estrogen receptor alpha by S118 phosphorylation involves a ligand-dependent interaction with TFIIH and participation of CDK7. *Mol Cell*. 2000;6:127–137.
- Zhang H, Christensen CL, Dries R, et al. CDK7 inhibition potentiates genome instability triggering anti-tumor immunity in small cell lung cancer. *Cancer Cell*. 2020;37:37–54.
- Wang J, Zhang R, Lin Z, et al. CDK7 inhibitor THZ1 enhances antiPD-1 therapy efficacy via the p38alpha/MYC/PD-L1 signaling in non-small cell lung cancer. *J Hematol Oncol*. 2020;13:99.
- Mi Z, Song Y, Cao X, et al. Super-enhancer-driven metabolic reprogramming promotes cystogenesis in autosomal dominant polycystic kidney disease. *Nat Metab*. 2020;2:717–731.
- Yang B, Zhang H, Li N, et al. Discovery of novel N-(5-(Pyridin-3-yl)-1H-indazol-3-yl)benzamide derivatives as potent cyclin-dependent

- kinase 7 inhibitors for the treatment of autosomal dominant polycystic kidney disease. *J Med Chem.* **2022**;65:15770–15788.
23. Diab S, Yu MF, Wang SD. CDK7 inhibitors in cancer therapy: the sweet smell of success? *J Med Chem.* **2020**;63:7458–7474.
 24. Li ZM, Liu G, Gao Y, et al. Targeting CDK7 in oncology: the avenue forward. *Pharmacol Therapeut.* **2022**;240:1–16. .
 - **Recent review on CDK7, its role in cancer and current progress in CDK7 inhibitors**
 25. Teng Y, Lu K, Zhang Q, et al. Recent advances in the development of cyclin-dependent kinase 7 inhibitors. *Eur J Med Chem.* **2019**;183:111641.
 26. Ali S, Heathcote DA, Kroll SHB, et al. The development of a selective cyclin-dependent kinase inhibitor that shows antitumor activity. *Cancer Res.* **2009**;69:6208–6215.
 27. Wang BY, Liu QY, Cao J, et al. Selective CDK7 inhibition with BS-181 suppresses cell proliferation and induces cell cycle arrest and apoptosis in gastric cancer. *Drug Des Devel Ther.* **2016**;10:1181–1189.
 28. Greber BJ, Remis J, Ali S, et al. 2.5 A-resolution structure of human CDK-activating kinase bound to the clinical inhibitor ICEC0942. *Biophys J.* **2021**;120:677–686.
 29. Hazel P, Kroll SH, Bondke A, et al. Inhibitor selectivity for cyclin-dependent kinase 7: a structural, thermodynamic, and modelling study. *ChemMedchem.* **2017**;12:372–380.
 30. Krebs MG, Lord S, Kenny L, et al. 230MO First in human, modular study of samuraciclib (CT7001), a first-in-class, oral, selective inhibitor of CDK7, in patients with advanced solid malignancies. *Ann Oncol.* **2021**;32:S458.
 31. Howell SJ, Krebs MG, Lord S, et al. 265P Study of samuraciclib (CT7001), a first-in-class, oral, selective inhibitor of CDK7, in combination with fulvestrant in patients with advanced hormone receptor positive HER2 negative breast cancer (HR+BC). *Ann Oncol.* **2021**;32:S477–8.
 32. Kelso TW, Baumgart K, Eickhoff J, et al. Cyclin-dependent kinase 7 controls mRNA synthesis by affecting stability of preinitiation complexes, leading to altered gene expression, cell cycle progression, and survival of tumor cells. *Mol Cell Biol.* **2014**;34:3675–3688.
 33. Kwiatkowski N, Zhang T, Rahl PB, et al. Targeting transcription regulation in cancer with a covalent CDK7 inhibitor. *Nature.* **2014**;511:616–620.
 34. Olson CM, Liang Y, Leggett A, et al. Development of a selective Cdk7 covalent inhibitor reveals predominant cell-cycle phenotype. *Cell Chem Biol.* **2019**;26:792–803.
 35. Greber BJ, Perez-Bertoldi JM, Lim K, et al. The cryoelectron microscopy structure of the human CDK-activating kinase. *Proc Natl Acad Sci U S A.* **2020**;117:22849–22857.
 36. Christensen CL, Kwiatkowski N, Abraham BJ, et al. Targeting transcriptional additions in small cell lung cancer with a covalent CDK7 inhibitor. *Cancer Cell.* **2014**;26:909–922.
 37. Eliades P, Abraham BJ, Ji ZY, et al. High MITF expression is associated with super-enhancers and suppressed by CDK7 inhibition in melanoma. *J Invest Dermatol.* **2018**;138:1582–1590.
 38. Zhou L, Zhang Y, Sharma K, et al. Targeting transcriptional regulation in multiple myeloma with a covalent CDK7 inhibitor THZ1. *Cancer Res.* **2018**;78:4836.
 39. Wang Y, Zhang T, Kwiatkowski N, et al. CDK7-dependent transcriptional addiction in triple-negative breast cancer. *Cell.* **2015**;163:174–186.
 40. Hu S, Marineau JJ, Rajagopal N, et al. Discovery and characterization of SY-1365, a selective, covalent inhibitor of CDK7. *Cancer Res.* **2019**;79:3479–3491.
 41. Hodgson G, Johannessen L, Rajagopal N, et al. Sy-1365, a potent and selective CDK7 inhibitor, exhibits anti-tumor activity in preclinical models of hematologic malignancies, and demonstrates interactions with the BCL-XL/BCL2 mitochondrial apoptosis signaling pathway in leukemia. *Blood.* **2017**;130:2651.
 42. Rajagopal N, Hodgson G, Hu S, et al. Abstract P1-09-08: BCL2L1 (BCL-XL) expression and MYC super-enhancer positivity predict sensitivity to the covalent CDK7 inhibitor SY-1365 in triple negative breast cancer (TNBC) cell lines. *Cancer Res.* **2018**;78:1098.
 43. Konstantinopoulos PA, Hodgson G, Rajagopal N, et al. Abstract 1525: sY-1365, a selective CDK7 inhibitor, exhibits potent antitumor activity against ovarian cancer models in vitro and in vivo. *Cancer Res.* **2018**;78:1525.
 44. Hu S, Ke N, Ren Y, et al. Abstract 1151: sY-1365, a potent and selective CDK7 inhibitor, exhibits promising anti-tumor activity in multiple preclinical models of aggressive solid tumors. *Cancer Res.* **2017**;77:1151.
 45. Shapiro G, Papadopoulos KP, Do KT, et al. Trial design of a first-in-human phase 1 evaluation of SY-1365, a first-in-class selective CDK7 inhibitor, with initial expansions in ovarian and breast cancer. *J Clin Oncol.* **2018**;36:TPS2600.
 46. Juric D, Papadopoulos KP, Tolcher A, et al. Proof-of-mechanism based on target engagement and modulation of gene expression following treatment with SY-1365, a first-in-class selective CDK7 inhibitor in Phase 1 patients with advanced cancer. *Eur J Cancer.* **2018**;103:E19.
 47. Syros Pharmaceuticals, Inc. Prioritizing development of SY-5609, its oral CDK7 inhibitor, and discontinuing further development of SY-1365, its intravenous CDK7 inhibitor. *WO2020093011 (2019)*.
 48. Marineau JJ, Hamman KB, Hu SH, et al. Discovery of SY-5609: A selective, noncovalent inhibitor of CDK7. *J Med Chem.* **2022**;65:1458–1480.
 49. Syros Pharmaceuticals, Inc. Inhibitors of cyclin-dependent kinase 7 (CDK7). *WO2020093011 (2020)*.
 - **Patent describing discovery of clinical candidate SY-5609**
 50. Murray BW, Guo C, Piraino J, et al. Small-molecule p21-activated kinase inhibitor PF-3758309 is a potent inhibitor of oncogenic signaling and tumor growth. *Proc Natl Acad Sci U S A.* **2010**;107:9446–9451.
 51. Rudolph J, Crawford JJ, Hoeflich KP, et al. Inhibitors of p21-activated kinases (PAKs). *J Med Chem.* **2015**;58:111–129.
 52. Kalan S, Amat R, Schachter MM, et al. Activation of the p53 transcriptional program sensitizes cancer cells to Cdk7 inhibitors. *Cell Rep.* **2017**;21:467–481.
 53. Minzel W, Venkatachalam A, Fink A, et al. Small molecules co-targeting cKialpha and the transcriptional kinases CDK7/9 control AML in preclinical models. *Cell.* **2018**;175:171–185.
 54. Chen R, Hassankhani R, Long Y, et al. Discovery of potent inhibitors of cyclin-dependent kinases 7 and 9: design, synthesis, structure-activity relationship analysis and biological evaluation. *Chem Med Chem.* **2023**;18:e202200582.
 55. Yu D, Jeon Y, Park D, et al. Abstract 4855: development of highly selective CDK7 inhibitor Q901 for solid tumors. *Cancer Res.* **2020**;80:4855.
 56. Yu D, Jeon Y, Park D, et al. Abstract 1953: q901, a selective CDK7 inhibitor, a potential new strategy for primary and CDK4/6 inhibitor resistant ER-positive breast cancer. *Cancer Res.* **2021**;81:1953.
 57. Yu D, Jeon Y, Lee S-J, et al. Abstract 2574: q901; a highly selective covalent cdk7 inhibitor inducing substantial anti-tumor effect in a broad spectrum of solid tumor lineages. *Cancer Res.* **2022**;82:2574.
 58. Satyam LK, Poddutoori R, Thiyagarajan S, et al. Potent anti-tumor activity of AUR102, a selective covalent inhibitor of CDK7. *Eur J Cancer.* **2020**;138:S47.
 59. Shapiro G, Barve MA, Bhavne MA, et al. A phase 1 dose-escalation and expansion-cohort study of the oral CDK7 inhibitor XL102 as a single-agent and in combination therapy in patients (pts) with advanced solid tumors. *J Clin Oncol.* **2022**;40:TPS3176.
 60. Choi YJ, Lee H, Kim DS, et al. Discovery of a novel CDK7 inhibitor YPN-005 in small cell lung cancer. *Eur J Pharmacol.* **2021**;907:174298.
 61. Koo B-K, Choi E-J, Hur E-H, et al. Antileukemic activity of YPN-005, a CDK7 inhibitor, inducing apoptosis through c-MYC and FLT3 suppression in acute myeloid leukemia. *Heliyon.* **2022**;8:e11004.
 62. Matsushita T, Onuma K, Sunamoto H, et al. Abstract LB-111: in vitro anti-cancer activity of UD-017, a novel potent & highly selective CDK7 reversible inhibitor. *Cancer Res.* **2017**;77:111.
 63. Onuma K, Aga Y, Ogi S, et al. Preclinical in vitro and in vivo study of UD-017, a novel highly selective and orally available CDK7 inhibitor, in a variety of cancers. *J Clin Oncol.* **2017**;35:e14086.
 64. Aga Y, Ogi S, Onuma K, et al. Abstract 4837: evaluation of anticancer activities of UD-017, a novel selective and orally available CDK7 inhibitor, in blood cancers. *Cancer Res.* **2018**;78:4837.

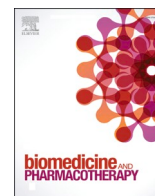
65. Aga Y, Matsushita T, Ogi S, et al. Novel oral derivative UD-017, a highly selective CDK7 inhibitor, exhibits anticancer activity by inducing cell-cycle arrest and apoptosis in human colorectal cancer. *Hiroshima J Med Sci.* 2020;69:23–31.
66. Matsushita T, Ogi S, Onuma K, et al. Abstract 4835: uD-017, a novel highly selective and orally active CDK7 inhibitor, shows a significant anticancer activity in patient-derived cancers. *Cancer Res.* 2018;78:4835.
67. Gao Y, Volegova M, Nasholm N, et al. Synergistic anti-tumor effect of combining selective CDK7 and BRD4 inhibition in neuroblastoma. *Front Oncol.* 2021;11:773186.
68. Chongqing Medical University. CDK kinase inhibitor and application thereof. CN113880772A. 2022.
69. Longtaishen Pharmaceutical Technology (Nanjing) Co., Ltd. Heteroaryl compound, preparation method, pharmaceutical composition and application thereof. CN110698460. 2020.
70. Ancureall Pharmaceutical (Shanghai) Co., Ltd. Pyrimidine compound, preparation method therefor and medical use thereof. WO2019157959. 2019.
71. Suzhou Sinovent Pharmaceutical Technology Co., Ltd. Pyrimidinamine compound, preparation method and application thereof. CN111269217. 2020.
72. Suzhou Sinovent Pharmaceutical Technology Co., Ltd. Polycyclic compound, preparation method and application thereof. CN111303128. 2020.
73. Suzhou Sinovent Pharmaceutical Technology Co., Ltd. Heteroaromatic nitrile compound and application thereof. CN111393415. 2020.
74. Syros Pharmaceuticals, Inc. Inhibitors of cyclin-dependent kinase 7 (cdk7). WO2019143719. 2019.
75. Syros Pharmaceuticals, Inc. Inhibitors of cyclin-dependent kinase 7 (cdk7). WO2019143730. 2019.
76. Syros Pharmaceuticals, Inc. Methods of treating cancer in biomarker-identified patients with inhibitors of cyclin-dependent kinase 7. WO2021087138. 2021.
77. Syros Pharmaceuticals, Inc. Methods of treating cancer in biomarker-identified patients with non-covalent inhibitors of cyclin-dependent kinase. WO2020093006. 2020.
78. Syros Pharmaceuticals, Inc. Methods of treating cancer in patients with an anomalous KRAS gene or deletions within chromosome. WO2021243280. 2021.
79. Syros Pharmaceuticals, Inc. Dosing regimens for cyclin-dependent kinase 7 (CDK7) inhibitors. WO2022082056. 2022.
- **Results of phase I clinical trials of SY-5609.**
80. GT Apeiron Therapeutics, Ltd. Preparation of heteroaromatic compound, pharmaceutical composition and use thereof. WO2022134641. 2022.
81. GT Apeiron Therapeutics, Ltd. Aromatic heterocyclic compound, and pharmaceutical composition and application thereof. WO2022134642. 2022.
82. GT Apeiron Therapeutics, Ltd. Aromatic heterocyclic compound, and pharmaceutical composition and application thereof. TW202225162. 2022.
83. Marineau JJ, Zahler R, Ciblat S, et al. Inhibitors of cyclin dependent kinase 7 (CDK7). WO2018013867. 2018.
84. TYK Medicines, Inc. Compound useful as cdk7 kinase inhibitor and use thereof. WO2022017533. 2022.
85. Jiangsu Hengrui Pharmaceuticals Co., Ltd., Shanghai Hengrui Pharmaceutical Co., Ltd. Pyrimidine derivative, preparation method thereof and application thereof in medicine. CN114907406. 2022.
86. Jiangsu Simcere Pharmaceutical Co., Ltd. Inhibitors of cyclin dependent kinase 7 (CDK7). CN114907407. 2022.
87. Guangzhou Fermion Technology Co., Ltd. Pyrimidyl derivative, preparation method therefor and use thereof. WO2022063212. 2022.
88. Newsoara Biopharma Co., Ltd. Nitrogen-containing heterocyclic compound and application thereof. WO2022089444. 2022.
89. Shanghai Lingda Biomedical Co., Ltd., Shanghai Lingji Biological Technology Co., Ltd. Compound with CDK kinase inhibitory activity, pharmaceutical composition and use thereof. CN114605390. 2022.
90. Beijing Guohong Biomedical Technology Co., Ltd. Heterocyclic compound and pharmaceutical composition thereof and use thereof. WO2021000957. 2021.
91. Carrick Therapeutics, Ltd., Cancer Research Technology, Ltd., Imperial Innovations, Ltd. 4-[[[(7-aminopyrazolo[1,5-a]pyrimidin-5-yl)amino]methyl]piperidin-3-ol compounds as CDK inhibitors. WO2019057825. 2019.
92. Carrick Therapeutics, Ltd. 4-[[[(7-aminopyrazolo[1,5-a]pyrimidin-5-yl)amino]methyl]piperidin-3-ol compounds and their therapeutic use. WO2021122745. 2021.
93. Carrick Therapeutics, Ltd. Substituted pyrazolo[1,5-a]pyrimidine-7-amine compounds as CDK inhibitors and their therapeutic use. WO2022263604. 2022.
94. The Translational Genomics Research Institute. Trisubstituted pyrazolo [1,5-a]pyrimidine compounds as CDK7 inhibitors. WO2020186196. 2020.
95. Eli Lilly and Company. Compounds useful for inhibiting cdk7. WO2019099298. 2019.
- **Patent describing discovery of clinical candidate LY3405105.**
96. Longtaishen Medical Technology (Nanjing) Co., Ltd. Cdk kinase inhibitor, preparation method therefor, pharmaceutical composition, and application. WO2022033552. 2022.
97. Suzhou Sinoway Pharmaceutical Technology Co., Ltd. Pyrimidopyrazole compound, and preparation method and application thereof. CN111393447. 2020.
98. Eli Lilly and Company. Compounds useful for inhibiting CDK7. WO2021242602. 2021.
99. Tianjin University of Science and Technology. Class of biperidine derivatives as antitumor drug. WO2020108407. 2020.
100. Suzhou Sinovent Pharmaceuticals Co., Ltd. Heterocyclic compound, and pharmaceutical composition thereof, preparation method therefor, intermediate thereof and application thereof. WO2021121390. 2021.
101. Taizhou EOC Pharma Co., Ltd. A cyclin-dependent kinase inhibitor. WO2022206795. 2022.
102. Qurient Co., Ltd., Pyrazolo-triazine and/or pyrazolo-pyrimidine derivatives as selective inhibitor of cyclin dependent kinase. WO2019197549. 2019.
103. Qurient Co., Ltd., Pharmaceutically active pyrazolo-triazine and/or pyrazolo-pyrimidine derivatives. WO2019197546. 2019.
104. Qurient Co., Ltd. Compounds having cyclin-dependent kinase(cdk)-inhibitory function. WO2022117504. 2022.
105. Qurient Co., Ltd. Compounds for degradation of cyclin-dependent kinase 7 (CDK7). WO2022248682. 2022.
- **Some of patented compound showed excellent degradation of CDK7 already at low nanomolar concentrations.**
106. Longtaishen Pharmaceutical Technology (Nanjing) Co., Ltd. CDK kinase inhibitor, preparation method, pharmaceutical composition and application thereof. CN112125908. 2020.
107. Shanghai Lingda Biomedical Co., Ltd. Amino-substituted aromatic heterocyclic pyrazole compounds, preparation method and application. CN114805361. 2022.
108. The Translational Genomics Research Institute. Imidazopyridazine and imidazopyrazine compounds as inhibitors of CDK7. WO2022061155. 2022.
109. ScinnoHub Pharmaceutical Co., Ltd. Heterocyclic compound and derivative thereof. WO2021249417. 2021.
110. Dana-Farber Cancer Institute, Inc. Inhibitors of cyclin-dependent kinase 7 and uses thereof. WO2021016388. 2021.
111. Dana-Farber Cancer Institute, Inc. Inhibitors of cyclin-dependent kinase 7 and uses thereof. WO2020140098. 2020.
112. Dana-Farber Cancer Institute, Inc. Degraders of cyclin-dependent kinase 7 (CDK7) and uses thereof. WO2021026109. 2021.
113. Ube Industries, Ltd. Dihydropyrrlopyrazole derivative. WO2020100944. 2020.
114. Yungjin Pharm. Co., Ltd. Novel thiazole derivatives and pharmaceutically acceptable salts thereof. WO2020060112. 2020.
115. Yungjin Pharm. Co., Ltd. Novel CDK7 inhibitory compound or pharmaceutically acceptable salt thereof. WO2021182914. 2021.

116. Yungjin Pharm. Co., Ltd. Pharmaceutical composition for preventing or treating cancer comprising azole derivatives or pharmaceutically acceptable salt thereof. WO2021182918. 2021.
117. Aurigene Discovery Technologies Limited. Process for preparing a CDK inhibitor. WO2022229835. 2022.
118. Aurigene Discovery Technologies Limited. Cancer therapy using a combination of CDK7 inhibitor with an anti-microtubule agent. WO2022084930. 2022.
119. Longtaishen Pharmaceutical Technology (Nanjing) Co., Ltd. Compound, preparation method, pharmaceutical composition and application thereof. CN110590747. 2019.
120. Janssen Pharmaceutica NV. Tricyclic pyridines as cyclin-dependent kinase 7 (CDK7) inhibitors. WO2022189387. 2022.
121. Janssen Pharmaceutica NV. Tricyclic pyrimidines as cyclin-dependent kinase 7 (CDK7) inhibitors. WO2022136174. 2022.
122. Kinnate Biopharma Inc. Inhibitors of cyclin-dependent kinases. WO2019213403. 2019.
123. Janssen Pharmaceutica NV. Cyclin-dependent kinase 7 (CDK7) non-covalent inhibitors. WO2022064009. 2022.
124. Ganuza M, Saiz-Ladera C, Canamero M, et al. Genetic inactivation of Cdk7 leads to cell cycle arrest and induces premature aging due to adult stem cell exhaustion. EMBO J. 2012;31:2498–2510.
125. Wu D, Zhang ZY, Chen X, et al. Angel or Devil ?-CDK8 as the new drug target. Eur J Med Chem. 2021;213:113043.
126. Kung JE, Jura N. Structural basis for the non-catalytic functions of protein kinases. Structure. 2016;24(1):7–24.

PŘÍLOHA II

Kovalová M, Havlíček L, Djukic S, Škerlová J, Peřina M, Pospíšil T, Řezníčková E, Řezáčová P, Jorda R, Kryštof V. (2023) Characterization of new highly selective pyrazolo 4,3-d pyrimidine inhibitor of CDK7. *Biomed Pharmacother* 161, 114492

<https://doi.org/10.1016/j.biopha.2023.114492>



Characterization of new highly selective pyrazolo[4,3-d]pyrimidine inhibitor of CDK7

Markéta Kovalová^a, Libor Havlíček^b, Stefan Djukic^c, Jana Škerlová^c, Miroslav Peřina^a, Tomáš Pospíšil^d, Eva Řezníčková^a, Pavlína Řezáčová^c, Radek Jorda^a, Vladimír Kryštof^{a,e,*}

^a Department of Experimental Biology, Faculty of Science, Palacký University Olomouc, Šlechtitelů 27, 78371 Olomouc, Czech Republic

^b Isotope Laboratory, Institute of Experimental Botany, Czech Academy of Sciences, Vídeňská 1083, 14220 Prague, Czech Republic

^c Institute of Organic Chemistry and Biochemistry of the Czech Academy of Sciences, Flemingovo nám. 2, 16610 Prague, Czech Republic

^d Department of Chemical Biology, Faculty of Science, Palacký University Olomouc, Šlechtitelů 27, 78371 Olomouc, Czech Republic

^e Institute of Molecular and Translational Medicine, Faculty of Medicine and Dentistry, Palacký University Olomouc, Hněvotínská 5, 77900 Olomouc, Czech Republic

ARTICLE INFO

Keywords:

Cyclin-dependent kinase 7
pyrazolo[4,3-d]pyrimidine
Selectivity
Inhibitor

ABSTRACT

Targeting cyclin-dependent kinase 7 (CDK7) provides an interesting therapeutic option in cancer therapy because this kinase participates in regulating the cell cycle and transcription. Here, we describe a new trisubstituted pyrazolo[4,3-d]pyrimidine derivative, LGR6768, that inhibits CDK7 in the nanomolar range and displays favourable selectivity across the CDK family. We determined the structure of fully active CDK2/cyclin A2 in complex with LGR6768 at 2.6 Å resolution using X-ray crystallography, revealing conserved interactions within the active site. Structural analysis and comparison with LGR6768 docked to CDK7 provides an explanation of the observed biochemical selectivity, which is linked to a conformational difference in the biphenyl moiety. In cellular experiments, LGR6768 affected regulation of the cell cycle and transcription by inhibiting the phosphorylation of cell cycle CDKs and the carboxy-terminal domain of RNA polymerase II, respectively. LGR6768 limited the proliferation of several leukaemia cell lines, triggered significant changes in protein and mRNA levels related to CDK7 inhibition and induced apoptosis in dose- and time-dependent experiments. Our work supports previous findings and provides further information for the development of selective CDK7 inhibitors.

1. Introduction

Cyclin-dependent kinase 7 (CDK7) is a serine-threonine kinase that plays a crucial role in regulating the cell cycle and transcription, linking these processes together. CDK7 forms a trimeric complex with cyclin H and MAT1, which is called a CDK-activating complex (CAK), that is responsible for activating CDK1 and CDK2 by phosphorylating their T-loops at T160 and T161, respectively. Moreover, CDK7 regulates transcription as a part of the general transcription factor TFIIF, which is recruited to a Mediator–preinitiation complex responsible for phosphorylating the carboxy-terminal domain of RNA polymerase II at serine 5, which facilitates the initiation of transcription [1].

While cell cycle CDKs or cyclins are often amplified or overexpressed in cancer, the involvement of transcriptional CDKs (tCDK) in the initiation and development of cancer is unclear. It was proposed that CDK7 and other tCDKs are necessary for the expression of highly expressed antiapoptotic genes, genes controlled by oncogenic transcription factors

and fusion chimaeras (e.g., MYC, MLL1-AF9), and genes associated with cancer-specific super-enhancer elements. It was recently discovered that the genes encoding tCDKs in cancers are usually characterized by a loss in copy numbers. Among others, CDK7 showed the most significant copy-number loss across more than 10,000 assessed tumours [2]. These genetic alterations are correlated with increased sensitivity of cancer cells to DNA-damaging agents, which is mechanistically linked to the repression of genes encoding for the DNA damage response proteins. Due its essential roles in cell proliferation and transcription, CDK7 has become intensively studied as a possible target in cancer treatment.

In the last decade, several selective CDK7 inhibitors have been developed, which function either as traditional ATP competitors or as irreversible inhibitors. Currently, six compounds are in clinical studies (Fig. 1). BS-181 was described as the first noncovalent selective CDK7 inhibitor [3] built on a pyrazolo[1,5-a]pyrimidine scaffold. Preclinical studies have shown its antitumour activity on several tumour types, but BS-181 exerts poor drug-like properties [4–6]. By modifying BS-181, the

* Corresponding author at: Department of Experimental Biology, Faculty of Science, Palacký University Olomouc, Šlechtitelů 27, 78371 Olomouc, Czech Republic.
E-mail address: vladimir.krystof@upol.cz (V. Kryštof).

clinical candidate samuraciclib (also known as ICEC0942 or CT7001) was produced with improved selectivity towards CDK7 and strong antitumour effects in breast and colorectal cancer xenografts [7]. Further analogues of BS-181, LDC4297 and LDC3140, were built on the pyrazolo[1,5-*a*][1,3,5]triazine scaffold and displayed high specificity to CDK7 and selectivity [8]. Recently, indolylpyrimidine SY-5609 was reported as a subnanomolar, highly selective, noncovalent and orally available inhibitor of CDK7 with favourable ADME properties and is currently being evaluated in phase I clinical trials [9].

Selective CDK7 inhibition can be achieved by targeting reactive Cys312 residue outside the ATP pocket. THZ1 was described as the first covalent nanomolar CDK7 inhibitor [10] and was tested on many cancer models [11–15]. Unfortunately, THZ1 exhibited short plasma stability, but its position isomer THZ2 showed improved pharmacokinetics and antitumour activities [16]. Subsequent development led to the discovery of structurally related SY-1365 (mevociclib) [17], the first CDK7 covalent inhibitor that entered clinical trials. Its antitumour properties were observed in several xenograft models, either as monotherapy or in combination with venetoclax [17]. The combination of the THZ1 warhead and core from the PAK4 inhibitor PF-3758309 also led to the development of YKL-5-124 [18]. Although YKL-5-124 showed potency similar to that of THZ1, the compound induced a different phenotype in cancer cells and did not change global RNA polymerase II phosphorylation, probably due to its kinase selectivity profile.

Recently, other CDK7 inhibitors have been introduced, some of which have already entered clinical trials, namely, LY3405105, Q901 and XL102. Nevertheless, limited information about their mode of action, kinase selectivity or structure has been disclosed [19–23].

We have previously reported several series of potent 3,5,7-trisubstituted pyrazolo[4,3-*d*]pyrimidine CDK inhibitors with strong anticancer activity *in vitro* and *in vivo* [24–27]. Recently, we also showed the

ability of some pyrazolo[4,3-*d*]pyrimidines to act as molecular glue, causing rapid and selective proteasome-dependent degradation of cyclin K [28]. In the current study, we describe that the change of the 4-phenylbenzyl ring to a 2-phenylbenzyl at the 7 position of pyrazolo[4,3-*d*]pyrimidine confers a significant change in the desired selectivity for CDK7. Here, we introduce the novel CDK7 inhibitor LGR6768, confirm its preference for CDK7 and describe its antiproliferative effect on several leukaemia cell lines.

2. Results and discussion

2.1. Compound design and structural rationale

The design of LGR6768 (5-(piperidin-4-yl)thio-3-isopropyl-7-(2-phenylbenzyl)amino-1(2)*H*-pyrazolo[4,3-*d*]pyrimidine) was inspired by the binding of previously described 3,5,7-trisubstituted pyrazolo[4,3-*d*]pyrimidines in the CDK2/cyclin cavity (PDB: 3PJ8, 6GVA, 7QHL) [24, 25, 28]. Conserved isopropyl at position 3 was retained, whereas incorporation of the piperidine-thio chain at position 5 and the biphenyl moiety at position 7 partly reflected the structures of known CDK7 inhibitors [8, 29]. Compound LGR6768 was then synthesized as described previously by two subsequent reactions from pyrazolo[4,3-*d*]pyrimidine-5,7-dithiol [25, 27]; for details, see Fig. S1.

To understand the selectivity, we wanted to compare the orientation of the ligand in CDK2 and CDK7. Due to technical issues with structure determination of CDK7 co-crystals, we decided to model the binding of LGR6768 to CDK7, following an accepted approach [30]. We first determined the crystal structure of fully active Thr160-phosphorylated CDK2 with cyclin A2 (residues 175–432) in complex with LGR6768 at 2.6 Å resolution (PDB: 8B54) to confirm the orientation in the CDK2 active site cavity. Data collection and refinement statistics are listed in

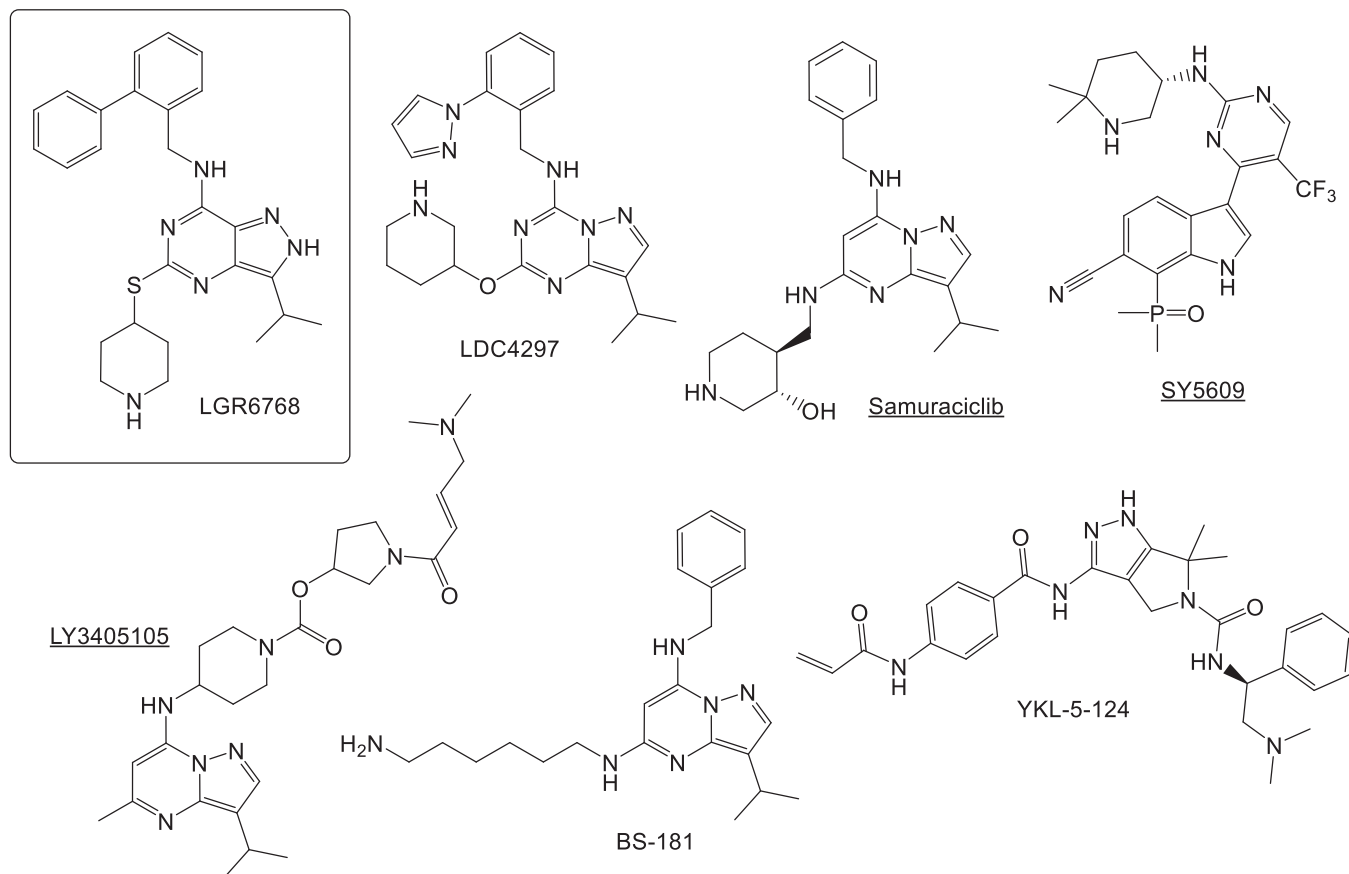


Fig. 1. Structure of LGR6768 and some known CDK7 inhibitors (the underlined inhibitors were registered in clinical trials).

Table S1, and the electron density maps are shown in Fig. S2. The pyrazolo[4,3-*d*]pyrimidine core of the inhibitor forms direct hydrogen bonds with Glu81 and Leu83 residues. In addition, water-mediated hydrogen bonds are formed between N4 of the inhibitor core and the Lys33, Glu51, and Asn132 side chains, as well as the main-chain nitrogen of Asp145. The thioether-linked piperidine moiety adopts a twisted-boat conformation that is stabilized by a hydrogen bond with Gln131, together with additional water-mediated interactions with the Asp86 carboxyl. The biphenyl moiety is oriented towards the active site opening, forming hydrophobic interactions with Ile10, Asp86, Lys89 and Phe82 (Fig. 2B, Fig. S3). Finally, the isopropyl substituent is buried into the hydrophobic pocket, interacting with Val64, Leu134, Ala144, and the gatekeeper Phe80 (Fig. S3).

Next, molecular docking of LGR6768 into the cryo-EM structure of CDK7 (PDB: 7B50) was performed to explain its selectivity for CDK7. The best binding pose of the inhibitor in the active site of CDK7 ($\Delta G_{\text{Vina}} = -9.4$ kcal/mol) is very similar to that in CDK2 (Fig. 2A, B); the pyrazolo[4,3-*d*]pyrimidine core forms direct hydrogen bonds with Asp92 and Met94. However, key differences were observed when comparing the binding of LGR6768 in the active cavity of CDK2 and CDK7. Generally, the active site cavity of CDK7 is much wider and more open to a possible interaction (Fig. 2C). This could be the reason why LGR6768 is in a more relaxed conformation in CDK7 than in CDK2 and why the piperidine moiety points deeper in the cavity to interact with Asp155. Next, the isopropyl group of LGR6768 protrudes into the analogical hydrophobic pocket in CDK7 interacting with Ala39, Ile75 and the gatekeeper Phe91 (Fig. 2B, Fig. S3). However, the isopropyl group is rotated by approx. 180° between the crystal structure in CDK2 and the modelled pose in CDK7, similar to inhibitor BS-181 in CDK7 [3]. The most evident difference in the binding pose of LGR6768 is the switched/flipped orientation of the biphenyl moiety, which points towards the active site opening in the CDK2 crystal structure but is oriented to the other side of the opening in the modelled pose in CDK7, pointing to the surface at the very edge of the active site cavity. Structural differences between CDK2 and CDK7 at the edge of the binding cavity could explain the opposite orientations of the biphenyl substituent. First, the cavity opening widens due to the substitution of Lys89 in CDK2 by Val100 in CDK7. More importantly, residue Glu8 in CDK2 forms a hump on the surface of the cavity edge; this conformation clashes with the biphenyl moiety binding mode observed in CDK7, in which the biphenyl outer ring points towards the surface due to homologous Asp16, which is oriented away from the cavity opening (Fig. 2C). In addition, the

substitution of Ile10 in CDK2 by Leu18 in CDK7 seems to be important as well, since one of the terminal methyl groups of Leu18 in CDK7 points towards the outer phenyl ring of LGR6768. The biphenyl moiety of LGR6768 forms extensive hydrophobic interactions with CDK7 residues Leu18, Phe93, Thr96 and Val100 (Fig. 2A, Fig. S3). Of note, the different orientations of the biphenyl moiety in CDK2 and CDK7 correspond well with the different orientations of the benzylamine substituent of samuraciclib observed in the same kinases. These were termed the “ring-up” and “ring-down” conformations, which are related by a rotation by $\sim 120^\circ$, and were explained by the same structural differences between CDK2 and CDK7 [31]. Based on the previous knowledge, we believe that the biphenyl substituent position and interaction are key for the potency and selectivity of LGR6768 towards CDK7.

2.2. Kinase selectivity

The selectivity profiling of LGR6768 was performed on a panel of 50 kinases, including known off-targets of other structurally related pyrazolo[4,3-*d*]pyrimidines [25,28] or isosteres, such as roscovitine or CR8 [32]. Given the high structural similarity within the CDK family, we also evaluated LGR6768 against 14 CDKs to assess its selectivity across them. The compound was applied at a $1 \mu\text{M}$ concentration, and the experiment confirmed selective reduction of the enzymatic activity of CDK7 to 4%. Only a few other kinases were significantly inhibited under the same settings, including CDK16 from the CDK family (Fig. 3A) and CK1 δ (both with 19% residual activity) (Fig. S4). Dose-dependent measurement revealed potent inhibition of recombinant CDK7 at low nanomolar concentrations with $\text{IC}_{50} = 20$ nM, which was at least 12-fold lower than for other CDKs (Table S2). Finally, the selectivity profile of LGR6768 for selected CDKs was compared to that of other nanomolar CDK7 inhibitors, namely, THZ1, LDC4297 and samuraciclib (Fig. 3B). Our results indicate that LDC4297 and samuraciclib have a lower selectivity index than LGR6768. However, the apparently lower selectivity of THZ1 compared to published data [10,33] could be due to the experimental conditions set for non-covalent compounds (short reaction time, no preincubation). These results indicate the reasonable kinase selectivity of our candidate.

CDK7 is involved in regulating the cell cycle as CAK (CDK activating kinase) by activating phosphorylation of the T-loop of CDK1 and CDK2 at threonines 161 and 162, respectively. Immunoblotting analysis revealed that LGR6768 downregulates the phosphorylation of both CDKs in a dose- (Fig. 3C) and time-dependent (Fig. 3D) manner in the

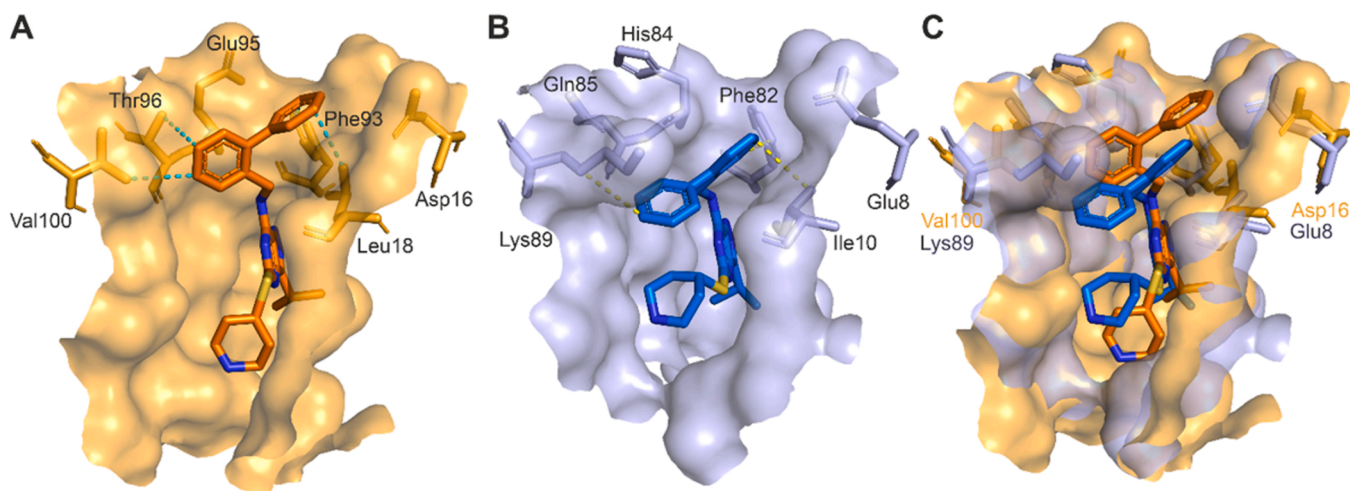


Fig. 2. LGR6768 binding poses in the active sites of CDK7 and CDK2. (A) LGR6768 docked into the CDK7 cryo-EM structure (PDB: 7B50). (B) CDK2 co-crystal structure with LGR6768 (PDB: 8B54). (C) Alignment of both binding poses and cavities of CDK7 and CDK2 shows structural differences in CDK7 (orange) and CDK2 (blue). Selected protein residues forming the edge of the cavity are shown as sticks. Hydrophobic interactions of the biphenyl moiety of LGR6768 with protein residues are shown as dashed lines. Ligand heteroatoms are blue (nitrogens) and yellow (sulfur).

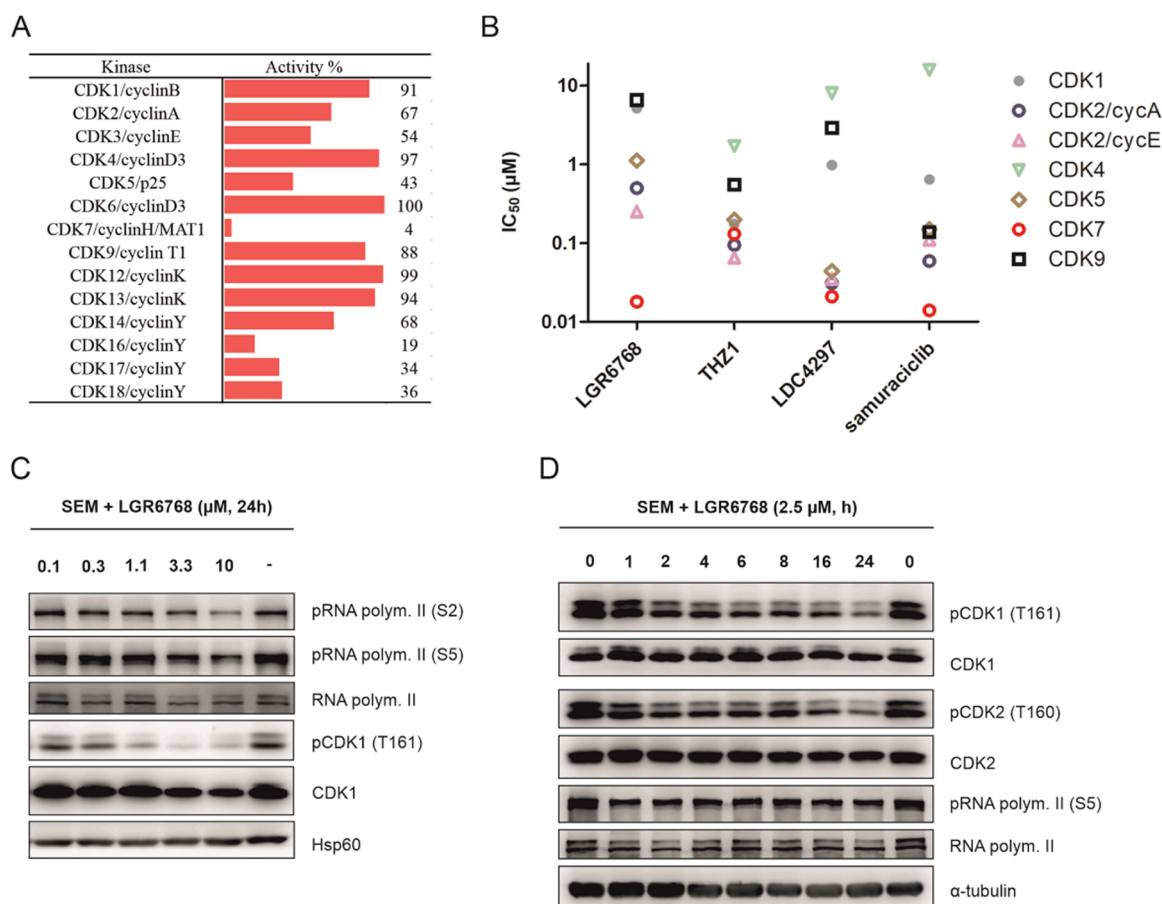


Fig. 3. (A) CDK selectivity profile of LGR6768 assayed at 1 µM concentration. (B) Comparison of kinase inhibition values of selected CDKs for LGR6768 and selected CDK7 inhibitors. IC₅₀ values > 20 µM are not shown. (C, D) Immunoblotting analysis of CDK7-related proteins in the SEM cell line treated for the indicated times with LGR6768. Hsp60 and tubulin protein expression marked equal protein loading.

SEM cell line. Moreover, we also observed the expected dephosphorylation of RNA polymerase II (Fig. 3C, D), although not as dramatic as was caused by the less selective CDK7 inhibitor THZ1 [10]. In fact, our results resemble those obtained with the CDK7 inhibitor YKL-5-124, which exhibited little effect on RNA polymerase II phosphorylation [18].

2.3. Antiproliferative and proapoptotic effects of LGR6768

Several CDK7 inhibitors showed antileukaemic effects in both AML and ALL cell lines [5,10,11,17], and SY-1365 also showed antitumour activity in AML xenografts [17]. Therefore, we profiled LGR6768 on a panel of 10 cell lines derived from haematological malignancies (5 AML cell lines, 3 ALL cell lines, 1 lymphoma, 1 CML). The observed activities reached GI₅₀ values between 0.44 and 4.4 µM except for K562 and CCRF-CEM cells (GI₅₀ > 5 µM). Antiproliferative properties in seven selected cancer cell lines derived from different origins (breast, prostate, melanoma) showed higher GI₅₀ values than those in AML and ALL cell lines, suggesting the antileukaemic potential of LGR6768 (Fig. 4A). Known CDK7 inhibitors THZ1 [10] and SY-1365 [17] show higher antiproliferative activity in leukaemia cell lines than LGR6768. However, unlike LGR6768, these inhibitors both covalently bind to CDK7, and THZ1 also inhibits CDK12/13, which may explain the increased potency against cell lines.

The cell cycle phenotype caused by inhibition of CDK7 usually leads to a reduction in the number of S-phase cells and concomitant accumulation of cells in the G1 or G2/M phase of the cell cycle, which is specific for each cell line and the concentration of inhibitor [34]. One-day treatment with compound LGR6768 led to dose-dependent G1

arrest in both the SEM and MOLM-13 cell lines already observed at mid-nanomolar concentrations (Fig. 4B). Significant apoptosis accompanied by G2/M arrested cells was observed solely at 10 µM. The effect of LGR6768 on the cell cycle of the most sensitive MOLM-13 cells showed a time-dependent tendency and deepened to low-nanomolar concentrations during the 3-day experiment (Fig. S5).

Furthermore, we investigated the proapoptotic effect of LGR6768 in MV4-11, MOLM-13, and SEM cell lines. Cells were treated with increasing doses of LGR6768 for 24 h and examined for apoptotic markers. As presented in Fig. 5A, immunoblotting revealed only a moderate effect of LGR6768 on the tested cell lines, as documented by PARP-1 cleavage and detection of caspase-7 and caspase-9 fragments, mostly at 10 µM. Additionally, LGR6768 caused downregulation of the antiapoptotic protein Mcl-1 to a lesser extent, while no changes in Bcl-2 levels were detected, probably explaining its higher stability. In concordance with immunoblotting, a fluorometric caspase-3/7 activity assay confirmed the proapoptotic effect of LGR6768 in MOLM-13 and SEM cell lines after 24 h of treatment (Fig. 5B).

2.4. Effect of LGR6768 on transcription targets

Furthermore, we investigated the inhibition of transcription in treated cells by analysing newly synthesized transcripts involved in apoptosis (e.g., Bcl-2, Mcl-1) or playing roles as oncogenic drivers in various haematological malignancies (e.g., RUNX, Myc, Myb). Those genes were previously established as genes sensitive to inhibition of global transcription and as fundamental genes important in targeting triple-negative breast cancer [16]. Their negative modulation by CDK7

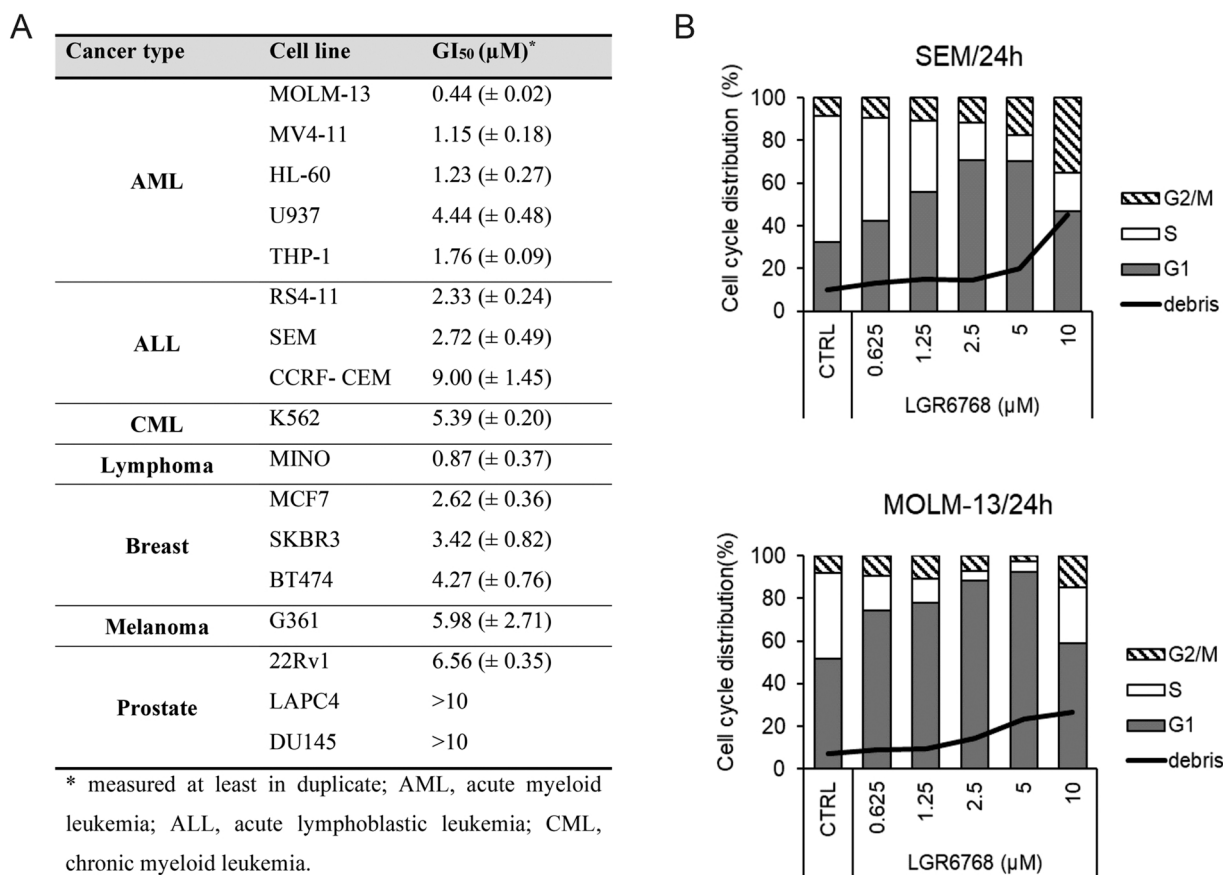


Fig. 4. (A) Antiproliferative activity of LGR6768. (B) Effect of LGR6768 on cell cycle distribution in the SEM and MOLM-13 cell lines. Cells were treated for 24 h with increasing concentrations of LGR6768 or vehicle.

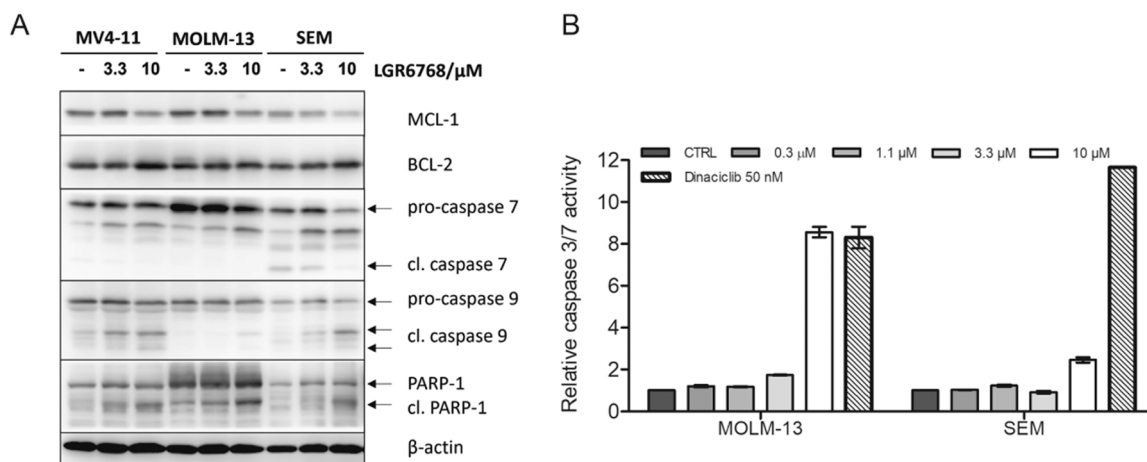


Fig. 5. Proapoptotic effect of LGR6768. (A) Immunoblotting analysis of apoptosis-related proteins. MV4-11, MOLM-13 and SEM cells were treated for 24 h with increasing concentrations of LGR6768. The actin level marked equal protein loading. (B) Activity of caspases 3/7 in MOLM-13 and SEM cell lines treated with LGR6768, dinaciclib or vehicle for 24 h.

inhibitors was highlighted in several studies, and as an example, targeting Jurkat ALL cells with low doses of THZ-1 was explained by diminishing the RUNX1-driven transcriptional program [16].

Transcriptional changes in mRNAs of anti-apoptotic genes *Mcl-1* and *Bcl-2* were observed to be suppressed with increasing doses of LGR6768 in SEM and MOLM-13 cell lines. These changes were examined after 4 h of treatment and demonstrate the rapid action of the inhibitor and the ability to induce apoptosis. Most of the other transcripts were down-regulated in a dose-dependent manner to 50% values. *MYC* expression

decreased rapidly in MOLM-13 cells to < 1%, which could be explained by the highest sensitivity of MOLM-13 cells to LGR6768 (Fig. 6).

3. Conclusion

In recent years, CDK7 has emerged as an attractive target in cancer therapy due to its role in regulating both the cell cycle and transcription. Here, we describe the development of compound LGR6768, a new pyrazolo[4,3-d]pyrimidine derivative that potently and selectively

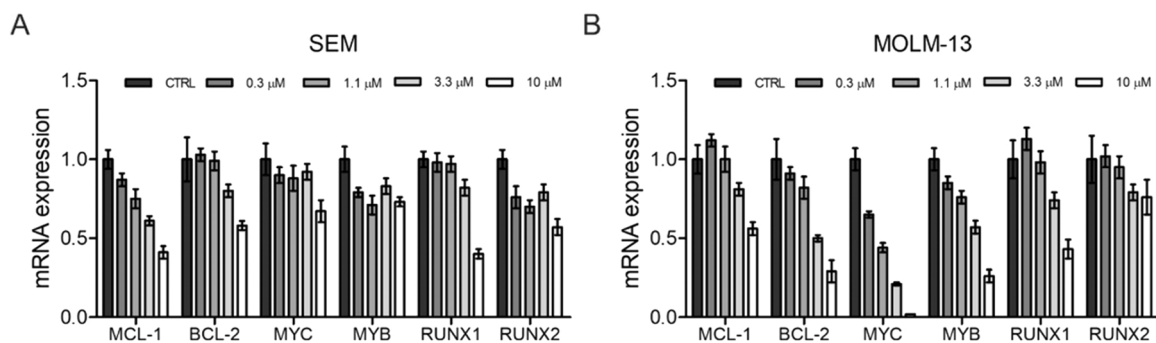


Fig. 6. LGR6768 downregulates the expression of transcription factors and apoptosis-related genes in the SEM (A) and MOLM-13 (B) cell lines. Cells were treated with increasing concentrations of LGR6768 or vehicle for 4 h. Relative expression levels were normalized to GAPDH and RPL13A genes (MOLM-13) or GAPDH and B2M genes (SEM).

inhibits CDK7. The selective targeting of CDK7 was confirmed by biochemical kinase profiling and supported by structural analysis. LGR6768 showed antileukaemic potential and downregulated the phosphorylation of CDK7 substrates, including CDK1, CDK2 and RNA polymerase CTD. Cell cycle analysis revealed a blockage in the G1 phase after treatment, and higher concentrations led to the induction of apoptosis accompanied by G2/M block, caspase activation, PARP-1 cleavage, and downregulation of the expression of antiapoptotic proteins at both the mRNA and protein levels. Moreover, LGR6768 downregulated the expression of several oncogenic drivers of haematological malignancies, indicating that targeting CDK7 is worth further exploration as a new therapeutic modality.

4. Experimental section

NMR spectra were recorded on a JEOL ECA-500 spectrometer operating at frequencies of 500.16 MHz (^1H) and 125.76 MHz (^{13}C) or on JEOL-ECZ 400/R spectrometer operating at frequencies of 399.78 MHz (^1H) and 100.53 MHz (^{13}C). ^1H NMR and ^{13}C NMR chemical shifts were referenced to the solvent signals; ^1H : δ (residual CHCl_3) = 7.25 ppm, δ (residual $\text{DMSO} - d_5$) = 2.50 ppm; ^{13}C : δ (CDCl_3) = 77.23 ppm, δ ($\text{DMSO} - d_6$) = 39.52 ppm. Chemical shifts are given on the δ scale [ppm], and coupling constants are given in Hz. Melting points were determined on a Kofler block and are uncorrected. Reagents were of analytical grade from standard commercial sources or were synthesized according to the referenced procedure. Thin layer chromatography (TLC) was carried out using aluminum sheets with silica gel F254 from Merck. Spots were visualized under UV light (254 nm). ESI mass spectra were determined using a Waters Micromass ZMD mass spectrometer (solution of sample in MeOH, direct inlet, coin voltage in the range of 10–20 V, trace amounts of HCOOH or NH_4OH were used to influence ionization). Column chromatography was performed using Merck silica gel Kieselgel 60 (230–400 mesh). All compounds gave satisfactory elemental analyses ($\pm 0.4\%$).

4.1. 3-Isopropyl-5-methylsulfanyl-7-(2-phenylbenzyl)amino-1(2H)-pyrazolo[4,3-d]pyrimidine (2)

A solution of 7-chloro-3-isopropyl-5-methylsulfanyl-1(2H)-pyrazolo[4,3-d]pyrimidine **1** [24] (700 mg, 2.88 mmol), 2-phenylbenzylamine (0.56 g, 3.15 mmol) and 0.4 mL trimethylamine in 10 mL acetonitrile was heated with stirring at 70 °C for 8 h. The solution was evaporated to dryness in vacuum, and the residue was purified by column chromatography on silica gel, stepwise with 2% and 4% MeOH in CHCl_3 . The product was obtained as white crystals from CHCl_3 (763 mg, 68% yield), m.p. 82–86 °C, MS ESI⁺ 390.2 [M + H]⁺, ESI⁻ 388.1 [M - H]⁻. ^1H NMR (500 MHz; CDCl_3): δ = 1.27 (d, J = 7.0 Hz, 6 H, $-\text{CH}(\text{CH}_3)_2$); 1.43 (s, 3 H, CH_3); 2.39 (s, 3 H, CH_3); 3.20 (sept., J = 7.0 Hz, 1 H, $-\text{CH}(\text{CH}_3)_2$); 7.72 (d, J = 5.2 Hz, 2 H, $\text{NH}-\text{CH}_2-$); 6.77 (s, 1 H, $\text{NH}-\text{CH}_2-$); 7.16–7.25

(m, 4 H, H_{Ar}); 7.28–7.33 (m, 4 H, H_{Ar}); 7.37 (d, J = 7.3 Hz, 1 H, H_{Ar}); ^{13}C (125 MHz; CDCl_3): δ = 14.3, 21.4, 26.0, 26.8, 42.2, 127.1, 127.6, 128.1, 128.5, 128.9, 130.0, 135.0, 140.4, 141.6, 163.2. Anal. Calcd. ($\text{C}_{22}\text{H}_{23}\text{N}_5\text{S}$) C, 67.84; H, 5.95; N, 17.98; S, 8.23. Found: C, 67.70; H, 6.06; N, 17.74; S, 8.15.

4.2. 3-Isopropyl-7-(2-phenylbenzyl)amino-1(2H)-pyrazolo[4,3-d]pyrimidin-5-thiol (3)

3-Isopropyl-5-methylsulfanyl-7-(2-phenylbenzyl)amino-1(2H)-pyrazolo[4,3-d]pyrimidine **2** (0.383 g, 1 mmol) was dissolved in 2.65 mL of HMPA and sodium (56 mg, 2.5 eq.) was added under argon. The reaction mixture was stirred for 3 h, and during this time, the temperature was continuously increased to 105 °C. For another 3 h, the reaction mixture was maintained at 105 °C. The solution was cooled to 5 °C, and water (8 mL) was added. The solution was acidified by adding 5 N HCl. The precipitated crude product was isolated by filtration and purified by column chromatography on silica gel, stepwise with 1%, 2% and 3% MeOH in CHCl_3 . The product was obtained as yellow crystals (140 mg, 37% yield), m.p. 130–136 °C, MS ESI⁺ 376.1 [M + H]⁺, ESI⁻ 374.1 [M - H]⁻. NMR ^1H (500 MHz; $\text{DMSO} - d_6$): δ = 1.24 (d, J = 6.9 Hz, 6 H, $-\text{CH}(\text{CH}_3)_2$); 3.40–3.47 (m, 1 H, $-\text{CH}(\text{CH}_3)_2$); 4.64 (d, J = 5.5 Hz, 2 H, $\text{NH}-\text{CH}_2-$); 7.21–7.58 (m, 9 H, H_{Ar}); 9.02 (s, 1 H, NH). ^{13}C (125 MHz; $\text{DMSO} - d_6$): δ = 21.9, 24.0, 41.2, 127.1, 127.2, 127.6, 128.4, 129.2, 129.9, 135.5, 140.3, 141.0, 179.1. Anal. Calcd. ($\text{C}_{21}\text{H}_{21}\text{N}_5\text{S}$) C, 67.17; H, 5.64; N, 18.65; S, 8.54. Found: C, 66.83; H, 5.61; N, 18.99; S, 8.85.

4.3. 5-Piperidin-4-ylthio-3-isopropyl-7-(2-phenylbenzyl)amino-1(2H)-pyrazolo[4,3-d]pyrimidine (4, LGR6768)

A solution of 3-isopropyl-7-(2-phenylbenzyl)amino-1(2H)-pyrazolo[4,3-d]pyrimidin-5-thiol **3** (98 mg, 0.26 mmol), 1-Boc-4-bromopiperidine (85 mg, 0.32 mmol) and KOH (25 mg, 0.45 mmol) in 2 mL of DMF was stirred for 12 h at room temperature. The solution was evaporated under vacuum, and the product was purified by column chromatography (stepwise 0.8%, 1.5% and 2% MeOH in CHCl_3). The Bocylated product was dissolved in 0.5 mL MeOH, and then 0.5 mL of 10 N aq. HCl was added, and the solution was stirred for 1/2 h at 40 °C. The solution was evaporated under vacuum, and the rest was repeatedly evaporated with abs. EtOH until the product was obtained as an amorphous colourless glass foam (47 mg, 39% yield). MS ESI⁺ 459.2 [M + H]⁺, ESI⁻ 457.1 [M - H]⁻. ^1H NMR (400 MHz, $\text{DMSO} - d_6$) δ = 1.35 (d, J = 7.0 Hz, 6 H, $-\text{CH}(\text{CH}_3)_2$), 1.42–1.54 (m, 2 H, $-\text{CH}_2-$), 1.96–1.98 (m, 2 H, $-\text{CH}_2-$), 2.57–2.60 (m, 2 H, $-\text{CH}_2-$), 2.95–2.96 (m, 2 H, $-\text{CH}_2-$), 3.23 (sept., J = 6.9 Hz, 1 H, $-\text{CH}(\text{CH}_3)_2$), 3.68 (tt, J = 10.4, 3.5 Hz, 2 H, $-\text{CH}_2-\text{S}-$), 4.58 (d, J = 4.3, 2 H, $\text{Ar}-\text{CH}_2-\text{NH}-$), 7.23–7.29 (m, 1 H, Ar), 7.33–7.40 (m, 3 H, Ar), 7.44 (d, J = 4.0, 5 H, Ar), 8.60 (s, 1 H, $-\text{NH}$). ^{13}C NMR (100 MHz, $\text{DMSO} - d_6$) δ = 21.7, 26.2, 31.6, 40.1, 41.4, 44.7, 127.2, 127.3, 127.6, 127.9, 128.3, 129.0, 129.8, 135.7, 138.8, 140.3,

141.0, 146.4, 149.8, 159.8. Anal. Calcd. (C₂₆H₃₀N₆S. HCl) C, 63.08; H, 6.31; Cl, 7.16; N 16.97; S, 6.48, Found: C, 62.81; H, 6.67; N, 16.63; S, 6.23.

4.4. Crystallization, diffraction data collection, structure determination and analyses

CDK2/cyclin A2 protein was concentrated to 13.3 mg/mL in a buffer composed of 40 mM HEPES, 200 mM NaCl, and 0.02% monothioglycerol, pH 8.5, and mixed with 100 mM LGR6768 (in 100% DMSO). The final protein:inhibitor molar ratio was 1:3. Incubation was performed for 45 min on ice, and the sample was clarified by centrifugation at 4 °C (22,000 g, 15 min). Crystals were obtained at 18 °C using the sitting-drop vapour diffusion technique in Swissci 96-well 3-drop plates (Molecular Dimensions) and the Oryx8 robot (Douglas Instruments). The reservoir solution was created by mixing 23 µL of Morpheus (Molecular Dimensions) [35] condition #35 containing 10% w/v PEG 4000, 20% v/v glycerol, 0.03 M NaNO₃, 0.03 M Na₂HPO₄, 0.03 M (NH₄)₂SO₄, 0.1 M Tris/Bicine pH 8.5 with 9 µL of JCSG⁺ (Qiagen) condition #29 containing 0.8 M sodium phosphate monobasic monohydrate, 0.8 M potassium phosphate monobasic, 0.1 M sodium HEPES, pH 7.5 [36]. Crystallization drops were prepared by mixing 100 nL of the protein-inhibitor complex and 200 nL of the reservoir solution. A plate-shaped crystal, size 150 µm × 100 µm × 10 µm, appeared after 3 days and was fished and flash-cooled in liquid N₂ after 5 days.

A complete dataset at 2.6 Å resolution was collected at 100 K at beamline MX14.1 operated by Helmholtz-Zentrum Berlin (HZB) at the BESSY II electron storage ring (Berlin-Adlershof, Germany) [37]. The dataset was processed using the program XDS [38], and the structure was solved by the molecular replacement method using MolRep version 11.2.08 [39] with the CDK2/cyclin A2 complex available in the Protein Data Bank (PDB) under the code 6GVA [25] as the search model. Model refinement was performed using REFMAC 5.8.0352 from the CCP4 package version 8.0.002 [40] in combination with manual refinement in WinCoot version 0.9.8.1 [41]. The ligand model and restraints were prepared using the Ligand Builder feature in WinCoot [41]. Data collection and refinement statistics are shown in Table S1. The structural model was validated using MolProbity [42] and wwPDB [43] validation servers. Structural analysis was conducted using LigPlot+ [44] and the PISA server [45]. The figures were prepared using PyMol version 2.5.3 [46]. Atomic coordinates and structure factors were deposited into the PDB under the code 8B54.

4.5. Molecular modelling

Molecular modelling was performed on the cryo-EM structure of CDK7 (PDB: 7B5O). The 3D structure of LGR6768 was obtained from the co-crystal structure with CDK2/cyclin A2 (deposited as PDB: 8B54). Polar hydrogens were added to the ligand and protein with the AutoDock Tools program, and rigid docking was performed using AutoDock Vina 1.059 [47]. Interactions between LGR6768 and CDK7 were determined using BIOVIA Discovery Studio Visualizer 2021 (Dassault Systemes). Other figures were generated using PyMOL ver. 2.0.4 (Schrodinger, LLC).

4.6. Cell culture and viability assay

Human cell lines were obtained from the European Collection of Authenticated Cell Culture, German Collection of Microorganisms and Cell Cultures, Cell Line Service, and American Tissue Culture Collection or were kindly gifted by Jan Bouchal from Palacký University Olomouc (see Table S3 for more details and the cultivation conditions). The cells were grown in appropriate media supplemented with 10% foetal bovine serum, streptomycin (100 µg/mL), penicillin (100 IU/mL) and glutamine (4 mM) and stored in a humidified incubator at 37 °C and in 5% CO₂.

For viability assays, the cells were seeded into 96-well plates and treated in triplicate with 6 different concentrations of LGR6768 for 72 h. After the treatment, the resazurin solution (Sigma Aldrich) was added for 4 h, and then the signal of resorufin was measured using a Fluoroskan Ascent microplate reader (Labsystems) at 544 nm/590 nm (excitation/emission). The GI₅₀ (the drug concentration that is lethal for 50% of cells) was calculated from the dose response curves in Origin 6.0 software.

4.7. Kinase inhibition assay and selectivity profiling

The kinase inhibition assay was performed as previously described [48]. Briefly, all tested kinases were incubated with specific substrates in the presence of ATP, 0.05 µCi [³³P]ATP and the LGR6768 compound in a final volume of 10 µL. The reaction was stopped by adding 3% aq. H₃PO₄. Aliquots were spotted onto P-81 phosphocellulose (Whatman), washed three times with 0.5% aq. H₃PO₄ and air-dried. Kinase inhibition was quantified using a FLA-7000 digital image analyser (Fujifilm). The drug doses required to decrease kinase activities by 50%, represented by the IC₅₀ values, were determined from —dose—response curves.

Kinase selectivity profiling was performed by Eurofins Discovery. The tested compound was assayed at a single concentration (1 µM) at ATP concentrations equal to K_m.

4.8. Immunoblotting and antibodies

Cell lysates were separated by —SDS—PAGE and electroblotted onto nitrocellulose membranes. The membranes were blocked, incubated with primary antibodies overnight, washed and incubated with secondary antibodies conjugated with peroxidase (Cell Signalling). Peroxidase activity was detected using Super-Signal West Pico reagents (Merck) using a CCD camera LAS-4000 (FujiFilm). The specific antibodies were purchased from Cell Signalling (anti-caspase 7; anti-caspase 9; anti-cdc2; anti-CDK2, clone 78B2; anti-cyclin A2, clone BF683; anti-cyclin B1, clone V152; anti-HSP60, clone D6F1; anti-Mcl-1, clone D35A5; anti-PARP, clone 46D11), Santa Cruz Biotechnology (anti-β-actin, clone C4; anti-caspase-3; anti-p-Cdc2 p34 (Thr 161); anti-p-CDK2 (Thr 160)) or Merck (anti-Bcl-2, clone Bcl-2-100; anti-α-tubulin, clone DM1A).

4.9. Caspase 3/7 activity assay

Cell lysates were incubated with 100 µM Ac-DEVD-AMC (Enzo Life Sciences), which is a substrate for caspases 3 and 7, in assay buffer (25 nM PIPES, 2 mM MgCl₂, 2 mM EGTA, 5 mM DTT, pH 7.3). The fluorescent signal of the product was measured at 355 nm/460 nm (excitation/emission) using a Fluoroskan Ascent microplate reader (Labsystems).

4.10. Cell cycle analysis

After harvesting, the cells were then washed with PBS, fixed with 70% ethanol, denatured with 2 M HCl and neutralized. After staining with propidium iodide, the cells were analysed by flow cytometry using a 488 nm laser (BD FACS Verse with BD FACSuite software, version 1.0.6.). Cell cycle distribution was analysed using ModFit LT (Verity Software House, version 4.1.7).

4.11. RNA isolation and qPCR

Total RNA was isolated via an RNeasy plus mini kit (QIAGEN) according to the manufacturer's instructions. The concentration and purity of isolated RNA were measured on a DeNovix DS-11 spectrophotometer. Isolated RNA (0.5–1 µg) was then used for reverse transcription into first strand cDNA via a SensiFast cDNA synthesis kit

(Bioline). RNA spike I (TATAA) was used as an inhibition control of the transcription reaction. Quantitative PCR was carried out with a SensiFAST SYBR No-Rox Kit (Bioline) on a CFX96 Real-time PCR Detection System. Suitable primers were designed via Primer BLAST [49] and synthesized by Genetech Biotech. Raw data were analysed using CFX Maestro 2.2, and relative normalized expression was commutated by the $\Delta\Delta C_T$ method [50]. Expression was normalized to GAPDH and RPL13A in the MOLM-13 cell line or GAPDH and B2M in the SEM cell line. Those pairs of genes were found to be the most stable for concrete cell lines using CFX Maestro 2.2 software.

List of used primers: BCL-2 (F: ATGTGTGTGGAGAGCGTCA, R: ACAGCCAGGAGAAATCAAACAG); GAPDH: (F: TCCAAAATCAAGTG GGGCGA, R: TGGTTCACACCCATGACGAA); MCL-1 (F: AGTTGTACCG GCAGTCC, R: TTTGATGTCCAGTTCCGAAG); MYB (F: TCTCCAGT-CATGTTCCATACCC, R: TGTGTGGTCTGTGTTGGTAGC); MYC (F: TACAACACCCGAGCAAGGAC, R: AGCTAACGTTGAGGGGCATC); RPL 13A (F: CGACAAGAAAAAGCGGATGG, R: TTCTTTCTCTCTCTCC TCC); RUNX1 (F: CACTGTGATGGCTGGCAATG, R: CTTGCGGTGGGT TTGTGAAG); RUNX2 (F: TCTGGCCTTCCACTCTCAGT, R: TGGCAGG-TAGGTGTGGTAGT); HOXA9 (F: CCGTACTGACTATGCTTGTGGT, R: ACTCTTTCTCCAGTTCCAGGG).

CRedit authorship contribution statement

Markéta Kovalová: Investigation, Writing – original draft, Visualization. **Libor Havlíček:** Investigation, Methodology. **Stefan Djukic:** Investigation, Visualization, Writing - original draft. **Jana Škerlová:** Data curation, Supervision, Writing - review & editing. **Miroslav Perina:** Formal analysis, Visualization. **Tomáš Pospíšil:** Investigation. **Eva Řezníčková:** Investigation, Validation. **Pavla Rezacová:** Project administration, Supervision, Writing – review & editing. **Radek Jorda:** Investigation, Writing – review & editing, Visualization. **Vladimír Krýstof:** Project administration, Supervision, Funding acquisition, Writing – review & editing.

Data Availability

Data will be made available on request.

Acknowledgements

Authors would like to thank Veronika Vojáčková for excellent technical support. Diffraction data have been collected on BL14.1 at the BESSY II electron storage ring operated by the Helmholtz-Zentrum Berlin. The work was supported by the European Union - Next Generation EU (The project National Institute for Cancer Research, Programme EXCELES, Project No. LX22NPO5102), Czech Science Foundation (23–05462S) and Palacký University Olomouc (IGA_PRF_2022_007).

Appendix A. Supporting information

Supplementary data associated with this article can be found in the online version at [doi:10.1016/j.biopha.2023.114492](https://doi.org/10.1016/j.biopha.2023.114492).

References

[1] S.J. Vervoort, J.R. Devlin, N. Kwiatkowski, M. Teng, N.S. Gray, R.W. Johnstone, Targeting transcription cycles in cancer, *Nat. Rev. Cancer* 22 (2022) 5–24, <https://doi.org/10.1038/s41568-021-00411-8>.

[2] W. Shan, J. Yuan, Z. Hu, J. Jiang, Y. Wang, N. Loo, L. Fan, Z. Tang, T. Zhang, M. Xu, Y. Pan, J. Lu, M. Long, J.L. Tanyi, K.T. Montone, Y. Fan, X. Hu, Y. Zhang, L. Zhang, Systematic characterization of recurrent genomic alterations in cyclin-dependent kinases reveals potential therapeutic strategies for cancer treatment, *Cell Rep.* 32 (2020), 107884, <https://doi.org/10.1016/j.celrep.2020.107884>.

[3] S. Ali, D.A. Heathcote, S.H. Kroll, A.S. Jogalekar, B. Scheiper, H. Patel, J. Brackow, A. Siwicki, M.J. Fuchter, M. Periyasamy, R.S. Tolhurst, S.K. Kanneganti, J. P. Snyder, D.C. Liotta, E.O. Aboagye, A.G. Barrett, R.C. Coombes, The development of a selective cyclin-dependent kinase inhibitor that shows antitumor activity,

Cancer Res 69 (2009) 6208–6215, <https://doi.org/10.1158/0008-5472.CAN-09-0301>.

[4] H. Ma, D.C. Dean, R. Wei, F.J. Hornicek, Z. Duan, Cyclin-dependent kinase 7 (CDK7) is an emerging prognostic biomarker and therapeutic target in osteosarcoma, *Ther. Adv. Musculoskelet. Dis.* 13 (2021). [doi:10.1177/1759720X21995069](https://doi.org/10.1177/1759720X21995069).

[5] S.Y. Park, K.Y. Kim, D.Y. Jun, S.K. Hwang, Y.H. Kim, G(1) cell cycle arrest and extrinsic apoptotic mechanisms underlying the anti-leukemic activity of CDK7 inhibitor BS-181, *Cancers (Basel)* 12 (2020), <https://doi.org/10.3390/cancers12123845>.

[6] B.Y. Wang, Q.Y. Liu, J. Cao, J.W. Chen, Z.S. Liu, Selective CDK7 inhibition with BS-181 suppresses cell proliferation and induces cell cycle arrest and apoptosis in gastric cancer, *Drug Des. Devel. Ther.* 10 (2016) 1181–1189, <https://doi.org/10.2147/DDDT.S86317>.

[7] H. Patel, M. Periyasamy, G.P. Sava, A. Bondke, B.W. Slafer, S.H.B. Kroll, M. Barbazanges, R. Starkey, S. Ottaviani, A. Harrod, E.O. Aboagye, L. Buluwela, M. J. Fuchter, A.G.M. Barrett, R.C. Coombes, S. Ali, ICEC0942, an orally bioavailable selective inhibitor of CDK7 for cancer treatment, *Mol. Cancer Ther.* 17 (2018) 1156–1166, <https://doi.org/10.1158/1535-7163.MCT-16-0847>.

[8] T.W. Kelso, K. Baumgart, J. Eickhoff, T. Albert, C. Antrecht, S. Lemcke, B. Klebl, M. Meisterernst, Cyclin-dependent kinase 7 controls mRNA synthesis by affecting stability of preinitiation complexes, leading to altered gene expression, cell cycle progression, and survival of tumor cells, *Mol. Cell Biol.* 34 (2014) 3675–3688, <https://doi.org/10.1128/MCB.00595>.

[9] J.J. Marineau, K.B. Hamman, S. Hu, S. Alnemy, J. Mihalich, A. Kabro, K. M. Whitmore, D.K. Winter, S. Roy, S. Ciblat, N. Ke, A. Savinainen, A. Wilsily, G. Malojcic, R. Zahler, D. Schmidt, M.J. Bradley, N.J. Waters, C. Chuaqui, Discovery of SY-5609: a selective, noncovalent inhibitor of CDK7, *J. Med. Chem.* 65 (2022) 1458–1480, <https://doi.org/10.1021/acs.jmedchem.1c01171>.

[10] N. Kwiatkowski, T. Zhang, P.B. Rahl, B.J. Abraham, J. Reddy, S.B. Ficarro, A. Dastur, A. Amzallag, S. Ramaswamy, B. Tesar, C.E. Jenkins, N.M. Hannett, D. McMillin, T. Sanda, T. Sim, N.D. Kim, T. Look, C.S. Mitsiades, A.P. Weng, J. R. Brown, C.H. Benes, J.A. Marto, R.A. Young, N.S. Gray, Targeting transcription regulation in cancer with a covalent CDK7 inhibitor, *Nature* 511 (2014) 616–620, <https://doi.org/10.1038/nature13393>.

[11] T. Abudurehman, J. Xia, M.H. Li, H. Zhou, W.W. Zheng, N. Zhou, R.Y. Shi, J. M. Zhu, L.T. Yang, L. Chen, L. Zheng, K. Xue, K. Qing, C.W. Duan, CDK7 inhibitor THZ1 induces the cell apoptosis of B-cell acute lymphocytic leukemia by perturbing cellular metabolism, *Front Oncol.* 11 (2021), 663360, <https://doi.org/10.3389/fonc.2021.663360>.

[12] F. Cayrol, P. Praditsuktavorn, T.M. Fernando, N. Kwiatkowski, R. Marullo, M. N. Calvo-Vidal, J. Phillip, B. Pera, S.N. Yang, K. Takpradit, L. Roman, M. Gaudiano, R. Crescenzo, J. Ruan, G. Inghirami, T. Zhang, G. Cremaschi, N.S. Gray, L. Cerchietti, THZ1 targeting CDK7 suppresses STAT transcriptional activity and sensitizes T-cell lymphomas to BCL2 inhibitors, *Nat. Commun.* 8 (2017) 14290, <https://doi.org/10.1038/ncomms14290>.

[13] F. Liu, W. Jiang, Y. Sui, W. Meng, L. Hou, T. Li, M. Li, L. Zhang, J. Mo, J. Wang, Y. Zhao, L. Zhang, J. Ma, Y. Tang, CDK7 inhibition suppresses aberrant hedgehog pathway and overcomes resistance to smoothened antagonists, *Proc. Natl. Acad. Sci. U. S. A.* 116 (2019) 12986–12995, <https://doi.org/10.1073/pnas.1815780116>.

[14] S. Sampathi, P. Acharya, Y. Zhao, J. Wang, K.R. Stengel, Q. Liu, M.R. Savona, S. W. Hiebert, The CDK7 inhibitor THZ1 alters RNA polymerase dynamics at the 5' and 3' ends of genes, *Nucleic Acids Res* 47 (2019) 3921–3936, <https://doi.org/10.1093/nar/gkz127>.

[15] C. Wang, H. Jin, D. Gao, L. Wang, B. Evers, Z. Xue, G. Jin, C. Lieftink, R. L. Beijersbergen, W. Qin, R. Bernards, A CRISPR screen identifies CDK7 as a therapeutic target in hepatocellular carcinoma, *Cell Res* 28 (2018) 690–692, <https://doi.org/10.1038/s41422-018-0020-z>.

[16] Y. Wang, T. Zhang, N. Kwiatkowski, B.J. Abraham, T.I. Lee, S. Xie, H. Yuzugullu, T. Von, H. Li, Z. Lin, D.G. Stover, E. Lim, Z.C. Wang, J.D. Iglehart, R.A. Young, N. S. Gray, J.J. Zhao, CDK7-dependent transcriptional addiction in triple-negative breast cancer, *Cell* 163 (2015) 174–186, <https://doi.org/10.1016/j.cell.2015.08.063>.

[17] S. Hu, J.J. Marineau, N. Rajagopal, K.B. Hamman, Y.J. Choi, D.R. Schmidt, N. Ke, L. Johannessen, M.J. Bradley, D.A. Orlando, S.R. Alnemy, Y. Ren, S. Ciblat, D. K. Winter, A. Kabro, K.T. Sprott, J.G. Hodgson, C.C. Fritz, J.P. Carulli, T.E. Di, E. R. Olson, Discovery and characterization of SY-1365, a selective, covalent inhibitor of CDK7, *Cancer Res* 79 (2019) 3479–3491, <https://doi.org/10.1158/0008-5472.CAN-19-0119>.

[18] C.M. Olson, Y. Liang, A. Leggett, W.D. Park, L. Li, C.E. Mills, S.Z. Elsarrag, S. B. Ficarro, T. Zhang, R. Duster, M. Geyer, T. Sim, J.A. Marto, P.K. Sorger, K. D. Westover, C.Y. Lin, N. Kwiatkowski, N.S. Gray, Development of a selective CDK7 covalent inhibitor reveals predominant cell-cycle phenotype, *Cell Chem. Biol.* 26 (2019) 792–803, <https://doi.org/10.1016/j.chembiol.2019.02.012>.

[19] Y.J. Choi, D.H. Kim, D.H. Yoon, C. Suh, C.M. Choi, J.C. Lee, J.Y. Hong, J.K. Rho, Efficacy of the novel CDK7 inhibitor QS1189 in mantle cell lymphoma, *Sci. Rep.* 9 (2019) 7193, <https://doi.org/10.1038/s41598-019-43760-z>.

[20] Y.J. Choi, H. Lee, D.S. Kim, D.H. Kim, M.H. Kang, Y.H. Cho, C.M. Choi, J. Yoo, K. O. Lee, E.K. Choi, J.C. Lee, J.K. Rho, Discovery of a novel CDK7 inhibitor YPN-005 in small cell lung cancer, *Eur. J. Pharm.* 907 (2021), 174298, <https://doi.org/10.1016/j.ejphar.2021.174298>.

[21] B.K. Koo, E.J. Choi, E.H. Hur, J.H. Moon, J.Y. Kim, H.S. Park, Y. Choi, J.H. Lee, K. H. Lee, E.K. Choi, J. Kim, J.H. Lee, Antileukemic activity of YPN-005, a CDK7 inhibitor, inducing apoptosis through c-MYC and FLT3 suppression in acute myeloid leukemia, *Heliyon* 8 (2022), e11004, <https://doi.org/10.1016/j.heliyon.2022.e11004>.

- [22] S.K. Satyam, R. Poddutoori, S. Thiagarajan, S. Mukherjee, L.N. Kaza, K. Charamanna, S. Marappan, D. Samiulla, N.K. Tiwari, T. Devaraja, A. Aravind, A. A. Dhudashiya, R. Booher, G. Dagainakatte, T. Antony, S. Chelur, K. Nellore, S. Giri, M. Ramachandra, S. Samajdar, Potent anti-tumor activity of AUR102, a selective covalent inhibitor of CDK7 (2020), *Eur. J. Cancer* 138S2 (2020) S1–S62, [https://doi.org/10.1016/S0959-8049\(20\)31201-6](https://doi.org/10.1016/S0959-8049(20)31201-6).
- [23] D. Yu, Y. Jeon, S.J. Lee, J. Kim, K. Nam, Q901; a highly selective covalent cdk7 inhibitor inducing substantial anti-tumor effect in a broad spectrum of solid tumor lineages, Abstract 2574.(2022), *Cancer Res* 82 (12 Supplement) (2022), <https://doi.org/10.1158/1538-7445.AM2022-2574>.
- [24] R. Jorda, L. Havlicek, I.W. McNae, M.D. Walkinshaw, J. Voller, A. Sturc, J. Navratilova, M. Kuzma, M. Mistrik, J. Bartek, M. Strnad, V. Krystof, Pyrazolo [4,3-d]pyrimidine bioisostere of roscovitine: evaluation of a novel selective inhibitor of cyclin-dependent kinases with antiproliferative activity, *J. Med. Chem.* 54 (2011) 2980–2993, <https://doi.org/10.1021/jm200064p>.
- [25] R. Jorda, L. Havlicek, A. Sturc, D. Tuskova, L. Daumova, M. Alam, J. Skerlova, M. Nekardova, M. Perina, T. Pospisil, J. Siroka, L. Urbanek, P. Pachel, P. Rezacova, M. Strnad, P. Klener, V. Krystof, 3,5,7-substituted pyrazolo[4,3-d]pyrimidine inhibitors of cyclin-dependent kinases and their evaluation in lymphoma models, *J. Med. Chem.* 62 (2019) 4606–4623, <https://doi.org/10.1021/acs.jmedchem.9b00189>.
- [26] E. Reznickova, S. Weitensteiner, L. Havlicek, R. Jorda, T. Gucky, K. Berka, V. Bazgier, S. Zahler, V. Krystof, M. Strnad, Characterization of a pyrazolo[4,3-d]pyrimidine Inhibitor of cyclin-dependent kinases 2 and 5 and aurora A with pro-apoptotic and anti-angiogenic activity in vitro, *Chem. Biol. Drug Des.* 86 (2015) 1528–1540, <https://doi.org/10.1111/cbdd.12618>.
- [27] L. Vymetalova, L. Havlicek, A. Sturc, Z. Skraskova, R. Jorda, T. Pospisil, M. Strnad, V. Krystof, 5-Substituted 3-isopropyl-7-[4-(2-pyridyl)benzyl]amino-1(2)H-pyrazolo[4,3-d]pyrimidines with anti-proliferative activity as potent and selective inhibitors of cyclin-dependent kinases, *Eur. J. Med. Chem.* 110 (2016) 291–301, <https://doi.org/10.1016/j.ejmech.2016.01.011>.
- [28] R. Jorda, L. Havlicek, M. Perina, V. Vojackova, T. Pospisil, S. Djukic, J. Skerlova, J. Gruz, N. Renesova, P. Klener, P. Rezacova, M. Strnad, V. Krystof, 3,5,7-substituted pyrazolo[4,3-d]pyrimidine inhibitors of cyclin-dependent kinases and cyclin K degraders, *J. Med. Chem.* 65 (2022) 8881–8896, <https://doi.org/10.1021/acs.jmedchem.1c02184>.
- [29] Pyrazolo - triazine derivatives as selective cyclin-dependent kinase inhibitors, WO2013128028A1, 2013.
- [30] P. Hazel, S.H. Kroll, A. Bondke, M. Barbazanges, H. Patel, M.J. Fuchter, R. C. Coombes, S. Ali, A.G. Barrett, P.S. Freemont, Inhibitor selectivity for cyclin-dependent kinase 7: a structural, thermodynamic, and modelling study, *ChemMedChem* 12 (2017) 372–380, <https://doi.org/10.1002/cmdc.201600535>.
- [31] B.J. Greber, J. Remis, S. Ali, E. Nogales, 2.5 Å-resolution structure of human CDK-activating kinase bound to the clinical inhibitor ICEC0942, *Biophys. J.* 120 (2021) 677–686, <https://doi.org/10.1016/j.bpj.2020.12.030>.
- [32] K. Bettayeb, N. Oumata, A. Echalié, Y. Ferandin, J.A. Endicott, H. Galons, L. Meijer, CR8, a potent and selective, roscovitine-derived inhibitor of cyclin-dependent kinases, *Oncogene* 27 (2008) 5797–5807, <https://doi.org/10.1038/onc.2008.191>.
- [33] C.I. Wells, J.D. Vasta, C.R. Corona, J. Wilkinson, C.A. Zimprich, M.R. Ingold, J. E. Pickett, D.H. Drewry, K.M. Pugh, M.K. Schwinn, B.B. Hwang, H. Zegzouti, K.V. M. Huber, M. Cong, P.L. Meisenheimer, T.M. Willson, M.B. Rogers, Quantifying CDK inhibitor selectivity in live cells, *Nat. Commun.* 11 (2020) 2743, <https://doi.org/10.1038/s41467-020-16559-0>.
- [34] G.P. Sava, H. Fan, R.C. Coombes, L. Buluwela, S. Ali, CDK7 inhibitors as anticancer drugs, *Cancer Metastasis. Rev.* 39 (2020) 805–823, <https://doi.org/10.1007/s10555-020-09885-8>.
- [35] F. Gorrec, The MORPHEUS protein crystallization screen, *J. Appl. Crystallogr* 42 (2009) 1035–1042, <https://doi.org/10.1107/S0021889809042022>.
- [36] R. Page, S.K. Grzechnik, J.M. Canaves, G. Spraggon, A. Kreusch, P. Kuhn, R. C. Stevens, S.A. Lesley, Shotgun crystallization strategy for structural genomics: an optimized two-tiered crystallization screen against the *Thermotoga maritima* proteome, *Acta Crystallogr. D. Biol. Crystallogr.* 59 (2003) 1028–1037, <https://doi.org/10.1107/s0907444903007790>.
- [37] U. Mueller, N. Darowski, M.R. Fuchs, R. Forster, M. Hellmig, K.S. Paithankar, S. Puhlinger, M. Steffien, G. Zocher, M.S. Weiss, Facilities for macromolecular crystallography at the Helmholtz-Zentrum Berlin, *J. Synchrotron Radiat.* 19 (2012) 442–449, <https://doi.org/10.1107/S0909049512006395>.
- [38] W. Kabsch, XDS, *Acta Crystallogr. D. Biol. Crystallogr.* 66 (2010) 125–132, <https://doi.org/10.1107/S0907444909047337>.
- [39] A. Vagin, A. Teplyakov, MOLREP: an automated program for molecular replacement, *J. Appl. Cryst.* 30 (1997) 1022–1025, <https://doi.org/10.1107/S0021889897006766>.
- [40] G.N. Murshudov, A.A. Vagin, E.J. Dodson, Refinement of macromolecular structures by the maximum-likelihood method, *Acta Crystallogr. D. Biol. Crystallogr.* 53 (1997) 240–255, <https://doi.org/10.1107/S0907444996012255>.
- [41] P. Emsley, K. Cowtan, Coot: model-building tools for molecular graphics, *Acta Crystallogr. D. Biol. Crystallogr.* 60 (2004) 2126–2132, <https://doi.org/10.1107/S0907444904019158>.
- [42] V.B. Chen, W.B. Arendall III, J.J. Headd, D.A. Keedy, R.M. Immormino, G.J. Kapral, L.W. Murray, J.S. Richardson, D.C. Richardson, MolProbity: all-atom structure validation for macromolecular crystallography, *Acta Crystallogr. D. Biol. Crystallogr.* 66 (2010) 12–21, <https://doi.org/10.1107/S0907444909042073>.
- [43] H. Berman, K. Henrick, H. Nakamura, Announcing the worldwide Protein Data Bank, *Nat. Struct. Biol.* 10 (2003) 980, <https://doi.org/10.1038/nsb1203-980>.
- [44] R.A. Laskowski, M.B. Swindells, LigPlot+: multiple ligand-protein interaction diagrams for drug discovery, *J. Chem. Inf. Model* 51 (2011) 2778–2786, <https://doi.org/10.1021/ci200227u>.
- [45] E. Krissinel, K. Henrick, Inference of macromolecular assemblies from crystalline state, *J. Mol. Biol.* 372 (2007) 774–797, <https://doi.org/10.1016/j.jmb.2007.05.022>.
- [46] Schrodinger, L.L.C., The PyMOL Molecular Graphics System, Version 1.3r1 in, Schrodinger, LCC. 2010;
- [47] O. Trott, A.J. Olson, AutoDock Vina: improving the speed and accuracy of docking with a new scoring function, efficient optimization, and multithreading, *J. Comput. Chem.* 31 (2010) 455–461, <https://doi.org/10.1002/jcc.21334>.
- [48] R. Jorda, D. Hendrychova, J. Voller, E. Reznickova, T. Gucky, V. Krystof, How selective are pharmacological inhibitors of cell-cycle-regulating cyclin-dependent kinases, *J. Med. Chem.* 61 (2018) 9105–9120, <https://doi.org/10.1021/acs.jmedchem.8b00049>.
- [49] J. Ye, G. Coulouris, I. Zaretskaya, I. Cutcutache, S. Rozen, T.L. Madden, Primer-BLAST: a tool to design target-specific primers for polymerase chain reaction, *Bmc. Bioinforma.* 13 (2012) 134, <https://doi.org/10.1186/1471-2105-13-134>.
- [50] K.J. Livak, T.D. Schmittgen, Analysis of relative gene expression data using real-time quantitative PCR and the 2(-Delta Delta C(T)) Method, *Methods* 25 (2001) 402–408, <https://doi.org/10.1006/meth.2001.1262>.

Supplementary information

Characterization of new highly selective pyrazolo[4,3-*d*]pyrimidine inhibitor of CDK7

Markéta Kovalová¹, Libor Havlíček², Stefan Djukic³, Jana Škerlová³, Miroslav Peřina¹, Tomáš Pospíšil⁴, Eva Řezníčková¹, Pavlína Řezáčová³, Radek Jorda¹, Vladimír Kryštof^{1,5}

¹ Department of Experimental Biology, Faculty of Science, Palacký University Olomouc, Šlechtitelů 27, 78371 Olomouc, Czech Republic

² Isotope Laboratory, Institute of Experimental Botany, Czech Academy of Sciences, Vídeňská 1083, 14220 Prague, Czech Republic

³ Institute of Organic Chemistry and Biochemistry of the Czech Academy of Sciences, Flemingovo nám. 2, 16610 Prague, Czech Republic

⁴ Department of Chemical Biology, Faculty of Science, Palacký University Olomouc, Šlechtitelů 27, 78371 Olomouc, Czech Republic

⁵ Institute of Molecular and Translational Medicine, Faculty of Medicine and Dentistry, Palacký University Olomouc, Hněvotínská 5, 77900 Olomouc, Czech Republic

Content

1. Synthesis of LGR6768 and crystal structure description

Figure S1-S3, Table S1

2. Kinase selectivity

Figure S4, Table S2

3. Further cellular tests

Figure S5

4. NMR spectra

5. Cultivation condition of used cell lines

Table S3

Synthesis of LGR6768 and crystal structure description

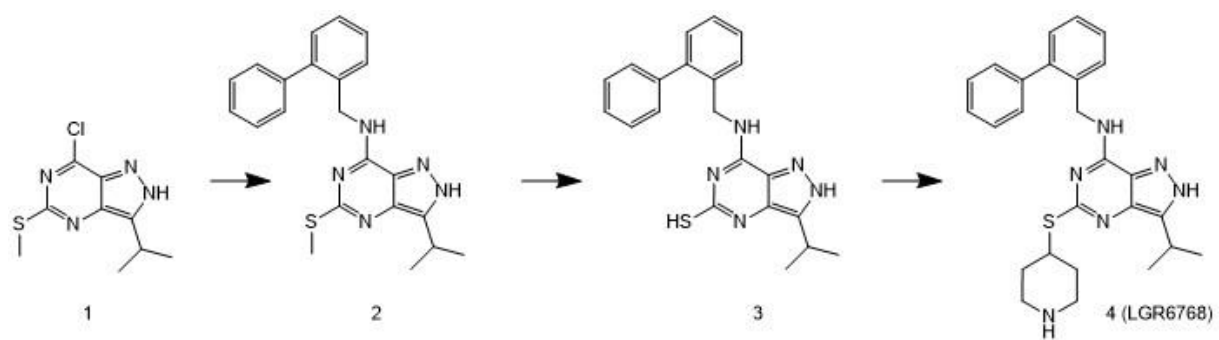


Figure S1: Synthesis of LGR6768

Table S1: X-ray data collection and refinement statistics

Data collection statistics	
Space group	$P2_12_12_1$
Cell parameters a, b, c [Å]; α , β , γ [°]	73.02, 134.99, 163.96 90.00, 90.00, 90.00
Wavelength [Å]	0.918
Resolution [Å]	50.00-2.60 (2.76-2.60)
Unique reflections	50,620 (8,027)
Multiplicity	13.6 (14.2)
Completeness [%]	99.9 (100)
R_{meas} [%] ^a	61.3 (290.3)
$CC_{(1/2)}$ [%] ^b	98.8 (71.7)
Average $I/\sigma(I)$	5.42 (1.01)
Wilson B [Å ²] ^c	39.44
Refinement statistics	
Resolution range [Å]	49.56-2.60 (2.68-2.60)
No. of reflections in working set	49,156 (3,539)
No. of reflections in test set	1,460 (105)
R value [%] ^d	23.3 (40.3)
R-free value [%] ^e	28.7 (39.8)
RMSD deviation from ideal bond length [Å]	0.011
RMSD deviation from ideal bond angle [°]	1.596
Number of protein atoms	8,845
Number of water molecules	314
Number of other non-protein atoms	98
Mean B value [Å ²]	39.61
Residues in Ramachandran favored regions [%] ^f	96.47
Residues in Ramachandran allowed regions [%] ^f	99.63

^a R_{meas} defined in ref. [1]. ^b $CC_{(1/2)}$ is Pearson's correlation coefficient determined on the data set randomly split in half [2]. ^cWilson B by the Scheck program from the CCP4 suite [3]. ^dR-value = $\frac{\sum |F_o - F_c|}{\sum |F_o|}$, where F_o and F_c are the observed and calculated structure factors, respectively. ^e R_{free} is

equivalent to the R-value but is calculated for 5% of the reflections chosen at random and omitted from the refinement process [4]. ^fAs determined by MolProbity [5].

The asymmetric unit of the crystal contains two CDK2/cyclin A2 heterodimers (protein chains A/B and C/D). All the residues are modeled into the electron density map, except for disordered residues 39-40 in chains A and C, as well as residues 175-176 in chain B and 175-177 in chain D. Inhibitor LGR6768 was modeled into well-defined electron density in both active sites with full occupancy (Figure S2). The RMSD for the superposition of the C α atoms for the two heterodimers is 0.154 Å² and the conformation of the active site residues and the ligand poses in the two heterodimers are almost identical. Heterodimer A/B was used to describe protein – inhibitor interactions.

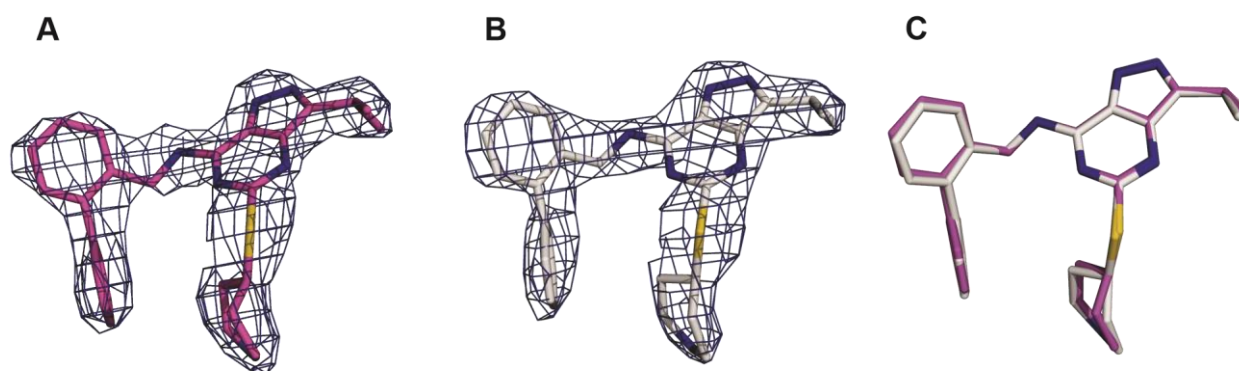


Figure S2: Electron density for the inhibitor LGR6768 in the active site A (panel A) and C (panel B). A superposition of the inhibitor molecules bound in the two active sites is shown in panel C. The inhibitor is shown as sticks with carbon atoms in magenta (active site A) and gray (active site C), nitrogen atoms are blue, and sulfur atoms yellow; *2Fo-Fc* maps are shown as blue mesh at 1.3 σ .

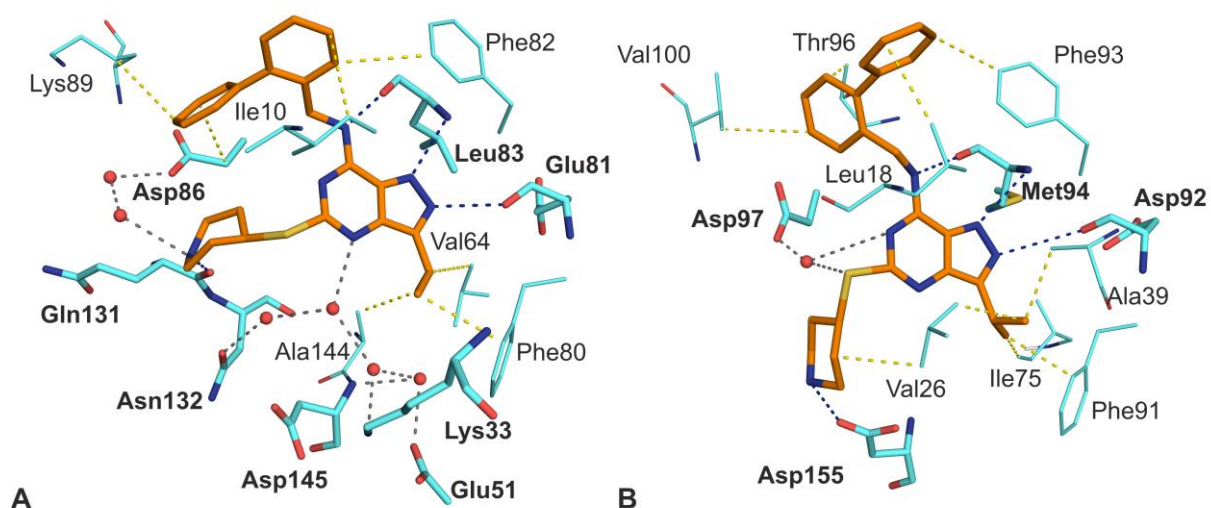


Figure S3: LGR6768 in the active site of CDK2 (crystal structure, panel A) and CDK7 (molecular docking, panel B). Interacting residues are shown as sticks with H-bond forming residues labelled with bold font and other residues with regular font. Direct H-bonds are shown as blue dashed lines, water-mediated H-bonds as grey dashed lines, and hydrophobic interactions as yellow dashed lines. Carbon atoms are cyan (protein) and orange (inhibitor). Nitrogen atoms are blue, oxygen atoms red, sulphur atoms are yellow, and waters are shown as red spheres. Residues Ala31 Val18, and Leu134 from CDK2, and Leu144 from CDK7 were not shown for clarity. Structure of LGR6768 in complex with CDK2 has been deposited to the PDB under the code 8B54.

Kinase selectivity

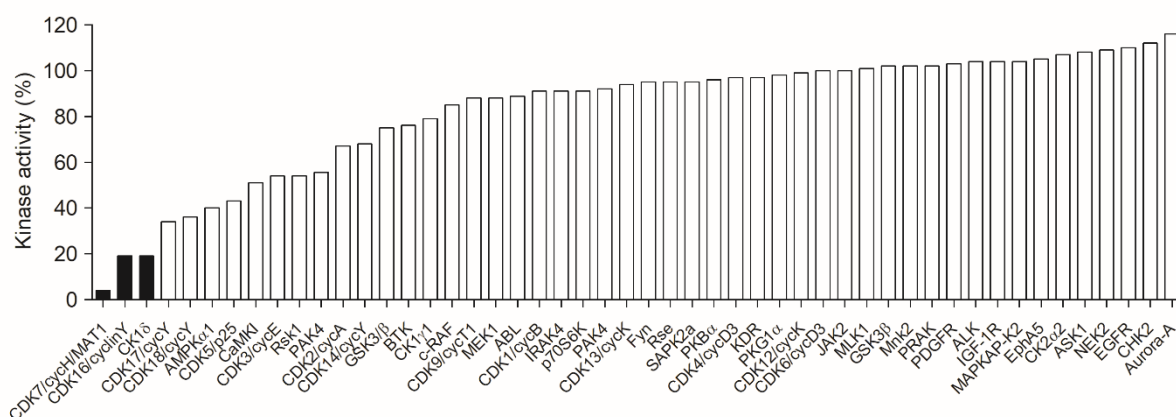


Figure S4: Selectivity profiling of LGR6768. The compound was applied in a single 1 μ M concentration on 50 kinases.

Table S2: CDK selectivity profile of LGR6768

kinase	IC ₅₀ (μ M)*
CDK1/cyclin B	5.14 (\pm 0.97)
CDK2/cyclin A	0.50 (\pm 0.05)
CDK2/cyclin E	0.25 (\pm 0.01)
CDK4/cyclin D1	>20
CDK5/p25	1.12 (\pm 0.1)
CDK7/cyclin H/MAT1	0.02 (\pm 0.02)
CDK9/cyclin T	6.55 (\pm 1.70)

* – measured at least in duplicate

Further cellular tests

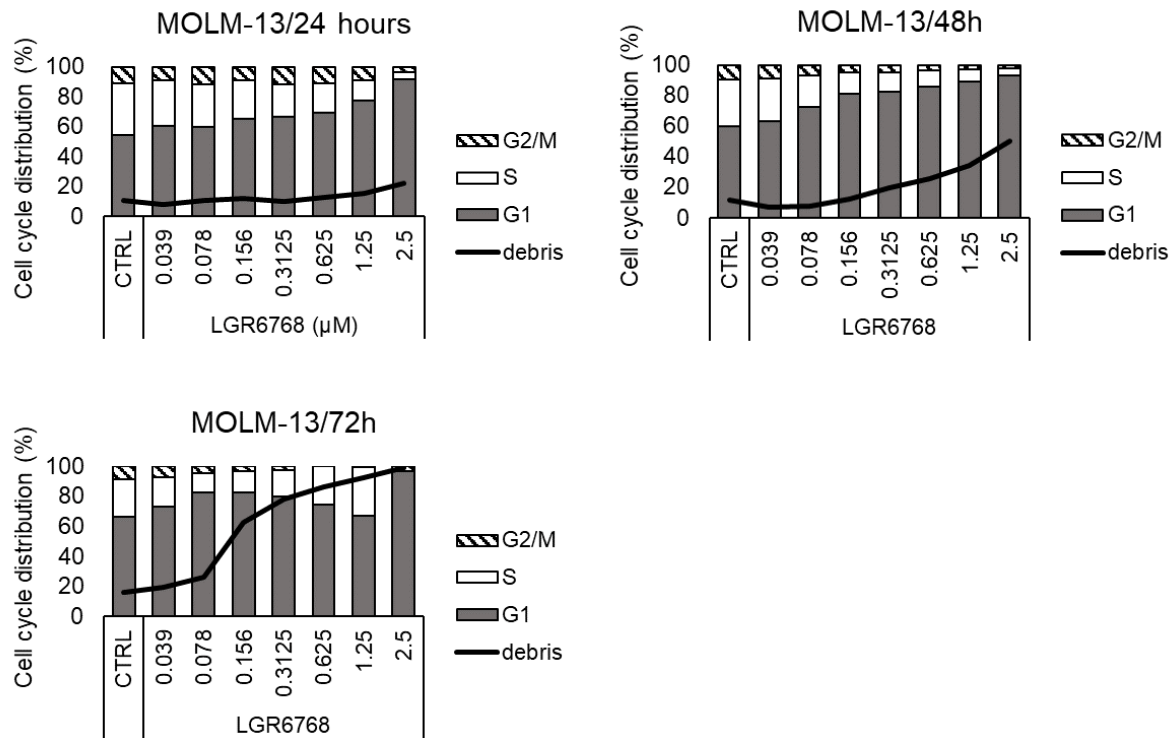
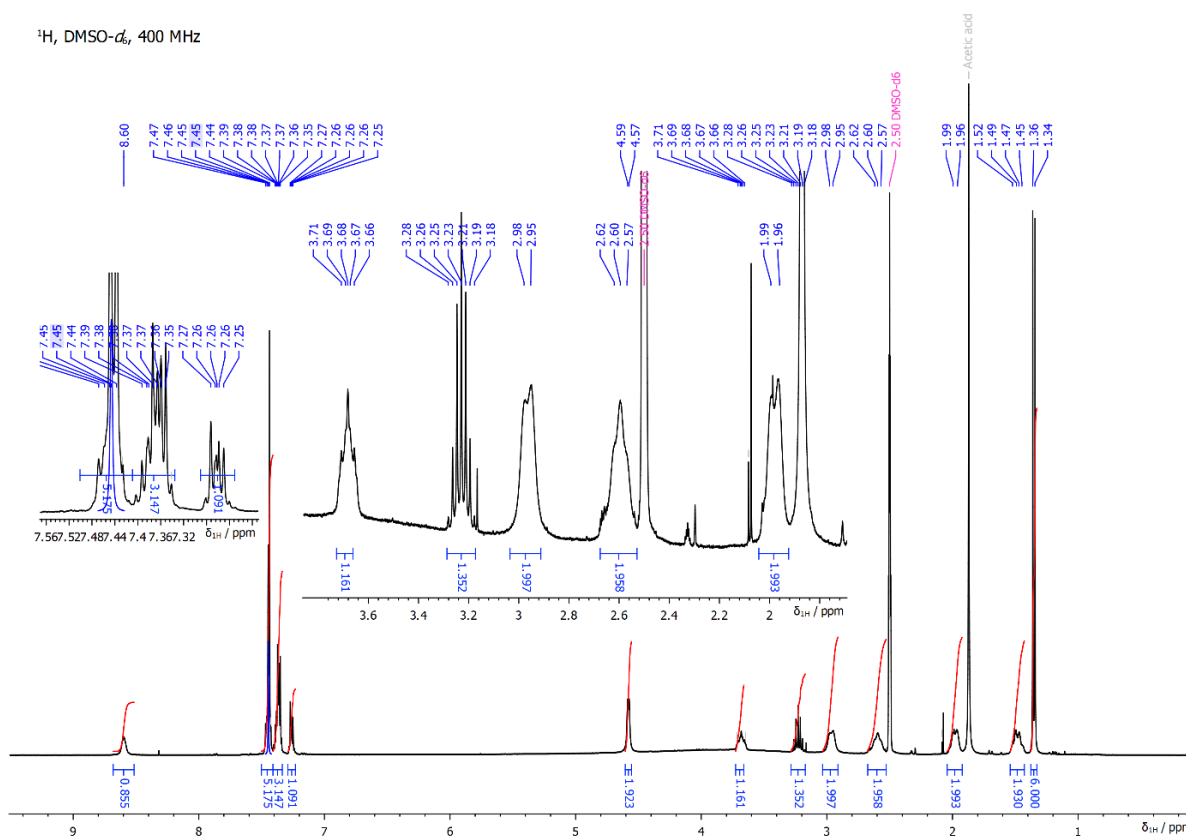


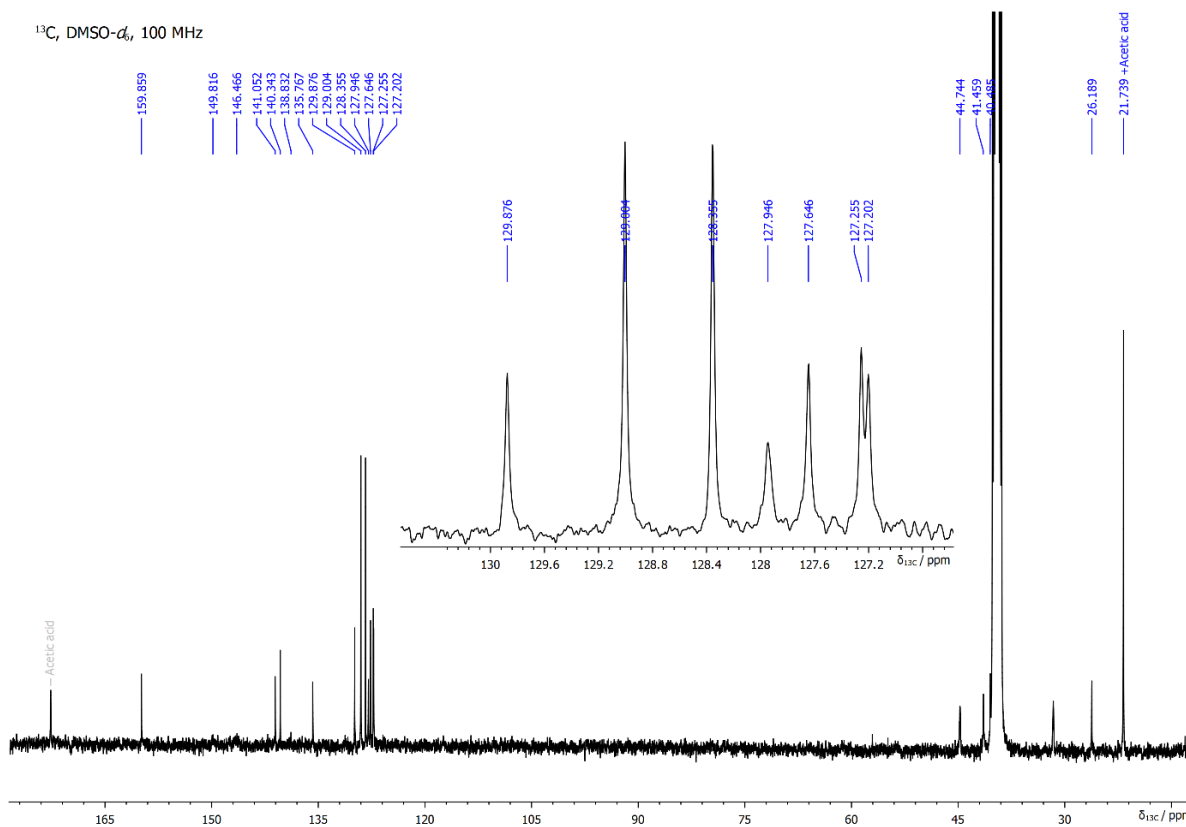
Figure S5: Effect of LGR6768 on cell cycle in MOLM-13 cell line. Cells were treated for 24, 48, or 72 hours with an increasing concentration of LGR6768 or vehicle.

NMR Spectra

¹H, DMSO-d₆, 400 MHz



¹³C, DMSO-d₆, 100 MHz



Cultivation conditions of used cell lines

Table S3: Used cell lines with source and culture media

Cell line	Cancer type	Source	Used medium
22Rv1	Prostate	Jan Bouchal*	RPMI
BT474	Breast	Jan Bouchal*	DMEM
CCFR- CEM	ALL	ECACC	RPMI
DU145	Prostate	Jan Bouchal*	RPMI
G361	Melanoma	ECACC	DMEM
HL-60	AML	ECACC	IMDM
K562	CML	ECACC	DMEM
LAPC4	Prostate	Jan Bouchal*	DMEM
MCF7	Breast	ECACC	DMEM
MINO	Lymphoma	ATCC	RPMI
MOLM-13	AML	DSMZ	RPMI
MV4-11	AML	Cell line service	RPMI
RS4-11	ALL	DSMZ	α -MEM
SEM	ALL	DSMZ	IMDM
SKBR3	Breast	ATCC	DMEM
THP-1	AML	DSMZ	RPMI
U937	AML	DSMZ	RPMI

AML – acute myeloid leukemia, ALL – acute lymphoblastic leukemia, CML – chronic myeloid leukemia; ATCC - American Tissue Culture Collection; DSMZ - German Collection of Microorganisms and Cell Cultures; ECACC - European Collection of Authenticated Cell Culture;

* Cells were kindly gifted by Jan Bouchal from Palacký University Olomouc.

Supplementary references

1. Diederichs, K. & Karplus, P. A. (1997) Improved R-factors for diffraction data analysis in macromolecular crystallography, *Nature structural biology*. **4**, 269-75.
2. Karplus, P. A. & Diederichs, K. (2012) Linking crystallographic model and data quality, *Science*. **336**, 1030-1033.
3. Collaborative Computational Project, N. (1994) The CCP4 suite: programs for protein crystallography, *Acta crystallographica Section D, Biological crystallography*. **50**, 760-3.
4. Brunger, A. T. (1992) Free R value: a novel statistical quantity for assessing the accuracy of crystal structures, *Nature*. **355**, 472-5.
5. Chen, V. B., Arendall, W. B., 3rd, Headd, J. J., Keedy, D. A., Immormino, R. M., Kapral, G. J., Murray, L. W., Richardson, J. S. & Richardson, D. C. (2010) MolProbity: all-atom structure validation for macromolecular crystallography, *Acta crystallographica Section D, Biological crystallography*. **66**, 12-21.

PŘÍLOHA III

Břehová, P., Řezníčková, E., Škach, K., Jorda, R., Dejmek, M., Vojáčková, V., Šála, M, **Kovalová, M.**, Dračínský, M., Dolníková, A., Strmeň, T., Kinnertová, M., Chalupský, K., Dvořáková, A., Gucký, T., Mertlíková Kaiserová, H, Klener, P., Nencka, R., Kryštof, V. (2023). Inhibition of FLT3-ITD Kinase in Acute Myeloid Leukemia by New Imidazo[1,2-*b*]pyridazine Derivatives Identified by Scaffold Hopping. *J Med Chem*, 66(16), 11133-11157.

<https://doi.org/10.1021/acs.jmedchem.3c00575>

Inhibition of FLT3-ITD Kinase in Acute Myeloid Leukemia by New Imidazo[1,2-*b*]pyridazine Derivatives Identified by Scaffold Hopping

Petra Břehová,[†] Eva Řezníčková,[†] Kryštof Škach, Radek Jorda, Milan Dejmek, Veronika Vojáčková, Michal Šála, Markéta Kovalová, Martin Dračínský, Alexandra Dolníková, Timotej Strmeň, Monika Kinnertová, Karel Chalupský, Alexandra Dvořáková, Tomáš Gucký, Helena Mertlíková Kaiserová, Pavel Klener, Radim Nencka,* and Vladimír Kryštof*

Cite This: *J. Med. Chem.* 2023, 66, 11133–11157

Read Online

ACCESS |



Metrics & More

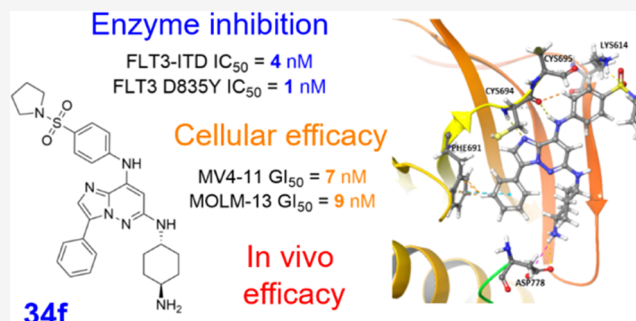


Article Recommendations



Supporting Information

ABSTRACT: FLT3 kinase is a potential drug target in acute myeloid leukemia (AML). Patients with FLT3 mutations typically have higher relapse rates and worse outcomes than patients without FLT3 mutations. In this study, we investigated the suitability of various heterocycles as central cores of FLT3 inhibitors, including thieno[3,2-*d*]pyrimidine, pyrazolo[1,5-*a*]pyrimidine, imidazo[4,5-*b*]pyridine, pyrido[4,3-*d*]pyrimidine, and imidazo[1,2-*b*]pyridazine. Our assays revealed a series of imidazo[1,2-*b*]pyridazines with high potency against FLT3. Compound 34f showed nanomolar inhibitory activity against recombinant FLT3-ITD and FLT3-D835Y (IC₅₀ values 4 and 1 nM, respectively) as well as in the FLT3-ITD-positive AML cell lines MV4-11, MOLM-13, and MOLM-13 expressing the FLT3-ITD-D835Y mutant (GI₅₀ values of 7, 9, and 4 nM, respectively). In contrast, FLT3-independent cell lines were much less sensitive. In vitro experiments confirmed suppression of FLT3 downstream signaling pathways. Finally, the treatment of MV4-11 xenograft-bearing mice with 34f at doses of 5 and 10 mg/kg markedly blocked tumor growth without any adverse effects.



INTRODUCTION

Acute myeloid leukemia (AML) is a malignant clonal disorder of the hematopoietic system characterized by infiltration of the bone marrow, peripheral blood, and other tissues by abnormally differentiated blasts of myeloid lineage.^{1,2} Although AML can occur at any age, it is the most common acute type of leukemia in adults and increases in incidence with age. The five-year overall survival of patients diagnosed with AML is estimated to be less than 50%.³ Despite the growing number of drugs available for the treatment of AML, the need for efficient therapeutic strategies persists. Advances in molecular cancer biology have resulted in the identification of potential therapeutic targets for the treatment of AML. Mutations of the FMS-like tyrosine kinase 3 (FLT3) gene occur in approximately 30% of AML cases. Patients with FLT3 mutations have higher relapse rates and worse outcomes for both overall survival and disease-free survival in comparison with patients without FLT3 mutations.

FLT3 is a membrane-bound cytokine receptor closely related to KIT, FMS, and PDGFR. Binding to an extracellular ligand results in receptor dimerization and autophosphorylation of tyrosine residues in the intracellular domain, which activates downstream signaling pathways, including RAS/MAPK, JAK/STATS, and PI3K/AKT/mTOR. These path-

ways promote the growth, proliferation, survival, and differentiation of myeloid cells.^{4,5}

Internal tandem duplication (ITD), which represents the most common group of FLT3 mutations, occurs in 20–25% of all AML patients. ITD promotes ligand-independent dimerization and downstream signaling.^{6,7} Point mutations in the tyrosine kinase domain (FLT3-TKD) are approximately twice less prevalent. TKD mutations stabilize the kinase in its active conformation. Both FLT3-ITD and FLT3-TKD mutations can cause ligand-independent FLT3 kinase activation and promote cell proliferation, resulting in a high leukemic burden.

As mutated FLT3 is considered an attractive target for the treatment of AML, several small-molecule inhibitors have been investigated as potential therapeutics.^{8–10} First-generation inhibitors comprise nonspecific receptor tyrosine kinase inhibitors, such as sunitinib, sorafenib, and midostaurin,

Received: March 31, 2023

Published: August 3, 2023



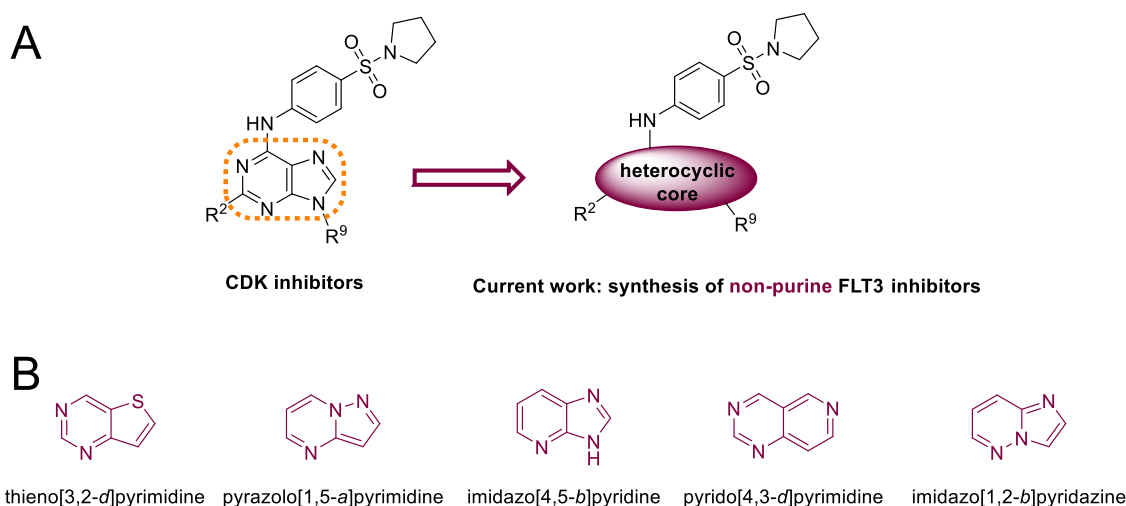
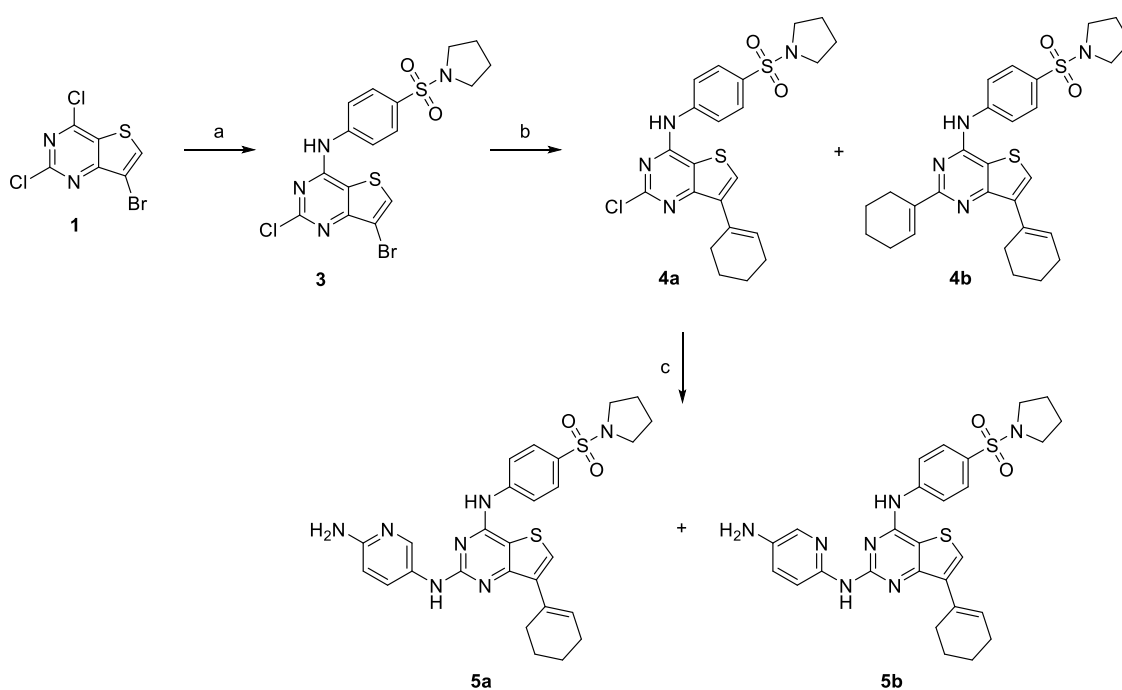


Figure 1. Structural modifications of kinase inhibitors leading to (A) FLT3 inhibitors and (B) heterocyclic cores explored in this study.

Scheme 1. Synthesis of Thieno[3,2-*d*]pyrimidine Derivatives^a



^aReagents and conditions: (a) 4-(pyrrolidin-1-ylsulfonyl)aniline (**2**), *t*-BuOK, *N,N*-dimethylformamide (DMF), 0 °C; (b) cyclohex-1-en-1-ylboronic acid, Cs₂CO₃, Pd(dppf)Cl₂-dichloromethane (DCM), dioxane, water, 95 °C; and (c) 2,5-diaminopyridine hydrochloride, Cs₂CO₃, XPhos Pd G2, DMF, 95 °C.

originally developed for other indications. A second generation of more selective and efficient inhibitors, which exhibit lower toxicity and off-target effects, has also been developed. These inhibitors, which include quizartinib, crenolanib, and gilteritinib, produce significant responses in AML patients.

In our previous studies, we investigated trisubstituted purines as kinase inhibitors and carbocyclic nucleoside derivatives with CDK2 inhibitory activity, among other analogues.¹¹ We revealed that some of these compounds display nanomolar inhibitory potency toward FLT3 kinase (unpublished observation, Supporting Information, Table S1). These findings are substantiated in another of our studies, which found that trisubstituted purine derivatives are potent FLT3 inhibitors that selectively block the proliferation of AML

cell lines harboring FLT3-ITD mutations.¹² In order to identify potent and selective FLT3 inhibitors, we focused on synthesizing heterocyclic mimics of the purine base bearing similar substitution patterns as the parent purine derivatives. We designed trisubstituted derivatives containing various heterocyclic cores (Figure 1B) and then evaluated their inhibitory effects on FLT3 kinase *in vitro* and *in vivo*.

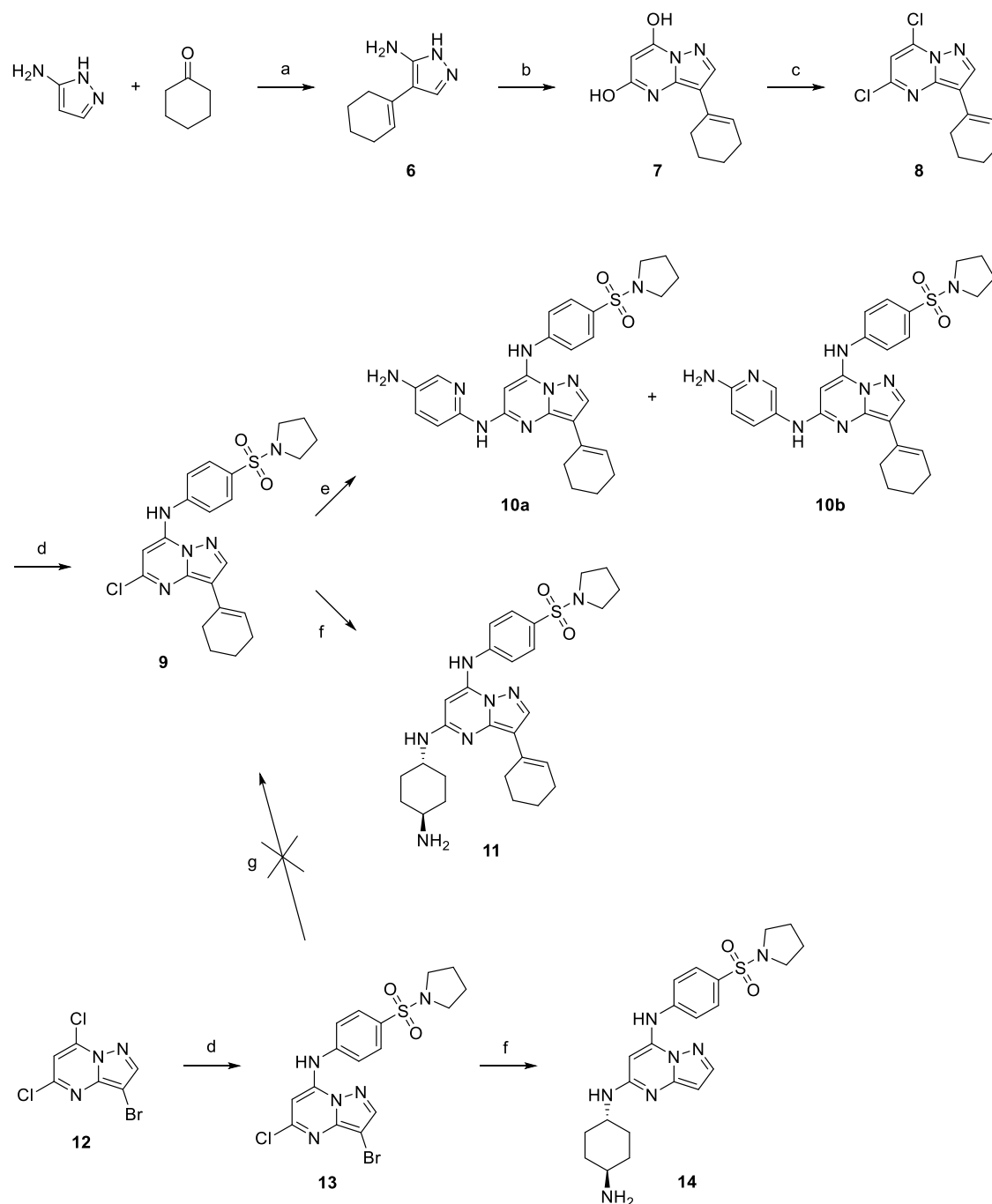
RESULTS AND DISCUSSION

Trisubstituted purines were previously described as potent CDK and FLT3-ITD kinase inhibitors.^{12–15} In order to explore this understudied chemical space and generate new active compounds, we designed new isosteric trisubstituted derivatives of several heterocyclic cores, including thieno[3,2-

Table 1. Kinase-Inhibitory and Antiproliferative Activities of Thieno[3,2-*d*]pyrimidine Derivatives

	IC ₅₀ (μM) ^a			GI ₅₀ (μM) ^a						
	FLT3-ITD	FLT3-D835Y	CDK2/E	MV4-11	MOLM-13	SEM	CEM	NOMO-1	ML-2	K562
4a	>20	NT	>20	1.765	3.260	>6.25	>6.25	>10	>10	9.890
4b	>20	NT	>20	2.570	6.010	4.400	>6.25	8.945	6.775	8.533
5a	5.098	NT	17.204	1.665	2.180	1.467	7.490	8.030	4.243	6.595
5b	>20	NT	>20	2.705	6.075	2.595	>10	>10	7.335	>10

^aFor standard deviation (SD) values, see Table S3 in the Supporting Information. NT = not tested.

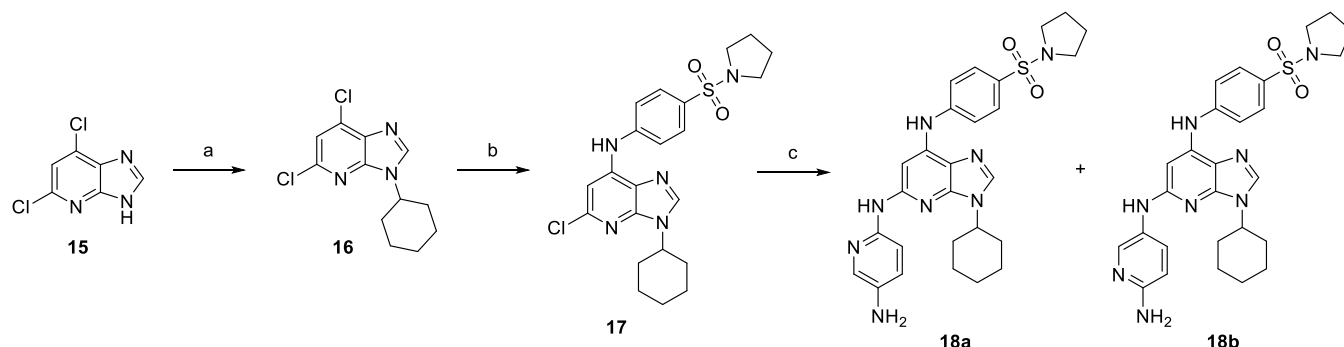
Scheme 2. Synthesis of Pyrazolo[1,5-*a*]pyrimidine Derivatives^a

^aReagents and conditions: (a) AcOH, RT; (b) Na, CH₂(COOEt)₂, EtOH, reflux; (c) POCl₃, *N,N*-dimethylaniline, 80 °C; (d) 4-(pyrrolidin-1-ylsulfonyl)aniline (2), *t*-BuOK, DMF, 0 °C; (e) 2,5-diaminopyridine hydrochloride, Cs₂CO₃, Pd₂(dba)₃, Xantphos, DMF, 120 °C; (f) *trans*-1,4-diaminocyclohexane, *N*-methylpyrrolidone (NMP), 210 °C; and (g) cyclohex-1-en-1-ylboronic acid, Cs₂CO₃, Pd(dppf)Cl₂·DCM, dioxane, water, 95 °C.

Table 2. Kinase-Inhibitory and Antiproliferative Activities of Pyrazolo[1,5-*a*]pyrimidine Derivatives

	IC ₅₀ (μM) ^a			GI ₅₀ (μM) ^a						
	FLT3-ITD	FLT3-D835Y	CDK2/E	MV4-11	MOLM-13	SEM	CEM	NOMO-1	ML-2	K562
9	>20	NT	>20	7.360	3.285	1.575	3.595	>10	>10	>10
10a	10.612	NT	>20	>10	>10	>10	>10	>10	>10	>10
10b	2.507	NT	>20	5.737	3.280	9.840	>10	>10	>10	>10
11	0.540	0.109	0.774	1.817	2.553	5.510	>10	>10	>10	>10
14	0.623	0.272	0.100	0.690	1.413	7.905	>10	>10	>10	>10

^aFor SD values, see Table S3 in the Supporting Information. NT = not tested.

Scheme 3. Synthesis of Imidazo[4,5-*b*]pyridine Derivatives^a

^aReagents and conditions: (a) cyclohexanol, Ph₃P, diisopropyl azodicarboxylate (DIAD), dioxane, RT; (b) 4-(pyrrolidin-1-ylsulfonyl)aniline (**2**), *t*-BuOK, DMF, 0 °C; and (c) 2,5-diaminopyridine hydrochloride, Cs₂CO₃, Pd₂(dba)₃, Xantphos, DMF, 115 °C.

d]pyrimidine,^{16–18} pyrazolo[1,5-*a*]pyrimidine,^{19–21} imidazo[4,5-*b*]pyridine,²² pyrido[4,3-*d*]pyrimidine,²³ and imidazo[1,2-*b*]pyridazine^{24,25} (Figure 1B). All of the prepared compounds were tested for their inhibitory activity against recombinant FLT3-ITD and CDK2/E. The most active compounds were screened against the FLT3-D835Y mutant, which is the most common resistance initiator in AML patients treated with clinically approved FLT3 inhibitors. To evaluate the FLT3-dependent mechanism of action, compounds were further screened for antiproliferative activity in a panel of human leukemia cell lines. Two AML cell lines, MV4-11 and MOLM-13, characterized by the presence of FLT3-ITD (full FLT3-dependency) and SEM, an acute lymphoblastic leukemia (ALL) cell line overexpressing FLT3-wt (with partial dependency on FLT3 signaling), were supplemented with four FLT3-independent cell lines. These included the AML-derived cell lines NOMO-1 and ML-2, the ALL-derived cell line CEM, and chronic myeloid leukemia (CML)-derived K562 cells.

Synthesis and Activity of Thieno[3,2-*d*]pyrimidines. Thieno[3,2-*d*]pyrimidine derivatives (Scheme 1) were prepared from 7-bromo-2,4-dichloro-thieno[3,2-*d*]pyrimidine (**1**).²⁶ Reaction with 4-(pyrrolidin-1-ylsulfonyl)aniline (**2**) in the presence of *t*-BuOK at 0 °C afforded substituted derivative **3**. Subsequent Suzuki cross-coupling proceeded smoothly and afforded monoderivative **4a** as a major product together with dialkylated compound **4b**. Buchwald–Hartwig cross-coupling of chloro derivative **4a** produced a mixture of two isomers **5a** and **5b** in 10 and 25% yield, respectively. Heating of **4a** with *trans*-1,4-cyclohexyldiamine led to the decomposition of the starting material; only traces of the product were detected (data not shown).

Compounds containing the thieno[3,2-*d*]pyrimidine core did not display significant inhibitory activity against recombinant FLT3-ITD. Their antiproliferative activities against

leukemic cell lines varied mainly within the micromolar range (see Table 1).

Synthesis and Activity of Pyrazolo[1,5-*a*]pyrimidines. First, the cyclohexenyl ring in pyrazolo[1,5-*a*]pyrimidine derivatives (Scheme 2) had to be installed by cyclization of 4-(cyclohex-1-en-1-yl)-1*H*-pyrazol-5-amine (**6**) with diethyl malonate^{29,30} due to the low reactivity of bromo derivative **13** in the subsequent Suzuki cross-coupling reaction. Dihydroxy derivative **7** was refluxed in POCl₃ to give dichloro derivative **8**, which was further converted to sulfonamide **9**. Buchwald–Hartwig cross-coupling of **9** with 2,5-diaminopyridine afforded derivatives **10a** and **10b** in moderate yields. Heating of **9** with *trans*-1,4-cyclohexyldiamine gave compound **11**. However, heating of **13** with *trans*-1,4-cyclohexyldiamine at 210 °C overnight afforded debrominated amino derivative **14**.

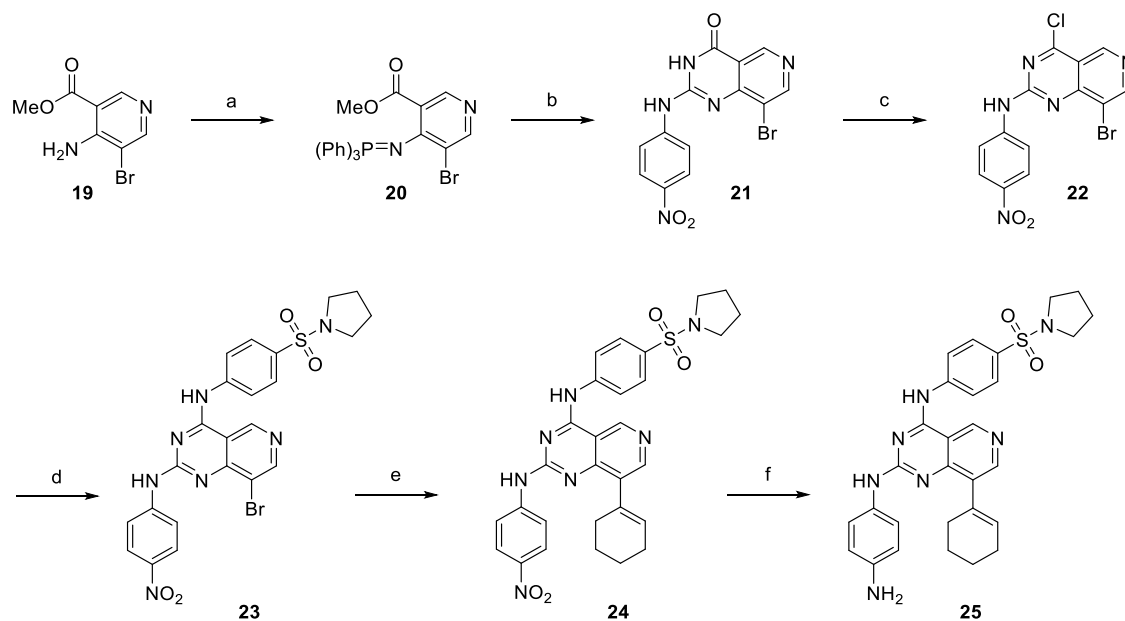
Compounds from the pyrazolo[1,5-*a*]pyrimidine series showed poor potency against the tested recombinant kinases. Their antiproliferative activities did not reach measurable values in most of the compounds (GI₅₀ > 10 μM; Table 2). Only disubstituted pyrazolo[1,5-*a*]pyrimidine derivative **14** bearing 4-(pyrrolidin-1-ylsulfonyl)aniline and aminocyclohexylamino substituents in positions 7 and 5, respectively, and trisubstituted derivative **11** bearing an additional cyclohexenyl in position 3 showed submicromolar activities against FLT3-ITD and CDK2. Also, FLT3-ITD-positive MV4-11 and MOLM-13 cell lines were more sensitive to treatment than FLT3-independent cell lines, indicating the FLT3-dependent mechanism of action (Table 2).

Synthesis and Activity of Imidazo[4,5-*b*]pyridine Derivatives. Imidazo[4,5-*b*]pyridine derivatives (Scheme 3) were prepared by alkylation of commercially available 5,7-dichloro-1*H*-imidazo[4,5-*b*]pyridine (**15**) under Mitsunobu conditions.^{31,32} Further substitution with aniline substituent and Buchwald–Hartwig amination with 2,5-diaminopyridine afforded derivatives **18a** and **18b** (Scheme 3).

Table 3. Kinase-Inhibitory and Antiproliferative Activities of Imidazo[4,5-*b*]pyridine Derivatives

	IC ₅₀ (μM) ^a			GI ₅₀ (μM) ^a						
	FLT3-ITD	FLT3-D835Y	CDK2/E	MV4-11	MOLM-13	SEM	CEM	NOMO-1	ML-2	K562
17	2.453	NT	>20	5.520	3.075	>10	>10	>10	9.530	>10
18a	0.430	0.479	>20	1.877	1.540	2.380	>10	>10	>10	>10
18b	0.134	0.392	>20	0.735	0.335	1.565	>10	8.565	5.835	8.180

^aFor SD values, see Table S3 in the Supporting Information. NT = not tested.

Scheme 4. Synthesis of Pyrido[4,3-*d*]pyrimidine Derivatives^a

^aReagents and conditions: (a) Ph₃P, Br₂, triethylamine (TEA), DCM, 0 °C to RT; (b) (i) 4-nitrophenyl isocyanate, tetrahydrofuran (THF), RT; (ii) NH₃, RT; (c) POCl₃, *N,N*-dimethylaniline; (d) 4-(pyrrolidin-1-ylsulfonyl)aniline (**2**), *t*-BuOK, DMF, 0 °C; (e) cyclohex-1-en-1-ylboronic acid, Cs₂CO₃, Pd(dppf)Cl₂·DCM, DMF, water, 80 °C; and (f) Pd/C (10% wt), H₂, 15 bar, RT.

Table 4. Kinase-Inhibitory and Antiproliferative Activities of Pyrido[4,3-*d*]pyrimidine Derivatives

	IC ₅₀ (μM) ^a			GI ₅₀ (μM) ^a						
	FLT3-ITD	FLT3-D835Y	CDK2/E	MV4-11	MOLM-13	SEM	CEM	NOMO-1	ML-2	K562
23	>20	NT	>20	3.900	1.675	1.340	3.365	7.510	8.295	8.710
24	>20	NT	>20	>10	>10	>10	>10	>10	>10	>10
25	1.907	NT	>20	6.560	4.520	7.350	>10	>10	>10	9.530

^aFor SD values, see Table S3 in the Supporting Information. NT = not tested.

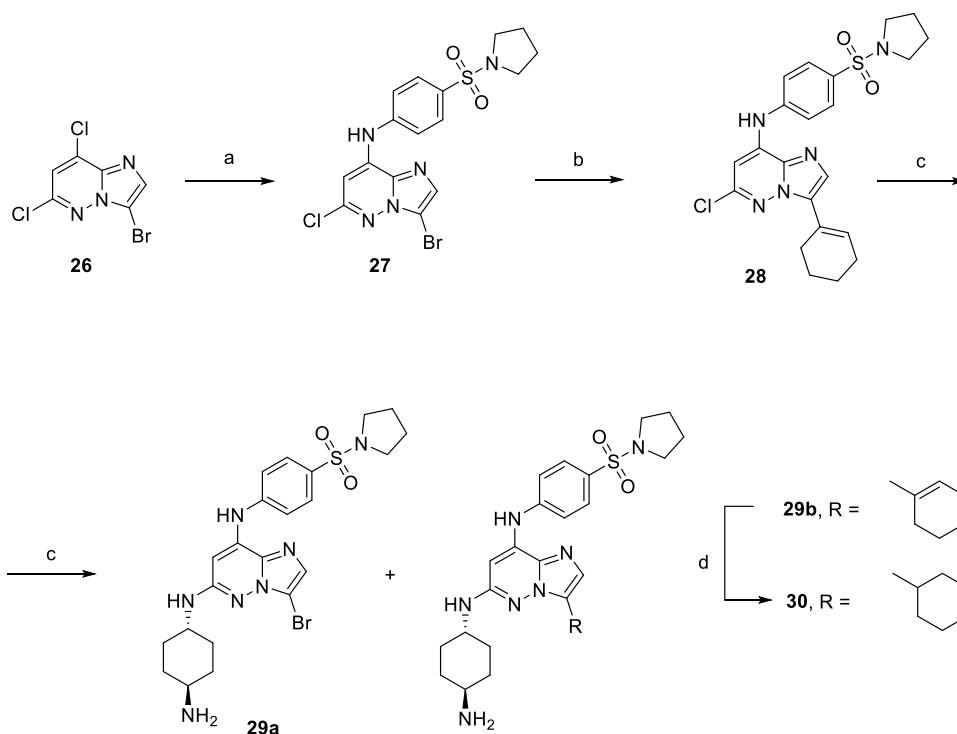
Imidazo[4,5-*b*]pyridine derivatives **18a** and **18b** with 4-(pyrrolidin-1-ylsulfonyl)aniline substituent in position 7, cyclohexyl moiety in position 3, and 6-aminopyridin-2/3-yl in position 5 displayed submicromolar activities against recombinant FLT3-ITD and FLT3-D835Y (Table 3). Moreover, antiproliferative activities established in the panel of leukemia cell lines indicated an FLT3-dependent mechanism of action. Nevertheless, the rather weak potency of these molecules required further modification of the heterocycle core.

Synthesis and Activity of Pyrido[4,3-*d*]pyrimidines. Pyrido[4,3-*d*]pyrimidine derivatives (Scheme 4) were prepared according to a procedure described by Jansa et al.³³ Activation of bromonicotinate with triphenylphosphine and ring closure with isocyanate afforded derivative **21**. Chlorination and subsequent substitution with an aniline derivative afforded compound **23**, which reacted with cyclohexene-1-boronic acid to give derivative **24** in a high yield. Final reduction with H₂

(15 bar) on Pd/C for 2 days afforded amino derivative **25** with an unsaturated cyclohexene ring. However, modification of the pyrido[4,3-*d*]pyrimidine core proved counterproductive, given the prepared compounds failed to show any promising activity (Table 4).

Synthesis and Activity of Imidazo[1,2-*b*]pyridazines.

Finally, we focused on imidazo[1,2-*b*]pyridazine derivatives (Scheme 5). We started with 3-bromo-6-chloro derivative **27**. However, it showed very poor reactivity under Suzuki cross-coupling conditions and afforded only a small amount of **28** together with the starting material as an inseparable mixture. Next, we treated the mixture with 1,4-*trans*-cyclohexendiamine, separated the products by reverse phase chromatography, and isolated compounds **29a** and **29b**. Unsaturated derivative **29b** was hydrogenated by H₂ on Pd/C to give **30** (Scheme 5). Attempts to prepare 2,5-diaminopyridine derivatives using the Buchwald–Hartwig reaction failed, and 6-chloro derivative **28** proved poorly reactive.

Scheme 5. Synthesis of Imidazo[1,2-*b*]pyridazine Derivatives^a

^aReagents and conditions: (a) 4-(pyrrolidin-1-ylsulfonyl)aniline (**2**), *t*-BuOK, DMF, 0 °C; (b) cyclohex-1-en-1-ylboronic acid, Cs₂CO₃, Pd(dppf)Cl₂-DCM, dioxane, water, 95 °C; (c) *trans*-1,4-diaminocyclohexane, NMP, 210 °C; and (d) Pd/C (10% wt), H₂, EtOAc, MeOH, 15 bar, RT.

Table 5. Kinase-Inhibitory and Antiproliferative Activities of Imidazo[1,2-*b*]pyridazine Derivatives

	IC ₅₀ (μM) ^a			GI ₅₀ (μM) ^a						
	FLT3-ITD	FLT3-D835Y	CDK2/E	MV4-11	MOLM-13	SEM	CEM	NOMO-1	ML-2	KS62
29a	0.002	0.002	0.003	0.0001	0.004	0.008	0.623	0.240	0.118	0.320
29b	0.005	0.004	0.037	0.001	0.024	0.225	1.073	1.380	0.596	0.722
30	0.006	0.012	0.211	0.279	0.070	0.655	1.910	4.875	3.100	1.363

^aFor SD values, see Table S3 in the Supporting Information.

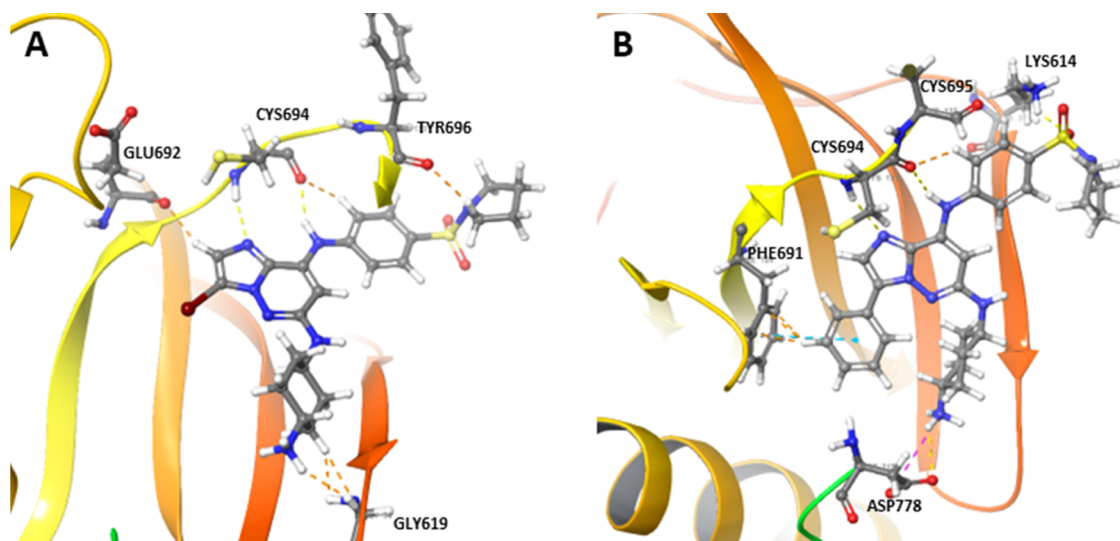


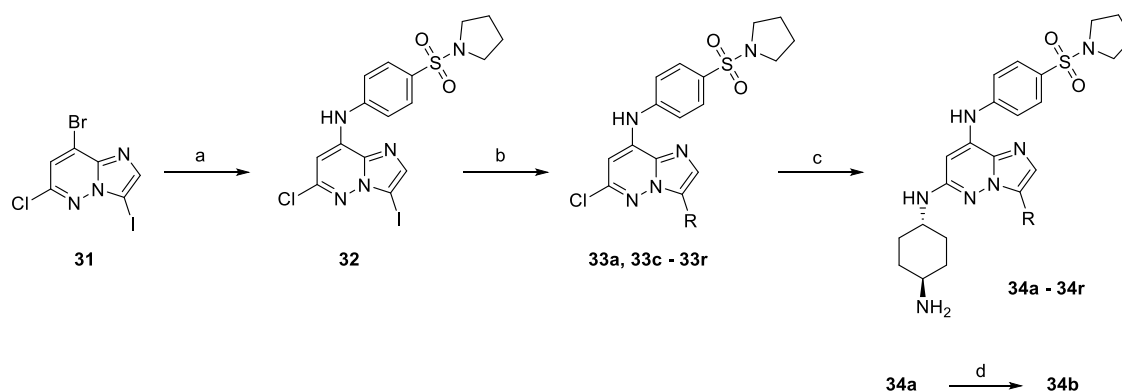
Figure 2. Docked binding poses of (A) compound **29a** and (B) its phenyl derivative **34f** in the active FLT3 site.

The first candidates of the imidazo[1,2-*b*]pyridazine series shared the 4-(pyrrolidin-1-ylsulfonyl)aniline substituent in

position 8 and the *trans*-1,4-diaminocyclohexyl substituent in position 6. Substituents in position 3 included Br (**29a**),

Table 6. Substituted Imidazo[1,2-*b*]pyridazine Derivatives in Position 3 of the Heterocyclic Core

Compd.	R	Compd.	R
33a	34a	33j	34j
-	34b	33k	34k
33c	34c	33l	34l
33d	34d	33m	34m
33e	34e	33n	34n
33f	34f	33o	34o
33g	34g	33p	34p
33h	34h	33q	34q
33i	34i	33r	34r

Scheme 6. Synthesis of Imidazo[1,2-*b*]pyridazine Derivatives Modified in Position 3^a

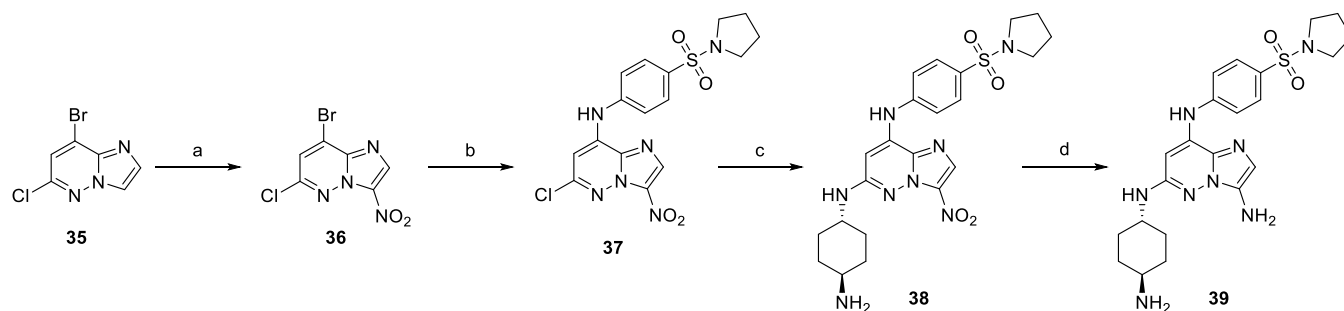
^aReagents and conditions: (a) 4-(pyrrolidin-1-ylsulfonyl)aniline (2), *t*-BuOK, DMF, 0 °C; (b) for 33a and 33f–33r: boronic acid, Cs₂CO₃, Pd(dppf)Cl₂·DCM, dioxane, water, 95 °C; for 33c and 33d: alkylzinc bromide, Pd(dppf)Cl₂·DCM, THF, 45 °C; for 33e: Pd₂(dba)₃, XPhos, DABAL-Me₃, 60 °C; (c) *trans*-1,4-diaminocyclohexane, NMP, 210 °C; and (d) Pd/C (10% wt), H₂, EtOAc, MeOH, 15 bar, RT.

cyclohexyl (30), and cyclohexenyl (29b). These compounds displayed promising inhibitory activities against the tested recombinant kinases within the nanomolar range. Antiproliferative activities confirmed that these compounds employed an FLT3-dependent mechanism of action: FLT3-dependent MV4-11 and MOLM-13, as well as SEM cell lines, were several times more sensitive than FLT3-independent cell lines (Table 5).

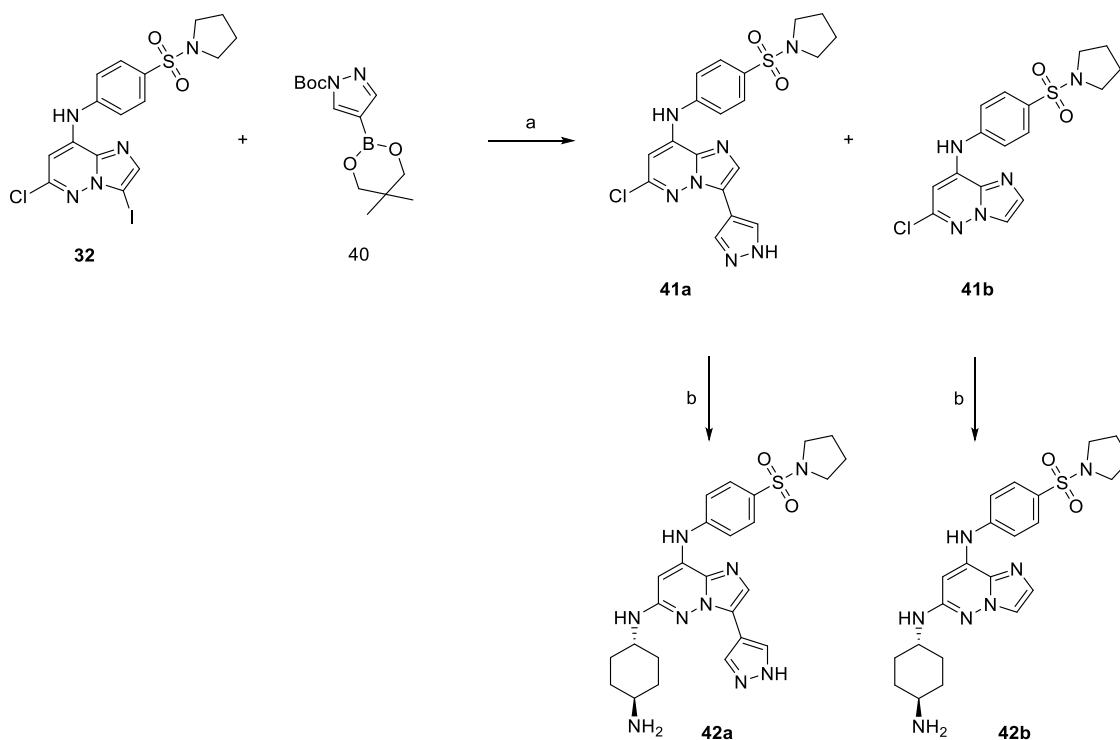
In the first part of this study, we identified new compounds by scaffold hopping and evaluated central cores as suitable replacements for the purine scaffold. As the most promising inhibitory activities were observed for imidazo[1,2-*b*]pyridazine derivatives, we decided to extend the series and modify the substituent in position 3 of the core. We performed a docking study using the active site of FLT3 to predict the binding poses of imidazo[1,2-*b*]pyridazine derivatives bearing aliphatic and aromatic substituents. We based the structures of the proposed ligands on the most potent inhibitor identified up to this point in the study, compound 29a (Figure 2A). Various aliphatic and aromatic substituents were placed in position 3 of

the heterocycle to induce interaction with a pocket lined by A642, K644, V675, F691, and L767. Proposed analogues of 29a were docked in silico, and the binding affinity of each compound was evaluated using Glide built-in scoring functions (Table S2, Supporting Information). In agreement with previously published docking studies,¹² our results confirmed that the most important residues participating in the interaction are K614, C694, N765, and D778. Another residue that proved important was F691 in the hydrophobic cavity, which presumably interacts with aromatic residues such as phenyl in 34f (Figure 2B), pyrazole, or other hydrophobic species. A docking study also suggests that the binding mode of our molecules is similar to that of type I FLT3 inhibitors.

Based on our preliminary biological results and in silico docking analysis, we extended the imidazo[1,2-*b*]pyridazine series and prepared derivatives substituted in position 3 with various aliphatic and aromatic substituents (Table 6, Schemes 6–8). As the phenyl derivative 34f showed activity toward FLT3-ITD-positive kinase in the single-digit nanomolar range together with high selectivity in comparison with CDK2, we

Scheme 7. Synthesis of the 3-Aminoimidazo[1,2-*b*]pyridazine Derivative^a

^aReagents and conditions: (a) H₂SO₄, HNO₃, 0 °C to RT; (b) 4-(pyrrolidin-1-ylsulfonyl)aniline (**2**), *t*-BuOK, DMF, 0 °C; (c) *trans*-1,4-diaminocyclohexane, NMP, 210 °C; and (d) SnCl₂, EtOH, reflux.

Scheme 8. Synthesis of the 3-(1*H*-Pyrazole-4-yl)imidazo[1,2-*b*]pyridazine Derivative^a

^aReagents and conditions: (a) Na₂CO₃, Pd(dppf)Cl₂·DCM, dioxane, water, 100 °C and (b) *trans*-1,4-diaminocyclohexane, NMP, 210 °C.

extended our study to phenyl derivatives substituted at various positions in the phenyl ring (Table 6, entries g–p). The series was prepared from 3-iodo derivative **32** (Scheme 6),³⁴ which is more reactive than 3-bromo derivative **27** used in the previous synthesis (Scheme 5).

While the reaction of **32** with sodium azide did not proceed (data not shown), 3-amino derivative **39** was synthesized via 3-nitro intermediate **36** by nitration³⁵ of imidazo[1,2-*b*]pyridazine **35** and further substitution of the heterocyclic core (Scheme 7).

Finally, the 3-pyrazolo derivative was prepared by Suzuki coupling of 3-iodo derivative **32** and protected 1*H*-pyrazole-4-yl-boronic acid (**40**). The reaction gave a mixture of deprotected product **41a** and dehalogenated starting material **41b**. Reaction with *trans*-1,4-diaminocyclohexane afforded compounds **42a** and **42b**, respectively (Scheme 8).

We explored the structure–activity relationship using a diverse series of compounds bearing the conserved 4-

(pyrrolidin-1-ylsulfonyl)aniline substituent in position 8 (Table 7). Although a number of compounds featuring chloro substitution in position 6 were tested against FLT3-ITD as well, our results confirmed (Table S4, Supporting Information) that the introduction of the *trans*-1,4-diaminocyclohexyl substituent into this position is crucial for the anti-FLT3 activity of imidazo[1,2-*b*]pyridazines.

Compounds lacking the substituent in position 3 (**42b**) or containing a small polar amino group (**39**) are among the less potent in the series displaying IC₅₀ values against FLT3-ITD within a high nanomolar range. The introduction of small aliphatic substituents (methyl in **34e**, isopropyl in **34d**, isobutyl in **34c**), cyclic aliphatic substituents (**34b**, **34a**, **30**, **29b**), or furanyl (**34r**) and thienyl (**34q**) resulted in low nanomolar activity against recombinant FLT3-ITD as well as FLT3-D835Y. These results correspond with the potent antiproliferative activities in MV4-11 and MOLM-13 cell lines within a nanomolar concentration range. In contrast,

Table 7. Kinase-Inhibitory and Antiproliferative Activities of Imidazo[1,2-*b*]pyridazine Derivatives

	IC ₅₀ (μM) ^a			GI ₅₀ (μM) ^a						
	FLT3-ITD	FLT3-D835Y	CDK2	MV4-11	MOLM-13	SEM	CEM	NOMO-1	ML-2	K562
34a	0.007	0.004	0.196	0.005	0.007	0.372	3.800	8.430	5.780	6.870
34b	0.005	0.002	0.005	0.008	0.007	0.235	0.917	0.620	0.480	0.885
34c	0.008	0.002	0.083	0.028	0.030	0.453	3.727	2.435	1.078	1.725
34d	0.004	0.001	0.011	0.005	0.009	0.210	0.810	0.848	0.490	0.635
34e	0.009	0.002	0.093	0.005	0.007	0.132	0.683	0.700	0.455	1.310
34f	0.004	0.001	0.493	0.007	0.009	0.140	1.768	4.275	3.030	1.525
34g	0.001	0.002	2.119	0.045	0.040	0.283	2.645	5.223	3.505	1.640
34h	0.002	0.002	0.961	0.073	0.176	1.060	6.170	>10	6.865	1.010
34i	0.002	0.006	1.435	0.060	0.027	0.877	6.380	5.085	4.220	2.255
34j	0.001	0.001	0.234	0.023	0.030	0.150	1.690	5.030	2.050	1.063
34k	0.001	0.002	0.037	0.017	0.019	0.590	1.940	0.865	0.325	2.120
34l	0.004	0.011	1.443	0.156	0.200	1.031	1.570	5.025	3.923	1.505
34m	0.013	0.025	6.587	0.790	0.410	1.335	4.750	4.260	3.310	1.550
34n	0.001	0.002	0.366	0.042	0.025	0.168	0.760	0.393	0.245	1.655
34o	0.231	0.569	3.428	0.710	0.935	2.525	8.990	9.035	4.475	>10
34p	0.142	0.834	2.435	1.183	1.160	1.500	8.400	2.385	2.000	4.128
34q	0.001	0.003	0.082	0.002	0.004	0.381	1.400	1.455	0.440	1.470
34r	0.001	0.002	0.031	0.001	0.001	0.399	1.030	0.755	0.270	0.570
39	0.333	0.268	1.116	1.557	2.213	>10	>10	>10	>10	>10
42a	0.002	0.001	0.031	0.006	0.011	0.823	7.363	1.745	0.370	9.850
42b	0.106	0.014	0.178	0.039	0.097	0.523	1.423	4.733	3.650	5.545

^aFor SD values, see Table S3 in the Supporting Information.

FLT3-independent cell lines were several orders of magnitude less sensitive. On the other hand, these compounds showed very strong potency against CDK2, where the inhibitory ratio of CDK2 and FLT3-ITD was between 1 and 82. These results indicate the lower selectivity of these molecules.

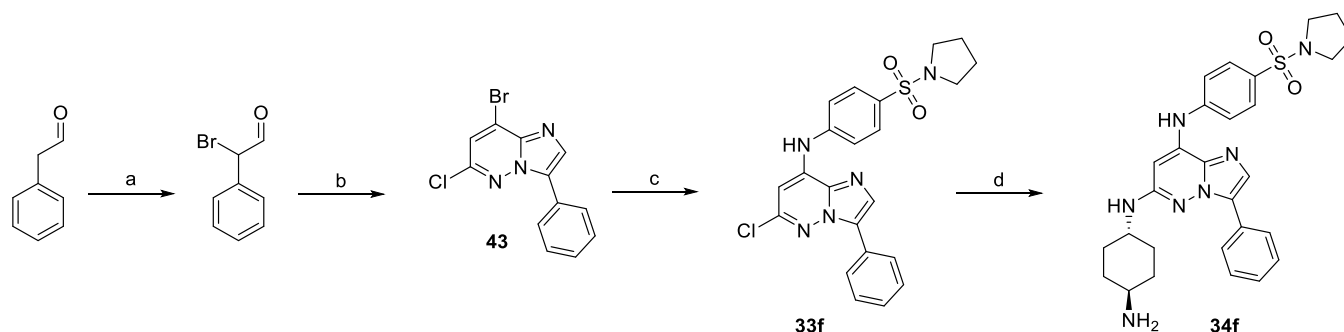
As described in the literature,¹³ larger substituents in position 9 of the purine ring lead to decreased activity of trisubstituted purines toward CDK2. Further, our docking analysis suggests that phenyl substituent may successfully bind to the FLT3-ITD active site. Therefore, we focused on derivatives bearing phenyl substituent (34f) and its substituted derivatives (34g–34p) in position 3 of the imidazo[1,2-*b*]pyridazine ring to improve the selectivity of the compounds over CDK2. Compounds containing phenyl (34f), 4- and 3-methoxyphenyl (34g and 34h, respectively), 3,4-dimethoxyphenyl (34i), 4-fluorophenyl (34j), 3-fluoro-4-hydroxyphenyl (34k), 4-cyanophenyl (34n), and 4-trifluoromethyl- or 4-trifluoromethoxyphenyl (34l and 34m, respectively) retained FLT3 inhibitory activity within low nanomolar ranges. However, as expected, CDK2 inhibitory activity dropped dramatically to micromolar or submicromolar concentrations in most compounds (except for 34k, which displayed an anti-CDK2 IC₅₀ value of 37 nM). A ratio between CDK2 and FLT3-ITD of more than 200 highlighted the improved selectivity of these substances, albeit accompanied by a slight decrease in antiproliferative activity. Nevertheless, these compounds still exhibited potency against FLT3-ITD-positive AML cell lines, whereas FLT3-independent cell lines were far less sensitive. This confirms the FLT3-dependent mechanism of action.

On the other hand, dimethylcarbamoyl and dimethylsulfonyl substituents of compounds 34o and 34p, respectively, probably affected the binding of compounds into active sites of the tested kinases and resulted in reduced activity. For example, IC₅₀ values increased more than 100-fold in comparison with the values of other members of the group.

From all of the prepared compounds, 34f was selected as the tool compound for further biochemical and mechanistic evaluation. This molecule showed single-digit nanomolar IC₅₀ values against recombinant FLT3-ITD and FLT3-D835Y (0.004 and 0.001 μM, respectively), whereas CDK2 was nearly 250 times less sensitive. FLT3-ITD-inhibitory activity of 34f was comparable to the standards quizartinib (0.010 ± 0.004 μM) and gilteritinib (0.012 ± 0.001 μM). Although 34f shows promising potency also against FLT3-D835Y (0.001 μM), comparable to the clinically approved gilteritinib (0.002 ± 0.0003 μM), quizartinib is more than 100 times less potent against FLT3-D835Y than 34f (0.136 ± 0.002 μM for quizartinib). The same trend was also observed for FLT3-ITD-F691L. While 34f and gilteritinib showed low nanomolar IC₅₀ values (0.004 ± 0.003 and 0.010 ± 0.005 μM, respectively), quizartinib lost its potency against this mutant variant of FLT3 (>5 μM).

In addition to its outstanding FLT3 inhibitory activity, 34f displayed strong antiproliferative efficacy in the FLT3-ITD-positive MV4-11 and MOLM-13 cell lines (0.013 and 0.020 μM, respectively). In contrast, GI₅₀ values measured in FLT3-independent cell lines were in the micromolar range (Table 7). Our results of antiproliferative activities were comparable to the data obtained for quizartinib and gilteritinib. The GI₅₀ values for FLT3-ITD-positive cell lines varied in the nanomolar range for both quizartinib (MV4-11: 0.003 ± 0.001 μM; MOLM-13: 0.004 ± 0.004 μM) and gilteritinib (MV4-11: 0.026 ± 0.009 μM; MOLM-13: 0.034 ± 0.013 μM). FLT3-independent cell lines treated with quizartinib were not significantly affected by concentrations up to 10 μM, and the GI₅₀ values obtained for gilteritinib varied in the micromolar range (CEM: 2.771 ± 0.229 μM, NOMO-1: 1.601 ± 0.226 μM, K562: 2.254 ± 0.486 μM).

Synthesis of 34f on a Larger Scale. Compound 34f was selected for in vivo experiments in mice, requiring the preparation of hundreds of milligrams of the material. Given

Scheme 9. Synthesis of 34f on a Larger Scale^a

^aReagents and conditions: (a) Br₂, 1,4-dioxane, 0 °C to RT; (b) 3-amino-4-bromo-6-chloropyridazine, EtOH, 85 °C; (c) *t*-BuOK, amine (2), DMF, 0 °C; and (d) *trans*-1,4-diaminocyclohexane, NMP, 200 °C.

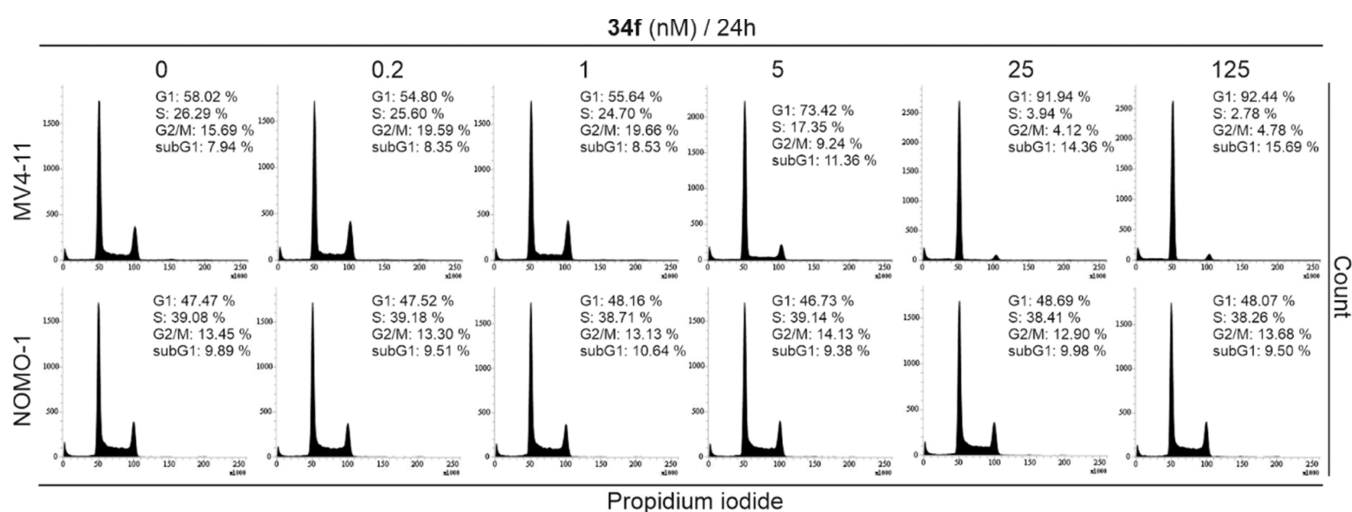


Figure 3. Cell cycle analysis of MV4-11 and NOMO-1 cells treated with 34f for 24 h.

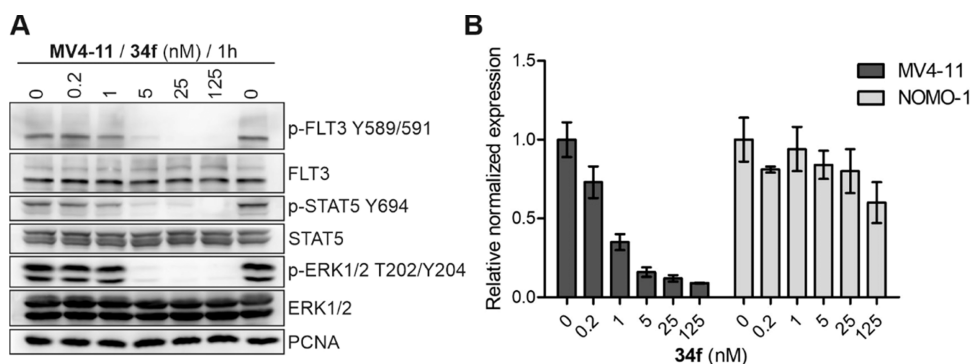


Figure 4. (A) Immunoblotting analysis of FLT3 and its downstream signaling pathways in MV4-11 treated with 34f for 1 h. (B) Relative normalized expression of the MYC gene in MV4-11 and NOMO-1 cells treated with 34f for 4 h.

that Suzuki cross-coupling of 3-iodo derivative **32** gave products in relatively low yields from 15 to 30% and upscaling of the reaction proved problematic, we developed an alternative synthetic procedure employing phenylacetaldehyde (Scheme 9). Bromination³⁶ and subsequent cyclization with 3-aminopyridazine gave compound **43** in a 50% yield after two steps. Further substitution with aniline and amine gave **34f** in a 20% overall yield after four steps. This synthetic strategy, starting from cheap substituted acetaldehyde, proved suitable for the synthesis of larger quantities of 3-substituted imidazo[1,2-*b*]pyridazine derivatives.

Cellular Effects of 34f. Specific FLT3 inhibition induces G1 arrest of FLT3-dependent AML cells but does not affect other cell lines (FLT3-independent). This was validated by flow cytometry analysis of FLT3-ITD-positive MV4-11 cells treated for 24 h with nanomolar concentrations of 34f. The number of G1 cells increased in a dose-dependent manner (Figure 3), but the NOMO-1 cell line was not affected within the same 34f concentration range (Figure 3). These results were comparable to the effects seen in MV4-11 and NOMO-1 cells treated with both quizartinib and gilteritinib (Figures S1, S2). The primary cause of this phenomenon is the blocking of FLT3-subordinate

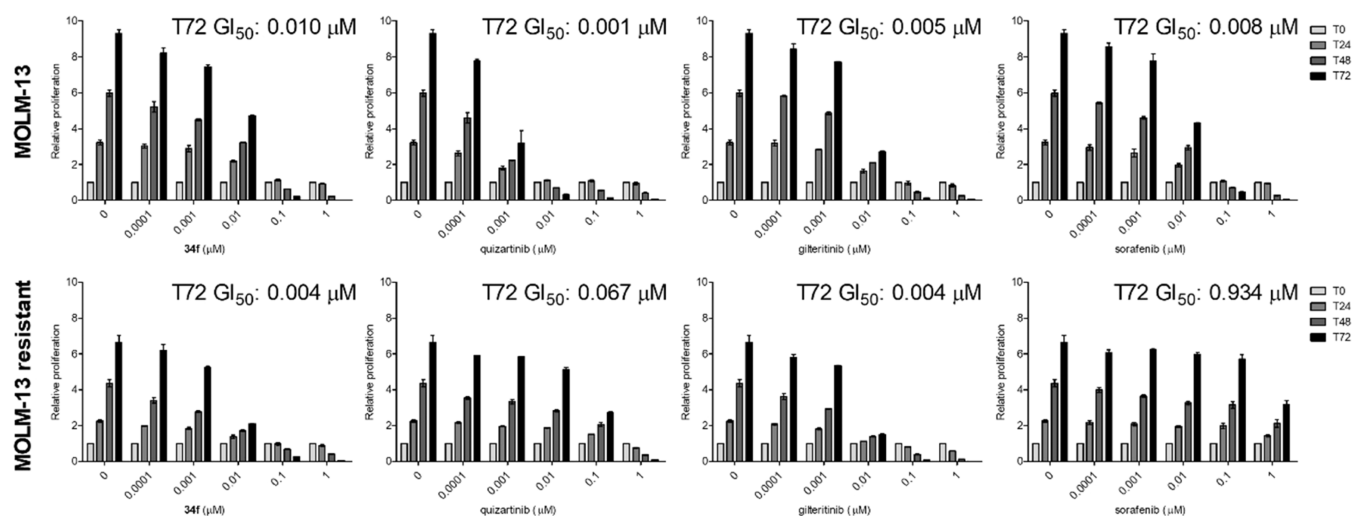


Figure 5. Antiproliferative activity of **34f** in the MOLM-13 cell line and its clone expressing FLT3-ITD-D835Y (MOLM-13 resistant). Quizartinib, gilteritinib, and sorafenib were used as standards. T72 GI_{50} = 50% growth inhibition concentration determined at the final point of the experiment after 72 h of treatment.

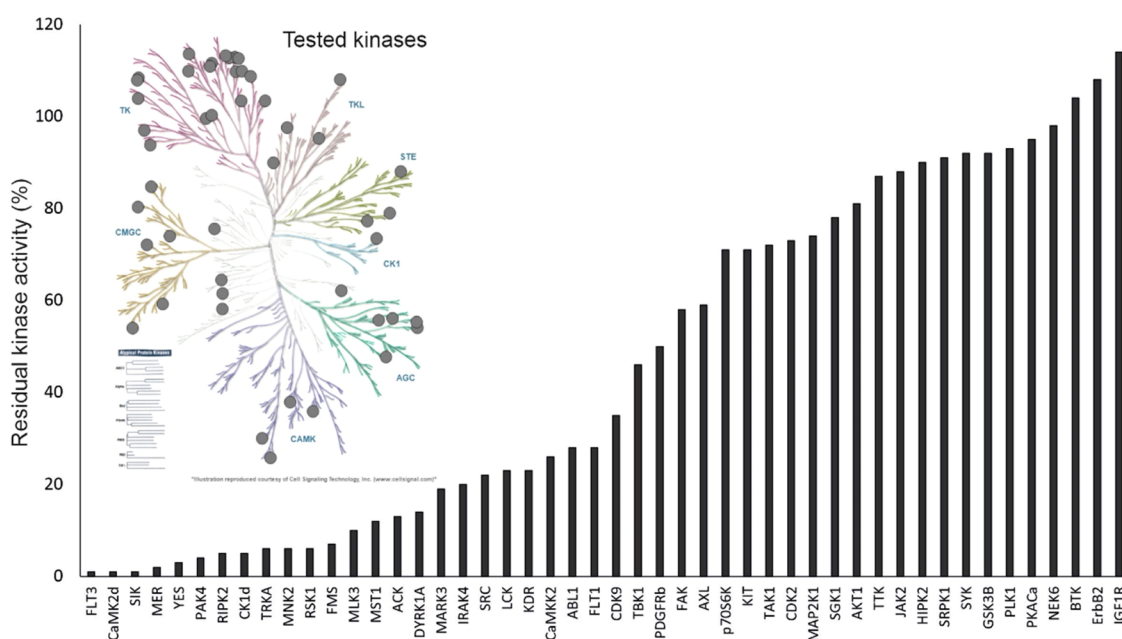


Figure 6. Kinase selectivity profiling of **34f**. The efficacy of **34f** at 100 nM concentration was compared with 48 human kinases across the kinome (coverage shown in the phylogenetic tree).

signaling pathways, which are of crucial importance in cell proliferation. Dose-dependent attenuation of phosphorylation of FLT3 as well as its downstream targets, Y694 of STAT5 and T202/Y204 of ERK1/2, was confirmed after 1 h of treatment with **34f** in MV4-11 cells. This demonstrated the FLT3-dependent mechanism of action (Figure 4) and efficacy comparable to quizartinib and gilteritinib (Figures S3A, S4A).

Expression analysis of the MYC gene, a key transcription factor and common oncogene whose deregulation often contributes to the development of hematological malignancies, further confirmed the FLT3-dependent mechanism of action of **34f**. MYC transcript levels were significantly reduced by **34f** in treated MV4-11 cells, whereas they remained more stable in FLT3-independent NOMO-1 cells. Comparable effects were also observed in cells treated with quizartinib (Figure S3B) as

well as gilteritinib (Figure S4B), a finding consistent with previously reported studies.³⁷

One of the most common obstacles to FLT3-inhibitor therapy of AML is the development of drug resistance. Therefore, we used the MOLM-13 cell line and its resistant clone expressing the FLT3-ITD-D835Y mutant to evaluate the effect of the lead compound **34f** on proliferation. FLT3 inhibitors sorafenib, gilteritinib, and quizartinib were used for comparison. The graphs of the relative proliferation of MOLM-13 cells (Figure 5) show that compound **34f**, as well as quizartinib, gilteritinib, and sorafenib, blocked proliferation in a time-dependent manner at low nanomolar concentrations. The antiproliferative ability of compound **34f** was also confirmed in MOLM-13-resistant cells with the D835Y mutation; the GI_{50} value obtained after 72 h treatment did not change significantly (0.010 and 0.004 μ M in MOLM-13

and its resistant variant, respectively). A similar outcome was also observed for clinically approved gilteritinib. In contrast, the efficacy of quizartinib and sorafenib dramatically decreased, and the GI_{50} values increased significantly.

Kinase Selectivity of 34f. The preliminary kinase selectivity of **34f** in the panel of 48 kinases selected across the human kinome demonstrated the outstanding inhibitory activity of this compound against FLT3 (Figure 6). The IC_{50} values for the most important off-targets were determined (Table S5). Although **34f** also inhibits other kinases, it notably does not target KIT kinase, which is one of the most common off-targets of the known FLT3 inhibitors. Simultaneous inhibition of FLT3 and KIT results in myelosuppression,³⁸ which complicates the clinical use of these compounds. Therefore, avoiding KIT inhibition is a crucial goal in the development of novel FLT3 inhibitors. Kinase selectivity profiling demonstrated that **34f** at a concentration of 100 nM reduced KIT activity to 71% (in comparison with 1% obtained for FLT3). A subsequent concentration-dependent experiment showed that the IC_{50} value of **34f** for KIT kinase is 680 nM (Table S5), a hundred times higher than for FLT3. These results indicate a favorable inhibitory ratio among these kinases. Hence, we decided to verify this finding using the Kasumi-1 cell line, which is characterized by activating N822K point mutation in KIT. Based on an evaluation of the antiproliferative properties of **34f**, the GI_{50} value measured in Kasumi-1 was $0.188 \pm 0.019 \mu\text{M}$, which was more than 18 times higher than the GI_{50} values obtained for quizartinib in Kasumi-1 ($0.010 \pm 0.004 \mu\text{M}$) and for **34f** in FLT3-ITD MV4-11 cells ($0.007 \pm 0.004 \mu\text{M}$). The GI_{50} value determined for gilteritinib in Kasumi-1 cells was $0.124 \pm 0.013 \mu\text{M}$. The limited ability of **34f** to block KIT activity was also confirmed by immunoblotting. At a concentration of 125 nM, **34f** only partially reduced the phosphorylation of two tyrosine residues (Y703 and Y719) of the KIT kinase and T202/Y204 in the KIT downstream ERK1/2 (Figure S5).

Plasma and Microsomal Stability of 34f. In vitro stability of **34f** in blood plasma and liver microsomes (from human and mouse sources) was tested prior to in vivo experiments in order to predict the clearance of compounds in the whole organism. Propranolol and verapamil were used as reference compounds for plasma and microsomal stability, respectively, demonstrating the usual stability profiles.

Compound **34f** was stable in both human and mouse plasma for up to 120 min of incubation (Figure 7A). As for microsomal stability, a slow decay by approximately 25% at 45 min was observed (Figure 7B). The calculated intrinsic clearance (CL_{int} ; Table S6) values were $18 \mu\text{mol}/\text{min}/\text{mL}$ for human microsomes and $13 \mu\text{mol}/\text{min}/\text{mL}$ for mouse microsomes, indicating that the compound falls within the low-to-moderate clearance category. Overall, the metabolic stability of **34f** was considered acceptable for in vivo experiments.

In Vivo Efficacy of 34f. Encouraged by these results, we performed in vivo experiments on immunodeficient mice bearing subcutaneous MV4-11 xenografts, the widely accepted simple in vivo model. As shown in Figure 8A, tumor growth was blocked in groups of mice treated repeatedly with intraperitoneal injections of **34f** at doses of 5 and 10 mg/kg. By the end of the drug administration (day 7), the tumor growth rate remained restricted. On the other hand, our vehicle-treated control group of mice exhibited a steep increase in tumor size. For this reason, the experiment in this cohort had to be terminated prematurely. In addition to displaying

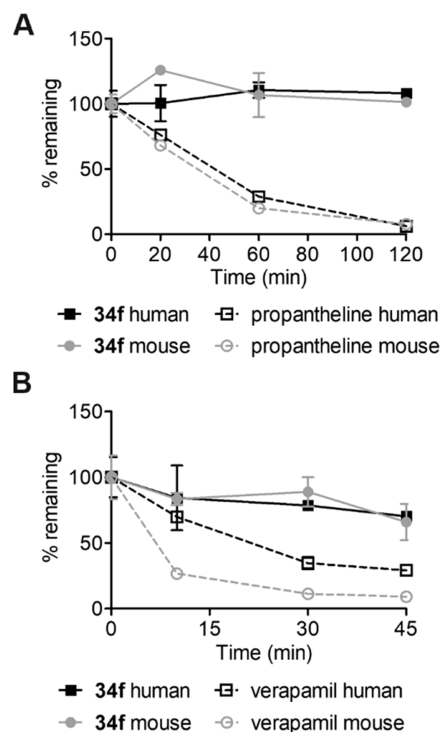


Figure 7. (A) Plasma and (B) microsomal stability of **34f**. Propranolol bromide and verapamil were used as standards to determine plasma stability and microsomal stability, respectively.

strong anticancer efficacy in vivo, **34f** administration had no adverse effect on mouse weight during the experiment (Figure 8B).

Moreover, immunoblotting analysis of MV4-11 xenografts exposed for 6 or 24 h to **34f** at a dose of 10 mg/kg revealed reduced phosphorylation of FLT3 at Y589/S91 and of STAT5 at Y694 in most of the analyzed tumors in comparison with vehicle-treated mice, thus confirming the FLT3-dependent mechanism of action of **34f** in vivo (Figure 9).

In addition, the pharmacokinetic properties of **34f** were determined in mice following intraperitoneal administration at a dose of 10 mg/kg. The results showed that **34f** has a half-life of 71.3 min, including the absorption and elimination phases. The compound reaches a maximal plasma concentration of 384 pg/mL (722 nmol/L) after approximately 49 min following administration. For the details, see the Supporting information.

CONCLUSIONS

In this study, we investigated the suitability of several series of heterocyclic derivatives as potential FLT3 kinase inhibitors. Compounds derived from the imidazo[1,2-*b*]pyridazine heterocyclic core proved to be potent inhibitors of FLT3 kinase, and modification of position 3 resulted in a pronounced effect on activity and selectivity in comparison with CDK2. In the extensive structure–activity relationship (SAR), the 3-phenyl substituent and some of its derivatives (e.g., 3- or 4-methoxyphenyl, 4-fluorophenyl, or 4-(trifluoromethyl)phenyl) displayed activity toward FLT3 within a single-digit nanomolar range, where the selectivity ratio for CDK2/FLT3-ITD was more than 200. Candidate compound **34f** showed high antiproliferative efficacy in the FLT3-ITD-positive AML cell lines MV4-11 and MOLM-13 (7 and 9 nM, respectively) as

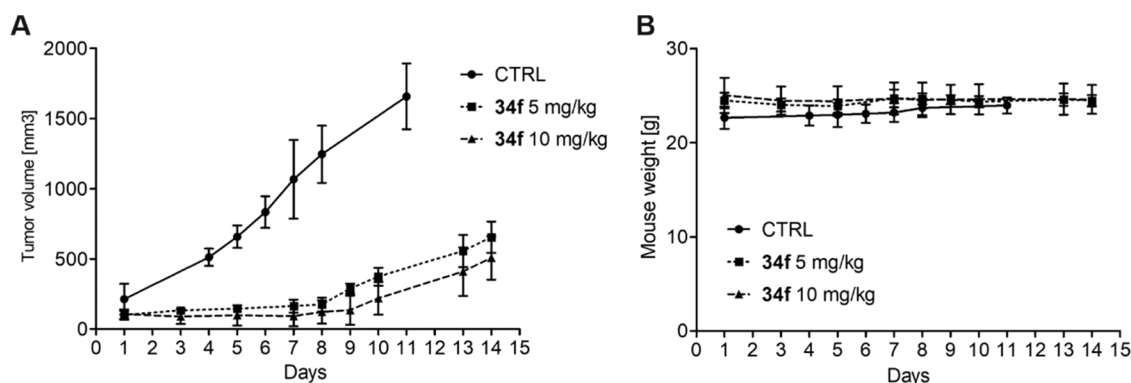


Figure 8. In vivo efficacy of **34f**. (A) Growth of subcutaneous MV4-11 xenografts (mean volume \pm SD) in groups of mice treated with **34f** (5 and 10 mg/kg) or a vehicle only every other day until day 7 (4 doses) by intraperitoneal administration. (B) The weight of mice (mean \pm SD) during the experiment.

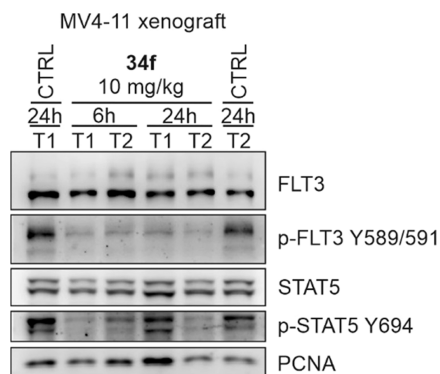


Figure 9. Immunoblotting analysis of MV4-11 subcutaneous xenografts exposed to **34f** for 6 or 24 h.

well as in the MOLM-13 variant bearing the FLT3-ITD-D835Y mutation (4 nM) in comparison with low sensitivity of FLT3-independent cell lines, proving the FLT3-dependent mechanism of action. Immunoblotting and flow cytometry analysis confirmed the blocking of signaling pathways subordinate to FLT3 as well as induced G1 arrest of FLT3-dependent MV4-11 AML cells. As the derivative **34f** showed sufficient plasma and microsomal stability, we continued with in vivo experiments in immunodeficient mice bearing subcutaneous MV4-11 xenografts. We observed a strong effect of **34f** on tumor growth without any side effects on mouse weight. Additionally, immunoblotting analysis of MV4-11 xenografts confirmed reduced phosphorylation of FLT3 at Y589/591 and of STAT5 at Y694 in the analyzed tumors, confirming the FLT3-dependent mode of action in vivo. In summary, we found a novel substitution pattern of imidazo-[1,2-*b*]pyridazine that shows excellent potency toward FLT3 kinase in vitro and in vivo without any pronounced side effects. The activity displayed by this series of compounds, mainly the derivatives **34f**, **34g**, **34h**, **34i**, **34j**, **34l**, **34n**, and **34m**, indicates their suitability for further development as potential AML drug candidates.

EXPERIMENTAL SECTION

Starting compounds and reagents were purchased from commercial suppliers (Sigma-Aldrich, Fluorochem, Acros Organics, Carbosynth, TCI) and used without further purification. Dry tetrahydrofuran was distilled with lithium aluminum hydride pellets under an argon atmosphere. Analytical thin-layer chromatography (TLC) was performed on silica gel pre-coated aluminum plates with a fluorescent

indicator (Merck 60 F₂₅₄). Flash column chromatography was carried out using Teledyne ISCO CombiFlash Nextgen. Preparative HPLC purification was performed on the INGOS HPLC system (LCD5000 and LCP5020 modules, chromatography column: Luna 5 μ m C18(2) 100 Å). Mass spectra, UV absorbency, and purity of compounds were measured on the Waters UPLC-MS system, consisting of the Waters UPLC H-Class Core System (Waters Acquity UPLC BEH C18 1.7 mm column, 2.1 mm \times 100 mm), the Waters Acquity UPLC PDA detector, and the Waters SQD2 mass spectrometer. The universal LC method was used (eluent H₂O/CH₃CN, gradient 0–100%, run length 4 min or 7 min) in conjunction with the MS method (ESI+ and/or ESI–, cone voltage = 30 V, mass detector range 100–1000 Da for standard cases and 500–1600 Da for larger molecules). High-resolution mass spectra were measured on the LTQ Orbitrap XL spectrometer (Thermo Fisher Scientific). NMR spectra were obtained using the Bruker Avance III HD 500 MHz spectrometer operating at 125.7 MHz for ¹³C and 500 MHz for ¹H. The spectra were referenced to solvent residual signals (dimethyl sulfoxide (DMSO): 2.50 for ¹H and 39.70 for ¹³C, CDCl₃: 7.26 for ¹H and 77.16 for ¹³C). The assignment of hydrogen and carbon spectra was based on a combination of one-dimensional (1D) and two-dimensional (2D) experiments (¹H–¹³C APT, ¹H–¹H COSY, ¹H–¹³C HSQC, and ¹H–¹³C HMBC). The purity of the final compounds was determined by ultra-performance liquid chromatography–mass spectrometry (UPLC-MS) and was 95% or higher, with the exception of compounds **5b**, **10**, **25**, **34n**, and **39** due to the problematic separation of highly polar compounds; nevertheless, the purity was still higher than 90%.

Molecular Docking. A docking study was performed using Schrödinger built-in modules. The homology model of the active DFG-in conformation of FLT3 (based on the crystal structure of FLT3 kinase,³⁹ PDB 1RJB, resolution 2.10 Å) was used.¹² The structure was optimized prior to docking using the Schrödinger Protein Preparation Wizard Maestro Suite (version 12.9.123, release 2021-3). Inconsistencies in the structure, such as missing hydrogens, incorrect bond orders, and poor orientation of amino-acid side chains, were rectified during the optimization process. The LigPrep module was used to convert two-dimensional structures to three-dimensional (3D), correct improper bond distances and bond orders, ionize compounds to correspond with pH 7 \pm 1, and minimize ligand energy. Structures generated by LigPrep were then used for ligand docking. Ligand docking was performed using the Schrödinger Grid-based Ligand Docking with Energetics (Glide) Suite 2021 application. Receptor grid generation was based on the ligand from the original PDB structure. The default selection of 20 poses per ligand was set for Glide. Extra precision (XP) mode was selected for the Glide redocking stage.

General Procedure 1 (GP1): Reaction with 4-(1-Pyrrolidinylsulfonyl)aniline (2). The heterocyclic derivative (1 mmol) and aniline (**2**) (1.25 mmol) in DMF (5 mL) were treated dropwise with *t*-BuOK (1 M in THF, 2.5 mL, 2.5 mmol) at 0 °C; the

resulting mixture was stirred at the same temperature for 30 min. The mixture was diluted with EtOAc, washed with saturated NH_4Cl and water, dried over MgSO_4 , and evaporated. The residue was purified by RP FC ($\text{H}_2\text{O}/\text{ACN}$) and dried.

General Procedure 2 (GP2): Reaction with *Trans*-1,4-diaminocyclohexane. The heterocyclic derivative (1 mmol) and *trans*-1,4-diaminocyclohexane (10 mmol) in NMP (2.5 mL) were heated in a tightly sealed 4 mL vial at 210 °C overnight. The mixture was diluted with DMSO (2 mL) and directly applied to the RP FC ($\text{H}_2\text{O}/\text{ACN}$ + 0.1% of formic acid). Products containing fractions were evaporated and codistilled with water; the final compound was dried in vacuo or freeze-dried from dioxane.

General Procedure 3 (GP3): Suzuki Cross-Coupling with Boronic Acids. Heteroaryl bromide or iodide (1 equiv), boronic acid (1.2 equiv), Cs_2CO_3 (3 equiv), and $\text{Pd}(\text{dppf})\text{Cl}_2\cdot\text{DCM}$ (0.1 equiv) in dioxane/water (9:1, 5 mL to 1 mmol of the aryl halogenide) under an argon atmosphere were heated at 95 °C for 4 to 12 h. After the solvent was evaporated, the residue was purified by FC (c-hexane/EtOAc + 10% of MeOH, 0–50%), repurified by RP FC ($\text{H}_2\text{O}/\text{ACN}$ + 0.1% formic acid), evaporated, and codistilled with water and EtOH.

7-Bromo-2-chloro-N-[4-(1-pyrrolidinylsulfonyl)phenyl]thieno[3,2-d]pyrimidin-4-amine (3). Prepared from 7-bromo-2,4-dichlorothieno[3,2-d]pyrimidine according to GP1. Pale brown solid, yield 54%. MS (ESI): $m/z = 472.9$ [$\text{M} + \text{H}$] $^+$. ^1H NMR (DMSO- d_6): $\delta = 10.65$ (s, 1H, NH); 8.54 (s, 1H, H-6); 8.08–8.02 (m, 2H, H-2'); 7.87–7.82 (m, 2H, H-3'); 3.16 (m, 4H, NCH_2); 1.67 (m, 4H, CH_2) ppm. ^{13}C NMR (DMSO- d_6): $\delta = 158.02$ (C-7a); 156.41 (C-4); 155.65 (C-2); 142.42 (C-1'); 133.62 (C-6); 130.98 (C-4'); 128.35 (C-3'); 121.41 (C-2'); 115.06 (C-4a); 107.49 (C-7); 47.83 (N- CH_2); 24.72 (CH_2 -pyrrol.) ppm. HRMS (ESI): m/z calculated for $\text{C}_{16}\text{H}_{15}\text{O}_2\text{N}_4\text{BrClS}_2$ 472.95028, found 472.95051.

2-Chloro-7-(cyclohex-1-en-1-yl)-N-[4-(1-pyrrolidinylsulfonyl)phenyl]thieno[3,2-d]pyrimidin-4-amine (4a) and 2,7-Bis-(Cyclohex-1-en-1-yl)-N-[4-(1-pyrrolidinylsulfonyl)phenyl]thieno[3,2-d]pyrimidin-4-amine (4b). Compound 3 (500 mg, 1.05 mmol), 1-cyclohex-1-en-1-ylboronic acid (140 mg, 1.11 mmol), and Cs_2CO_3 (923 mg, 3.15 mmol) in degassed dioxane (18 mL) and water (2 mL) were treated with $\text{Pd}(\text{dppf})\text{Cl}_2\cdot\text{CH}_2\text{Cl}_2$ (73 mg, 0.1 mmol) under an argon atmosphere and heated at 95 °C for 4 h. The solvent was evaporated, after which the residue was purified by FC (c-hex/EtOAc + 10% MeOH) and repurified by RP FC ($\text{H}_2\text{O}/\text{ACN}$) to give 4a (340 mg, 68%) and disubstituted product 4b (60 mg, 10%).

4a. White solid. MS (ESI): $m/z = 475.1$ [$\text{M} + \text{H}$] $^+$. ^1H NMR (DMSO- d_6): $\delta = 10.39$ (s, 1H, NH); 8.09 (s, 1H, H-6); 8.05 (d, 2H, $J = 8.7$ Hz, H-2'); 7.82 (d, 2H, $J = 8.7$ Hz, H-3'); 7.05 (s, 1H, H-2''); 3.17 (m, 4H, NCH_2); 2.45 (m, 2H, H-6''); 2.22 (m, 2H, H-3''); 1.74 (m, 2H, H-5''); 1.69–1.58 (m, 6H, CH_2 -pyrrol., H-4'') ppm. ^{13}C NMR (DMSO- d_6): $\delta = 159.31$ (C-7a); 155.74 (C-4); 155.14 (C-2); 142.78 (C-1'); 136.22 (C-1''); 130.54 (C-4'); 130.04 (C-6); 128.33 (C-3'); 127.79 (C-2''); 121.19 (C-2'); 116.24 (C-4a); 47.86 (N CH_2); 27.32 (C-6''); 25.17 (C-3''); 24.74 (CH_2 -pyrrol.); 22.41 (C-5''); 21.65 (C-4'') ppm. HRMS (ESI): m/z calculated for $\text{C}_{22}\text{H}_{24}\text{O}_2\text{N}_4\text{ClS}_2$ 475.10237, found 475.10219.

4b. White solid. MS (ESI): $m/z = 521.1$ [$\text{M} + \text{H}$] $^+$. ^1H NMR (DMSO- d_6): $\delta = 9.84$ (s, 1H, NH); 8.20 (m, 2H, H-2'); 7.94 (s, 1H, H-6); 7.80 (m, 2H, H-3'); 7.38 (m, 1H, H-2''); 7.21 (m, 1H, H-2'''); 3.15 (m, 4H, NCH_2); 2.58 (m, 2H, H-6''); 2.50 (m, 2H, H-6'''); 2.29 (m, 2H, H-3''); 2.24 (m, 2H, H-3'''); 1.72 (m, 4H, H-5'', H-5'''); 1.65 (m, 8H, CH_2 -pyrrol., H-4'', H-4''') ppm. ^{13}C NMR (DMSO- d_6): $\delta = 160.62$ (C-2); 158.81 (C-7a); 154.14 (C-4); 144.10 (C-1'); 136.70 (C-7); 136.10 (C-1''); 132.00 (C-6); 130.52 (C-1'''); 128.92 (C-4'); 128.23 (C-3'); 127.73 (C-2''); 127.36 (C-2''); 120.04 (C-2'); 114.99 (C-4a); 47.79 (N CH_2); 27.26 (C-6''); 25.61 (C-3''); 25.33 (C-6'''); 25.18 (C-3'''); 24.66 (CH_2 -pyrrol.); 22.49 (C-5'', C-5'''); 21.83 (C-4''); 21.79 (C-4''') ppm. HRMS (ESI): m/z calculated for $\text{C}_{28}\text{H}_{33}\text{O}_2\text{N}_4\text{S}_2$ 521.20394, found 521.20358.

***N*²-(6-Aminopyridin-3-yl)-7-(cyclohex-1-en-1-yl)-*N*⁴-[4-(1-pyrrolidinylsulfonyl)phenyl]thieno[3,2-d]pyrimidin-2,4-diamine (5a) and *N*²-(5-Aminopyridin-2-yl)-7-(cyclohex-1-en-1-yl)-*N*⁴-[4-(1-pyrrolidinylsulfonyl)phenyl]thieno[3,2-d]pyrimidin-2,4-diamine**

(5b). Compound 4a (300 mg, 0.63 mmol), 2,5-diaminopyridine hydrochloride (185 mg, 1 mmol), and Cs_2CO_3 (1012.5 mg, 3.15 mmol) in dry DMF were treated with the XPhos Pd G2 precatalyst (50 mg, 0.063 mmol) under an argon atmosphere; the resulting mixture was heated at 95 °C overnight. The mixture was diluted with EtOAc, washed with sat. NH_4Cl , and dried over MgSO_4 . EtOAc was evaporated, and the residue was purified by FC (c-hex/EtOAc + 10% MeOH). Final separation by RP FC ($\text{H}_2\text{O}/\text{ACN}$ with 0.1% of formic acid) afforded 5a (pale brown solid, 40 mg, yield 10%) and 5b (pale brown solid, 87 mg, yield 25%).

5a. MS (ESI): $m/z = 548.14$ [$\text{M} + \text{H}$] $^+$. ^1H NMR (DMSO- d_6): $\delta = 9.74$ (bs, 1H, NH-1'); 8.87 (bs, 1H, NH-py); 8.18 (m, 3H, H-2', H-6py); 7.84 (s, 1H, H-6); 7.81 (m, 1H, H-4py); 7.70 (d, 2H, $J = 8.8$ Hz, H-3'); 7.18 (m, 1H, H-2''); 6.52 (d, 1H, $J = 8.9$ Hz, H-3py); 3.14 (m, 4H, NCH_2); 2.45 (m, 2H, H-6''); 2.22 (m, 2H, H-3''); 1.74 (m, 2H, H-5''); 1.65 (m, 6H, H-4'', CH_2 -pyrrol.) ppm. ^{13}C NMR (DMSO- d_6): $\delta = 159.95$ (C-2py); 157.86 (C-2); 154.92 (C-7a); 144.16 (C-1'); 135.99 (C-1''); 138.38 (C-6py); 130.63 (C-7); 132.23 (C-4py); 127.74 (C-4'); 128.06 (C-3'); 127.69 (C-6); 127.46 (C-5py); 126.82 (C-2''); 120.32 (C-2'); 108.66 (C-4a); 107.89 (C-3py); 47.89 (N CH_2); 27.32 (C-6''); 25.26 (C-3''); 24.71 (CH_2 -pyrrol.); 22.58 (C-5''); 21.82 (C-4'') ppm. HRMS (ESI): m/z calculated for $\text{C}_{27}\text{H}_{30}\text{O}_2\text{N}_7\text{S}_2$ 548.18969, found 548.18942.

5b. MS (ESI): $m/z = 548.16$ [$\text{M} + \text{H}$] $^+$. ^1H NMR (DMSO- d_6): $\delta = 11.38$ (bs, 1H, NH-1'); 10.65 (bs, 1H, NH-py); 8.17 (s, 1H, H-6); 8.16 (m, 2H, H-2'); 7.83 (m, 2H, H-3'); 7.64 (d, 1H, $J = 2.7$ Hz, H-6py); 7.52 (dd, 1H, $J = 9.1, 2.7$ Hz, H-4py); 7.38 (d, 1H, $J = 9.1$ Hz, H-3py); 6.55 (m, 1H, H-2''); 3.17 (m, 4H, NCH_2); 2.46 (m, 2H, H-6''); 2.35 (m, 2H, H-3''); 1.80 (m, 2H, H-5''); 1.73 (m, 2H, H-4''); 1.67 (m, 4H, CH_2 -pyrrol.) ppm. ^{13}C NMR (DMSO- d_6): $\delta = 155.44$ (C-2); 153.53 (C-7a); 151.88 (C-4); 142.52 (C-1'); 141.57 (C-2py); 140.91 (C-5py); 134.74 (C-1''); 131.35 (C-6); 131.13 (C-4'); 130.40 (C-7); 130.21 (C-4py); 128.23 (C-3'); 127.48 (C-2''); 122.50 (C-6py); 122.09 (C-2'); 115.73 (C-3py); 111.64 (C-4a); 47.89 (N CH_2); 28.08 (C-6''); 25.38 (C-3''); 24.77 (CH_2 -pyrrol.); 22.43 (C-5''); 21.63 (C-4'') ppm. HRMS (ESI): m/z calculated for $\text{C}_{27}\text{H}_{30}\text{O}_2\text{N}_7\text{S}_2$ 548.18969, found 548.18945.

3-Amino-4-(cyclohex-1-en-1-yl)pyrazole (6). Compound 6 was prepared according to a previously described procedure.^{28,29} White solid, yield 23%. MS (ESI): $m/z = 164.1$ [$\text{M} + \text{H}$] $^+$. ^1H NMR (350 K, DMSO- d_6): $\delta = 11.25$ (bs, NH); 7.24 (s, 1H, H-3); 5.75 (m, 1H, H-2'); 4.27 (bs, 2H, NH_2); 2.21 (m, 2H, H-6'); 2.12 (m, 2H, H-3''); 1.67 (m, 2H, H-5'); 1.58 (m, 2H, H-4') ppm. ^{13}C NMR (350 K, DMSO- d_6): $\delta = 150.49$ (C-5); 129.41 (C-1'); 125.95 (C-3); 118.98 (C-2'); 108.32 (C-4); 27.84 (C-6'); 24.89 (C-3''); 22.54 (C-5''); 21.86 (C-4'') ppm. HRMS (ESI): m/z calculated for $\text{C}_9\text{H}_{14}\text{N}_3$ 164.11822, found 164.11821.

3-(Cyclohex-1-en-1-yl)-5,7-dichloropyrazolo[1,5-a]pyrimidine (8). Sodium (0.394 g, 17.15 mmol, 2.5 equiv) was dissolved in dry EtOH (17 mL), followed by the addition of 6 (1.12 g, 6.86 mmol, 1 equiv) and diethyl malonate (1.0 mL, 6.86 mmol, 1 equiv); the resulting mixture was refluxed for 8 h. The mixture was cooled to RT, and the precipitated solids were filtered, dissolved in water, and acidified with 1 M HCl to pH 2. Solids were then filtered off, washed with water, and dried in vacuo. The mother liquor was evaporated to half its volume and acidified with 1 M HCl. Next, a further portion of the white solid product was filtered, washed with water, and dried. White solid, yield 1.23 g (76%). MS (ESI): $m/z = 232.2$ [$\text{M} + \text{H}$] $^+$. Next, the product was directly treated with POCl_3 (5 mL) and *N,N*-dimethylaniline (0.74 mL, 5.8 mmol, 1.5 equiv). The mixture was heated at 80 °C for 5 h, cooled down to RT, and carefully poured over crushed ice under vigorous stirring. The product was extracted with DCM, which was then washed with water and dried over MgSO_4 . Purification by FC (c-hex/EtOAc + 10% MeOH, 0–20%) provided a yellow solid of 8 (0.60 g, 46%). MS (ESI): $m/z = 268.08$ [$\text{M} + \text{H}$] $^+$. ^1H NMR (CDCl_3): $\delta = 8.17$ (s, 1H, H-8); 6.92 (s, 1H, H-1); 6.64 (m, 1H, H-2'); 2.51 (m, 2H, H-6'); 2.26 (m, 2H, H-3'); 1.81 (m, 2H, H-5'); 1.69 (m, 2H, H-4') ppm. ^{13}C NMR (CDCl_3): $\delta = 148.18$ and 139.83 (C-5 and C-7); 143.60 (C-2); 127.15 (C-1'); 126.01 (C-2'); 114.69 (C-3); 108.40 (C-6); 27.57 (C-6'); 25.75 (C-3'); 22.86 (C-

5'); 22.23 (C-4') ppm. HRMS (ESI): m/z calculated for $C_{12}H_{12}N_3Cl_2$ 268.04028, found 268.04033.

5-Chloro-3-(cyclohex-1-en-1-yl)- N^7 -(4-(1-pyrrolidinylsulfonyl)phenyl)pyrazolo[1,5-*a*]pyrimidin-7-amine (9). Prepared from **8** according to **GP1**. White solid, yield 59%. MS (ESI): m/z = 458.03 [M + H]⁺. ¹H NMR (CDCl₃): δ = 8.36 (s, 1H, NH); 8.04 (s, 1H, H-2); 7.94 (d, 2H, *J* = 8.7 Hz, H-3''); 7.50 (d, 2H, *J* = 8.7 Hz, H-2''); 6.68 (m, 1H, H-2'); 6.48 (s, 1H, H-6); 3.30 (m, 4H, NCH₂); 2.52 (m, 2H, H-6'); 2.26 (m, 2H, H-3''); 1.84–1.78 (m, 6H, H-5', CH₂-pyrrol.); 1.70 (m, 2H, H-4') ppm. ¹³C NMR (CDCl₃): δ = 150.90 (C-7); 143.61 (C-3a); 143.29 (C-5); 141.66 (C-2); 140.27 (C-1''); 134.55 (C-4''); 129.65 (C-3''); 127.54 (C-1'); 124.87 (C-2'); 122.23 (C-2''); 113.22 (C-3); 87.33 (C-6); 48.12 (NCH₂); 27.63 (C-6'); 25.74 (C-3'); 25.46 (CH₂-pyrrol.); 22.95 (C-5'); 22.34 (C-4') ppm. HRMS (ESI): m/z calculated for $C_{22}H_{25}O_2N_5ClS$ 458.14120, found 458.14112.

N^5 -(5-Aminopyridin-2-yl)-3-(cyclohex-1-en-1-yl)- N^7 -(4-(1-pyrrolidinylsulfonyl)phenyl)pyrazolo[1,5-*a*]pyrimidine-5,7-diamine (10a) and N^5 -(6-Aminopyridin-3-yl)-3-(cyclohex-1-en-1-yl)- N^7 -(4-(1-pyrrolidinylsulfonyl)phenyl)pyrazolo[1,5-*a*]pyrimidine-5,7-diamine (10b). Compound **9** (450 mg, 0.98 mmol), 2,5-diaminopyridine (537 mg, 2.95 mmol), and Cs₂CO₃ (2.56 g, 7.8 mmol) in dry DMF (20 mL) under an argon atmosphere were treated with Pd₂(dba)₃ (90 mg, 0.098 mmol) and Xantphos (114 mg, 0.2 mmol); the resulting mixture was heated at 120 °C overnight. The mixture was diluted with EtOAc, washed with sat. NH₄Cl, dried over MgSO₄, and evaporated. After the residue was purified by FC (c-hex/EtOAc + 10% MeOH), isomers were separated by RP FC (H₂O/ACN + 0.1% TFA), evaporated, codistilled with water, and freeze-dried from dioxane.

10a. Off-white foam, yield 126 mg (24%). MS (ESI): m/z = 531.50 [M + H]⁺. ¹H NMR (DMSO-*d*₆): δ = 9.85 (s, 1H, NH-7); 9.40 (s, 1H, NH-5); 7.99 (H-2); 7.97 (d, 1H, *J*(py-3,4) = 9.1 Hz, py-3); 7.82 (m, 2H, H-3''); 7.70–7.67 (m, 3H, H-2'', py-6); 7.00 (dd, *J*(py-4,3) = 8.9 Hz, *J*(py-4,6) = 2.9 Hz, py-4); 6.75 (s, 1H, H-6); 6.64 (m, 1H, H-2'); 4.93 (s, 2H, NH₂); 3.17 (m, 4H, NCH₂); 2.50 (m, 2H, H-6''); 2.22 (m, 2H, H-3''); 1.79–1.66 (m, 8H, H-5'', H-4'', CH₂-pyrrol.) ppm. ¹³C NMR (DMSO-*d*₆): δ = 153.73 (C-5); 144.42 (C-3a); 144.11 (py-5); 143.27 (C-1''); 143.11 (C-7); 140.31 (C-8); 140.25 (py-2); 133.52 (py-6); 130.75 (C-4''); 128.93 (C-3''); 128.76 (C-1'); 123.07 (py-4); 121.86 (C-2''); 120.17 (C-2'); 113.68 (py-3); 108.07 (C-3); 78.57 (C-6); 48.08 (NCH₂); 27.23 (C-6'); 25.31 (C-3'); 24.96 (CH₂-pyrrol.); 22.83 (C-5'); 22.36 (C-4') ppm. HRMS (ESI): m/z calculated for $C_{27}H_{31}O_2N_8S$ 531.22852, found 531.22812. Purity was 90% due to complications with purification.

10b. Off-white foam, yield 100 mg (19%). MS (ESI): m/z = 531.4 [M + H]⁺. ¹H NMR (DMSO-*d*₆): δ = 9.81 (s, 1H, NH-7); 8.96 (s, 1H, NH-5); 8.29 (d, 1H, *J*(py-6,4) = 2.7 Hz, py-6); 7.96 (s, 1H, H-2); 7.83 (m, 2H, H-3''); 7.76 (dd, 1H, *J*(py-4,3) = 8.8 Hz, *J*(py-4,6) = 2.7 Hz, py-4); 7.68 (m, 2H, H-2''); 6.58 (m, 1H, H-2'); 6.45 (d, 1H, *J*(py-3,4) = 8.9 Hz, py-3); 6.12 (s, 1H, H-6); 5.62 (bs, 2H, NH₂); 3.17 (m, 4H, NCH₂); 2.45 (m, 2H, H-6'); 2.19 (m, 2H, H-3'); 1.74–1.61 (m, 8H, H-5', 4', CH₂-pyrrol.) ppm. ¹³C NMR (DMSO-*d*₆): δ = 155.59 (py-2); 154.57 (C-5); 144.60 (C-3a); 143.40 (C-7); 143.12 (C-1''); 140.29 (C-2); 137.50 (C-6); 130.97 (C-4''); 130.56 (py-4); 129.04 (C-3''); 128.75 (C-1'); 127.58 (py-5); 122.11 (C-2''); 119.98 (C-2'); 107.91 (C-3); 107.69 (py-3); 77.87 (C-6); 48.07 (NCH₂); 27.20 (C-6'); 25.36 (C-3'); 24.97 (CH₂-pyrrol.); 22.83 (C-5'); 22.36 (C-4') ppm. HRMS (ESI): m/z calculated for $C_{27}H_{31}O_2N_8S$ 531.22852, found 531.22831.

N^5 -((1*R*,4*R*)-4-Aminocyclohexyl)-3-(cyclohex-1-en-1-yl)- N^7 -(4-(pyrrolidin-1-ylsulfonyl)phenyl)pyrazolo[1,5-*a*]pyrimidine-5,7-diamine (11). Prepared from **9** according to **GP2**. Brown solid, yield 68%. MS (ESI): m/z = 536.3 [M + H]⁺. ¹H NMR (DMSO-*d*₆): δ = 9.66 (bs, 1H, NH); 7.88 (s, 1H, H-2); 7.85 (bd, 2H, *J* = 5.4 Hz, NH₂); 7.80 (m, 2H, H-3'); 7.63 (m, 2H, H-2'); 7.02 (bs, 1H, NH); 6.62 (m, 1H, H-2''); 5.96 (s, 1H, H-6); 3.75 (m, 1H, c-hex-1); 3.16 (m, 4H, NCH₂); 3.04 (m, 1H, c-hex-4); 2.45 (m, 2H, H-6''); 2.17 (m, 2H, H-3''); 2.11 (m, 2H, c-hex-2a); 1.99 (m, 2H, c-hex-3a); 1.73–1.66 (m, 6H, H-5'', CH₂-pyrrol.); 1.62 (m, 2H, H-4''); 1.42 (m, 2H, c-hex-3b); 1.23 (m, 2H, c-hex-2b) ppm. ¹³C NMR (DMSO-*d*₆): δ = 156.18 (C-

7); 143.04 (C-1'); 139.76 (C-2); 130.55 (C-4'); 128.78 (C-3'); 128.74 (C-1''); 121.63 (C-2''); 119.23 (C-2''); 106.78 (C-8); 76.73 (C-6); 48.76 and 48.60 (c-hex-1,4); 47.83 (NCH₂); 29.76 and 29.19 (c-hex-2,3); 26.85 (C-6''); 25.12 (C-3''); 24.74 (CH₂-pyrrol.); 22.65 (C-5''); 22.20 (C-4'') ppm.

3-Bromo-5-chloro- N -(4-(1-pyrrolidinylsulfonyl)phenyl)pyrazolo[1,5-*a*]pyrimidine-7-amine (13). Prepared from 3-bromo-5,7-dichloropyrazolo[1,5-*a*]pyrimidine³⁰ according to **GP1**. Off-white solid, yield 85%. MS (ESI): m/z = 456.01 [M + H]⁺. ¹H NMR (DMSO-*d*₆): δ = 10.80 (bs, 1H, NH); 8.44 (s, 1H, H-2); 7.88 (m, 2H, H-3'); 7.72 (m, 2H, H-2'); 6.54 (s, 1H, H-6); 3.18 (m, 4H, NCH₂); 1.69 (m, 4H, CH₂-pyrrol.) ppm. ¹³C NMR (DMSO-*d*₆): δ = 151.83 (C-7); 145.44 (C-5); 144.57 (C-3a); 144.26 (C-2); 140.92 (C-1'); 133.0 (C-4'); 128.91 (C-3'); 123.83 (C-2'); 88.02 (C-6); 82.07 (C-3); 47.84 (NCH₂); 24.75 (CH₂-pyrrol.) ppm. HRMS (ESI): m/z calculated for $C_{16}H_{16}O_2N_5BrClS$ 455.98911, found 455.98889.

N^5 -((1*R*,4*R*)-4-Aminocyclohexyl)- N^7 -(4-(1-pyrrolidinylsulfonyl)phenyl)pyrazolo[1,5-*a*]pyrimidine-5,7-diamine (14). Prepared from **13** according to **GP2**. Off-white foam, yield 41%. MS (ESI): m/z = 456.34 [M + H]⁺. ¹H NMR (DMSO-*d*₆): δ = 10.23 (bs, NH-1'); 7.99 (d, 1H, *J*(2,3) = 2.1 Hz, H-2); 7.94 (m, 3H, NH, NH₂); 7.86 (d, 2H, *J*(3',2') = 8.7 Hz, H-3'); 7.66 (d, 2H, *J*(2',3') = 8.7 Hz, H-2'); 6.17 (d, 1H, *J*(3,2) = 2.1 Hz, H-3); 5.89 (s, 1H, H-6); 3.69 (m, 1H, N-CH-1'); 3.17 (m, 4H, NCH₂); 3.04 (m, 1H, N-CH-4''); 2.03–1.95 (m, 4H, H-2'a, H-3'a); 1.69 (m, 4H, CH₂-pyrrol.); 1.43 (m, 2H, H-3'b); 1.28 (m, 2H, H-2'b) ppm. ¹³C NMR (DMSO-*d*₆): δ = 158.52 (C-7); 158.19 (C-5); 154.33 (C-9); 143.35 (C-2); 141.97 (C-1'); 132.05 (C-4'); 128.85 (C-3'); 123.20 (C-2'); 91.28 (C-2); 75.08 (C-6); 48.42 (N-CH-1', 4'); 47.85 (NCH₂); 29.87 and 28.94 (C-2'', 3'') ppm. HRMS (ESI): m/z calculated for $C_{22}H_{30}O_2N_7S$ 456.21762, found 456.21743.

5,7-Dichloro-3-cyclohexyl-3H-imidazo[4,5-*b*]pyridine (16). 5,7-Dichloro-3H-imidazo[4,5-*b*]pyridine (0.9 g, 4.8 mmol) was codistilled with toluene and dry dioxane. Cyclohexanol (4.9 mL, 47.8 mmol) and Ph₃P (3.77 g, 14.36 mmol) were added, and the mixture was then flushed with argon. Dry degassed dioxane (24 mL) was added together with DIAD (2.8 mL, 14.36 mmol) in a dropwise manner; the resulting mixture was stirred at RT overnight. The solvent was evaporated, the product was isolated by FC (c-hex/EtOAc + 10% MeOH), and the final compound was repurified by RP FC (H₂O/ACN)⁺. ¹H NMR (DMSO-*d*₆): δ = 8.71 (s, 1H, H-8); 7.61 (s, 1H, H-1); 4.45 (tt, 1H, *J* = 11.8, 3.8 Hz, H-1'); 2.03 (m, 2H, H-2'a); 1.93–1.79 (m, 4H, H-2'b, H-3'a); 1.71 (m, 1H, H-4'a); 1.47 (m, 2H, H-3'b); 1.27 (m, 1H, H-4'b) ppm. ¹³C NMR (DMSO-*d*₆): δ = 146.01 (C-4); 144.83 (C-8); 143.89 (C-2); 135.05 (C-6); 131.93 (C-5); 117.76 (C-1); 54.15 (C-1'); 32.17 (C-2'); 25.02 (C-3'); 24.75 (C-4') ppm. HRMS (ESI): m/z calculated for $C_{12}H_{14}N_4Cl_2$ 270.05593, found 270.05579.

5-Chloro-3-cyclohexyl- N -(4-(pyrrolidin-1-ylsulfonyl)phenyl)-3H-imidazo[4,5-*b*]pyridin-7-amine (17). Prepared according to **GP1**. White solid, yield 80%. MS (ESI): m/z = 460.1 [M + H]⁺. ¹H NMR (DMSO-*d*₆): δ = 9.78 (s, 1H, NH); 8.44 (s, 1H, H-8); 7.75 (d, 2H, *J* = 8.8 Hz, H-3'); 7.56 (d, 2H, *J* = 8.8 Hz, H-2'); 6.98 (s, 1H, H-1); 4.40 (tt, 1H, *J* = 12.2, 4.0 Hz, H-1''); 3.14 (m, 2H, NCH₂); 2.03 (m, 2H, H-2'a); 1.84–1.94 (m, 4H, H-2'b, 3'a); 1.66–1.73 (m, 5H, H-4'b, CH₂-pyrrol.); 1.47 (m, 2H, H-3'b); 1.26 (m, 1H, H-4'a) ppm. ¹³C NMR (DMSO-*d*₆): δ = 146.11 (C-4); 145.36 (C-2); 144.49 (C-1'); 142.69 (C-6); 140.42 (C-8); 129.26 (C-4''); 128.81 (C-3'); 123.94 (C-5); 119.74 (C-2''); 101.31 (C-1); 53.48 (C-1''); 47.78 (NCH₂); 32.38 (C-2''); 25.11 (C-3''); 24.82 (C-4''); 24.68 (CH₂-pyrrol.) ppm. HRMS (ESI): m/z calculated for $C_{22}H_{27}O_2N_5ClS$ 460.15685, found 460.15658.

N^5 -(5-Aminopyridin-2-yl)-3-(cyclohexyl)-3H-imidazo[4,5-*b*]pyridine-5,7-diamine (18a) and N^5 -(6-Aminopyridin-3-yl)-3-(cyclohexyl)- N^7 -(4-(pyrrolidin-1-ylsulfonyl)phenyl)-3H-imidazo[4,5-*b*]pyridine-5,7-diamine (18b). Compound **17** (250 mg, 0.54 mmol), 2,5-diaminopyridine (297 mg, 1.63 mmol), and Cs₂CO₃ (1.42 g, 4.35 mmol) in dry DMF (12 mL) under an argon atmosphere were treated with Pd₂(dba)₃ (50 mg,

0.054 mmol) and Xantphos (63 mg, 0.11 mmol); the resulting mixture was then heated at 115 °C overnight. The mixture was diluted with EtOAc, washed with sat. NH₄Cl, dried over MgSO₄, and evaporated. After the residue was purified by FC (c-hex/EtOAc + 10% MeOH), isomers were separated by RP FC (H₂O/ACN + 0.1% TFA), evaporated, codistilled with water, and freeze-dried from dioxane.

18a. Pale brown foam, yield 47 mg (16%). MS (ESI): *m/z* = 533.2 [M + H]⁺. ¹H NMR (DMSO-*d*₆): δ = 10.97 (s, 1H, NH); 9.76 (s, 1H, NH); 8.38 (s, 1H, H-8); 7.78 (3, 2H, H-3'); 7.70 (d, 1H, *J* = 2.7 Hz, py-6); 7.66 (dd, 1H, *J* = 9.27, 2.7 Hz, py-4); 7.59 (m, 2H, H-2'); 7.34 (d, 1H, *J* = 9.4 Hz, py-3); 6.85 (s, 1H, H-1); 4.72 (m, 1H, H-1''); 3.16 (m, 2H, NCH₂); 2.12 (m, 2H, H-2''a); 1.87–1.92 (m, 4H, H-2''b, 3''a); 1.78 (m, 1H, H-4''b); 1.59 (m, 4H, CH₂-pyrrol.); 1.56 (m, 2H, H-3''b); 1.29 (m, 1H, H-4''a) ppm. ¹³C NMR (DMSO-*d*₆): δ = 150.57 (C-2); 144.73 (C-1'); 143.62 (C-4); 142.86 (C-6); 138.34 (C-8); 133.50 (py-4); 129.23 (C-4'); 129.14 (py-6); 128.87 (C-3'); 121.30 (C-5); 119.91 (C-2'); 115.63 (py-3); 89.99 (C-1); 53.32 (C-1''); 47.82 (NCH₂); 32.45 (C-2''); 25.08 (C-3''); 24.73 (C-4''), CH₂-pyrrol.) ppm. HRMS (ESI): *m/z* calculated for C₂₇H₃₃O₂N₈S 533.24417, found 533.24380.

18b. Pale brown foam, yield 40 mg (14%). MS (ESI): *m/z* = 533.2 [M + H]⁺. ¹H NMR (DMSO-*d*₆): δ = 9.46 (s, 1H, NH); 9.33 (s, 1H, NH); 8.83 (d, 1H, *J* = 2.5 Hz, py-6); 8.34 (s, 1H, H-8); 7.90 (dd, 1H, *J* = 9.5, 2.5 Hz, py-4); 7.75 (d, 2H, *J* = 8.8 Hz, H-3'); 7.68 (bs, 2H, NH₂); 7.53 (d, 2H, *J* = 8.8 Hz, H-2'); 7.03 (d, 1H, *J* = 9.5 Hz, py-3); 6.65 (s, 1H, H-1); 4.41 (m, 1H, H-1''); 3.14 (m, 2H, NCH₂); 2.08 (m, 2H, H-2''a); 1.86–1.95 (m, 4H, H-2''b, 3''a); 1.67–1.75 (m, 5H, H-4''b, CH₂-pyrrol.); 1.52 (m, 2H, H-3''b); 1.32 (m, 1H, H-4''a) ppm. ¹³C NMR (DMSO-*d*₆): δ = 152.71 (C-2); 149.42 (py-2); 145.34 (C-1'); 144.88 (C-4); 141.41 (C-6); 137.33 (py-4); 137.10 (C-8); 129.36 (py-5); 128.92 (C-3'); 128.35 (C-4'); 120.67 (py-4); 119.00 (C-2'); 118.78 (C-5); 114.06 (py-3); 90.10 (C-1); 54.03 (C-1''); 47.81 (NCH₂); 32.21 (C-2''); 25.17 (C-3''); 24.95 (C-4''); 24.71 (CH₂-pyrrol.) ppm. HRMS (ESI): *m/z* calculated for C₂₇H₃₃O₂N₈S 533.24417, found 533.24380.

8-Bromo-2-(4-nitrophenylamino)pyrido[4,3-*d*]pyrimidin-4(3*H*)-one (21). Compound **20** was prepared as previously described.³³ In freshly distilled THF (100 mL), **20** (6.2 g, 13 mmol) was treated with 4-nitrophenyl isocyanate (4.14 g, 25 mmol) under an argon atmosphere at RT. The mixture was stirred at RT for 2 h (TLC showed complete consumption of the starting material) and diluted with 100 mL of THF. Next, NH₃ was bubbled through the mixture for 2 min, and the resulting mixture was stirred at RT overnight. Poorly soluble solids were filtered, washed with THF, and dried. Bright yellow powder, yield 3.1 g (68%). MS (ESI): *m/z* = 362 [M + H]⁺. ¹H NMR (DMSO-*d*₆, 353 K): δ = 8.97 (s, 1H, H-7); 8.73 (s, 1H, H-5); 8.28 (m, 2H, H-2'); 8.20 (m, 2H, H-3') ppm. ¹³C NMR (DMSO-*d*₆, 353 K): δ = 165.55 (C-4); 155.35 (C-2); 153.56 (C-8a); 152.37 (C-5); 147.89 (C-7); 146.20 (C-1'); 141.12 (C-4'); 124.45 (C-3'); 118.81 (C-2'); 116.57 and 116.45 (C-8 and C-4a) ppm.

8-Bromo-N²-(4-nitrophenyl)-N⁴-(4-(1-pyrrolidinylsulfonyl)phenyl)pyrido[4,3-*d*]pyrimidine-2,4-diamine (23). Compound **20** (3 g, 8 mmol) in POCl₃ (75 mL) was treated with *N,N*-dimethylaniline (2.1 mL, 17 mmol). The reaction mixture was refluxed for 20 h, cooled to RT, and poured slowly over ice. The solids were filtered and washed with water. Red solid, yield 2.8 g (89%). MS (ESI): *m/z* = 379.9 [M + H]⁺. The chloro derivative was converted to **23** according to **GP1**. Dark red solid, yield 32%. MS (ESI): *m/z* = 570.0 [M + H]⁺. ¹H NMR (DMSO-*d*₆): δ = 10.52 (bs, 1H, NH-2); 10.48 (bs, 1H, NH-4); 9.62 (s, 1H, H-5); 8.93 (s, 1H, H-7); 8.21–8.30 (m, 6H, H-2', H-2'', H-3''); 7.87 (d, 2H, *J* = 8.8 Hz, H-3'); 3.19 (m, 4H, NCH₂); 1.68 (m, 4H, CH₂-pyrrol.) ppm. ¹³C NMR (DMSO-*d*₆): δ = 158.58 (C-2); 158.14 (C-4); 153.20 (C-8a); 151.46 (C-7); 146.38 (C-1''); 146.36 (C-5); 142.62 (C-1'); 141.20 (C-4''); 128.15 (C-3''); 124.72 (C-3''); 122.26 (C-2'); 119.08 (C-2''); 117.43 (C-8); 110.45 (C-4a); 47.85 (NCH₂); 24.74 (CH₂-pyrrol.) ppm. HRMS (ESI): *m/z* calculated for C₂₃H₂₁O₄N₇BrS 570.05536, found 570.05564.

8-(1-Cyclohexen-1-yl)-N²-(4-nitrophenyl)-N⁴-(4-(1-pyrrolidinylsulfonyl)phenyl)pyrido[4,3-*d*]pyrimidine-2,4-diamine

(24). Compound **23** (170 mg, 0.3 mmol), cyclohex-1-en-1-ylboronic acid (113 mg, 0.9 mmol), Cs₂CO₃ (583 mg, 1.8 mmol), and Pd(dppf)Cl₂·DCM (49 mg, 0.06 mmol) in DMF (13 mL) and water (2 mL) under an argon atmosphere were heated at 80 °C overnight. The mixture was diluted with EtOAc, washed with sat. NH₄Cl, and dried over MgSO₄. Purification by RP FC (H₂O/ACN + 0.1% TFA) afforded a yellow solid (160 mg, 94%). MS (ESI): *m/z* = 572.2 [M + H]⁺. ¹H NMR (DMSO-*d*₆): δ = 10.33 (bs, 1H, NH); 10.26 (bs, 1H, NH); 9.58 (s, 1H, H-5); 8.44 (s, 1H, H-7); 8.30 (d, 2H, *J* = 8.2 Hz, H-2'); 8.23 (d, 2H, *J* = 9.1 Hz, H-2''); 8.14 (d, 2H, *J* = 8.9 Hz, H-3''); 7.84 (d, 2H, *J* = 8.2 Hz, H-3'); 5.89 (m, 1H, H-2'''); 3.18 (m, 4H, NCH₂); 2.50 (m, 2H, H-6'''); 2.26 (m, 2H, H-3'''); 1.82 (m, 2H, H-5'''); 1.76 (m, 2H, H-4'''); 1.68 (m, 4H, CH₂-pyrrol.) ppm. ¹³C NMR (DMSO-*d*₆): δ = 158.62 (C-2); 156.86 (C-4); 153.18 (C-8a); 148.91 (C-7); 146.94 (C-1''); 146.31 (C-5); 143.07 (C-1'); 140.77 (C-4''); 134.61 (C-8); 130.50 (C-1'''); 128.14 (C-3'); 127.83 (C-2''); 124.58 (C-3''); 121.83 (C-2'); 118.42 (C-2''); 108.56 (C-4a); 47.85 (NCH₂); 28.79 (C-6'''); 25.35 (C-3'''); 24.74 (CH₂-pyrrol.); 22.74 (C-5'''); 21.90 (C-4''') ppm. HRMS (ESI): *m/z* calculated for C₂₉H₃₀O₄N₇S 572.20745, found 572.20707.

8-(1-Cyclohexen-1-yl)-N²-(4-aminophenyl)-N⁴-(4-(1-pyrrolidinylsulfonyl)phenyl)pyrido[4,3-*d*]pyrimidine-2,4-diamine (25). Compound **24** (60 mg, 0.1 mmol) in EtOAc (5 mL) and EtOH (1 mL) was treated with Pd/C (10% wt, 14 mg) and stirred under a hydrogen atmosphere (15 bar) for 2 days. The mixture was filtered, the solvent was evaporated, and the residue was purified by RP FC (H₂O/ACN + 0.1% TFA) to give an off-white solid (35 mg, 58%). MS (ESI): *m/z* = 542.2 [M + H]⁺. ¹H NMR (DMSO-*d*₆): δ = 10.55 (bs, 1H, NH); 10.25 (bs, 1H, NH); 9.68 (s, 1H, H-5); 8.42 (s, 1H, H-7); 8.34 (d, 2H, *J* = 8.2 Hz, H-2'); 7.93 (d, 2H, *J* = 9.1 Hz, H-2''); 7.83 (m, 2H, H-3''); 7.11 (m, 2H, H-3'); 6.01 (m, 1H, H-2'''); 3.17 (m, 4H, NCH₂); 2.50 (m, 2H, H-6'''); 2.25 (m, 2H, H-3'''); 1.79–1.71 (m, 4H, H-5''', H-4'''); 1.67 (m, 4H, CH₂-pyrrol.) ppm. ¹³C NMR (DMSO-*d*₆): δ = 158.37 (C-2); 158.05 (C-4); 157.21 (C-8a); 140.91 (C-5); 139.61 (C-7); 133.27 (C-8); 128.92 (C-2''); 127.95 (C-3''); 121.47 (C-2'); 121.15 (C-2''); 120.18 (C-3'); 115.36 (C-4a); 47.87 (NCH₂); 28.06 (C-6'''); 25.29 (C-3''); 24.74 (CH₂-pyrrol.); 22.48 (C-5'''); 21.65 (C-4''') ppm. HRMS (ESI): *m/z* calculated for C₂₉H₃₂O₂N₇S 542.23327, found 542.23275. Purity was 93% due to complications with purification.

3-Bromo-6-chloro-N-(4-(1-pyrrolidinylsulfonyl)phenyl)imidazo[1,2-*b*]pyridazin-8-amine (27). Prepared according to **GP1** from 3-bromo-6,8-dichloroimidazo[1,2-*b*]pyridazine.^{40,41} White solid, yield 52%. MS (ESI): *m/z* = 455.9 [M + H]⁺. ¹H NMR (DMSO-*d*₆): δ = 10.34 (bs, 1H, NH); 7.83 (m, 3H, H-2, H-3'); 7.70 (m, 2H, H-2'); 6.84 (s, 1H, H-7); 3.16 (m, 4H, NCH₂); 1.68 (m, 4H, CH₂-pyrrol.) ppm. ¹³C NMR (DMSO-*d*₆): δ = 148.54 (C-6); 142.63 (C-1'); 139.75 (C-8); 133.16 (C-9); 131.64 (C-2); 131.49 (C-4'); 128.88 (C-3'); 122.01 (C-2'); 101.16 (C-3); 95.23 (C-7); 47.81 (NCH₂); 24.72 (CH₂-pyrrol.) ppm. HRMS (ESI): *m/z* calculated for C₁₆H₁₆O₂N₃BrClS 455.98911, found 455.98873.

N⁶-((1*r*,4*r*)-4-Aminocyclohexyl)-3-bromo-N⁸-(4-(1-pyrrolidinylsulfonyl)phenyl)imidazo[1,2-*b*]pyridazine-6,8-diamine (29a) and N⁶-((1*r*,4*r*)-4-Aminocyclohexyl)-3-(1-cyclohexene-1-yl)-N⁸-(4-(1-pyrrolidinylsulfonyl)phenyl)imidazo[1,2-*b*]pyridazine-6,8-diamine (29b). Compound **27** (520 mg, 1.14 mmol), cyclohex-1-en-1-ylboronic acid (158 mg, 1.25 mmol), and XPhos Pd G2 (45 mg, 0.057 mmol) in degassed dioxane (18 mL) were treated with an aqueous solution of K₃PO₄ (0.5 M, 4.56 mL, 2.28 mmol) under an argon atmosphere and heated at 95 °C overnight. After the solvent was evaporated, the residue was purified by FC (c-hex/EtOAc + 10% MeOH) and repurified by RP FC (H₂O/ACN) to give an inseparable mixture of starting material and compound **28** in a ratio of approximately 5:3, 490 mg. MS (ESI): *m/z* = 458.4 [M + H]⁺. The resulting mixture (310 mg) was converted according to **GP2** to the corresponding aminocyclohexyl derivatives **29a** and **29b**, which were finally separated by RP FC (H₂O/ACN + 0.1% formic acid).

29a. Off-white solid, 10 mg. MS (ESI): *m/z* = 534.3 [M + H]⁺. ¹H NMR (DMSO-*d*₆): δ = 9.48 (s, 1H, NH); 7.83 (d, 2H, *J* = 5.4 Hz, NH₂); 7.77 (m, 2H, H-3'); 7.59 (m, 2H, H-2'); 7.47 (s, 1H, H-2);

6.66 (d, 1H, $J = 7.0$ Hz, NH); 6.45 (s, 1H, H-7); 3.57 (m, 1H, H-1"); 3.15 (m, 4H, NCH₂); 3.04 (m, 1H, H-4"); 2.15 (m, 2H, H-2"); 1.99 (m, 2H, H-3"); 1.67 (m, 4H, CH₂-pyrrol.); 1.43 (m, 2H, H-3"); 1.25 (m, 2H, H-2") ppm. ¹³C NMR (DMSO-*d*₆): $\delta = 154.83$ (C-6); 144.41 (C-1'); 137.03 (C-8); 132.27 (C-9); 129.39 (C-4'); 128.7 (C-3', C-2); 120.26 (C-2'); 99.62 (C-3); 88.36 (C-7); 48.71 and 48.64 (C-1", C-4"); 47.78 (NCH₂); 29.69 (C-2"); 29.15 (C-3"); 24.70 (CH₂-pyrrol.) ppm. HRMS (ESI): m/z calculated for C₂₂H₂₃O₂N₅BrS 534.12813, found 534.12767.

29b-HCOOH. Off-white solid, 30 mg. MS (ESI): $m/z = 536.2$ [M + H]⁺. ¹H NMR (DMSO-*d*₆): $\delta = 8.45$ (s, 1H, HCOOH); 7.75 (m, 2H, H-3'); 7.59 (m, 2H, H-2'); 7.35 (s, 1H, H-2); 7.17 (m, 1H, H-2-c-hex); 6.52 (d, 1H, $J = 6.5$ Hz, NH); 6.42 (s, 1H, H-7); 3.46 (m, 1H, H-1"); 3.14 (m, 4H, NCH₂); 2.89 (m, 1H, H-4"); 2.46 (m, 2H, H-6-c-hex); 2.25 (m, 2H, H-3-c-hex); 2.14 (m, 2H, H-2") a); 1.96 (m, 2H, H-3") a); 1.74 (m, 2H, H-5-c-hex); 1.64–1.69 (m, 6H, H-4-c-hex, CH₂-pyrrol.); 1.35 (m, 2H, H-3") b); 1.22 (m, 2H, H-2") b) ppm. ¹³C NMR (DMSO-*d*₆): $\delta = 165.59$ (HCOOH); 153.79 (C-6); 144.73 (C-1'); 136.87 (C-8); 132.41 (C-9); 128.90 (C-4'); 128.76 (C-3'); 126.61 (C-2); 125.75 (C-3); 123.94 (C-2-c-hex); 119.85 (C-2'); 87.79 (C-7); 49.66 (C-1"); 48.91 (C-4"); 47.78 (NCH₂); 30.79 (C-2"); 29.99 (C-3"); 26.22 (C-6-c-hex); 25.14 (C-3-c-hex); 24.69 (CH₂-pyrrol.); 22.34 (C-5-c-hex); 21.77 (C-4-c-hex) ppm. HRMS (ESI): m/z calculated for C₂₈H₃₈O₂N₇S 536.28022, found 536.27977.

N⁶-(1*r*,4*r*)-4-Aminocyclohexyl)-3-(cyclohexan-1-yl)-N⁸-(4-(1-pyrrolidinylsulfonyl)phenyl)imidazo[1,2-*b*]pyridazine-6,8-diamine (30). Compound **29b** (100 mg, 0.18 mmol) in a mixture of EtOAc (3 mL) and MeOH (1 mL) was treated with Pd/C (10% loading, 20 mg) and stirred under a hydrogen atmosphere (15 bar) for 2 days. The mixture was filtered, evaporated, purified by RP FC (H₂O/ACN + 0.1% formic acid), and freeze-dried from dioxane to give 70 mg of **30**. MS (ESI): $m/z = 538.5$ [M + H]⁺. ¹H NMR (DMSO-*d*₆): $\delta = 8.45$ (s, 1H, FA); 7.75 (m, 2H, H-3'); 7.58 (m, 2H, H-2'); 7.09 (s, 1H, H-2); 6.42 (d, 1H, $J = 6.5$ Hz, NH); 6.37 (s, 1H, H-7); 3.49 (m, 1H, H-1"); 3.14 (m, 4H, NCH₂); 2.91 (m, 2H, H-4", H-1-c-hex); 2.15 (m, 2H, H-2") a); 2.05 (m, 2H, H-3") a); 1.96 (m, 2H, H-2a-c-hex); 1.79 (m, 2H, H-3a-c-hex); 1.73 (m, 1H, H-4a-c-hex); 1.67 (m, 4H, CH₂-pyrrol.); 1.52 (m, 2H, H-3") b); 1.36 (m, 4H, H-2b-c-hex, H-3b-c-hex); 1.22 (m, 3H, H-4b-c-hex, H-2") b) ppm. ¹³C NMR (DMSO-*d*₆): $\delta = 165.52$ (FA); 153.66 (C-6); 144.84 (C-1'); 136.95 (C-8); 133.32 (C-3); 131.27 (C-9); 128.79 (C-3'); 128.74 (C-4'); 124.39 (C-7); 119.78 (C-2'); 87.62 (C-2); 49.43 (C-1"); 49.84 (C-4"); 47.77 (NCH₂); 33.80 (C-1-c-hex); 30.67 (C-2-c-hex); 30.43 (C-3"); 30.02 (C-2"); 20.95 (C-3, C-4-c-hex); 24.88 (CH₂-pyrrol.) ppm. HRMS (ESI): m/z calculated for C₂₈H₄₀O₂N₇S 538.29587, found 538.29535.

6-Chloro-3-iodo-N-(4-(1-pyrrolidinylsulfonyl)phenyl)imidazo[1,2-*b*]pyridazin-8-amine (32). Compound **32** was prepared according to **GP1** from 8-bromo-6-chloro-3-iodoimidazo[1,2-*b*]pyridazine^{40,41} White solid, yield 58%. MS (ESI): $m/z = 503.8$ [M + H]⁺. ¹H NMR (DMSO-*d*₆): $\delta = 10.27$ (bs, 1H, NH); 7.83 (m, 2H, H-3'); 7.81 (s, 1H, H-2); 7.68 (m, 2H, H-2'); 6.83 (s, 1H, H-7); 3.16 (m, 4H, NCH₂); 1.68 (m, 4H, CH₂-pyrrol.) ppm. ¹³C NMR (DMSO-*d*₆): $\delta = 148.21$ (C-6); 142.80 (C-1'); 139.51 (C-8); 137.58 (C-2); 134.49 (C-9); 131.38 (C-4'); 128.92 (C-3'); 121.92 (C-2'); 95.35 (C-7); 72.66 (C-3); 47.86 (NCH₂); 24.76 (CH₂-pyrrol.) ppm. HRMS (ESI): m/z calculated for C₁₆H₁₆O₂N₅ClIS 503.97524, found 503.97476.

6-Chloro-3-(1-cyclopentene-1-yl)-N-(4-(1-pyrrolidinylsulfonyl)phenyl)imidazo[1,2-*b*]pyridazine-8-amine (33a). Prepared from **32** and cyclopent-1-en-1-ylboronic acid according to **GP3**. White solid, yield 57%. MS (ESI): $m/z = 444.3$ [M + H]⁺. ¹H NMR (DMSO-*d*₆): $\delta = 10.25$ (s, 1H, NH); 7.83 (d, 2H, $J = 8.7$ Hz, H-3'); 7.69 (m, 3H, H-2', H-2); 6.85 (t, 1H, $J = 2.2$ Hz, H-2"); 6.83 (s, 1H, H-7); 3.16 (m, 4H, NCH₂); 2.79 (m, 2H, H-5"); 2.57 (m, 2H, H-3"); 1.95 (m, 2H, H-4"); 1.68 (m, 4H, CH₂-pyrrol.) ppm. ¹³C NMR (DMSO-*d*₆): $\delta = 147.42$ (C-6); 142.92 (C-1'); 139.44 (C-8); 133.32 (C-9); 131.13 (C-4'); 130.39 (C-2); 128.90 (C-3'); 127.53 (C-2"); 121.71 (C-2'); 94.84 (C-7); 47.82 (NCH₂); 33.51 and 33.33 (C-3" and C-5"); 24.72

(CH₂-pyrrol.); 22.00 (C-4") ppm. HRMS (ESI): m/z calculated for C₂₁H₂₃O₂N₅ClIS 444.12555, found 444.12518.

6-Chloro-3-(propan-2-yl)-N-(4-(1-pyrrolidinylsulfonyl)phenyl)imidazo[1,2-*b*]pyridazine-8-amine (33d). Compound **32** (500 mg, 1 mmol) and Pd(dppf)Cl₂·DCM (81 mg, 0.1 mmol) in dry THF under an argon atmosphere were treated with 2-propylzinc bromide (0.5 M in THF, 3 mL, 1.5 mmol) at RT for 1 h, quenched with sat. NH₄Cl, diluted with EtOAc, washed with sat. NH₄Cl, and dried over MgSO₄. FC (c-hexane/EtOAc + 10% MeOH) afforded a white solid (120 mg, 29%). MS (ESI): $m/z = 420.2$ [M + H]⁺. ¹H NMR (DMSO-*d*₆): $\delta = 10.20$ (bs, 1H, NH); 7.82 (m, 2H, H-3'); 7.69 (m, 2H, H-2'); 7.50 (d, 1H, $J(2,1'') = 0.7$ Hz, H-2); 6.75 (s, 1H, H-7); 3.16 (m, 4H, NCH₂); 3.33 (m, 1H, H-1"); 1.69 (m, 4H, CH₂-pyrrol.); 1.35 (d, 6H, $J(\text{CH}_3, 1'') = 6.9$ Hz, CH₃) ppm. ¹³C NMR (DMSO-*d*₆): $\delta = 147.04$ (C-6); 143.03 (C-1'); 139.50 (C-8); 135.67 (C-3); 132.03 (C-9); 131.01 (C-4'); 128.89 (C-3'); 127.09 (C-2); 121.66 (C-2'); 94.02 (C-7); 47.81 (NCH₂); 24.72 (CH₂-pyrrol.); 23.68 (C-1"); 20.65 (C-2") ppm. HRMS (ESI): m/z calculated for C₁₉H₂₃O₂N₅ClIS 420.12555, found 420.12517.

6-Chloro-3-methyl-N-(4-(1-pyrrolidinylsulfonyl)phenyl)imidazo[1,2-*b*]pyridazine-8-amine (33e). Compound **32** (600 mg, 1.2 mmol), Pd₂(dba)₃ (109 mg, 0.12 mmol), and XPhos (114 mg, 0.24 mmol) in THF under an argon atmosphere were treated with DABAL-Me₃ (0.25 M in THF, 5.7 mL, 1.43 mmol); the mixture was then heated at 60 °C overnight. Another portion of DABAL-Me₃ (5.7 mL) was added, after which the mixture was again heated at 60 °C for a further 4 h. The mixture was cooled to RT and quenched with sat. NH₄Cl at 0 °C, diluted with EtOAc, and filtered through Celite. FC (c-hex/EtOAc + 10% MeOH, 0–60%) and RP FC (H₂O/ACN + 0.1% of formic acid) afforded **33e** (33 mg, 7%). MS (ESI): $m/z = 392.2$ [M + H]⁺. ¹H NMR (DMSO-*d*₆): $\delta = 10.18$ (bs, 1H, NH); 7.82 (m, 2H, H-3'); 7.68 (m, 2H, H-2'); 7.50 (d, 1H, $J(2, \text{CH}_3) = 1.0$ Hz, H-2); 6.75 (s, 1H, H-7); 3.16 (m, 4H, NCH₂); 2.45 (d, 3H, $J(\text{CH}_3, 2) = 1.0$ Hz, CH₃); 1.68 (m, 4H, CH₂-pyrrol.) ppm. ¹³C NMR (DMSO-*d*₆): $\delta = 147.18$ (C-6); 143.05 (C-1'); 139.37 (C-8); 131.83 (C-9); 130.97 (C-4'); 129.39 (C-2); 128.89 (C-3'); 125.89 (C-3); 121.60 (C-2'); 93.94 (C-7); 47.82 (NCH₂); 24.73 (CH₂-pyrrol.); 8.51 (CH₃) ppm. HRMS (ESI): m/z calculated for C₁₇H₁₉O₂N₅ClIS 392.09425, found 392.09408.

6-Chloro-3-phenyl-N-(4-(1-pyrrolidinylsulfonyl)phenyl)imidazo[1,2-*b*]pyridazin-8-amine (33f). Method A. Prepared from **32** and phenylboronic acid according to **GP3**. White solid, yield 29%. MS (ESI): $m/z = 454.3$ [M + H]⁺. ¹H NMR (DMSO-*d*₆): $\delta = 10.31$ (s, 1H, NH); 8.15 (s, 1H, H-2); 8.09 (m, 2H, H-2"); 7.84 (m, 2H, H-3'); 7.72 (m, 2H, H-2'); 7.54 (t, 2H, $J = 7.8$ Hz, H-3"); 7.41 (m, 1H, H-4"); 6.86 (s, 1H, H-7); 3.17 (m, 4H, NCH₂); 1.69 (m, 4H, CH₂-pyrrol.) ppm. ¹³C NMR (DMSO-*d*₆): $\delta = 147.45$ (C-6); 142.84 (C-1'); 139.67 (C-8); 133.34 (C-9); 131.14 (C-4'); 130.34 (C-2); 128.85 (C-3'); 128.69 (C-3"); 128.06 (C-1"); 127.98 (C-4"); 126.41 (C-2"); 121.77 (C-2'); 94.81 (C-7); 47.76 (NCH₂); 24.66 (CH₂-pyrrol.) ppm. HRMS (ESI): m/z calculated for C₂₂H₂₁O₂N₅ClIS 454.10990, found 454.11032.

Method B. Prepared from **43** and **2** according to **GP1**, yield 80%.

6-Chloro-3-(4-methoxyphenyl)-N-(4-(1-pyrrolidinylsulfonyl)phenyl)imidazo[1,2-*b*]pyridazin-8-amine (33g). Prepared from **32** and 4-methoxyphenylboronic acid according to **GP3**. White solid, yield 30%. MS (ESI): $m/z = 484.2$ [M + H]⁺. ¹H NMR (DMSO-*d*₆): $\delta = 10.28$ (s, 1H, NH); 8.05 (s, 1H, H-2); 8.01 (m, 2H, H-2"); 7.84 (m, 2H, H-3'); 7.71 (m, 2H, H-2'); 7.10 (m, 2H, H-3"); 6.82 (s, 1H, H-7); 3.82 (s, 3H, OCH₃); 3.17 (m, 4H, NCH₂); 1.69 (m, 4H, CH₂-pyrrol.) ppm. ¹³C NMR (DMSO-*d*₆): $\delta = 159.05$ (C-4"); 147.34 (C-6); 142.96 (C-1'); 139.64 (C-8); 132.87 (C-9); 131.11 (C-4'); 129.52 (C-2); 128.89 (C-3'); 128.76 (C-3); 128.00 (C-2"); 121.74 (C-2'); 120.54 (C-1"); 114.20 (C-3"); 94.50 (C-7); 55.23 (OCH₃); 47.82 (NCH₂); 24.72 (CH₂-pyrrol.) ppm. HRMS (ESI): m/z calculated for C₂₃H₂₃O₃N₅ClIS 484.12046, found 484.12032.

6-Chloro-3-(3-methoxyphenyl)-N-(4-(1-pyrrolidinylsulfonyl)phenyl)imidazo[1,2-*b*]pyridazin-8-amine (33h). Prepared from **32** and 3-methoxyphenylboronic acid according to **GP3**. White solid, yield 28%. MS (ESI): $m/z = 484.26$ [M + H]⁺. ¹H NMR (DMSO-

*d*₆): δ = 10.31 (s, 1H, NH); 8.20 (s, 1H, H-2); 7.84 (m, 2H, H-3'); 7.68–7.73 (m, 4H, H-2', 2'', 6''); 7.45 (m, 1H, H-5''); 6.98 (ddd, 1H, J = 8.2, 2.6 and 0.9 Hz, H-4''); 6.86 (s, 1H, H-7); 3.84 (s, 3H, OCH₃); 3.17 (m, 4H, NCH₂); 1.69 (m, 4H, CH₂-pyrrol.) ppm. ¹³C NMR (DMSO-*d*₆): δ = 159.39 (C-3''); 147.48 (C-6); 142.91 (C-1'); 139.73 (C-8); 133.51 (C-9); 131.20 (C-4'); 130.76 (C-2); 129.88 (C-5''); 129.34 (C-1''); 128.92 (C-3'); 128.47 (C-3); 121.84 (C-2'); 118.69 (C-6''); 113.37 (C-4''); 112.05 (C-2''); 94.86 (C-7); 55.19 (OCH₃); 47.83 (NCH₂); 24.74 (CH₂-pyrrol.) ppm. HRMS (ESI): *m/z* calculated for C₂₃H₂₃O₃N₅ClS 484.12046, found 484.12033.

6-Chloro-3-(3,4-dimethoxyphenyl)-N-(4-(1-pyrrolidinylsulfonyl)phenyl)imidazo[1,2-*b*]pyridazin-8-amine (33i). Prepared from **32** and 3,4-dimethoxyphenylboronic acid according to **GP3**. White solid, yield 19%. MS (ESI): *m/z* = 514.0 [M + H]⁺. ¹H NMR (DMSO-*d*₆): δ = 10.29 (s, 1H, NH); 8.13 (s, 1H, H-2); 7.84 (m, 2H, H-3'); 7.73–7.70 (m, 3H, H-2', H-6''); 7.64 (d, 1H, J = 2.0 Hz, H-2''); 7.12 (d, 1H, J = 8.6 Hz, H-5''); 6.83 (s, 1H, H-7); 3.85 (s, 3H, OCH₃); 3.82 (s, 3H, OCH₃); 3.17 (m, 4H, NCH₂); 1.69 (m, 4H, CH₂-pyrrol.) ppm. ¹³C NMR (DMSO-*d*₆): δ = 148.79 and 148.72 (C-3'', C-4''); 147.29 (C-6); 142.95 (C-1'); 139.62 (C-8); 132.94 (C-9); 131.13 (C-4'); 129.81 (C-2); 128.88 (C-3'); 128.77 (C-3); 121.72 (C-2'); 120.70 (C-1''); 119.14 (C-6''); 111.93 (C-2''); 110.44 (C-5''); 94.49 (C-7); 55.63 and 55.57 (OCH₃); 47.81 (NCH₂); 24.72 (CH₂-pyrrol.) ppm. HRMS (ESI): *m/z* calculated for C₂₄H₂₅O₄N₅ClS 514.13103, found 514.13070.

6-Chloro-3-(4-fluorophenyl)-N-(4-(1-pyrrolidinylsulfonyl)phenyl)imidazo[1,2-*b*]pyridazin-8-amine (33j). Prepared from **32** and 4-fluorophenylboronic acid according to **GP3**. White solid, yield 46%. MS (ESI): *m/z* = 472.19 [M + H]⁺. ¹H NMR (DMSO-*d*₆): δ = 10.32 (s, 1H, NH); 8.15–8.12 (m, 3H, H-2, H-2''); 7.83 (m, 2H, H-3'); 7.71 (m, 2H, H-2'); 7.38 (m, 2H, H-3''); 6.85 (s, 1H, H-7); 3.17 (m, 4H, NCH₂); 1.69 (m, 4H, CH₂-pyrrol.) ppm. ¹³C NMR (DMSO-*d*₆): δ = 161.66 (d, J = 245.9 Hz, C-4''); 147.53 (C-6); 142.86 (C-1'); 139.74 (C-8); 133.29 (C-9); 131.23 (C-4'); 130.34 (C-2); 128.90 (C-3'); 128.64 (d, J = 8.2 Hz, C-2''); 127.85 (C-3); 124.69 (d, J = 3.2 Hz, C-1''); 121.84 (C-2'); 115.74 (d, J = 21.7 Hz, C-3''); 94.83 (C-7); 47.82 (NCH₂); 24.72 (CH₂-pyrrol.) ppm. HRMS (ESI): *m/z* calculated for C₂₂H₂₀O₂N₅ClFS 472.10048, found 472.10037.

6-Chloro-3-(3-fluoro-4-methoxyphenyl)-N-(4-(1-pyrrolidinylsulfonyl)phenyl)imidazo[1,2-*b*]pyridazin-8-amine (33k). Prepared from **32** and 3-fluoro-4-methoxyphenylboronic acid according to **GP3**. White solid, yield 52%. MS (ESI): *m/z* = 502.2 [M + H]⁺. ¹H NMR (DMSO-*d*₆): δ = 10.29 (s, 1H, NH); 8.15 (s, 1H, H-2); 7.98 (dd, J = 13.0, 2.1 Hz, H-2''); 7.92 (m, 1H, H-6''); 7.84 (m, 2H, H-3'); 7.71 (m, 2H, H-2'); 7.33 (t, 1H, J = 9.0 Hz, H-5''); 6.84 (s, 1H, H-7); 3.91 (s, 3H, OCH₃); 3.17 (m, 4H, NCH₂); 1.69 (m, 4H, CH₂-pyrrol.) ppm. ¹³C NMR (DMSO-*d*₆): δ = 151.26 (d, J = 243.0 Hz, C-3''); 147.45 (C-6); 146.79 (d, J = 10.7 Hz, C-4''); 142.84 (C-1'); 139.67 (C-8); 133.17 (C-9); 131.21 (C-4'); 130.14 (C-2); 128.86 (C-3'); 127.44 (d, J = 2.1 Hz, C-3); 122.86 (d, J = 3.3 Hz, C-6''); 121.79 (C-2'); 121.00 (d, J = 7.7 Hz, C-1''); 114.12 (d, J = 2.2 Hz, C-5''); 113.81 (d, J = 20.3 Hz, C-2''); 94.69 (C-7); 56.09 (OCH₃); 47.79 (NCH₂); 24.72 (CH₂-pyrrol.) ppm. HRMS (ESI): *m/z* calculated for C₂₃H₂₂O₃N₅ClFS 502.11104, found 502.11063.

6-Chloro-3-(4-(trifluoromethyl)phenyl)-N-(4-(1-pyrrolidinylsulfonyl)phenyl)imidazo[1,2-*b*]pyridazin-8-amine (33l). Prepared from **32** and 4-(trifluoromethyl)phenylboronic acid according to **GP3**. White solid, yield 40%. MS (ESI): *m/z* = 521.95 [M + H]⁺. ¹H NMR (DMSO-*d*₆): δ = 10.35 (s, 1H, NH); 8.34 (m, 2H, H-2''); 8.32 (s, 1H, H-2); 7.89 (m, 2H, H-3''); 7.85 (m, 2H, H-3'); 7.72 (m, 2H, H-2'); 7.10 (s, 1H, H-7); 3.17 (m, 4H, NCH₂); 1.69 (m, 4H, CH₂-pyrrol.) ppm. ¹³C NMR (DMSO-*d*₆): δ = 147.77 (C-6); 142.75 (C-1'); 139.84 (C-8); 134.13 (C-9); 132.15 (C-1''); 131.73 (C-2); 131.39 (C-4'); 128.89 (C-2''); 127.78 (d, J = 31.9 Hz, C-4'); 127.21 (C-3); 126.59 (C-3'); 125.66 (d, J = 3.9 Hz, C-3''); 121.93 (C-2'); 95.34 (C-7); 47.81 (NCH₂); 24.72 (CH₂-pyrrol.) ppm. HRMS (ESI): *m/z* calculated for C₂₃H₂₀O₂N₅ClF₃S 522.09728, found 522.09690.

6-Chloro-3-(4-(trifluoromethoxy)phenyl)-N-(4-(1-pyrrolidinylsulfonyl)phenyl)imidazo[1,2-*b*]pyridazin-8-amine

(33m). Prepared from **32** and 4-(trifluoromethoxy)phenylboronic acid according to **GP3**. White solid, yield 87%. MS (ESI): *m/z* = 538.2 [M + H]⁺. ¹H NMR (DMSO-*d*₆): δ = 10.33 (s, 1H, NH); 8.22 (m, 2H, H-2''); 8.20 (s, 1H, H-2); 7.84 (m, 2H, H-3'); 7.72 (m, 2H, H-2'); 7.54 (m, 2H, H-3''); 6.86 (s, 1H, H-7); 3.17 (m, 4H, NCH₂); 1.69 (m, 4H, CH₂-pyrrol.) ppm. ¹³C NMR (DMSO-*d*₆): δ = 147.64 (C-6); 142.80 (C-1'); 139.80 (C-8); 133.62 (C-9); 131.32 (C-4'); 130.89 (C-2); 128.88 (C-3'); 128.25 (C-2''); 127.49 (C-1''); 127.42 (C-3); 121.89 (C-2'); 121.39 (C-3''); 95.04 (C-7); 47.80 (NCH₂); 24.71 (CH₂-pyrrol.) ppm. HRMS (ESI): *m/z* calculated for C₂₃H₂₀O₃N₅ClF₃S 538.09220, found 538.09181.

6-Chloro-3-(4-cyanophenyl)-N-(4-(1-pyrrolidinylsulfonyl)phenyl)imidazo[1,2-*b*]pyridazin-8-amine (33n). Prepared from **32** and 4-cyanophenylboronic acid according to **GP3**. White solid, yield 46%. MS (ESI): *m/z* = 479.02 [M + H]⁺. ¹H NMR (DMSO-*d*₆): δ = 10.35 (s, 1H, NH); 8.37 (s, 1H, H-2); 8.34 (m, 2H, H-2''); 7.97 (m, 2H, H-3''); 7.83 (m, 2H, H-3'); 7.71 (m, 2H, H-2'); 6.89 (s, 1H, H-7); 3.17 (m, 4H, NCH₂); 1.69 (m, 4H, CH₂-pyrrol.) ppm. ¹³C NMR (DMSO-*d*₆): δ = 147.74 (C-6); 142.62 (C-1'); 139.76 (C-8); 134.36 (C-9); 132.39 (C-3''); 132.56 (C-1''); 132.22 (C-2); 131.35 (C-4'); 128.81 (C-3'); 126.81 (C-3); 126.18 (C-2''); 121.88 (C-2'); 118.76 (CN); 109.66 (C-4''); 95.41 (C-7); 47.73 (NCH₂); 24.64 (CH₂-pyrrol.) ppm. HRMS (ESI): *m/z* calculated for C₂₃H₂₀O₂N₆ClS 479.10515, found 479.10473.

6-Chloro-3-(3-(*N,N*-dimethylcarbamoyl)phenyl)-N-(4-(1-pyrrolidinylsulfonyl)phenyl)imidazo[1,2-*b*]pyridazin-8-amine (33o). Prepared from **32** and 3-(*N,N*-dimethylcarbamoyl)phenylboronic acid according to **GP3**. White solid, yield 28%. MS (ESI): *m/z* = 525.3 [M + H]⁺. ¹H NMR (DMSO-*d*₆): δ = 10.34 (s, 1H, NH); 8.24 (s, 1H, H-2); 8.16 (dt, 1H, J = 7.9, 1.4 Hz, H-6''); 8.13 (m, 1H, H-2''); 7.84 (m, 2H, H-3''); 7.72 (m, 2H, H-2'); 7.60 (t, 1H, J = 7.8 Hz, H-5''); 7.43 (dt, 1H, J = 7.7, 1.4 Hz, H-4''); 6.87 (s, 1H, H-7); 3.17 (m, 4H, NCH₂-pyrrol.); 3.03 and 3.00 (2 × s, 2 × 3H, NCH₃); 1.69 (m, 4H, CH₂-pyrrol.) ppm. ¹³C NMR (DMSO-*d*₆): δ = 169.73 (CO); 147.59 (C-6); 142.86 (C-1'); 139.79 (C-8); 136.91 (C-3'); 133.60 (C-9); 131.25 (C-4'); 130.87 (C-2); 128.92 (C-3''); 128.83 (C-5''); 128.13 (C-1''); 128.06 (C-3); 127.17 (C-6''); 126.47 (C-4''); 124.78 (C-2''); 121.87 (C-2'); 94.98 (C-7); 47.83 (NCH₂-pyrrol.); 37.69 (NCH₃); 34.83 (NCH₃); 24.73 (CH₂-pyrrol.) ppm. HRMS (ESI): *m/z* calculated for C₂₅H₂₆O₃N₆ClS 525.14701, found 525.14670.

6-Chloro-3-(3-(*N,N*-dimethylsulfamoyl)phenyl)-N-(4-(1-pyrrolidinylsulfonyl)phenyl)imidazo[1,2-*b*]pyridazin-8-amine (33p). Prepared from **32** and 3-(*N,N*-dimethylsulfamoyl)phenylboronic acid according to **GP3**. White solid, yield 27%. MS (ESI): *m/z* = 561.2 [M + H]⁺. ¹H NMR (DMSO-*d*₆): δ = 10.38 (s, 1H, NH); 8.55 (t, 1H, J = 1.8 Hz, H-2''); 8.36 (dt, 1H, J = 7.8, 1.5 Hz, H-6''); 8.33 (s, 1H, H-2); 7.85 (m, 2H, H-3'); 7.81 (t, 1H, J = 7.8 Hz, H-5''); 7.76 (dt, 1H, J = 7.9, 1.5 Hz, H-4''); 7.72 (m, 2H, H-2'); 6.90 (s, 1H, H-7); 3.17 (m, 4H, NCH₂); 2.70 (s, 6H, NCH₃); 1.69 (m, 4H, CH₂-pyrrol.) ppm. ¹³C NMR (DMSO-*d*₆): δ = 147.76 (C-6); 142.80 (C-1'); 139.90 (C-8); 135.35 (C-3''); 133.97 (C-9); 131.38 (C-2); 131.36 (C-4); 130.69 (C-6''); 129.94 (C-5''); 129.27 (C-1''); 128.95 (C-3'); 127.03 (C-3); 126.63 (C-4''); 124.71 (C-2''); 121.95 (C-2'); 95.29 (C-7); 47.85 (NCH₂-pyrrol.); 37.71 (NCH₃); 24.75 (CH₂-pyrrol.) ppm. HRMS (ESI): *m/z* calculated for C₂₄H₂₆O₄N₆ClS₂ 561.11400, found 561.11371.

6-Chloro-3-(thiophen-3-yl)-N-(4-(1-pyrrolidinylsulfonyl)phenyl)imidazo[1,2-*b*]pyridazin-8-amine (33q). Prepared from **32** and 3-thienylboronic acid according to **GP3**. White solid, yield 36%. MS (ESI): *m/z* = 460.3 [M + H]⁺. ¹H NMR (DMSO-*d*₆): δ = 10.30 (s, 1H, NH); 8.32 (dd, 1H, J = 2.9, 1.3 Hz, H-4''); 8.18 (s, 1H, H-2); 7.84 (m, 2H, H-3''); 7.81 (m, 1H, H-2''); 7.74 (m, 1H, H-5''); 7.71 (m, 2H, H-2'); 6.86 (s, 1H, H-7); 3.17 (m, 4H, NCH₂); 1.69 (m, 4H, CH₂-pyrrol.) ppm. ¹³C NMR (DMSO-*d*₆): δ = 147.59 (C-6); 142.86 (C-1'); 139.61 (C-8); 132.73 (C-9); 131.20 (C-4'); 129.89 (C-2); 128.86 (C-3'); 128.15 (C-3); 126.74 (C-5''); 126.08 (C-2''); 125.63 (C-3''); 121.78 (C-2'); 121.42 (C-4''); 94.72 (C-7); 47.78 (NCH₂); 24.69 (CH₂-pyrrol.) ppm. HRMS (ESI): *m/z* calculated for C₂₀H₁₉O₂N₅ClS₂ 460.06632, found 460.06611.

6-Chloro-3-(furan-3-yl)-N-(4-(1-pyrrolidinylsulfonyl)phenyl)imidazo[1,2-b]pyridazin-8-amine (33r). Prepared from **32** and 3-furanylboronic acid according to **GP3**. White solid, yield 27%. MS (ESI): $m/z = 444.3$ $[M + H]^+$. 1H NMR (DMSO- d_6): $\delta = 10.30$ (s, 1H, NH); 8.40 (dd, 1H, $J = 1.6, 0.8$ Hz, H-2''); 8.07 (s, 1H, H-2); 7.86 (m, 1H, H-5''); 7.83 (m, 2H, H-3''); 7.71 (m, 2H, H-2''); 7.16 (dd, 1H, $J = 1.8, 0.8$ Hz, H-4''); 6.84 (s, 1H, H-7); 3.17 (m, 4H, NCH₂-pyrrol.); 1.69 (m, 4H, CH₂-pyrrol.) ppm. ^{13}C NMR (DMSO- d_6): $\delta = 147.68$ (C-6); 143.84 (C-5''); 142.87 (C-1'); 139.57 (C-8); 139.15 (C-2''); 132.87 (C-9); 131.22 (C-4'); 129.30 (C-2); 128.88 (C-3'); 122.79 (C-3); 121.78 (C-2'); 113.56 (C-3''); 108.56 (C-4''); 94.59 (C-7); 47.80 (NCH₂); 24.71 (CH₂-pyrrol.) ppm. HRMS (ESI): m/z calculated for C₂₀H₁₉O₃N₃ClS 444.08916, found 444.08910.

N⁶-((1*r*,4*r*)-4-Aminocyclohexyl)-3-(1-cyclopentan-1-yl)-N⁸-(4-(1-pyrrolidinylsulfonyl)phenyl)imidazo[1,2-b]pyridazine-6,8-diamine (34a). Prepared from **33a** according to **GP2**. White solid, yield 46%. MS (ESI): $m/z = 522.5$ $[M + H]^+$. 1H NMR (DMSO- d_6): $\delta = 9.44$ (bs, 1H, NH); 7.98 (d, 2H, $J = 5.0$ Hz, NH₂); 7.76 (m, 2H, H-3'); 7.59 (m, 2H, H-2'); 7.39 (s, 1H, H-2); 6.86 (m, 1H, c-pent-2); 6.67 (d, 1H, $J(NH,1'') = 6.8$ Hz, NH); 6.49 (s, 1H, H-7); 3.53 (m, 1H, H-1''); 3.14 (m, 4H, NCH₂); 3.07 (m, 1H, H-4''); 2.75 (m, 2H, c-pent-5); 2.56 (m, 2H, c-pent-3); 2.18 (m, 2H, H-2'a); 1.91–2.03 (m, 4H, H-3'a, c-pent-4); 1.67 (m, 4H, CH₂-pyrrol.); 1.46 (m, 2H, H-3'b); 1.26 (m, 2H, H-2'b) ppm. ^{13}C NMR (DMSO- d_6): $\delta = 154.34$ (C-6); 144.62 (C-1'); 136.80 (C-8); 132.50 (C-9); 130.11 (c-pent-1); 129.06 (C-4'); 128.81 (C-3'); 127.50 (C-2); 125.71 (C-3); 125.02 (c-pent-2); 119.96 (C-2'); 88.37 (C-7); 49.21 (C-4''); 48.76 (C-1''); 47.81 (NCH₂); 33.46 (c-pent-5); 33.31 (c-pent-3); 29.64 (C-2''); 29.18 (C-3''); 24.72 (CH₂-pyrrol.); 22.15 (c-pent-4) ppm. HRMS (ESI): m/z calculated for C₂₇H₃₆O₂N₇S 522.26457, found 522.26499.

N⁶-((1*r*,4*r*)-4-Aminocyclohexyl)-3-(cyclopentan-1-yl)-N⁸-(4-(1-pyrrolidinylsulfonyl)phenyl)imidazo[1,2-b]pyridazine-6,8-diamine (34b). Compound **34a** (60 mg) in MeOH (5 mL) was treated with Pd/C (10% loading, 15 mg); the mixture was then stirred under a hydrogen atmosphere (10 bar) for 2 days. The mixture was filtered through Celite and then evaporated and freeze-dried from dioxane to give **34b** as an off-white solid (45 mg, 75%). MS (ESI): $m/z = 524.5$ $[M + H]^+$. 1H NMR (DMSO- d_6): $\delta = 9.55$ (bs, 1H, NH); 8.01 (d, 2H, $J = 4.8$ Hz, NH₂); 7.78 (m, 2H, H-3'); 7.55 (m, 2H, H-2'); 7.48 (s, 1H, H-2); 6.82 (bs, 1H, NH); 6.58 (s, 1H, H-7); 3.53 (m, 1H, H-1''); 3.35 (m, 1H, c-pent-1); 3.15 (m, 4H, NCH₂); 3.06 (m, 1H, H-4''); 1.98–2.16 (m, 6H, H-2'a, c-pent-2, c-pent-5); 1.75–1.82 (m, 6H, H-3'a, c-pent-4, c-pent-3); 1.67 (m, 4H, CH₂-pyrrol.); 1.44 (m, 2H, H-3'b); 1.25 (m, 2H, H-2'b) ppm. ^{13}C NMR (DMSO- d_6): $\delta = 154.57$ (C-6); 144.19 (C-1'); 135.77 (C-8); 132.50 (C-9); 132.88 (C-3); 130.07 (C-9); 129.58 (C-4'); 128.98 (C-3'); 121.50 (C-2); 120.04 (C-2'); 90.05 (C-7); 49.05 (C-4''); 48.70 (C-1''); 47.82 (NCH₂); 34.60 (c-pent-1); 30.25 (c-pent-2, c-pent-5); 29.54 (C-2''); 29.08 (C-3''); 25.11 (c-pent-5, c-pent-4); 24.73 (CH₂-pyrrol.) ppm. HRMS (ESI): m/z calculated for C₂₇H₃₈O₂N₇S 524.28022, found 524.28043.

N⁶-((1*r*,4*r*)-4-Aminocyclohexyl)-3-(2-methylpropan-1-yl)-N⁸-(4-(1-pyrrolidinylsulfonyl)phenyl)imidazo[1,2-b]pyridazine-6,8-diamine (34c). Compound **32** (500 mg, 1 mmol) and Pd(dppf)Cl₂·DCM (81 mg, 0.1 mmol) in freshly distilled THF (5 mL) were treated with isobutylzinc bromide (0.5 M solution in THF, 4 mL, 2 mmol) under an argon atmosphere; the mixture was then heated at 45 °C overnight. The mixture was diluted with EtOAc, washed with sat. NH₄Cl, and dried over MgSO₄. FC (c-hex/EtOAc + 10% MeOH) afforded an inseparable mixture of **33c** and a dialkylated side product (310 mg, ratio approximately 3:1 of **33c** to side product). MS (ESI): $m/z = 434.1$ $[M + H]^+$. The mixture was treated with *trans*-1,4-diaminocyclohexane according to **GP2** and freeze-dried from dioxane. White foam, 85 mg of **34c**. MS (ESI): $m/z = 512.5$ $[M + H]^+$. 1H NMR (DMSO- d_6): $\delta = 8.42$ (s, HCOOH); 7.75 (d, 2H, $J = 8.8$ Hz, H-3'); 7.58 (d, 2H, $J = 8.8$ Hz, H-2'); 7.14 (s, 1H, H-2); 6.44 (d, 1H, $J = 6.7$ Hz, NH); 6.37 (s, 1H, H-7); 3.50 (m, 1H, H-1''); 3.14 (m, 4H, NCH₂); 3.01 (m, 1H, H-4''); 2.67 (d, 2H, $J = 6.7$ Hz, CH₂-isobutyl); 2.14 (m, 2H, H-2'a); 2.07 (m, 1H, CH-isobutyl); 1.98 (m, 2H, H-3'a); 1.67 (m, 4H, CH₂-pyrrol.); 1.41 (m, 2H, H-3'b); 1.22 (m, 2H,

H-2''b); 0.92 (d, 6H, $J = 6.7$ Hz, CH₃-isobutyl) ppm. ^{13}C NMR (DMSO- d_6): $\delta = 165.46$ (HCOOH); 153.81 (C-6); 144.83 (C-1'); 136.95 (C-8); 131.16 (C-9); 128.82 (C-4'); 128.78 (C-3'); 127.69 (C-3); 126.95 (C-2); 119.83 (C-2'); 87.54 (C-7); 49.06 (C-1''); 48.83 (C-4''); 47.79 (NCH₂); 32.23 (CH₂-isobutyl); 29.81 (C-2''); 29.61 (C-3''); 26.74 (CH-isobutyl); 24.70 (CH₂-pyrrol.); 22.38 (CH₃-isobutyl) ppm. HRMS (ESI): m/z calculated for C₂₆H₃₈O₂N₇S 512.28022, found 512.27985.

N⁶-((1*r*,4*r*)-4-Aminocyclohexyl)-3-(propan-2-yl)-N⁸-(4-(1-pyrrolidinylsulfonyl)phenyl)imidazo[1,2-b]pyridazine-6,8-diamine (34d). Prepared from **33d** according to **GP2**, isolated as a salt with formic acid, and freeze-dried from water. White foam, yield 46%. MS (ESI): $m/z = 498.46$ $[M + H]^+$. 1H NMR (DMSO- d_6): $\delta = 8.47$ (bs, 1H, FA); 7.75 (m, 2H, H-3'); 7.88 (m, 2H, H-2'); 7.11 (d, 1H, $J(2,1'') = 0.7$ Hz, H-2); 6.42 (d, 1H, $J(NH,1'') = 7.0$ Hz, NH); 6.39 (s, 1H, H-7); 3.52 (dt, $J = 7.5, 3.9$ Hz, H-1''); 3.21 (m, 1H, CH-*ipr*.); 3.14 (m, 4H, NCH₂); 2.89 (tt, 1H, $J = 11.1, 4.0$ Hz, H-4''); 2.12 (m, 2H, H-2'a); 1.94 (m, 2H, H-3'a); 1.67 (m, 4H, CH₂-pyrrol.); 1.34 (d, 6H, $J(CH_3,CH) = 6.9$ Hz, CH₃-*ipr*.); 1.17–1.31 (m, 4H, H-3''b, H-2''b) ppm. ^{13}C NMR (DMSO- d_6): $\delta = 165.98$ (FA); 153.80 (C-6); 144.85 (C-1'); 136.92 (C-8); 134.25 (C-3); 131.49 (C-9); 128.78 (C-3'); 128.12 (C-4'); 124.23 (C-2); 119.80 (C-2'); 87.69 (C-7); 49.14 (C-4''); 48.96 (C-1''); 47.80 (NCH₂); 30.83 and 30.10 (C-2'', C-3''); 24.72 (CH₂-pyrrol.); 24.12 (CH-*ipr*.); 20.53 (CH₃) ppm. HRMS (ESI): m/z calculated for C₂₅H₃₆O₂N₇S 498.26457, found 498.26412.

N⁶-((1*r*,4*r*)-4-Aminocyclohexyl)-3-methyl-N⁸-(4-(1-pyrrolidinylsulfonyl)phenyl)imidazo[1,2-b]pyridazine-6,8-diamine (34e). Prepared from **33e** according to **GP2**, isolated as a salt with formic acid, and freeze-dried from water. Off-white foam, yield 87%. MS (ESI): $m/z = 470.44$ $[M + H]^+$. 1H NMR (DMSO- d_6): $\delta = 8.43$ (bs, 1H, NH); 7.75 (m, 2H, H-3'); 7.58 (m, 2H, H-2'); 7.15 (s, 1H, H-2); 6.43 (d, 1H, $J(NH,1'') = 7.1$ Hz, NH); 6.39 (s, 1H, H-7); 3.55 (m, 1H, H-1''); 3.15 (m, 4H, NCH₂); 2.97 (m, 1H, H-4''); 2.35 (s, 3H, CH₃); 2.13 (m, 2H, H-2'a); 1.99 (m, 2H, H-3'a); 1.67 (m, 4H, CH₂-pyrrol.); 1.41 (m, 2H, H-3'b); 1.23 (m, 2H, H-2'b) ppm. ^{13}C NMR (DMSO- d_6): $\delta = 154.10$ (C-6); 144.87 (C-1'); 136.84 (C-8); 131.21 (C-9); 128.79 (C-3'); 128.76 (C-4'); 126.54 (C-2); 124.38 (C-3); 119.74 (C-2'); 87.60 (C-7); 48.71 and 48.68 (C-4'', C-1''); 47.81 (NCH₂); 30.02 (C-2''); 29.74 (C-3''); 24.72 (CH₂-pyrrol.); 8.57 (CH₃) ppm. HRMS (ESI): m/z calculated for C₂₃H₃₂O₂N₇S 470.23327, found 470.23288.

N⁶-((1*r*,4*r*)-4-Aminocyclohexyl)-3-phenyl-N⁸-(4-(1-pyrrolidinylsulfonyl)phenyl)imidazo[1,2-b]pyridazine-6,8-diamine (34f). Prepared from **33f** according to **GP2** and freeze-dried from dioxane. White foam, yield 52%. MS (ESI): $m/z = 532.5$ $[M + H]^+$. 1H NMR (DMSO- d_6): $\delta = 9.50$ (s, 1H, NH); 8.21 (m, 2H, Ph-2); 7.90 (s, 1H, H-2); 7.88 (bd, 2H, $J = 4.5$ Hz, NH₂); 7.78 (m, 2H, H-3'); 7.61 (m, 2H, H-2'); 7.45 (dd, 2H, $J = 8.4, 7.1$ Hz, Ph-3); 7.35 (1H, Ph-4); 6.72 (bs, 1H, NH); 6.51 (s, 1H, H-7); 3.56 (m, 1H, H-1''); 3.15 (m, 4H, NCH₂); 3.08 (m, 1H, H-4''); 2.19 (m, 2H, H-2'a); 2.02 (m, 2H, H-3'a); 1.68 (m, 4H, CH₂-pyrrol.); 1.48 (m, 2H, H-3'b); 1.28 (m, 2H, H-2'b) ppm. ^{13}C NMR (DMSO- d_6): $\delta = 154.23$ (C-6); 144.54 (C-1'); 137.05 (C-8); 132.51 (C-9); 129.48 (Ph-1); 129.22 (C-4'); 128.83 (C-3'); 128.37 (Ph-3); 127.54 (C-3); 127.32 (Ph-4); 127.05 (C-2); 125.86 (Ph-2); 120.12 (C-2'); 88.45 (C-7); 49.40 (C-4''); 48.77 (C-1''); 47.81 (NCH₂); 29.63 (C-2''); 29.21 (C-3''); 24.72 (CH₂-pyrrol.) ppm. HRMS (ESI): m/z calculated for C₂₈H₃₄O₂N₇S 532.24892, found 532.24922.

N⁶-((1*r*,4*r*)-4-Aminocyclohexyl)-3-(4-methoxyphenyl)-N⁸-(4-(1-pyrrolidinylsulfonyl)phenyl)imidazo[1,2-b]pyridazine-6,8-diamine (34g). Prepared from **33g** according to **GP2**. Off-white solid, yield 62%. MS (ESI): $m/z = 562.4$ $[M + H]^+$. 1H NMR (DMSO- d_6): $\delta = 9.45$ (bs, 1H, NH); 8.39 (bs, 1H, FA); 8.14 (m, 2H, H-2''); 7.78–7.75 (m, 3H, H-2); 7.61 (m, 2H, H-3''); 7.02 (m, 2H, H-3''); 6.63 (bd, 1H, $J = 6.5$ Hz, NH); 6.45 (s, 1H, H-7); 3.832 (s, 3H, OCH₃); 3.55 (m, 1H, c-hex-1); 3.15 (m, 4H, NCH₂); 3.03 (m, 1H, c-hex-4); 2.17 (m, 2H, c-hex-2a); 2.02 (m, 2H, c-hex-3a); 1.68 (m, 4H, CH₂); 1.49 (m, 2H, c-hex-3b); 1.26 (m, 2H, c-hex-2b) ppm. ^{13}C NMR (DMSO- d_6): $\delta = 158.23$ (C-4''); 154.03 (C-6); 144.70 (C-1''); 137.12 (-8); 132.25 (C-9); 129.02 (C-4'); 128.77 (C-3''); 127.47 (C-

3); 127.22 (C-2''); 126.83 (C-2); 122.25 (C-1''); 119.98 (C-2'); 113.79 (C-3''); 87.82 (C-7); 55.16 (OCH₃); 49.46 (c-hex-4); 48.65 (c-hex-1); 47.79 (NCH₂); 29.81 and 29.64 (c-hex-2, 3); 24.70 (CH₂) ppm. HRMS (ESI): *m/z* calculated for C₂₉H₃₆O₃N₇S 562.25949, found 562.25957.

N⁶-((1*r*,4*r*)-4-Aminocyclohexyl)-3-(3-methoxyphenyl)-N⁸-(4-(1-pyrrolidinylsulfonyl)phenyl)imidazo[1,2-*b*]pyridazine-6,8-diamine (34h). Prepared from 33h according to GP2. Off-white solid, yield 58%. MS (ESI): *m/z* = 562.5 [M + H]⁺. ¹H NMR (DMSO-*d*₆): δ = 8.41 (bs, 1H, FA); 7.90 (dd, 1H, *J* = 2.6, 1.6 Hz, H-2''); 7.88 (s, 1H, H-2); 7.77 (m, 2H, H-3'); 7.73 (dt, 1H, *J* = 8.0, 1.1 Hz, H-6''); 7.62 (m, 2H, H-2'); 7.35 (t, 1H, *J* = 8.0 Hz, H-5''); 6.89 (ddd, 1H, *J* = 8.3, 2.6, 0.9 Hz, H-4''); 6.63 (d, 1H, *J* = 6.7 Hz, NH); 6.49 (s, 1H, H-7); 3.85 (s, 3H, OCH₃); 3.57 (m, 1H, c-hex-1); 3.15 (m, 4H, NCH₂-pyrrol.); 3.01 (m, 1H, c-hex-4); 2.18 (m, 2H, c-hex-2a); 2.00 (m, 2H, c-hex-3a); 1.69 (m, 4H, CH₂-pyrrol.); 1.43 (m, 4H, c-hex-3b); 1.27 (m, 4H, c-hex-2b) ppm. ¹³C NMR (DMSO-*d*₆): δ = 165.28 (FA); 159.36 (C-3''); 154.19 (C-6); 144.63 (C-1''); 137.13 (C-8); 132.91 (C-9); 130.88 (C-1''); 129.38 (C-5''); 129.12 (C-4''); 128.78 (C-3''); 128.23 (C-2); 127.34 (C-3); 120.07 (C-2''); 118.06 (C-6''); 112.56 (C-4''); 111.16 (C-2''); 88.17 (C-7); 55.22 (OCH₃); 49.19 (c-hex-1); 48.67 (c-hex-4); 47.79 (NCH₂-pyrrol.); 29.91 and 29.73 (c-hex-2, 3); 24.71 (CH₂-pyrrol.) ppm. HRMS (ESI): *m/z* calculated for C₂₉H₃₆O₃N₇S 562.25949, found 562.25907.

N⁶-((1*r*,4*r*)-4-Aminocyclohexyl)-3-(3,4-dimethoxyphenyl)-N⁸-(4-(1-pyrrolidinylsulfonyl)phenyl)imidazo[1,2-*b*]pyridazine-6,8-diamine (34i). Prepared from 33i according to GP2. Off-white solid, yield 35%. MS (ESI): *m/z* = 592.50 [M + H]⁺. ¹H NMR (DMSO-*d*₆): δ = 9.44 (bs, 1H, NH); 8.37 (bs, 2H, NH₂); 7.82 (d, 1H, *J* = 2.1 Hz, H-2''); 7.79–7.75 (m, 3H, H-2, H-3'); 7.70 (dd, 1H, *J* = 8.4, 2.0 Hz, H-6''); 7.62 (m, 2H, H-2'); 7.03 (d, 1H, *J* = 8.6 Hz, H-5''); 6.57 (d, 1H, *J* = 7.1 Hz, NH); 6.46 (s, 1H, H-7); 3.87 and 3.81 (s, 3H, OCH₃); 3.61 (m, 1H, c-hex-1); 3.15 (m, 4H, NCH₂); 3.02 (m, 1H, c-hex-4); 2.15 (m, 2H, c-hex-2a); 1.99 (m, 2H, c-hex-3a); 1.68 (m, 4H, CH₂-pyrrol.); 1.41 (m, 2H, c-hex-3b); 1.26 (m, 2H, c-hex-2b) ppm. ¹³C NMR (DMSO-*d*₆): δ = 154.15 (C-6); 148.56 and 148.03 (C-3'', C-4''); 144.69 (C-1''); 137.07 (C-8); 132.42 (C-9); 129.03 (C-4''); 128.78 (C-3''); 127.71 (C-3); 127.28 (C-2); 122.50 (C-1''); 119.98 (C-2''); 118.58 (C-6''); 111.81 (C-5''); 109.98 (C-2''); 87.97 (C-7); 55.75 and 55.56 (2 × OCH₃); 48.77 and 48.61 (c-hex-1 and 4); 47.79 (NCH₂); 29.95 and 29.55 (c-hex-2 and 3); 24.70 (CH₂-pyrrol.) ppm. HRMS (ESI): *m/z* calculated for C₃₀H₃₈O₄N₇S 592.27005, found 592.26955.

N⁶-((1*r*,4*r*)-4-Aminocyclohexyl)-3-(4-fluorophenyl)-N⁸-(4-(1-pyrrolidinylsulfonyl)phenyl)imidazo[1,2-*b*]pyridazine-6,8-diamine (34j). Prepared from 33j according to GP2. Off-white solid, yield 69%. MS (ESI): *m/z* = 550.37 [M + H]⁺. ¹H NMR (DMSO-*d*₆): δ = 8.42 (bs, 1H, NH); 8.26 (dd, 2H, *J* = 8.9, 5.6 Hz, H-2''); 7.84 (s, 1H, H-2); 7.77 (m, 2H, H-3'); 7.62 (m, 2H, H-2''); 7.29 (t, 2H, *J* = 8.9 Hz, H-3''); 6.68 (d, 1H, *J* = 6.7 Hz, NH); 6.48 (s, 1H, H-7); 3.54 (m, 1H, c-hex-1); 3.15 (m, 4H, NCH₂); 3.02 (m, 1H, c-hex-4); 2.15 (m, 2H, c-hex-2a); 2.01 (m, 2H, c-hex-3a); 1.68 (m, 4H, CH₂); 1.48 (m, 2H, c-hex-3b); 1.26 (m, 2H, c-hex-2b) ppm. ¹³C NMR (DMSO-*d*₆): δ = 160.97 (d, *J* = 244.3 Hz, C-4''); 154.17 (C-6); 144.61 (C-1''); 137.21 (C-8); 132.63 (C-9); 129.15 (C-4''); 128.77 (C-3''); 127.81 (d, *J* = 7.8 Hz, C-2''); 127.72 (C-2); 126.60 (C-3); 126.24 (d, *J* = 3.2 Hz, C-1''); 120.10 (C-2''); 115.21 (d, *J* = 21.2 Hz, C-3''); 88.07 (C-7); 49.51 (c-hex-1); 48.66 (c-hex-4); 47.79 (NCH₂); 29.89 (c-hex-2, 3); 24.70 (CH₂) ppm. HRMS (ESI): *m/z* calculated for C₂₈H₃₃O₂N₇FS 550.23950, found 550.23942.

N⁶-((1*r*,4*r*)-4-Aminocyclohexyl)-3-(3-fluoro-4-hydroxyphenyl)-N⁸-(4-(1-pyrrolidinylsulfonyl)phenyl)imidazo[1,2-*b*]pyridazine-6,8-diamine (34k). Prepared from 33k according to GP2. Heating of the reaction mixture at high temperatures in basic media led to the cleavage of a methoxy group and hydroxy derivative 34k, which was isolated as a major product. Off-white solid, yield 38%. MS (ESI): *m/z* = 566.5 [M + H]⁺. ¹H NMR (DMSO-*d*₆): δ = 8.42 (bs, 1H, FA); 8.13 (dd, 1H, *J* = 13.6, 2.1 Hz, H-2''); 7.78–7.72 (m, 4H, H-2, H-3', H-6''); 7.61 (m, 2H, H-2'); 7.05 (m, 1H, H-5''); 6.64 (d, 1H, *J* = 6.4 Hz, NH); 6.45 (s, 1H, H-7); 3.52 (m, 1H, c-hex-1); 3.15 (m, 4H, NCH₂-pyrrol.); 3.03 (m, 1H, c-hex-4); 2.21 (m, 2H, c-hex-2a); 2.02

(m, 2H, c-hex-3a); 1.68 (m, 4H, CH₂-pyrrol.); 1.46 (m, 2H, c-hex-3b); 1.28 (m, 2H, c-hex-2b) ppm. ¹³C NMR (DMSO-*d*₆): δ = 154.10 (C-6); 150.80 (d, *J* = 239.3 Hz, C-3''); 144.66 (C-1''); 144.32 (d, *J* = 12.0 Hz, C-4''); 137.12 (C-8); 132.31 (C-9); 129.06 (C-4''); 128.77 (C-3''); 127.00 (C-2); 126.76 (d, *J* = 2.0 Hz, C-3); 122.18 (d, *J* = 2.9 Hz, H-6''); 120.93 (d, *J* = 7.4 Hz, C-1''); 120.02 (C-2''); 117.84 (d, *J* = 3.4 Hz, C-5''); 113.41 (d, *J* = 21.5 Hz, C-2''); 87.84 (C-7); 49.54 (c-hex-1); 48.74 (c-hex-4); 47.79 (NCH₂-pyrrol.); 29.82 (c-hex-2); 29.65 (c-hex-3); 24.70 (CH₂-pyrrol.) ppm. HRMS (ESI): *m/z* calculated for C₂₈H₃₃O₃N₇FS 566.23441, found 566.23436.

N⁶-((1*r*,4*r*)-4-Aminocyclohexyl)-3-(4-(trifluoromethyl)phenyl)-N⁸-(4-(1-pyrrolidinylsulfonyl)phenyl)imidazo[1,2-*b*]pyridazine-6,8-diamine (34l). Prepared from 33l according to GP2. Off-white solid, yield 71%. MS (ESI): *m/z* = 600.37 [M + H]⁺. ¹H NMR (DMSO-*d*₆): δ = 8.50 (d, 2H, *J* = 8.2 Hz, H-2''); 8.47 (s, 1H, FA); 8.05 (s, 1H, H-2); 7.78 (m, 4H, H-3', 3''); 7.62 (m, 2H, H-2'); 6.77 (d, 1H, *J* = 6.8 Hz, NH); 6.52 (s, 1H, H-7); 3.58 (m, 1H, c-hex-1); 3.15 (m, 4H, NCH₂); 2.97 (m, 1H, c-hex-4); 2.17 (m, 2H, c-hex-2a); 2.01 (m, 2H, c-hex-3a); 1.68 (m, 4H, CH₂); 1.50 (m, 2H, c-hex-3b); 1.25 (m, 2H, c-hex-2b) ppm. ¹³C NMR (DMSO-*d*₆): δ = 165.71 (FA); 154.41 (C-6); 144.54 (C-1''); 137.29 (C-8); 133.73 (C-1''); 133.55 (C-9); 129.43 (C-2); 129.28 (C-4''); 128.84 (C-3''); 126.64 (d, *J* = 32.0 Hz, C-4''); 125.96 (C-3); 125.66 (C-2''); 125.25 (d, *J* = 4.4 Hz, C-3''); 120.27 (C-2''); 88.48 (C-7); 49.61 (c-hex-1); 48.77 (c-hex-4); 47.83 (NCH₂); 30.19 and 29.95 (c-hex-2 and 3); 24.74 (CH₂) ppm. HRMS (ESI): *m/z* calculated for C₂₉H₃₃O₂N₇F₃S 600.23631, found 600.23582.

N⁶-((1*r*,4*r*)-4-Aminocyclohexyl)-3-(4-(trifluoromethoxy)phenyl)-N⁸-(4-(1-pyrrolidinylsulfonyl)phenyl)imidazo[1,2-*b*]pyridazine-6,8-diamine (34m). Prepared from 33m according to GP2. Off-white solid, yield 61%. MS (ESI): *m/z* = 616.4 [M + H]⁺. ¹H NMR (DMSO-*d*₆): δ = 8.48 (bs, 1H, FA); 8.37 (d, 2H, *J* = 9.0 Hz, H-2''); 7.92 (s, 1H, H-2); 7.78 (m, 2H, H-3'); 7.62 (m, 2H, H-2'); 7.44 (m, 2H, H-3''); 6.68 (d, 1H, *J* = 6.7 Hz, NH); 6.50 (s, 1H, H-7); 3.56 (m, 1H, c-hex-1); 3.15 (m, 4H, NCH₂-pyrrol.); 2.90 (m, 1H, c-hex-4); 2.15 (m, 2H, c-hex-2a); 1.97 (m, 2H, c-hex-3a); 1.68 (m, 4H, CH₂-pyrrol.); 1.43 (m, 2H, c-hex-3b); 1.25 (m, 2H, c-hex-2b) ppm. ¹³C NMR (DMSO-*d*₆): δ = 154.31 (C-6); 146.79 (d, *J* = 2.0 Hz, C-4''); 144.57 (C-1''); 137.20 (C-8); 133.01 (C-9); 129.21 (C-4''); 129.11 (C-3); 128.77 (C-3''); 128.40 (C-2); 127.25 (C-2''); 126.11 (C-1''); 120.98 (C-3''); 120.16 (C-2''); 88.28 (C-7); 49.64 (c-hex-1); 48.96 (c-hex-4); 47.79 (NCH₂-pyrrol.); 30.95 (c-hex-3); 30.08 (c-hex-2); 24.70 (CH₂-pyrrol.) ppm. HRMS (ESI): *m/z* calculated for C₂₉H₃₃O₃N₇F₃S 616.23122, found 616.23077.

N⁶-((1*r*,4*r*)-4-Aminocyclohexyl)-3-(4-cyanophenyl)-N⁸-(4-(1-pyrrolidinylsulfonyl)phenyl)imidazo[1,2-*b*]pyridazine-6,8-diamine (34n). Prepared from 33n according to GP2. Off-white solid, yield 28%. MS (ESI): *m/z* = 557.49 [M + H]⁺. ¹H NMR (DMSO-*d*₆): δ = 8.48 (d, 2H, *J* = 8.7 Hz, H-2''); 8.44 (s, 1H, FA); 8.09 (s, 1H, H-2); 7.88 (m, 2H, H-3''); 7.78 (m, 2H, H-3'); 7.62 (m, 2H, H-2'); 6.78 (d, 1H, *J* = 6.7 Hz, NH); 6.52 (s, 1H, H-7); 3.57 (m, 1H, c-hex-1); 3.15 (m, 4H, NCH₂); 3.02 (m, 1H, c-hex-4); 2.15 (m, 2H, c-hex-2a); 2.02 (m, 2H, c-hex-3a); 1.68 (m, 4H, CH₂); 1.52 (m, 2H, c-hex-3b); 1.27 (m, 2H, c-hex-2b) ppm. ¹³C NMR (DMSO-*d*₆): δ = 165.41 (FA); 154.39 (C-6); 144.44 (C-1''); 137.30 (C-8); 134.18 (C-1''); 133.77 (C-9); 132.27 (C-3''); 130.00 (C-2); 129.38 (C-4''); 128.78 (C-3''); 125.75 (C-3); 125.62 (C-2''); 120.30 (C-2''); 119.02 (CN); 108.50 (C-4''); 88.56 (C-7); 49.61 (c-hex-4); 48.66 (c-hex-1); 47.79 (NCH₂); 29.84 and 29.79 (c-hex-2 and 3); 24.71 (CH₂) ppm. HRMS (ESI): *m/z* calculated for C₂₉H₃₃O₂N₈S 557.24417, found 557.24377. Purity was 93.7% due to complications with purification.

N⁶-((1*r*,4*r*)-4-Aminocyclohexyl)-3-(3-(*N,N*-dimethylcarbamoyl)phenyl)-N⁸-(4-(1-pyrrolidinylsulfonyl)phenyl)imidazo[1,2-*b*]pyridazine-6,8-diamine (34o). Prepared from 33o according to GP2. Off-white solid, yield 54%. MS (ESI): *m/z* = 603.5 [M + H]⁺. ¹H NMR (DMSO-*d*₆): δ = 8.43 (s, 1H, FA); 8.26 (m, 1H, H-2''); 8.24 (m, 1H, H-6''); 7.94 (s, 1H, H-2); 7.78 (m, 2H, H-3'); 7.62 (m, 2H, H-2'); 7.50 (td, 1H, *J* = 7.6, 0.9 Hz, H-5''); 7.32 (dt, 1H, *J* = 7.6, 1.4 Hz, H-4''); 6.64 (d, 1H, *J* = 6.5 Hz, NH); 6.50 (s, 1H, H-7); 3.48 (m, 1H, c-hex-1); 3.15 (m, 4H, NCH₂-pyrrol.); 3.03 (s, 3H, NCH₃); 2.97–2.92 (m, 4H, NCH₃, c-hex-4); 2.18 (m, 2H, c-hex-2a); 1.97 (m,

2H, c-hex-3a); 1.68 (m, 4H, CH₂-pyrrol.); 1.38 (m, 2H, c-hex-3b); 1.25 (m, 2H, c-hex-2b) ppm. ¹³C NMR (DMSO-*d*₆): δ = 170.05 (CO); 154.32 (C-6); 144.59 (C-1'); 137.13 (C-3''); 136.98 (C-8); 133.02 (C-9); 129.71 (C-1''); 129.30 (C-2); 129.17 (C-4'); 128.78 (C-3'); 128.36 (C-5''); 126.83 (C-3); 126.17 (C-6''); 125.07 (C-4''); 123.77 (C-2''); 120.11 (C-2'); 88.28 (C-7); 49.46 (c-hex-1); 48.88 (c-hex-4); 47.79 (NCH₂-pyrrol.); 30.28 (c-hex-3); 30.05 (c-hex-2); 24.70 (CH₂-pyrrol.) ppm. HRMS (ESI): m/z calculated for C₃₁H₃₉O₃N₈S 603.28603, found 603.28597.

N⁶-((1*r*,4*r*)-4-Aminocyclohexyl)-3-(3-(*N,N*-dimethylsulfamoyl)phenyl)-N⁸-(4-(1-pyrrolidinylsulfonyl)phenyl)imidazo[1,2-*b*]pyridazine-6,8-diamine (34p). Prepared from 33p according to GP2. Off-white solid, yield 58%. MS (ESI): m/z = 639.48 [M + H]⁺. ¹H NMR (DMSO-*d*₆): δ = 8.73 (t, 1H, *J* = 1.8 Hz, H-2''); 8.47 (dt, 1H, *J* = 7.7, 1.6 Hz, H-6''); 8.39 (bs, 1H, FA); 8.04 (s, 1H, H-2); 7.78 (m, 2H, H-3'); 7.72 (t, 1H, *J* = 7.8 Hz, H-5''); 7.67 (dt, 1H, *J* = 7.8, 1.5 Hz, H-4''); 7.62 (m, 2H, H-2'); 6.64 (d, 1H, *J* = 7.5 Hz, NH); 6.53 (s, 1H, H-7); 3.66 (m, 1H, c-hex-1); 3.15 (m, 4H, NCH₂-pyrrol.); 2.97 (m, 1H, c-hex-4); 2.67 (s, 6H, NCH₃); 2.15 (m, 2H, c-hex-2a); 1.97 (m, 2H, c-hex-3a); 1.68 (m, 4H, CH₂-pyrrol.); 1.51 (m, 2H, c-hex-3b); 1.26 (m, 2H, c-hex-2b) ppm. ¹³C NMR (DMSO-*d*₆): δ = 154.58 (C-6); 144.50 (C-1'); 137.16 (C-8); 135.14 (C-3''); 133.49 (C-9); 130.76 (C-1''); 129.59 (C-6''); 129.48 (C-5''); 129.28 (C-4'); 129.10 (C-2); 128.79 (C-3'); 125.93 (C-3); 125.49 (C-4''); 123.81 (C-2''); 120.20 (C-2'); 88.64 (C-7); 48.81 (c-hex-1); 48.46 (c-hex-4); 47.80 (NCH₂-pyrrol.); 37.70 (NCH₃); 30.23 (c-hex-2); 29.59 (c-hex-3); 24.71 (CH₂-pyrrol.) ppm. HRMS (ESI): m/z calculated for C₃₀H₃₉O₄N₈S₂ 639.25302, found 639.25276.

N⁶-((1*r*,4*r*)-4-Aminocyclohexyl)-3-(thiophen-3-yl)-N⁸-(4-(1-pyrrolidinylsulfonyl)phenyl)imidazo[1,2-*b*]pyridazine-6,8-diamine (34q). Prepared from 33q according to GP2. Off-white solid, yield 32%. MS (ESI): m/z = 538.2 [M + H]⁺. ¹H NMR (DMSO-*d*₆): δ = 8.45 (bs, 1H, FA); 8.34 (dd, 1H, *J* = 3.0, 1.2 Hz, H-4''); 7.86 (s, 1H, H-2); 7.76–7.80 (m, 3H, H-3', H-2''); 7.68 (m, 1H, H-2''); 7.62 (m, 2H, H-2'); 6.69 (d, 1H, *J* = 6.8 Hz, NH); 6.49 (s, 1H, H-7); 3.63 (m, 1H, c-hex-1); 3.16 (m, 4H, NCH₂); 2.99 (m, 1H, c-hex-4); 2.20 (m, 2H, c-hex-2a); 2.02 (m, 2H, c-hex-3a); 1.69 (m, 4H, CH₂-pyrrol.); 1.49 (m, 2H, c-hex-3b); 1.27 (m, 2H, c-hex-2b) ppm. ¹³C NMR (DMSO-*d*₆): δ = 154.47 (C-6); 144.68 (C-1'); 137.12 (C-8); 132.13 (C-9); 129.88 (C-4'); 129.14 (C-3); 128.80 (C-3'); 128.01 (C-2); 127.32 (C-5''); 126.06 (C-2''); 124.85 (C-3''); 120.06 (C-2'); 118.89 (C-4''); 88.01 (C-7); 49.50 (c-hex-1); 48.80 (c-hex-4); 47.80 (NCH₂); 30.16 and 29.95 (c-hex-2, 3); 224.72 (CH₂-pyrrol.) ppm. HRMS (ESI): m/z calculated for C₂₆H₃₂O₂N₇S₂ 538.20534, found 538.20500.

N⁶-((1*r*,4*r*)-4-Aminocyclohexyl)-3-(furan-3-yl)-N⁸-(4-(1-pyrrolidinylsulfonyl)phenyl)imidazo[1,2-*b*]pyridazine-6,8-diamine (34r). Prepared from 33r according to GP2. Off-white solid, yield 57%. MS (ESI): m/z = 522.4 [M + H]⁺. ¹H NMR (DMSO-*d*₆): δ = 8.41 (s, 1H, FA); 8.37 (dd, 1H, *J* = 1.7, 0.7 Hz, H-2''); 7.80 (t, 1H, *J* = 1.7 Hz, H-5''); 7.77 (m, 2H, H-3'); 7.73 (s, 1H, H-2); 7.61 (m, 2H, H-2'); 7.10 (dd, 1H, *J* = 1.9, 0.7 Hz, H-4''); 6.68 (d, 1H, *J* = 6.8 Hz, NH); 6.46 (s, 1H, H-7); 3.60 (m, 1H, c-hex-1); 3.15 (m, 4H, NCH₂-pyrrol.); 3.02 (m, 1H, c-hex-4); 2.19 (m, 2H, c-hex-2a); 2.03 (m, 2H, c-hex-3a); 1.68 (m, 4H, CH₂-pyrrol.); 1.49 (m, 2H, c-hex-3b); 1.27 (m, 2H, c-hex-2b) ppm. ¹³C NMR (DMSO-*d*₆): δ = 165.35 (FA); 154.51 (C-6); 144.64 (C-1'); 137.06 (C-8); 132.25 (C-9); 129.10 (C-4'); 128.78 (C-3'); 126.56 (C-2); 121.84 (C-3); 120.03 (C-2'); 114.89 (C-3''); 108.44 (C-4''); 87.79 (C-7); 49.35 (c-hex-1); 48.64 (c-hex-4); 47.80 (NCH₂-pyrrol.); 29.85 and 29.79 (c-hex-2 and 3); 24.71 (CH₂-pyrrol.) ppm. HRMS (ESI): m/z calculated for C₂₆H₃₂O₃N₇S 522.22819, found 522.22793.

6-Chloro-3-nitro-N-(4-(1-pyrrolidinylsulfonyl)phenyl)imidazo[1,2-*b*]pyridazine-8-amine (37). In concentrated sulfuric acid (10 mL), 8-bromo-3-chloroimidazo[1,2-*b*]pyridazine (1 g, 4.3 mmol) was treated with HNO₃ (1.5 mL) at 0 °C. The resulting mixture was stirred at RT for 5 h, poured over ice, extracted with EtOAc, washed with sat. NaHCO₃ and water, and dried over MgSO₄. MS (ESI): m/z = 277.0 [M + H]⁺. The crude product was converted to 37 according to GP1. Yellow solid, yield 72%. MS (ESI): m/z = 423.2 [M + H]⁺.

¹H NMR (DMSO-*d*₆): δ = 10.60 (s, 1H, NH); 8.76 (s, 1H, H-2); 7.86 (m, 2H, H-3'); 7.71 (m, 2H, H-2'); 7.11 (s, 1H, H-7); 3.17 (m, 4H, NCH₂); 1.69 (m, 4H, CH₂-pyrrol.) ppm. ¹³C NMR (DMSO-*d*₆): δ = 150.22 (C-6); 142.08 (C-1'); 140.20 (C-8); 134.94 (C-9); 134.89 (C-3); 134.43 (C-2); 132.08 (C-4'); 128.95 (C-3'); 122.41 (C-2'); 98.91 (C-7); 47.84 (NCH₂); 24.75 (CH₂-pyrrol.) ppm. HRMS (ESI): m/z calculated for C₁₆H₁₆O₄N₆ClS 423.06368, found 423.06343.

N⁶-((1*r*,4*r*)-4-Aminocyclohexyl)-3-amino-N⁸-(4-(1-pyrrolidinylsulfonyl)phenyl)imidazo[1,2-*b*]pyridazine-6,8-diamine (39). Compound 37 (200 mg, 0.47 mmol) was converted to amine 38 according to GP2. Off-white solid, yield 100 mg (42%). MS (ESI): m/z = 501.4 [M + H]⁺. Crude 38 (80 mg, 0.16 mmol) in EtOH (13 mL) was treated with SnCl₂ (121 mg, 0.64 mmol) and heated at 75 °C for 2 h. The mixture was diluted with EtOAc and extracted with NaOH. RP FC (H₂O/ACN + 0.1% formic acid) afforded 39 (40 mg, 53%) as a salt with formic acid. MS (ESI): m/z = 471.4 [M + H]⁺. ¹H NMR (DMSO-*d*₆): δ = 9.22 (bs, 1H, NH); 8.40 (s, 1H, HCOOH); 7.72 (m, 2H, H-3'); 7.55 (m, 2H, H-2'); 6.59 (s, 1H, H-2); 6.29 (d, 1H, *J*(NH,1'') = 7.2 Hz, NH); 6.21 (s, 1H, H-7); 3.61 (m, 1H, H-1''); 3.13 (m, 4H, NCH₂); 2.96 (m, 1H, H-4''); 2.13 (m, 2H, H-2'a); 1.98 (m, 2H, H-3'a); 1.66 (m, 4H, CH₂-pyrrol.); 1.44 (m, 2H, H-3'b); 1.20 (m, 2H, H-2'b) ppm. ¹³C NMR (DMSO-*d*₆): δ = 165.40 (HCOOH); 153.69 (C-6); 145.15 (C-1'); 136.63 (C-8); 134.71 (C-3); 128.76 (C-3'); 128.29 (C-4'); 125.87 (C-9); 119.38 (C-2'); 110.49 (C-2); 86.01 (C-7); 48.73 (C-4''); 48.39 (C-1''); 47.99 (NCH₂); 30.17 (C-2''); 29.65 (C-3''); 24.70 (CH₂-pyrrol.) ppm. HRMS (ESI): m/z calculated for C₂₂H₃₁O₂N₈S 471.22852, found 471.22859. Purity was 90.55% due to complications of purification.

6-Chloro-3-(1*H*-pyrazole-4-yl)-N-(4-(1-pyrrolidinylsulfonyl)phenyl)imidazo[1,2-*b*]pyridazine-8-amine (41a) and 6-Chloro-N-(4-(1-pyrrolidinylsulfonyl)phenyl)imidazo[1,2-*b*]pyridazine-8-amine (41b). Compounds 32 (600 mg, 1.2 mmol) and 40 (667 mg, 2.4 mmol), Pd(dppf)Cl₂-DCM (97.3 mg, 0.12 mmol), and Na₂CO₃ (379 mg, 3.57 mmol) in a dioxane/water mixture (9:1, 20 mL) under an argon atmosphere were heated at 100 °C overnight. Compound 40 (200 mg) and Pd(dppf)Cl₂-DCM (48 mg) were added; the mixture was heated for a further 24 h. The mixture was then diluted with EtOAc, washed with sat. NH₄Cl, and dried over MgSO₄. FC (c-hex/EtOAc + 10% MeOH) and repurification by RP FC (H₂O/ACN) afforded compounds 41a (white solid, 160 mg, 30%) and 41b (white solid, 70 mg, 16%).

41a. MS (ESI): m/z = 444.2 [M + H]⁺. ¹H NMR (DMSO-*d*₆): δ = 13.19 (bs, 1H, NH-1''); 10.27 (s, 1H, NH-8); 8.41 and 8.17 (bs, 1H, H-3', H-5''); 8.00 (s, 1H, H-2); 7.83 (m, 2H, H-3'); 7.71 (m, 2H, H-2'); 6.80 (s, 1H, H-7); 3.17 (m, 4H, NCH₂); 1.69 (m, 4H, CH₂-pyrrol.) ppm. ¹³C NMR (DMSO-*d*₆): δ = 147.49 (C-6); 143.00 (C-1'); 139.50 (C-8); 136.69 and 125.68 (C-3', C-5''); 132.05 (C-9); 131.05 (C-4'); 128.90 (C-3'); 128.00 (C-2); 123.61 (C-3); 121.68 (C-2'); 108.44 (C-4''); 94.15 (C-7); 47.82 (NCH₂); 24.73 (CH₂-pyrrol.) ppm. HRMS (ESI): m/z calculated for C₁₉H₁₉O₂N₇ClS 444.10040, found 444.10013.

41b. MS (ESI): m/z = 378.2 [M + H]⁺. ¹H NMR (DMSO-*d*₆): δ = 10.26 (s, 1H, NH); 8.19 (d, 1H, *J*(3,2) = 1.2 Hz, H-3); 7.83 (m, 2H, H-3'); 7.70 (d, 1H, *J*(2,3) = 1.3 Hz, H-2); 7.69 (m, 2H, H-2'); 6.77 (s, 1H, H-7); 3.16 (m, 4H, NCH₂); 1.69 (m, 4H, CH₂-pyrrol.) ppm. ¹³C NMR (DMSO-*d*₆): δ = 147.43 (C-6); 142.90 (C-1'); 139.50 (C-8); 132.26 (C-9); 131.46 (C-2); 131.17 (C-4'); 128.89 (C-3'); 121.82 (C-2'); 118.25 (C-3); 94.65 (C-7); 47.81 (NCH₂); 24.72 (CH₂-pyrrol.) ppm. HRMS (ESI): m/z calculated for C₁₆H₁₇O₂N₅ClS 378.07860, found 378.07837.

N⁶-((1*r*,4*r*)-4-Aminocyclohexyl)-3-(1*H*-pyrazole-4-yl)-N⁸-(4-(1-pyrrolidinylsulfonyl)phenyl)imidazo[1,2-*b*]pyridazine-6,8-diamine (42a). Prepared from 41a according to GP2 and isolated as a salt with formic acid. White solid, yield 60%. MS (ESI): m/z = 522.4 [M + H]⁺. ¹H NMR (DMSO-*d*₆): δ = 9.44 (bs, 1H, NH); 8.46 (s, 1H, HCOOH); 8.27 (s, 2H, NH₂); 7.77 (m, 2H, H-3'); 7.66 (s, 1H, H-2); 7.61 (m, 2H, H-2'); 6.61 (d, 1H, *J* = 6.8 Hz, NH); 6.44 (s, 1H, H-7); 6.61 (d, 1H, *J*(NH,CH) = 6.8 Hz, NH); 6.44 (s, 1H, H-7); 3.62 (m, 1H, H-1''); 3.15 (m, 4H, NCH₂); 3.02 (m, 1H, H-4''); 2.20 (m, 2H, H-2'a); 2.03 (m, 2H, H-3'a); 1.68 (m, 4H, CH₂-pyrrol.); 1.51

(m, 2H, H-3''b); 1.27 (m, 2H, H-2''b) ppm. ^{13}C NMR (DMSO- d_6): δ = 165.67 (HCOOH); 154.33 (C-6); 144.79 (C-1'); 137.01 (C-8); 131.42 (C-9); 128.91 (C-4'); 128.81 (C-4''); 125.18 (C-2); 122.62 (C-3); 119.91 (C-2'); 110.02 (C-1'''); 87.52 (C-7); 49.36 (C-4''); 48.73 (C-1''); 47.82 (NCH₂); 29.88 (C-2''); 29.80 (C-3''); 24.73 (CH₂-pyrrol.) ppm. HRMS (ESI): m/z calculated for C₂₅H₃₂O₂N₉S 522.23942, found 522.23932.

N⁶-((1*r*,4*r*)-4-Aminocyclohexyl)-N⁸-(4-(1-pyrrolidinylsulfonyl)-phenyl)imidazo[1,2-*b*]pyridazine-6,8-diamine (42b). Prepared from **41b** according to GP2. White solid, yield 46%. MS (ESI): m/z = 456.37 [M + H]⁺. ^1H NMR (DMSO- d_6): δ = 8.46 (s, 1H, FA); 7.79 (d, 1H, J(3,2) = 1.1 Hz, H-3); 7.75 (m, 2H, H-3'); 7.59 (m, 2H, H-2'); 7.32 (d, J(2,3) = 1.1 Hz, H-2); 6.45 (d, 1H, J(NH,1'') = 7.4 Hz, NH); 3.51 (dtt, 1H, J = 7.4, 3.6, 11.0 Hz, H-1''); 3.14 (m, 4H, NCH₂); 2.91 (tt, 1H, J = 11.4, 4.0 Hz, H-4''); 2.06 (dd, 2H, J = 13.0, 4.0 Hz, H-2''a); 1.95 (m, 2H, H-3''a); 1.67 (m, 4H, CH₂-pyrrol.); 1.39 (m, 2H, H-3''b); 1.21 (m, 2H, H-2''b) ppm. ^{13}C NMR (DMSO- d_6): δ = 165.83 (FA); 154.42 (C-6); 144.72 (C-1'); 136.88 (C-8); 131.64 (C-9); 128.98 (C-4'); 128.79 (C-3'); 128.58 (C-2); 120.00 (C-2'); 117.23 (C-3); 88.43 (C-7); 48.69 (C-4'); 48.45 (C-1'); 47.81 (NCH₂); 30.23 and 30.19 (C-2'', C-3''); 24.72 (CH₂-pyrrol.) ppm. HRMS (ESI): m/z calculated for C₂₂H₃₀O₂N₇S 456.21762, found 456.21756.

8-Bromo-6-chloro-3-phenylimidazo[1,2-*b*]pyridazine (43). Phenylacetaldehyde (4 g, 33.28 mmol) in 1,4-dioxane (10 mL) was slowly treated with bromine (1.79 mL, 35 mmol) at 0 °C and left to warm to RT. The mixture was then diluted with DCM, washed with sat. Na₂S₂O₃ and water, dried over MgSO₄, filtered, and evaporated to half its volume. The dark brown residue was treated with 3-amino-4-bromo-6-chloropyridazine (5 g, 24 mmol), after which the mixture was refluxed overnight, evaporated, and purified by FC (c-hex/EtOAc/MeOH). Crystallization from the EtOAc and c-hex mixture afforded a yellow crystalline product (2.3 g, 49%). MS (ESI): m/z = 308.03 [M + H]⁺. ^1H NMR (DMSO- d_6): δ = 8.33 (s, 1H, H-2); 8.06 (m, 2H, H-3'); 7.97 (s, 1H, H-7); 7.55 (m, 2H, H-2'); 7.45 (m, 1H, H-4') ppm. ^{13}C NMR (DMSO- d_6): δ = 145.27 (C-6); 137.63 (C-9); 133.68 (C-2); 129.53 (C-3); 128.82 (C-3'); 128.58 (C-4'); 127.44 (C-1'); 126.65 (C-2'); 124.20 (C-8); 120.81 (C-7) ppm. HRMS (ESI): m/z calculated for C₁₂H₈N₃BrCl 307.95846, found 307.95865.

Kinase-Inhibitory Assays. FLT3-ITD and FLT3-D835Y were purchased from ProQinase, FLT3-ITD-F691L was purchased from Signalchem, and CDK2/Cyclin E was produced in Sf9 insect cells in-house. Activities of compounds against recombinant kinases were analyzed as described previously.^{12,42} Briefly, the kinase reactions were assayed with the peptide substrate (1 mg/mL AGLT (poly(Ala, Glu, Lys, Tyr) 6:2:5:1 hydrobromide)) for FLT3-ITD and FLT3-D835Y, with 1 mg/mL myelin basic protein for FLT3-ITD-F691L or with 1 mg/mL histone H1 for CDK2 in the presence of 1/1/12.5/15 μM ATP (for FLT3-ITD/D835Y/ITD-F691L/CDK2), 0.05 μCi [γ -³²P]ATP, and the test compound in a final volume of 10 μL in a reaction buffer for FLT3-ITD, FLT3-D835Y, and CDK2 (60 mM HEPES–NaOH, pH 7.5, 3 mM MgCl₂, 3 mM MnCl₂, 3 μM Na-orthovanadate, 1.2 mM DTT, 2.5 $\mu\text{g}/50$ μL PEG_{20,000}) or for FLT3-ITD-F691L (40 mM Tris-HCl, pH 7.4, 20 mM MgCl₂, 0.1 mg/mL BSA, 50 μM DTT).

The protein kinase selectivity of compound **34f** at a single concentration (100 nM) against 48 enzymes, as well as the determination of IC₅₀ values for the relevant off-targets, was determined at Eurofins Discovery. The kinome tree was generated using KinMap.⁴³ Illustration reproduced courtesy of Cell Signaling Technology, Inc. (www.cellsignal.com).

Cell Culture and Proliferation Assay. Human cell lines were obtained from the German Collection of Microorganisms and Cell Cultures (MOLM-13, NOMO-1, ML-2), the Cell Lines Service (MV4-11), and the European Collection of Authenticated Cell Cultures (CEM, K562), and were cultivated according to the providers' instructions. Briefly, MV4-11, MOLM-13, CEM, NOMO-1, and ML-2 were maintained in RPMI-1640 medium, SEM in IMDM, and K562 in DMEM. The cell culture medium was supplemented with 10% fetal bovine serum, penicillin (100 U/mL),

and streptomycin (100 $\mu\text{g}/\text{mL}$); cells were cultivated at 37 °C in 5% CO₂. A MOLM-13-resistant cell line (provided by Prof. Julhash Uddin Kazi) was obtained by long-term exposure to increasing concentrations of sorafenib (up to 1 μM); NGS revealed an FLT3-ITD-D835Y mutation (data not shown).

For antiproliferative assays, cells were seeded into 96-well plates in appropriate densities and subsequently treated with test compounds. After the incubation period, resazurin (Merck) solution was added for 4 h. Fluorescence of resorufin corresponding to live cells was measured at 544/590 nm (excitation/emission) using a Fluoroskan Ascent microplate reader (Labsystems).

Cell Cycle Analysis. Leukemia cells were seeded and, after a preincubation period, treated with tested compounds for 24 h. After staining with propidium iodide, DNA content was analyzed by flow cytometry using a 488 nm laser (BD FACSVerser with BD FACSuite software, version 1.0.6). Cell cycle distribution was analyzed using ModFit LT (Verity Software House).

Immunoblotting. After the preparation of cell lysates, proteins were separated on sodium dodecyl sulfate (SDS)-polyacrylamide gels and electroblotted onto nitrocellulose membranes. After blocking, proteins were incubated first with specific primary antibodies and subsequently with peroxidase-conjugated secondary antibodies. Peroxidase activity was detected using SuperSignal West Pico reagents (Thermo Fisher Scientific) and the LAS-4000 CCD camera system (Fujifilm). The following specific antibodies were purchased from Cell Signaling Technology: anti-FLT3 (8F2), anti-phospho-FLT3 Y589/S91 (30D4), anti-STAT5 (D2O6Y), anti-phospho-STAT5 Y694, anti-ERK1/2, anti-phospho-ERK1/2 (T202/Y204), anti-c-KIT (D13A2), anti-phospho-c-KIT Y703 (D12E12), and anti-phospho-c-KIT Y719. Anti-PCNA (clone PC-10) was generously gifted by Dr. Bořivoj Vojtěšek.

RNA Isolation and qPCR. Total RNA was isolated using the RNeasy Plus Mini Kit (QIAGEN) according to the manufacturer's instructions. RNA concentration and purity were measured using the DS-11 Series Spectrophotometer (DeNovix). RNA was transcribed into first-strand cDNA using the SensiFAST cDNA Synthesis Kit (Bioline). Quantitative RT-PCR was carried out on the CFX96 Touch Real-Time PCR Detection System (Bio-Rad) and the SensiFAST SYBR No-ROX Kit (Bioline). Suitable primers were designed using Primer-BLAST⁴⁴ and synthesized by Generi Biotech. Primary data were analyzed using CFX Maestro Software 2.2 (Bio-Rad). Relative gene expressions were determined using the delta-delta Ct method.⁴⁵ Expression of the MYC gene was normalized per the GAPDH and RPL13 genes, which were determined to be the most stable according to CFX Maestro Software 2.2 (Bio-Rad).

Primers used: GAPDH (F: TCCAAATCAAGTGGGGCGA; R: TGTTTCACACCCATGACGAA), MYC (F: TACAACACCCGAGCAAGGAC; R: AGCTAACGTTGAGGGGGCATT), RPL13A (F: C G A C A A G A A A A A G C G G A T G G ; R : TTCTCTTTCCTCTTCTCCTCC).

Plasma Stability Assay. To determine plasma stability, 5 μM of the given compound was incubated with human pooled plasma from 50 donors (Biowest) for 20, 60, and 120 min at 37 °C. The reactions were terminated by adding four volumes of ice-cold methanol. The samples were then mixed vigorously and left at –20 °C for 30 min before being centrifuged. The supernatants were diluted with four volumes of 30% methanol in water and then analyzed using the Echo MS system (SCIEX). Zero time points were prepared by adding ice-cold methanol to the compound prior to the addition of plasma.

Microsomal Stability Assay. A microsomal stability assay was performed using 0.5 mg/mL of pooled human liver microsomes (Thermo Fisher Scientific) and 5 μM compounds in 90 mM TRIS-Cl buffer (pH 7.4) containing 2 mM NADPH and 2 mM MgCl₂ for 10, 30, and 45 min at 37 °C. The reactions were terminated by the addition of four volumes of ice-cold methanol, mixed vigorously, and left at –20 °C for 30 min; the samples were then centrifuged. The supernatants were diluted with four volumes of 30% methanol in water and then analyzed using the Echo MS system (SCIEX). Zero time points were prepared by adding ice-cold methanol to the mixture of compounds and cofactors prior to the addition of microsomes.

In Vivo Efficacy. The experimental design was approved by the Institutional Animal Care and Use Committee (Charles University, MSMT-37334/2020-4). Immunodeficient adult female NOD.Cg-Prkdcscid112rgtm1Wjl/SzJ mice (referred to as NSG mice) purchased from the Jackson Laboratory were preserved in a pathogen-free environment in individually ventilated cages and provided with sterilized food and water. NSG mice were subcutaneously inoculated with MV4-11 cells. After all mice developed palpable tumors, they were stratified into cohorts (6 mice per group) with comparable calculated tumor volumes. Therapy involving **34f** (5 and 10 mg/kg dissolved in 5% DMSO in saline, intraperitoneal administration, final volume 500 μ L per mouse) was then initiated. Three perpendicular dimensions (in millimeters) were measured with a digital caliper. Tumor volumes were calculated using the following formula: $\pi/6 \times \text{length} \times \text{width} \times \text{height}$. The experiment was terminated when the tumors reached a maximum diameter of 20 mm. For the purpose of immunoblotting analysis, mice that had developed tumors were treated with a 10 mg/kg intraperitoneal dose of **34f** for 6 or 24 h. The mice were then euthanized, and the tumors were processed for further analysis.

■ ASSOCIATED CONTENT

SI Supporting Information

The Supporting Information is available free of charge at <https://pubs.acs.org/doi/10.1021/acs.jmedchem.3c00575>.

Activities of purine derivatives and intermediates; kinase-inhibitory and antiproliferative activities with standard deviations; additional in vitro data with quizartinib, gilteritinib, and **34f**; further kinase selectivity profiling; microsomal clearance; pharmacokinetic study; NMR spectra; and HPLC traces (PDF)

29a docked to FLT3 (PDB)

34f docked to FLT3 (PDB)

Molecular formula strings (CSV)

■ AUTHOR INFORMATION

Corresponding Authors

Radim Nencka – Institute of Organic Chemistry and Biochemistry of the Czech Academy of Sciences, 16000 Prague, Czech Republic; Phone: +420 220 183 265; Email: radim.nencka@uochb.cas.cz

Vladimír Kryštof – Department of Experimental Biology, Faculty of Science, Palacký University Olomouc, 78371 Olomouc, Czech Republic; Institute of Molecular and Translational Medicine, Faculty of Medicine and Dentistry, Palacký University Olomouc, 77900 Olomouc, Czech Republic; orcid.org/0000-0001-5838-2118; Phone: +420 585 634 854; Email: vladimir.krystof@upol.cz

Authors

Petra Břehová – Institute of Organic Chemistry and Biochemistry of the Czech Academy of Sciences, 16000 Prague, Czech Republic; orcid.org/0000-0001-5353-889X

Eva Rezníčková – Department of Experimental Biology, Faculty of Science, Palacký University Olomouc, 78371 Olomouc, Czech Republic; orcid.org/0000-0003-4773-2850

Kryštof Škach – Institute of Organic Chemistry and Biochemistry of the Czech Academy of Sciences, 16000 Prague, Czech Republic; orcid.org/0000-0002-7558-6961

Radek Jorda – Department of Experimental Biology, Faculty of Science, Palacký University Olomouc, 78371 Olomouc, Czech Republic; orcid.org/0000-0002-4905-7126

Milan Dejmeš – Institute of Organic Chemistry and Biochemistry of the Czech Academy of Sciences, 16000 Prague, Czech Republic; orcid.org/0000-0002-8195-971X

Veronika Vojáčková – Department of Experimental Biology, Faculty of Science, Palacký University Olomouc, 78371 Olomouc, Czech Republic; orcid.org/0000-0003-0946-3274

Michal Šála – Institute of Organic Chemistry and Biochemistry of the Czech Academy of Sciences, 16000 Prague, Czech Republic

Markéta Kovalová – Department of Experimental Biology, Faculty of Science, Palacký University Olomouc, 78371 Olomouc, Czech Republic

Martin Dračinský – Institute of Organic Chemistry and Biochemistry of the Czech Academy of Sciences, 16000 Prague, Czech Republic

Alexandra Dolníková – Institute of Pathological Physiology, First Faculty of Medicine, Charles University, 12108 Prague, Czech Republic

Timotej Strmeň – Institute of Organic Chemistry and Biochemistry of the Czech Academy of Sciences, 16000 Prague, Czech Republic

Monika Kinnertová – Department of Experimental Biology, Faculty of Science, Palacký University Olomouc, 78371 Olomouc, Czech Republic

Karel Chalupský – Institute of Organic Chemistry and Biochemistry of the Czech Academy of Sciences, 16000 Prague, Czech Republic

Alexandra Dvořáková – Institute of Organic Chemistry and Biochemistry of the Czech Academy of Sciences, 16000 Prague, Czech Republic

Tomáš Gucký – Department of Experimental Biology, Faculty of Science, Palacký University Olomouc, 78371 Olomouc, Czech Republic

Helena Mertlíková Kaiserová – Institute of Organic Chemistry and Biochemistry of the Czech Academy of Sciences, 16000 Prague, Czech Republic

Pavel Klener – Institute of Pathological Physiology, First Faculty of Medicine, Charles University, 12108 Prague, Czech Republic

Complete contact information is available at: <https://pubs.acs.org/doi/10.1021/acs.jmedchem.3c00575>

Author Contributions

[†]P.B. and E.Ř. contributed equally.

Notes

The authors declare no competing financial interest.

■ ACKNOWLEDGMENTS

This work was supported by the Ministry of Health of the Czech Republic (grant NU20-05-00472), the Czech Academy of Sciences (RVO: 61388963), the European Union—Next Generation EU (National Institute for Cancer Research, EXCELES, LX22NPO5102), the Czech Science Foundation (23-05462S), Palacký University Olomouc (IGA_PrF_2023_012), and Charles University, Prague (student research project SVV 260634/2023). The authors

wish to thank Prof. Julhash Uddin Kazi (Lund University) for providing the resistant MOLM-13 cell line.

■ ABBREVIATIONS USED

ACN, acetonitrile; AML, acute myeloid leukemia; CDK, cyclin-dependent kinase; EGFR, epidermal growth factor receptor; FA, formic acid; FC, flash column chromatography; FLT3, FMS-like tyrosine kinase 3; ITD, internal tandem duplication; JAK, Janus kinase; MAPK, mitogen-activated protein kinase; PARP-1, poly(ADP-ribose) polymerase 1; PDGFR, platelet-derived growth factor receptor; PI3K, phosphatidylinositol 3-kinase; RP FC, reversed-phase flash column chromatography; STAT, signal transducer and activator of transcription; TRK, tropomyosin receptor kinase; UPLC, ultra-performance liquid chromatography

■ REFERENCES

- (1) Döhner, H.; Weisdorf, D. J.; Bloomfield, C. D. Acute Myeloid Leukemia. *N. Engl. J. Med.* **2015**, *373*, 1136–1152.
- (2) Short, N. J.; Rytting, M. E.; Cortes, J. E. Acute Myeloid Leukaemia. *Lancet* **2018**, *392*, 593–606.
- (3) Prada-Arismendy, J.; Arroyave, J. C.; Röthlisberger, S. Molecular Biomarkers in Acute Myeloid Leukemia. *Blood Rev.* **2017**, *31*, 63–76.
- (4) Kazi, J. U.; Rönstrand, L. FMS-like Tyrosine Kinase 3/FLT3: From Basic Science to Clinical Implications. *Physiol. Rev.* **2019**, *99*, 1433–1466.
- (5) Gilliland, D. G.; Griffin, J. D. The Roles of FLT3 in Hematopoiesis and Leukemia. *Blood* **2002**, *100*, 1532–1542.
- (6) Daver, N.; Schlenk, R. F.; Russell, N. H.; Levis, M. J. Targeting FLT3 Mutations in AML: Review of Current Knowledge and Evidence. *Leukemia* **2019**, *33*, 299–312.
- (7) Stirewalt, D. L.; Kopecky, K. J.; Meshinchi, S.; Engel, J. H.; Pogosova-Agadjanian, E. L.; Linsley, J.; Slovak, M. L.; Willman, C. L.; Radich, J. P. Size of FLT3 Internal Tandem Duplication Has Prognostic Significance in Patients with Acute Myeloid Leukemia. *Blood* **2006**, *107*, 3724–3726.
- (8) Sutamtewagul, G.; Vigil, C. E. Clinical Use of FLT3 Inhibitors in Acute Myeloid Leukemia. *OncoTargets Ther.* **2018**, *Volume 11*, 7041–7052.
- (9) Thomas, C. M.; Campbell, P. FLT3 Inhibitors in Acute Myeloid Leukemia: Current and Future. *J. Oncol. Pharm. Pract.* **2019**, *25*, 163–171.
- (10) Zhong, Y.; Qiu, R. Z.; Sun, S. L.; Zhao, C.; Fan, T. Y.; Chen, M.; Li, N. G.; Shi, Z. H. Small-Molecule Fms-like Tyrosine Kinase 3 Inhibitors: An Attractive and Efficient Method for the Treatment of Acute Myeloid Leukemia. *J. Med. Chem.* **2020**, *63*, 12403–12428.
- (11) Köprülüoğlu, C.; Dejmek, M.; Šála, M.; Ajani, H.; Hřebabecský, H.; Fanfrlík, J.; Jorda, R.; Dračinský, M.; Procházková, E.; Šácha, P.; et al. Optimization of Norbornyl-Based Carbocyclic Nucleoside Analogs as Cyclin-Dependent Kinase 2 Inhibitors. *J. Mol. Recognit.* **2020**, *33*, No. e2842.
- (12) Gucký, T.; Řezníčková, E.; Radošová Muchová, T.; Jorda, R.; Klejová, Z.; Malínková, V.; Berka, K.; Bazgier, V.; Ajani, H.; Lepšík, M.; et al. Discovery of N 2 -(4-Amino-Cyclohexyl)-9-Cyclopentyl- N 6 -(4-Morpholin-4-ylmethyl-Phenyl)- 9H-Purine-2,6-Diamine as a Potent FLT3 Kinase Inhibitor for Acute Myeloid Leukemia with FLT3 Mutations. *J. Med. Chem.* **2018**, *61*, 3855–3869.
- (13) Chang, Y.-T.; Gray, N. S.; Rosania, G. R.; Sutherlin, D. P.; Kwon, S.; Norman, T. C.; Sarohia, R.; Leost, M.; Meijer, L.; Schultz, P. G. Synthesis and Application of Functionally Diverse 2,6,9-Trisubstituted Purine Libraries as CDK Inhibitors. *Chem. Biol.* **1999**, *6*, 361–375.
- (14) Zatloukal, M.; Jorda, R.; Gucký, T.; Řezníčková, E.; Voller, J.; Pospíšil, T.; Malínková, V.; Adamcová, H.; Kryštof, V.; Strnad, M. Synthesis and in Vitro Biological Evaluation of 2,6,9-Trisubstituted Purines Targeting Multiple Cyclin-Dependent Kinases. *Eur. J. Med. Chem.* **2013**, *61*, 61–72.
- (15) Gucký, T.; Jorda, R.; Zatloukal, M.; Bazgier, V.; Berka, K.; Řezníčková, E.; Béres, T.; Strnad, M.; Kryštof, V. A Novel Series of Highly Potent 2,6,9-Trisubstituted Purine Cyclin-Dependent Kinase Inhibitors. *J. Med. Chem.* **2013**, *56*, 6234–6247.
- (16) Ali, E. M. H.; Abdel-Maksoud, M. S.; Oh, C. H. Thieno[2,3-d]Pyrimidine as a Promising Scaffold in Medicinal Chemistry: Recent Advances. *Bioorg. Med. Chem.* **2019**, *27*, 1159–1194.
- (17) Wang, R.; Yu, S.; Zhao, X.; Chen, Y.; Yang, B.; Wu, T.; Hao, C.; Zhao, D.; Cheng, M. Design, Synthesis, Biological Evaluation and Molecular Docking Study of Novel Thieno[3,2-d]Pyrimidine Derivatives as Potent FAK Inhibitors. *Eur. J. Med. Chem.* **2020**, *188*, 112024.
- (18) Islam, F.; Quadery, T. M. Therapeutic Potential, Synthesis, Patent Evaluation and SAR Studies of Thieno[3,2-d]Pyrimidine Derivatives: Recent Updates. *Curr. Drug Targets* **2021**, *22*, 1944–1963.
- (19) Al-Azmi, A. Pyrazolo[1,5-a]Pyrimidines: A Close Look into Their Synthesis and Applications. *Curr. Org. Chem.* **2019**, *23*, 721–743.
- (20) Cherukupalli, S.; Karpoomath, R.; Chandrasekaran, B.; Hampannavar, G. A.; Thapliyal, N.; Palakollu, V. N. An Insight into Synthetic and Medicinal Aspects of Pyrazolo[1,5-a]Pyrimidine Scaffold. *Eur. J. Med. Chem.* **2017**, *126*, 298–352.
- (21) Jorda, R.; Paruch, K.; Kryštof, V. Cyclin-Dependent Kinase Inhibitors Inspired by Roscovitine: Purine Bioisosteres. *Curr. Pharm. Des.* **2012**, *18*, 2974–2980.
- (22) Bavetsias, V.; Crumpler, S.; Sun, C.; Avery, S.; Atrash, B.; Faisal, A.; Moore, A. S.; Kosmopoulou, M.; Brown, N.; Sheldrake, P. W.; et al. Optimization of Imidazo[4,5-b]Pyridine-Based Kinase Inhibitors: Identification of a Dual FLT3/Aurora Kinase Inhibitor as an Orally Bioavailable Preclinical Development Candidate for the Treatment of Acute Myeloid Leukemia. *J. Med. Chem.* **2012**, *55*, 8721–8734.
- (23) Elattar, K. M.; Doğru Mert, B. Recent Developments in the Chemistry of Bicyclic 6-6 Systems: Chemistry of Pyrido[4,3-d]Pyrimidines. *RSC Adv.* **2016**, *6*, 71827–71851.
- (24) Garrido, A.; Vera, G.; Delaye, P. O.; Enguehard-Gueiffier, C. Imidazo[1,2-b]Pyridazine as Privileged Scaffold in Medicinal Chemistry: An Extensive Review. *Eur. J. Med. Chem.* **2021**, *226*, No. 113867.
- (25) Kusakabe, K. I.; Ide, N.; Daigo, Y.; Itoh, T.; Yamamoto, T.; Hashizume, H.; Nozu, K.; Yoshida, H.; Tadano, G.; Tagashira, S.; et al. Discovery of Imidazo[1,2-b]Pyridazine Derivatives: Selective and Orally Available Mps1 (TTK) Kinase Inhibitors Exhibiting Remarkable Antiproliferative Activity. *J. Med. Chem.* **2015**, *58*, 1760–1775.
- (26) Tor, Y.; Del Valle, S.; Jaramillo, D.; Srivatsan, S. G.; Rios, A.; Weizman, H. Designing New Isomorphous Fluorescent Nucleobase Analogues: The Thieno[3,2-d]Pyrimidine Core. *Tetrahedron* **2007**, *63*, 3608–3614.
- (27) Myers, S. M.; Bawn, R. H.; Bisset, L. C.; Blackburn, T. J.; Cottyn, B.; Molyneux, L.; Wong, A. C.; Cano, C.; Clegg, W.; Harrington, R. W.; et al. High-Throughput Screening and Hit Validation of Extracellular-Related Kinase 5 (ERK5) Inhibitors. *ACS Comb. Sci.* **2016**, *18*, 444–455.
- (28) Winters, G.; Sala, A.; De Paoli, A.; Conti, M. Reaction of Cyclic Ketones with 5-Aminopyrazoles and 5-Aminoisoxazoles. *Synthesis* **1984**, *1984*, 1050–1052.
- (29) Fraley, M. E.; Hoffman, W. F.; Rubino, R. S.; Hungate, R. W.; Tebben, A. J.; Rutledge, R. Z.; McFall, R. C.; Huckle, W. R.; Kendall, R. L.; Coll, K. E.; Thomas, K. A. Synthesis and Initial SAR Studies of 3,6-Disubstituted Pyrazolo[1,5-a]Pyrimidines: A New Class of KDR Kinase Inhibitors. *Bioorg. Med. Chem. Lett.* **2002**, *12*, 2767–2770.
- (30) Kosugi, T.; Mitchell, D. R.; Fujino, A.; Imai, M.; Kambe, M.; Kobayashi, S.; Makino, H.; Matsueda, Y.; Oue, Y.; Komatsu, K.; et al. Mitogen-Activated Protein Kinase-Activated Protein Kinase 2 (MAPKAP-K2) as an Antiinflammatory Target: Discovery and in Vivo Activity of Selective Pyrazolo[1,5-a]Pyrimidine Inhibitors Using

a Focused Library and Structure-Based Optimization Approach. *J. Med. Chem.* **2012**, *55*, 6700–6715.

(31) Klejch, T.; Keough, D. T.; Chavchich, M.; Travis, J.; Skácel, J.; Pohl, R.; Janeba, Z.; Edstein, M. D.; Avery, V. M.; Guddat, L. W.; Hocková, D. Sulfide, Sulfoxide and Sulfone Bridged Acyclic Nucleoside Phosphonates as Inhibitors of the Plasmodium Falciparum and Human 6-Oxopurine Phosphoribosyltransferases: Synthesis and Evaluation. *Eur. J. Med. Chem.* **2019**, *183*, No. 111667.

(32) Dvořáková, H.; Holý, A. Synthesis and Biological Effects of N-(2-Phosphonomethoxyethyl) Derivatives of Deazapurine Bases. *Collect. Czech. Chem. Commun.* **1993**, *58*, 1419–1429.

(33) Jansa, P.; Kvasnica, M.; Mackman, R. L. Fused Pyrimidine Compounds for the Treatment of HIV. International Patent WO2016/105532, 30 June 2016.

(34) Mejdrová, I.; Chalupská, D.; Plačková, P.; Müller, C.; Šála, M.; Klíma, M.; Baumlová, A.; Hřebabeký, H.; Procházková, E.; Dejmek, M.; et al. Rational Design of Novel Highly Potent and Selective Phosphatidylinositol 4-Kinase III β (PI4KB) Inhibitors as Broad-Spectrum Antiviral Agents and Tools for Chemical Biology. *J. Med. Chem.* **2017**, *60*, 100–118.

(35) Terme, T.; Maldonado, J.; Crozet, M. P.; Vanelle, P.; Galtier, C.; Gueiffier, A. Synthesis of 2-Substituted-3-Nitroimidazo[1, 2-b]Pyridazines as Potential Biologically Active Agents. *J. Heterocycl. Chem.* **2002**, *39*, 173–177.

(36) Trabanco-Suarez, A. A.; Tresadern, G. J.; Vega Ramiro, J. A.; Cid-Nunez, J. M. Imidazo[1,2-a]Pyridine Derivatives and Their Use as Positive Allosteric Modulators of MGLUR2 Receptors. International Patent WO2009/062676 A2, 22 May 2009.

(37) Kim, K. T.; Baird, K.; Davis, S.; Piloto, O.; Levis, M.; Li, L.; Chen, P.; Meltzer, P.; Small, D. Constitutive Fms-like Tyrosine Kinase 3 Activation Results in Specific Changes in Gene Expression in Myeloid Leukaemic Cells. *Br. J. Haematol.* **2007**, *138*, 603–615.

(38) Warkentin, A. A.; Lopez, M. S.; Lasater, E. A.; Lin, K.; He, B. L.; Leung, A. Y. h.; Smith, C. C.; Shah, N. P.; Shokat, K. M. Overcoming Myelosuppression Due to Synthetic Lethal Toxicity for FLT3-Targeted Acute Myeloid Leukemia Therapy. *eLife* **2014**, *3*, No. e03445.

(39) Griffith, J.; Black, J.; Faerman, C.; Swenson, L.; Wynn, M.; Lu, F.; Lippke, J.; Saxena, K. The Structural Basis for Autoinhibition of FLT3 by the Juxtamembrane Domain. *Mol. Cell* **2004**, *13*, 169–178.

(40) Šála, M.; Hollinger, K. R.; Hollinger, K. R.; Hollinger, K. R.; Thomas, A. G.; Dash, R. P.; Tallon, C.; Tallon, C.; Veeravalli, V.; Veeravalli, V.; et al. Novel Human Neutral Sphingomyelinase 2 Inhibitors as Potential Therapeutics for Alzheimer's Disease. *J. Med. Chem.* **2020**, *63*, 6028–6056.

(41) Colombano, G.; Caldwell, J. J.; Matthews, T. P.; Bhatia, C.; Joshi, A.; McHardy, T.; Mok, N. Y.; Newbatt, Y.; Pickard, L.; Strover, J.; et al. Binding to an Unusual Inactive Kinase Conformation by Highly Selective Inhibitors of Inositol-Requiring Enzyme 1 α Kinase-Endoribonuclease. *J. Med. Chem.* **2019**, *62*, 2447–2465.

(42) Jorda, R.; Hendrychová, D.; Voller, J.; Řezníčková, E.; Gucký, T.; Kryštof, V. How Selective Are Pharmacological Inhibitors of Cell-Cycle-Regulating Cyclin-Dependent Kinases? *J. Med. Chem.* **2018**, *61*, 9105–9120.

(43) Eid, S.; Turk, S.; Volkamer, A.; Rippmann, F.; Fulle, S. KinMap: a Web-based Tool for Interactive Navigation through Human Kinome Data. *BMC Bioinf.* **2017**, *18*, No. 16.

(44) Ye, J.; Coulouris, G.; Zaretskaya, I.; Cutcutache, I.; Rozen, S.; Madden, T. L. Primer-BLAST: A Tool to Design Target-Specific Primers for Polymerase Chain Reaction. *BMC Bioinf.* **2012**, *13*, No. 134.

(45) Livak, K. J.; Schmittgen, T. D. Analysis of Relative Gene Expression Data Using Real-Time Quantitative PCR and the 2- $\Delta\Delta$ CT Method. *Methods* **2001**, *25*, 402–408.

Recommended by ACS

Discovery of Novel 1,3-Diphenylpyrazine Derivatives as Potent S-Phase Kinase-Associated Protein 2 (Skp2) Inhibitors for the Treatment of Cancer

Kun Zhang, Hong-Min Liu, et al.

MAY 19, 2023

JOURNAL OF MEDICINAL CHEMISTRY

READ 

Design and Optimization of Novel Benzimidazole- and Imidazo[4,5-b]pyridine-Based ATM Kinase Inhibitors with Subnanomolar Activities

Teodor Dimitrov, Stefan Laufer, et al.

MAY 25, 2023

JOURNAL OF MEDICINAL CHEMISTRY

READ 

Discovery of Potent DYRK2 Inhibitors with High Selectivity, Great Solubility, and Excellent Safety Properties for the Treatment of Prostate Cancer

Kai Yuan, Peng Yang, et al.

FEBRUARY 17, 2023

JOURNAL OF MEDICINAL CHEMISTRY

READ 

Discovery of Pyrimidinediamine Derivatives as Potent Methuosis Inducers for the Treatment of Triple-Negative Breast Cancer

Jia He, Yihua Chen, et al.

MAY 22, 2023

JOURNAL OF MEDICINAL CHEMISTRY

READ 

Get More Suggestions >

PŘÍLOHA IV

Řezníčková E, Krajčovičová S, Peřina M, **Kovalová M**, Sural M, Kryštof V.
(2022) Modulation of FLT3-ITD and CDK9 in acute myeloid leukaemia cells by
novel proteolysis targeting chimera (PROTAC). *Eur J Med Chem* 243, 114792

<https://doi.org/10.1016/j.ejmech.2022.114792>



Research paper

Modulation of FLT3-ITD and CDK9 in acute myeloid leukaemia cells by novel proteolysis targeting chimera (PROTAC)

Eva Řezníčková^{a,1}, Soňa Krajčovičová^{b,1}, Miroslav Peřina^a, Markéta Kovalová^a,
Miroslav Soural^{b,**}, Vladimír Kryštof^{a,c,*}

^a Department of Experimental Biology, Faculty of Science, Palacký University Olomouc, Šlechtitelů 27, 78371, Olomouc, Czech Republic

^b Department of Organic Chemistry, Faculty of Science, Palacký University Olomouc, 17. Listopadu 12, 77146, Olomouc, Czech Republic

^c Institute of Molecular and Translational Medicine, Faculty of Medicine and Dentistry, Palacký University Olomouc, Hněvotínská 5, 77900, Olomouc, Czech Republic



ARTICLE INFO

Keywords:

Acute myeloid leukaemia

FLT3

CDK9

Proteolysis targeting chimera (PROTAC)

ABSTRACT

Oncogenic mutations in gene encoding FLT3 kinase are often detected in acute myeloid leukaemia (AML) patients, and several potent kinase inhibitors have been developed. However, the FLT3 inhibitor treatment often leads to the resistance development and subsequent relapse. Targeted degradation of oncogenic protein kinases has emerged as a feasible pharmacological strategy, providing more robust effect over traditional competitive inhibitors. Based on previously developed competitive inhibitor of FLT3 and CDK9, we have designed and prepared a novel pomalidomide-based PROTAC. A series of biochemical and cellular experiments showed selectivity towards FLT3-ITD bearing AML cells and confirmed proteasome-dependent mechanism of action. Dual FLT3-ITD and CDK9 protein degradation resulted in the block of FLT3-ITD downstream signalling pathways, apoptosis activation and cell cycle arrest of FLT3-ITD AML cells. Moreover, transcriptional repression caused by CDK9 degradation significantly reduced expression of crucial genes involved in AML pathogenesis. The obtained results indicate the beneficial impact of simultaneous FLT3-ITD/CDK9 degradation for AML therapy.

1. Introduction

Acute myeloid leukaemia (AML) is a haematological malignant disease characterized by high numbers of abnormally differentiated immature myeloid cells infiltrated in the blood, bone marrow and other tissues [1]. It is the most frequent type of acute leukaemia in adults, causing 62% of all leukaemia related deaths [2]. Evaluating the genetic background of AML patients revealed that several frequently mutated genes play a crucial role in the disease's development [1], including FMS-like tyrosine kinase 3 (FLT3, CD135). FLT3 is one of the 56 human receptor tyrosine kinases (RTKs), and its expression is almost exclusively bound to haematopoietic stem and progenitor cells, where it is involved in the regulation of their proper maturation and function in normal haematopoiesis. Activating mutations in the FLT3 gene can be detected in one-third of AML patients ranking them among the most common drivers of the disease [3]. Internal tandem duplications (ITDs) in the juxtamembrane domain, as well as point mutations in the tyrosine

kinase domain (TKD), disrupt FLT3 autoinhibitory function and allow clonal expansion of immature blood progenitors [3]. As these findings revealed FLT3 plays a crucial role in AML pathology, the extensive research into the field of FLT3 inhibition was initiated. The first generation of FLT3 inhibitors (e.g. midostaurin, sorafenib, sunitinib) displayed a broad spectrum of kinase inhibition. This was extended over time by a second generation of more selective FLT3 inhibitors (e.g. quizartinib, gilteritinib, FF-10101). Several candidates from both generations successfully underwent clinical trials and being approved for AML treatment (midostaurin [4] and gilteritinib [5] received FDA approval, and quizartinib [6] was approved by regulatory authority in Japan). Nevertheless, the duration of FLT3 inhibitor-induced response is frequently limited due to the resistance development and subsequent relapse [7].

Strategies trying to deal with the resistance onset after FLT3 inhibitor therapy including combinations with conventional chemotherapy or haematopoietic stem cell transplantations are currently tested [8],

* Corresponding author. Department of Experimental Biology, Faculty of Science, Palacký University Olomouc, Šlechtitelů 27, 78371, Olomouc, Czech Republic.

** Corresponding author.

E-mail addresses: miroslav.soural@upol.cz (M. Soural), vladimir.krystof@upol.cz (V. Kryštof).

¹ Both authors contributed equally.

however novel approaches are still needed. Specific degradation of FLT3 via proteolysis targeting chimeras (PROTACs) could provide an alternative approach to overcome the limitations in AML treatment associated with the fast mutational rate of FLT3 gene. First described in 2001 [9], PROTACs are heterobifunctional conjugates consisting of a protein of interest (POI) binder interconnected to a ligand capable of E3 ubiquitin ligase engagement. PROTACs form a ternary complex with both these proteins resulting in polyubiquitination of the POI and inducing its degradation via proteasome. PROTACs provide some advantages over conventional kinase inhibitors. For example, owing to PROTAC's ability to work as a catalyser to degrade a target protein and given that E3 ligases have high enzymatic turnover, the cells usually require only low PROTAC exposure to give high cellular and in vivo efficacy. In addition, the effects can have long duration, so the drug exposure could be lower. And finally, some target enzymes display non-enzymatic scaffolding functions, which cannot be addressed by simple inhibition [10].

FLT3-recruiting PROTACs have been developed by groups of Gray [11] and Crews [12] in 2018 whose conjugates were based on FLT3-selective inhibitor quizartinib linked to cereblon (CRBN) and von Hippel-Lindau (VHL) ligands, respectively (Fig. 1A and B). Two other PROTACs based on tyrosine kinase inhibitor dovitinib [13] or experimental pyrrolo[2,3-*d*]pyrimidine derivative [14] were developed later on. These studies demonstrate that FLT3-ITD is amenable to degradation and that FLT3-targeting PROTACs provide efficacious compounds, further confirming the potential of this approach.

Although FLT3 as the most common driver of AML is undoubtedly suitable therapeutic option, the urgent need for more effective therapy expands the range of discussed targets for drug intervention including CDK9 [15]. Serine-threonine protein kinase CDK9 is a key regulator of transcriptional initiation and elongation having a great impact on levels of key pro-survival and apoptotic factors. Several studies highlight positive effect of CDK9 inhibition alone [16,17] or with simultaneous inhibition of other target including FLT3 [18]. Combination with other compounds such as Bcl-2 inhibitor venetoclax [19,20] in different haematological malignancies counting AML have been reported as well.

Encouraged by these facts, we decided to incorporate a potent kinase inhibitor from the recently described 2,6,9-trisubstituted purine series [21] into PROTAC conjugate. The lead compound of the 2,6,9-trisubstituted purine series showed significant selectivity to AML cell lines bearing the FLT3-ITD mutation. It blocked the autophosphorylation of FLT3 and inhibited its downstream signalling leading to G1 cell cycle phase arrest and apoptosis [21]. In addition to outstanding FLT3 inhibitory properties, it also displayed activity towards CDK9. In this

manuscript, we describe a PROTAC based on purine inhibitor **BPA311**, targeting both FLT3 and CDK9, two independent relevant AML cellular targets, with strong activity and selectivity towards FLT3-ITD expressing AML cell lines.

2. Results and discussion

2.1. Molecular design

Molecular docking studies, as well as inspections of available co-crystals with analogous kinase inhibitors [22–24], have indicated the orientation of **BPA311** (Fig. 1C) in the ATP active site of FLT3 and CDK9 kinases (Fig. 1D). Importantly, 4-ethyl-piperazin-1-yl-phenyl moiety of the compound pointed outward from the active site, thus the *N*-ethyl-piperazine part provided a rational option for enlarging the ethyl chain to a linker bound to pomalidomide, a CRBN ligand successfully applied in several protein kinase targeting PROTACs. Next, a suitable way of conjugation was established, as is known that the linker composition and its attachment to the ligand play a critical role in the successful development of PROTAC degraders [25,26]. The current synthetic toolbox offers a number of strategies for PROTAC construction; however, for practical reasons, we initially applied the readily available thalidomide-preloaded resin (TPR) [27], which enables fast and simple conjugation with the reactive amine-containing inhibitors. For this purpose, compound 7, with the free piperazine moiety, was synthesized (Scheme 1) and subjected to conjugation using TPR which provided the corresponding PROTAC **S19** (see Scheme S1 and Fig. S1 in Supplementary material for details). Nevertheless, a negative outcome was detected in the degradation assay (Fig. S1B) pointing to a non-optimal structure of the PROTAC conjugate. Subsequently, instead of the typical “trial-and-error” approach, consisting of the preparation of a series of PROTACs with different linker lengths, we attempted to rationally design the optimal structure using molecular modelling and clues from the previously reported degraders [11,12,28]. The outcome of this procedure clearly indicated the need for a shorter linker, and eventually changing the type of attachment. Consequently, PROTAC **13** (Fig. 1E and Scheme 2) was designed with the spacer resembling the structure of quizartinib-CRBN PROTAC (Fig. 1A) [11].

2.2. Preparation of PROTAC components: modified BPA311 and pomalidomide-glycine (Pom-Gly)

The synthetic strategy started with derivatization of 1-(4-

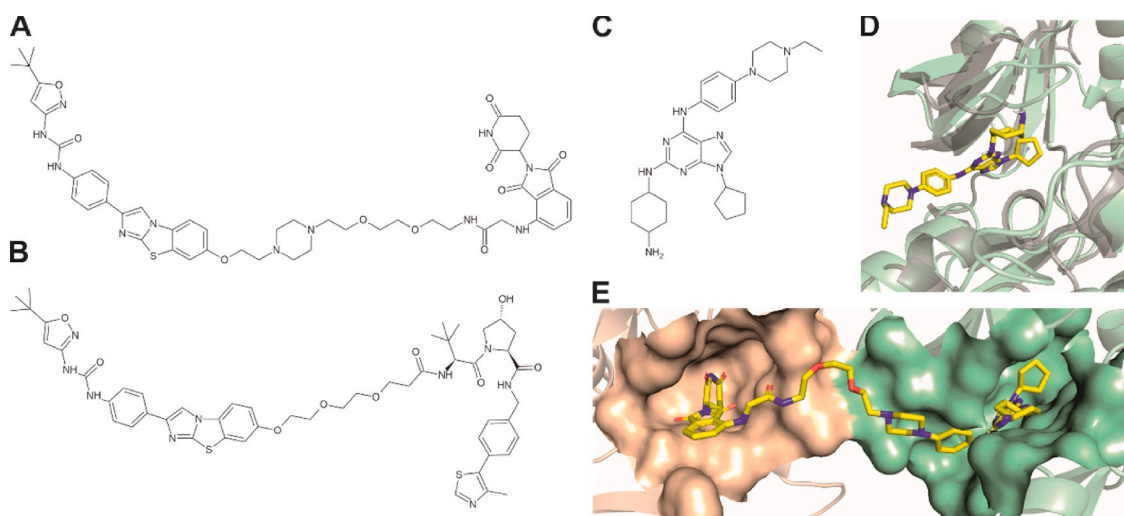
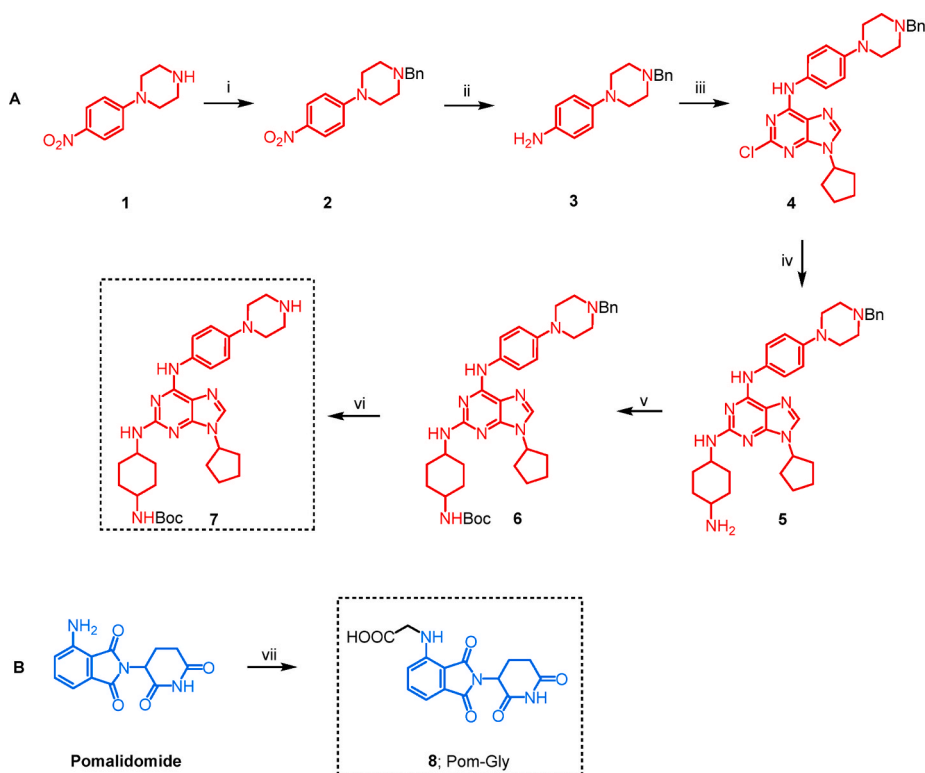
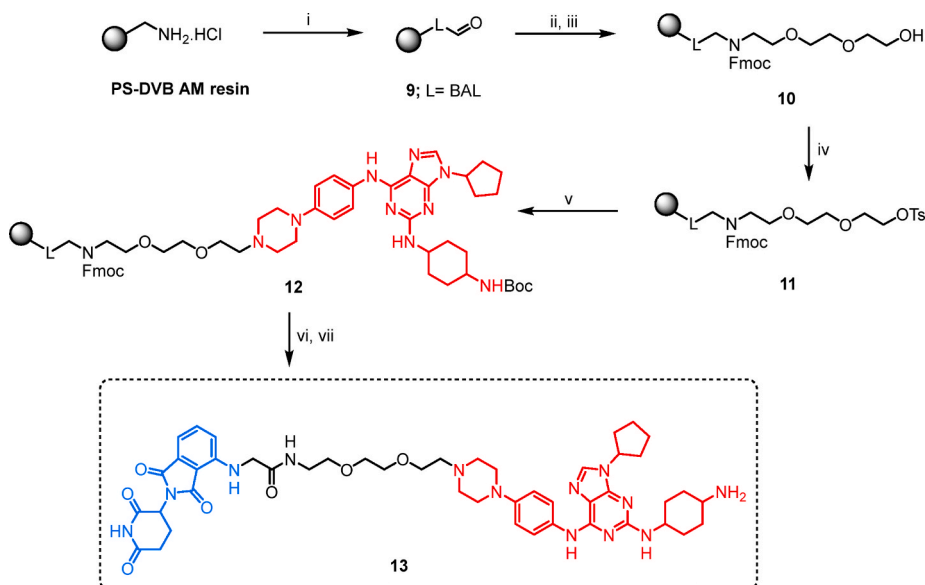


Fig. 1. Published FLT3 PROTAC conjugates: Quizartinib linked to CRBN (A) and VHL (B) ligands. Design of PROTAC: (C) Structure of FLT3-ITD/CDK9 inhibitor **BPA311**. (D) Overlay of FLT3 (green) and CDK9 (grey) with **BPA311** in the active site. (E) Predicted binding of PROTAC **13** (yellow) to FLT3 (green) and CRBN (orange).



Scheme 1. Synthesis of purine ligand **7** and modified pomalidomide **8**. *Reagents and conditions:* (i) benzyl bromide, K_2CO_3 , DMF/ CH_3CN , $50^\circ C$, 3 h; (ii) PtO_2 , ethanol/THF, r.t., 90 min; (iii) 2,6-dichloro-9-cyclopentyl purine, *N,N*-diisopropylethylamine (DIPEA), DMSO, $120^\circ C$, 16 h; (iv) *trans*-1,4-diaminocyclohexane, DIPEA, diethylene glycol diethyl ether, $160^\circ C$, 24 h; (v) Boc_2O , Et_3N , 4-(dimethylamino)pyridine (DMAP), THF, r.t., 16 h; (vi) NH_4HCO_2 , Pd/C, ethanol, $80^\circ C$, 16 h; (vii) glyoxylic acid, Bu_2SnCl_2 , phenyl silane, THF, reflux, 16 h.



Scheme 2. Synthesis of PROTAC **13**. *Reagents and conditions:* (i) 4-(4-formyl-3-methoxyphenoxy)butanoic acid, 1-hydroxybenzotriazole (HOBT), *N,N'*-diisopropylcarbodiimide (DIC), DMF/ CH_2Cl_2 , r.t., 16 h; (ii) 2-(2-(2-aminoethoxy)ethoxy)ethan-1-ol, DMF/AcOH, r.t., 16 h then $NaBH(OAc)_3$, DMF/AcOH, r.t., 4 h; (iii) Fmoc-OSu, CH_2Cl_2 , r.t., 16 h; (iv) tosyl chloride (TsCl), Et_3N , DMAP, CH_2Cl_2 , r.t., 16 h; (v) **7**, DIPEA, DMF, $70^\circ C$, 16 h; (vi) a) 1,8-diazabicyclo[5.4.0]undec-7-ene (DBU)/ CH_2Cl_2 , r.t., 10 min, b) **8**, HOBT, DIC, DMF, r.t., 16 h; (vii) TFA/ CH_2Cl_2 , r.t., 2 h.

nitrophenyl)piperazine **1**. This compound was in two steps converted to 4-(*N*-benzyl)piperazine aniline **3**, which underwent regioselective aromatic nucleophilic substitution with 2,6-dichloro-9-cyclopentyl-purine to yield intermediate **4** (Scheme 1A). The choice of benzyl protecting group was carefully envisioned for orthogonal manipulation in the presence of acid-labile *t*-butoxycarbonyl (Boc) group later in the sequence.

Installation of cyclohexyl diamine motif to the C^2 purine position was inspired by our previous work [29]. However, the Buchwald-Hartwig cross-coupling was not successful in this case and only starting material **4** was recovered under various conditions. In contrast, using large excess of diamine at harsh conditions ($160^\circ C$) yielded the desired

intermediate **5** (Scheme 1A). The diamine moiety was then protected with the Boc protecting group, removable under acidic conditions during the cleavage of the final PROTAC from the resin (see later in the text, Scheme 2). Finally, deprotection of the benzyl group under ammonium formate-promoted *in situ* hydrogenation in a presence of palladium on activated charcoal (Pd/C) yielded final purine ligand **7** (Scheme 1A). The modification of pomalidomide was achieved by silane-based direct reductive amination [30] with glyoxylic acid that yielded Pom-Gly **8** (Scheme 1B).

2.3. Preparation of the PROTAC

To prepare the desired conjugate, the solid-phase synthesis was used as it allowed simple and fast preparation of the targeted compound in a multistep sequence without the need of tedious purification. The synthesis started from commercially available amino methyl polystyrene (PS-DVB AM) resin which was in the first step equipped with backbone amide linker (BAL) using 4-(4-formyl-3-methoxyphenoxy)butanoic acid (Scheme 2). Subsequent reductive amination in the presence of 2-(2-aminoethoxy)ethoxy)ethan-1-ol and NaBH(OAc)₃ was followed by protection with fluorenylmethyloxycarbonyl (Fmoc) protecting group which yielded intermediate **10**. After tosylation, the nucleophilic substitution with prepared purine ligand **7** yielded intermediate **12**. The reaction proceeded smoothly; however, high temperature was needed to reach full conversion to the product. Notably, we also observed partial cleavage of Fmoc during this step, due to the excess of DIPEA used. A quantitative deprotection was accomplished with the mixture of DBU/CH₂Cl₂, which proved itself as the superior alternative to standard piperidine/DMF cocktail [27]. Acylation with Pom-Gly **8** was followed by cleavage from the resin with concomitant removal of Boc protecting group which yielded desired PROTAC **13** (Scheme 2).

2.4. Antiproliferative activity and protein kinase selectivity

PROTAC **13** displayed significant antiproliferative selectivity against AML cell lines bearing FLT3-ITD mutation (MV4-11 and MOLM-13) with the GI₅₀ values ranging in nanomolar concentrations while the GI₅₀ values obtained for the FLT3-independent leukaemic cells were at least 20 times higher. Although potency of PROTAC **13** did not improve over parent **BPA311**, it maintained the selectivity towards the FLT3-ITD expressing leukaemic cells (Table 1). Importantly, a twofold difference in the GI₅₀ values measured in MV4-11 and CRBN-deficient MV4-11 [31] suggested the activity at least partly associated with CRBN-dependent mechanism of action.

The selectivity of PROTAC **13** was compared to its parent compound **BPA311** in the panel of 46 kinases across the human kinome at 100 nM concentration. The results indicated that PROTAC **13** maintained the activity of parent molecule towards FLT3 (2% residual activity in both compounds) as well as CDK9 (3% and 8% residual activity, respectively) (Fig. S2).

2.5. Cellular effects

Conventional FLT3-kinase inhibitors act through inhibition of the FLT3 autophosphorylation and subsequent dampening of its downstream signalling pathways, namely MAPK-ERK and STAT5 pathways. This results in block of proliferation of FLT3-dependent cells while such compounds do not affect other cells. However, additional effects of these compounds can be seen in the levels of FLT3 protein itself. Cells bearing

Table 1
Antiproliferative activity of PROTAC **13** and compound **BPA311** in panel of leukaemic cell lines.

cell line	GI ₅₀ ± SD (µM) ^a	
	PROTAC 13	BPA311
MV4-11	0.047 ± 0.029	0.009 ± 0.007
MV4-11 CRBN-def.	0.119 ± 0.039	0.008 ± 0.004
MOLM-13	0.042 ± 0.031	0.008 ± 0.011
RS4-11	1.014 ± 0.208	0.295 ± 0.062
HL60	6.122 ± 2.383	1.520 ± 0.074
U937	9.507 ± 0.641	0.695 ± 0.224
THP-1	9.993 ± 0.012	0.681 ± 0.139
Kasumi-1	>10	0.534 ± 0.001
CEM	>10	1.278 ± 0.073
K562	>10	2.070 ± 0.490

^a GI₅₀ determined after 72 h cultivation.

FLT3-ITD mutation are characterized by predominant intracellular localization of the immature 130-kDa form of FLT3, which is not fully glycosylated [32,33]. Long-term treatment with FLT3 inhibitors induces glycosylation, maturation, and subsequent FLT3 translocation to the cell surface and its anchoring to the cytoplasmic membrane. Moreover, these changes are linked with increased FLT3 protein levels caused by elevated FLT3 mRNA expression [33] having a potential impact on a resistance development in the long-term perspective [34]. This outcome was proved in our experiment performed on MV4-11 cells bearing the FLT3-ITD mutation (Fig. 2A). Overnight treatment with FLT3 inhibitors quizartinib and sorafenib reduced the autophosphorylation of FLT3 at Y589/591 and suppressed signalling of its downstream pathways that was proved by decreased phosphorylation of ERK1/2 at T202/Y204 as well as STAT5 at Y694. A similar effect was observed after treatment with PROTAC **13** that proved the binding of the conjugate into the FLT3 active site. Quizartinib as well as sorafenib significantly increased the total level of FLT3, on the other hand, levels of FLT3 after treatment with low nanomolar concentrations of PROTAC **13** remained comparable with endogenous levels in untreated cells; concentrations of 100 nM and higher induced FLT3 degradation. The degradation of protein levels in a concentration-dependent manner was observed also in the case of CDK9, which were not affected by quizartinib nor sorafenib. Comparable results were obtained in heterozygous FLT3-ITD cell line MOLM-13 (Fig. S3).

To confirm a CRBN-dependent mechanism of action, the previous experiment was repeated using CRBN-deficient MV4-11 (Fig. 2B and S4) [31]. Identical results were obtained with control samples of quizartinib- and sorafenib-treated cells. Both inhibitors blocked the FLT3-dependent signalling efficiently and induced upregulation of FLT3 protein. Absence of CRBN resulted in the prevention of E3 ligase engagement of PROTAC **13**. Target proteins were not ubiquitinated and their levels were not decreased by proteasome-mediated degradation. While the CDK9 levels remained unaltered, the concentration-dependent stabilization of FLT3 that is typical for FLT3 kinase inhibitors was observed.

In addition, proapoptotic effects of PROTAC **13** depending on CRBN levels in MV4-11 cells were evaluated. Activities of caspases 3 and 7, key executioner players of apoptotic cascade, were measured in MV4-11 as well as CRBN-deficient MV4-11 cells treated with PROTAC **13**, quizartinib and sorafenib for 16 h using the fluorescently labelled peptide substrate Ac-DEVD-AMC (Fig. 3). In MV4-11 cells, we observed massive concentration-dependent activation of caspases upon PROTAC **13** treatment that was in line with cleavage of protein PARP-1, a substrate of caspases (Fig. 2). Contrary to this, 100 nM concentrations of quizartinib and sorafenib showed only minimal effect on activation of caspases in MV4-11 cells. In CRBN-deficient MV4-11 cells, PROTAC **13**-induced activation of caspases was not observed and measured activities were at the endogenous level of the untreated control sample. These results were repeated by an alternative approach and complemented with MOLM-13 (FLT3-ITD) and THP-1 (FLT3 wild-type) cell lines confirming the sensitivity of FLT3-ITD bearing cells to targeted degradation of FLT3 and CDK9 (Fig. S5).

These results were also confirmed using flow cytometry analysis (Fig. S6). Although the effect of PROTAC **13** on cell cycle phase distribution was comparable between MV4-11 and CRBN-deficient MV4-11 cells, and we observed concentration-dependent increase of the cells arrested in the G1 phase of the cell cycle that is typical for FLT3 inhibition, the MV4-11 cells were far more sensitive to the treatment. Higher tested concentrations induced apoptosis in the MV4-11 cells resulting in the massive increase of the subG1 population, while the CRBN-deficient counterpart cells were not affected and the proapoptotic effect of PROTAC **13** was not confirmed in this model. These results suggest that the cells are more sensitive to degradation of the target proteins rather than only to kinase inhibition.

The effect of PROTAC **13** on CDK9, a key transcriptional regulator, has a potential to be transmitted into the reduced expression of genes

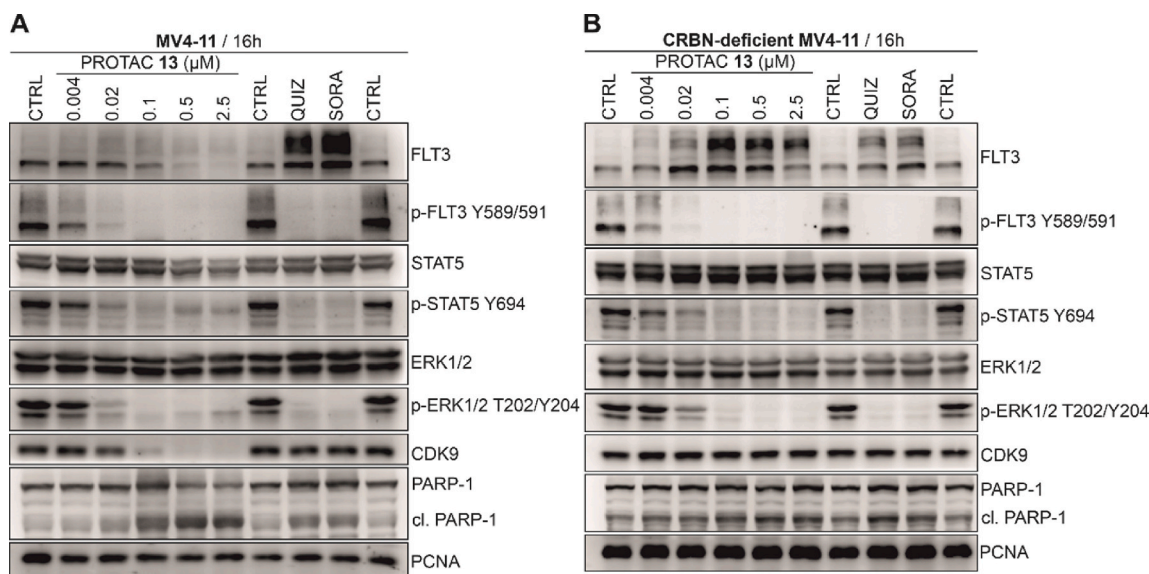


Fig. 2. Immunoblotting analysis of MV4-11 (A) and CRBN-deficient MV4-11 (B) cells treated with PROTAC 13. Quizartinib (QUIZ) and sorafenib (SORA) at 0.1 μ M concentration were used as controls.

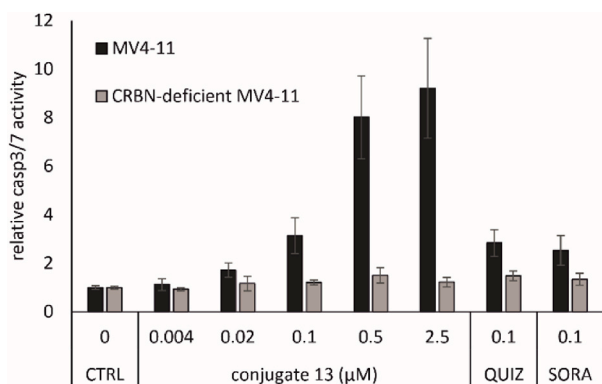


Fig. 3. Induction of apoptosis in MV4-11 and CRBN-deficient MV4-11 cells treated with PROTAC 13, quizartinib (QUIZ) and sorafenib (SORA).

involved in AML pathogenesis. To confirm this we selected genes essential for haematopoiesis, apoptosis and AML initiation including HOXA9, MEIS1, MCL-1, Bcl-2, Myc and Myb whose expression, moreover, often correlates with poor prognosis of the disease. MV4-11 cells were treated for 4 h with increasing concentrations of PROTAC 13, which showed dose-dependent ability to affect significantly the expression of all studied genes (Fig. 4). On the other hand, quizartinib and sorafenib did not show such a strong impact. These results indicate another potential therapeutic benefit of CDK9 targeting in AML. In addition, levels of FLT3 transcripts were not affected by PROTAC 13 treatment further confirming its mechanism of action.

To further verify the PROTAC-mediated mechanism of action, MV4-11 cells were pre-treated with 4-hydroxythalidomide as the CRBN ligand to limit the ternary complex formation. 4-Hydroxythalidomide itself had no impact on MV4-11 cells, levels of target proteins remained unaltered and FLT3 signalling pathway was not affected as well. PROTAC 13 induced massive degradation of FLT3 and CDK9. While the 4-hydroxythalidomide pre-treatment did not affect the binding of PROTAC 13 into the kinase active sites, as proved by inhibition of FLT3 autophosphorylation as well as reduction of downstream signalling pathways, the CRBN binding site was blocked and thus the ternary complex formation was abolished. The CDK9 degradation caused by PROTAC 13 was significantly reduced by 4-hydroxythalidomide pre-treatment, and FLT3

levels were even elevated, as is typical for standard FLT3 kinase inhibitors (Fig. 5A).

Interestingly, the proapoptotic effect of PROTAC 13 that was confirmed using caspase-3/7 fluorimetric-based assay in MV4-11 treated lysates was shown to be repressed by 4-hydroxythalidomide pre-treatment and activity of caspase-3/7 in these samples remained significantly lower (Fig. 5B). These results further proved beneficial properties of PROTAC 13.

Alternatively, PROTAC-induced effects should be abolished by proteasome inhibition. Nevertheless, proteasome inhibitors are known to induce degradation of FLT3-ITD in AML cells [35], complicating the experimental setup. We therefore decided to find a suitable compound tool which, in the proper concentration, would block proteasome activity without adverse effects on FLT3-ITD and CDK9 levels. Among the tested inhibitors (data not shown), results of MG132 at concentration of 200 nM were the most convenient. In MV4-11 cells treated with MG132 alone, we observed significantly increased levels of polyubiquitinated proteins indicating proteasome function failure, while the CDK9 and FLT3 protein levels were not decreased dramatically in comparison to untreated control cells. The observed degradation of target proteins caused by PROTAC 13 was diminished when the MV4-11 cells were pre-treated for 90 min with MG132 prior to PROTAC 13 treatment (Fig. 6). These results confirm the proteasome-dependent degradation of the target proteins caused by our conjugate.

3. Conclusion

AML belongs to the most devastating haematological malignancies whose onset was shown to be often linked to oncogenic mutations in the gene encoding FLT3. Internal tandem duplications and mutations in the kinase domain in FLT3 can be detected in a third of all patients with AML diagnosis. Although several kinase inhibitors showing potency and selectivity towards FLT3-ITD expressing AML were developed, their efficacy is often reduced by resistance development and relapse of the disease. This can be avoided by use of resistance-overcoming inhibitors of new generations or by co-targeting of FLT3 and other relevant target, which plays a role in cancer cells survival. Emerging PROTAC-mediated protein degradation offers another potential therapeutic strategy enabling elimination of oncogenic targets by a mechanism different from available competitive kinase inhibition.

By combining our previously reported FLT3/CDK9 kinase inhibitor

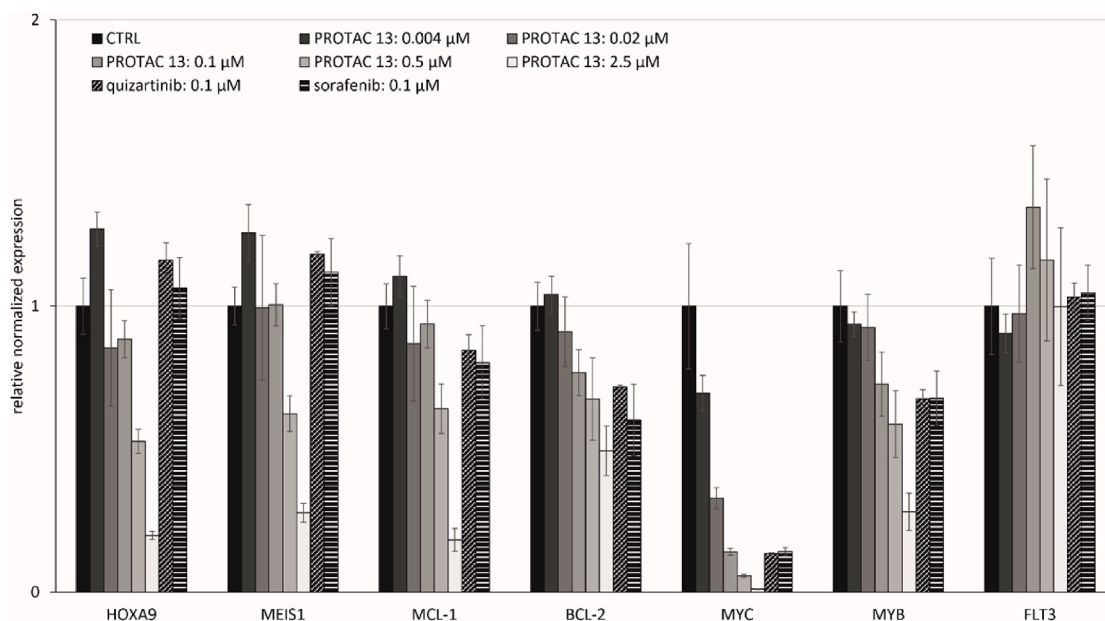


Fig. 4. Relative normalized expression of HOXA9, MEIS1, MCL-1, BCL-2, MYC, MYB and FLT3 genes in MV4-11 cells. MV4-11 cells were treated with PROTAC 13, quizartinib or sorafenib for 4 h. Gene expressions were normalized per GAPDH and RPL13A genes.

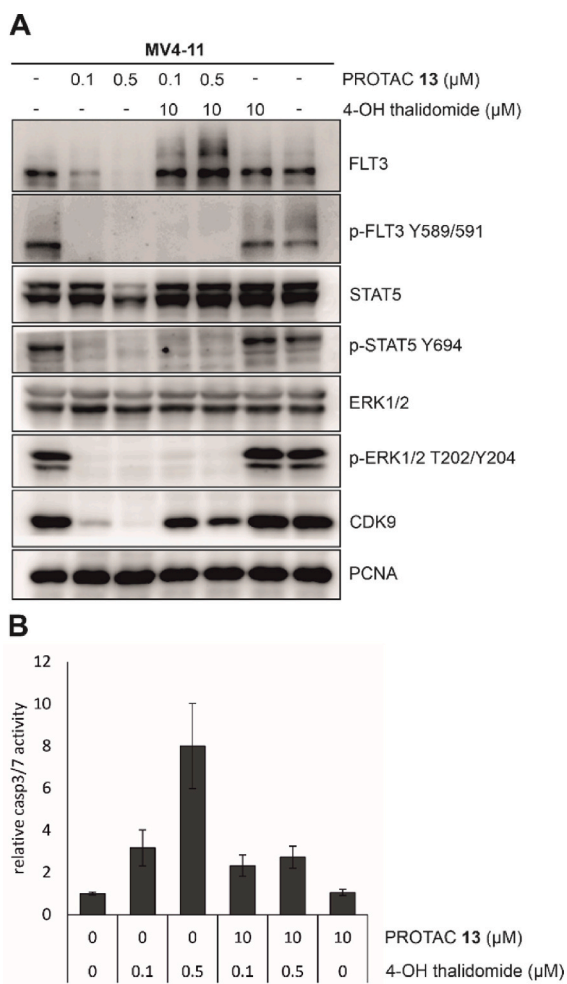


Fig. 5. Effects of PROTAC 13 on levels of FLT3 and CDK9 (A) as well as its proapoptotic activities (B) in MV4-11 cells are reversed by competition with 4-hydroxythalidomide. Cells were pre-treated with 10 μM 4-hydroxythalidomide for 90 min and treated with PROTAC 13 for further 16 h.

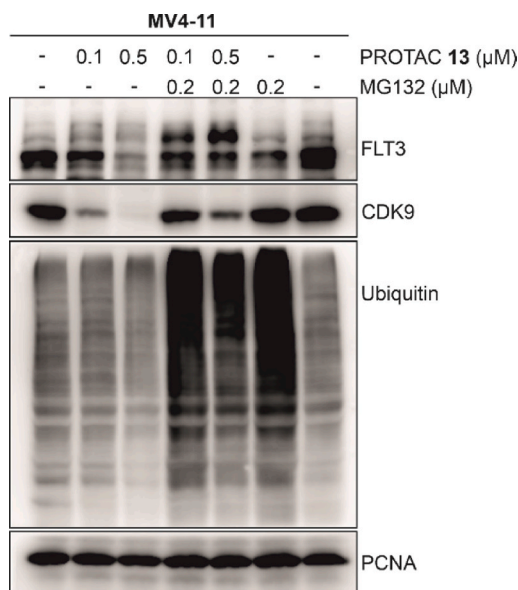


Fig. 6. Inhibition of proteasome blocks the degradation of FLT3 and CDK9 caused by PROTAC 13 in MV4-11 cells. Cells were pre-treated with 0.2 μM MG132 for 90 min and treated with PROTAC 13 for further 16 h.

with CRBN-ligand pomalidomide, we have obtained PROTAC 13 showing significant selectivity towards FLT3-ITD-mutated AML cells. Although potency of PROTAC 13 did not improve over parent inhibitor, it acted by a new CRBN-dependent mechanism of action. PROTAC 13 efficiently blocked FLT3 and its downstream signalling pathways that are important for proliferation as well as survival of FLT3-dependent leukaemic cells. In addition, transcriptional repression caused by CDK9 degradation reduced expression of genes playing crucial roles in AML pathogenesis and correlating with poor disease prognosis. Results indicate that FLT3-ITD expressing cells are more sensitive to FLT3 and CDK9 degradation caused by PROTAC 13-mediated mechanism of action than only to their kinase inhibition. This induces activation of an apoptotic cascade and cell death. We believe that the simultaneous

degradation of FLT3 and CDK9 could be the beneficial option for AML therapy.

4. Experimental section

4.1. General information

All reagents were of reagent grade and used without further purification. Solvents and chemicals were purchased from Sigma-Aldrich (US), Acros Organics (Belgium) or Fluorochem (UK). Anhydrous solvents were dried over 4 Å molecular sieves or stored as received from commercial suppliers.

Reactions on solid-phase were performed in plastic syringes, each equipped with a porous disk, using a manually operated synthesizer (Torviq, US), unless otherwise stated. The volume of wash solvent was 10 mL per 1 g of resin. For washing, resin slurry was shaken with the fresh solvent for at least 1 min before changing the solvent. Resin-bound intermediates were dried under a stream of nitrogen for prolonged storage and/or quantitative analysis. For the UHPLC-MS analysis a sample of resin (~5 mg) was treated with CH₂Cl₂/TFA (1:1, 1 mL, v/v), the cleavage cocktail was evaporated under a stream of nitrogen, and cleaved compounds extracted into CH₃CN/H₂O (1:1, 1 mL, v/v).

Reactions in solution-phase were performed in round-bottom flasks fitted with rubber septa under positive pressure of nitrogen or in ace-pressure tubes, unless otherwise stated. All reactions were monitored by UHPLC-MS analysis. Thin-layer chromatography (TLC) plates using aluminium plates precoated with silica gel (silica gel 60 F₂₅₄, Merck, US) impregnated with a fluorescent indicator were visualized by exposure to ultraviolet light ($\lambda = 254$ nm) and/or by submersion in aqueous ceric ammonium molybdate (CAM) solution followed by brief heating. Column chromatography was performed using silica gel (60 Å, 230–400 mesh, Sigma-Aldrich).

Prior to HPLC separation (column Phenomenex Gemini, 50 × 2.00 mm, 3 µm particles, C¹⁸), the samples were injected by direct infusion into the mass spectrometer using autosampler. Mobile phase was isocratic 80% CH₃CN and 20% 0.01 M ammonium acetate in H₂O or 95% methanol +5% H₂O + 0.1% formic acid and flow 0.3 mL/min.

4.2. Instrumentation

UHPLC-MS analyses were carried out on UHPLC-MS system consisting of UHPLC chromatograph Acquity with photodiode array detector and single quadrupole mass spectrometer (Waters, US), using X-Select C¹⁸ column at 30 °C and flow rate of 0.6 mL/min. Mobile phase was (A) 0.01 M ammonium acetate in H₂O, and (B) CH₃CN, linearly programmed from 10% A to 80% B over 2.5 min, kept for 1.5 min. The column was re-equilibrated with 10% of solution B for 1 min. The ESI source operated at discharge current of 5 µA, vaporizer temperature of 350 °C and capillary temperature of 200 °C. HPLC purification was carried out on C¹⁸ reverse phase column (YMC Pack ODS-A, 20 × 100 mm, 5 µm particles), gradient was formed from CH₃CN and 0.01 M ammonium acetate in H₂O, flow rate 15 mL/min. For lyophilization of residual solvents at -110 °C the ScanVac Coolsafe 110-4 was used.

HRMS analyses were performed using LC chromatograph (Dionex Ultimate 3000, Thermo Fischer Scientific, US) and Exactive Plus Orbitrap high-resolution mass spectrometer (Thermo Fischer Scientific, US) operating at positive full scan mode (120 000 FWHM) in the range of 100–2000 *m/z*. The settings for electrospray ionization were as follows: oven temperature of 150 °C and source voltage of 3.6 kV. The acquired data were internally calibrated with phthalate as a contaminant in methanol (*m/z* 297.15909). Samples were diluted to a final concentration of 0.1 mg/mL in CH₃CN/H₂O (9:1, v/v).

NMR spectra were recorded on JEOL ECX500 spectrometer at magnetic field strengths of 11.75 T with operating frequencies 500.16 MHz (for ¹H) and 125.77 MHz (for ¹³C) at 27 °C. Chemical shifts (δ) are reported in parts per million (ppm) and coupling constants (*J*) are reported

in Hertz (Hz). The ¹H and ¹³C NMR chemical shifts (δ in ppm) were referenced to the residual signals of DMSO-*d*₆ [2.50 (¹H) and 39.52 (¹³C)]. The residual signal of ammonium acetate (from HPLC purification) exhibited signal at 1.90 ppm (¹H) and at 21.3 ppm and 172.0 ppm (¹³C). Abbreviations in NMR spectra: app – apparent, br s – broad singlet, d – doublet, dd – doublet of doublets, m – multiplet, p – pentet, s – singlet, t – triplet.

4.3. Experimental procedures

4.3.1. Procedure for benzylation

To a stirred solution of 1-(4-nitrophenyl)piperazine **1** (1 g, 4.83 mmol, 1 eq) in anhydrous DMF/CH₃CN (3:1, 15 mL, v/v) were added benzyl bromide (860 µL, 7.24 mmol, 1.5 eq) and K₂CO₃ (1.3 g, 9.66 mmol, 2 eq). The reaction mixture was stirred at 50 °C for 3 h after which UHPLC-MS confirmed full conversion to compound **2**. The reaction mixture was concentrated, diluted with aq. NH₄Cl (250 mL), and extracted with EtOAc (3 × 250 mL). Organic extracts were combined, dried over MgSO₄, filtered, and evaporated under reduced pressure. The crude product was purified by column chromatography (CH₂Cl₂/EtOAc 1:1, v/v) to afford compound **2** as yellow solid (931 mg, 65% yield).

4.3.2. Procedure for reduction of nitro group

The starting material **2** (359 mg, 1.21 mmol, 1 eq) was dissolved in a mixture of anhydrous ethanol/THF (3:1, 8 mL v/v) and properly flushed with nitrogen for 15 min. Then, PtO₂ (192 mg, 0.85 mmol, 0.7 eq) was added, and the resulting mixture was stirred at ambient temperature under positive pressure of hydrogen. UHPLC-MS analysis was used to confirm the full conversion to the corresponding product after 90 min. The reaction mixture was diluted with methanol, and residual PtO₂ was filtered off. The residual solvents were evaporated under reduced pressure, and crude product **3** (510 mg, 1.91 mmol) was used to the next step without further purification.

4.3.3. Procedure for alkylation of 2,6-dichloropurine

2,6-dichloro-9-cyclopentyl purine was prepared by previously published procedure [29].

4.3.4. Procedure for aromatic nucleophilic substitution with **3**

To a stirred solution of **3** (510 mg, 1.91 mmol, 1.1 eq) in anhydrous DMSO (8 mL) were added 2,6-dichloro-9-cyclopentyl purine (446 mg, 1.73 mmol, 1 eq) and DIPEA (315 µL, 1.91 mmol, 1.1 eq). The reaction mixture was stirred at 120 °C for 16 h after which UHPLC-MS confirmed full conversion to product **4**. The reaction mixture was cooled down to ambient temperature, diluted with aq. NH₄Cl (200 mL), and extracted with EtOAc (3 × 200 mL). Organic extracts were combined, dried over MgSO₄, filtered and evaporated under reduced pressure. The crude product was purified by column chromatography (CH₂Cl₂/MeOH gradually eluted from 15:1 to 5:1, v/v) to afford compound **4** as pale brown solid (501 mg, 60% yield).

4.3.5. Procedure for aromatic nucleophilic substitution with diamine

Starting material **4** (254 mg, 0.52 mmol, 1 eq) in ace-pressure tube was dissolved in diethylene glycol diethyl ether (4 mL). Then, solid *trans*-1,4-diamino cyclohexane (2.9 g, 26 mmol, 50 eq) was added at once to the solution of starting material, followed by addition of DIPEA (2.5 mL). The reaction mixture was vigorously stirred at 160 °C for 22 h after which UHPLC-MS confirmed full conversion to product **5**. The reaction mixture was cooled down to ambient temperature, diluted with CH₃CN (20 mL) upon which residual solid precipitated and was filtered off. The residual solvents were concentrated under reduced pressure and lyophilized overnight. The crude product was purified by column chromatography (CH₂Cl₂/7 M NH₃ in MeOH 10:1, v/v) to afford compound **5** as pale brown solid (200 mg, 67% yield).

4.3.6. Procedure for protection with Boc

To a stirred solution of starting material **5** (126 mg, 0.22 mmol, 1 eq) and Et₃N (50 μ L, 0.35 mmol, 1.6 eq) in anhydrous THF (2 mL) at 0 °C was added DMAP (4 mg, 0.03 mmol, 15 mol%) in anhydrous THF (500 μ L). The reaction mixture was stirred for 3 min when solution of Boc₂O (60 mg, 0.27 mmol, 1.2 eq) in anhydrous THF (500 μ L) was added and the mixture was warmed up to ambient temperature. The reaction mixture was stirred for 16 h after which UHPLC-MS confirmed full conversion to product **6**. The residual solvents were evaporated under reduced pressure and crude product was purified by column chromatography (CH₂Cl₂/MeOH 10:1, v/v) to obtain compound **6** as colourless oil (135 mg, 92% yield).

4.3.7. Procedure for cleavage of benzyl group

To a stirred solution of NH₄HCO₂ (504 mg, 8 mmol) in anhydrous ethanol (15 mL) was added solution of starting material **6** (146 mg, 0.22 mmol, 1 eq) in anhydrous ethanol (5 mL) and palladium on activated charcoal (10% of Pd, 26 mg, 0.24 mmol, 1.1 eq). The resulting mixture was stirred at 80 °C for 36–42 h after which UHPLC-MS confirmed full conversion to product **7**. The reaction mixture was cooled down to ambient temperature, diluted with ethanol and residual catalyst was filtered off. The solvents were evaporated, and the crude product was purified by column chromatography (CH₂Cl₂/MeOH gradually eluted from 15:1 to 5:1, v/v) to obtain compound **7** as a pale yellow solid (86 mg, 68% yield).

4.3.8. Procedure for reductive amination in solution phase

Pomalidomide (250 mg, 0.92 mmol, 1 eq) was dissolved in THF (15 mL), followed by addition of glyoxylic acid monohydrate (421 mg, 4.57 mmol, 5 eq) and Bu₂SnCl₂ (278 mg, 0.92 mmol, 1 eq). The mixture was vigorously stirred for 20 min at ambient temperature and then phenyl silane (562 μ L, 4.57 mmol, 5 eq) was slowly added. The reaction mixture was heated up to reflux and stirred for 22 h after which UHPLC-MS analysis confirmed full conversion to product **8**. The mixture was cooled down to ambient temperature, diluted with aq. NH₄Cl (200 mL) and extracted with EtOAc (3 \times 200 mL). Organic extracts were combined, dried over MgSO₄, filtered and evaporated under reduced pressure. The crude product was purified by column chromatography (CH₂Cl₂/MeOH/AcOH 10:1:0.2, v/v) to afford compound **8** as yellow solid (260 mg, 86% yield).

4.3.9. Procedure for preparation of BAL resin

Amino methyl polystyrene resin (1 g, loading 0.98 mmol/g) was swollen in CH₂Cl₂ (10 mL) for 30 min, washed with DMF (3 \times 10 mL), neutralized in DMF/piperidine (5:1, 10 mL) for additional 30 min and then again washed with DMF (5 \times 10 mL). 4-(4-formyl-3-methoxyphenoxy)butanoic acid (700 mg, 2.94 mmol) and HOBt (450 mg, 2.94 mmol) were dissolved in DMF/CH₂Cl₂ (1:1, 10 mL, v/v) and DIC (460 μ L, 2.94 mmol) was added. The resulting solution was added to the polypropylene fritted syringe with amino methyl polystyrene resin. The reaction slurry was shaken at ambient temperature for 16 h, followed by wash with DMF (3 \times 10 mL) and CH₂Cl₂ (3 \times 10 mL). Negative bromophenol blue test confirmed quantitative acylation of the resin.

4.3.10. Procedure for reductive amination and Fmoc-protection on solid-phase

BAL resin **9** (500 mg, loading 0.98 mmol/g) was swollen in CH₂Cl₂ (5 mL) for 30 min, then washed with anhydrous THF (3 \times 5 mL) and anhydrous DMF (3 \times 5 mL). The solution of 2-(2-(2-aminoethoxy)ethoxy)ethan-1-ol (338 μ L, 2.45 mmol) in DMF/AcOH (10:1, 5 mL, v/v) was added to polypropylene fritted syringe with BAL resin **9** and it was shaken for 16 h at ambient temperature. Then, NaBH(OAc)₃ (309 mg, 1.47 mmol) in DMF/AcOH (20:1, 5 mL, v/v) was added portion wise (3 \times 103 mg) to the reaction mixture during the period of 4 h. The reaction slurry was shaken at ambient temperature for 16 h, followed by washing with DMF (5 \times 5 mL), CH₂Cl₂ (3 \times 5 mL), neutralization with DMF/Et₃N

(10:1, 5 mL, v/v) for additional 30 min and final wash with CH₂Cl₂ (3 \times 5 mL). Fmoc-OSu (1 g, 3 mmol) was dissolved in CH₂Cl₂ (5 mL) and added to the polypropylene fritted syringe with resin. The reaction slurry was shaken at ambient temperature for 16 h, followed by washing with CH₂Cl₂ (5 \times 5 mL). Subsequent cleavage from the resin and UHPLC-MS analysis confirmed the presence of desired product **10**. (ESI+ 373, 469 (trifluoroacetate)) Loading after this step (0.40 mmol/g) was determined as follows: the sample of resin **10** (~30 mg) was washed with CH₂Cl₂ (5 \times 3 mL) and MeOH (3 \times 3 mL), dried under a stream of nitrogen and divided into two portions (2 \times 12 mg). Both samples were treated with CH₂Cl₂/TFA (1:1, 1 mL, v/v) for 1 h, after which the cleavage cocktail was evaporated under a stream of nitrogen. Cleaved compounds were dissolved in CH₃CN/H₂O (1:1, 1 mL, v/v), diluted four times, and analyzed by ultra-high performance liquid chromatography coupled with mass spectrometry and ultraviolet detection (UHPLC/MS/UV). Loading of the resin was calculated with the use of an external standard (Fmoc-Ala-OH, 0.5 mg/mL).

4.3.11. Procedure for tosylation

Resin **10** (500 mg) was swollen in CH₂Cl₂ (5 mL) for 30 min and then washed with CH₂Cl₂ (3 \times 5 mL). Tosyl chloride (285 mg, 1.5 mmol), Et₃N (209 μ L, 1.5 mmol) and DMAP (61 mg, 0.5 mmol) were dissolved in dry CH₂Cl₂ (5 mL) and added to the propylene fritted syringe with resin **10**. The reaction slurry was shaken at ambient temperature for 16 h, followed by washing with DMF (5 \times 5 mL) and CH₂Cl₂ (3 \times 5 mL). Subsequent cleavage from the resin and UHPLC-MS analysis confirmed the presence of desired product **11**. (ESI+ 527).

4.3.12. Procedure for nucleophilic substitution with 7

Resin **11** (250 mg) was swollen in CH₂Cl₂ (5 mL) for 30 min, washed with CH₂Cl₂ (3 \times 5 mL) and added to the ace-pressure tube with solution of purine ligand **7** (86 mg, 0.15 mmol) and DIPEA (247 μ L, 1.5 mmol) in DMF (2.5 mL). The reaction slurry was stirred at 70 °C for 16 h, followed by washing with DMF (5 \times 5 mL) and CH₂Cl₂ (3 \times 5 mL). Subsequent cleavage from the resin and UHPLC-MS analysis confirmed the presence of desired product **12**. (ESI- 828).

4.3.13. Procedure for deprotection of Fmoc on resin

Resin (250 mg) was swollen in CH₂Cl₂ (3 mL) for 30 min and then washed with DMF (3 \times 3 mL). The freshly prepared solution of CH₂Cl₂/DBU (1:1, 3 mL, v/v) was added to polypropylene fritted syringe with the resin. The reaction slurry was shaken at ambient temperature for 10 min, followed by washing with CH₂Cl₂ (3 \times 3 mL), THF (3 \times 3 mL) and CH₂Cl₂ (3 \times 3 mL). Resin was used directly into the next step without further analysis.

4.3.14. Procedure for acylation with 8 and final cleavage from the resin

Resin **12** (250 mg) was swollen in CH₂Cl₂ (3 mL) for 30 min and then washed with CH₂Cl₂ (3 \times 3 mL). Pom-Gly **8** (165 mg, 0.5 mmol) and HOBt (72 mg, 0.5 mmol) were dissolved in DMF (2.5 mL), followed by addition of DIC (80 μ L, 0.5 mmol). The mixture was added to the propylene fritted syringe with resin **12** and the reaction slurry was shaken at ambient temperature for 16 h, followed by washing with DMF (5 \times 5 mL) and CH₂Cl₂ (3 \times 5 mL). Subsequent cleavage from the resin and UHPLC-MS analysis confirmed the presence of desired product **13**.

4.3.15. Final cleavage from the resin prior to HPLC purification

The corresponding resin (250 mg) was swollen in CH₂Cl₂ (3 mL). Solution of CH₂Cl₂/TFA (1:1, 6 mL, v/v) was added to polypropylene fritted syringe with resin. The reaction slurry was shaken at ambient temperature for 2 h and then washed with CH₂Cl₂/TFA (1:1, 3 \times 3 mL, v/v) and CH₂Cl₂ (3 \times 3 mL). The cleavage cocktail with combined washes were evaporated under a stream of nitrogen, the crude product was dissolved in CH₃CN/H₂O (3:1, 5 mL, v/v) and purified by RP-HPLC to afford final compound **13** as yellowish oil (2 mg, 2% overall yield calculated from **10**).

4.4. Molecular modeling

Molecular docking of **BPA311** was performed with the FLT3 DFG-in model published previously [21] and with crystal structure of phosphorylated CDK9/cyclin T (PDB: 7NWK) co-crystalised with imidazo[4,5-*b*]pyridine ATP-competitive inhibitor.

Next, we prepared 3D structures of FLT3-CRBN and CDK9-CRBN based on a previously published crystal complexes of BRD4-CRBN and BTK-CRBN [36] constructed by molecular modelling in PROsettaC [37]. BTK was replaced by FLT3 or CDK9 based on structural alignment and homologous complexes with increasing distance between kinase domain and CRBN were obtained. These complexes were used as targets for docking of the PROTAC to find the optimal distance between the kinase and CRBN proteins in which both heads of the PROTAC were oriented properly with same interactions as in docking into protein monomers. The 3D structures of all compounds were obtained and their energy was minimized by molecular mechanics with Avogadro 1.90.0, a software for the characterization of chemical structures. Polar hydrogens were added to ligands and proteins with the AutoDock Tools program [38] and docking studies were performed using AutoDock Vina 1.05 [39]. Figures were generated using Pymol ver. 2.0.4 (Schrödinger, LLC).

4.5. Kinase-selectivity profiling

Protein kinase selectivity of **BPA311** and PROTAC **13** was evaluated at a single concentration (100 nM) by screening against 46 enzymes at Eurofins Discovery.

4.6. Cell cultures and viability assay

Human cell lines were obtained from the German Collection of Microorganisms (MOLM-13, RS4-11, Kasumi-1, THP-1, U937), European Collection of Authenticated Cell Cultures (K562), Cell lines service (MV4-11) or were generously gifted by G. E. Winter (CRBN-deficient MV4-11) and were cultivated according to the provider's instructions. Briefly, cells were maintained in RPMI-1640 medium (or DMEM for K562) supplemented with 10% fetal bovine serum, penicillin (100 U/mL), and streptomycin (0.1 mg/mL) at 37 °C in 5% CO₂.

For the viability assays, cells were treated in triplicate with six different doses of each compound for 72 h. After treatments, resazurin (Sigma Aldrich) solution was added for 4 h, and fluorescence of resorufin corresponding to live cells was measured at 544 nm/590 nm (excitation/emission) using a Fluoroskan Ascent microplate reader (Labsystems). The GI₅₀ value, the drug concentration lethal to 50% of the cells, was calculated from the dose response curves that resulted from the assays.

4.7. Immunoblotting

Cell lysates were prepared, and then proteins were separated on SDS-polyacrylamide gels and electroblotted onto nitrocellulose membranes. After blocking, overnight incubation with specific primary antibodies, and incubation with peroxidase-conjugated secondary antibodies, peroxidase activity was detected with Super-Signal West Pico reagents (Thermo Scientific) using a CCD camera LAS-4000 (Fujifilm). The specific antibodies were purchased from Cell signaling (anti-FLT3, clone 8F2; anti-phospho-FLT3 Y589/591, clone 30D4; anti-STAT5; anti-phospho-STAT5 Y694; anti-ERK1/2; anti-phospho-ERK1/2 T202/Y204; anti-PARP-1, clone 46D11; peroxidase-conjugated secondary antibodies), Santa Cruz Biotechnology (anti-CDK9, clone D-7), DAKO (anti-ubiquitin), Atlas Antibodies (anti-CRBN) or were generously gifted by Dr. B. Vojtěšek (anti-PCNA, clone PC-10).

4.8. Flow cytometry

Asynchronously growing cells were seeded and, after a

preincubation period, treated with tested compounds for 24 h. After the staining with propidium iodide, DNA content was analyzed by flow cytometry using a 488 nm laser (BD FACS Verse with software BD FACSuite™, version 1.0.6.). Cell cycle distribution was analyzed using ModFit LT (Verity Software House).

4.9. Caspase 3/7 assay

Cell lysates were incubated with 100 μM Ac-DEVD-AMC (Enzo Life Sciences) as a substrate of caspases 3 and 7 in the assay buffer (25 mM PIPES, 2 mM EGTA, 2 mM MgCl₂, 5 mM DTT, pH 7.3). The fluorescence of the product was measured using a Fluoroskan Ascent microplate reader (Labsystems) at 355/460 nm (ex/em).

Alternatively, cellular caspase-3/7 activity was measured according to a previously published procedure [40]. Cells were cultivated in a 96-well plate and treated with increasing concentrations of compounds for 16 h. After incubation, 3 × caspase-3/7 assay buffer (150 mM HEPES pH 7.4, 450 mM NaCl, 150 mM KCl, 30 mM MgCl₂, 1.2 mM EGTA, 1.5% Nonidet P40, 0.3% CHAPS, 30% sucrose, 30 mM DTT, 3 mM PMSF) containing 150 μM peptide substrate Ac-DEVD-AMC (Enzo Life Sciences) was added. After 4 h incubation, the caspase-3/7 activity was measured using a Fluoroskan Ascent microplate reader (Labsystems) at 346 nm/442 nm (ex/em).

4.10. RNA isolation and qPCR

Total RNA was isolated using RNeasy plus mini kit (QIAGEN) according to the manufacturer's instruction, and RNA concentration and purity was measured by DeNovix DS-11 spectrophotometer. RNA was transcribed into first-strand cDNA using SensiFast cDNA Synthesis Kit (Bioline). Quantitative RT-PCR was carried out on CFX96 Real-Time PCR Detection System (Biorad) with a SensiFAST SYBR No-Rox Kit (Bioline). The suitable primers were designed using Primer-BLAST [41] and synthesized by Geni Biotech. Primary data were analyzed using Bio-rad CFX Manager. Relative gene expression levels were determined using delta delta Ct method [42]. Expressions were normalized per GAPDH and RPL13A genes which were determined as the most stable by RefFinder Software [43].

Used primers: BCL-2 (F: ATGTGTGTGGAGAGCGTCA; R: ACAGC-CAGGAGAAATCAAACAG); FLT3 (F: GGAATGGGTGCTTTGCGATT; R: CAGCACCTTATGTCCGTC); GAPDH (F: TCCAAAAT-CAAGTGGGGCGA; R: TGGTTCACACCCATGACGAA); HOXA9 (F: CCTGACTGACTATGCTTGTGGT; R: ACTCTTTCTCCAGTCCAGGG); MEIS-1 (F: CGTCACAAAAGCGTGCCAT; R: ATGGT-GAGTCCCGTGTCTTG); MCL-1 (F: AGTTGTACCGGCAGTCG; R: TTTGATGTCCAGTTTCCGAAG); MYB (F: TCTCCAGTCATGTTCCA-TACCC; R: TGTGTGTTCTGTGTGGTAGC); MYC (F: TACAA-CACCCGAGCAAGGAC; R: AGCTAACGTTGAGGGGCATC); RPL13A (F: CGACAAGAAAAGCGGATGG; R: TTCTCTTCTCTCTCTCTCC).

Author contributions

E.Ř., M.P. and M.K. performed cellular experiments, S.K. and M.S. prepared and analyzed compounds, M.P. and V.K. analyzed binding modes, E.Ř., S.K., M.S. and V.K. designed the study and wrote the manuscript.

Declaration of competing interest

The authors declare that they have no known competing financial interests or personal relationships that could have appeared to influence the work reported in this paper.

Data availability

Data will be made available on request.

Acknowledgements

Authors thank Georg E. Winter for providing CRBN-deficient MV4-11 cells and Sophie Day-Riley for grammar proofreading corrections. The work was supported by the European Union - Next Generation EU (The project National Institute for Cancer Research, Programme EXCELES, ID No. LX22NPO5102), Czech Science Foundation (19-09086S) and Palacký University Olomouc (IGA_2022_007).

Appendix A. Supplementary data

Supplementary data to this article can be found online at <https://doi.org/10.1016/j.ejmech.2022.114792>.

References

- H. Döhner, D.J. Weisdorf, C.D. Bloomfield, Acute myeloid leukemia, *N. Engl. J. Med.* 373 (2015) 1136–1152, <https://doi.org/10.1056/NEJMra1406184>.
- R.M. Shallis, R. Wang, A. Davidoff, X. Ma, A.M. Zeidan, Epidemiology of acute myeloid leukemia: recent progress and enduring, *Blood Rev.* 36 (2019) 70–87, <https://doi.org/10.1016/j.blre.2019.04.005>.
- J.U. Kazi, L. Rönstrand, FMS-Like tyrosine kinase 3/FLT3: from basic science to clinical implications, *Physiol. Rev.* 99 (2019) 1433–1466, <https://doi.org/10.1152/physrev.00029.2018>.
- M. Levis, Midostaurin approved for FLT3-mutated AML, *Blood* 129 (2017) 3403–3406, <https://doi.org/10.1182/blood-2017-05-782292>.
- S. Dhillon, Gilteritinib: first global approval, *Drugs* 79 (2019) 331–339, <https://doi.org/10.1007/s40265-019-1062-3>.
- K. Kidoguchi, M. Shibusawa, T. Tanimoto, A critical appraisal of Japan's new drug approval process: a case study of FLT3-ITD inhibitor quizartinib, *Invest. N. Drugs* 39 (2021) 1457–1459, <https://doi.org/10.1007/s10637-021-01151-0>.
- M. Wu, C. Li, X. Zhu, FLT3 inhibitors in acute myeloid leukemia, *J. Hematol. Oncol.* 11 (2018) 133, <https://doi.org/10.1186/s13045-018-0675-4>.
- S.S.Y. Lam, A.Y.H. Leung, Overcoming resistance to FLT3 inhibitors in the treatment of FLT3-mutated AML, *Int. J. Mol. Sci.* 21 (2020) 1537, <https://doi.org/10.3390/ijms21041537>.
- K.M. Sakamoto, K.B. Kim, A. Kumagai, F. Mercurio, C.M. Crews, R.J. Deshaies, Protacs: chimeric molecules that target proteins to the Skp1-Cullin-F box complex for ubiquitination and degradation, *Proc. Natl. Acad. Sci. USA* 98 (2001) 8554–8559, <https://doi.org/10.1073/pnas.141230798>.
- S.J. Hughes, A. Testa, N. Thompson, I. Churcher, The rise and rise of protein degradation: opportunities and challenges ahead, *Drug Discov. Today* 26 (2021) 2889–2897, <https://doi.org/10.1016/j.drudis.2021.08.006>.
- H.T. Huang, D. Dobrovolsky, J. Paulk, G. Yang, E.L. Weisberg, Z.M. Doctor, D. L. Buckley, J.H. Cho, E. Ko, J. Jang, K. Shi, H.G. Choi, J.D. Griffin, Y. Li, S.P. Treon, E.S. Fischer, J.E. Bradner, L. Tan, N.S. Gray, A chemoproteomic approach to query the degradable kinome using a multi-kinase degrader, *Cell Chem. Biol.* 25 (2018) 88–99, <https://doi.org/10.1016/j.chembiol.2017.10.005>, e6.
- G.M. Burslem, J. Song, X. Chen, J. Hines, C.M. Crews, Enhancing antiproliferative activity and selectivity of a FLT-3 inhibitor by proteolysis targeting chimera conversion, *J. Am. Chem. Soc.* 140 (2018) 16428–16432, <https://doi.org/10.1021/jacs.8b10320>.
- S. Cao, L. Ma, Y. Liu, M. Wei, Y. Yao, C. Li, R. Wang, N. Liu, Z. Dong, X. Li, M. Li, X. Wang, C. Yang, G. Yang, Proteolysis-targeting chimera (PROTAC) modification of dovitinib enhances the antiproliferative effect against FLT3-ITD-positive acute myeloid leukemia cells, *J. Med. Chem.* 64 (2021) 16497–16511, <https://doi.org/10.1021/acs.jmedchem.1c00996>.
- Y. Chen, X. Yuan, M. Tang, M. Shi, T. Yang, K. Liu, D. Deng, L. Chen, Degrading FLT3-ITD protein by proteolysis targeting chimera (PROTAC), *Bioorg. Chem.* 119 (2022), 105508, <https://doi.org/10.1016/j.bioorg.2021.105508>.
- S. Boffo, A. Damato, L. Alfano, A. Giordano, CDK9 inhibitors in acute myeloid leukemia, *J. Exp. Clin. Cancer Res.* 37 (2018) 36, <https://doi.org/10.1186/s13046-018-0704-8>.
- X. Han, N. Song, A. Saidahmatov, P. Wang, Y. Wang, X. Hu, W. Kan, W. Zhu, L. Gao, M. Zeng, Y. Wang, C. Li, J. Li, H. Liu, Y. Zhou, J. Wang, Rational design and development of novel CDK9 inhibitors for the treatment of acute myeloid leukemia, *J. Med. Chem.* 64 (2021) 14647–14663, <https://doi.org/10.1021/acs.jmedchem.1c01148>.
- T. Yin, M.J. Lallena, E.L. Kreklau, K.R. Fales, S. Carballares, R. Torres, G. N. Wshart, R.T. Ajamie, D.M. Cronier, P.W. Iversen, T.I. Meier, R.T. Foreman, D. Zeckner, S.E. Sissons, B.W. Halstead, A.B. Lin, G.P. Donoho, Y. Qian, S. Li, S. Wu, A. Aggarwal, X.S. Ye, J.J. Starling, R.B. Gaynor, A. de Dios, J. Du, A novel CDK9 inhibitor shows potent antitumor efficacy in preclinical hematologic tumor models, *Mol. Cancer Therapeut.* 13 (2014) 1442–1456, <https://doi.org/10.1158/1535-7163.MCT-13-0849>.
- A.T. Anshabo, L. Bantie, S. Diab, J. Lenjisa, A. Kebede, Y. Long, G. Heinemann, J. Karanjia, B. Noll, S.K.C. Basnet, M. Li, R. Milne, H. Albrecht, S. Wang, An orally bioavailable and highly efficacious inhibitor of CDK9/FLT3 for the treatment of acute myeloid leukemia, *Cancers* 14 (2022) 1113, <https://doi.org/10.3390/cancers14051113>.
- D.C. Phillips, S. Jin, G.P. Gregory, Q. Zhang, J. Xue, X. Zhao, J. Chen, Y. Tong, H. Zhang, M. Smith, S.K. Tahir, R.F. Clark, T.D. Penning, J.R. Devlin, J. Shortt, E. D. Hsi, D.H. Albert, M. Konopleva, R.W. Johnstone, J.D. Levenson, A.J. Souers, A novel CDK9 inhibitor increases the efficacy of venetoclax (ABT-199) in multiple models of hematologic malignancies, *Leukemia* 34 (2020) 1646–1657, <https://doi.org/10.1038/s41375-019-0652-0>.
- D.A. Luedtke, Y. Su, J. Ma, X. Li, S.A. Buck, H. Edwards, L. Polin, J. Kushner, S. H. Dzinic, K. White, H. Lin, J.W. Taub, Y. Ge, Inhibition of CDK9 by voruciclib synergistically enhances cell death induced by the Bcl-2 selective inhibitor venetoclax in preclinical models of acute myeloid leukemia, *Signal Transduct. Targeted Ther.* 5 (2020) 17, <https://doi.org/10.1038/s41392-020-0112-3>.
- T. Gucký, E. Řezníčková, T. Radošová Muchová, R. Jorda, Z. Klejová, V. Malínková, K. Berka, V. Bazgier, H. Ajani, M. Lepšík, V. Divoký, V. Krýstof, Discovery of N-2-(4-Amino-cyclohexyl)-9-cyclopentyl-N 6-(4-morpholin-4-ylmethyl-phenyl)-9H-purine-2,6-diamine as a potent FLT3 kinase inhibitor for acute myeloid leukemia with FLT3 mutations, *J. Med. Chem.* 61 (2018) 3855–3869, <https://doi.org/10.1021/acs.jmedchem.7b01529>.
- T. Gucký, R. Jorda, M. Zatloukal, V. Bazgier, K. Berka, E. Řezníčková, T. Béres, M. Strnad, V. Krýstof, A novel series of highly potent 2,6,9-trisubstituted purine cyclin-dependent kinase inhibitors, *J. Med. Chem.* 56 (2013) 6234–6247, <https://doi.org/10.1021/jm4006884>.
- R. Jorda, L. Havlíček, A. Šturd, D. Tušková, L. Daumová, M. Alam, J. Škerlová, M. Nekardová, M. Peřina, T. Pospíšil, J. Široká, L. Urbánek, P. Pachel, P. Řezáčová, M. Strnad, P. Klener, V. Krýstof, 3,5,7-Substituted pyrazolo[4,3-d]pyrimidine inhibitors of cyclin-dependent kinases and their evaluation in lymphoma models, *J. Med. Chem.* 62 (2019) 4606–4623, <https://doi.org/10.1021/acs.jmedchem.9b00189>.
- D. Dalgarno, T. Stehle, S. Narula, P. Schelling, M.R. van Schravendijk, S. Adams, L. Andrade, J. Keats, M. Ram, L. Jin, T. Grossman, I. MacNeil, C. Metcalf 3rd, W. Shakespeare, Y. Wang, T. Keenan, R. Sundaramoorthi, R. Bohacek, M. Weigle, T. Sawyer, Structural basis of Src tyrosine kinase inhibition with a new class of potent and selective trisubstituted purine-based compounds, *Chem. Biol. Drug Des.* 67 (2006) 46–57, <https://doi.org/10.1111/j.1747-0285.2005.00316.x>.
- D.P. Bondeson, B.E. Smith, G.M. Burslem, A.D. Buhimschi, J. Hines, S. Jaime-Figueroa, J. Wang, B.D. Hamman, A. Ishchenko, C.M. Crews, Lessons in PROTAC design from selective degradation with a promiscuous warhead, *Cell Chem. Biol.* 25 (2018) 78–87, <https://doi.org/10.1016/j.chembiol.2017.09.010>, e5.
- B.E. Smith, S.L. Wang, S. Jaime-Figueroa, A. Harbin, J. Wang, B.D. Hamman, C. M. Crews, Differential PROTAC substrate specificity dictated by orientation of recruited E3 ligase, *Nat. Commun.* 10 (2019) 131, <https://doi.org/10.1038/s41467-018-08027-7>.
- S. Krajčovičová, R. Jorda, D. Hendrychová, V. Krýstof, M. Sural, Solid-phase synthesis for thalidomide-based proteolysis-targeting chimeras (PROTAC), *Chem. Commun.* 55 (2019) 929–932, <https://doi.org/10.1039/c8cc08716d>.
- C.M. Olson, B. Jiang, M.A. Erb, Y. Liang, Z.M. Doctor, Z. Zhang, T. Zhang, N. Kwiatkowski, M. Boukhali, J.L. Green, W. Haas, T. Nomanbhoy, E.S. Fischer, R. A. Young, J.E. Bradner, G.E. Winter, N.S. Gray, Pharmacological perturbation of CDK9 using selective CDK9 inhibition or degradation, *Nat. Chem. Biol.* 14 (2018) 163–170, <https://doi.org/10.1038/nchembio.2538>.
- S. Krajčovičová, T. Gucký, D. Hendrychová, V. Krýstof, M. Sural, A stepwise approach for the synthesis of folic acid conjugates with protein kinase inhibitors, *J. Org. Chem.* 82 (2017) 13530–13541, <https://doi.org/10.1021/acs.joc.7b02650>.
- S. Krajčovičová, J. Hlaváč, K. Vychodilová, Polymer-supported synthesis of N-substituted anthranilates as the building blocks for preparation of N-arylated 3-hydroxyquinolin-4(1H)-ones, *RSC Adv.* 11 (2021) 9362–9365, <https://doi.org/10.1039/d1ra01308d>.
- M. Brand, B. Jiang, S. Bauer, K.A. Donovan, Y. Liang, E.S. Wang, R.P. Nowak, J. C. Yuan, T. Zhang, N. Kwiatkowski, C.A. Müller, E.S. Fischer, N.S. Gray, G. E. Winter, Homolog-selective degradation as a strategy to probe the function of CDK6 in AML, *Cell Chem. Biol.* 26 (2019) 300–306, <https://doi.org/10.1016/j.chembiol.2018.11.006>, e9.
- D.E. Schmidt-Arras, A. Böhmer, B. Markova, C. Choudhary, H. Serve, F.D. Böhmer, Tyrosine phosphorylation regulates maturation of receptor tyrosine kinases, *Mol. Cell Biol.* 25 (2005) 3690–3703, <https://doi.org/10.1128/MCB.25.9.3690-3703.2005>.
- K. Reiter, H. Polzer, C. Krupka, A. Maiser, B. Vick, M. Rothenberg-Thurley, K. H. Metzler, D. Dörfel, H.R. Salih, G. Jung, E. Nößner, I. Jeremias, W. Hiddemann, H. Leonhardt, K. Spiekermann, M. Subklewe, P.A. Greif, Tyrosine kinase inhibition increases the cell surface localization of FLT3-ITD and enhances FLT3-directed immunotherapy of acute myeloid leukemia, *Leukemia* 32 (2018) 313–322, <https://doi.org/10.1038/leu.2017.257>.
- E. Weisberg, A. Ray, E. Nelson, S. Adamia, R. Barrett, M. Sattler, C. Zhang, J. F. Daley, D. Frank, E. Fox, J.D. Griffin, Reversible resistance induced by FLT3 inhibition: a novel resistance mechanism in mutant FLT3-expressing cells, *PLoS One* 6 (2011), e25351, <https://doi.org/10.1371/journal.pone.0025351>.
- C. Larrue, E. Saland, H. Boutzen, F. Vergez, M. David, C. Joffre, M.A. Hospital, J. Tamburini, E. Delabesse, S. Manenti, J.E. Sarry, C. Récher, Proteasome inhibitors induce FLT3-ITD degradation through autophagy in AML cells, *Blood* 127 (2016) 882–892, <https://doi.org/10.1182/blood-2015-05-646497>.
- A. Zorba, C. Nguyen, Y. Xu, J. Starr, K. Borzilleri, J. Smith, H. Zhu, K.A. Farley, W. Ding, J. Schiemer, X. Feng, J.S. Chang, D.P. Uccello, J.A. Young, C.N. Garcia-Irrizary, L. Czabaniuk, B. Schuff, R. Oliver, J. Montgomery, M.M. Hayward, J. Coe, J. Chen, M. Niosi, S. Luthra, J.C. Shah, Delineating the role of cooperativity in the design of potent PROTACs for BTK, *Proc. Natl. Acad. Sci. USA* 31 (2018) E7285–E7292, <https://doi.org/10.1073/pnas.1803662115>.

- [37] D. Zaidman, J. Prilusky, N. London, ProsettaC, Rosetta based modeling of PROTAC mediated ternary complexes, *J. Chem. Inf. Model.* 60 (2020) 4894–4903, <https://doi.org/10.1021/acs.jcim.0c00589>.
- [38] G.M. Morris, R. Huey, W. Lindstrom, M.F. Sanner, R.K. Belew, D.S. Goodsell, A. J. Olson, AutoDock4 and AutoDockTools4: automated docking with selective receptor flexibility, *J. Comput. Chem.* 30 (2009) 2785–2791, <https://doi.org/10.1002/jcc.21256>.
- [39] O. Trott, A.J. Olson, AutoDock Vina, Improving the speed and accuracy of docking with a new scoring function, efficient optimization, and multithreading, *J. Comput. Chem.* 31 (2009) 455–461, <https://doi.org/10.1002/jcc.21334>.
- [40] R.A. Carrasco, N.B. Stamm, B.K.R. Patel, One-step cellular caspase-3/7 assay, *Biotechniques* 34 (2003) 1064–1067, <https://doi.org/10.2144/03345dd02>.
- [41] J. Ye, G. Coulouris, I. Zaretskaya, I. Cutcutache, S. Rozen, T.L. Madden, Primer-Blast, A tool to design target-specific primers for polymerase chain reaction, *BMC Bioinf.* 13 (2012) 134, <https://doi.org/10.1186/1471-2105-13-134>.
- [42] K.J. Livak, T.D. Schmittgen, Analysis of relative gene expression data using real-time quantitative PCR and the 2(-Delta Delta C(T)) Method, *Methods* 25 (2001) 402–408, <https://doi.org/10.1006/meth.2001.1262>.
- [43] F. Xie, P. Xiao, D. Chen, L. Xu, B. Zhang, miRDeepFinder: a miRNA analysis tool for deep sequencing of plant small RNAs, *Plant Mol. Biol.* 80 (2012) 75–84, <https://doi.org/10.1007/s11103-012-9885-2>.

Supplementary Material

Modulation of FLT3-ITD and CDK9 in acute myeloid leukaemia cells by novel proteolysis targeting chimera (PROTAC)

Eva Řezníčková^a, Soňa Krajčovičová^b, Miroslav Peřina^a, Markéta Kovalová^a, Miroslav Sural^{b*}, Vladimír Kryštof^{a,c*}

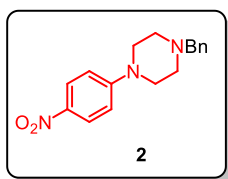
- a Department of Experimental Biology, Faculty of Science, Palacký University Olomouc, Šlechtitelů 27, 78371 Olomouc, Czech Republic
- b Department of Organic Chemistry, Faculty of Science, Palacký University Olomouc, 17. Listopadu 12, 77146 Olomouc, Czech Republic
- c Institute of Molecular and Translational Medicine, Faculty of Medicine and Dentistry, Palacký University Olomouc, Hněvotínská 5, 77900 Olomouc, Czech Republic

*corresponding authors

email addresses: miroslav.sural@upol.cz; vladimir.krystof@upol.cz

Analytical data

- **1-benzyl-4-(4-nitrophenyl)piperazine 2**

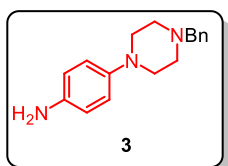


$^1\text{H NMR}$ (500 MHz, $\text{DMSO-}d_6$): δ 8.07 – 8.02 (m, 2H), 7.34 – 7.32 (m, 4H), 7.28 – 7.25 (m, 1H), 7.01 – 6.98 (m, 2H), 3.52 (s, 2H), 3.46 – 3.43 (m, 4H), 2.51 – 2.47 (m, 4H, *overlap with solvent*) ppm.

$^{13}\text{C NMR}$ (126 MHz, $\text{DMSO-}d_6$): δ 154.6, 137.7, 136.8, 128.8, 128.1, 127.0, 125.6, 112.5, 61.7, 52.0, 46.3 ppm.

HRMS (ESI): m/z calcd for $\text{C}_{17}\text{H}_{19}\text{N}_3\text{O}_2$ $[\text{M}+\text{H}]^+ = 298.1550$, found $[\text{M}+\text{H}]^+ = 298.1550$.

- **4-(4-benzylpiperazin-1-yl)aniline 3**

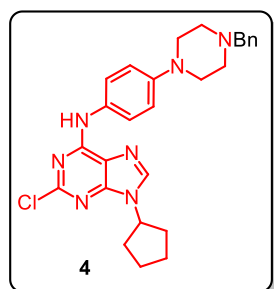


$^1\text{H NMR}$ (500 MHz, $\text{DMSO-}d_6$): δ 7.34 – 7.31 (m, 4H), 7.28 – 7.23 (m, 1H), 6.68 – 6.65 (m, 2H), 6.50 – 6.46 (m, 2H), 4.53 (s, 2H), 3.50 (s, 2H), 2.92 – 2.87 (m, 4H), 2.49 – 2.47 (m, 4H, *overlap with solvent*) ppm.

$^{13}\text{C NMR}$ (126 MHz, $\text{DMSO-}d_6$): δ 142.4, 142.0, 138.1, 128.8, 128.1, 126.8, 117.8, 114.7, 62.0, 52.8, 50.3 ppm.

HRMS (ESI): m/z calcd for $\text{C}_{17}\text{H}_{22}\text{N}_3$ $[\text{M}+\text{H}]^+ = 268.1808$, found $[\text{M}+\text{H}]^+ = 268.1808$.

- **N-(4-(4-benzylpiperazin-1-yl)phenyl)-2-chloro-9-cyclopentyl-9H-purine-6-amine 4**

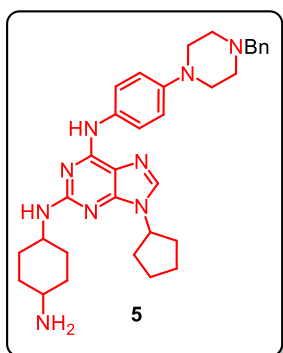


$^1\text{H NMR}$ (500 MHz, $\text{DMSO-}d_6$): δ 10.02 (s, 1H), 8.34 (s, 1H), 7.62 – 7.55 (m, 2H), 7.34 – 7.33 (m, 4H), 7.28 – 7.21 (m, 1H), 6.93 – 6.90 (m, 2H), 4.83 – 4.80 (m, 1H), 3.53 – 3.51 (m, 2H), 3.13 – 3.11 (m, 4H), 2.53 – 2.50 (m, 4H, *overlap with solvent*), 2.20 – 2.13 (m, 2H), 2.01 – 1.93 (m, 2H), 1.90 – 1.83 (m, 2H), 1.74 – 1.66 (m, 2H) ppm.

$^{13}\text{C NMR}$ (126 MHz, $\text{DMSO-}d_6$) δ 152.4, 152.2, 150.3, 147.5, 140.2, 130.3, 128.8, 128.8, 128.1, 126.9, 122.5, 118.8, 115.4, 62.0, 55.4, 52.5, 48.9, 31.9, 23.4 ppm.

HRMS (ESI): m/z calcd for $\text{C}_{27}\text{H}_{31}\text{ClN}_7$ $[\text{M}+\text{H}]^+ = 488.2324$, found $[\text{M}+\text{H}]^+ = 488.2327$.

- **N²-(4-aminocyclohexyl)-N⁶-(4-(4-benzylpiperazin-1-yl)phenyl)-9-cyclopentyl-9H-purine-2,6-diamine 5**

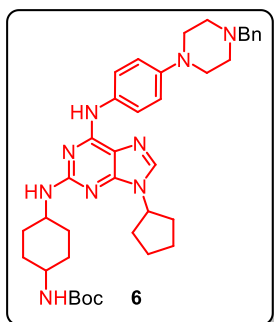


$^1\text{H NMR}$ (500 MHz, $\text{DMSO-}d_6$): δ 9.04 (br s, 1H), 7.81 – 7.74 (m, 3H), 7.30 – 7.29 (m, 4H), 7.23 – 7.21 (m, 1H), 6.83 – 6.79 (m, 2H), 6.21 (app s, 1H), 4.67 (p, $J = 7.6$ Hz, 1H), 3.61 – 3.55 (m, 1H), 3.49 – 3.38 (m, 5H), 3.04 – 3.02 (m, 4H), 2.51 – 2.48 (m, 4H, *overlap with solvent*), 2.09 – 2.02 (m, 2H), 1.98 – 1.91 (m, 4H), 1.86 – 1.81 (m, 2H), 1.78 – 1.73 (m, 2H), 1.66 – 1.63 (m, 2H), 1.23 – 1.20 (m, 2H) ppm.

¹³C NMR (126 MHz, DMSO-*d*₆): δ 158.1, 152.0, 146.2, 138.0, 136.1, 132.6, 128.8, 128.1, 126.9, 121.1, 115.6, 113.9, 65.5, 62.0, 52.6, 49.9, 49.0, 35.1, 31.7, 31.2, 23.7 ppm.

HRMS (ESI): *m/z* calcd for C₃₃H₄₄N₉ [M+H]⁺ = 566.3714, found [M+H]⁺ = 566.3715.

- ***tert*-butyl-(4-((6-((4-(4-benzylpiperazin-1-yl)phenyl)amino)-9-cyclopentyl-9H-purine-2-yl)amino)cyclohexyl)carbamate 6**

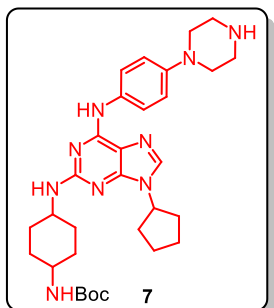


¹H NMR (500 MHz, DMSO-*d*₆): δ 9.09 (br s, 1H), 7.83 – 7.81 (m, 3H), 7.34 – 7.31 (m, 3H), 7.29 – 7.24 (m, 1H), 6.87 – 6.85 (m, 2H), 6.73 – 6.71 (m, 1H), 6.30 (app s, 1H), 4.69 – 4.66 (m, 1H), 3.63 – 3.57 (m, 1H), 3.53 (br s, 2H), 3.32 (s, 3H), 3.25 – 3.17 (m, 1H), 3.09 – 3.07 (m, 4H), 2.54 – 2.52 (m, 4H, overlap with solvent), 2.11 – 2.06 (m, 2H), 2.01 – 1.97 (m, 4H), 1.91 – 1.80 (m, 4H), 1.71 – 1.62 (m, 2H), 1.35 (s, 9H), 1.30 – 1.27 (m, 2H) ppm.

¹³C NMR (126 MHz, DMSO-*d*₆): δ 158.1, 154.8, 152.0, 151.4, 146.3, 138.0, 136.1, 135.6, 132.6, 128.8, 128.1, 126.9, 121.0, 115.6, 77.3, 68.2, 62.0, 52.6, 49.0, 48.9, 31.7, 31.6, 31.2, 28.2, 27.3, 23.7 ppm.

HRMS (ESI): *m/z* calcd for C₃₈H₅₂N₉O₂ [M+H]⁺ = 666.4238, found [M+H]⁺ = 666.4236.

- ***tert*-butyl-(4-((9-cyclopentyl-6-((4-(piperazin-1-yl)phenyl)amino)-9H-purin-2-yl)amino)cyclohexyl)carbamate 7**

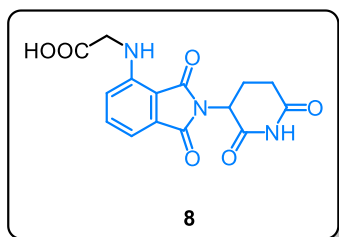


¹H NMR (500 MHz, DMSO-*d*₆): δ 9.10 (s, 1H), 7.83 – 7.82 (m, 3H), 6.87 – 6.85 (m, 2H), 6.75 – 6.73 (m, 1H), 6.30 (app s, 1H), 4.67 (p, *J* = 7.6 Hz, 1H), 3.63 – 3.58 (m, 1H), 3.25 – 3.19 (m, 1H, overlap with solvent), 3.03 (t, *J* = 5.0 Hz, 3H), 2.91 (t, *J* = 4.9 Hz, 3H), 2.12 – 2.06 (m, 2H), 1.99 – 1.95 (m, 4H), 1.90 – 1.81 (m, 4H), 1.71 – 1.63 (m, 2H), 1.39 (s, 9H), 1.31 – 1.26 (m, 2H) ppm.

¹³C NMR (126 MHz, DMSO-*d*₆): δ 158.1, 154.8, 151.8, 146.6, 136.2, 132.7, 121.0, 115.7, 77.3, 49.6, 48.9, 45.2, 31.7, 31.6, 31.2, 28.2, 23.7 ppm.

HRMS (ESI): *m/z* calcd for C₃₁H₄₆N₉O₂ [M+H]⁺ = 576.3769, found [M+H]⁺ = 576.3768.

- **(2-(2,6-dioxopiperidin-3-yl)-1,3-dioxoisindolin-4-yl)glycine 8**

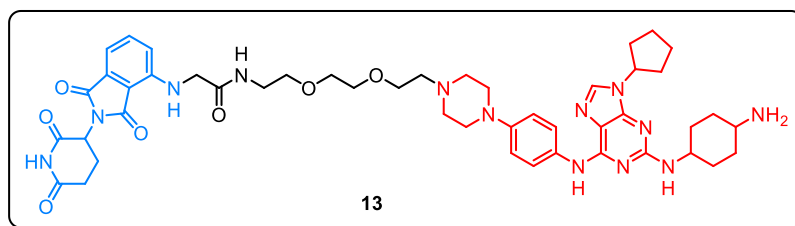


¹H NMR (500 MHz, DMSO-*d*₆): δ 11.05 (br s, 1H), 7.54 (dd, *J* = 8.5, 7.1 Hz, 1H), 7.04 – 7.03 (m, 1H), 6.96 – 6.94 (m, 1H), 6.82 (t, *J* = 5.8 Hz, 1H), 5.03 (dd, *J* = 12.9, 5.5, 1H), 4.14 – 4.00 (m, 2H), 3.86 – 3.80 (m, 1H), 2.89 – 2.81 (m, 1H), 2.55 – 2.53 (m, 1H, overlap with solvent), 2.04 – 1.98 (m, 1H) ppm. ¹³C NMR (126 MHz, DMSO-*d*₆): δ 172.7, 170.0, 168.7,

167.2, 145.7, 136.0, 132.0, 117.7, 110.9, 109.5, 48.5, 30.9, 27.2, 25.6, 22.1 ppm.

HRMS (ESI): *m/z* calcd for C₁₅H₁₄N₃O₆ [M+H]⁺ = 332.0877, found [M+H]⁺ = 332.0877.

- **PROTAC 13**



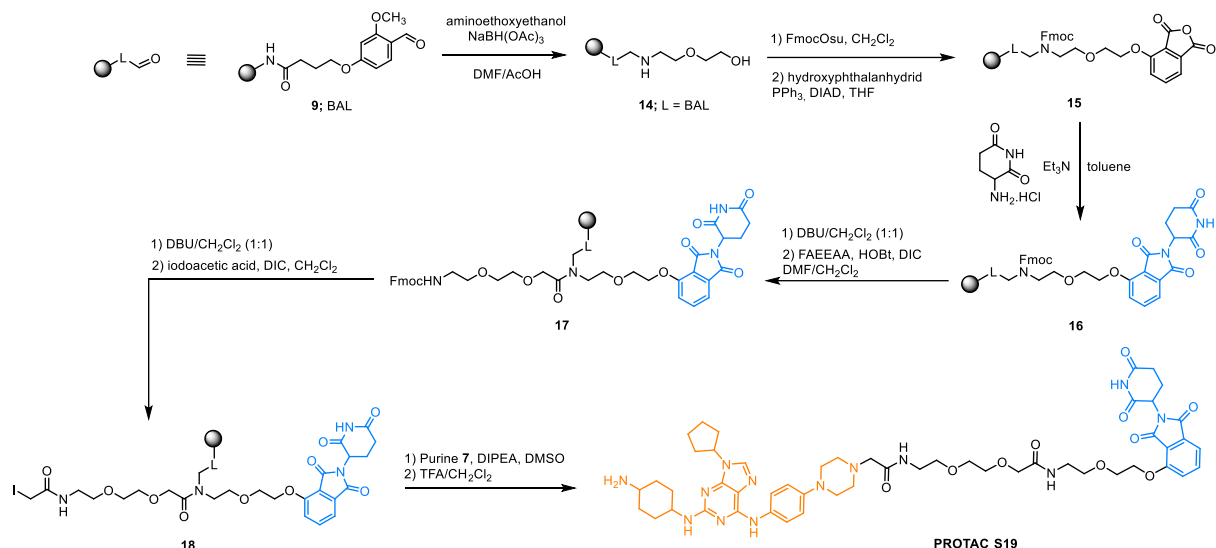
¹H NMR (500 MHz, DMSO-*d*₆): δ 9.12 (br s, 1H), 8.16 – 8.14 (m, 1H), 7.87 – 7.79 (m, 2H), 7.61 – 7.56 (m, 1H), 7.08 – 7.06 (m, 1H), 6.96 – 6.93 (m, 1H), 6.87 – 6.84 (m, 2H), 6.39 (br s, 1H), 5.07 (dd, *J* = 13.2, 5.3 Hz, 1H), 4.68 – 4.66 (m, 1H), 3.94 – 3.84 (m, 2H), 3.71 – 3.65 (m, 1H), 3.61 – 3.58 (m, 1H) 3.55 – 3.51 (m, 6H), 3.45 – 3.43 (m, 3H), 3.30 – 3.26 (m, 10H, *overlap with solvent*) 3.05 (t, *J* = 4.8 Hz, 3H), 2.91 – 2.85 (m, 1H), 2.57 – 2.55 (m, 3H, *overlap with solvent*), 2.10 – 1.90 (m, 12H), 1.69 – 1.66 (m, 2H), 1.31 – 1.24 (m, 2H) ppm.

¹³C NMR (126 MHz, DMSO-*d*₆): δ 172.7, 171.8, 170.0, 168.6, 168.5, 167.2, 146.3, 145.7, 136.1, 132.0, 121.0, 117.4, 115.5, 110.9, 109.8, 106.9, 70.5, 69.5, 68.9, 68.3, 57.2, 54.9, 53.1, 49.0, 48.5, 45.1, 43.5, 31.7, 30.9, 30.2, 30.2, 22.1 ppm.

Note: quaternary carbons adjacent to nitrogen atoms on purine scaffold were not visible, as they are usually broad and difficult to observe due to the lack of polarisation transfer between these atoms

HRMS (ESI): *m/z* calcd for C₄₇H₆₂N₁₃O₇ [M+H]⁺ = 920.4890, found [M+H]⁺ = 920.4892 (460.7482).

Preparation of inactive PROTAC conjugate S19



Scheme S1.

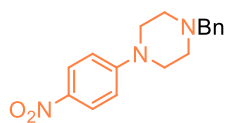
PROTAC **S19** have been prepared from amino methyl polystyrene resin with BAL linker in 10 steps (Scheme **S1**) as pale yellow oil (3 mg, 3% overall yield from **16**) in accordance with previously published procedure [1].

- **PROTAC S19**

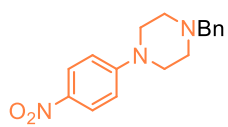
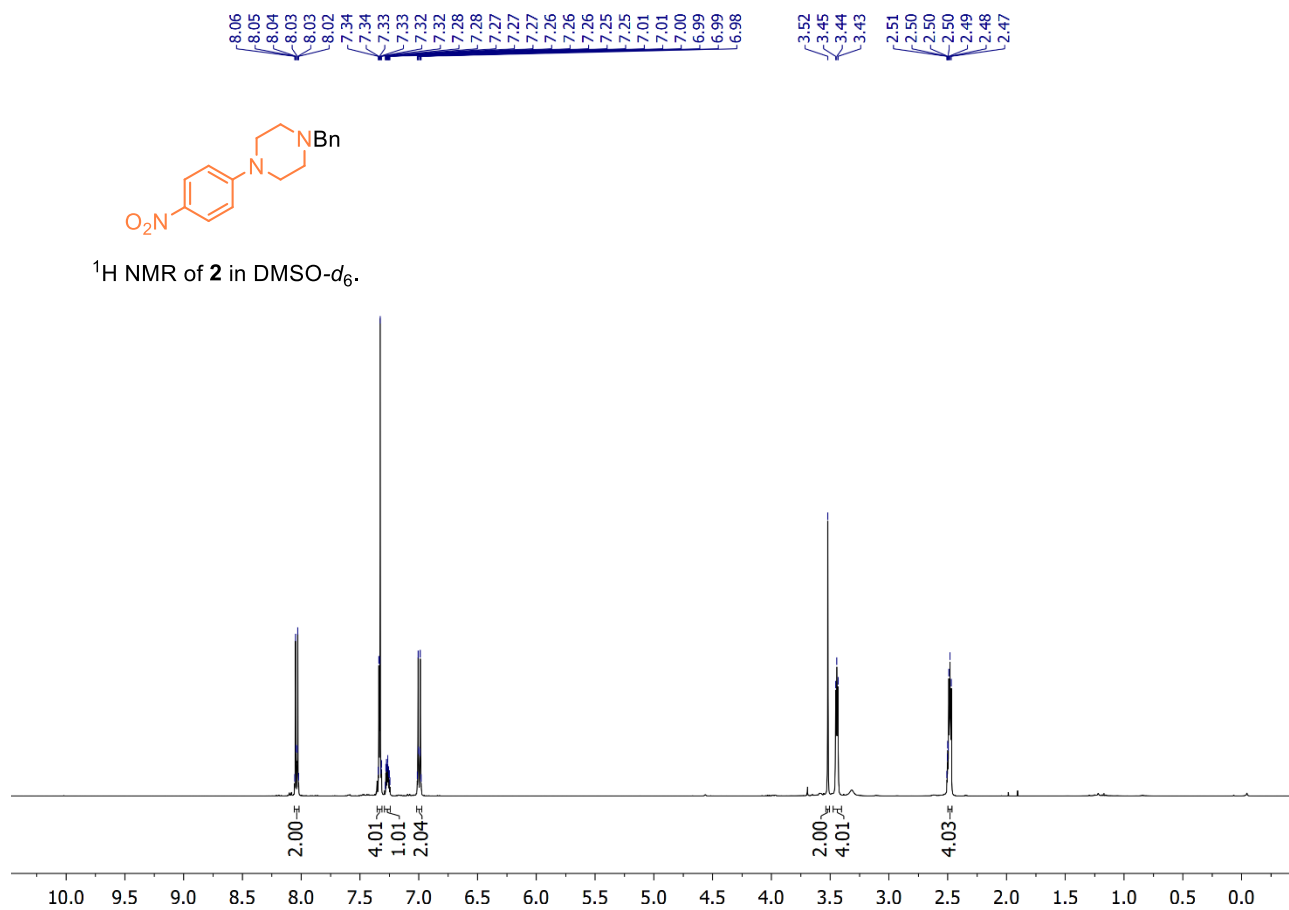
¹H NMR (500 MHz, DMSO-*d*₆) δ 11.09 (s, 1H), 9.21 (br s, 1H), 7.99 – 7.93 (m, 3H), 7.93 – 7.77 (m, 5H), 7.68 (t, *J* = 5.9 Hz, 1H), 7.52 – 7.50 (m, 1H), 7.47 – 7.44 (m, 1H), 7.33 – 7.29 (m, 1H), 7.21 – 7.18 (m, 1H), 7.11–7.07 (m, 1H), 6.92 – 6.90 (m, 2H), 6.44 (br s, 1H), 5.08 (dd, *J* = 12.8, 5.5 Hz, 1H), 4.69 (t, *J* = 7.5 Hz, 1H), 4.36 – 4.30 (m, 2H), 3.88 (s, 2H), 3.81 – 3.77 (m, 2H), 3.60 – 3.50 (m, 8H), 3.48 – 3.46 (m, 4H), 3.33 – 3.30 (m, 6H), 3.01 – 2.97 (m, 2H), 2.90 – 2.85 (m, 1H), 2.14 – 1.94 (m, 10H), 1.90 – 1.85 (m, 2H), 1.71–1.63 (m, 2H), 1.49 – 1.42 (m, 2H), 1.35 – 1.27 (m, 2H) ppm.

¹³C NMR (126 MHz, DMSO-*d*₆): δ 172.7, 169.9, 169.3, 166.8, 165.2, 158.4, 158.2, 157.9, 157.7, 156.8, 155.8, 151.9, 137.0, 133.2, 121.1, 120.8, 120.0, 118.4, 116.3, 116.1, 116.0, 115.4, 113.6, 70.1, 69.9, 69.4, 69.2, 68.7, 68.7, 68.3, 51.9, 48.9, 48.7, 40.6, 38.5, 38.0, 31.7, 30.9, 30.0, 29.4, 23.2, 22.0 ppm.

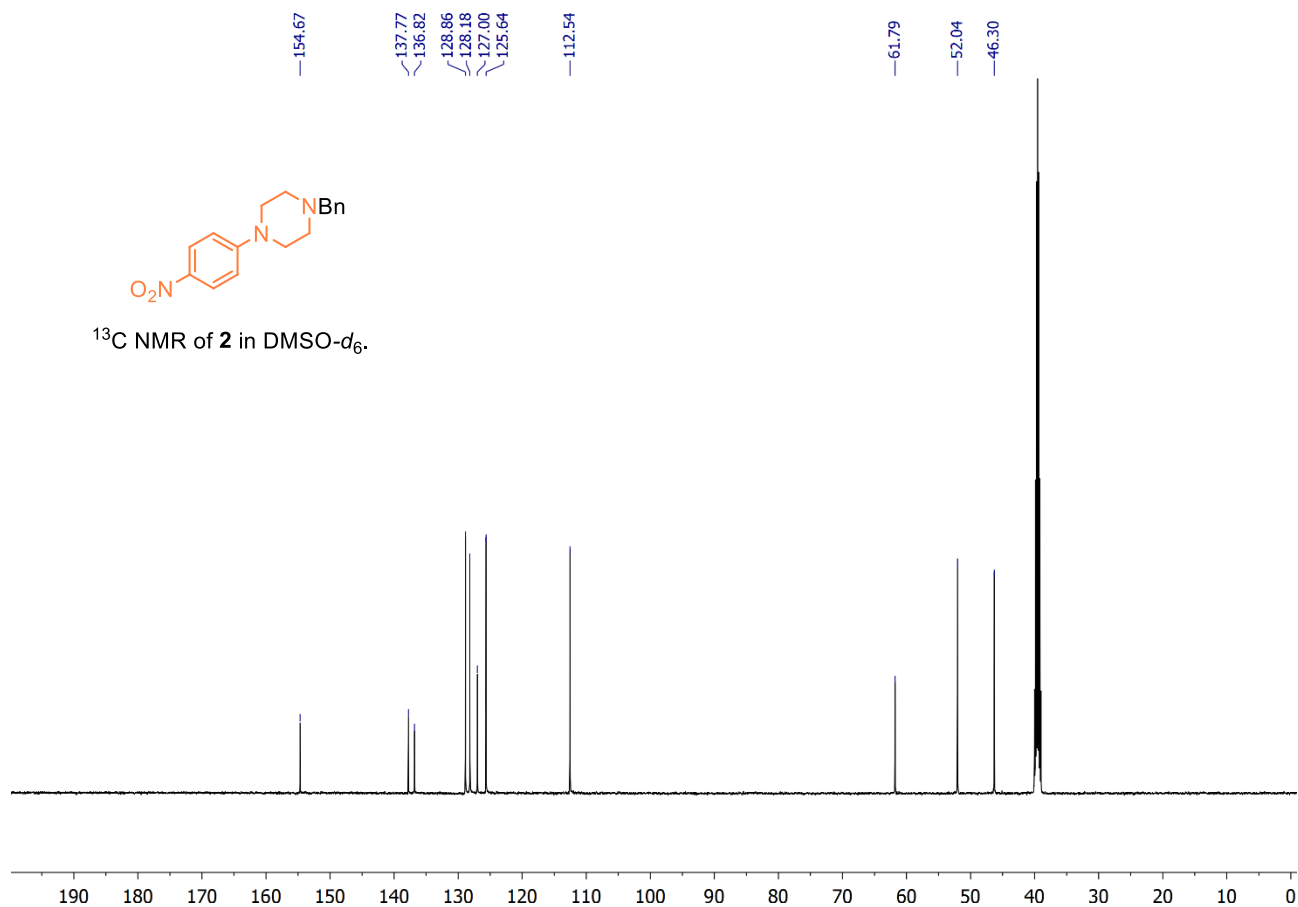
NMR spectra



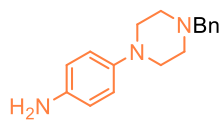
^1H NMR of **2** in $\text{DMSO-}d_6$.



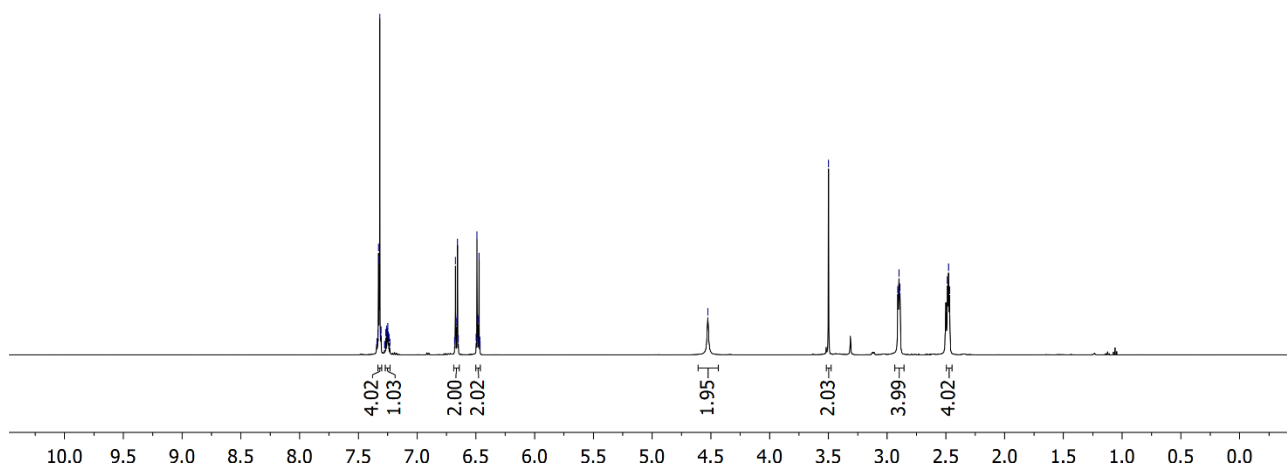
^{13}C NMR of **2** in $\text{DMSO-}d_6$.



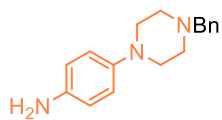
7.34 7.33 7.33 7.32 7.32 7.31 7.28 7.27 7.27 7.26 7.26 7.25 7.25 7.24 7.24 7.23 6.68 6.67 6.67 6.66 6.66 6.65 6.50 6.49 6.49 6.48 6.48 6.47 6.47 6.46 4.53 3.50 2.91 2.90 2.89 2.49 2.48 2.47



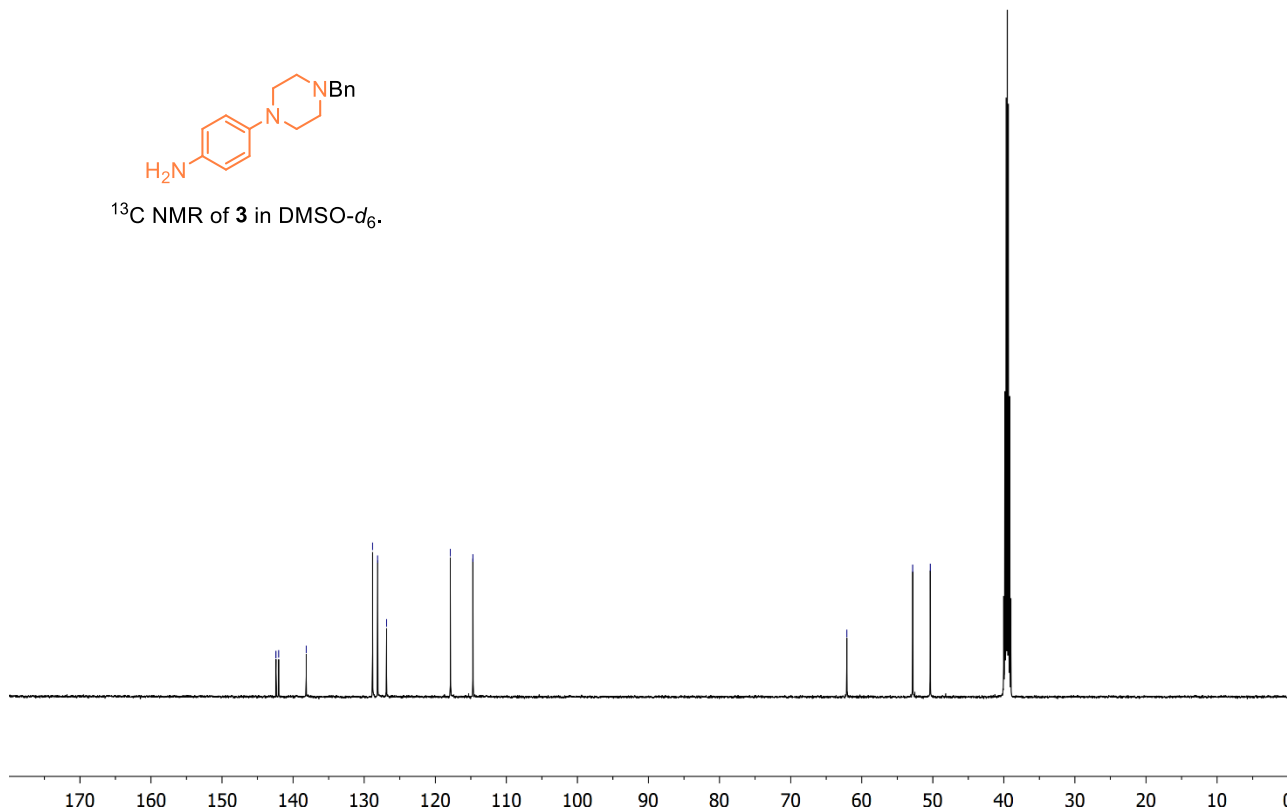
^1H NMR of **3** in $\text{DMSO-}d_6$.

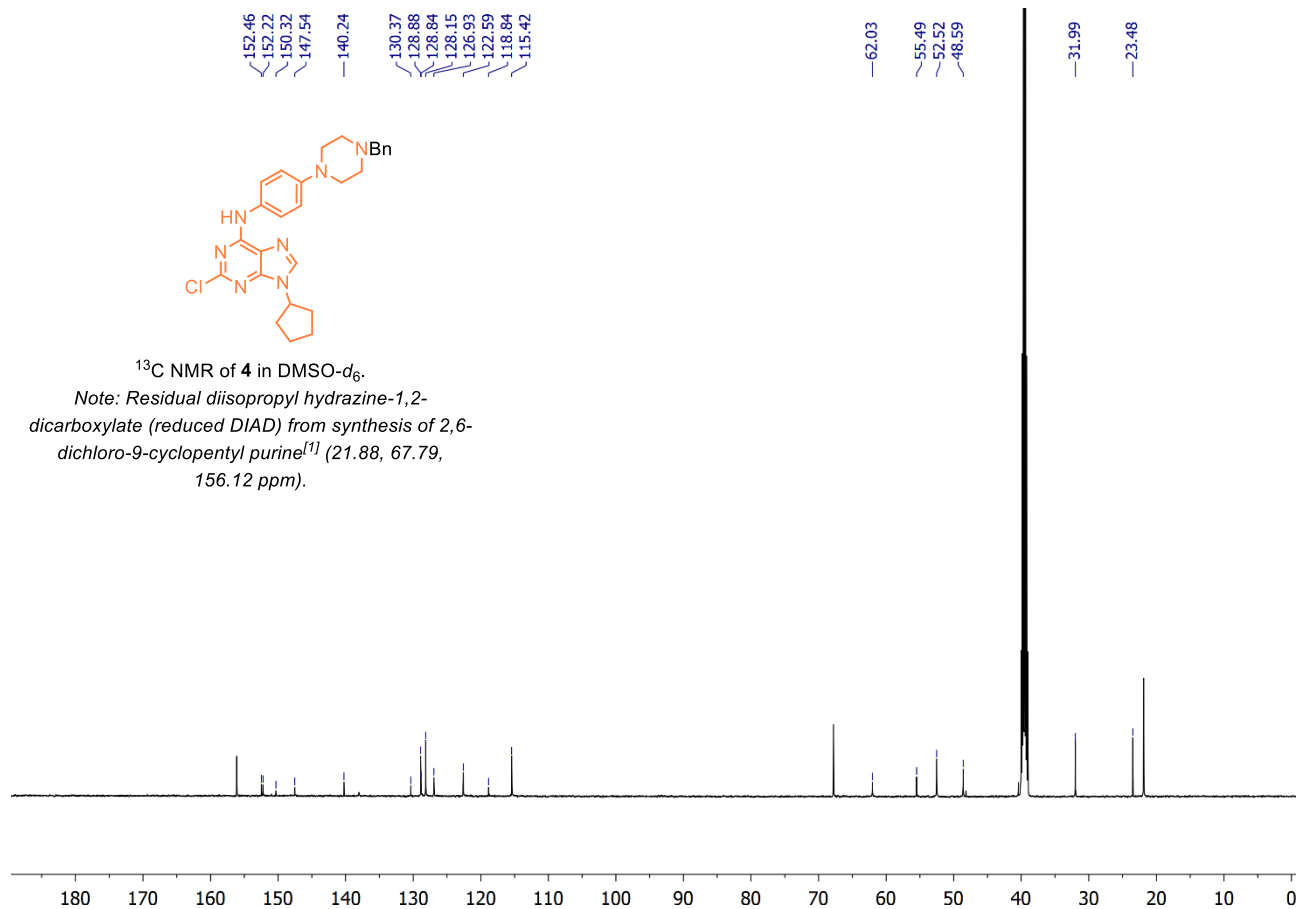
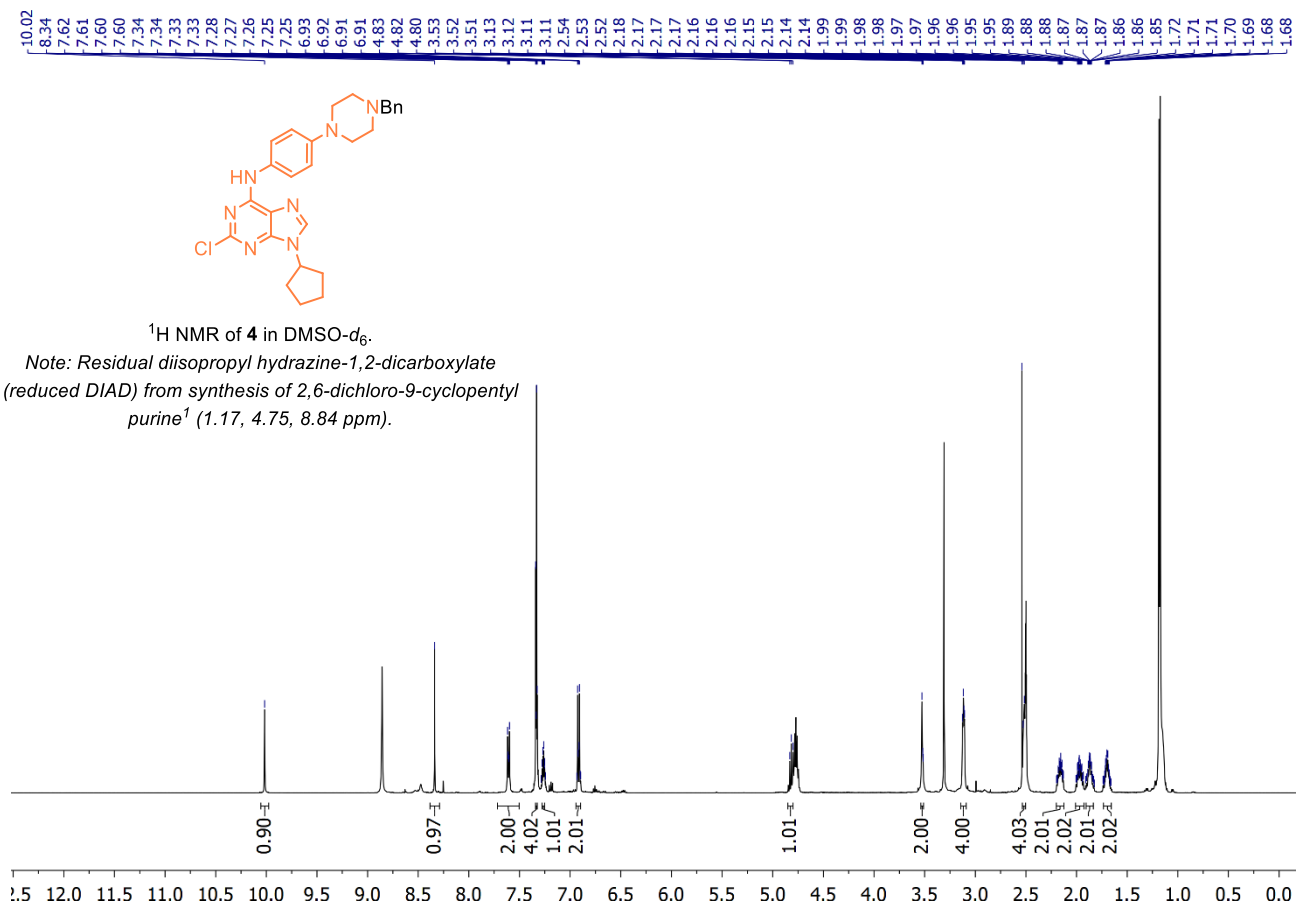


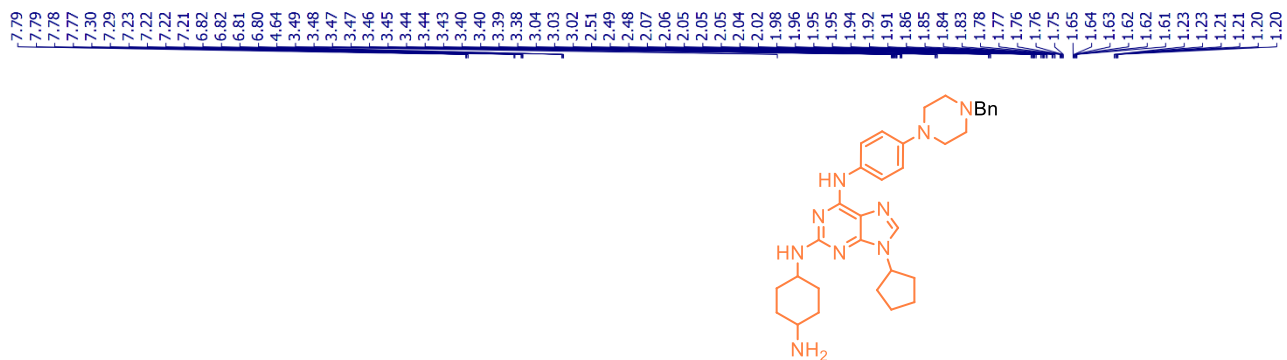
142.41 142.04 138.16 128.82 128.12 126.86 117.86 114.70 62.09 52.83 50.35



^{13}C NMR of **3** in $\text{DMSO-}d_6$.

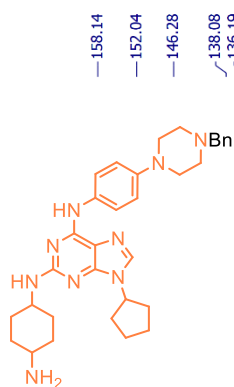
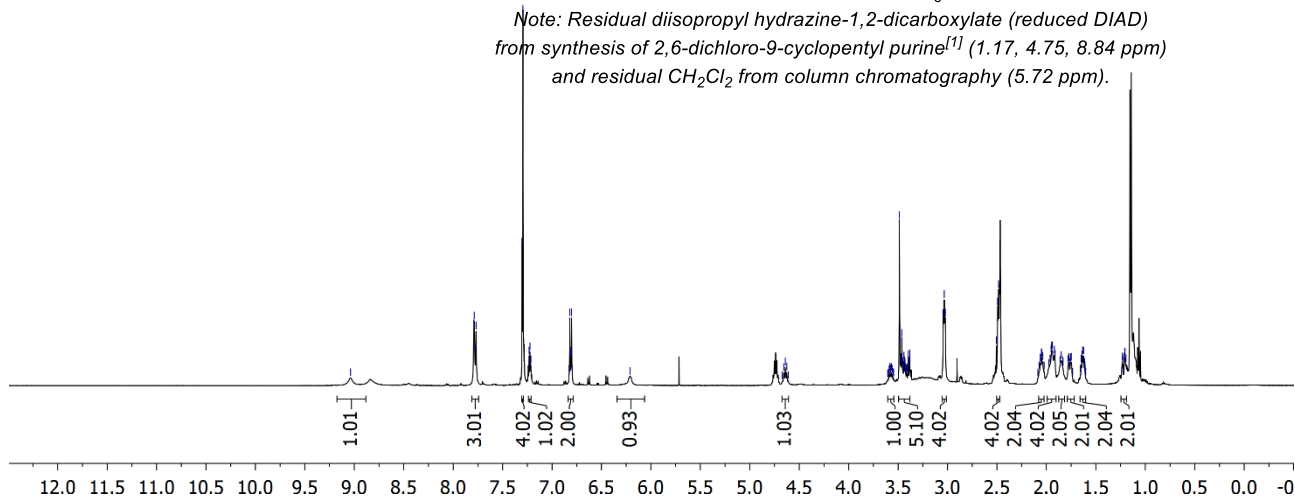






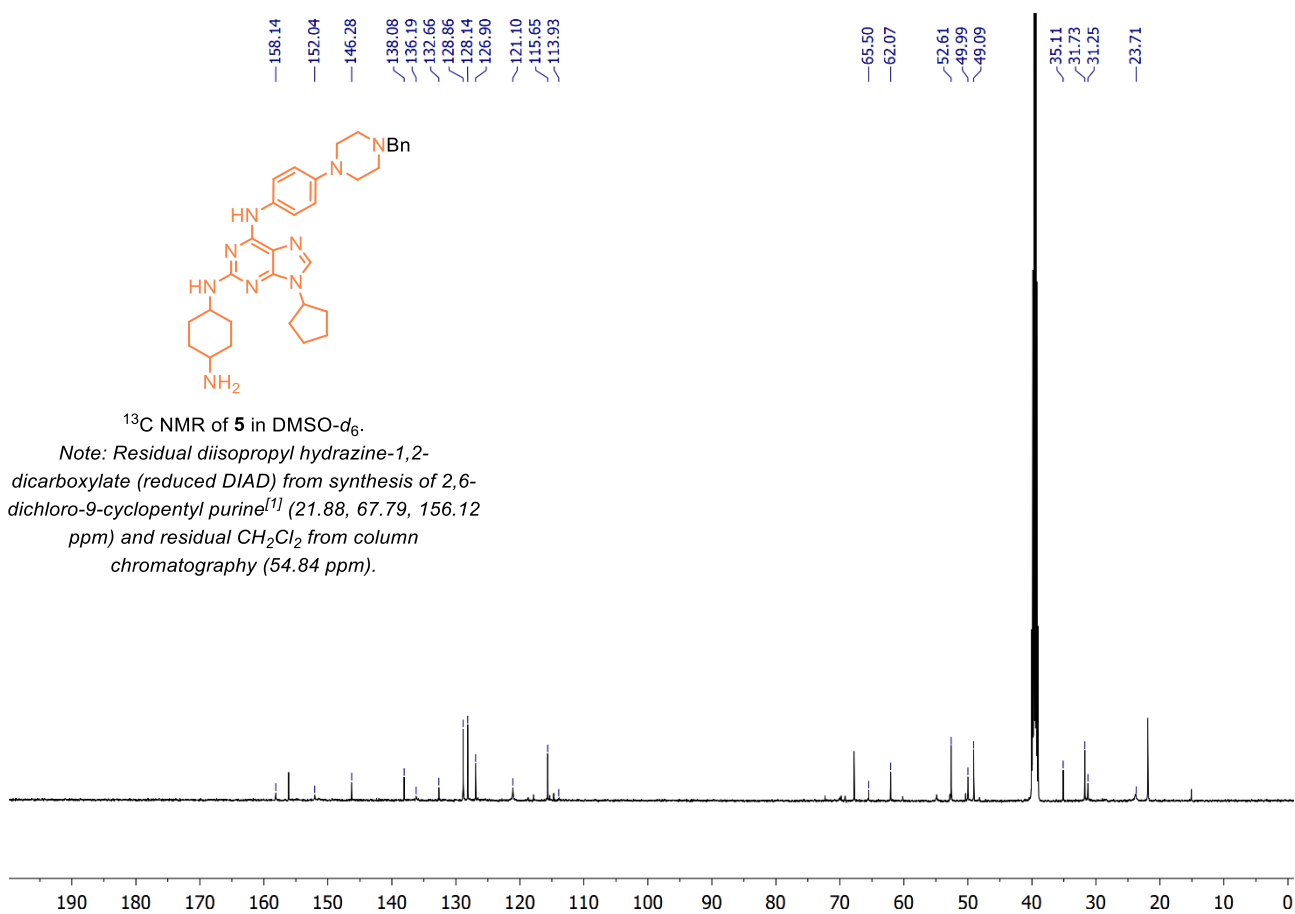
¹H NMR of **5** in DMSO-d₆.

Note: Residual diisopropyl hydrazine-1,2-dicarboxylate (reduced DIAD) from synthesis of 2,6-dichloro-9-cyclopentyl purine^[1] (1.17, 4.75, 8.84 ppm) and residual CH₂Cl₂ from column chromatography (5.72 ppm).

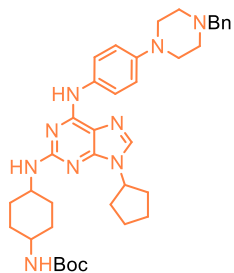


¹³C NMR of **5** in DMSO-d₆.

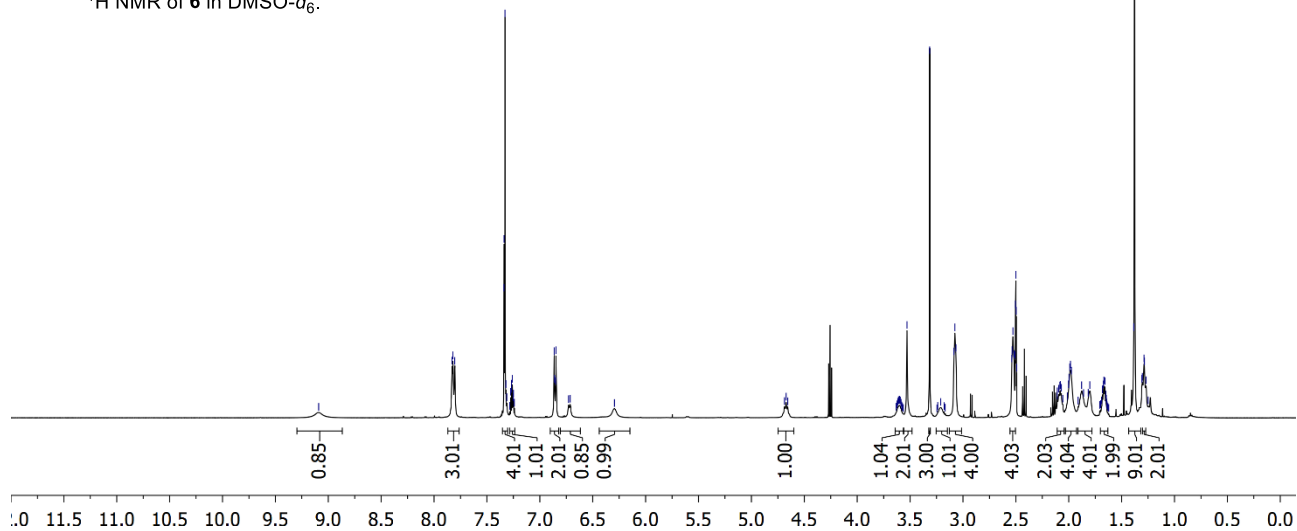
Note: Residual diisopropyl hydrazine-1,2-dicarboxylate (reduced DIAD) from synthesis of 2,6-dichloro-9-cyclopentyl purine^[1] (21.88, 67.79, 156.12 ppm) and residual CH₂Cl₂ from column chromatography (54.84 ppm).



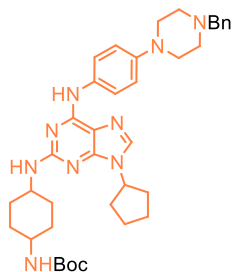
7.83
7.82
7.80
7.34
7.34
7.34
7.33
7.33
7.32
7.31
7.28
7.27
7.27
7.26
7.25
7.25
6.87
6.86
6.85
6.85
6.73
6.73
6.71
4.67
3.61
3.60
3.59
3.53
3.31
3.09
3.08
3.07
2.54
2.53
2.53
2.52
2.51
2.50
2.50
2.50
2.49
2.11
2.11
2.09
2.08
2.08
2.07
2.06
2.01
2.00
2.00
1.99
1.98
1.97
1.88
1.86
1.82
1.80
1.68
1.67
1.66
1.65
1.65
1.64
1.38
1.38
1.31
1.30
1.29
1.28
1.27
1.25



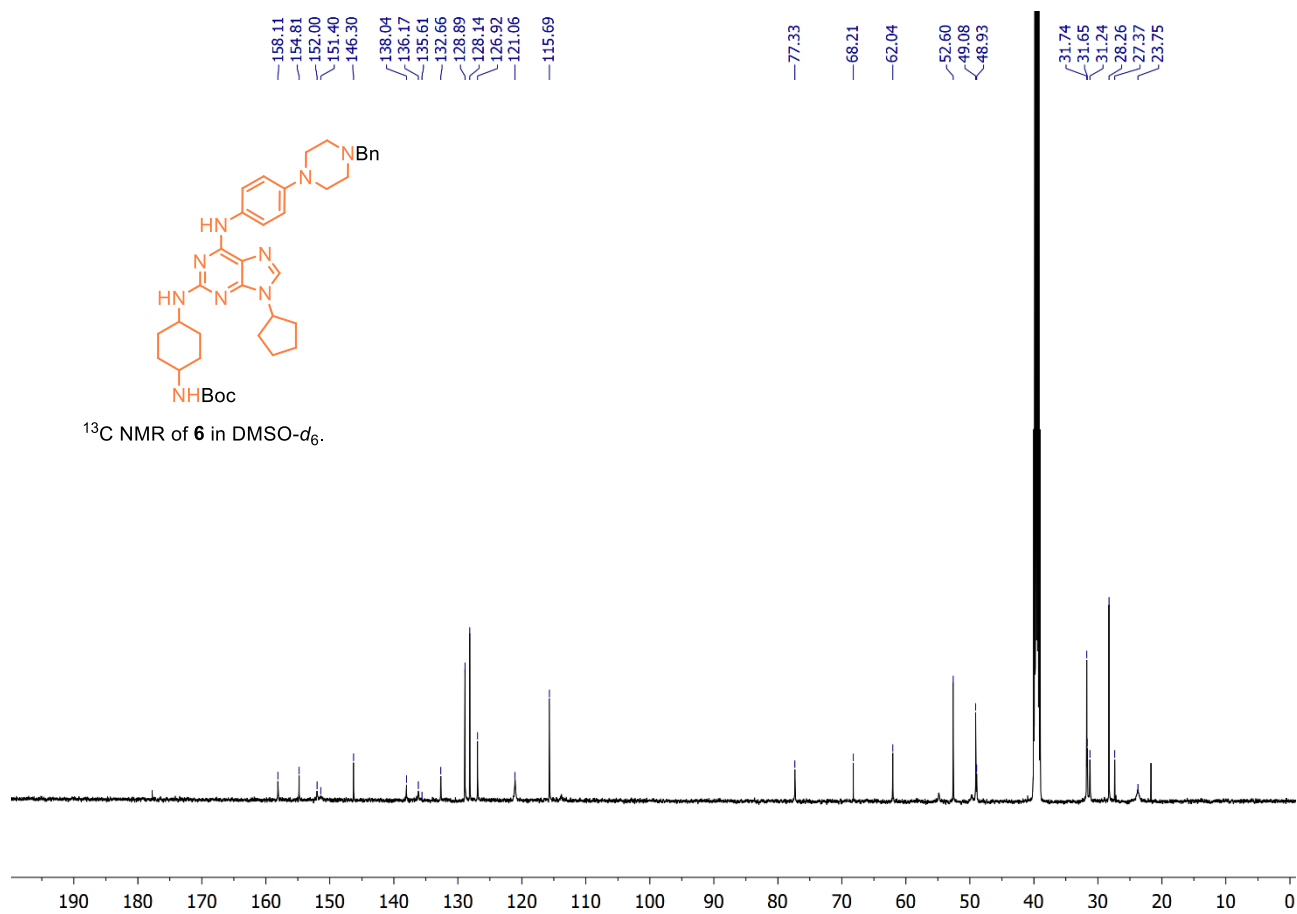
^1H NMR of **6** in $\text{DMSO-}d_6$.

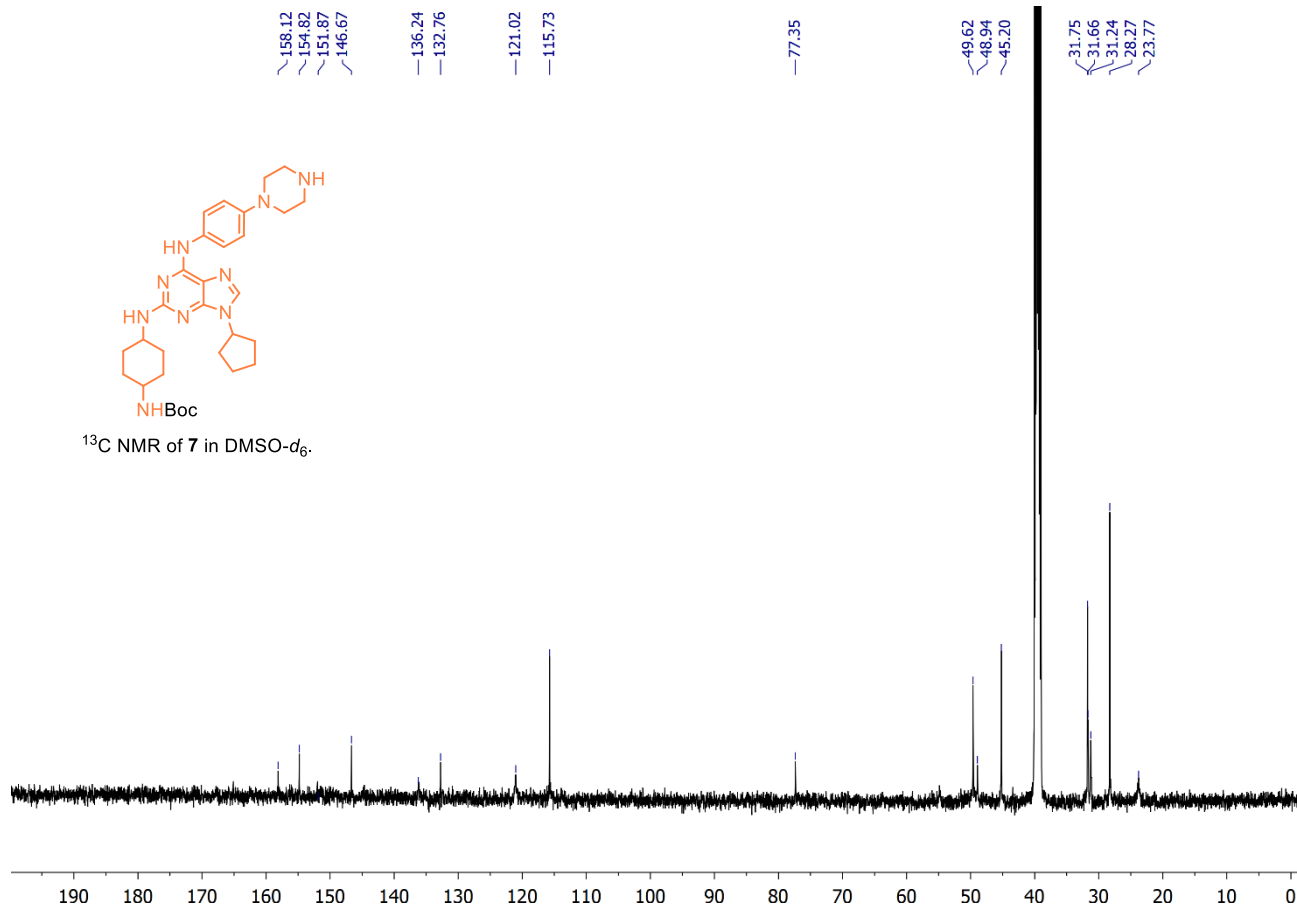
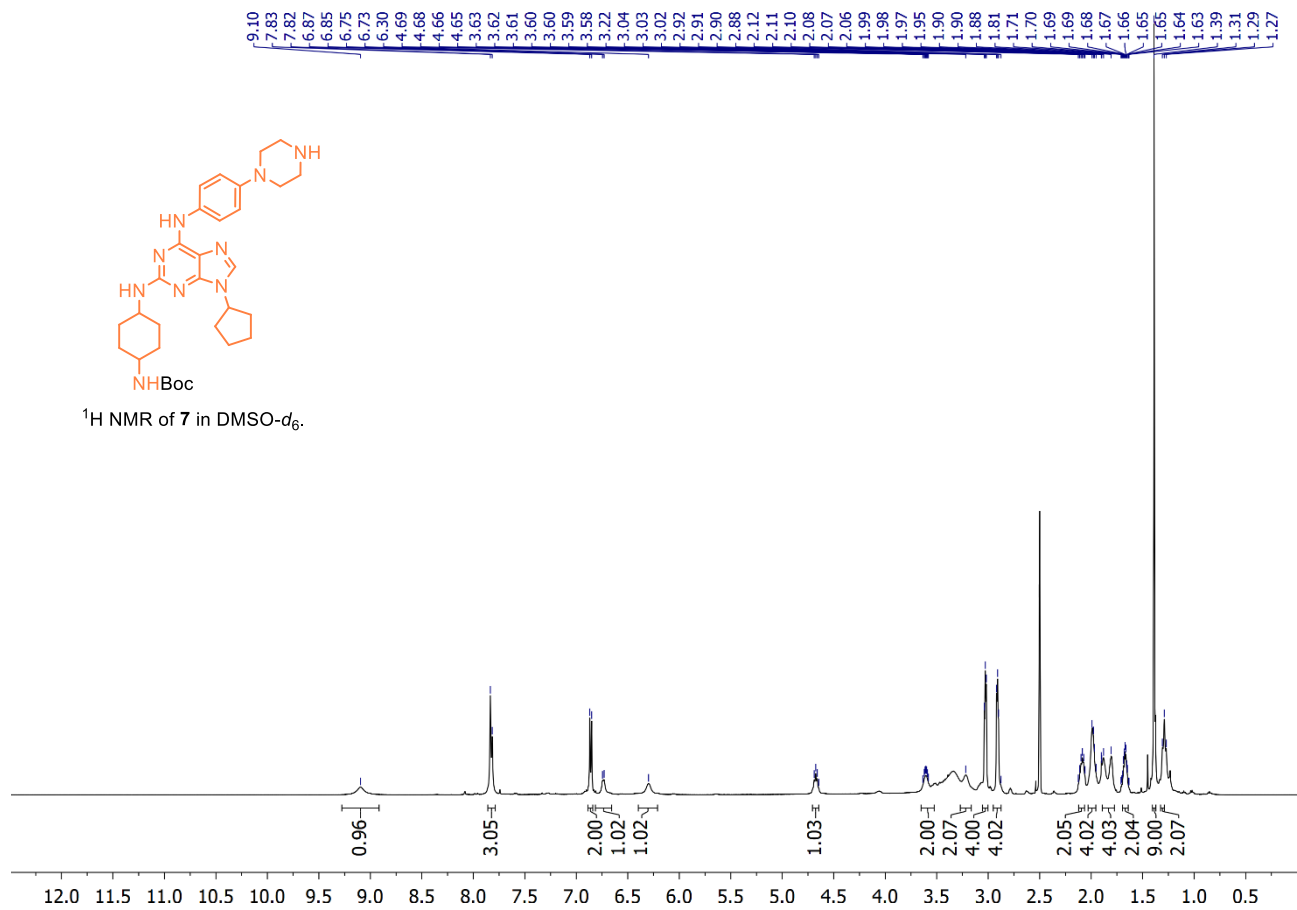


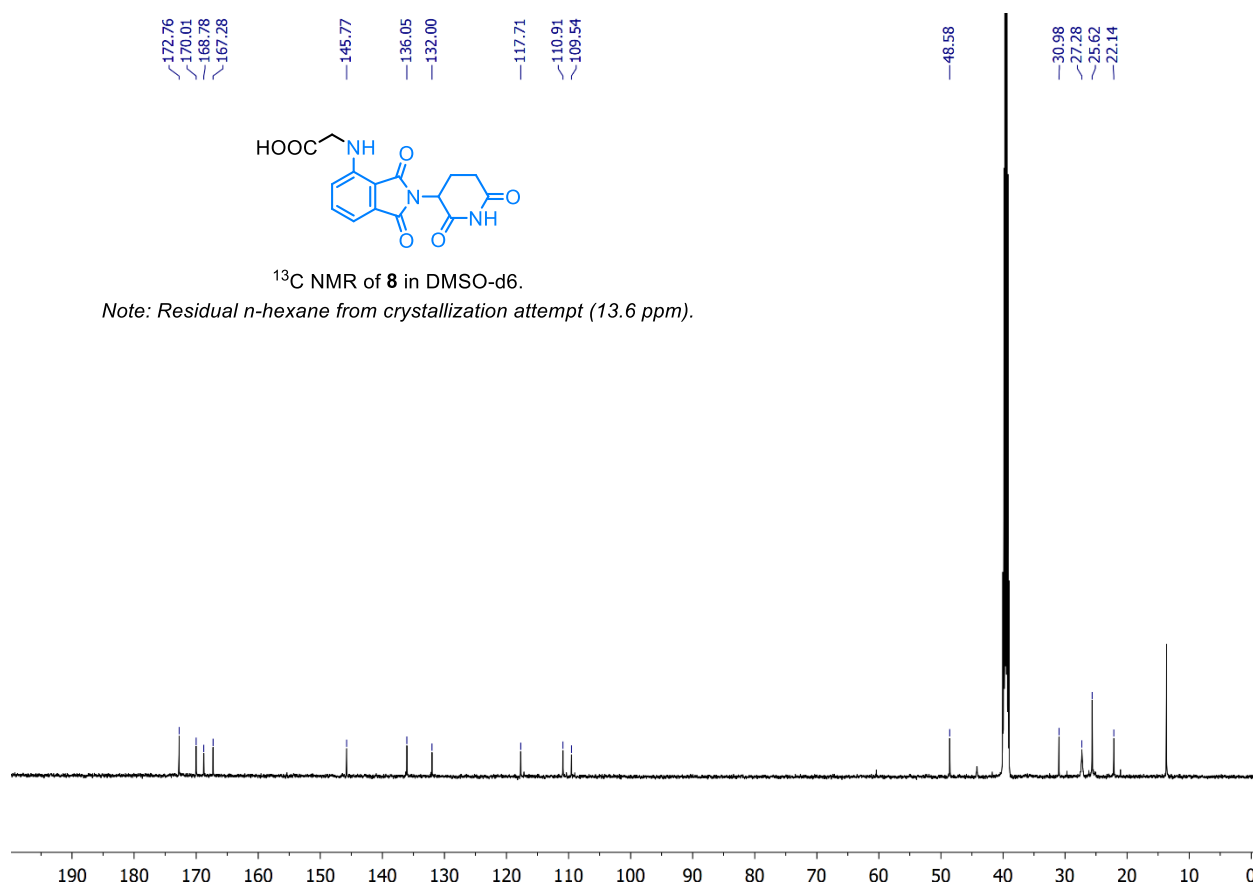
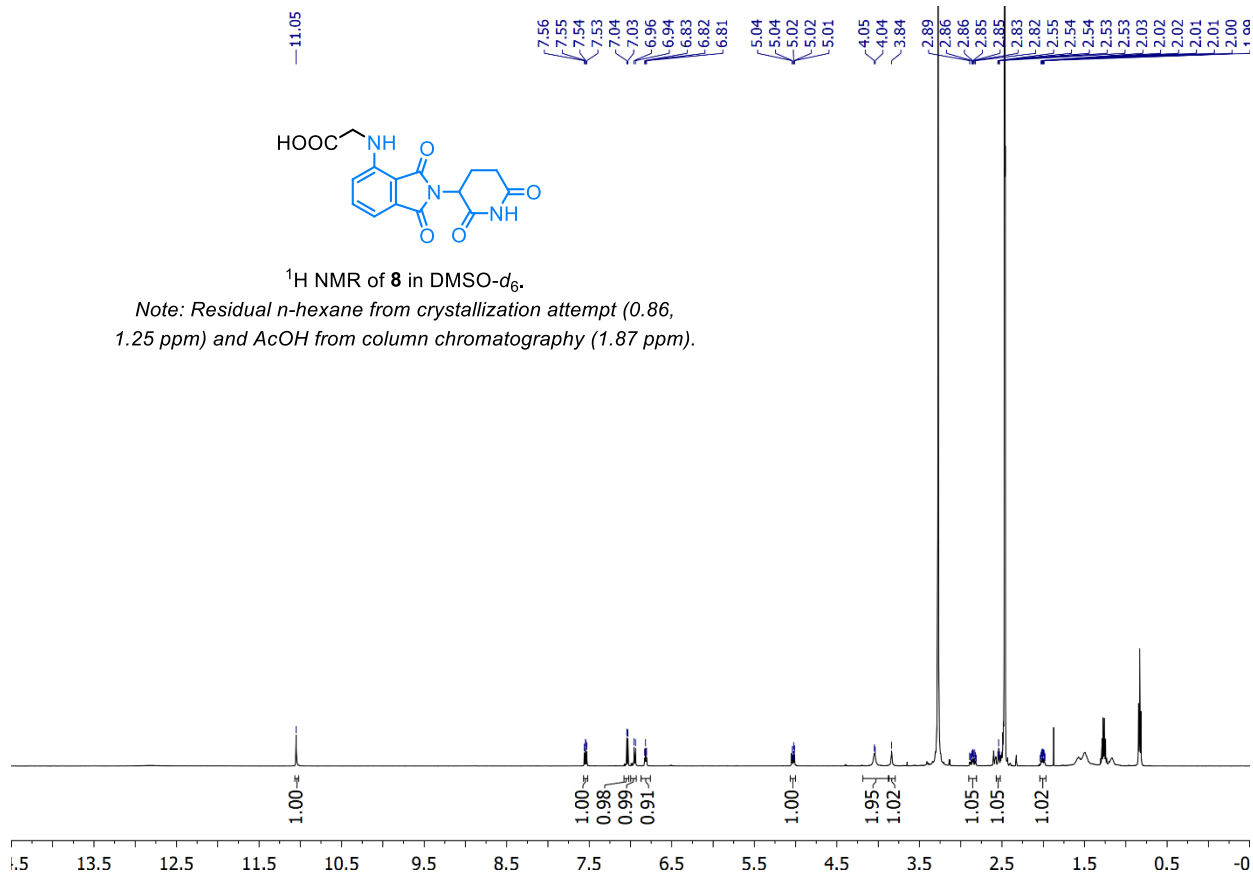
158.11
154.81
152.00
151.40
146.30
138.04
136.17
135.61
132.66
128.89
128.14
126.92
121.06
115.69

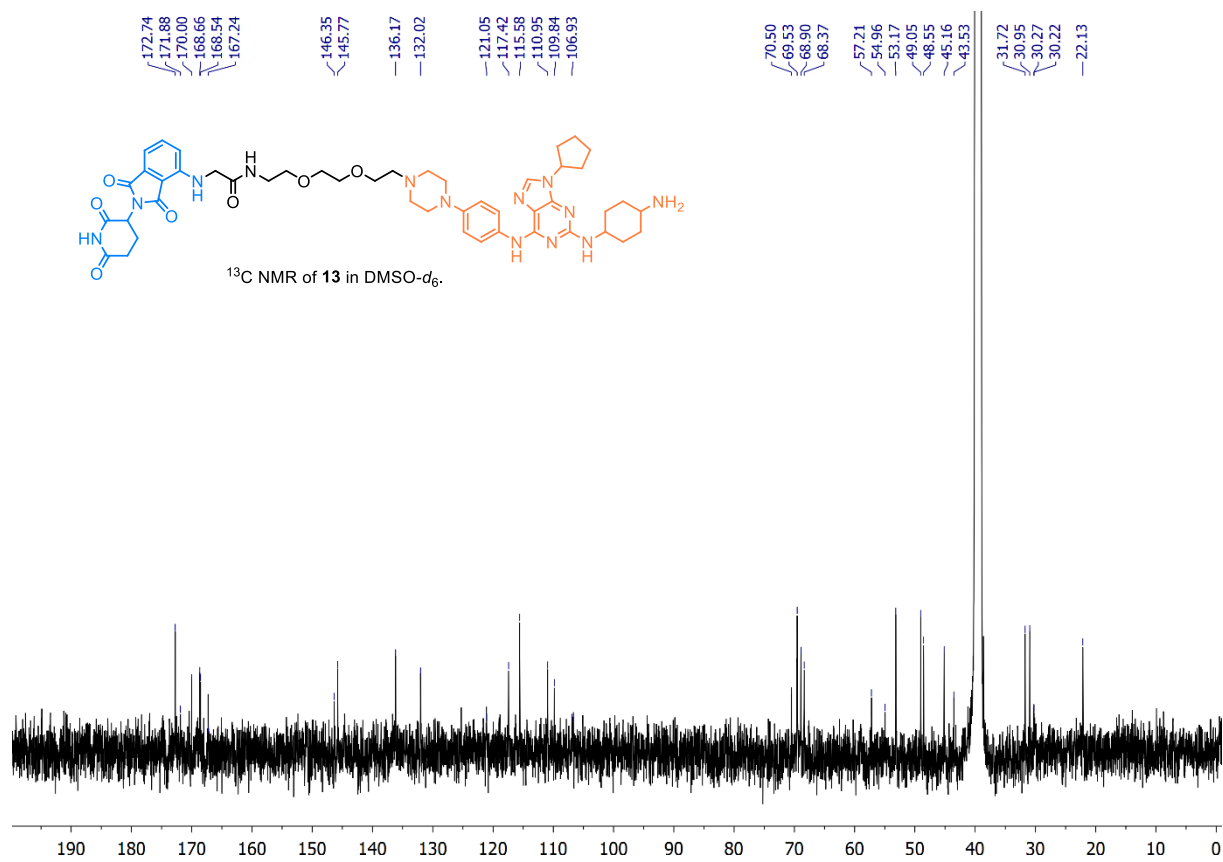
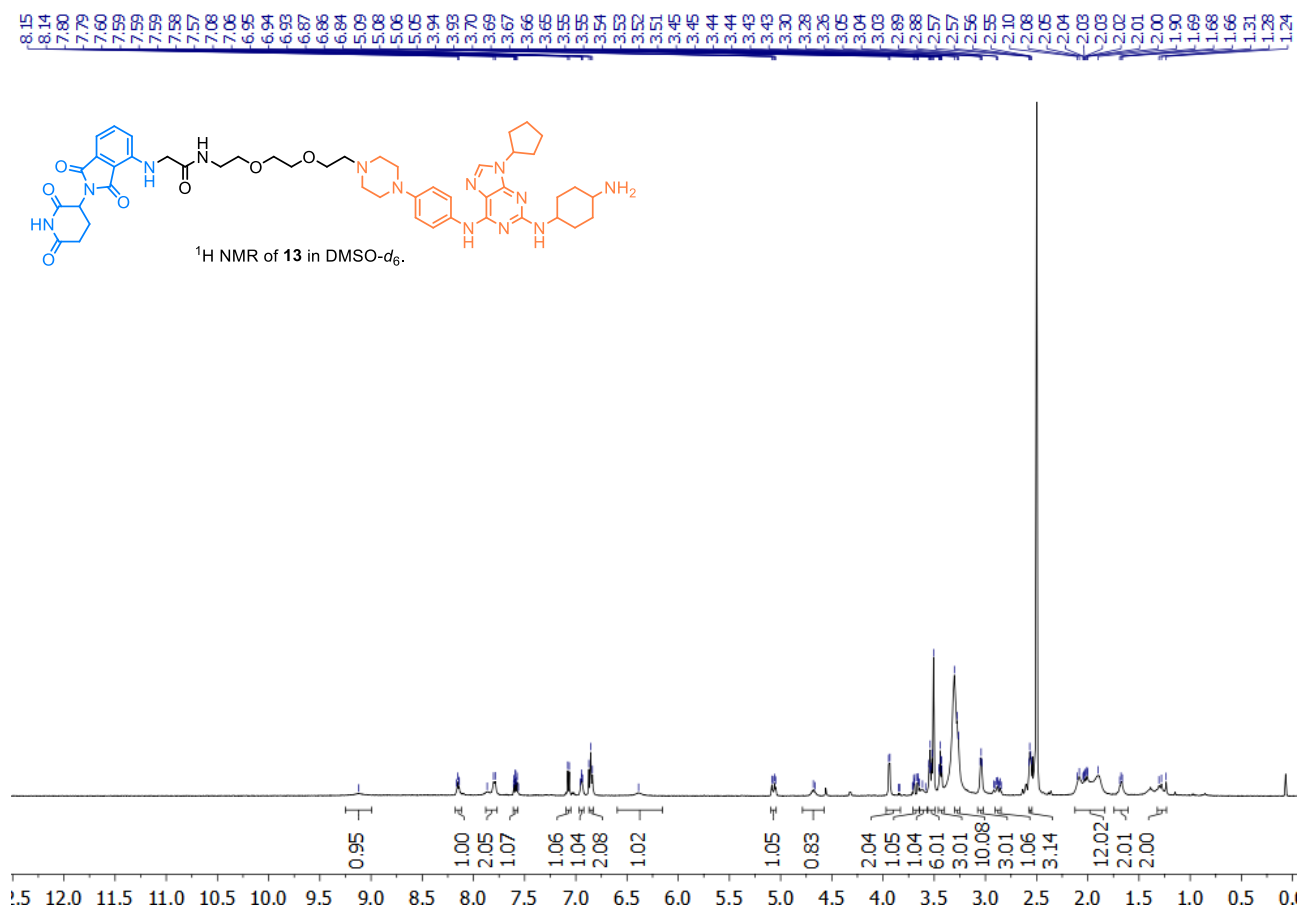


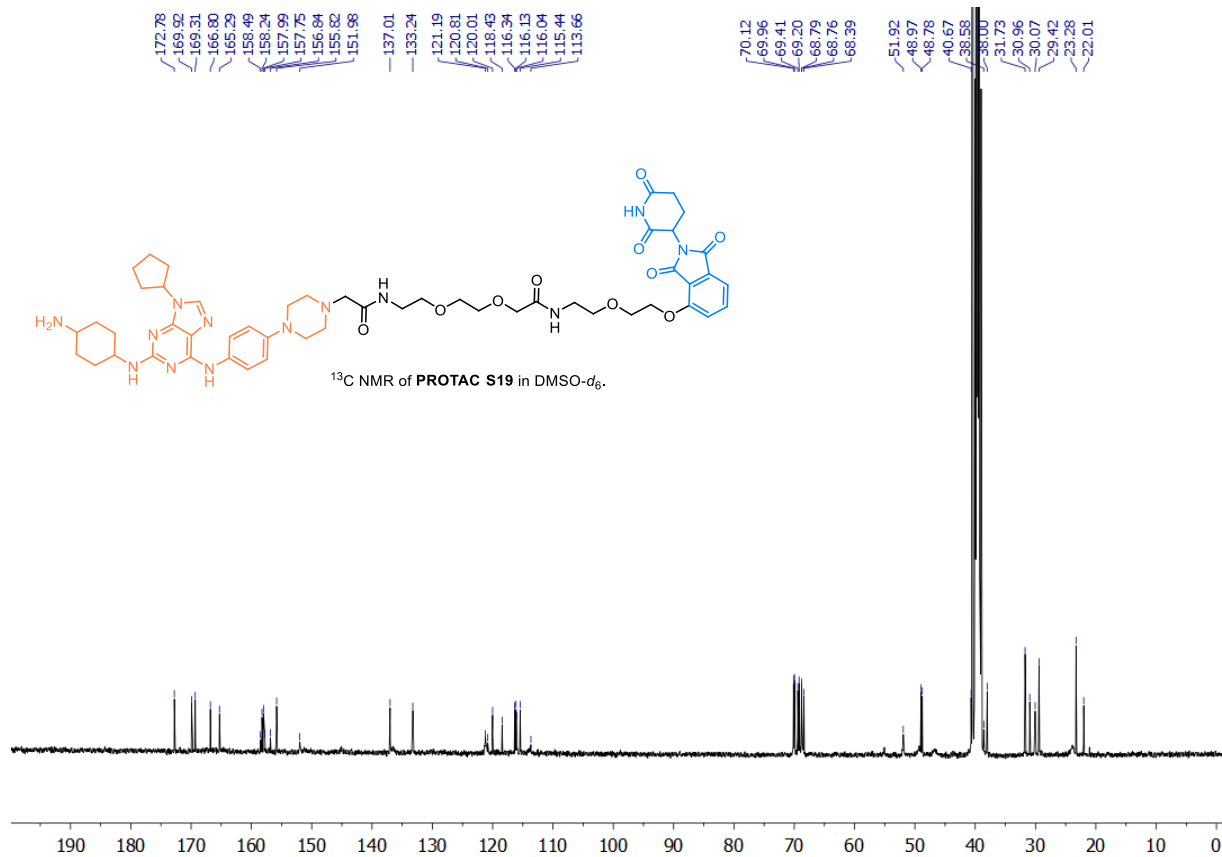
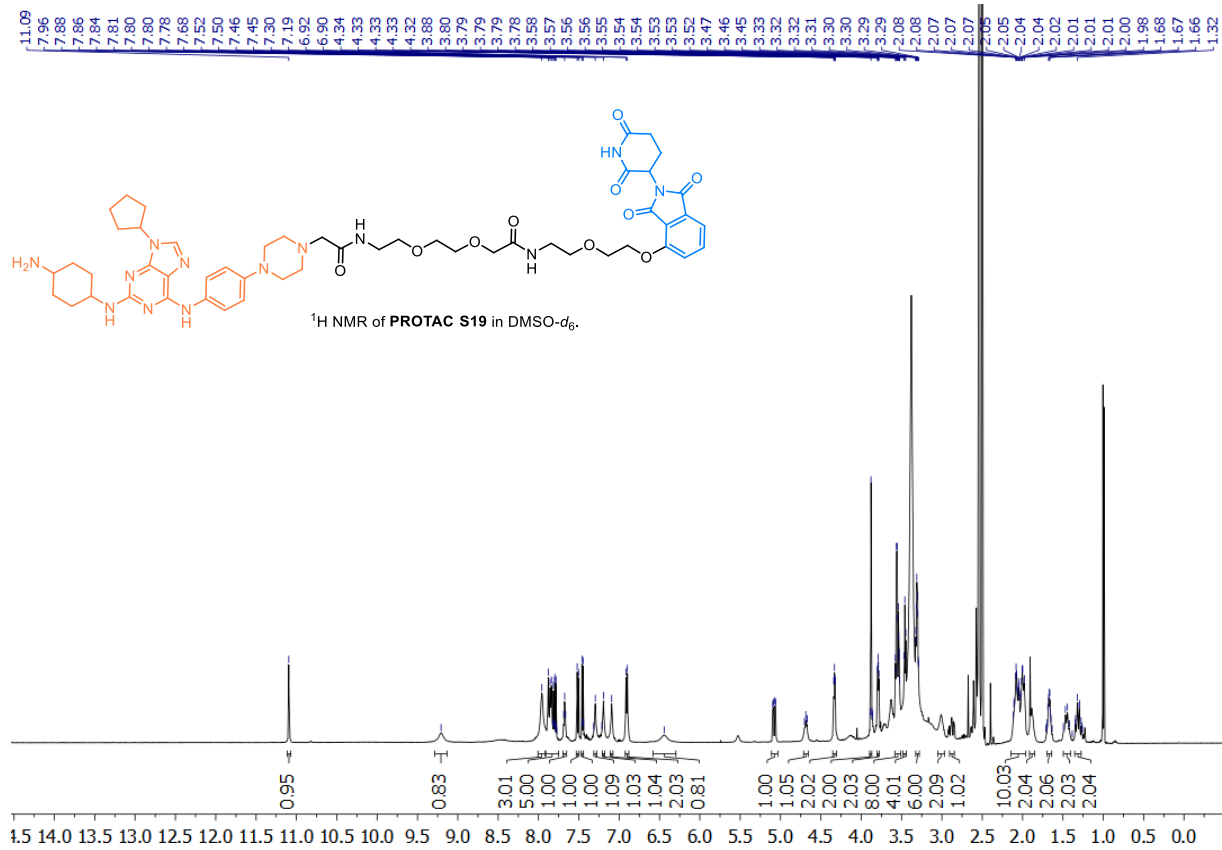
^{13}C NMR of **6** in $\text{DMSO-}d_6$.





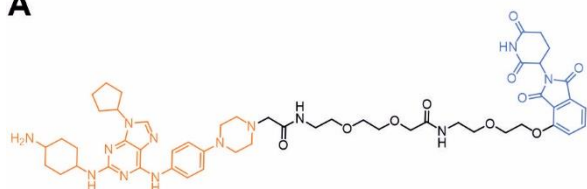






Supplementary figures

A



B

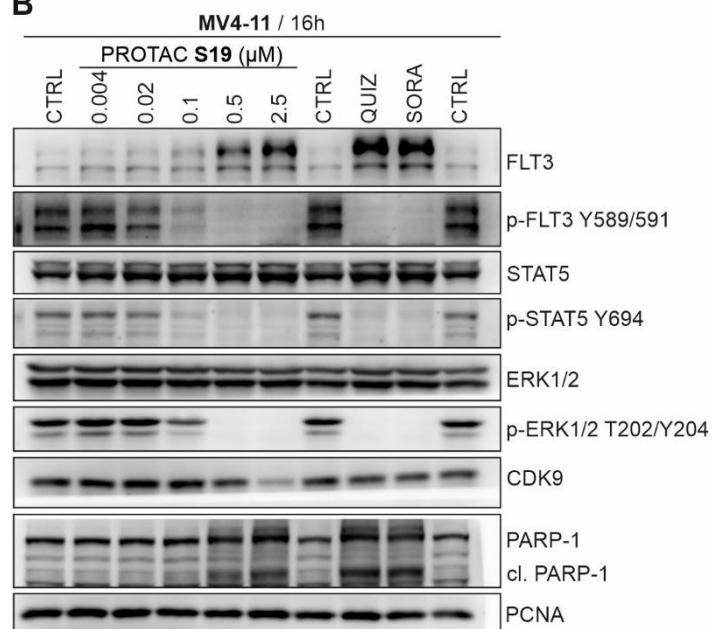


Fig. S1. (A) Structure of **PROTAC S19** and (B) its effect on the MV4-11 cells. Quizartinib (QUIZ) and sorafenib (SORA) at 0.1 μM concentration were used as controls.

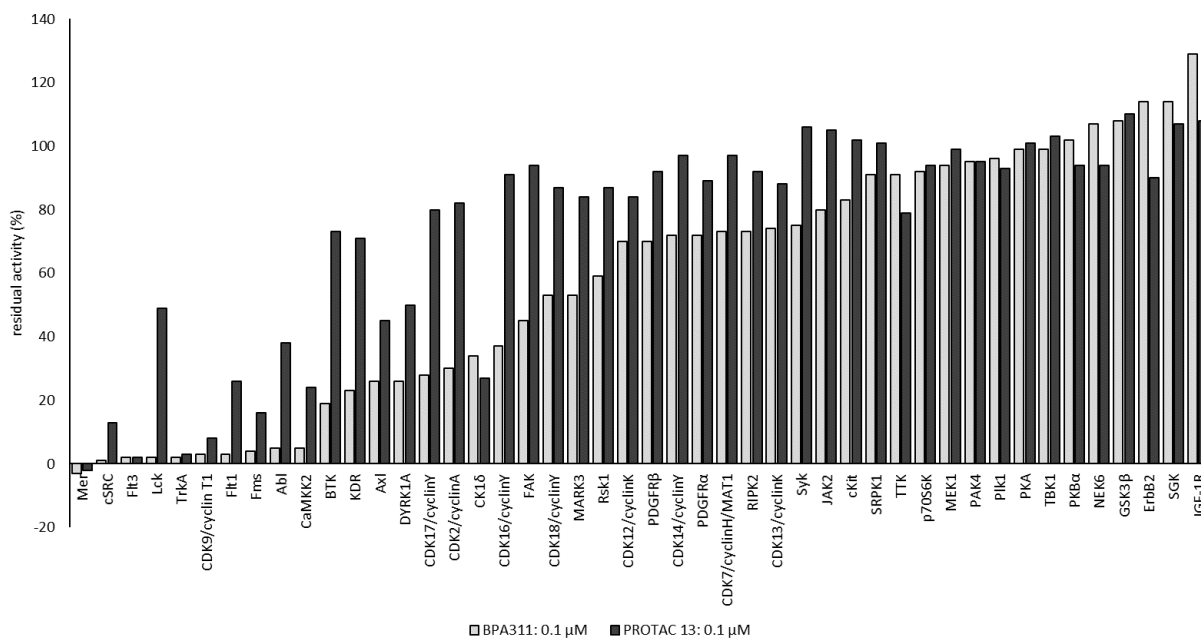


Fig. S2. Protein kinase selectivity of **BPA311** compare to **PROTAC 13**.

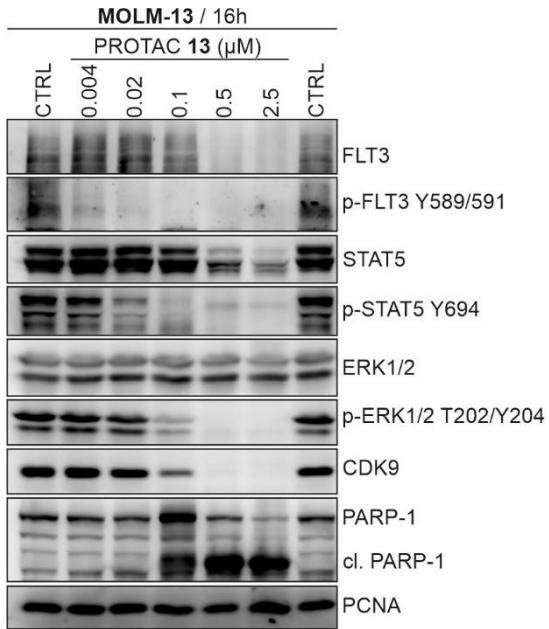


Fig. S3. Immunoblotting analysis of MOLM-13 cells treated with PROTAC 13.

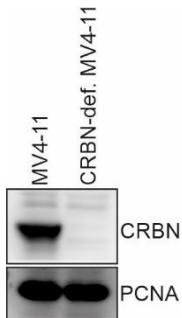


Fig. S4. The CRBN level in MV4-11 and CRBN-deficient MV4-11 cells.

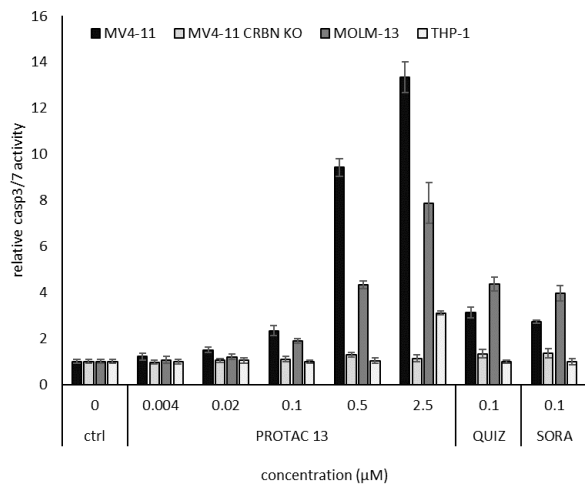


Fig. S5. Induction of apoptosis in MV4-11, CRBN-deficient MV4-11, MOLM-13 and THP-1 cells treated with PROTAC 13, quizartinib (QUIZ) and sorafenib (SORA) for 16 hours.

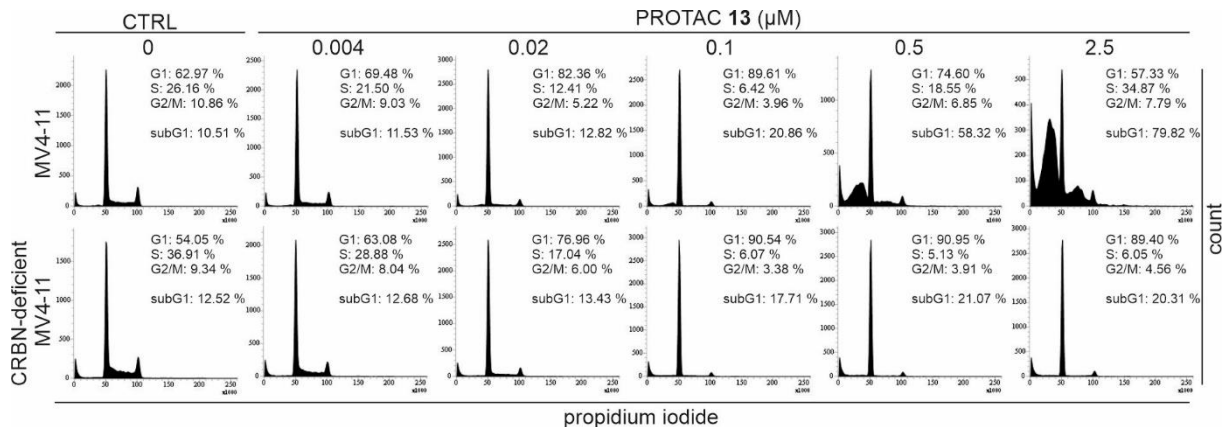


Fig. S6. Cell cycle analysis of MV4-11 and CRBN-deficient MV4-11 cells treated with indicated concentrations of PROTAC 13 for 16 hours.

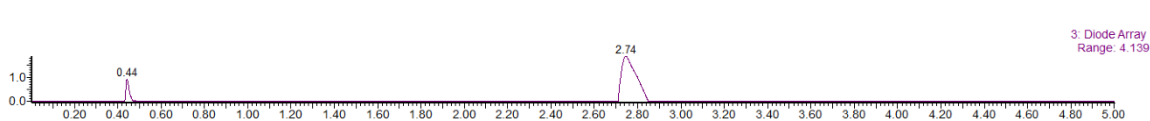


Fig. S7. UV-HPLC traces of PROTAC 13.

Reference

- [1] S. Krajcovicova, R. Jorda, D. Hendrychova, V. Krystof, M. Soural, Solid-phase synthesis for thalidomide-based proteolysis-targeting chimeras (PROTAC), *Chem. Commun. (Camb)*. 55 (2019) 929-932. <https://doi.org/10.1039/c8cc08716d>.

UNIVERZITA PALACKÉHO V OLOMOUCI

Přírodovědecká fakulta

Katedra experimentální biologie



Autoreferát k disertační práci

**Molekulární mechanismus působení vybraných
inhibitorů proteinkinas**

Mgr. Markéta Kovalová

B1527 Biologie

1501V019 Experimentální biologie

Olomouc 2024

Tato disertační práce byla vypracována v rámci prezenčního studia doktorského studijního programu Experimentální biologie 1501V019 na Přírodovědecké fakultě Univerzity Palackého v Olomouci. Školícím pracovištěm byla Laboratoř růstových regulátorů, Přírodovědecká fakulta, Univerzita Palackého v Olomouci.

Uchazeč: Mgr. Markéta Kovalová

Školitel: prof, RNDr. Vladimír Kryštof, Ph.D.
Katedra experimentální biologie
Přírodovědecká fakulta, Univerzita Palackého v Olomouci

Oponenti: doc. RNDr. Milan URBAN Ph.D.
Ústav molekulární a translační medicíny
Lékařská fakulta, Univerzita Palackého v Olomouci

doc. Mgr. Martin Trbušek, Dr.
Oddělení genetiky a molekulární biologie
Lékařská fakulta, Masarykova univerzita

Stanovisko k disertační práci vypracovala Laboratoř růstových regulátorů, Přírodovědecká fakulta, Univerzita Palackého v Olomouci.

Obhajoba se koná dne 29.1.2024 před komisí pro obhajoby disertačních prací v programu Experimentální biologie v seminární místnosti budovy..... Přírodovědecké fakulty Univerzity Palackého v Olomouci-Holici, Šlechtitelů 27.

S vlastní disertací je možno se seznámit 14 dní před obhajobou v knihovně biologických kateder Přírodovědecké fakulty Univerzity Palackého v Olomouci-Holici.

prof. Ing. Miroslav Strnad, CSc. DSc.

Předseda komise pro obhajoby disertačních prací ve studijním programu EXBIO, Přírodovědecká fakulta, Univerzita Palackého v Olomouci

Souhrn

Cyklin dependentní kinasy (CDK) představují klíčové regulátory nejen transkripčního cyklu a jejich funkce je v nádorových buňkách často narušena. To, společně s transkripční závislostí nádorů, představuje slibné důvody pro využití inhibice transkripčních CDK v nádorové terapii a v posledních letech byla představena řada slibných tCDK inhibitorů. První část této disertační práce je zaměřena na využití již známých inhibitorů tCDK v léčbě leukemií s KMT2A translokací, jejichž aplikace by mohla být přínosem ve srovnání se standardizovanou léčbou. V druhé části práce je představen nový trisubstituovaný pyrazolo[4,3-*d*]pyrimidinový derivát, LGR6768, který inhiboval CDK7 v nanomolárních koncentracích. Tento inhibitor vykazoval slibné antileukemické účinky a jeho aplikace ovlivnila buněčný cyklus i transkripci a vedla k apoptose nádorových buněk. Poslední část této práce vychází z optimalizace duálního FLT3 a CDK9 inhibitoru. Ta vedla k vývoji nového ATP-kompetitivního FLT3 inhibitoru a také duálního degradéru FLT3/CDK9, jejichž testování a charakterizace byla zaměřena na leukemie s FLT3-ITD mutací.

Obsah

Souhrn.....	3
1 Úvod a cíle práce.....	5
2 Metodika	7
2.1 Buněčné kultury	7
2.2 Analýza cytotoxicity.....	8
2.3 Analýza exprese genů.....	8
2.4 Analýza buněčného cyklu	8
2.5 SDS PAGE a imunodetekce	9
2.6 Detekce aktivity kaspas 3/7	9
3 Komentované výsledky a diskuze.....	10
3.1 Inhibitory CDK v léčbě leukemií s <i>KMT2A</i> translokací	10
3.2 CDK7 jako potenciální terapeutický cíl	15
3.3 Od CDK inhibice k inhibici FLT3	21
4 Závěr	26
5 Seznam použité literatury.....	29
6 Přehled publikační činnosti.....	33
7 Summary	35

1 Úvod a cíle práce

Proteinkinasy představují klíčové regulátory široké škály buněčných procesů včetně regulace proliferace a diferenciaci buněk, transkripce, apoptosy či buněčného metabolismu. Zprostředkovávají přenos γ -fosfátové skupiny z ATP na cílový substrát vedoucí ke konformační změně substrátu a ovlivnění jeho aktivity. Deregulace proteinkinas, způsobená změnami v expresi či mutacemi, je pozorována u řady onemocnění včetně nádorových, neurodegenerativních či zánětlivých (Manning *et al.*, 2002; Rask-Andersen *et al.*, 2014)

Mezi proteinkinasy patří i rodina cyklin-dependentních kinas (CDK). Jedná se o skupinu serin/threonin kinas, jejichž katalytická aktivita je závislá na regulační podjednotce, kterým je obvykle protein cyklin. V genomu člověka bylo popsáno 21 genů kódujících CDK a většina z nich specificky váže pouze jeden nebo několik málo z 30 známých cyklinů. Na základě strukturních a funkčních studií byly CDK rozděleny do dvou podrodin – CDK regulující buněčný cyklus (CDK1-6 a CDK14-18) a CDK regulující transkripci (CDK7-13, CDK19 a CDK20) (Malumbres *et al.*, 2009; Malumbres, 2014; Wood *et al.*, 2018). Mimo tyto hlavní dva procesy jsou však zapojeny do regulace široké plejády dalších buněčných procesů, jako jsou například opravy DNA (Blazek *et al.*, 2011; Nepomuceno *et al.*, 2017), sestřih RNA (Hu *et al.*, 2003), epigenetické modifikace (Ebmeier *et al.*, 2017) či neurogeneze (Jessberger *et al.*, 2009) a spermatogeneze (Mikolcevic *et al.*, 2012). Struktura CDK je dvoulaločná, obdobně jako struktura většiny kinas. Menší amino-terminální lalok je tvořený primárně β -skládanými listy. Ty jsou spojené flexibilní pantovou oblastí s α -helixy tvořící větší karboxy-terminální lalok. Mezi tyto oblasti je vmezeřeno konzervativní aktivní místo složené z ATP-vazebné domény, cyklin-vazebné domény a T-aktivační smyčky (Whittaker *et al.*, 2017; Wood *et al.*, 2018).

Pro svoji esenciální roli a častou deregulaci v rámci nádorových onemocnění představují CDK slibné terapeutické cíle již několik dekád. Vývoj selektivních inhibitorů však komplikuje vysoká strukturní similarita a konzervativnost ATP-vazebné domény. První ATP-kompetitivní inhibitory vykazovaly velmi omezenou selektivitu, což společně s nedostatečným pochopením mechanismu účinku vedlo k jejich toxicitě a u většiny z nich také k selhání v klinických testováních. Nicméně v průběhu let byla objevena řada strukturních odlišností mezi jednotlivými CDK, které umožnily vývoj nových selektivních, nejen ATP-kompetitivních, inhibitorů. Některé již byly schváleny pro léčbu (např. CDK4/6 specifické inhibitory palbociclib, abemaciclib, ribociclib a trilaciclib) a velká řada z nich je testována v klinických studiích (Whittaker *et al.*, 2017; Zhang *et al.*, 2021).

Tato disertační práce je zaměřena na charakterizaci nových nízkomolekulárních inhibitorů transkripčních cyklin-dependentních kinas, které byly navrženy a připraveny na pracovišti školitele, s cílem pochopit jejich mechanismu účinku a ověřit možnosti jejich využití jako protinádorová léčiva se zaměřením na leukemická onemocnění.

2 Metodika

2.1 Buněčné kultury

Lidské nádorové linie byly získány z European Collection of Authenticated Cell Culture, German Collection of Microorganisms and Cell Cultures, Cell Line Service, American Tissue Culture Collection nebo byly darovány doc. Janem Bouchalem z Univerzity Palackého v Olomouci. Všechny buněčné linie byly kultivovány ve vhodném médiu doplněné o 10% fetální bovinní sérum, streptomycin (100 µg/ml), penicilin (100 IU/ml) a glutamin (4 mM) a kultivovány v 37°C a 5% CO₂. Seznam použitých buněčných linií s kultivačním médiem a zdrojem je shrnut v Tab. 1.

Tab. 1: Seznam použitých lidských nádorových linií

Buněčná linie	Nádorový typ	Zdroj	Kultivační médium
22Rv1	karcinom prostaty	LF UP*	RPMI
BT474	karcinom prsu	LF UP*	DMEM
CCFR-CEM	ALL	ECACC	RPMI
DU145	karcinom prostaty	LF UP*	RPMI
G361	Melanom	ECACC	DMEM
HL-60	AML	ECACC	IMDM
K562	CML	ECACC	DMEM
LAPC4	karcinom prostaty	LF UP*	DMEM
MCF7	karcinom prsu	ECACC	DMEM
MINO	Lymfom	ATCC	RPMI
ML-2	AML	DMSZ	RPMI
MOLM-13	AML	DSMZ	RPMI
MV4-11	AML	Cell line service	RPMI
RS4-11	ALL	DSMZ	α-MEM
SEM	ALL	DSMZ	IMDM
SKBR3	karcinom prsu	ATCC	DMEM
THP-1	AML	DSMZ	RPMI
U937	AML	DSMZ	RPMI

AML – akutní myeloidní leukemie; ALL – akutní lymfoblastická leukemie; CML – chronická myeloidní leukemie; ATCC - American Tissue Culture Collection; DSMZ - German Collection of Microorganisms and Cell Cultures; ECACC - European Collection of Authenticated Cell Culture

* Buňky byly získány z Ústavu patologie Lékařské fakulty Univerzity Palackého Olomouc.

2.2 Analýza cytotoxicity

Pro analýzu cytotoxických účinků studovaných látek byla použita metoda Calcein AM, která je založena na hydrolýze calceinu AM intracelulárními esterasami živých buněk na silně fluorescenční calcein.

Buněčné linie byly vysazeny do 96-jamkové mikrotitrační desky a následující den byly ovlivněny požadovanými koncentracemi testovaných látek. Po 72hodinové inkubaci byl ke vzorkům přidán roztok Calceinu AM a po další 4hodinové inkubaci byla změřena fluorescence při 485/538 nm (excitace/emise) na fluorimetru Fluoreskan Ascent (Labsystem).

2.3 Analýza exprese genů

Buněčné linie určené pro analýzu exprese genů byly vysazeny na Petriho kultivační misky, ovlivněny testovanými látkami o příslušné koncentraci, sklizeny do lyzačního pufru a zamrazeny v -80 °C. Následovala izolace RNA pomocí RNeasy plus mini kitu (QIAGEN). V rámci izolace byla ze vzorků odstraněna gDNA. Koncentrace RNA byla stanovena pomocí spektrofotometru DeNovix. Stabilita RNA byla ověřena pomocí agarózové elektroforézy. Vzorky s intaktní RNA obsahovaly 2 jasné bandy odpovídající 28S a 18S RNA. Vyizolovaná RNA byla přepsána do cDNA pomocí SensiFAST cDNA Synthesis Kit (Bioline). Pro ověření efektivity transkripce byl do vzorku přidán RNA spike I (TATAA). Vlastní analýza genové exprese byla provedena pomocí qPCR za využití SensiFAST SYBR No-ROX kitu (Bioline) na přístroji CFX96 Real-time PCR Detection System (Biorad). Používané primery byly navrženy pomocí programu Primer Blast (Ye *et al.*, 2012) a nasyntetizovány firmou Generi biotech. Raw data byla vyhodnocena v programu CFX Maestro Software (Biorad Laboratories, ver 2.2) a relativní normalizovaná exprese byla stanovena pomocí metody delta delta Ct (Livak *et Schmittgen*, 2001). Exprese studovaných genů byla vztažena vždy k minimálně 2 referenčním genům, jejichž exprese byla v rámci daných experimentálních podmínek vyhodnocena jako nejstabilnější pomocí programů CFX Maestro Software (Biorad Laboratories, ver 2.2) nebo RefFinder (Xie *et al.*, 2012; Xie *et al.*, 2023). Sekvence použitých primerů jsou specifikovány v příslušných publikacích.

2.4 Analýza buněčného cyklu

Testované buněčné linie byly vysazeny na Petriho kultivační misky a následující den byly ovlivněny testovanými látkami. Po 24/48/72hodinové inkubaci byly buňky sklizeny a fixovány

ve vychlazeném 70% ethanolu přes noc. Následující den proběhla rehydratace vzorků v PBS, denaturace pomocí 2M HCl s 0,5% Tritonem X-100 a neutralizace pomocí 0,1M Na₂B₄O₇ (pH = 8,5). Vzorky byly poté značeny propidium jodidem (výsledná koncentrace 100 µg/ml) po dobu půl hodiny s následným měřením relativního obsah jaderné DNA pomocí průtokové cytometrie s využitím přístroje BD FACS Verse (FACSuite software, verze 1.0.6.) a 488 nm excitačního laseru. Pro analýzu buněčného cyklu byl použit software ModFit LT (Verity Software House, verze 4.1.7).

2.5 SDS PAGE a imunodetekce

Vzorky určené pro imunodetekci proteinů byly ovlivněny testovanými látkami, sklizeny a poté 20 minut lyzovány v extrakčním RIPA pufru (20 mM TRIS pH = 7,4; 100 mM NaCl; 2 mM EGTA; 5 mM EDTA; 0,2% Nonidet P-40 pH = 7,4; před použitím přidáno: 1 mM DTT; 1 mM PMSF; 1 mM Na₂VO₃; 2 mM NaF; 0,5 µg/ml leupeptin a 2 µg/ml aprotinin). Následně byly vzorky sonikovány pomocí ultrazvukového homogenizátoru a zcentrifugovány. Koncentrace proteinů v lyzátu byla stanovena spektrofotometrickou Bradfordovou metodou (Bradford, 1976). Pro vyrovnání koncentrace byly vzorky doplněny o vzorkovací pufr (0,3 M TRIS pH = 6,8; 10% SDS; 50% glycerol; 0,05% bromfenolová modř; 5% 2-merkaptoethanol) a poté byly denaturovány při 95 °C po dobu 3 minut.

Proteiny byly separovány s využitím polyakrylamidové elektroforézy za denaturujících podmínek a poté byly přeneseny na nitrocelulosovou membránu pomocí metody western blotting. Membrány byly blokovány v 3% BSA, inkubovány s primárními protilátkami přes noc, promyty a nakonec inkubovány se sekundárními protilátkami konjugovanými s křenovou peroxidasou. Aktivita peroxidasy byla detekována s využitím Super-Signal West Pico reagents (Merck) a CCD kamery LAS-4000 (FujiFilm). Použité protilátky jsou vždy specifikovány v příslušné publikaci.

2.6 Detekce aktivity kaspas 3/7

Buněčné lyzáty určené pro detekci aktivity kaspas 3/7 byly napipetovány do 96-jamkové mikrotitrační destičky s výslednou koncentrací proteinů 15 µg. Ke vzorkům byl přidán fluorescenčně značený substrát Ac-DEVD-AMC (Enzo Life Sciences) a reakční pufr (25 nM PIPES, 2 mM MgCl₂, 2 mM EGTA, 5 mM DTT, pH 7.3). Po inkubaci při laboratorní teplotě ve tmě následovala detekce fluorescenčního signálu při 355/460 nm (excitace/emise) s využitím fluorimetru Fluoreskan Ascent (Labsystem).

3 Komentované výsledky a diskuze

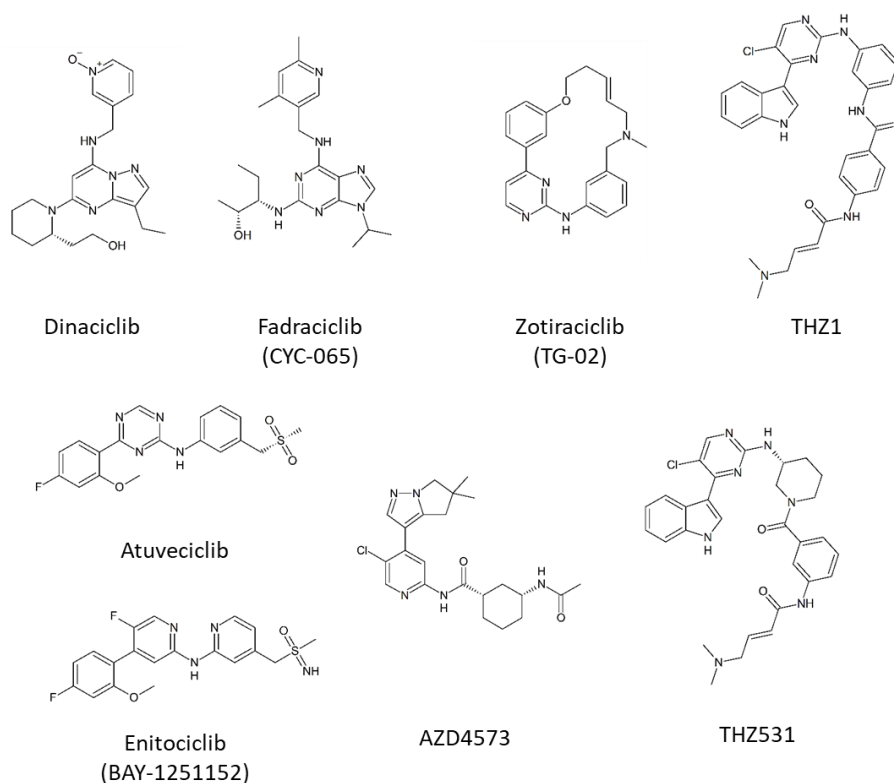
3.1 Inhibitory CDK v léčbě leukemií s *KMT2A* translokací

Inhibitory tCDK skrývají velký potenciál v protinádorové léčbě (Huang *et al.*, 2022; Li *et al.*, 2022; Vervoort *et al.*, 2022). Vzhledem k tomu, že CDK9 je v některých případech zapojena do *KMT2A*-r patogeneze, mohla by její selektivní inhibice představovat další terapeutický přístup v léčbě leukemií s *KMT2A* translokací. Tento typ leukemií je charakteristický špatnou odpovědí na standardizovaný léčebný protokol zejména u pacientů s ALL. Vývoj nových cílených léčiv, případně znovu-využití již schválených, by mohlo vést k zefektivnění léčby těchto leukemií (Tsakaneli et Williams, 2021; Górecki *et al.*, 2023; Kamens *et al.*, 2023).

Dílčím cílem práce bylo prověřit možnost využití inhibitorů tCDK pro léčbu leukemií s *KMT2A* translokacemi. Pro tuto část práce bylo zvoleno 8 různých CDK inhibitorů zahrnující pan-selektivní inhibitory, ale i selektivní inhibitory CDK7, CDK9 nebo CDK12/13. Selektivita jednotlivých inhibitorů popsána v původních publikacích je shrnuta v Tab. 2, jejich struktury jsou znázorněny na Obr. 1.

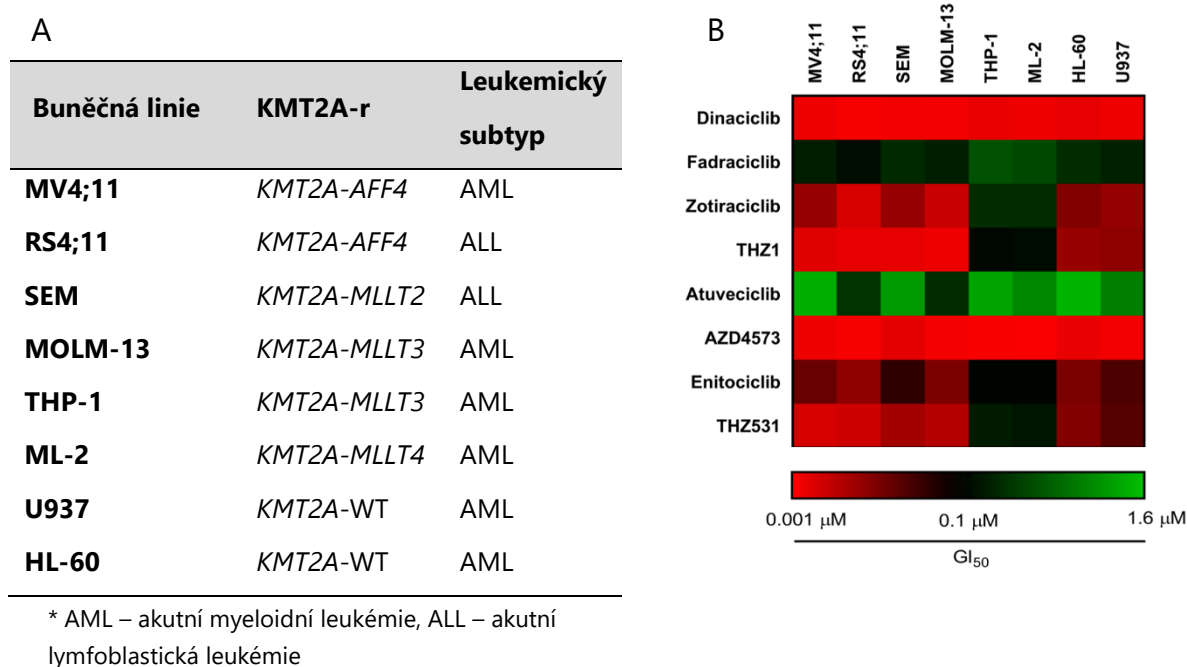
Tab. 2: Testované inhibitory CDK a jejich primárně uváděné kinasové cíle

Inhibitor	Publikované cíle	Primární publikace
Dinaciclib	CDK1, CDK2, CDK5, CDK9	(Parry <i>et al.</i> , 2010)
Fadraciclib	CDK2, CDK5, CDK9	(Frame <i>et al.</i> , 2020)
Zotiraciclib	CDK2, JAK, FLT3	(William <i>et al.</i> , 2012)
THZ1	CDK7	(Kwiatkowski <i>et al.</i> , 2014)
Atuveciclib	CDK9	(Lücking <i>et al.</i> , 2017)
AZD4573	CDK9	(Barlaam <i>et al.</i> , 2018)
Enitociclib	CDK9	(Luecking <i>et al.</i> , 2017)
THZ531	CDK12, CDK13	(Zhang <i>et al.</i> , 2016)



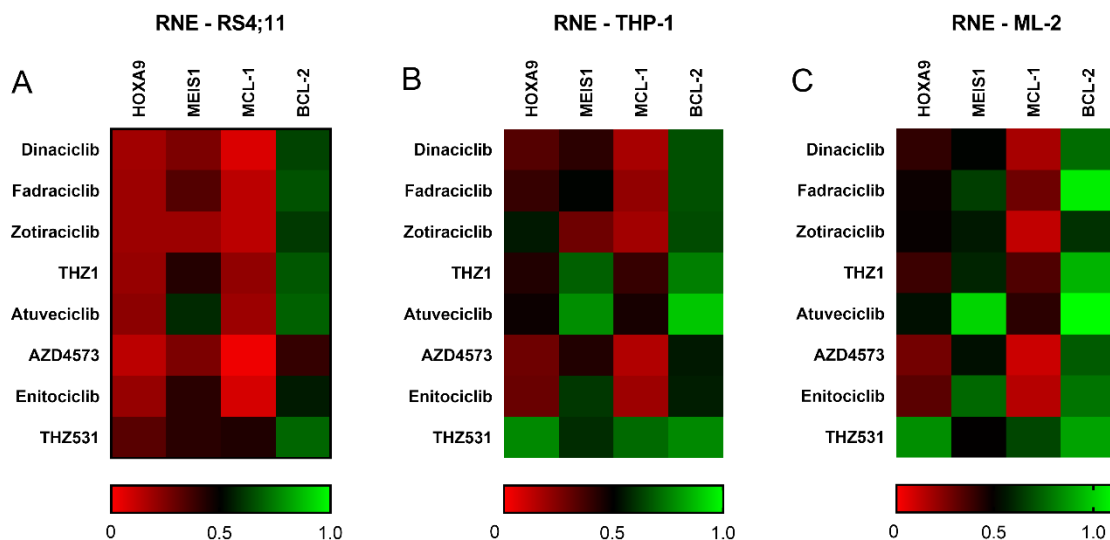
Obr. 1: Struktury použitých inhibitorů

Tyto látky byly nejprve testovány pro svou antiproliferační aktivitu na panelu leukemických linií zahrnující linie s translokací genu *KMT2A* (*KMT2A-r*) a i s původní nemutovanou variantou (*KMT2A-WT*) (Obr. 2A). Většina inhibitorů vykazovala na všech použitých leukemických liniích antiproliferační aktivitu s hodnotami GI_{50} v nanomolárních až submikromolárních koncentracích (Obr. 2B). V rámci *KMT2A-r* linií nebyl pozorován vliv fúzního partnera na citlivost vůči studovaným inhibitorům. Navíc tyto linie vykazovaly obdobnou citlivost jako linie *KMT2A-WT*, a to i v případě CDK9 selektivních inhibitorů. Přičemž u těchto inhibitorů byla očekávána vyšší citlivost vzhledem k patogenezi *KMT2A-r* leukemií.



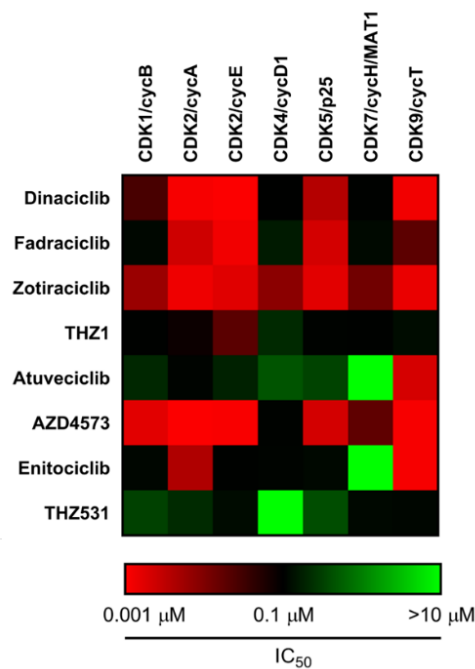
Obr. 2: (A) Seznam použitých buněčných linií. (B) Grafické znázornění antiproliferační aktivity testovaných inhibitorů na buněčných liniích *KMT2A-r* nebo *KMT2A-WT*.

Dále byl studován vliv testovaných látek na expresi genů zapojených do patogeneze *KMT2A-r* leukemií (*HOXA9*, *MEIS-1*) a apoptosy (*MCL-1*, *BCL-2*) (Armstrong *et al.*, 2002; Wong *et al.*, 2007; Faber *et al.*, 2009). Látky byly testovány na třech buněčných liniích s rozdílnou translokací genu *KMT2A*, konkrétně RS4;11, THP-1 a ML-2. V případě buněčné linie RS4;11 je přítomný fúzní partner (*AFF4*) součástí SEC, podobně jako P-TEFb (Lin *et al.*, 2010). Taktéž byly popsány interakce mezi *MLLT3*, nacházející se u linie THP-1, a komponentami transkripčního aparátu (Erfurth *et al.*, 2004; Monroe *et al.*, 2011). Navíc *MLLT3* patří mezi nejčastější fúzní partnery genu *KMT2A* (Meyer *et al.*, 2023). Testované látky byly aplikovány na buněčné linie v koncentraci 1 μM po dobu 2 hodin. Většina aplikovaných látek vedla k poklesu exprese genů *HOXA9* a *MCL-1* (Obr. 3). Oproti tomu například exprese genu *BCL-2* zůstala ve většině případů stabilní, což pravděpodobně souvisí s jeho vyšší stabilitou. Nicméně při porovnání efektu jednotlivých inhibitorů na studované geny nebyl ani zde pozorován výrazně odlišný efekt selektivních CDK9 inhibitorů ve srovnání s ostatními CDK inhibitory. Pozorovaný efekt spíše koreloval s cytotoxickými účinky použitých inhibitorů. Podobně byl studován vliv inhibitorů na hladiny fosforylace RNAPII a hladiny proteinů Mcl-1 a MEIS-1 u linií s *KMT2A* translokací. Předběžné výsledky imunoanalýzy také neodhalily specifický efekt CDK9 inhibitorů u *KMT2A-r* leukemických linií.



Obr. 3: Grafické znázornění relativní normalizované exprese studovaných genů po aplikaci vybraných inhibitorů u linií (A) RS4;11, (B) THP-1 a (C) ML-2. Látky byly aplikovány po dobu 2 hodin v koncentraci 1 μ M. Expresse genů byla normalizovaná ke genům *RPL13A* a *ACTB* v případě linie RS4;11, genům *RPL13A* a *GAPDH* v případě linie THP-1 a genům *RPL13A* a *B2M* v případě linie ML-2.

Získané výsledky nenaznačily žádný specifický efekt inhibice CDK9 u buněčných linií nesoucí translokaci v genu *KMT2A*. Nicméně v průběhu prováděných experimentů byla publikována studie Wells *et al.* (2020), zaměřující se na selektivitu známých CDK inhibitorů. V této studii bylo poukázáno na problematiku neselektivity inhibitorů, které jsou často popisovány jako selektivní, a to včetně některých inhibitorů zahrnutých v této práci. Podobné zjištění o nesprávně popisované selektivitě inhibitorů byla taktéž publikována kolektivem z pracoviště školitele (Jorda *et al.*, 2018; Hendrychová *et al.*, 2021). Z tohoto důvodu jsme se rozhodli otestovat selektivitu vybraných inhibitorů interním standardizovaným kinetickým testem. Naše výsledky korelují s výsledky Wells *et al.* (2020) a zejména u inhibitoru AZD4573 byla zjištěna jeho omezená selektivita (Obr. 4).



Obr. 4: Grafické znázornění inhibičních aktivit vybraných inhibitorů na panelu CDK.

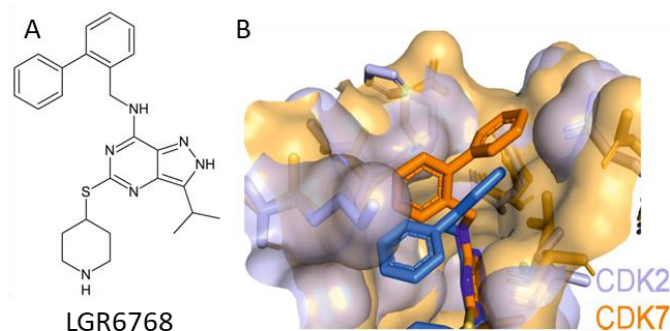
Z důvodu nedostatečné selektivity většiny použitých inhibitorů a také neprůkaznosti prozatímních výsledků jsme se rozhodli v této práci nepokračovat. Z testovaných látek vykazovaly inhibitory atuveciclib a enitociclib vyšší míru selektivity vůči CDK9. CDK9 inhibovaly v nanomolárních koncentracích a hodnoty IC_{50} pro další CDK byly alespoň 10x vyšší. Lze tedy předpokládat, že pokud by selektivní inhibice CDK9 vedla ke specifickému účinku u *KMT2A*-r leukemií, byl by tento efekt pozorován alespoň u těchto inhibitorů. Podobnou studii se zaměřením na CDK9 inhibitory u *KMT2A*-r leukemií provedli (Garcia-Cuellar *et al.*, 2014). Tato studie je zaměřena zejména na účinky flavopiridolu a inhibitoru PC585, kdy popisuje benefiční inhibici CDK9 u *KMT2A*-r leukemií. Flavopiridol je však pan-selektivní inhibitor CDK a i přesto, že PC585 je popisován jako vysoce selektivní CDK9 inhibitor, data potvrzující takovéto tvrzení nebyla publikována. Pozorované výsledky nelze tedy s jistotou přisuzovat inhibici CDK9. Nicméně jak naše, tak data publikovaná ve studii Garcia-Cuellar *et al.* (2014) mohou naznačovat, že selektivní i neselektivní inhibice CDK9 by mohla být u leukemií s *KMT2A*-r translokací benefiční, a to zejména ve srovnání se standardizovanou léčbou, která má velmi často pouze malou účinnost. Pro přesné pochopení mechanismu účinku CDK případně CDK9 inhibitorů u *KMT2A*-r leukemií je však potřeba provést další testování.

3.2 CDK7 jako potenciální terapeutický cíl

Cyklin-dependentní kinasa 7, jakožto duální regulátor transkripce i buněčného cyklu, představuje slibný terapeutický cíl v protinádorové léčbě. Zvýšená exprese CDK7 byla popsána v řadě nádorů, jako je například triple-negativní karcinom prsu, karcinom ovarií či hepatocelulární karcinom. Často také koreluje s agresivitou tumoru a horší prognózou pacientů. V posledním desetiletí byla představena celá řada selektivních CDK7 inhibitorů a šest z nich je aktuálně v klinickém testování (shrnutí v **(Kovalová *et al.*, 2023a; Příloha I)**).

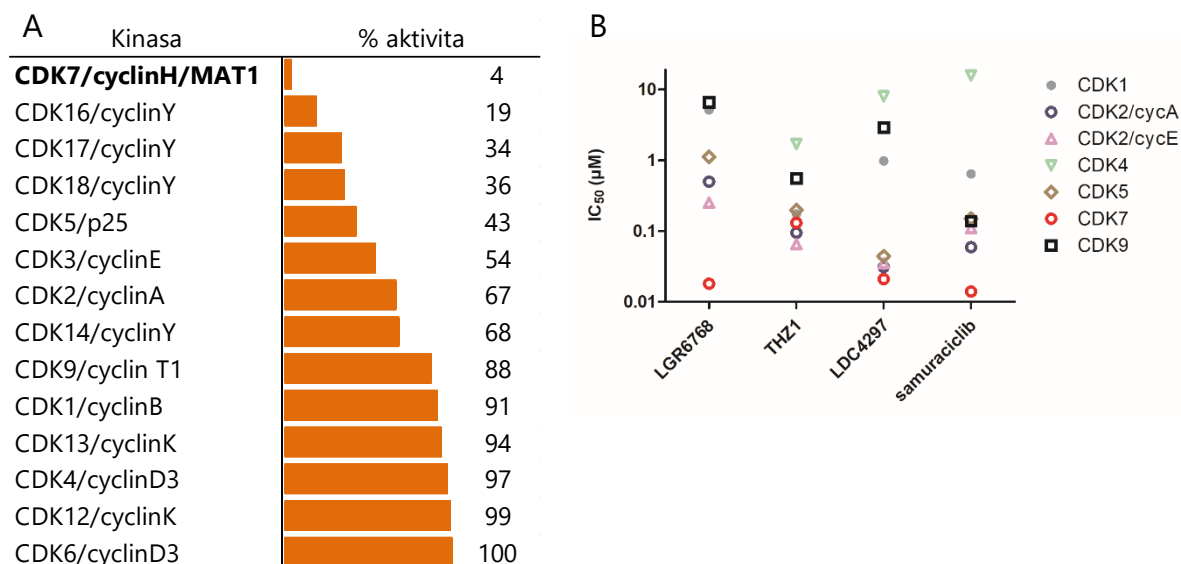
V dřívějších pracích publikovaných autory z pracoviště školitele bylo popsáno několik sérií velmi účinných 3,5,7-trisubstituovaných pyrazolo[4,3-*d*]pyrimidinů, které jakožto panselektivní CDK inhibitory vykazovaly silné protinádorové účinky *in vitro* a *in vivo* (Jorda *et al.*, 2011; Řezníčková *et al.*, 2015; Vymětalová *et al.*, 2016; Jorda *et al.*, 2019). Optimalizací těchto látek vznikl nový trisubstituovaný derivát pyrazolo[4,3-*d*]pyrimidinu, LGR6768 (Obr. 5A), který selektivně inhibuje CDK7 (**Kovalová *et al.*, 2023b; Příloha II**).

Pro pochopení selektivity byla nejprve porovnána jeho orientace v aktivním místě CDK2 a CDK7 na základě nově určené struktury kokrystalu (PDB ID 8B54), resp. modelu. I přes strukturní podobnost CDK2 a CDK7 byly pozorovány změny ve vazebné pozici LGR6768 v aktivních místech. Aktivní místo CDK7 je mnohem širší a otevřenější možným vazbám. LGR6768 je tedy v mnohem relaxovanější pozici a piperidinová část zasahuje hlouběji do aktivního místa. Hlavní rozdíl je v orientaci bifenyly. V případě CDK2 bifenyly směřuje do aktivního místa, kdežto u CDK7 se nachází na jeho okraji a směřuje ven. Tyto změny v orientaci by mohly být způsobeny rozdíly ve struktuře okraje aktivního místa mezi CDK2 a CDK7. Odlišná orientace bifenyly koresponduje s rozdílnými orientacemi benzylaminového substituentu u samuraciclibu, pozorovanými taktéž mezi CDK2 a CDK7 (Greber *et al.*, 2021). Důležitá je také mimo jiné substituce Ile10 (CDK2) za Leu18 (CDK7), s nímž bifenylový substituent vytváří hydrofobní interakce. Získané výsledky (Obr. 5B) naznačují, že pro selektivitu LGR6768 vůči CDK7 je klíčová orientace a interakce bifenylového substituentu.



Obr. 5: (A) Struktura látky LGR6768. (B) Srovnání vazebné pozice LGR6768 v CDK7 (oranžová) a CDK2 (modrá).

Pro stanovení selektivity bylo provedeno komerční kinomové testování na panelu 50 kinas, které zahrnovaly známé vedlejší cíle příbuzných pyrazolo[4,3-*d*]pyrimidinů (Jorda *et al.*, 2019) a purinových isosterů, jako jsou roscovitín a CR8 (Bettayeb *et al.*, 2008). Kinomové testování potvrdilo selektivní redukci aktivity CDK7 na 4 % a to při aplikování 1 μ M koncentrace látky. Pouze dvě další kinasy byly signifikantně inhibovány – CDK16 (Obr. 6A) a CK1 δ (**Příloha II, Fig S4**), obě s residuální aktivitou 19 %. Vzhledem k vysoké strukturní podobnosti v rámci rodiny CDK byla látka LGR6768 také testována interním standardizovaným kinetickým testem pro určení selektivity vůči některým CDK. Koncentračně závislé měření prokázalo potentní inhibici CDK7 v nízkých nanomolárních hodnotách s $IC_{50} = 20$ nM, přičemž hodnota byla nejméně 12x nižší než hodnoty IC_{50} pro zbylé testované CDK (**Příloha II, Tab S2**). Nakonec byla selektivita LGR6768 porovnána s dalšími CDK7 inhibitory, konkrétně THZ1, LDC4297 a samuracilibem (Obr. 6B). Látka LGR6768 vykazovala vyšší míru selektivity v porovnání s inhibitory LDC4297 a samuracilibem.



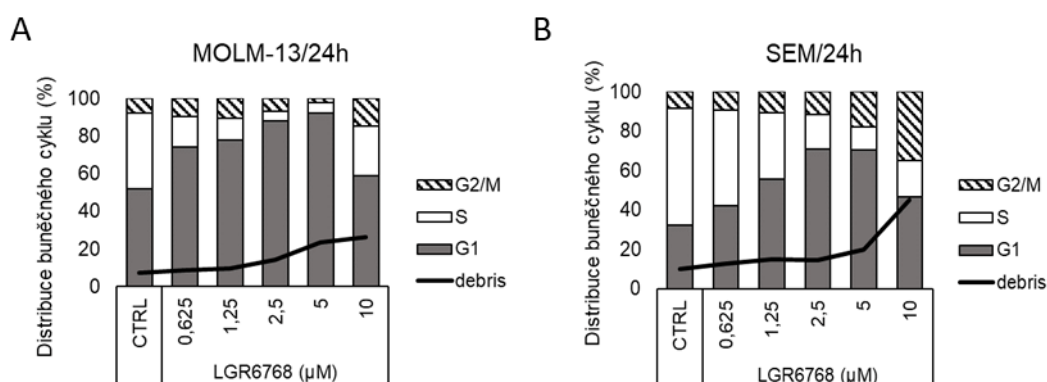
Obr. 6: (A) Selektivita LGR6768 vůči CDK při aplikaci látky v koncentraci 1 μM . (B) Srovnání inhibice vybraných CDK látkou LGR6768 a vybranými známými CDK7 inhibitory.

CDK7, jakožto součást CAK, je zapojena do regulace buněčného cyklu skrz fosforylaci T-smyčky CDK1 a CDK2 v místech Thr161, respektive Thr162. Imunoanalýza na buněčné nádorové linii SEM ukázala pokles ve fosforylaci obou kinas v závislosti na koncentraci (**Příloha II, Fig. 3C**) a době působení (**Příloha II, Fig. 3D**) aplikované látky LGR6768. Byla taktéž pozorována očekávaná defosforylace CTD RNAPII (**Příloha II, Fig. 3C, D**). Detekovaný pokles nebyl tak dramatický jako u méně selektivního CDK7 inhibitoru THZ1 (Kwiatkowski *et al.*, 2014) a naše výsledky více odpovídají novému selektivnímu inhibitoru YKL-5-124, který vykazoval pouze minimální efekt na fosforylaci CTD RNAPII (Olson *et al.*, 2019).

V předchozích studiích vykazovaly některé CDK7 inhibitory antileukemické účinky na AML i ALL liniích a taktéž AML xenograftech (Kwiatkowski *et al.*, 2014; Hu *et al.*, 2019; Park *et al.*, 2020; Abudureheman *et al.*, 2021). Z tohoto důvodu byla látka LGR6768 testována na panelu buněčných linií 10 hematologických malignit (5 AML, 3 ALL, 1 lymfom, 1 CML). Pozorovaná antiproliferační aktivita látky u leukemických buněčných linií dosahovala hodnot GI_{50} v rozmezí od 0,44 μM po 4,4 μM . Výjimku tvořily méně citlivé linie K562 a CCRF-CEM ($\text{GI}_{50} > 5 \mu\text{M}$). Látka byla testována také na buněčných liniích odvozených od jiných nádorových typů (karcinom prsu, prostaty, melanom). Tyto buněčné linie vykazovaly nižší citlivost vůči LGR6768 ve srovnání s AML a ALL liniemi, což naznačuje antileukemický potenciál látky (**Příloha II, Fig. 4A**). Ve srovnání se známými CDK7 inhibitory THZ1 (Kwiatkowski *et al.*, 2014) a SY-1365 (Hu *et al.*, 2019) vykazuje látka LGR6768 slabší

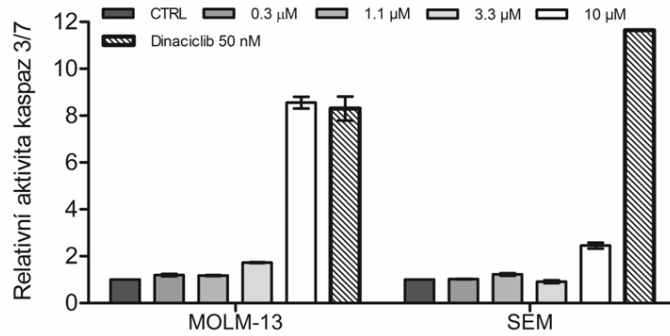
antiproliferační aktivitu. Nicméně obě tyto látky jsou kovalentními inhibitory, na rozdíl od LGR6768. To by mohlo vysvětlovat vyšší potenci látek vůči nádorovým buněčným liniím.

Inhibice CDK7 často vede k narušení buněčného cyklu, což je doprovázeno poklesem počtu buněk v S-fázi, a naopak nárůstem počtu buněk v G1 či G2/M fázi v závislosti na buněčné linii a koncentraci inhibitoru (Ali *et al.*, 2009; Kelso *et al.*, 2014; Choi *et al.*, 2019; Olson *et al.*, 2019; Marineau *et al.*, 2022; Gaur *et al.*, 2023). Aplikace látky po dobu jednoho dne vedla ke koncentračně závislému G1 bloku u linie SEM i MOLM-13 již v nejnižších koncentracích (Obr. 7). Nejvyšší aplikovaná koncentrace (10 μM) pak vedla k signifikantní apoptose doprovázené G2/M blokem.



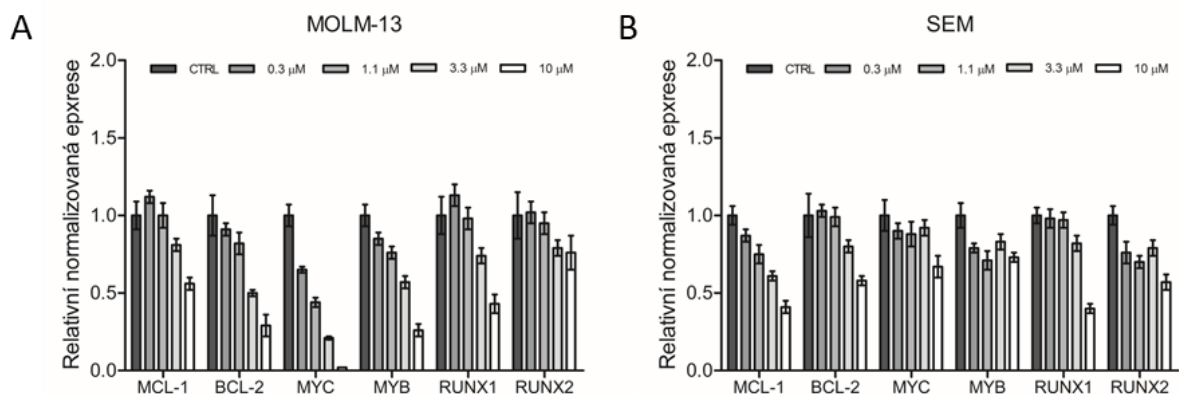
Obr. 7: Vliv LGR6768 na buněčný cyklus linií (A) MOLM-13 a (B) SEM po 24 hodinách.

Pro-apoptický efekt látky byl dále studován pomocí imunoanalýzy na buněčných liniích MV4-11, MOLM-13 a SEM (**Příloha II, Fig. 5A**). Látka byla aplikována po dobu 24 hodin ve vzrůstající koncentraci. Efekt látky byl pozorován pouze v nejvyšší aplikované koncentraci (10 μM), kdy bylo detekováno štěpení apoptického markeru PARP-1 a také fragmenty caspasy-7 a caspasy-9. Aplikace látky vedla také k mírnému snížení hladiny anti-apoptického proteinu Mcl-1, avšak hladiny anti-apoptického proteinu Bcl-2 zůstaly stabilní. To je pravděpodobně způsobeno jeho vyšší stabilitou. Podobné výsledky již byly popsány u jiných CDK7 inhibitorů (Kwiatkowski *et al.*, 2014; Patel *et al.*, 2018; Hu *et al.*, 2019; Gaur *et al.*, 2023). Pro-apoptický účinek látky byl v souladu s imunoanalýzou potvrzen i fluorimetrickým kaspasovým testem, a to na buněčných liniích MOLM-13 i SEM po 24hodinovém ovlivnění látkou LGR6768 (Obr. 8).



Obr. 8: Relativní aktivita kaspaz 3/7 v buněčných liniích MOLM-13 a SEM po ovlivnění látkou LGR6768 nebo dinacilbem po dobu 24 hodin.

Vzhledem ke změnám na proteinové úrovni byl studován vliv látky LGR6768 na expresi genů hrající významnou roli při apoptose, hematopoese nebo v AML patogenezi (*BCL-2*, *MCL-1*, *RUNX*, *MYC*, *MYB*) (Obr. 9). U většiny těchto genů byly již dříve popsány změny v transkripci vlivem působení některých inhibitorů tCDK (Kwiatkowski *et al.*, 2014; Zeng *et al.*, 2018; Hu *et al.*, 2019; Cidado *et al.*, 2020; Abudurehman *et al.*, 2021). Vzrůstající dávky LGR6768 vedly k poklesu exprese anti-apoptických genů *MCL-1* a *BCL-2*. Změny byly detekovány již po 4 hodinách, což naznačuje rychlou inhibici a schopnost indukovat apoptosu. U většiny genů došlo alespoň k dvojnásobnému poklesu exprese, který byl koncentračně závislý. V případě genu *MYC* u linie MOLM-13 došlo k rapidnímu poklesu exprese na < 1 % hladiny exprese kontrol. To by mohlo být vysvětleno vysokou sensitivitou linie MOLM-13 k látce LGR6768.



Obr. 9: Relativní normalizovaná exprese genů souvisejících s apoptosou a kódující transkripční faktory souvisejících s patogenezi hematologických malignit u buněčných linií (A) MOLM-13 a (B) SEM. Buňky byly ovlivněny vzrůstající koncentrací látky LGR6768 po dobu 4 hodin. Exprese genů byla normalizovaná k referenčním genům *GAPDH* a *RPL13A* (MOLM-13) nebo *GAPDH* a *B2M* (SEM).

Vzhledem k duální roli při regulaci buněčného cyklu i transkripce představuje cílení na CDK7 zajímavou terapeutickou možností v léčbě nádorových onemocnění (Diab *et al.*, 2020; Li *et al.*, 2022; **Kovalová *et al.*, 2023a; Příloha I**). V této části byla popsána látka LGR67468, nový pyrazolo[4,3-*d*]pyrimidinový derivát, který účinně a selektivně inhibuje CDK7. Účinky této látky odpovídají dalším popsaným CDK7 inhibitorům (Hu *et al.*, 2019; Olson *et al.*, 2019; Gaur *et al.*, 2023).

3.3 Od CDK inhibice k inhibici FLT3

Poslední část této práce je věnována studiu mechanismu působení duálních inhibitorů kinas s antileukemickými účinky, ať již na bázi konvenčních ATP kompetitivních inhibitorů, nebo na bázi proteolýzy indukujícího chimérodního konjugátu (PROTAC), který indukuje specifickou degradaci cílových kinas, konkrétně CDK9 a onkogenní kinasy FLT3.

FMS-like tyrosin kinasa (FLT3) je jednou z 56 receptorových tyrosin kinas (RTS). Její exprese je asociována primárně s ranými hematopoetickými buňkami a je nezbytná pro proliferaci a diferenciaci hematopoetických progenitorů (Kazi *et Rönstrand*, 2019). Zhruba u 30 % pacientů s AML je detekována aktivační mutace ve *FLT3*. Nejčastěji se jedná o interní tandemovou duplikaci (ITD) v juxtamembránové doméně, která vede k dimerizaci FLT3 bez přítomnosti ligandu. Méně časté jsou bodové mutace v kinasové doméně, které způsobují konstitutivní aktivaci FLT3 (Meshinchi *et Appelbaum*, 2009; Daver *et al.*, 2021). Vzhledem k významu FLT3 v patologii AML došlo v posledních letech k vývoji několika FLT3 inhibitorů. Přičemž midostaurin (Levis, 2017), gilteretinib (Dhillon, 2019) a quizartinib (Zarrinkar *et al.*, 2009) byly již schváleny FDA pro léčbu AML pacienty s FLT3 mutací. Nicméně odpověď na FLT3 inhibitory je často limitována rozvojem rezistence.

Výchozím bodem pro tuto část práce byla série 2,6,9-trisubstituovaných purinů, které silně inhibovaly CDK a některé z nich také FLT3 (Gucký *et al.*, 2018). Jedna z neúčinnějších modelových látek této série (BPA311) inhibovala cílové kinasy v nanomolárních koncentracích a podobně vysoká účinnost byla pozorována také v leukemických buňkách exprimujících onkogenní variantu *FLT3*-ITD. Modifikací struktury BPA311 byly získány další nové látky s odlišným mechanismem účinku – kompetitivní inhibitor **34f** (Břehová *et al.*, 2023; Příloha III) a proteolýzu indukující chimérodní konjugát PROTAC 13 (Řezníčková *et al.*, 2022; Příloha IV).

Nové kompetitivní inhibitory byly získány racionální modifikací již výše zmíněných trisubstituovaných purinů (Gucký *et al.*, 2018); konkrétně byly navrženy, připraveny a studovány isosterní trisubstituované deriváty s rozdílnými heterocyklickými jádry místo purinu jako jsou thieno[3,2-*d*]pyrimidiny, pyrazolo[1,5-*a*]pyrimidiny, imidazo[4,5-*b*]pyridiny, pyrido[4,3-*d*]pyrimidiny a imidazo[1,2-*b*]pyridaziny (Břehová *et al.*, 2023; Příloha III). Všechny látky byly testovány pro svou inhibiční aktivitu vůči rekombinantní *FLT3*-ITD, CDK2 a některé i CDK9. Cílem bylo potlačení CDK inhibiční aktivity a zvýšení aktivity vůči FLT3.

Z připravených látek vykazovaly nejzajímavější aktivity deriváty imidazo[1,2-*b*]pyridazinů a pro detailnější charakterizaci účinků byla z této skupiny vybrána látka **34f**. Interní standardizované kinetické testování odhalilo účinnou inhibici rekombinantní *FLT3*-ITD již v nanomolárních koncentracích. Oproti látce BPA311 z předchozí série došlo rovněž k vylepšení selektivity. Kinasy CDK2 a CDK9 byly inhibovány sub-mikromolárními koncentracemi (Tab. 3), o řád vyššími než látkou BPA311. Inhibiční aktivita **34f** vůči *FLT3*-ITD byla také srovnatelná se známými inhibitory, jako jsou quizartinib (0,010 μ M) a gilteritinib (0,012 μ M).

Tab. 3: Inhibiční aktivita látky **34f** a inhibitoru BPA 311

Inhibitor	IC ₅₀ ± SD (μM)		
	FLT3-IDT	CDK2	CDK9
34f	0,004 ± 0,002	0,493 ± 0,091	0,146 ± 0,054
BPA 311	0,002 ± 0,001	0,028 ± 0,009	0,037 ± 0,009

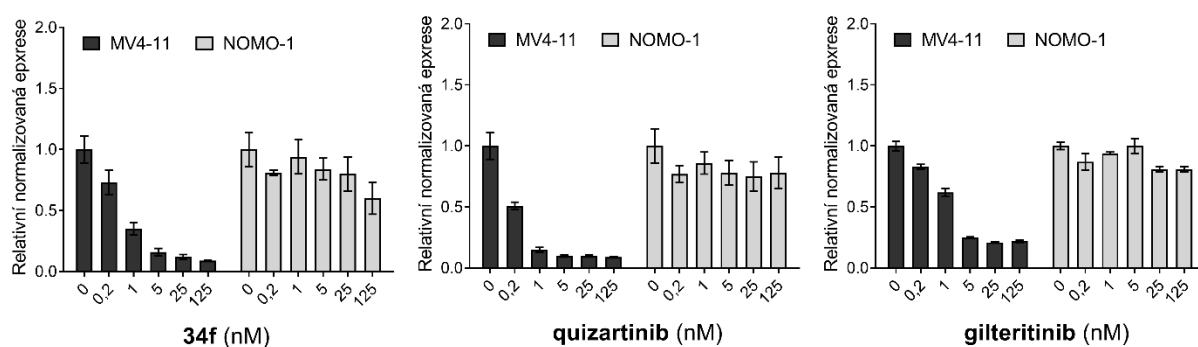
Antiproliferační aktivita látek byla testována na souboru 7 hematologických malignit. Soubor zahrnoval linie nesoucí *FLT3*-ITD, které jsou plně závislé na *FLT3* signalizaci (MV4-11, MOLM-13) a také několik *FLT3* independentních linií (Tab. 4; **Příloha III, Tab. 7**). Látka **34f** vykazovala silnou antiproliferační aktivitu na *FLT3*-ITD buněčných liniích MV4-11 a MOLM-13 s hodnotami GI₅₀ v jednotkách nanomolů, oproti tomu linie nezávislé na *FLT3* signalizaci byly inhibovány s hodnotami GI₅₀ v jednotkách mikromolů. Získané výsledky antiproliferační aktivity byly srovnatelné se standardními *FLT3* inhibitory (quizartinib a gilteritinib).

Tab. 4: Antiproliferační aktivita látky **34f** a standardních *FLT3* inhibitorů

Buněčná linie	GI ₅₀ ± SD (μM)		
	34f	quizartinib	gilteritinib
MV4-11	0,007 ± 0,004	0,003 ± 0,001	0,026 ± 0,009
MOLM-13	0,009 ± 0,006	0,004 ± 0,004	0,034 ± 0,013
CCRF-CEM	1,768 ± 0,261	> 10	2,771 ± 0,229
NOMO-1	4,275 ± 0,818	> 10	1,601 ± 0,226

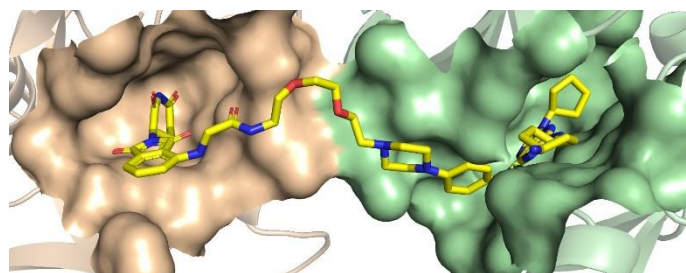
Další analýza potvrdila *FLT3*-dependentní mechanismus účinku látky **34f**. Aplikace látky ve vzrůstajících koncentracích po dobu 1 hodiny vedla ke koncentračně závislému

poklesu fosforylace FLT3 a také podřízených proteinů u buněčné linie MV4-11 (**Příloha III, Fig. 4A**). Aktivační mutace *FLT3-ITD* vede k narušení exprese specifického setu genů včetně například zvýšení exprese genu *MYC* (Kim *et al.*, 2007; Ohanian *et al.*, 2014; Basit *et al.*, 2018; Bogdanov *et al.*, 2023). Taktéž se jedná o klíčový onkogen, jehož deregulace často přispívá k rozvoji hematologických malignit. Aplikace látky **34f** po dobu 4 hodin vedla k signifikantnímu poklesu exprese genu *MYC* u FLT3-dependenční linie MV4-11, oproti tomu exprese tohoto genu nebyla výrazně ovlivněna u FLT3-independentní linie NOMO-1. Podobný efekt byl pozorován také po aplikaci inhibitorů quizaritinibu a gilteritinibu (Obr. 10).



Obr. 10: Relativní normalizovaná exprese genu *MYC* u buněčných linií MV4-11 a NOMO-1. Buňky byly ovlivněny látkou **34f** či komerčním inhibitorem quizaritinibem nebo gilteritinibem po dobu 4 hodin. Exprese genů byla normalizovaná ke genům *GAPDH* a *RPL13A*.

Druhá část práce, věnovaná charakterizaci účinku PROTAC, taktéž vychází z duálních kompetitivních inhibitorů CDK a FLT3 (Gucký *et al.*, 2018). Jejich konverze na PROTAC vycházela z molekulárního modelování, jímž byla určena orientace látky BPA311 v aktivních místech kinas CDK9 a FLT3. Ethylový zbytek mířící ven z aktivního místa byl zvolen vhodným místem pro prodloužení linkerem propojující BPA311 a pomalidomid, který byl vybrán jakožto známý a používaný ligand ubiquitinligasy CRBN (**Řezníčková *et al.*, 2022; Příloha IV**). Délka a chemická struktura linkeru byla navržena opět pomocí molekulárního modelování a částečně byla inspirována předešlými publikacemi (Burslem *et al.*, 2018; Huang *et al.*, 2018; Olson *et al.*, 2018).



Obr. 11: Predikovaná vazba látky PROTAC 13 (žlutá) do FLT3 (zelená) a CRBN (oranžová).

Získaný PROTAC 13 (Obr. 11) vykazoval slibnou antiproliferační aktivitu na buněčných liniích AML nesoucích *FLT3*-ITD (MV4-11, MOLM-13) s hodnotami GI_{50} v nanomolárních koncentracích. Naopak hodnoty GI_{50} u leukemických liniích bez *FLT3*-ITD byly alespoň 20x vyšší (Tab. 5; **Příloha IV, Tab. 1**). Ve srovnání s parentální látkou BPA311 nedošlo ke zlepšení antiproliferační aktivity, nicméně byla zachována citlivost a selektivita buněčných linií s *FLT3*-ITD (**Příloha IV, Tab. 1**). Podobně byla také zachována aktivita parentální látky vůči FLT3 (2% residuální aktivita) a CDK9 (3% a 8% residuální aktivita) (**Příloha IV, Fig S2**).

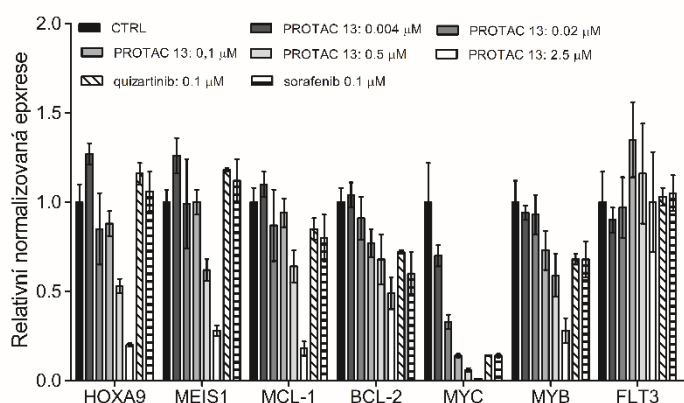
Tab. 5: Antiproliferační aktivita látky PROTAC 13 na panelu leukemických linií

Buněčná linie	$IC_{50} \pm SD$ (μM)
	PROTAC 13
MV4-11	0,047 \pm 0,029
MOLM-13	0,119 \pm 0,031
RS4;11	1,014 \pm 0,208
HL60	6,122 \pm 2,383
THP-1	9,993 \pm 0,012

Vliv PROTAC 13 na hladiny proteinů FLT3 a CDK9 byl následně ověřován pomocí imunoanalýzy. Látka byla testována na buněčné linii MV4-11 a její aplikace přes noc vedla ke koncentračně závislé degradaci proteinů FLT3 a CDK9, a to již od 100 nM (**Příloha IV, Fig. 2A**). Oproti tomu aplikace standardních FLT3 inhibitorů quizartinibu a sorafenibu neovlivnila CDK9, a naopak vedla k nárůstu hladiny FLT3 proteinu. Tento efekt je pozorován při dlouhodobém ovlivnění FLT3 inhibitory (Reiter *et al.*, 2018) a potenciálně může mít vliv na rozvoj rezistence (Weisberg *et al.*, 2011).

Efekt PROTAC 13 na CDK9, jakožto klíčového regulátoru transkripce, lze pozorovat na poklesu exprese genů zapojených do patogeneze AML. Pro potvrzení mechanismu účinku byly vybrány geny hrající roli při hematopoese, apoptose a iniciaci AML jako jsou *HOXA9*,

MEIS-1, *MCL-1*, *BCL-2*, *MYC* a *MYB*. Aplikace látky PROTAC 13 na buněčnou linii MV4-11 po dobu 4 hodin vedla ke koncentračně závislému poklesu exprese studovaných genů (Obr. 22). Zároveň však aplikace látky neovlivnila expresi genu *FLT3*, což potvrzuje její mechanismus účinku. Pro srovnání efektu látky s komerčními FLT3 inhibitory byla linie MV4-11 ovlivněna také sorafenibem a quizartinibem. Nicméně v jejich případě nebyl pozorován tak silný efekt inhibice na expresi vybraných genů, což naznačuje potenciální terapeutický benefit inhibice CDK9 u AML.



Obr. 12: Relativní normalizovaná exprese genů zapojených do AML patogeneze u buněčné linie MV4-11. Buňky byly ovlivněny látkou PROTAC 13 či komerčními inhibitory quizartinibem nebo sorafenibem po dobu 4 hodin. Exprese genů byla normalizovaná ke genům *GAPDH* a *RPL13A*.

Akutní myeloidní leukemie je agresivním typem leukemií a zhruba u třetiny pacientů se nachází onkogenní mutace v genu *FLT3*. Pro tyto typy leukemie již bylo schváleno použití některých FLT3 inhibitorů (Zarrinkar *et al.*, 2009; Levis, 2017; Dhillon, 2019) a další jsou v klinickém testování. Dlouhodobá aplikace těchto inhibitorů je však doprovázena rozvojem rezistence (Wu *et al.*, 2018). V rámci této disertační práce byl popsán nový imidazo[1,2-*b*]pyridazinový inhibitor FLT3 (látko **34f**) a také proteolýzu indukující chimérický konjugát, PROTAC 13, který selektivně degraduje FLT3 a CDK9. Strukturní optimalizací došlo u řady látek k omezení inhibice CDK, což naznačuje, že CDK9 inhibiční aktivita nemusí být klíčová pro aktivitu látek. Naopak primární roli zde pravděpodobně hraje inhibice FLT3. I přesto však experimenty s PROTAC 13 naznačují, že selektivní degradace CDK9 může být významným příspěvkem k účinnosti.

4 Závěr

Nádorové buňky často vykazují transkripční závislost a jsou tedy kriticky dependentní na kontinuální expresi transkriptů s krátkým poločasem rozpadu. Příkladem mohou být transkripty antiapoptických genů nebo klíčových onkogenních transkripčních faktorů. Společně s častou deregulací exprese transkripčních CDK (tCDK) to představuje pádné důvody pro zkoumání tCDK jako možných terapeutických cílů v onkologii. Tahle možnost je studována již řadu let od vývoje první generace pan-selektivních CDK inhibitorů, které blokovaly nejen buněčný cyklus, ale také inhibovaly tCDK. Tyto první inhibitory často pozbývaly biochemickou selektivitu. Jejich toxicita byla způsobena ovlivněním většího množství cílů a taktéž jejich aplikace komplikovala pochopení důležitosti tCDK v protinádorové odpovědi. I přesto významně přispěly k vnímání tCDK jako slibných terapeutických cílů. Intenzivní výzkum částečně vyřešil problematiku selektivity, alespoň vůči některým CDK. Příkladem mohou být palbociclib nebo ribociclib selektivně cílicí na CDK4/6, a které byly eventuálně schválené jako protinádorová léčiva. Tato skutečnost potvrdila, že dostatečné selektivity lze dosáhnout i u velmi příbuzných enzymů, jako jsou CDK. Také to podnítilo vývoj řady nových selektivnějších inhibitorů zaměřujících se nejen na tCDK.

První část této práce byla zaměřena na využití inhibitorů transkripčních CDK v léčbě leukemií s *KMT2A* translokací. Tyto translokace jsou časté zejména u kojenců do 1 roku a jejich následkem je deregulace transkripce řady klíčových onkogenů. Jedním z mechanismů deregulace je interakce fúzních partnerů se super-elongačním komplexem, který je složený z velké řady proteinů včetně CDK9 (Li et Song, 2021; Meyer *et al.*, 2023). Inhibice CDK9 by mohla být možným terapeutickým řešením. Část této práce se zaměřila na testování více či méně selektivních inhibitorů CDK zahrnujících i tři inhibitory, které byly popsány jako CDK9 selektivní. Ověřena byla jejich antiproliferační aktivita na panelu leukemických linií obsahujících jak linie s translokací genu *KMT2A* (*KMT2A-r*), tak linie obsahující nemutovanou variantu (*KMT2A-wt*). Dále byl studován vliv těchto inhibitorů na expresi genů a proteinů zapojených do patogeneze *KMT2A-r* leukemií. Předběžné výsledky žádného z těchto testů neodhalily specifický efekt CDK9 inhibitorů u *KMT2A-r* linií. Navíc u některých studovaných inhibitorů byla odhalena jejich nízká selektivita, což byl paralelně potvrzeno i nezávisle (Wells *et al.*, 2020). Ze získaných dat nelze jednoznačně určit, zdali cílená inhibice CDK9 byla významně efektivní u *KMT2A-r* leukemií. Nicméně i přesto byly testované buněčné linie citlivé k některým tCDK a jejich obecná inhibice by mohla být přínosem.

Druhá a hlavní část této práce byla zaměřena na inhibici CDK7. Vzhledem k duální roli při regulaci buněčného cyklu i transkripce, představuje cílení na CDK7 zajímavou terapeutickou možnost v léčbě nádorových onemocnění a již bylo popsáno několik kovalentních i kompetitivních inhibitorů, které selektivně inhibují CDK7. Několik z nich je aktuálně v klinickém testování (Patel *et al.*, 2018; Satyam *et al.*, 2020; Yu *et al.*, 2020; Marineau *et al.*, 2022). V této části byl popsán nový trisubstituovaný derivát pyrazolo[4,3-*d*]pyrimidinu, látka LGR6768, která účinně a selektivně inhibuje CDK7. Selektivita inhibice byla potvrzena kinetickými experimenty s rekombinantními enzymy a podpořena strukturní analýzou. LGR6768 ukázala antileukemický potenciál a její aplikace vedla ke snížení fosforylace substrátů CDK7, včetně CDK1, CDK2 a mírně i CTD RNAPII. Analýza buněčného cyklu ukázala blokaci v G1 fázi po aplikaci látky. Ve vyšších koncentracích došlo k indukci apoptosy doprovázené G2/M blokem, aktivací kaspas a štěpení proteinu PARP-1. Navíc, aplikace látky LGR6768 vedla ke snížení exprese hematologických onkogenů. Naše i další publikované výsledky naznačují, že inhibice CDK7 jako terapeutická možnost v léčbě nádorových onemocnění stojí za další zkoumání.

Poslední část byla zaměřena na akutní myeloidní leukemie s mutací *FLT3*-ITD, která souvisí s vyšší mírou relapsu a horší prognózou. Tato část práce vycházela z optimalizace dříve publikované látky BPA311 (Gucký *et al.*, 2018), která potently inhibovala CDK a *FLT3*. První optimalizací došlo k vývoji imidazo[1,2-*b*]pyridazinu, látky **34f**, u níž došlo k vylepšení selektivity vůči *FLT3*-ITD a potlačení její CDK inhibiční aktivity. Látka prokázala slibné antiproliferační účinky u buněčných liniích nesoucí *FLT3*-ITD srovnatelné se standardními inhibitory. Oproti tomu buněčné linie s nemutovanou formou *FLT3* vykazovaly několikanásobně nižší citlivost, což dokazuje *FLT3*-dependentní mechanismus účinku látky. Aplikace látky vedla také k narušení fosforylace *FLT3* a podřízené signalizace a také snížení exprese genu *MYC*. Druhou optimalizací vznikl proteolýzu indukující chimérický konjugát PROTAC 13, jakožto duální degradér CDK9 a *FLT3*. Tato látka taktéž vykazovala slibné antiproliferační účinky u buněčných liniích s *FLT3*-ITD a mechanismus účinku byl potvrzen pomocí imunoanalýzy, kde byla pozorována koncentračně závislá degradace cílových proteinů. Efekt látky, v souvislosti s cílovou degradací CDK9, byl prokázán pomocí analýzy exprese genů, kde byl pozorován pokles v expresi onkogenů zapojených do patogeneze AML.

Získaná data této dizertační práce přispívají k pochopení role inhibice tCDK v léčbě nádorových onemocnění a jsou v souladu s již dříve publikovanými daty. Přestože se transkripční inhibitory zaměřují na globální transkripci, jsou relativně selektivní vůči maligním buňkám. To je pravděpodobně způsobeno již zmíněnou citlivostí nádorových buněk

na kontinuální expresi specifických onkogenů. Stále je však třeba lépe porozumět molekulárním mechanismům, které řídí transkripční cyklus, a důsledkům jeho inhibice. Moderní techniky, jako je CRISPR/Cas9, mohou hrát důležitou roli v tomto poznání a také v racionálním designu nových terapeutických strategií pro léčbu nádorových onemocnění.

5 Seznam použité literatury

- Abudurehman, T., Xia, J., Li, M.-H., Zhou, H., Zheng, W.-W., Zhou, N., ... Duan, C.-W. (2021). CDK7 Inhibitor THZ1 Induces the Cell Apoptosis of B-Cell Acute Lymphocytic Leukemia by Perturbing Cellular Metabolism. *Frontiers in Oncology*, 11.
- Ali, S., Heathcote, D. A., Kroll, S. H. B., Jogalekar, A. S., Scheiper, B., Patel, H., ... Coombes, R. C. (2009). The Development of a Selective Cyclin-Dependent Kinase Inhibitor That Shows Antitumor Activity. *CANCER RESEARCH*, 69(15), 6208-6215.
- Armstrong, S. A., Staunton, J. E., Silverman, L. B., Pieters, R., den Boer, M. L., Minden, M. D., ... Korsmeyer, S. J. (2002). MLL translocations specify a distinct gene expression profile that distinguishes a unique leukemia. *Nature Genetics*, 30(1), 41-47.
- Barlaam, B., Savi, C. D., Drew, L., Ferguson, A. D., Ferguson, D., Gu, C., ... Shao, W. (2018). Abstract 1650: Discovery of AZD4573, a potent and selective inhibitor of CDK9 that enables transient target engagement for the treatment of hematologic malignancies. *CANCER RESEARCH*, 78, 1650-1650.
- Basit, F., Andersson, M., & Hultquist, A. (2018). The Myc/Max/Mxd Network Is a Target of Mutated Flt3 Signaling in Hematopoietic Stem Cells in Flt3-ITD-Induced Myeloproliferative Disease. *Stem Cells International*, 2018, 3286949.
- Bettayeb, K., Oumata, N., Echalié, A., Ferandin, Y., Endicott, J. A., Galons, H., & Meijer, L. (2008). CR8, a potent and selective, roscovitine-derived inhibitor of cyclin-dependent kinases. *Oncogene*, 27(44), 5797-5807.
- Blazek, D., Kohoutek, J., Bartholomeeusen, K., Johansen, E., Hulinkova, P., Luo, Z., ... Peterlin, B. M. (2011). The Cyclin K/Cdk12 complex maintains genomic stability via regulation of expression of DNA damage response genes. *Genes & Development*, 25(20), 2158-2172.
- Bogdanov, K., Kudryavtseva, E., Fomicheva, Y., Churkina, I., Lomaia, E., Girshova, L., ... Zaritskey, A. (2023). Shift of N-MYC Oncogene Expression in AML Patients Carrying the FLT3-ITD Mutation. *Pathophysiology*, 30(3), 296-313.
- Bradford, M. M. (1976). A rapid and sensitive method for the quantitation of microgram quantities of protein utilizing the principle of protein-dye binding. *Analytical Biochemistry*, 72(1), 248-254.
- Břehová, P., Řezníčková, E., Škach, K., Jorda, R., Dejmek, M., Vojáčková, V., ... Kryštof, V. (2023). Inhibition of FLT3-ITD Kinase in Acute Myeloid Leukemia by New Imidazo[1,2-b]pyridazine Derivatives Identified by Scaffold Hopping. *Journal of Medicinal Chemistry*, 66(16), 11133-11157.
- Burslem, G. M., Song, J., Chen, X., Hines, J., & Crews, C. M. (2018). Enhancing Antiproliferative Activity and Selectivity of a FLT-3 Inhibitor by Proteolysis Targeting Chimera Conversion. *Journal of the American Chemical Society*, 140(48), 16428-16432.
- Cidado, J., Boiko, S., Proia, T., Ferguson, D., Criscione, S. W., San Martin, M., ... Drew, L. (2020). AZD4573 Is a Highly Selective CDK9 Inhibitor That Suppresses MCL-1 and Induces Apoptosis in Hematologic Cancer Cells. *Clinical Cancer Research*, 26(4), 922-934.
- Daver, N., Venugopal, S., & Ravandi, F. (2021). FLT3 mutated acute myeloid leukemia: 2021 treatment algorithm. *Blood Cancer Journal*, 11(5), 104.
- Dhillon, S. (2019). Gilteritinib: First Global Approval. *Drugs*, 79(3), 331-339.
- Diab, S., Yu, M., & Wang, S. (2020). CDK7 Inhibitors in Cancer Therapy: The Sweet Smell of Success? *Journal of Medicinal Chemistry*, 63(14), 7458-7474.
- Ebmeier, C. C., Erickson, B., Allen, B. L., Allen, M. A., Kim, H., Fong, N., ... Taatjes, D. J. (2017). Human TFIIF Kinase CDK7 Regulates Transcription-Associated Chromatin Modifications. *Cell Reports*, 20(5), 1173-1186.
- Erfurth, F., Hemenway, C. S., de Erkenez, A. C., & Domer, P. H. (2004). MLL fusion partners AF4 and AF9 interact at subnuclear foci. *Leukemia*, 18(1), 92-102.
- Faber, J., Krivtsov, A. V., Stubbs, M. C., Wright, R., Davis, T. N., van den Heuvel-Eibrink, M., ... Armstrong, S. A. (2009). HOXA9 is required for survival in human MLL-rearranged acute leukemias. *Blood*, 113(11), 2375-2385.
- Frame, S., Saladino, C., MacKay, C., Atrash, B., Sheldrake, P., McDonald, E., ... Zheleva, D. (2020). Fadraciclib (CYC065), a novel CDK inhibitor, targets key pro-survival and oncogenic pathways in cancer. *PLOS ONE*, 15(7), e0234103.
- Garcia-Cuellar, M. P., Füller, E., Mäthner, E., Breitingner, C., Hetzner, K., Zeitlmann, L., ... Slany, R. K. (2014). Efficacy of cyclin-dependent-kinase 9 inhibitors in a murine model of mixed-lineage leukemia. *Leukemia*, 28(7), 1427-1435.
- Gaur, T., Poddutoori, R., Khare, L., Bagal, B., Rashmi, S., Patkar, N., ... Hasan, S. K. (2023). Novel covalent CDK7 inhibitor potently induces apoptosis in acute myeloid leukemia and synergizes with Venetoclax. *Journal of Experimental & Clinical Cancer Research*, 42(1), 186.

- Górecki, M., Koziol, I., Kopystecka, A., Budzyńska, J., Zawitkowska, J., & Lejman, M. (2023). Updates in KMT2A Gene Rearrangement in Pediatric Acute Lymphoblastic Leukemia. *Biomedicines*, *11*(3), 821.
- Greber, B. J., Remis, J., Ali, S., & Nogales, E. (2021). 2.5-resolution structure of human CDK-activating kinase bound to the clinical inhibitor ICEC0942. *Biophysical Journal*, *120*(4), 677-686.
- Gucký, T., Řezníčková, E., Radošová Muchová, T., Jorda, R., Klejová, Z., Malínková, V., ... Kryštof, V. (2018). Discovery of N2-(4-Amino-cyclohexyl)-9-cyclopentyl-N6-(4-morpholin-4-ylmethyl-phenyl)-9H-purine-2,6-diamine as a Potent FLT3 Kinase Inhibitor for Acute Myeloid Leukemia with FLT3 Mutations. *Journal of Medicinal Chemistry*, *61*(9), 3855-3869.
- Hendrychová, D., Jorda, R., & Kryštof, V. (2021). How selective are clinical CDK4/6 inhibitors? *Medicinal Research Reviews*, *41*(3), 1578-1598.
- Hu, D., Mayeda, A., Trembley, J. H., Lahti, J. M., & Kidd, V. J. (2003). CDK11 Complexes Promote Pre-mRNA Splicing *. *Journal of Biological Chemistry*, *278*(10), 8623-8629.
- Hu, S., Marineau, J. J., Rajagopal, N., Hamman, K. B., Choi, Y. J., Schmidt, D. R., ... Olson, E. R. (2019). Discovery and Characterization of SY-1365, a Selective, Covalent Inhibitor of CDK7. *CANCER RESEARCH*, *79*(13), 3479-3491.
- Huang, H.-T., Dobrovolsky, D., Paulk, J., Yang, G., Weisberg, E. L., Doctor, Z. M., ... Gray, N. S. (2018). A Chemoproteomic Approach to Query the Degradable Kinome Using a Multi-kinase Degradator. *Cell Chemical Biology*, *25*(1), 88-99.e86.
- Huang, Z., Wang, T., Wang, C., & Fan, Y. (2022). CDK9 inhibitors in cancer research. [10.1039/D2MD00040G]. *RSC Medicinal Chemistry*, *13*(6), 688-710.
- Choi, Y. J., Kim, D. H., Yoon, D. H., Suh, C., Choi, C.-M., Lee, J. C., ... Rho, J. K. (2019). Efficacy of the novel CDK7 inhibitor QS1189 in mantle cell lymphoma. *Scientific Reports*, *9*(1), 7193.
- Jessberger, S., Gage, F. H., Eisch, A. J., & Lagace, D. C. (2009). Making a neuron: Cdk5 in embryonic and adult neurogenesis. *Trends in Neurosciences*, *32*(11), 575-582.
- Jorda, R., Havlíček, L., McNae, I. W., Walkinshaw, M. D., Voller, J., Šturc, A., ... Kryštof, V. (2011). Pyrazolo[4,3-d]pyrimidine Bioisostere of Roscovitine: Evaluation of a Novel Selective Inhibitor of Cyclin-Dependent Kinases with Antiproliferative Activity. *Journal of Medicinal Chemistry*, *54*(8), 2980-2993.
- Jorda, R., Havlíček, L., Šturc, A., Tušková, D., Daumová, L., Alam, M., ... Kryštof, V. (2019). 3,5,7-Substituted Pyrazolo[4,3-d]pyrimidine Inhibitors of Cyclin-Dependent Kinases and Their Evaluation in Lymphoma Models. *Journal of Medicinal Chemistry*, *62*(9), 4606-4623.
- Jorda, R., Hendrychová, D., Voller, J., Řezníčková, E., Gucký, T., & Kryštof, V. (2018). How Selective Are Pharmacological Inhibitors of Cell-Cycle-Regulating Cyclin-Dependent Kinases? *Journal of Medicinal Chemistry*, *61*(20), 9105-9120.
- Kamens, J. L., Nance, S., Koss, C., Xu, B., Cotton, A., Lam, J. W., ... Gruber, T. A. (2023). Proteasome inhibition targets the KMT2A transcriptional complex in acute lymphoblastic leukemia. *Nature Communications*, *14*(1), 809.
- Kazi, J. U., & Rönstrand, L. (2019). FMS-like Tyrosine Kinase 3/FLT3: From Basic Science to Clinical Implications. *Physiological Reviews*, *99*(3), 1433-1466.
- Kelso, T. W. R., Baumgart, K., Eichhoff, J., Albert, T., Antrecht, C., Lemcke, S., ... Meisterernst, M. (2014). Cyclin-Dependent Kinase 7 Controls mRNA Synthesis by Affecting Stability of Preinitiation Complexes, Leading to Altered Gene Expression, Cell Cycle Progression, and Survival of Tumor Cells. *Molecular and Cellular Biology*, *34*(19), 3675-3688.
- Kim, K.-T., Baird, K., Davis, S., Piloto, O., Levis, M., Li, L., ... Small, D. (2007). Constitutive Fms-like tyrosine kinase 3 activation results in specific changes in gene expression in myeloid leukaemic cells. *British Journal of Haematology*, *138*(5), 603-615.
- Kovalová, M., Baraka, J. P., Mik, V., Jorda, R., Luo, L., Shao, H., & Kryštof, V. (2023a). A patent review of cyclin-dependent kinase 7 (CDK7) inhibitors (2018-2022). *Expert Opinion on Therapeutic Patents*, *33*(2), 67-87.
- Kovalová, M., Havlíček, L., Djukic, S., Škerlová, J., Peřina, M., Pospíšil, T., ... Kryštof, V. (2023b). Characterization of new highly selective pyrazolo[4,3-d]pyrimidine inhibitor of CDK7. *Biomedicine & Pharmacotherapy*, *161*, 114492.
- Kwiatkowski, N., Zhang, T., Rahl, P. B., Abraham, B. J., Reddy, J., Ficarro, S. B., ... Gray, N. S. (2014). Targeting transcription regulation in cancer with a covalent CDK7 inhibitor. *Nature*, *511*(7511), 616-620.
- Levis, M. (2017). Midostaurin approved for FLT3-mutated AML. *Blood*, *129*(26), 3403-3406.
- Li, X., & Song, Y. (2021). Structure, function and inhibition of critical protein-protein interactions involving mixed lineage leukemia 1 and its fusion oncoproteins. *Journal of Hematology & Oncology*, *14*(1), 56.
- Li, Z.-M., Liu, G., Gao, Y., & Zhao, M.-G. (2022). Targeting CDK7 in oncology: The avenue forward. *Pharmacology & Therapeutics*, *240*, 108229.

- Lin, C., Smith, E. R., Takahashi, H., Lai, K. C., Martin-Brown, S., Florens, L., ... Shilatifard, A. (2010). AFF4, a Component of the ELL/P-TEFb Elongation Complex and a Shared Subunit of MLL Chimeras, Can Link Transcription Elongation to Leukemia. *Molecular Cell*, 37(3), 429-437.
- Livak, K. J., & Schmittgen, T. D. (2001). Analysis of Relative Gene Expression Data Using Real-Time Quantitative PCR and the $2^{-\Delta\Delta CT}$ Method. *Methods*, 25(4), 402-408.
- Lücking, U., Scholz, A., Lienau, P., Siemeister, G., Kosemund, D., Bohlmann, R., ... Brands, M. (2017). Identification of Atuveciclib (BAY 1143572), the First Highly Selective, Clinical PTEFb/CDK9 Inhibitor for the Treatment of Cancer. *ChemMedChem*, 12(21), 1776-1793.
- Luecking, U. T., Scholz, A., Kosemund, D., Bohlmann, R., Briem, H., Lienau, P., ... Brands, M. (2017). Abstract 984: Identification of potent and highly selective PTEFb inhibitor BAY 1251152 for the treatment of cancer: from p.o. to i.v. application via scaffold hops. *CANCER RESEARCH*, 77, 984-984.
- Malumbres, M. (2014). Cyclin-dependent kinases. *Genome Biology*, 15(6), 122.
- Malumbres, M., Harlow, E., Hunt, T., Hunter, T., Lahti, J. M., Manning, G., ... Wolgemuth, D. J. (2009). Cyclin-dependent kinases: a family portrait. *Nature Cell Biology*, 11(11), 1275-1276.
- Manning, G., Whyte, D. B., Martinez, R., Hunter, T., & Sudarsanam, S. (2002). The Protein Kinase Complement of the Human Genome. *Science*, 298(5600), 1912-1934.
- Marineau, J. J., Hamman, K. B., Hu, S., Alnemy, S., Mihalich, J., Kabro, A., ... Chuaqui, C. (2022). Discovery of SY-5609: A Selective, Noncovalent Inhibitor of CDK7. *Journal of Medicinal Chemistry*, 65(2), 1458-1480.
- Meshinchi, S., & Appelbaum, F. R. (2009). Structural and Functional Alterations of FLT3 in Acute Myeloid Leukemia. *Clinical Cancer Research*, 15(13), 4263-4269.
- Meyer, C., Larghero, P., Almeida Lopes, B., Burmeister, T., Gröger, D., Sutton, R., ... Marschalek, R. (2023). The KMT2A recombinome of acute leukemias in 2023. *Leukemia*, 37(5), 988-1005.
- Mikolcevic, P., Sigl, R., Rauch, V., Hess, M. W., Pfaller, K., Barisic, M., ... Geley, S. (2012). Cyclin-Dependent Kinase 16/PCTAIRE Kinase 1 Is Activated by Cyclin Y and Is Essential for Spermatogenesis. *Molecular and Cellular Biology*, 32(4), 868-879.
- Monroe, S. C., Jo, S. Y., Sanders, D. S., Basrur, V., Elenitoba-Johnson, K. S., Slany, R. K., & Hess, J. L. (2011). MLL-AF9 and MLL-ENL alter the dynamic association of transcriptional regulators with genes critical for leukemia. *Experimental Hematology*, 39(1), 77-86.e75.
- Nepomuceno, T. C., Fernandes, V. C., Gomes, T. T., Carvalho, R. S., Suarez-Kurtz, G., Monteiro, A. N., & Carvalho, M. A. (2017). BRCA1 recruitment to damaged DNA sites is dependent on CDK9. *Cell Cycle*, 16(7), 665-672.
- Ohanian, M., Kantarjian, H. M., Rozovski, U., Loghavi, S., Huh, Y., Abruzzo, L., ... Cortes, J. E. (2014). Clinical significance of MYC expression in acute myeloid leukemia. *Journal of Clinical Oncology*, 32, 7094-7094.
- Olson, C. M., Jiang, B., Erb, M. A., Liang, Y., Doctor, Z. M., Zhang, Z., ... Gray, N. S. (2018). Pharmacological perturbation of CDK9 using selective CDK9 inhibition or degradation. *Nature Chemical Biology*, 14(2), 163-170.
- Olson, C. M., Liang, Y., Leggett, A., Park, W. D., Li, L., Mills, C. E., ... Gray, N. S. (2019). Development of a Selective CDK7 Covalent Inhibitor Reveals Predominant Cell-Cycle Phenotype. *Cell Chemical Biology*, 26(6), 792-803.e710.
- Park, S. Y., Kim, K. Y., Jun, D. Y., Hwang, S.-K., & Kim, Y. H. (2020). G1 Cell Cycle Arrest and Extrinsic Apoptotic Mechanisms Underlying the Anti-Leukemic Activity of CDK7 Inhibitor BS-181. *Cancers*, 12(12), 3845.
- Parry, D., Guzi, T., Shanahan, F., Davis, N., Prabhavalkar, D., Wiswell, D., ... Lees, E. M. (2010). Dinaciclib (SCH 727965), a Novel and Potent Cyclin-Dependent Kinase Inhibitor. *Molecular Cancer Therapeutics*, 9(8), 2344-2353.
- Patel, H., Periyasamy, M., Sava, G. P., Bondke, A., Slafer, B. W., Kroll, S. H. B., ... Ali, S. (2018). ICEC0942, an Orally Bioavailable Selective Inhibitor of CDK7 for Cancer Treatment. *Molecular Cancer Therapeutics*, 17(6), 1156-1166.
- Rask-Andersen, M., Zhang, J., Fabbro, D., & Schiöth, H. B. (2014). Advances in kinase targeting: current clinical use and clinical trials. *Trends in Pharmacological Sciences*, 35(11), 604-620.
- Reiter, K., Polzer, H., Krupka, C., Maiser, A., Vick, B., Rothenberg-Thurley, M., ... Greif, P. A. (2018). Tyrosine kinase inhibition increases the cell surface localization of FLT3-ITD and enhances FLT3-directed immunotherapy of acute myeloid leukemia. *Leukemia*, 32(2), 313-322.
- Řezníčková, E., Krajčovičová, S., Peřina, M., Kovalová, M., Sural, M., & Kryštof, V. (2022). Modulation of FLT3-ITD and CDK9 in acute myeloid leukaemia cells by novel proteolysis targeting chimera (PROTAC). *European Journal of Medicinal Chemistry*, 243, 114792.
- Řezníčková, E., Weitensteiner, S., Havlíček, L., Jorda, R., Gucký, T., Berka, K., ... Strnad, M. (2015). Characterization of a Pyrazolo[4,3-d]pyrimidine Inhibitor of Cyclin-Dependent Kinases 2 and 5 and

- Aurora A With Pro-Apoptotic and Anti-Angiogenic Activity In Vitro. *Chemical Biology & Drug Design*, 86(6), 1528-1540.
- Satyam, L. K., Poddutoori, R., Thiyagarajan, S., Mukherjee, S., Kaza, L. N., Charamanna, K., ... Samajdar, S. (2020). 170 Poster - Potent anti-tumor activity of AUR102, a selective covalent inhibitor of CDK7. *European Journal of Cancer*, 138, S47.
- Tsakaneli, A., & Williams, O. (2021). Drug Repurposing for Targeting Acute Leukemia With KMT2A (MLL)-Gene Rearrangements. *Frontiers in Pharmacology*, 12.
- Vervoort, S. J., Devlin, J. R., Kwiatkowski, N., Teng, M., Gray, N. S., & Johnstone, R. W. (2022). Targeting transcription cycles in cancer. *Nature Reviews Cancer*, 22(1), 5-24.
- Vymětalová, L., Havlíček, L., Štunc, A., Skrášková, Z., Jorda, R., Pospíšil, T., ... Kryštof, V. (2016). 5-Substituted 3-isopropyl-7-[4-(2-pyridyl)benzyl]amino-1(2)H-pyrazolo[4,3-d]pyrimidines with anti-proliferative activity as potent and selective inhibitors of cyclin-dependent kinases. *European Journal of Medicinal Chemistry*, 110, 291-301.
- Weisberg, E., Ray, A., Nelson, E., Adamia, S., Barrett, R., Sattler, M., ... Griffin, J. D. (2011). Reversible Resistance Induced by FLT3 Inhibition: A Novel Resistance Mechanism in Mutant FLT3-Expressing Cells. *PLOS ONE*, 6(9), e25351.
- Wells, C. I., Vasta, J. D., Corona, C. R., Wilkinson, J., Zimprich, C. A., Ingold, M. R., ... Robers, M. B. (2020). Quantifying CDK inhibitor selectivity in live cells. *Nature Communications*, 11(1), 2743.
- Whittaker, S. R., Mallinger, A., Workman, P., & Clarke, P. A. (2017). Inhibitors of cyclin-dependent kinases as cancer therapeutics. *Pharmacology & Therapeutics*, 173, 83-105.
- William, A. D., Lee, A. C. H., Goh, K. C., Blanchard, S., Poulsen, A., Teo, E. L., ... Dymock, B. W. (2012). Discovery of Kinase Spectrum Selective Macrocycle (16E)-14-Methyl-20-oxa-5,7,14,26-tetraazatetracyclo[19.3.1.1(2,6).1(8,12)]heptacos-1(25),2(26),3,5,8(27),9,11,16,21,23-decaene (SB1317/TG02), a Potent Inhibitor of Cyclin Dependent Kinases (CDKs), Janus Kinase 2 (JAK2), and Fms-like Tyrosine Kinase-3 (FLT3) for the Treatment of Cancer. *Journal of Medicinal Chemistry*, 55(1), 169-196.
- Wong, P., Iwasaki, M., Somervaille, T. C. P., So, C. W. E., & Cleary, M. L. (2007). Meis1 is an essential and rate-limiting regulator of MLL leukemia stem cell potential. *Genes & Development*, 21(21), 2762-2774.
- Wood, D. J., & Endicott, J. A. (2018). Structural insights into the functional diversity of the CDK–cyclin family. *Open Biology*, 8(9), 180112.
- Wu, M., Li, C., & Zhu, X. (2018). FLT3 inhibitors in acute myeloid leukemia. *Journal of Hematology & Oncology*, 11(1), 133.
- Xie, F., Wang, J., & Zhang, B. (2023). RefFinder: a web-based tool for comprehensively analyzing and identifying reference genes. *Functional & Integrative Genomics*, 23(2), 125.
- Xie, F., Xiao, P., Chen, D., Xu, L., & Zhang, B. (2012). miRDeepFinder: a miRNA analysis tool for deep sequencing of plant small RNAs. *Plant Molecular Biology*, 80(1), 75-84.
- Ye, J., Coulouris, G., Zaretskaya, I., Cutcutache, I., Rozen, S., & Madden, T. L. (2012). Primer-BLAST: A tool to design target-specific primers for polymerase chain reaction. *BMC Bioinformatics*, 13(1), 134.
- Yu, D., Jeon, Y., Park, D., Seo, M., Ahn, W., Kim, J., ... Nam, K. (2020). Abstract 4855: Development of highly selective CDK7 inhibitor Q901 for solid tumors. *CANCER RESEARCH*, 80(16_Supplement), 4855-4855.
- Zarrinkar, P. P., Gunawardane, R. N., Cramer, M. D., Gardner, M. F., Brigham, D., Belli, B., ... Bhagwat, S. S. (2009). AC220 is a uniquely potent and selective inhibitor of FLT3 for the treatment of acute myeloid leukemia (AML). *Blood*, 114(14), 2984-2992.
- Zeng, M., Kwiatkowski, N. P., Zhang, T., Nabet, B., Xu, M., Liang, Y., ... Gray, N. S. (2018). Targeting MYC dependency in ovarian cancer through inhibition of CDK7 and CDK12/13. *eLife*, 7, e39030.
- Zhang, M., Zhang, L., Hei, R., Li, X., Cai, H., Wu, X., ... Cai, C. (2021). CDK inhibitors in cancer therapy, an overview of recent development. *American journal of cancer research*, 11 5, 1913-1935.
- Zhang, T., Kwiatkowski, N., Olson, C. M., Dixon-Clarke, S. E., Abraham, B. J., Greifengberg, A. K., ... Gray, N. S. (2016). Covalent targeting of remote cysteine residues to develop CDK12 and CDK13 inhibitors. *Nature Chemical Biology*, 12(10), 876-884.

6 Přehled publikační činnosti

Seznam publikovaných prací:

- Publikace zahrnuté v této práci
 - I. **Kovalová, M.***, Baraka, JP.*, Mik, V., Jorda, R., Luo, L., Shao, H., Kryštof, V. (2023) A patent review of cyclin-dependent kinase 7 (CDK7) inhibitors (2018-2022). *Expert Opin Ther Patents* 33 (2), 67-87 *Sdílené prvouautorství
 - II. **Kovalová, M.**, Havlíček, L., Djukic, S., Škerlová, J., Peřina, M., Pospíšil, T., Řezníčková, E., Řezáčová, P., Jorda, R., Kryštof, V. (2023) Characterization of new highly selective pyrazolo 4,3-d pyrimidine inhibitor of CDK7. *Biomed Pharmacother* 161, 114492
 - III. Břehová, P., Řezníčková, E., Škach, K., Jorda, R., Dejmek, M., Vojáčková, V., Šála, M., **Kovalová, M.**, Dračínský, M., Dolníková, A., Strmeň, T., Kinnertová, M., Chalupský, K., Dvořáková, A., Gucký, T., Mertlíková Kaiserová, H, Klener, P., Nencka, R., Kryštof, V. (2023) Inhibition of FLT3-ITD Kinase in Acute Myeloid Leukemia by New Imidazo[1,2-b]pyridazine Derivatives Identified by Scaffold Hopping. *J Med Chem*, 66(16), 11133-11157.
 - IV. Řezníčková, E., Krajčovičová, S., Peřina, M., **Kovalová, M.**, Sural, M., Kryštof, V. (2022) Modulation of FLT3-ITD and CDK9 in acute myeloid leukaemia cells by novel proteolysis targeting chimera (PROTAC). *Eur J Med Chem* 243, 114792
- Další publikace
 - V. Peřina, M., Kiss, M. A., Mótyán, G., Szczyrbová, E., Eliáš, M., Študent, V., Kurfürstová, D., **Kovalová, M.**, Mada, L., Bouchal, J., Frank, Ě., Jorda, R. (2023) A-ring-fused pyrazoles of dihydrotestosterone targeting prostate cancer cells via the downregulation of the androgen receptor. *Eur J Med Chem* 249, 115086
 - VI. Barghash, R. F., Eldehna, W. M., **Kovalová, M.**, Vojáčková, V., Kryštof, V., Abdel-Aziz, H. A. (2022) One-pot three-component synthesis of novel pyrazolo 3,4-b pyridines as potent antileukemic agents. *Eur J Med Chem* 227, 113952

Konferenční příspěvky:

- Kovalová, M., Jorda, R., Kryštof, V.: TRANSCRIPTIONAL CDKs: The way to go? Chemistry and biology of phytohormones and related substances, 2019, květen 19.-21., Luhačovice, ČR. Ústní prezentace.
- Kovalová, M., Jorda, R., Havlíček, L., Řezníčková, E., Kryštof, V.: Transcriptional CDKs: potential targets in the treatment of leukemia. Chemistry and biology of phytohormones and related substances, 2021, září 12.-14., Malenovice, ČR. Ústní prezentace.
- Kovalová, M., Grebien, F., Kryštof, V.: Establishment of novel AML cellular models using CRISPR/Cas9 technologies. Chemistry and biology of phytohormones and related substances, 2022, květen 15.-17., Bystřice nad Pernštejnem, ČR. Ústní prezentace.
- Kovalová, M., Jorda, R., Havlíček, L., Řezníčková, E., Kryštof, V.: Transcriptional kinase CDK7 as a drug target. Chemistry and biology of phytohormones and related substances, 2023, květen 21-23, Velké Losiny, ČR. Ústní prezentace.

7 Summary

Cyclin-dependent kinases (CDK) are key regulators of the transcriptional cycle, and they are often deregulated in cancer cells. Together with the transcriptional addiction of tumours, this provides a promising rationale for the use of transcriptional CDK inhibitors in cancer therapy, and several promising tCDK inhibitors have been introduced in recent years. The first part of this thesis focuses on known inhibitors of tCDK in the treatment of leukaemia with KMT2A translocation, whose application could be beneficial compared to standard therapy. The second part presents a novel pyrazolo[4,3-d]pyrimidine derivative, LGR6768, which inhibited CDK7 in the nanomolar range. This inhibitor showed promising anti-leukaemic potential and its application affected cell cycle, transcription, and induced apoptosis of cancer cells. The last part of the thesis is based on the optimisation of dual FLT3/CDK9 inhibitor, which led to the development of new ATP-competitive FLT3 inhibitor and also dual FLT3/CDK9 degrader. The characterisation and testing of these compounds was focused on leukaemia with FLT3-IDT mutation.